DOC.20070928.0011

QA: QA

MDL-WIS-PA-000003 REV 03

September 2007

Seismic Consequence Abstraction

Prepared for:
U.S. Department of Energy
Office of Civilian Radioactive Waste Management
Office of Repository Development
1551 Hillshire Drive
Las Vegas, Nevada 89134-6321

Prepared by:
Sandia National Laboratories
OCRWM Lead Laboratory for Repository Systems
1180 Town Center Drive
Las Vegas, Nevada 89144

Under Contract Number
DE-AC04-94AL85000

DISCLAIMER

This report was prepared as an account of work sponsored by an agency of the United States Government. Neither the United States Government nor any agency thereof, nor any of their employees, nor any of their contractors, subcontractors or their employees, makes any warranty, express or implied, or assumes any legal liability or responsibility for the accuracy, completeness, or any third party's use or the results of such use of any information, apparatus, product, or process disclosed, or represents that its use would not infringe privately owned rights. Reference herein to any specific commercial product, process, or service by trade name, trademark, manufacturer, or otherwise, does not necessarily constitute or imply its endorsement, recommendation, or favoring by the United States Government or any agency thereof or its contractors or subcontractors. The views and opinions of authors expressed herein do not necessarily state or reflect those of the United States Government or any agency thereof.

QA: QA

Seismic Consequence Abstraction

MDL-WIS-PA-000003 REV 03

September 2007

Model Signature Page/Change History

Complete only applicable items.

1. Total Pages: 456

2. Type of Mathematical Model

☐ Process Model ☒ Abstraction Model ☐ System Model

Describe Intended Use of Model

The abstractions in this report define the mechanical response of the waste package and drip shield to seismic hazards. This report also provides a recommended methodology for including these abstractions in the seismic scenario class for the TSPA compliance case for the License Application.

3. Title

Seismic Consequence Abstraction

4. DI (including Rev. No.):

MDL-WIS-PA-000003 REV 03

	Printed Name	Signature	Date
5. Originator	Michael B. Gross		9/27/07
6. Independent Technical Reviewer for	Jean Younker	Ming Zhu	9/27/07
7. Checker	James Kam		9/27/07
8. QCS	Charles D. Beach		9/27/07
9. Responsible Manager/Lead	Cliff Howard		9/27/07
10. Responsible Manager	M. Kathryn Knowles For Paul R Dixon		9-27-07

11. Remarks

Change History

12. Revision No.	13. Description of Change
REV 00	Initial Issue.
REV 01	Initial abstractions have been modified for: 1. Damaged area on the waste package and drip shield is represented as a network of stress corrosion cracks, rather than a "plug" of material that can separate from an EBS component. 2. The effective area of the crack network for diffusive transport is defined. Arguments are provided to demonstrate that the physical morphology of the crack network will not allow a significant advective flux to pass through the drip shield or waste package. 3. A distribution for the maximum value of peak ground velocity is described and incorporated into the computational methodology for the seismic scenario. 4. Minor changes to the fault displacement damage abstraction because of changes in waste package design for the outer diameter of the outer barrier.

REV 01 (Continued)	Initial abstractions have been modified for (continued): 5. Changes in waste package temperature and waste package relative humidity if a drift collapses in the lithophysal zones are incorporated into the seismic scenario. The entire document was revised because of extensive changes. Changes to this version are too extensive to be indicated by change bars.
REV 02	The major changes to the abstractions and the computational algorithm for Revision 02 are as follows: 1. New abstractions for damaged area due to end-to-end impacts of adjacent waste packages have been developed. These new damage abstractions are based on the results from kinematic calculations for the response of multiple waste packages to vibratory ground motions. 2. New abstractions for damaged area due to waste package-pallet impacts have been developed. These new abstractions are based on the results with the original structural response calculations that are documented in Revision 01 of the Seismic Consequence Abstraction. 3. The computational algorithm for the seismic scenario class incorporates the recently developed bounded hazard curve for horizontal peak ground velocity at the emplacement drifts. Change bars have been dropped because the changes from REV 01 are extensive.
REV 03	The abstractions for the seismic scenario class have been modified for peak dose assessment, for the potential for failure of the waste package and drip shield, and for the TAD-bearing waste package. This report includes: 1. New abstractions for damaged area and rupture of the TAD-bearing waste package in response to vibratory ground motion. 2. New abstractions for damaged area and rupture of the CDSP waste package in response to vibratory ground motion. 3. New abstractions for accumulation of rubble in the lithophysal and nonlithophysal units of the repository in response to vibratory ground motion. 4. Fragility curves for the buckling of the drip shield framework and for the tearing of the drip shield plates under the static load from rockfall and the dynamic load from vibratory ground motion 5. New abstraction for the damaged area and failure of the drip shield plates from rock block impacts in nonlithophysal units in response to vibratory ground motion 6. New abstraction for the damaged area on the drip shield under the combined static load from rockfall and the dynamic load from vibratory ground motion 7. New abstraction for damage from fault displacement to the TAD-bearing waste package and the CDSP waste package. Change bars have been dropped because the changes from REV 02 are extensive.

CONTENTS

Page

CONTENTS (Continued)

Page

CONTENTS (Continued)

Page

INTENTIONALLY LEFT BLANK

FIGURES

Page

FIGURES (Continued)

Page

FIGURES (Continued)

Page

FIGURES (Continued)

Page

FIGURES (Continued)

Page

FIGURES (Continued)

Page

TABLES

Page

TABLES (Continued)

Page

TABLES (Continued)

Page

TABLES (Continued)

Page

ACRONYMS

BSC	Bechtel SAIC Company, LLC
CRWMS	Civilian Radioactive Waste Management System
DHLW	defense high-level radioactive waste
DIRS	Document Input Reference System
DOE	U.S. Department of Energy
DTN	data tracking number
EBS	Engineered Barrier System
ECRB	Enhanced Characterization of the Repository Block (cross-drift)
FEPs	features, events, and processes
g	the acceleration of gravity
g-load	acceleration measured as the number of g's
MCO	multicanister overpack
NRC	U.S. Nuclear Regulatory Commission
OCB	outer corrosion barrier (of the waste package)
PGA	peak ground acceleration
PGV	peak ground velocity
PGV-H1	the first horizontal component of peak ground velocity
PMA	Performance Margin Analysis
PSHA	Probabilistic Seismic Hazard Analysis
Q-Q	quantile-quantile (plot)
RST	residual stress threshold
SCC	stress corrosion cracking
SNF	spent nuclear fuel
SNL	Sandia National Laboratories
TAD	transportation, aging, and disposal (canister)
TSPA	total system performance assessment
TSPA-LA	TSPA for the license application
TWP	technical work plan

INTENTIONALLY LEFT BLANK

1. PURPOSE

The primary purpose of this report is to develop abstractions for the mechanical response of Engineered Barrier System (EBS) components to seismic hazards at a geologic repository at Yucca Mountain, Nevada, and to define the methodology for using these abstractions in the total system performance assessment (TSPA) for the license application (TSPA-LA). The abstractions and resulting methodology define the potential for seismic events to disrupt EBS components and affect repository performance over the time period for peak dose assessment. These disruptive effects are represented as a separate scenario class in TSPA, called the seismic scenario class. The seismic scenario class considers two modeling cases: (1) the seismic ground motion modeling case addresses the potential for seismic effects to damage waste packages and drip shields due to vibratory ground motion; and (2) the seismic fault displacement modeling case addresses the effects of fault displacements on waste packages and drip shields. These modeling cases explicitly represent the degradation of waste packages and drip shields from general corrosion and consider the potential for rockfall from multiple seismic events to partly fill or completely collapse emplacement drifts. If radionuclides are released from the EBS due to seismic events, their transport is defined by all of the nominal processes in the unsaturated and saturated zones around the repository.

The seismic hazards addressed herein are vibratory ground motion, fault displacement, and rockfall due to ground motion. The major EBS components addressed in this report are the drip shield and the waste package because failure of these components has the potential to form advective and diffusive pathways that result in the direct release of radionuclides from the EBS into the unsaturated zone. The drift invert and emplacement pallet are included in the structural response calculations for the EBS; however, it is not necessary to develop damage abstractions for the invert and pallet because they do not form new pathways for transport and release of radionuclides after seismic events. The waste package internals and the waste form are also considered in structural response calculations. The compliance case for the TSPA-LA is not taking credit for the fuel rod cladding as a barrier to radionuclide release, so a cladding damage abstraction is not needed for the compliance case. However, a cladding damage abstraction has been developed (see Appendix A) in support of the Performance Margin Analysis (PMA) for the TSPA-LA. The requirements for development of the abstractions and the computational algorithm for the TSPA are defined in *Technical Work Plan for: Calculation of Waste Package and Drip Shield Response to Vibratory Ground Motion and Revision of the Seismic Consequence Abstraction* (SNL 2007 [DIRS 179869]).

The development of these abstractions, which are collectively referred to as seismic damage abstractions, will provide a comprehensive representation of the mechanical response of EBS components after seismic events. The seismic damage abstractions consider (1) the use of the transportation, aging, and disposal (TAD) canister for commercial spent nuclear fuel; (2) the use of the codisposal waste package for defense high level waste (DHLW) and for U.S. Department of Energy (DOE) spent nuclear fuel (SNF); (3) the possibility that EBS components will become highly degraded by general corrosion during the time periods for peak dose assessment; and (4) the potential for multiple seismic events to occur during the time periods for peak dose assessment. The results from this development will address portions of U.S. Nuclear Regulatory Commission (NRC) integrated subissue ENG2, Mechanical Disruption of Engineered Barriers, including the acceptance criteria for this subissue defined in Section 2.2.1.3.2.3 of *Yucca*

Mountain Review Plan, Final Report (NRC 2003 [DIRS 163274]). The seismic damage abstractions documented in this report supersede the abstractions documented in previous versions of this report.

1.1 SCOPE

The scope of this report is limited to abstracting the mechanical response of EBS components to seismic hazards during the postclosure period and to defining the computational algorithms that use these abstractions in the seismic scenario class in the TSPA. The seismic hazards include rockfall induced by vibratory ground motion, so the accumulation of rockfall from multiple seismic events is included in the seismic damage abstractions. Seismic events may also change the thermal and hydrological environments in the drifts after a seismic event. However, changes to the thermal and hydrological environments after seismic events are addressed in *Multiscale Thermohydrologic Model* (SNL 2007 [DIRS 181383]), and are beyond the scope of this report.

The seismic damage abstractions are based on the results from kinematic and structural response calculations for the response of EBS components to vibratory ground motion[1] and from analyses for fault displacement. The kinematic and structural response calculations are not documented in this report; rather, the results from these calculations provide the input data that form the basis for the seismic damage abstractions. The major reports that provide input information for the seismic damage abstractions are identified in Table 1-1. The sources for direct input data and corroborating input data are identified in Table 4-1 and Table 6-1, respectively. The outputs from this report are identified in Section 8.1.

Table 1-1. Major References with Input Data for the Seismic Abstractions

Damage Process	Summary Report
Kinematic and structural response calculations for the response of waste packages and drip shields to vibratory ground motion and to rockfall induced by vibratory ground motion. These calculations also provide the basis for defining the peak acceleration of waste package internals and cladding during waste package-to-pallet impacts and during end-to-end impacts of adjacent waste packages.	*Mechanical Assessment of Degraded Waste Packages and Drip Shields Subject to Vibratory Ground Motion* (SNL 2007 [DIRS 178851])
Rockfall induced by vibratory ground motion.	*Drift Degradation Analysis* (BSC 2004 [DIRS 166107])
Limitation of horizontal peak ground velocity by the dynamic load-bearing capability of the rock at Yucca Mountain.	*Peak Ground Velocities for Seismic Events at Yucca Mountain, Nevada* (BSC 2005 [DIRS 170137])

[1] Vibratory ground motion is the time-dependent, three-dimensional motion of the earth during a seismic event. Each ground motion time history defines the displacement, velocity, and acceleration in three component directions as a function of time at a specific repository location. The three components of each ground motion time history are applied simultaneously to determine kinematic and structural response of EBS components. Ground motion amplitude is identified by the first horizontal component of the peak ground velocity (PGV), usually referred to as horizontal PGV or simply PGV in this document. This horizontal component may be oriented in the longitudinal direction (along the axis of the emplacement drift) or in the transverse direction (in the horizontal plane and perpendicular to the axis of the emplacement drift) for the structural response calculations. Note that the peak velocities for the second horizontal and vertical components of ground motion will vary substantially even when the PGV for the first horizontal component is at a fixed value. This intercomponent variability reflects the aleatory uncertainty inherent in vibratory ground motions. The process to generate the ground motion time histories is summarized in Section 6.4.2.

The seismic damage abstractions for EBS components include both model abstractions and scientific analyses. The abstractions for damage to the waste package and drip shield in response to vibratory ground motion and to rockfall induced by vibratory ground motion are treated as models because they rely on analyses of structural response over a range of ground motions that is wider than typically covered by seismic designs for buildings or nuclear power plants. These model abstractions have been validated to the requirements in SCI-PRO-006, *Models*, through an independent technical review and through a comparison of the individual abstractions to the data from validated computational models. The abstraction for damage from fault displacement and the calculations in Appendix D for the standoff distance from a known secondary fault are considered scientific analyses. The fault displacement damage abstraction is considered a calculation because it evaluates the performance of EBS components by comparing fault displacement with the clearances between EBS components and does not use a mathematical model. The calculation of the standoff distance from known secondary faults in Appendix D is based on established engineering practice and does not require mathematical model development. Section 6.14 provides further justification for the status of the fault displacement damage abstraction and the calculations in Appendix D.

A cladding damage abstraction is not part of the compliance case for the TSPA-LA because the TSPA is not taking credit for fuel rod cladding as a barrier to radionuclide release. However, the PMA for the TSPA-LA may investigate the impact of seismically-induced damage to cladding on repository performance. Appendix A includes a cladding damage abstraction to support the PMA for the TSPA-LA. This damage abstraction does not need validation because it is not included in the compliance case for the TSPA-LA.

The technical work plan (TWP) for this report (SNL 2007 [DIRS 179869], Section 1.1) identifies a commitment to resolve CR 5110 in this revision of *Seismic Consequence Abstraction*. CR 5110 was closed on July 18, 2006, and no further actions are necessary in this report. CR 10115 is not applicable to this report because Section 6.7.2 provides a calculation of the effective drift length for nonlithophysal rockfall. This report responds to many items in CR 9202, as documented in Table 1-2.

Table 1-2. Response to Issues in CR 9202 Relevant to This Report

Number	Title	Objective Evidence for Resolution
9202-001	Revise MDL-WIS-PA-000003 to use time-dependent thickness calculated by WAPDEG	Sections 6.5.1.5, 6.5.2.5, 6.6.1.5, 6.6.2.5, 6.9.6, and 6.10.2.7 incorporate the time-dependent thickness of the outer corrosion barrier (OCB) or drip shield components into the seismic damage abstractions. These thicknesses are calculated by other elements of the TSPA.
9202-002	Address Acceptance Criterion 5 in revision of MDL-WIS-PA-000003 REV 03	Criterion 5 is addressed in Sections 4.2 and 8.2 in this report.
9202-004	Indicate by administrat. change to calc. which assumptions require verification	The results in 000-00C-SSE0-00300-000-00A, *Drip Shield Structural Response to Rock Fall,* have been superseded by *Mechanical Assessment of Degraded Waste Packages and Drip Shields Subject to Vibratory Ground Motion* (SNL 2007 [DIRS 178851], Section 6.4.7). Administrative changes to 000-00C-SSE0-00300-000-00A are, therefore, not required.

Table 1-2. Response to Issues in CR 9202 Relevant to This Report (Continued)

Number	Title	Objective Evidence for Resolution
9202-005	Obtain both upper and lower bounds of yield strength from DTN	DTN: MO0702PASTRESS.002 [DIRS 180514], Table 8-1 in file *Model Output DTN.doc*, provides the upper and lower bound of the residual stress threshold (RST) for Alloy 22 (UNS N06022) (see Table 4-1).
9202-006	Document independence of reviewers in MDL-WIS-PA-000003 REV 03	Dr. Gabriel Toro has not been involved in any aspect of the development of the seismic damage abstractions, as noted in Section 7.2.2.
9202-008	Clarify values of peak ground velocity for 1E-4 annual exceedance	In Table 4-1, the precise value is 40.19 cm/sec, with a note that the value is often rounded to 0.40 m/s in the text.
9202-009	Use LS-DYNA to calculate WP-to-WP impact results in MDL-WIS-PA-000003 REV 03	A unified computational approach with LS-DYNA (V. 970.3858. STN: 10300-970.3858-02 [DIRS 172925]; V. 971.7600.398. STN: 10300-971.7600.398-00 [DIRS 178801]), involving kinematic analyses and damage catalogs for waste package-to-waste package impacts and for waste package-to-pallet impacts, forms the basis for the seismic damage abstractions in Sections 6.5 and 6.6 of this report. The LS-DYNA calculations are described in *Mechanical Assessment of Degraded Waste Packages and Drip Shields Subject to Vibratory Ground Motion* (SNL 2007 [DIRS 178851], Section 6.3).
9202-010	Improve transparency of documentation of methodology and abstraction	This report has been through extensive technical reviews and a licensing review.
9202-011	Compare quasi-static versus dynamic response of a drip shield	Section 6.8.3.1 discusses failure modes of the drip shield, as determined by quasi-static and dynamic calculations (SNL 2007 [DIRS 178851], Section 6.4.4).
9202-012	Determine failure modes of drip shield	Section 6.8.3.1 discusses failure modes of the drip shield, as determined by quasi-static and dynamic calculations (SNL 2007 [DIRS 178851], Section 6.4.4).
9202-013	Determine damage from waste package-to-drip-shield impacts	Section 6.8.5 describes the kinematics for waste package-to-drip shield impacts and discusses the potential for drip shield collapse or failure from these impacts.
9202-014	Correlate damage from WP-to-WP and WP-to-pallet collisions	A unified computational approach with LS-DYNA, involving kinematic analyses and damage catalogs for waste package-to-waste package impacts and for waste package-to-pallet impacts, forms the basis for the seismic damage abstractions in Sections 6.5 and 6.6 of this report. This unified approach eliminates the need to correlate damage from separate models for both types of impacts. Further details on the calculations are in *Mechanical Assessment of Degraded Waste Packages and Drip Shields Subject to Vibratory Ground Motion* (SNL 2007 [DIRS 178851], Section 6.3).

NOTE: WP is waste package; in this report, WP-to-WP impacts are referred to as end-to-end impacts between adjacent waste packages, and WP-to-pallet impacts are referred to as waste package-pallet impacts.

Appendix D of this report provides an analysis of the standoff distance that will ensure no damage to a waste package from displacement along a known secondary fault in the repository block. The requirement for this analysis arose after approval of the technical work plan (SNL 2007 [DIRS 179869]) for development of the seismic damage abstractions. The calculations in Appendix D are considered scientific analyses because they are based on a standard engineering approach. Section 6.14 provides a verification of the engineering approach and software that provide the basis for the scientific analyses in Appendix D. The calculations documented in Appendix D are the single deviation from the approved TWP for this activity.

This report does not address the performance of naval SNF during seismic events. The Naval Nuclear Propulsion Program Technical Support Document for the License Application will provide the seismic analysis for naval SNF. This report also does not address the preclosure response of EBS components to a seismic event.

1.2 LIMITATIONS

The major limitations of the postclosure abstractions for the seismic scenario class are as follows:

- Waste package internals are assumed to degrade as structural elements after the outcer corrosion barrier (OCB) is first damaged by a seismic event. More exactly, the internals degrade as a structural component by the time of the next seismic event after the first seismic event that breaches the waste package. This approach is conservative because a waste package with degraded internals has significantly greater deformation and probability of rupture relative to a waste package with intact internals (see Sections 6.5.1 versus 6.5.2 and 6.6.1 versus 6.6.2). However, this approach underestimates the structural capacity of stainless steel internal components, such as the 2-in-thick inner vessel or the TAD canister itself, during the initial 10,000-year period, which may be important for screening citicality issues.

- Spatial variability in the mechanical response of EBS components to vibratory ground motion has not been represented in the TSPA. In other words, damage to the waste package and drip shield from vibratory ground motion is constant throughout the repository for each seismic event (examples of this can be found in Sections 6.5.5, 6.6.5, 6.9.9, and 6.8.2.2). Although spatial variability is not included within the TSPA, it has been included in the kinematic calculations through the variability of friction factors on a package-by-package basis and in the abstraction of damaged areas for the two or three central waste packages in the kinematic calculations.

  Lack of spatial variability is not important for estimating the mean dose from the seismic scenario class. The mean dose is accurately estimated because the sum of the mean doses from groups of waste packages with different damage levels is equal to the mean of the sum of the doses from the individual groups. In other words, using a constant mean value for the damaged area is an accurate approach for calculating the mean total dose from the repository. On the other hand, the coefficient of variation (i.e., the variability about the mean) of the total dose over all realizations is overestimated without spatial variability. If damage to waste package or drip shield is constant and perfectly correlated everywhere in the repository, realizations with very high or very low

damaged areas produce a more extreme dose history than a realization with damaged areas that varies spatially between the high and low values.

- Structural response calculations for the waste package surrounded by rubble are based on the TAD-canister bearing waste package (referred to hereafter as the TAD-bearing waste package) with degraded internals. Section 6.9.10 provides the rationale for using the results for the TAD-bearing waste package with degraded internals for the codisposal waste package with degraded internals.

- The internals of the waste package surrounded by rubble are always degraded. The use of degraded internals is consistent with the fact that the waste package becomes surrounded by rubble at late times, after the drip shield plates have failed and allowed rubble to contact the waste package. The use of degraded internals is conservative because damage to a waste package with degraded internals is observed to be significantly greater than damage to a waste package with intact internals (see Sections 6.5.1 versus 6.5.2 and 6.6.1 versus 6.6.2).

2. QUALITY ASSURANCE

Analysis and modeling activities performed under *Technical Work Plan for: Calculation of Waste Package and Drip Shield Response to Vibratory Ground Motion and Revision of the Seismic Consequence Abstraction* (SNL 2007 [DIRS 179869]) are subject to the requirements of *Quality Assurance Requirements and Description* (DOE 2007 [DIRS 182051]) because they support the postclosure safety analysis and the performance assessment for the TSPA. Preparation of this model report and its supporting technical activities has been performed in accordance with the appropriate requirements of the quality assurance program and documented in accordance with the TWP (SNL 2007 [DIRS 179869]). The TWP was prepared in accordance with SCI-PRO-002, *Planning for Science Activities*.

This document has been prepared in accordance with SCI-PRO-006. No qualified software was used to develop the abstractions documented in this report, so IM-PRO-003, *Software Management,* is not applicable to the development of the seismic damage abstractions. However, the calculation in Appendix D is performed with qualified software and documented to meet the requirements of IM-PRO-003. Documents produced under the TWP will be submitted for technical, quality assurance, and management review under SCI-PRO-003, *Document Review*, as directed in the TWP. All data produced by the work documented in this model report will be submitted to and incorporated in the Technical Data Management System, in accordance with TST-PRO-001, *Submittal and Incorporation of Data to the Technical Data Management System*. The methods used to control the electronic management of data, as required by IM PRO-002, *Control of the Electronic Management of Information*, are identified in Section 8.4 of the TWP.

INTENTIONALLY LEFT BLANK

3. USE OF SOFTWARE

3.1 QUALIFIED SOFTWARE

No qualified software is used to develop the seismic damage abstractions. These abstractions are based on the results of kinematic calculations, structural response calculations, and rockfall analyses that are performed with qualified software. The major reports documenting these calculations are identified in Table 1-1. The qualified software programs for the structural response and rockfall calculations are not directly used in the abstraction process and are therefore not listed here.

The two-dimensional PFC2D V. 2.0 program (STN: 10828-2.0-00 [DIRS 161950]) was used to perform an analysis of the fault standoff distance that is documented in Appendix D of this report. The software tracking number, version, operating environment, and range of use for PFC2D is listed below, including any limitations on outputs from the software. PFC2D is appropriate for calculating the mechanical response of lithophysal rubble, as used in Appendix D and as explained in Section 6.14. PFC2D was obtained from Software Configuration Management in accordance with established procedures (e.g., IM-PRO-003). PFC2D was used within the range of its validation, as specified in the software qualification documentation in accordance with IM-PRO-003. The relevant information for PFC2D is as follows:

Software Title/Version: PFC2D V. 2.0

Software Tracking Number: 10828-2.0-00

Operating Environment: PC/Windows 2000

Brief Description of Software: PFC2D was used to characterize the behavior of a rubblized rock mass in the lithophysal units of the repository. PFC2D was selected for its capability of modeling the nonlinear response of a rubblized rock mass by combining the behaviors of individual grain particles to simulate the overall deformation of a rubblized rock mass with voids. There are no known limitations on outputs from PFC2D.

3.2 OTHER SOFTWARE

Microsoft Excel for Windows, Version Excel 97 SR-2, running under the Microsoft Windows 2000 Professional operating system on an IBM-compatible personal computer, has been used to develop the abstractions for damage from seismic hazards. The standard functions in Microsoft Excel, including its statistical package and its Solver, are sufficient for these analyses. No macros, codes, or software routines are required for or developed during this work. As used to develop abstractions, Microsoft Excel 97 SR-2 is not required to be qualified or documented in accordance with IM-PRO-003. The formulas, inputs to the formulas, and outputs from the formulas in the Excel spreadsheets that document the statistical analyses for the seismic damage abstractions are identified in the individual spreadsheets and in Appendix B, as required by SCI-PRO-006, Section 6.2, Item I.

All Microsoft Excel files that are relevant for the abstractions are included in the output data tracking numbers (DTNs) identified in Section 9.5 of this report.

4. INPUTS

4.1 DIRECT INPUT

Table 4-1 presents the direct input information for the seismic damage abstractions. The information in Table 4-1 has been categorized into nine areas that are relevant to the abstractions in this report: (1) residual stress threshold (RST) for Alloy 22 (UNS N06022); (2) the bounded hazard curve; (3) kinematic damage to the waste package; (4) damage to the waste package surrounded by rubble; (5) rubble and rockfall accumulation; (6) drip shield fragility; (7) damaged areas on the drip shield; (8) damage from fault displacement; and (9) damage to cladding from vibratory ground motion. The numerical values in Table 4-1 are presented with the same number of significant figures and in the same units as the data in the source, unless otherwise noted. The Group 1 files, Group 2 files, Group 3 worksheets, and Group 4 worksheets that are referenced in Table 4-1 are identified in footnotes at the end of Table 4-1. The intensity of a seismic event is defined in terms of the peak ground velocity of the first horizontal component of the ground motion, denoted as PGV-H1 or more simply as PGV in Table 4-1.

The technical product inputs identified in Table 4-1 are appropriate for the development of model abstractions and scientific analyses for the Seismic Scenario Class. Most items in Table 4-1 are based on the structural response calculations and coupled rockfall/structural response calculations that were performed specifically to provide the technical basis for the seismic damage abstractions for the Seismic Scenario Class. These calculations are documented in the reports listed in Table 1-1.

Section 8.2 identifies the uncertainties in input information and parameters for the damage analyses of EBS components and explains how these uncertainties are propagated into the seismic damage abstractions for the seismic scenario class.

Table 4-1. Direct Input Information

Input Data or Information	Value	Source
Residual Stress Thresholds:		
Residual stress threshold for Alloy 22.	90% to 105% of the yield strength of Alloy 22	DTN: MO0702PASTRESS.002 [DIRS 180514], Table 8-1 in the file *Model Output DTN.doc*
Bounded Hazard Curve:		
Bounded hazard curve for horizontal peak ground velocity at the waste emplacement level.	See DTN for data; numerical values identified in Table 6-3	DTN: MO0501BPVELEMP.001 [DIRS 172682], worksheet "Bounded Horizontal PGV Hazard" in the file *Bounded Horizontal Peak Ground Velocity Hazard at the Repository Waste Emplacement Level.xls*
Minimum annual exceedance frequency for TSPA.	"[C]*onsider only events that have at least one chance in 10,000 of occurring over 10,000 years"* or a minimum value of 1×10^{-8} per year	10 CFR [DIRS 180319], Part 63.114(d)

Table 4-1. Direct Input Information (Continued)

Input Data or Information	Value	Source
Kinematic Damage to the Waste Package:		
Damage statistics for waste package-to-waste package impacts for the TAD-bearing waste package, based on a sampling of vibratory ground motions at the 0.4 m/s, 1.05 m/s, 2.44 m/s, and 4.07 m/s PGV levels.	See DTN for data; numerical values identified in work-sheet "WP-WP Data" in the Group 1 files[1] in output DTN: MO0703PASDSTAT.001	DTN: LL0704PA048SPC.023 [DIRS 180735] File *NavalLong_TAD_ kinematic_analyses_DA_ summary.xls*
Damage statistics for waste package-to-pallet impacts for the TAD-bearing waste package, based on a sampling of vibratory ground motions at the 0.4 m/s, 1.05 m/s, 2.44 m/s, and 4.07 m/s PGV levels.	See DTN for data; numerical values identified in work-sheet "WP-Pallet Data" in the Group 1 files[1] in output DTN: MO0703PASDSTAT.001	DTN: LL0704PA048SPC.023 [DIRS 180735] File *NavalLong_TAD_ kinematic_analyses_DA_ summary.xls*
Statistics for probability of incipient rupture and for probability of rupture for the TAD-bearing waste package in response to vibratory ground motion.	See DTN for data; numerical values identified in Section 6.5.1.1 and Table 6-5	DTN: LL0703PA029SPC.014 [DIRS 179775] File *kinematic_analyses_ rupture_summary.xls* Worksheet: "Naval Long TAD Summary"
Damaged areas for the single TAD-bearing waste package calculations for Realization 4 at the 0.4 m/s PGV level.	See DTN for data; numerical values identified in Table 6-8.	DTN: LL0702PA055SPC.002 [DIRS 179406] File *NavalLong_TAD_1WP _analyses_DA_summary.xls*
Damage statistics for waste package-to-waste package impacts for the CDSP waste package, based on a sampling of vibratory ground motions at the 0.4 m/s, 1.05 m/s, 2.44 m/s, and 4.07 m/s PGV levels.	See DTN for data; numerical values identified in work-sheet "WP-WP Data" in the Group 2 files[2] in output DTN: MO0703PASDSTAT.001	DTN: LL0704PA049SPC.024 [DIRS 180736] File *CDSP_kinematic_ analyses_DA_summary.xls*
Damage statistics for waste package-to-pallet impacts for the CDSP waste package, based on a sampling of vibratory ground motions at the 0.4 m/s, 1.05 m/s, 2.44 m/s, and 4.07 m/s PGV levels.	See DTN for data; numerical values identified in work-sheet "WP-Pallet Data" in the Group 2 files[2] in output DTN: MO0703PASDSTAT.001	DTN: LL0704PA049SPC.024 [DIRS 180736] File *CDSP_kinematic_ analyses_DA_summary.xls*
Statistics for probability of incipient rupture and for probability of rupture for the CDSP waste package in response to vibratory ground motion.	See DTN for data; numerical values identified in Table 6-20	DTN: LL0703PA029SPC.014 [DIRS 179775] File *kinematic_analyses_ rupture_summary.xls* Worksheet: CDSP Summary
Damaged areas for the single CDSP waste package calculations for Realizations 3 and 4 at the 0.4 m/s PGV level.	See DTN for data; numerical values identified in Table 6-23.	DTN: LL0703PA007SPC.005 [DIRS 179644] File *CDSP_1WP_analyses _DA_summary.xls*
Nominal length of OCB for the TAD-bearing waste package.	5,691.38 mm	SNL 2007 [DIRS 179394], Table 4-3
Nominal length of OCB for the 5-DHLW/DOE SNF Long waste package.	5,145.28 mm	SNL 2007 [DIRS 179567], Table 4-9

Table 4-1. Direct Input Information (Continued)

Input Data or Information	Value	Source
Kinematic Damage to the Waste Package (Continued):		
Damaged areas for the 90% RST with material properties at 150°C from end-on and side-on impacts of a waste package on an elastic surface for impact velocities between 1 and 10 m/s and impact angles of 1° and 8°.	See Table 5 for data; numerical values identified in Table 6-13	BSC 2003 [DIRS 162293], Table 5
The median corrosion rate of Alloy 22 at 60°C, based on a medium uncertainty level in the distributions for general corrosion rate.	6.35 nm/yr	DTN: MO0612WPOUTERB.000 [DIRS 182035] File *BaseCase GC CDFs2.xls*, worksheet "Data," Cell L71
Damage to a Waste Package Surrounded by Rubble:		
Damage statistics for the TAD-bearing waste package surrounded by rubble with a 23-mm-thick OCB, based on a sampling of vibratory ground motions at the 0.4 m/s, 1.05 m/s, 2.44 m/s, and 4.07 m/s PGV levels.	See DTN for data; numerical values identified in the Group 3 worksheets[3] in the files in output DTN: MO0703PASDSTAT.001	DTN: MO0702POSTRUBB.000 [DIRS 179314], File *23mm.xls*
Damage statistics for the TAD-bearing waste package surrounded by rubble with a 17-mm-thick OCB, based on a sampling of vibratory ground motions at the 0.4 m/s, 1.05 m/s, 2.44 m/s, and 4.07 m/s PGV levels.	See DTN for data; numerical values identified in the Group 4 worksheets[4] in the files in output DTN: MO0703PASDSTAT.001	DTN: MO0702POSTRUBB.000 [DIRS 179314], File *17mm.xls*
Statistics for probability of puncture for a waste package surrounded by rubble in response to vibratory ground motion.	See DTN for data; numerical values identified in Table 6-42 and Table 6-43	DTN: MO0704PUNCTURE.000 [DIRS 180634], File *Puncture Probability Data – WP Surrounded by Rubble.xls*, worksheet "TAD Rubble Data"
Thickness of the OCB of the TAD waste package.	25.4 mm	SNL 2007 [DIRS 179394], Table 4-3
Thickness of the OCB of the 5-DHLW/DOE SNF-Long waste package.	25.4 mm	SNL 2007 [DIRS 179567], Table 4-9
Mass of a loaded TAD-bearing waste package.	162,055 lbm	SNL 2007 [DIRS 179394], Table 4-3
Mass of a loaded 5-DHLW/DOE SNF-Long waste package.	127,870 lbm	SNL 2007 [DIRS 179567], Table 4-9
Rubble and Rockfall Accumulation:		
Statistics for rubble volume per meter of drift in the lithophysal zones, based on a sampling of vibratory ground motions at the 0.4 m/s, 1.05 m/s, and 2.44 m/s PGV levels.	See DTN for data; numerical values identified in Table 6-28	DTN: MO0611ROCKFALL.000 [DIRS 178831], File *summary.xls*
LHS sampling for ground motion time history number and rock mass category number for the lithophysal realizations.	See Table for data; numerical values identified in Table 6-28	DTN: MO0301SPASIP27.004 [DIRS 161869], first 15 lines in Table I-3 in the file *Sampling_Description.doc*
Percent of emplacement drifts in lithophysal rock.	80% to 85%	SNL 2007 [DIRS 179466], Table 4-1, Item Number 01-03

Table 4-1. Direct Input Information (Continued)

Input Data or Information	Value	Source
Rubble and Rockfall Accumulation (Continued):		
Diameter of the emplacement drifts.	216-inches (5,486.4 mm)	SNL 2007 [DIRS 179354], Table 4-1, Item Number 01-10 and Figure 4-1
Nominal width of the drip shield.	2,535 mm	SNL 2007 [DIRS 179354], Table 4-2, item Number 07-01
Statistics for rock blocks in the nonlithophysal zones, based on a sampling of vibratory ground motions and fracture patterns at the 0.40 m/s PGV level.	See DTN for data	DTN: MO0703SUMM3DEC.000 [DIRS 179895], Worksheet "block information" in the file *nonlith rockfall characteristics in emplacement drifts with 1e-4 gm.xls*
Statistics for rock blocks in the nonlithophysal zones, based on a sampling of vibratory ground motions and fracture patterns at the 1.05 m/s PGV level.	See DTN for data; numerical values per realization in Table 6-31	DTN: MO0703SUMM3DEC.000 [DIRS 179895], Worksheets "rockfall per simulation" and "block information" in the file *nonlith rockfall characteristics in emplacement drifts with 1e-5 gm.xls*
Statistics for rock blocks in the nonlithophysal zones, based on a sampling of vibratory ground motions and fracture patterns at the 2.44 m/s PGV level.	See DTN for data; numerical values per realization in Table 6-31	DTN: MO0703SUMM3DEC.000 [DIRS 179895], Worksheets "rockfall per simulation" and "block information" in the file *nonlith rockfall characteristics in emplacement drifts with 1e-6 gm.xls*
Statistics for rock blocks in the nonlithophysal zones, based on a sampling of vibratory ground motions and fracture patterns at the 5.35 m/s PGV level.	See DTN for data; numerical values per realization in Table 6-31	DTN: MO0703SUMM3DEC.000 [DIRS 179895], Worksheets "rockfall per simulation" and "block information" in the file *nonlith rockfall characteristics in emplacement drifts with 1e-7 gm.xls*
Horizontal PGV for the 10^{-4} per year mean annual exceedance frequency on the unbounded hazard curve at Point B, the waste emplacement level.	40.19 cm/s, (sometimes rounded to 0.40 m/s in the text)	DTN: MO0404PGVRL104.000 [DIRS 170437], Cell A7 in "Sheet1" in file *10-4_PGV_Point B.xls*
Horizontal PGV for the 10^{-5} per year mean annual exceedance frequency on the unbounded hazard curve at Point B, the waste emplacement level.	1.05 m/s	DTN: MO0401SEPPGVRL.022 [DIRS 169099], Cell A7 in "Sheet1" in file *10-5_PGV_Point B.xls*
Horizontal PGV for the 10^{-6} per year mean annual exceedance frequency on the unbounded hazard curve at Point B, the waste emplacement level.	2.44 m/s	DTN: MO0303DPGVB106.002 [DIRS 162712], Cell A7 in "Sheet1" in file *10-6_PGV_Point B_Rev2.xls*
Horizontal PGV for the 10^{-7} per year mean annual exceedance frequency on the unbounded hazard curve at Point B, the waste emplacement level.	5.35 m/s	DTN: MO0210PGVPB107.000 [DIRS 162713], Cell A7 in "Sheet1" in file *10-7_PGV_Point B.xls*
Length in the 3DEC model for nonlithophysal rockfall.	25 meters	BSC 2004 [DIRS 166107], Section 6.3.1
Azimuthal angle for the drift in the 3DEC model for nonlithophysal rockfall.	75 degrees	BSC 2004 [DIRS 166107], Section 6.3.1.1
Length of solid continuum at the ends of the drift in 3DEC model for nonlithophysal rockfall.	2 meters	BSC 2004 [DIRS 166107], length scaled from Figure 6-34(f), based on 25-meter length of the 3DEC model (BSC 2004 [DIRS 166107], Section 6.3.1)

Table 4-1. Direct Input Information (Continued)

Input Data or Information	Value	Source
Drip Shield Fragility:		
Plastic load capacity of the drip shield plates for 5 mm, 10 mm, and 15 mm plate thicknesses.	See DTN for data; numerical values in Table 6-35	DTN: MO0701DRIPSHLD.000 [DIRS 182334], *3_4_5.zip*, File *summary DS plate fragility.xls,* worksheet "limit load"
Plastic load capacity of the drip shield framework for thickness reductions of 0 mm, 5 mm, and 10 mm.	See DTN for data; numerical values in Table 6-38	DTN: MO0701DRIPSHLD.000 [DIRS 182334], *3_4_5.zip*, File *summary DS framework fragility.xls,* worksheet "limit load"
Damaged areas for a collapsed drip shield on top of the TAD-bearing waste package.	See DTN for data; plot from the DTN is presented in Figure 6-77	DTN: MO0701DRIPSHLD.000 [DIRS 182334], File *summary WP loaded by DS.xls*
Average lithophysal rockfall load on the crown of the drip shield.	See DTN for data; numerical values in Table 6-34	MO0407MWDDSLCR.000 [DIRS 170873], File *final drip shield quasi-static pressures.xls*
Average lithophysal rockfall on each of 10 segments on the crown of the drip shield.	See DTN for data; numerical values in Table 6-37	MO0407MWDDSLCR.000 [DIRS 170873], File *final drip shield quasi-static pressures.xls*
First horizontal component of peak ground velocity (PGV-H1) at the 1.05 m/s PGV level for 17 ground motions.	See DTN for data; numerical values in Table 6-33	DTN: MO0402AVDTM105.001 [DIRS 168890], PGV-H1 from files *matxh1.vts in vts.zip*, where x = 01, 02, 03, …, 16, and 17
First horizontal component of peak ground velocity (PGV-H1) at the 2.44 m/s PGV level for 17 ground motions.	See DTN for data; numerical values in Table 6-33	DTN: MO0403AVDSC106.001 [DIRS 168891], PGV-H1 from files *matxh1.vts in vts.zip*, where x = 01, 02, 03, …, 16, and 17
First horizontal component of peak ground velocity (PGV-H1) at the 5.35 m/s PGV level for 17 ground motions.	See DTN for data; numerical values in Table 6-33	DTN: MO0403AVTMH107.003 [DIRS 168892], PGV-H1 from files *matxh1.vts in vts.zip*, where x = 01, 02, 03, …, 16, and 17
Frequency and magnitude of longitudinal impacts of the waste package into the bulkhead support beams on the underside of the crown of the drip shield.	See DTN for data; numerical values in Table 6-41	DTN: LL0704PA050SPC.025 [DIRS 180819], File *WPDS_kinematic_analyses _summary.xls*, worksheets "NLTAD Impacts Summary" and "CDSP Impacts Summary"
Magnitude of the lateral impact velocities for calculations of waste package-to-drip shield impacts.	6 m/s and 11 m/s	BSC 2005 [DIRS 173172], p. 5-49
Bounding lateral impact velocity at the 2.44 m/s PGV level.	6 m/s	BSC 2005 [DIRS 173172], Table 5-7
Results from structural response calculations for lateral impact of the waste package on the drip shield.	Even the extreme lateral impact velocity of 11 m/s does not cause catastrophic failure of the drip shield	BSC 2005 [DIRS 173172], Section VI-3.3
Results from structural response calculations for longitudinal impact of the waste package into the bulkhead support beam on the underside of the crown of the drip shield.	Longitudinal impact at 2.25 m/s may cause a section of one bulkhead to fail, but the drip shield remains structurally stable	BSC 2005 [DIRS 173172], Section VI-3.4.1 and Figure VI-40

Table 4-1. Direct Input Information (Continued)

Input Data or Information	Value	Source
Damaged Areas on the Drip Shield:		
Damaged areas on a drip shield plate with fixed boundary conditions at the middle stiffener and bulkhead.	See DTN for data; numerical values in Table 6-49 for the 5-mm plate thickness	DTN: MO0703PADSBLOC.000 [DIRS 179662], File *DS plate damage due to distributed loads.xls*, worksheet “Case 1 boundary condition”
Damaged areas on a drip shield plate that can move laterally and is fixed for rotations at the middle stiffener and bulkhead.	See DTN for data; numerical values in Table 6-49for the 10-mm and 15-mm plate thicknesses	DTN: MO0703PADSBLOC.000 [DIRS 179662], File *DS plate damage due to distributed loads.xls*, worksheet “Case 2 boundary condition”
Damaged areas on a quarter symmetry model of the drip shield from impacts by seven representative rock blocks.	See DTN for data; numerical values in Table 6-51	DTN: MO0703PADSBLOC.000 [DIRS 179662], File *DS damage due to large block impacts.xls*, worksheet “damage area”
Maximum plastic strain in the drip shield plates from impacts by seven representative rock blocks.	See DTN for data; numerical values in Table 6-51	DTN: MO0703PADSBLOC.000 [DIRS 179662], File *DS damage due to large block impacts.xls*, worksheet “max plate plastic strains”
Maximum plastic strain in the drip shield axial stiffeners from impacts by seven representative rock blocks.	See DTN for data; numerical values in Table 6-51	DTN: MO0703PADSBLOC.000 [DIRS 179662], File *DS damage due to large block impacts.xls*, worksheet “max stiffener plastic strains”
Maximum deflection of the drip shield axial stiffeners from impacts by seven representative rock blocks.	See DTN for data; numerical values in Table 6-51	DTN: MO0703PADSBLOC.000 [DIRS 179662], File *DS damage due to large block impacts.xls*, worksheet “stiffener displacements”
Nominal axial length of the drip shield.	5,805 mm	SNL 2007 [DIRS 179354], Table 4-2, item Number 07-01
Axial length of the drip shield connector (overlap) subassembly.	320 mm	SNL 2007 [DIRS 179354], Table 4-2, item Number 07-01
Mean value for the general corrosion rate for Titanium Grade 7 under benign conditions.	5.15 nm/yr	SNL 2007 [DIRS 180778], Table 8-1[a]
Mean value for the general corrosion rate for Titanium Grade 7 under aggressive conditions.	46.1 nm/yr	SNL 2007 [DIRS 180778], Table 8-1[a]
Fault Displacement Damage Abstraction:		
Schematic diagram of the emplacement drift cross section with key dimensions rounded to the nearest inch.	See source for data; numerical values in Figure 6-107	SNL 2007 [DIRS 179354], Figure 4-1
Height of the steel invert structure (maximum thickness of invert).	52 inches (1,320.8 mm)	SNL 2007 [DIRS 179354], Table 4-1, Item Number 01-10 and Figure 4-1
Clearance from crown of drip shield to roof of drift.	50 inches, rounded to the nearest inch	SNL 2007 [DIRS 179354], Table 4-2, Item Number 07-01 and Figure 4-1
Drip shield nominal height—exterior.	2,886 mm	SNL 2007 [DIRS 179354], Table 4-2, Item Number 07-01
Drip shield height—interior.	107 inches, rounded to the nearest inch (2,717.8 mm)	SNL 2007 [DIRS 179354], Table 4-2, Item Number 07-01, based on D2+D3 in Figure 4-1
Outside diameter of OCB of TAD-bearing waste package.	1,881.6 mm	SNL 2007 [DIRS 179394], Table 4-3
Outside diameter of OCB of Naval-Long waste package.	1,881.6 mm	SNL 2007 [DIRS 179567], Table 4-6

Table 4-1. Direct Input Information (Continued)

Input Data or Information	Value	Source
Fault Displacement Damage Abstraction (Continued):		
Outside diameter of OCB of Naval-Short waste package.	1,881.6 mm	SNL 2007 [DIRS 179567], Table 4-7
Outside diameter of OCB of 5-DHLW/DOE SNF Short waste package.	2,044.7 mm	SNL 2007 [DIRS 179567], Table 4-8
Outside diameter of OCB of 5-DHLW/DOE SNF Long waste package.	2,044.7 mm	SNL 2007 [DIRS 179567], Table 4-9
Outside diameter of OCB of 2-MCO/2-DHLW waste package.	1,749.3 mm	SNL 2007 [DIRS 179567], Table 4-10
Nominal length of TAD-bearing waste package.	5,850.1 mm	SNL 2007 [DIRS 179394], Table 4-3
Nominal length of Naval-Long waste package.	5,850.1 mm	SNL 2007 [DIRS 179567], Table 4-6
Nominal length of Naval Short waste package.	5,215.10 mm	SNL 2007 [DIRS 179567], Table 4-7
Nominal length of 5-DHLW/DOE SNF Short waste package.	3,697.4 mm	SNL 2007 [DIRS 179567], Table 4-8
Nominal length of 5-DHLW/DOE SNF Long waste package.	5,303.9 mm	SNL 2007 [DIRS 179567], Table 4-9
Nominal length of OCB of 2-MCO /2-DHLW waste package.	5,278.6 mm	SNL 2007 [DIRS 179567], Table 4-10
Clearance between top of TAD-bearing waste package and underside of drip shield peripheral bulkhead.	21 inches (836 mm)	SNL 2007 [DIRS 179354], Table 4-1, Item Number 02-02, based on dimension D3 in Figure 4-1 rounded to the nearest inch
Clearance between top of Naval waste package and underside of drip shield peripheral bulkhead.	21 inches (533 mm)	SNL 2007 [DIRS 179354], Table 4-1, Item Number 02-02, based on dimension D3 in Figure 4-1 rounded to the nearest inch
Clearance between top of 5-DHLW/DOE SNF waste package and underside of drip shield peripheral bulkhead.	14 inches (356 mm)	SNL 2007 [DIRS 179354], Table 4-1, Item Number 02-02, based on dimension D3 in Figure 4-1 rounded to the nearest inch
Clearance between top of 2-MCO/2-DHLW waste package and underside of drip shield peripheral bulkhead.	27 inches (686 mm)	SNL 2007 [DIRS 179354], Table 4-1, Item Number 02-02, based on dimension D3 in Figure 4-1 rounded to the nearest inch
Emplacement drift numbers intersected by the Sundance Fault.	1-2 1-3 1-4 1-5 1-6 2-1	DTN: MO0707FAULTEMP.000 [DIRS 182092] File *Output.xls*, with results summarized in the README file

Table 4-1. Direct Input Information (Continued)

Input Data or Information	Value	Source
Fault Displacement Damage Abstraction (Continued):		
Emplacement drift numbers intersected by the Drill Hole Wash Fault.	4-1 4-2 3-4W 3-5W 3-6W 3-7W 3-8W 3-9W1 3-9E1 3-10E1 3-11E1 3-12E1 3-13E1 3-14E 3-15E1 3-16E1 3-17E1	DTN: MO0707FAULTEMP.000 [DIRS 182092] File *Output.xls*, with results summarized in the README file
Emplacement drift numbers intersected by the Pagany Wash Fault.	3-1W 3-1E 3-2E 3-3E 3-4E 3-5E 3-6E1 3-7E1	DTN: MO0707FAULTEMP.000 [DIRS 182092] File *Output.xls*, with results summarized in the README file
Emplacement drift numbers Intersected by the Sever Wash Fault.	3-2 E	DTN: MO0707FAULTEMP.000 [DIRS 182092] File *Output.xls*, with results summarized in the README file
Emplacement drift numbers intersected by the western splay off the main Ghost Dance Fault.	2-17 2-18 2-19 2-20 2-21 2-22 2-23 2-24 2-25 2-26 2-27	DTN: MO0707FAULTEMP.000 [DIRS 182092] File *Output.xls*, with results summarized in the README file

Table 4-1. Direct Input Information (Continued)

Input Data or Information	Value	Source
Fault Displacement Damage Abstraction (Continued):		
Fault displacement hazard at Site 2 on the Solitario Canyon Fault.	Displ. (cm) / Mean Exceed. Freq. (1/yr) 0.1 2.42×10^{-05} 0.2 2.37×10^{-05} 0.5 2.30×10^{-05} 1 2.26×10^{-05} 2 2.19×10^{-05} 5 2.06×10^{-05} 10 1.86×10^{-05} 20 1.45×10^{-05} 50 6.95×10^{-06} 100 2.78×10^{-06} 200 8.41×10^{-07} 500 9.41×10^{-08}	DTN: MO0401MWDRPSHA.000 [DIRS 183046] File *./displ/tot_ haz/s2.frac_mean.gz*, with mean exceedance frequency rounded to three significant figures
Fault displacement hazard at Site 3 on the Drill Hole Wash Fault.	Displ. (cm) / Mean Exceed. Freq. (1/yr) 0.1 8.57×10^{-06} 0.2 7.86×10^{-06} 0.5 6.91×10^{-06} 1 5.98×10^{-06} 2 4.87×10^{-06} 5 3.06×10^{-06} 10 1.69×10^{-06} 20 7.38×10^{-07} 50 2.03×10^{-07} 100 5.94×10^{-08} 200 1.56×10^{-08} 500 1.69×10^{-09}	DTN: MO0401MWDRPSHA.000 [DIRS 183046] File *./displ/tot_ haz/s3.frac_mean.gz*, with mean exceedance frequency rounded to three significant figures
Fault displacement hazard at Site 4 on the Ghost Dance Fault.	Displ. (cm) / Mean Exceed. Freq. (1/yr) 0.1 9.30×10^{-06} 0.2 7.84×10^{-06} 0.5 6.86×10^{-06} 1 5.87×10^{-06} 2 4.69×10^{-06} 5 2.94×10^{-06} 10 1.63×10^{-06} 20 7.28×10^{-07} 50 1.82×10^{-07} 100 5.07×10^{-08} 200 1.18×10^{-08} 500 1.31×10^{-09}	DTN: MO0401MWDRPSHA.000 [DIRS 183046] File *./displ/tot_haz/*s4rev.frac_mean.gz, with mean exceedance frequency rounded to three significant figures

Table 4-1. Direct Input Information (Continued)

Input Data or Information	Value	Source
Fault Displacement Damage Abstraction (Continued):		
Fault displacement hazard at Site 5 on the Sundance Fault.	Displ. (cm) / Mean Exceed. Freq. (1/yr) 0.1 1.06×10^{-05} 0.2 9.21×10^{-06} 0.5 6.83×10^{-06} 1 4.77×10^{-06} 2 2.88×10^{-06} 5 1.23×10^{-06} 10 6.00×10^{-07} 20 2.72×10^{-07} 50 7.10×10^{-08} 100 1.94×10^{-08} 200 4.27×10^{-09} 500 4.72×10^{-10}	DTN: MO0401MWDRPSHA.000 [DIRS 183046] File ./displ/tot_haz/s5rev.frac_mean.gz, with mean exceedance frequency rounded to three significant figures
Fault displacement hazard at Site 7a, a generic repository location, approximately 100 m east of the Solitario Canyon Fault, with a hypothetical small fault with 2-m offset.	Displ. (cm) / Mean Exceed. Freq. (1/yr) 0.1 7.02×10^{-06} 0.2 5.47×10^{-06} 0.5 3.11×10^{-06} 1 1.72×10^{-06} 2 1.04×10^{-06} 5 4.58×10^{-07} 10 2.10×10^{-07} 20 8.63×10^{-08} 50 2.12×10^{-08} 100 5.43×10^{-09} 200 2.63×10^{-10} 500 1.41×10^{-11}	DTN: MO0401MWDRPSHA.000 [DIRS 183046] File *./displ/tot_ haz/s7a.frac_mean.gz,* with mean exceedance frequency rounded to three significant figures
Fault displacement hazard at Site 8a, a generic repository location, midway between the Solitario Canyon and Ghost Dance Faults, with a hypothetical small fault with a 2-m offset.	Displ. (cm) / Mean Exceed. Freq. (1/yr) 0.1 6.72×10^{-06} 0.2 5.26×10^{-06} 0.5 3.05×10^{-06} 1 1.70×10^{-06} 2 1.02×10^{-06} 5 4.52×10^{-07} 10 2.09×10^{-07} 20 8.91×10^{-08} 50 2.36×10^{-08} 100 6.17×10^{-09} 200 2.48×10^{-10} 500 1.28×10^{-11}	DTN: MO0401MWDRPSHA.000 [DIRS 183046] File *./displ/tot_ haz/s8a.frac_mean.gz*, with mean exceedance frequency rounded to three significant figures

Table 4-1. Direct Input Information (Continued)

Input Data or Information	Value	Source
Fault Displacement Damage Abstraction (Continued):		
Fault displacement hazard at Site 7b – a generic repository location, approximately 100 meters east of the Solitario Canyon Fault. Site 7b has a hypothetical shear with 10-cm offset.	Displ. (cm) / Mean Exceed. Freq. (1/yr) 0.1 2.95×10^{-06} 0.2 2.27×10^{-06} 0.5 1.49×10^{-06} 1 1.00×10^{-06} 2 5.81×10^{-07} 5 1.72×10^{-07} 10 6.02×10^{-09} 20 1.62×10^{-06}	DTN: MO0401MWDRPSHA.000 [DIRS 183046] Files *./displ/9ot_ haz/s7b.frac_mean.gz*, with mean exceedance frequency rounded to three significant figures
Fault displacement hazard at Site 7c – a generic repository location approximately 100 meters east of the Solitario Canyon Fault. Site 7c has a hypothetical fracture with no cumulative displacement.	Displ. (cm) / Mean Exceed. Freq. (1/yr) 0.1 1.10×10^{-06} 0.2 5.68×10^{-07} 0.5 1.91×10^{-07} 1 2.75×10^{-11} 2 1.48×10^{-17} 5 6.74×10^{-30}	DTN: MO0401MWDRPSHA.000 [DIRS 183046] File *./displ/tot_ haz/s7c.frac_mean.gz,* with mean exceedance frequency rounded to three significant figures
Fault displacement hazard at Site 7d – a generic repository location, approximately 100 meters east of the Solitario Canyon Fault. Site 7d is intact rock.	Displ. (cm) / Mean Exceed. Freq. (1/yr) 0.1 3.91×10^{-11} 0.2 2.47×10^{-15} 0.5 2.91×10^{-28} 1 1.00×10^{-30}	DTN: MO0401MWDRPSHA.000 [DIRS 183046] File */displ/tot_ haz/s7d.frac_mean.gz*, with mean exceedance frequency rounded to three significant figures
Fault displacement hazard at Site 8b – a generic repository location, midway between the Solitario Canyon and Ghost Dance Faults. Site 8b has a hypothetical shear with 10-cm offset.	Displ. (cm) / Mean Exceed. Freq. (1/yr) 0.1 2.71×10^{-06} 0.2 2.09×10^{-06} 0.5 1.38×10^{-06} 1 9.40×10^{-07} 2 5.67×10^{-07} 5 1.66×10^{-07} 10 5.16×10^{-09} 20 1.21×10^{-09}	DTN: MO0401MWDRPSHA.000 [DIRS 183046] File *./displ/tot_ haz/s8b.frac_mean.gz,* with mean exceedance frequency rounded to three significant figures
Fault displacement hazard at Site 8c – a generic repository location, midway between the Solitario Canyon and Ghost Dance Faults. Site 8c has a hypothetical fracture with no cumulative displacement.	Displ. (cm) / Mean Exceed. Freq. (1/yr) 0.1 1.03×10^{-06} 0.2 5.33×10^{-07} 0.5 1.79×10^{-07} 1 3.59×10^{-11} 2 1.47×10^{-17} 5 6.66×10^{-30}	DTN: MO0401MWDRPSHA.000 [DIRS 183046] File */displ/tot_ haz/s8c.frac_mean.gz,* with mean exceedance frequency rounded to three significant figures
Nominal quantity of TAD-bearing waste packages in design basis inventory.	7,483	DTN: MO0702PASTREAM.001 [DIRS 179925] File *DTN-Inventory-Rev00.xls*, worksheet "UNIT CELL," cells B14:L15

Table 4-1. Direct Input Information (Continued)

Input Data or Information	Value	Source
Fault Displacement Damage Abstraction (Continued):		
Nominal quantity of Naval-Long waste packages in design basis inventory.	310	DTN: MO0702PASTREAM.001 [DIRS 179925] File *DTN-Inventory-Rev00.xls*, worksheet "UNIT CELL," cells B14:L15
Nominal quantity of Naval-Short waste packages in design basis inventory.	90	DTN: MO0702PASTREAM.001 [DIRS 179925] File *DTN-Inventory-Rev00.xls*, worksheet "UNIT CELL," cells B14:L15
Nominal quantity of 5-DHLW/DOE SNF Short waste packages in design basis inventory.	1,207	DTN: MO0702PASTREAM.001 [DIRS 179925] File *DTN-Inventory-Rev00.xls*, worksheet "UNIT CELL," cells B14:L15
Nominal quantity of 5-DHLW/DOE SNF Long waste packages in design basis inventory (includes 1S/5L, 1L(Wide)/4L, and 1S(Wide)/4L configurations.	1,862	DTN: MO0702PASTREAM.001 [DIRS 179925] File *DTN-Inventory-Rev00.xls*, worksheet "UNIT CELL," cells B14:L15
Nominal quantity of 2-MCO/2-DHLW waste packages in design basis inventory.	210	DTN: MO0702PASTREAM.001 [DIRS 179925] File *DTN-Inventory-Rev00.xls*, worksheet "UNIT CELL," cells B14:L15
Damage to Cladding from Vibratory Ground Motion:		
Number of impacts of codisposal waste package with axial impact velocity greater than 4 m/s.	None at the 0.4 m/s and 1.05 m/s PGV levels; 1 out of 17 at the 2.44 m/s PGV level; 5 out of 17 at the 4.07 m/s PGV level	LL0706MG004SPC.001 [DIRS 182137] Worksheet "Max Vel CDSP-NavalLongTAD" in file *Catalog_analyses_accel.xls*
Number of impacts of TAD-bearing waste package with axial impact velocity greater than 6 m/s.	1 out of 17 at the 4.07 m/s PGV level; none at smaller PGV levels	LL0706MG004SPC.001 [DIRS 182137] Worksheet "Max Vel CDSP-NavalLongTAD" in file *Catalog_analyses_accel.xls*
Peak lateral acceleration of waste package internals from waste package-to-pallet impacts for the TAD-bearing or codisposal waste packages.	43 g's for a 10 m/s impact velocity	LL0706MG004SPC.001 [DIRS 182137] Worksheets "NavalLong TAD WPP" and "CDSP WPP" in file *Catalog_analyses_accel.xls*
Peak axial acceleration of waste package internals in the TAD-bearing waste package from TAD-to-TAD impacts.	72 g's for an impact velocity of 9 m/s	LL0706MG004SPC.001 [DIRS 182137] Worksheet "NavalLong TAD WPWP" in file *Catalog_analyses_accel.xls*
Peak axial acceleration of waste package internals in the TAD-bearing waste package from TAD-to-codisposal impacts.	75 g's for a 6 m/s impact velocity; 88 g's for a 9 m/s impact velocity	LL0706MG004SPC.001 [DIRS 182137] Worksheet "CDSP WPWP" in file *Catalog_ analyses_accel.xls*
Peak axial acceleration of waste package internals in the codisposal waste package from TAD-to-codisposal impacts.	75 g's for a 4 m/s impact velocity; 111 g's for a 6 m/s impact velocity; 164 g's for a 9 m/s impact velocity	LL0706MG004SPC.001 [DIRS 182137] Worksheet "CDSP WPWP" in file *Catalog_analyses_accel.xls*

Table 4-1. Direct Input Information (Continued)

Input Data or Information	Value	Source
Fault Displacement Standoff Analysis:		
Initial tangent modulus for tuff rubble.	50 MPa to 200 MPa	BSC 2005 [DIRS 173172], p. IX-15

Sources: [1] Group 1 files in output DTN: MO0703PASDSTAT.001 are *Kinematic Damage Abstraction 23-mm Intact.xls*, *Kinematic Damage Abstraction 23-mm Degraded.xls*, and *Kinematic Damage Abstraction 17-mm Degraded.xls*.

[2] Group 2 files in output DTN: MO0703PASDSTAT.001 are *CDSP Kinematic Damage Abstraction 23-mm Intact.xls*, *CDSP Kinematic Damage Abstraction 23-mm Degraded.xls*, and *CDSP Kinematic Damage Abstraction 17-mm Degraded.xls*.

[3] Group 3 worksheets in output DTN: MO0703PASDSTAT.001 are "Data at 0.40 mps PGV", "Data at 1.05 mps PGV", "Data at 2.44 mps PGV", and "Data at 4.07 mps PGV" in file *WP-Rubble Damage Abstraction 23-mm Degraded.xls*.

[4] Group 4 worksheets in output DTN: MO0703PASDSTAT.001 are "Data at 0.40 mps PGV", "Data at 1.05 mps PGV", "Data at 2.44 mps PGV", and "Data at 4.07 mps PGV" in file *WP-Rubble Damage Abstraction 17-mm Degraded.xls*.

NOTE: CDSP = codisposal; DHLW = defense high-level radioactive waste; WP = waste package.

4.2 CRITERIA

General programmatic requirements for this document are listed in *Technical Work Plan for: Calculation of Waste Package and Drip Shield Response to Vibratory Ground Motion and Revision of the Seismic Consequence Abstraction* (SNL 2007 [DIRS 179869]). This TWP specifies that this model report and the analyses described herein must adhere to the requirements of SCI-PRO-006, *Models*. The TWP also specifies that this model report must address the acceptance criteria in *Yucca Mountain Review Plan, Final Report* (NRC 2003 [DIRS 163274]).

Section 2.2.1.3.2.3, Mechanical Disruption of Engineered Barriers, of *Yucca Mountain Review Plan, Final Report* (NRC 2003 [DIRS 163274]) provides guidance regarding the acceptance criteria that may be used by the NRC staff to determine whether the technical requirements have been met by the seismic damage abstractions. The five general acceptance criteria in Section 2.2.1.3.2.3 are listed below, along with the subcriteria specifically addressed by this report. Where a subcriterion includes several components, only some components may be addressed. Section 8.2 provides a detailed discussion of how the seismic damage abstractions meet the applicable acceptance criteria from Section 2.2.1.3.2.3 of *Yucca Mountain Review Plan, Final Report* (NRC 2003 [DIRS 163274]).

Acceptance Criteria from Section 2.2.1.3.2.3, *Mechanical Disruption of Engineered Barriers*

Acceptance Criterion 1: System Description and Model Integration Are Adequate.

(1) Total system performance assessment adequately incorporates important design features, physical phenomena, and couplings, and uses consistent and appropriate assumptions throughout the mechanical disruption of engineered barrier abstraction process.

(2) The description of geological and engineering aspects of design features, physical phenomena, and couplings, that may affect mechanical disruption of engineered barriers, is adequate. For example, the description may include materials used in the construction of engineered barrier components, environmental effects (e.g., temperature, water chemistry, humidity, radiation) on these materials, and mechanical-failure processes and concomitant failure criteria used to assess the performance capabilities of these materials. Conditions and assumptions in the abstraction of mechanical disruption of engineered barriers are readily identified and consistent with the body of data presented in the description.

(3) The abstraction of mechanical disruption of engineered barriers uses assumptions, technical bases, data, and models that are appropriate and consistent with other related U.S. Department of Energy abstractions. For example, assumptions used for mechanical disruption of engineered barriers are consistent with the abstraction of degradation of engineered barriers as required in Section 2.2.1.3.1 of *Yucca Mountain Review Plan, Final Report* (NRC 2003 [DIRS 163274]). The descriptions and technical bases provide transparent and traceable support for the abstraction of mechanical disruption of engineered barriers.

(4) Boundary and initial conditions used in the total system performance assessment abstraction of mechanical disruption of engineered barriers are propagated throughout its abstraction approaches.

(5) Sufficient data and technical bases to assess the degree to which features, events, and processes have been included in this abstraction are provided.

Subcriterion (6) is not discussed here because it is related to transient criticality and beyond the scope of this report. Subcriterion (7) is not discussed here because there are no activities related to peer review or qualification of existing data discussed in this report.

Acceptance Criterion 2: Data Are Sufficient for Model Justification.

(1) Geological and engineering values, used in the license application to evaluate mechanical disruption of engineered barriers, are adequately justified. Adequate descriptions of how the data were used, interpreted, and appropriately synthesized into the parameters are provided.

(3) Data on geology of the natural system, engineering materials, and initial manufacturing defects, used in the total system performance assessment abstraction, are based on appropriate techniques. These techniques may include laboratory experiments, site-specific field measurements, natural analog research, and process-level modeling studies. As appropriate, sensitivity or uncertainty analyses used to support the U.S. Department of Energy total system performance assessment abstraction are adequate to determine the possible need for additional data.

(4) Engineered barrier mechanical failure models for disruption events are adequate. For example, these models may consider effects of prolonged exposure to the expected emplacement drift environment, material test results not specifically designed or

performed for the Yucca Mountain site, and engineered barrier component fabrication flaws.

Subcriterion (2) is not discussed here because data collection activities related to the geology of the natural system engineering materials, and initial manufacturing defects are beyond the scope of this report.

Acceptance Criterion 3: Data Uncertainty Is Characterized and Propagated Through the Model Abstraction.

(1) Models use parameter values, assumed ranges, probability distributions, and bounding assumptions that are technically defensible, reasonably account for uncertainties and variabilities, and do not result in an under-representation of the risk estimate.

(2) Process-level models used to represent mechanically disruptive events, within the emplacement drifts at the proposed Yucca Mountain repository, are adequate. Parameter values are adequately constrained by Yucca Mountain site data, such that the effects of mechanically disruptive events on engineered barrier integrity are not underestimated. Parameters within conceptual models for mechanically disruptive events are consistent with the range of characteristics observed at Yucca Mountain.

(3) Uncertainty is adequately represented in parameter development for conceptual models, process-level models, and alternative conceptual models considered in developing the assessment abstraction of mechanical disruption of engineered barriers. This may be done either through sensitivity analyses or use of conservative limits; and Review Plan for Safety Analysis Report 2.2-33.

Subcriterion (4) is not discussed here because an expert elicitation was not performed during the development of the seismic abstractions.

Acceptance Criterion 4: Model Uncertainty Is Characterized and Propagated Through the Model Abstraction.

(2) Consideration of conceptual model uncertainty is consistent with available site characterization data, laboratory experiments, field measurements, natural analog information and process-level modeling studies; and the treatment of conceptual model uncertainty does not result in an under-representation of the risk estimate.

(3) Appropriate alternative modeling approaches are investigated that are consistent with available data and current scientific knowledge, and appropriately consider their results and limitations using tests and analyses that are sensitive to the processes modeled.

Subcriterion (1) is not discussed here because alternate modeling approaches for features, events, and processes are beyond the scope of this report.

Acceptance Criterion 5: Model Abstraction Output Is Supported by Objective Comparisons.

(1) Models implemented in this total system performance assessment abstraction provide results consistent with output from detailed process-level models and/or empirical observations (laboratory and field testings and/or natural analogs).

(2) Outputs of mechanical disruption of engineered barrier abstractions reasonably produce or bound the results of corresponding process-level models, empirical observations, or both.

(3) Well-documented procedures, that have been accepted by the scientific community to construct and test the mathematical and numerical models, are used to simulate mechanical disruption of engineered barriers.

Subcriterion (4) is not discussed here because sensitivity studies or bounding analyses are not provided to the TSPA within this report.

4.3 CODES, STANDARDS, AND REGULATIONS

No engineering codes or engineering standards are applicable to the development of the seismic damage abstractions. The regulation that is applicable to the development of these abstractions is 10 CFR Part 63 [DIRS 180319], specifically 10 CFR 63.114, Requirements for Performance Assessment, which requires providing the technical basis for the data, models, parameter uncertainties, and alternative conceptual models that are included in the TSPA, and 10 CFR 63.115, Requirements for Multiple Barriers, which requires providing the technical basis for the barriers that are important to waste isolation. The technical basis, damage abstractions, parameter uncertainties, alternative conceptual models, and the computational methodology for the seismic damage abstractions are described in Sections 6.5 through 6.12. These abstractions provide a basis for evaluating the performance of the EBS barriers that are important for waste isolation in the seismic scenario class.

5. ASSUMPTIONS

5.1 PAGANY WASH AND SEVER WASH FAULT DISPLACEMENTS

Assumption: The fault displacement hazard curves for the Pagany Wash and Sever Wash Faults can be considered equal to the fault displacement hazard curve for the Drill Hole Wash Fault (DTN: MO0401MWDRPSHA.000 [DIRS 183046], File *./displ/tot_haz/s3.frac_mean.gz*).

Basis: The assumption of equivalency is justified by the results of field investigations that are summarized by Menges and Whitney (1996 [DIRS 106342], Section 4.2.4.10). The reasoning that supports the assumption of equivalency is as follows:

1. Previous geologic studies have consolidated discussion of the three faults based on similar characteristics and apparent similarity in fault development in response to the extensional environment. These faults are characterized as northwest-trending faults that are extensional structures related to the left-oblique component of displacement along the north-trending faults. They are, generally, strike-slip faults with a right lateral movement (Menges and Whitney 1996 [DIRS 106342], Section 4.2.4.10 and Table 4.2.1.2).

2. The field data for the three sites include surface exposures and trench studies for Pagany Wash Fault and Sever Wash Fault, and drill core data for the Drill Hole Wash Fault. Because of the existence of subsurface data, and consistent with the choice of representative locations used by the expert elicitation panel as presented in *Probabilistic Seismic Hazard Analysis for Fault Displacement and Vibratory Ground Motion at Yucca Mountain, Nevada (PSHA)* (CRWMS M&O 1998 [DIRS 103731], Section 4.3.2), it is reasonable to use the response of the Drill Hole Wash Fault as the basis for the seismic hazard.

3. None of the faults suggest displacement in Quaternary alluvial terraces, so it is appropriate to assume a low probability of significant displacement for these three faults (Menges and Whitney 1996 [DIRS 106342], Section 4.2.4.10).

4. The scale of vertical displacement is less than 5 m to 10 m for each structure (Menges and Whitney 1996 [DIRS 106342], Table 4.2.1.2), consistent with a maximum displacement of approximately 2 m for a single low probability event (CRWMS M&O 1998 [DIRS 103731], Figure 8-4).

5. Total fault length, an important factor in seismic hazard assessment, is similar for the three faults and ranges from 2 km for the Drill Hole Wash Fault to 4 km for the other faults (Menges and Whitney 1996 [DIRS 106342], Section 4.2.4.10).

6. Spatial orientation to the Solitario Canyon and Bow Ridge Faults, also an important factor in a hazard assessment, is similar for the three faults as illustrated in Figure 4.2.2 of *Seismotectonic Framework and Characterization of Faulting at Yucca Mountain, Nevada* and described by Menges and Whitney (1996 [DIRS 106342], Section 4.2.4.10). Spatial orientation to more distant seismic sources is also similar.

It is, therefore, reasonable to treat the Drill Hole Wash Fault, the Sever Wash Fault, and the Pagany Wash Fault in a similar manner with regard to the potential seismic hazard.

Confirmation Status: This assumption does not require confirmation. *Probabilistic Seismic Hazard Analyses for Fault Displacement and Vibratory Ground Motion at Yucca Mountain, Nevada* (CRWMS M&O 1998 [DIRS 103731]) defines fault displacement hazards at 15 faulting conditions within the immediate vicinity of Yucca Mountain. The PSHA did not characterize closely spaced faults separately because their displacements during a seismic event are expected to be similar. Assumption 5.1 follows the same approach used during the PSHA to characterize the response at representative fault locations (CRWMS M&O 1998 [DIRS 103731], Section 4.3.2).

Use in Model: This assumption is used in Section 6.11.3.

5.2 RANDOMNESS OF SEISMIC EVENTS

Assumption: Seismic events occur in a random manner, following a Poisson process, over long periods of time.

Basis: The assumption that the behavior of the earth is generally random (i.e., follows a Poisson process) is a common assumption in seismology. In other words, earthquakes are considered as independent events with regard to magnitude, time, and location. This assumption is similar to Assumption 6.4.2 in *Characterize Framework for Seismicity and Structural Deformation at Yucca Mountain, Nevada* (BSC 2004 [DIRS 168030]). Although there may be cases where sufficient data and information exist to depart from this assumption, the Poisson process is generally an effective representation of nature and represents a compromise between the complexity of natural processes, the availability of information, and the sensitivity of results of engineering relevance.

Confirmation Status: This assumption does not require confirmation because it is a common engineering assumption in seismology and because it is an implicit assumption in the development of hazard curves for the seismic scenario class (BSC 2004 [DIRS 168030], Section 6.4.2).

Use in Model: This assumption is used in Section 6.12.

5.3 RANGE OF BULKING FACTORS

Assumption: The range of bulking factors for the caved rock from seismic events is assumed to be 0.1 to 0.4.

Basis: The range of bulking factors for caved rock in the emplacement drifts has been estimated from published sources in the mining literature and from UDEC (V. 3.1. STN: 10173-3.1-00 [DIRS 161949]) calculations for lithophysal units. The bulking factor, B, is defined as the rubble volume, V_r, relative to its initial volume as intact rock, V_i (BSC 2004 [DIRS 166107], Section 6.4.2.5.2, Equation 6-11):

$$V_r = (1 + B)V_i, \qquad \text{(Eq. 5.3-1)}$$

An equivalent definition of the bulking factor is given by:

$$B = \frac{\phi}{1-\phi}, \qquad \text{(Eq. 5.3-2)}$$

where ϕ is the porosity of the caved rock.

The reported range of bulking factors is as follows:

- Laubscher (1994 [DIRS 179773]) recommends values of the swelling factor for caved rock as 1.16 for fine fragmentation, 1.12 for medium fragmentation and 1.08 for coarse fragmentation. The size scales for the lithophysal rubble and for the nonlithophysal rock blocks fit into the fine to medium category of fragmentation. The swelling factor is defined as (1 + *B*), where *B* is the bulking factor, implying bulking factors between 0.12 and 0.16 for caved rock.

- Duncan et al. (1980 [DIRS 161776], Table 5) report that porosity of the graded rock fill for dams is between 23 and 36%, which is equivalent to a bulking factor between 0.30 and 0.56. A graded rock fill is less applicable to caved rock than the other sources because its controlled distribution of gravel size is not representative of caved rock.

- An alternate approach is to evaluate the calculated bulking factors for lithophysal rock with the UDEC code. Using rock fragments with a characteristic length scale of 0.2 m, as is expected to occur in the lithophysal zones, the calculated bulking factor with UDEC varies between 0.19 and 0.25 (BSC 2004 [DIRS 166107], Table P-9). These values are consistent with the Laubscher value for fine fragmentation (1.16 − 1 = 0.16).

The range of bulking factors for the caved rock is assumed to be 0.1 to 0.4. This range of values encompasses the implied bulking factors from Laubscher (1994 [DIRS 179773]). This range of values encompasses the calculated bulking factors for lithophysal rock with the UDEC code. Finally, this range of values encompasses part of the data from Duncan et al. (1980 [DIRS 161776]) for graded rock fill for dams. The extreme bulking factors for a graded rock fill are expected to be less applicable to the ungraded caved rock from a seismic event than the other mining-related citations.

Confirmation Status: This assumption does not require confirmation because the recommended range for the bulking factor spans the full range of data, thereby preserving the uncertainty in this parameter.

Use in Model: This assumption is used in Sections 6.7.1.5 and 6.7.2.6.

5.4 DEGRADATION OF WASTE PACKAGE INTERNAL STRUCTURES

Assumption: Waste package internals are assumed to degrade as structural elements after the OCB is first damaged by a seismic event. More exactly, the internals degrade as a structural component for the TSPA by the time of the next seismic event after the first seismic event that breaches the waste package.

Basis: This approach is conservative because a waste package with degraded internals has significantly greater deformation and probability of rupture relative to a waste package with intact internals (see Sections 6.5.1 versus 6.5.2 and 6.6.1 versus 6.6.2). However, this approach underestimates the structural capacity of stainless steel internal components, such as the 2-in-thick inner vessel or the TAD canister itself, for screening of criticality-related issues during a 10,000-year period.

Confirmation Status: This assumption does not require confirmation because it is a bounding, assumption.

Use in Model: This assumption is used directly in Section 6.12.2 and indirectly in defining the computational model in Section 6.9.

5.5 ANGLE OF INTERNAL FRICTION FOR CAVED RUBBLE

Assumption: The angle of internal friction for caved rubble is assumed to be 35º. This value is consistent with data from direct shear testing of natural fractures of Topopah Spring tuff from the proposed repository site and is corroborated by information in the open literature.

Basis: A number of direct shear tests were performed on fractures obtained from 11.5-in diameter core samples that were drilled in the Enhanced Characterization of the Repository Block and in the Exploratory Studies Facility tunnels at the Yucca Mountain site at a low angle to either the smooth, subvertical cooling joints or to the rough and cohesive sub-horizontal vapor-phase partings of the Topopah Spring tuff. The experimental data are documented in (DTN: GS031083114222.002 [DIRS 177299]). From these data it is possible to plot the Coulomb slip envelope, from which the joint cohesion and angle of internal friction can be determined. The friction angle varies from 33.1° (DTN: GS031083114222.002 [DIRS 177299], File */gs93197311422_002.zip/65A-657-all-specimens.xls*, worksheet "Test Summary," Cell D39) to 45.7° (DTN: GS031083114222.002 [DIRS 177299], File */gs031083114222_002.zip/65A-642-all-specimens.xls*, worksheet "Test Summary," Cell D39. The higher values for the friction angle correspond to core with a sub-horizontal rough, vapor-phase parting and the lower values for the friction angle correspond to core with a smooth, sub-vertical cooling joint (BSC 2004 [DIRS 166107], Section 7.7.3.2).

The experimental data for the friction angle are corroborated by data from two sources. A friction angle of 35° is a typical value for quartz-rich rocks (Brady and Brown 1985 [DIRS 126811], p. 117), and a friction angle of 30° is a typical value for a smooth joint (Goodman 1980 [DIRS 101966], p. 158).

Based on this information, the friction angle of caved rubble is assumed to be 35°. The rubble particulates will have very rough surfaces and sharp projections, but are expected to have lower load bearing capacity and hence a smaller friction angle than an intact, vapor-phase parting which is characterized by continuous, anastomosing surfaces (BSC 2004 [DIRS 166107, Section 6.1.4.1, p. 6-15). The friction angle of 35° is slightly greater than the measured value for a smooth joint, 33.1°, consistent with the increased roughness of the caved rubble particulates relative to a smooth joint.

Confirmation Status: This assumption does not require confirmation because 35° is very close to the value for a smooth joint, which is a lower limit for this parameter.

Use in Model: This assumption is used directly in Appendix D.

INTENTIONALLY LEFT BLANK

6. MODEL DISCUSSION

6.1 INTRODUCTION

This section presents the abstractions for damage to EBS components due to seismic hazards in the postclosure repository environment. This section also presents the computational methodology for the seismic scenario class for the TSPA-LA. These abstractions and the computational methodology are the main outputs from this model report. The intended use of this output is to define the seismic scenario class for the (postclosure) compliance case for the TSPA-LA. The report includes discussion of:

- Abstractions for the kinematic response of the TAD-bearing waste package with 23-mm-thick outer corrosion barrier (OCB) and intact internals, with 23-mm-thick OCB and degraded internals, and with 17-mm-thick OCB and degraded internals in response to vibratory ground motion are described in Section 6.5.

- Abstractions for the kinematic response of the codisposal waste package with 23-mm-thick OCB and intact internals, with 23-mm-thick OCB and degraded internals, and with 17-mm-thick OCB and degraded internals in response to vibratory ground motion are described in Section 6.6.

- Abstractions for lithophysal rubble volume and nonlithophysal rockfall volume in response to vibratory ground motion are described in Section 6.7.

- Fragility curves for the drip shield plates in response to the combined loads from vibratory ground motion and from rockfall that accumulates on the drip shield are described in Sections 6.8.1 and 6.8.2.

- Fragility curves for the drip shield framework in response to the combined loads from vibratory ground motion and from rockfall that accumulates on the drip shield are described in Sections 6.8.1 and 6.8.3.

- Abstractions for the TAD-bearing and codisposal waste packages surrounded by rubble for the 23-mm-thick and 17-mm-thick OCBs with degraded internals in response to vibratory ground motion are described in Section 6.9.

- Abstraction for the drip shield, partly or completely surrounded by lithophysal rubble in response to vibratory ground motion, is described in Section 6.10.1.

- Abstraction for drip shield damage due to impact from large rock blocks induced by vibratory ground motion is described in Section 6.10.2. This abstraction is appropriate for drifts that are unfilled or partly filled and lie in nonlithophysal units.

- Damage to the waste package, drip shield, and fuel rod cladding from fault displacement is described in Section 6.11. The effect of fault displacement on cladding is not included in the TSPA compliance case because the TSPA is not taking credit for fuel rod cladding for the license application. However, the PMA for the license application may include a cladding damage abstraction, in which case cladding failure is relevant.

These abstractions and fragility curves are collectively referred to as seismic damage abstractions in this document. Preclosure mechanical response is not considered in this report.

6.1.1 EBS Components for Seismic Response

Figure 6-1 illustrates the major components of the EBS in a typical emplacement drift. The major EBS components addressed in this report are the drip shield and the waste package because failure of these components has the potential to form diffusive or advective transport pathways that release radionuclides into the unsaturated zone. The drift invert and emplacement pallet are included in the kinematic and structural response calculations for the seismic scenario class, but it is not necessary to develop damage abstractions for these components because they do not form new pathways for transport and release of radionuclides after strong vibratory ground-motion events. The waste package internals and mass of the waste form are considered in the structural response calculations but are not represented as separate damage abstractions because the TSPA compliance case for the TSPA-LA is not taking credit for the fuel rod cladding as a barrier to radionuclide release. Figure 6-1 shows the as-emplaced configuration of the EBS components, including the steel sets that will be added as ground support in some drifts. Steel sets are not considered in postclosure seismic analysis because their relatively rapid corrosion is anticipated to limit their effectiveness in the postclosure repository environment.

The effectiveness of these barriers is potentially compromised by the direct effects from an earthquake, including vibratory ground motion, fault displacement, and rockfall induced by ground motion. The effectiveness of these barriers is also potentially altered by environmental changes after an earthquake, including changes in seepage, temperature, and relative humidity as the emplacement drifts collapse and fill with rubble. The potential changes in seepage, temperature, and relative humidity are beyond the scope of this report.

6.1.2 Conceptual Model for Evolution of the EBS

The mechanical response of EBS components to a seismic event will be highly dependent on the in-drift configuration of EBS components and on the structural integrity of the EBS components at the time of the seismic event. For example, a low intensity seismic event may not cause any damage to EBS components if it occurs within the first 10,000 years after repository closure. But the same seismic event may result in failure of an EBS component at several hundred thousand years after repository closure because the structural integrity of EBS components may have been reduced by general corrosion. Similarly, the mechanical response of the drip shield in its initial configuration, as shown in Figure 6-2(a), may be quite different than its mechanical response in a collapsed drift, as shown in Figure 6-2(b), when the drip shield is covered by rockfall and may fail under the combined loads from rockfall and vibratory ground motion.

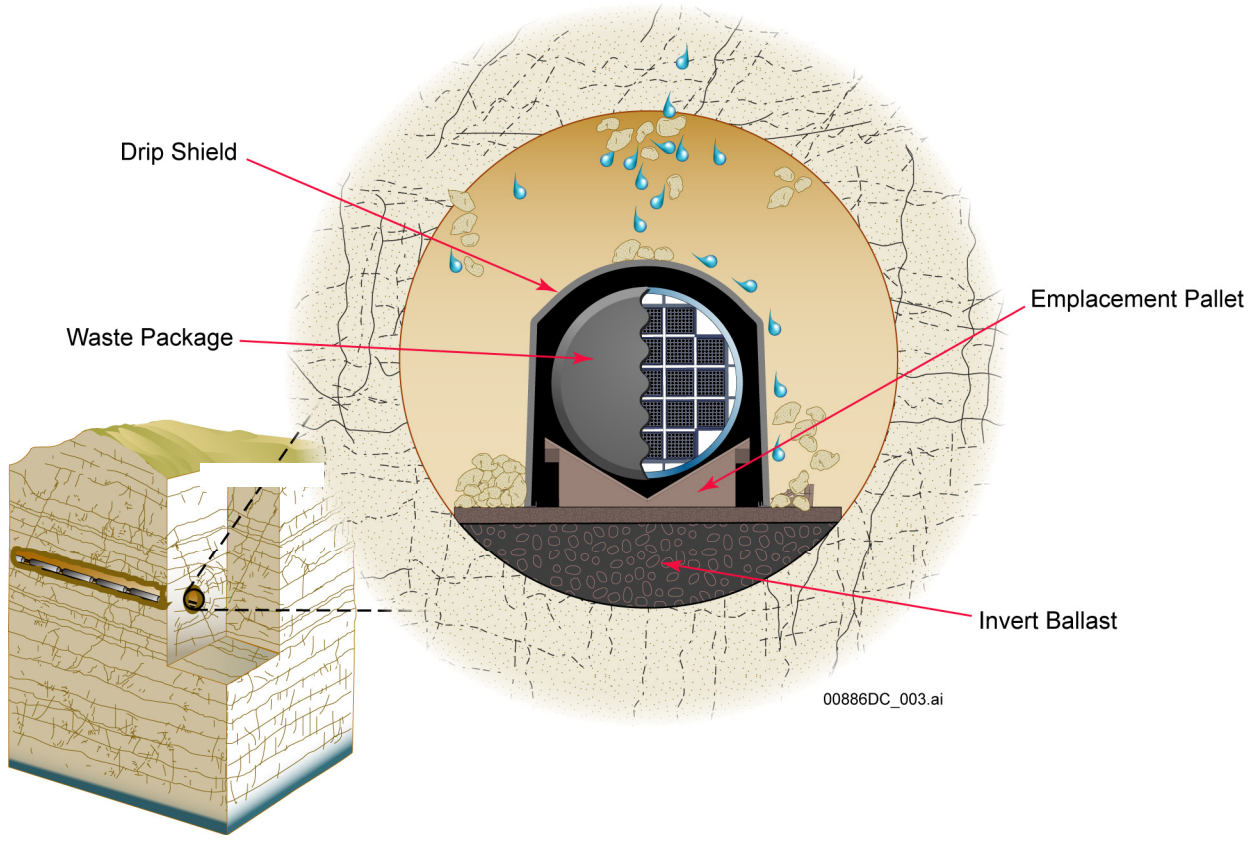

Source: Created for illustrative purposes only.

Figure 6-1. Schematic Diagram of the EBS Components in a Typical Emplacement Drift

The future configuration of the EBS components has been represented by three conceptual configurations, as shown in Figure 6-2. Figure 6-2(a) represents the as-emplaced EBS configuration, with an intact drip shield and minimal rockfall in the drifts. In this configuration, the waste packages can move freely beneath the drip shields. Figure 6-2(b) represents an intermediate state of the system where the legs of the drip shield have buckled under combined rockfall/seismic load, but the drip shield plates remain intact. In this configuration, the drip shield may collapse onto the waste package, inhibiting free movement of the waste package and emplacement pallet during the seismic event. Figure 6-2(c) represents the final state of the system, in which rubble surrounds the waste package after failure of the drip shield plates. The transition between these configurations is determined by fragility curves for the drip shield framework and plates (Section 6.8), based on the intensity of the seismic event, the thickness of drip shield components, and the load from accumulated rockfall at the time of the seismic event. A simplified isometric of the drip shield is presented in Figure 6-3.

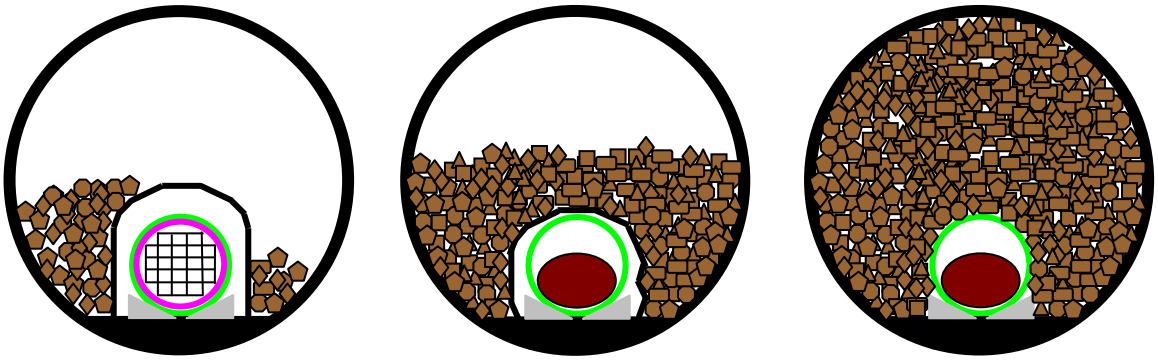

(a) Initial Configuration (b) After Drip Shield Collapse (c) After Drip Shield Plates Fail

Source: Created for illustrative purposes only.

Figure 6-2. Future Configurations of the EBS for Seismic Damage Abstractions

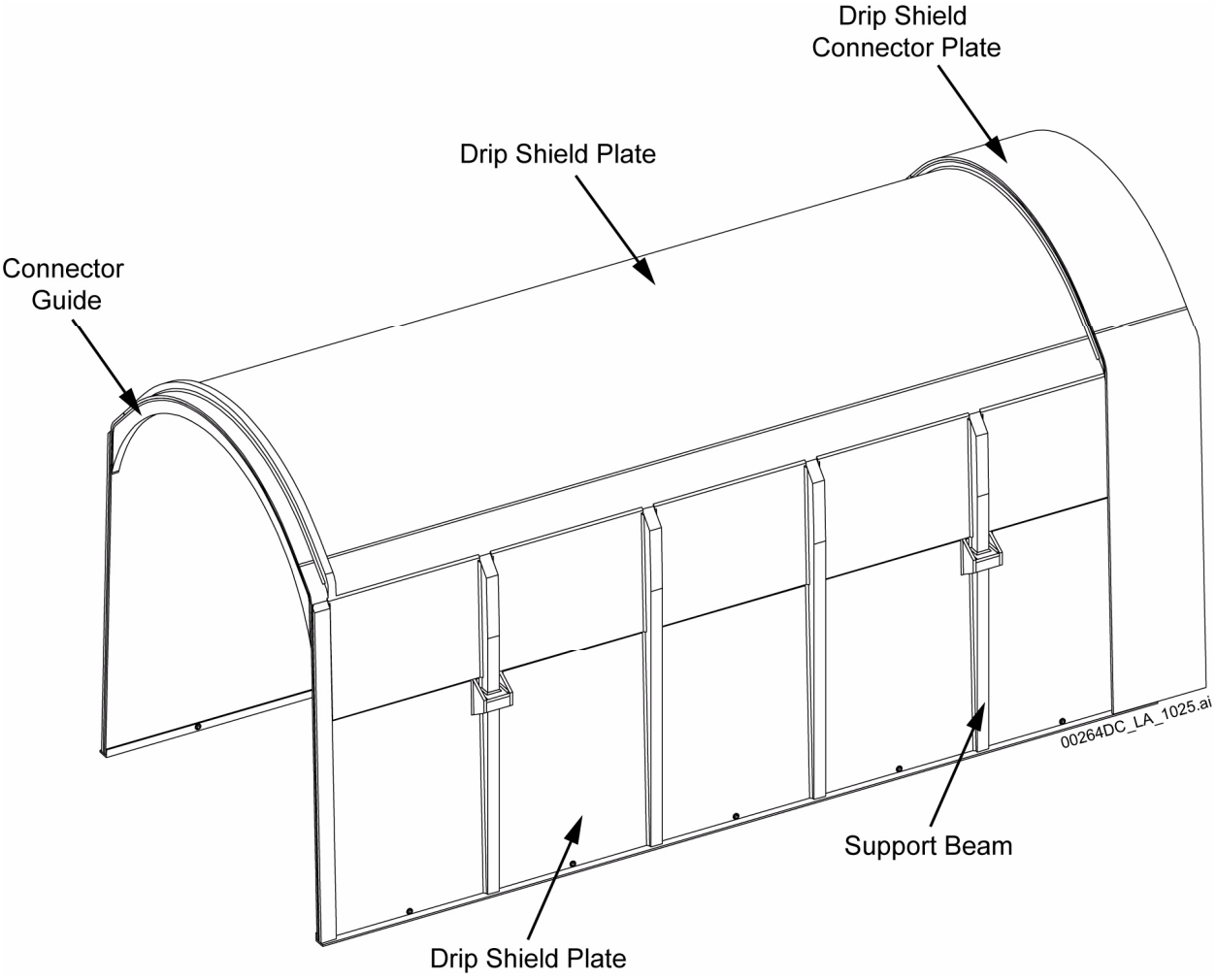

Source: Created for illustrative purposes only.

Figure 6-3. Simplified Isometric of the Drip Shield

The three states in Figure 6-2 provide a reasonable representation for the evolution of the EBS components. Figure 6-2(a) represents the as-emplaced configuration of the EBS components, with an intact drip shield and intact internals within the waste package. Both the waste package and drip shield can move freely in this configuration because there is only minimal rockfall to constrain the motion of the drip shield. Over time, some rockfall will accumulate from multiple seismic events, partly restricting the motion of the drip shields. However, the waste packages continue to move freely beneath the intact drip shields. The damage abstractions for this configuration are discussed in Sections 6.5 and 6.6 as the kinematic damage abstractions for the waste package. Sections 6.10.1 and 6.10.2 discuss the damage abstractions for the drip shield in the lithophysal and nonlithophysal units, respectively.

Figure 6-2(c) represents the late-time configuration of the EBS components, after the drip shields have failed from general corrosion. This late-time configuration is reasonable because the general corrosion rate for titanium alloys, although small, is significantly greater than the general corrosion rate for Alloy 22. In this situation, the titanium drip shield will degrade rapidly relative to the Alloy 22 outer corrosion barrier (OCB) of the waste package. In addition, significant rockfall volume is probably present in the drifts from multiple seismic events, and the waste package internals are likely to be degraded as structural elements at late times. It follows that, at late times, the waste package is likely to be directly surrounded by rubble without a drip shield, as shown in Figure 6-2(c). Note that the waste package internals in Figure 6-2(c) are degraded because seismic damage from previous events allows water vapor to enter the waste package through cracks in the OCB, leading to corrosion that degrades the internals as structural components. The damage abstractions for a waste package surrounded by rubble are discussed in Section 6.9 and for the drip shield surrounded by rubble in Section 6.10.1.

Drip shield failure determines the transition between the three states in Figure 6-2. Drip shield failure can result from general corrosion of the drip shield, static rockfall load on top of the drip shield, and the dynamic acceleration during a seismic event. The probability of drip shield failure is represented by fragility curves for two failure models of the drip shield: (1) buckling of the sidewalls of the drip shield and (2) rupture of the drip shield plates. Buckling of the sidewalls determines the transition from the first to the second state in Figure 6-2, and plate rupture determines the transition from the second to the third state in Figure 6-2. This order is appropriate because the probability of buckling the sidewalls is greater than the probability of plate rupture for the cases considered, all other factors (drip shield thickness, rockfall load, and intensity of the seismic event) being equal. This result is based on the fragility analysis documented in Section 6.8.

The timing of these transitions cannot be predicted as a deterministic value because of the uncertainty in the timing and intensity of individual seismic events, in the corrosion rates for titanium and Alloy 22, and in the accumulation of rockfall within the emplacement drifts. Drip shield failures from sidewall buckling or plate rupture will occur over a broad range of times in the compliance case for the TSPA, based on the Monte Carlo sampling for these parameters. While the timing of the transitions has a range of values, the individual states in Figure 6-2 are consistent with the start and end states for the evolution of the EBS components:

- The as-emplaced configuration in Figure 6-2(a) is expected to be applicable during at least the first 10,000 years after repository closure because there will be minimal

degradation of EBS components from general corrosion during 10,000 years and because a very high intensity earthquake is a very-low-probability event during a 10,000-year period. In fact, this initial configuration is expected to persist over a time period of several tens of thousands of years.

- The third configuration (Figure 6-2(c)) represents the late-time system configuration, after the drip shield has failed, the drifts have collapsed, and the waste package internals have failed as structural elements. This final state is consistent with the observations that: (1) the drip shield will degrade more rapidly than the Alloy 22 OCB of the waste package, (2) significant rockfall volume will accumulate in the drifts from multiple seismic events, and (3) waste package internals will begin corroding after first breach of the OCB, which allows corrosion to proceed once water vapor can enter the waste package.

It follows that the evolution illustrated in Figure 6-2 is consistent with the initial, as-emplaced configuration and with the final late-time configuration for EBS components. Since the start and end states of the system have now been defined, the remaining issue is to define reasonable intermediate state(s) of the system. The second configuration, Figure 6-2(b), is an intermediate state that is based on the observations that the titanium drip shield will corrode more rapidly than the Alloy 22 OCB, and that sidewall buckling is more probable than rupture of the drip shield plates. In effect, the drip shield is the weakest element in the system, and its response determines the preferred pathway between the start and end states of the system.

This intermediate state has several branches that are not illustrated in the simple schematic in Figure 6-2(b). These branches relate to waste package internals and to the potential for rupture or puncture of the OCB. Waste package internals are assumed to degrade as load-bearing elements after the OCB is first damaged by a seismic event. More exactly, the internals degrade as a structural component by the time of the next seismic event after the first seismic event that breaches the waste package (see Assumption 5.4, Section 5). The timing of the first seismic event that breaches the waste package is a strong function of waste package type. The TAD-bearing waste package has two independent stainless steel vessels, the inner vessel and its lids and the TAD canister itself. The codisposal waste package only has the inner vessel and its lids. The TAD-bearing waste package is demonstrably more robust than the codisposal waste package, based on a comparison of the probabilities of damage with intact internals in Sections 6.5.1.2 and 6.6.1.2. In this situation, a TAD-bearing waste package is likely to have intact internals (i.e., be undamaged) when the sidewalls of the drip shield buckle, while the codisposal waste package is likely to have degraded internals from damage during a prior seismic event when the sidewalls buckle. Figure 6-2(b) shows the configuration for a waste package with degraded internals, although the seismic damage abstractions represent the time-dependent transition from intact to degraded internals within the TSPA compliance case.

The potential for rupture or puncture of the OCB is also not illustrated in Figure 6-2 but is included in the seismic damage abstractions. The failure mechanism leading to rupture is postulated to be the accumulation of damage from high-velocity kinematic impacts. This is a postulated mechanism because the strain in the Alloy 22 OCB is always below the ultimate tensile strain from individual waste package-pallet impacts. However, the potential for more rapid general corrosion in localized regions of the OCB may produce weakened regions where

damage could accumulate from several seismic events with severe deformation of the waste package.

The failure mechanism leading to puncture is postulated to be collapse of the OCB around the degraded waste package internals. Although the waste package internals are assumed to degrade as structural elements after the OCB is first breached, large fragments of the stainless steel inner vessel and parts of the Zircaloy cladding are likely to persist for significant periods of time. The sharp edges or corners on these fragments may puncture a severely deformed OCB when it is loaded down by rockfall in the final state illustrated in Figure 6-2(c). Figure 6-2(a) and Figure 6-2(c) do not illustrate the potential for rupture or puncture, although the seismic damage abstractions represent the occurrence of these failures within the TSPA compliance case for the TSPA-LA.

The seismic damage abstractions are aligned with the mechanical response for each of the three states in Figure 6-2. The abstractions are identified in Figure 6-4, with the relevant section numbers in this report noted in parentheses.

6.1.3 Structural Response of EBS Components

Structural response and rockfall have been calculated with detailed finite-element, finite-difference, and discrete-element representations for future states of the EBS components (SNL 2007 [DIRS 178851]). Future states must be considered because the EBS components may degrade significantly or fail completely during the time scales for peak dose assessment. These future states represent the potential for general corrosion to influence the deformation and failure of the EBS components:

- Structural deformation or denting may produce high residual stresses in some areas of an EBS component. If the residual stress exceeds a threshold, then potential stress corrosion cracking (SCC) may form pathways for diffusive or possibly advective transport through the component. The areas with high residual stress are referred to as “damaged areas” throughout this document.

- These damaged areas are distinct from structural failure, which corresponds to a tear, rupture, or buckling of an EBS component. A rupture or tear in an EBS component partly or completely negates its effectiveness as a barrier to the inflow of seepage or the outward transport of radionuclides. Similarly, buckling of an EBS component may change the structural configuration and possibly change a component’s effectiveness as a barrier to seepage or rockfall.

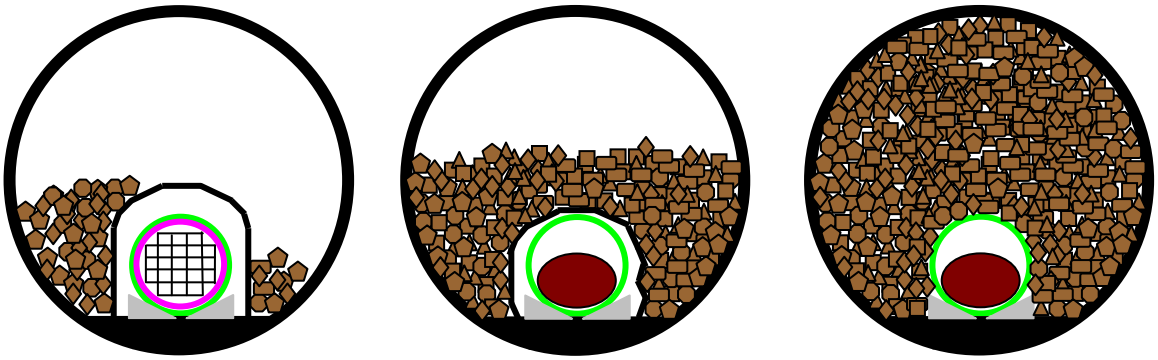

(a) Initial Configuration

- Kinematic damage abstractions for TAD-bearing waste package (6.5)
- Kinematic damage abstractions for CDSP waste package (6.6)
- Drip shield damage abstractions in lithophysal units (6.10.1)
- Drip shield damage abstraction for large rock blocks in nonlithophysal units (6.10.2)
- Rubble accumulation (6.7)

(b) After Drip Shield Collapse

- Fragility of drip shield framework (6.8.3)
- Damage for a waste package loaded by a collapsed drip shield (6.8.4)
- Drip shield damage abstraction in lithophysal units (6.10.1)
- Rubble accumulation (6.7)

(c) After Drip Shield Plates Fail

- Fragility of drip shield plates (6.8.2)
- Damage abstraction for TAD-bearing waste package surrounded by rubble (6.9)
- Rubble accumulation (6.7)

Source: Created for illustrative purposes only.

NOTE: Section numbers in this document are shown in parentheses.

Figure 6-4. Seismic Damage Abstractions Representing the Future EBS Configurations

6.1.3.1 Drip Shield Failure

The potential for drip shield failure (due to rupture or buckling) is important for the damage mechanisms on the waste package. When the drip shield is intact, waste packages can move freely beneath the drip shield during a seismic event. After the drip shield framework has buckled, the motion of the waste package may be restricted if the drip shield is surrounded by rockfall and is pressing down on the waste package. Similarly, rupture of the drip shield plates can restrict motion of the waste packages because rubble from drift collapse can fall through the drip shield and surround the waste packages. This response leads to three distinct damage mechanisms for the waste package. The first mechanism, referred to as "kinematic" damage, exists when the packages are free to move beneath the drip shield (see Figure 6-2(a)). The second and third damage mechanisms occur when the motion of the waste package is restricted, as shown in Figure 6-2(b) and Figure 6-2(c). These mechanisms are referred to as damage for a waste package beneath (loaded by) a buckled drip shield and damage for a waste package surrounded by rubble, respectively.

6.1.3.2 State of the Internals

The future state of the internal structures within the waste package is also important for the damage mechanisms. The internal structure within the TAD-bearing waste package includes a two-inch thick inner vessel of stainless steel, a TAD canister containing commercial spent nuclear fuel, and the basket structure that supports the fuel rod assemblies. The internal structure within the codisposal waste package includes a two-inch thick inner vessel of stainless steel and a structure that supports DHLW and DOE SNF assemblies. These internal structures may corrode much faster than Alloy 22, depending on the in-package chemical environment, the residual stress near welds in the inner vessel, and the potential for galvanic contact between the Alloy 22 OCB and the stainless steel inner vessel. Given the uncertainties related to these corrosion processes, the future state of the internals is represented as either intact or degraded. The internals remain intact structurally until the first breach[2] of the OCB, after which time they are treated as a degraded material with minimal strength and minimal cohesion. First breach may occur from SCC in the lid welds or in response to seismic events, as explained later in this section.

The seismic scenario assumes that the internals degrade as a structural (stress-bearing) component by the next seismic event after the OCB is first breached (see Assumption 5.4, Section 5). Since the Poisson frequency of seismic events is about 4.3×10^{-4} per year (see Step 2 in Section 6.12.2), the typical time interval between seismic events is about 2,300 years. While this assumption is appropriate for the TSPA, it may underestimate the structural integrity of the waste package internals for criticality studies, which consider the 10,000-year period after repository closure. During the first 10,000 years after repository closure, stainless steel internal structures are expected to remain structurally intact if in-package chemical conditions remain similar to a fresh water environment, which is the expected condition until after drip shield failure.

Since the internals may corrode slowly over many thousands of years, the potential for puncture of the waste package OCB by fragments of partly degraded internal components has been included in the damage abstraction for a waste package surrounded by rubble. Conceptually, a high-intensity ground motion may collapse the OCB against the partly degraded internals, possibly resulting in a tear or puncture from sharp or pointed fragments of the internals. The probability of puncture for a waste package surrounded by rubble is analyzed in Section 6.9.1.

6.1.3.3 Future States of the Waste Package

The finite-element and discrete-element models directly represent these future states through kinematic calculations (SNL 2007 [DIRS 178851], Section 6.3) and through calculations for a waste package surrounded by rubble (SNL 2007 [DIRS 178851], Section 6.5). The initial thickness of the OCB for the TAD-bearing or codisposal waste packages is 25.4 mm. Kinematic calculations have evaluated seismic-induced damage for three discrete states of the waste package, based on different degrees of degradation from general corrosion:

- 23-mm-thick OCB with intact internals

[2] "Breach" refers to any penetration of the OCB.

- 23-mm-thick OCB with degraded internals
- 17-mm-thick OCB with degraded internals.

The thickness of 23 mm is designed to represent the response of the waste package for the first few hundred thousand years after repository closure. The thickness of 17 mm is designed to represent the response of the waste package at the end of the peak dose assessment period, on the order of 1,000,000 years. The timing of the 23-mm or 17-mm thickness for the OCB is a probabilistic parameter that will vary in each realization of TSPA. The quoted times are simple estimates based on median corrosion rates (see Sections 6.5.1.2 and 6.5.2.2).

The damage calculations for the waste package surrounded by rubble are performed with a fully coupled two-dimensional representation of the lithophysal rubble, the OCB, and degraded internals. Seismic-induced damage is evaluated for two discrete states of the waste package:

- 23-mm-thick OCB with degraded internals
- 17-mm-thick OCB with degraded internals.

The timing for the 23-mm-thick and 17-mm-thick OCBs is similar to the previous paragraph.

The finite-element and discrete-element models for the waste package are based on the spatially averaged thickness of the OCB. While surface imperfections, residual stresses from welding, and local chemical environments may result in variable corrosion rates on the OCB, the spatially averaged thickness of the OCB is most relevant to the overall structural response of the waste package. The spatially averaged thickness of the OCB is a time-dependent input parameter that is used to interpolate between the seismic damage abstractions for the two or three discrete states of the waste package. It is determined by other elements of the TSPA using the general corrosion rates of EBS materials, independent of seismic events.

The finite-element and discrete-element calculations are based on four levels of horizontal peak ground velocity (PGV): 0.4 m/s, 1.05 m/s, 2.44 m/s, and 4.07 m/s. Each level is represented by 15 or 17 sets of three-component ground motions. The calculations for kinematic response and for a waste package surrounded by rubble use 17 sets of ground motions at each of the four PGV levels. The rockfall calculations for the nonlithophysal units (BSC 2004 [DIRS 166107]) predate the finite-element and discrete-element calculations in (SNL 2007 [DIRS 178851]) and were performed with 15 sets of ground motions at the 1.05 m/s, 2.44 m/s, and 5.35 m/s PGV levels. The 5.35 m/s PGV level was appropriate at that time because 5.35 m/s corresponds to the 10^{-7} annual exceedance frequency on the unbounded hazard curve. Additional details of the hazard curves are presented in Section 6.1.7.

The failure of the drip shield from rupture or buckling is also based on future states of the EBS (SNL 2007 [DIRS 178851], Section 6.4). For these calculations, the ultimate plastic load capacity of the drip shield is determined as a function of plate thickness, the static load from rubble in the drift, and the vertical peak ground acceleration. The plastic load capacity is determined with a quasi-static approach, avoiding the need to evaluate 17 sets of ground motions at multiple PGV levels. Finite-element calculations have also been performed to define the damaged areas on the drip shield as a function of vibratory ground motion and of rockfall induced by vibratory ground motion.

6.1.4 Damaged Area and Failure Mechanisms for EBS Components

Mechanical processes that occur during a significant seismic event (i.e., an event with the capacity to deform or rupture the waste package) have the potential to compromise the functionality of the waste packages and drip shields as barriers to radionuclide release. These mechanical processes include impacts between components caused by vibratory ground motion, impacts caused by rock blocks and rockfall induced by vibratory ground motions, and mechanical loading from fault displacement. As noted in Section 6.1.3, "damaged area" refers to a plastically deformed region with high residual stress. These damaged areas are distinct from structural failure, which corresponds to a tear, rupture, or buckling of an EBS component.

Under significant vibratory ground motions, impacts can occur between adjacent waste packages and between the waste package and its emplacement pallet, the surrounding drip shield, and the invert. Impacts can also occur between the drip shield and the emplacement pallet, the invert, and even the drift wall. Rockfall induced by vibratory ground motions can result in impacts on the drip shield in the postclosure period. Lithophysal rockfall induced by vibratory ground motion can result in static loads on the drip shield from the surrounding mass of fractured rock. Finally, mechanical loads may be generated by fault displacement within the repository block. In this case, EBS components may become pinned if fault displacement is greater than the available clearances between or around components.

These mechanical processes are associated with a number of potential failure mechanisms, each of which is discussed below:

- Dynamic loads have the potential to result in rupture (tearing) or puncture of a waste package if the local strain exceeds the ultimate tensile strain. A waste package that has been ruptured or punctured provides a potential pathway for seepage to flow into and for radionuclide transport out of the waste package.
- Impact-related dynamic loads may dent the waste package, resulting in permanent structural deformation with residual stress. High levels of residual tensile stress may lead to local degradation from potential SCC. Areas that are breached from corrosion processes provide a potential pathway for radionuclide transport out of the waste package.
- The static load from rockfall combined with the dynamic load during a seismic event may buckle the sidewalls of the drip shield or rupture the drip shield plates. Buckling of the sidewalls does not compromise the ability of the drip shield to deflect seepage and rockfall away from the waste package (see Section 6.7.3). Rupture of the plates compromises the capacity of the drip shield to deflect seepage and rockfall away from the waste package.
- The static load from rockfall combined with the dynamic load during a seismic event may deform the plates on the crown of the drip shield. High levels of residual tensile stress may lead to local degradation from potential SCC. Areas that are breached from corrosion processes provide a potential pathway for seepage through the drip shield.

- Impacts by large rock blocks in unfilled or partly filled drifts in nonlithophysal units may deform the drip shield and/or fail the plates and axial stiffeners on the crown of the drip shield. Failed plates provide a potential pathway for seepage through the drip shield.

- Vibratory ground motion may cause adjacent drip shields to separate if there is large vertical displacement between adjacent drip shields or if the welds holding the drip shield connector guides tear loose from the drip shield plates during the dynamic response. Separation compromises the capacity of the drip shield to deflect seepage and rockfall away from the waste package.

- Vibratory ground motion may cause waste package-to-drip shield impacts that could compromise the structural stability of the drip shield or tear the interior support bulkhead beneath the crown of the drip shield. A failed drip shield could provide a potential pathway for seepage through the drip shield.

- Large displacements on known faults in the repository block may shear waste packages and drip shields if the EBS components become pinned by the fault response. Sheared components provide potential pathways for flow into and radionuclide transport out of the damaged components.

The outer wall of the waste package is fabricated from Alloy 22, which is a very ductile material. The structural response calculations for the kinematic analyses indicate that a single waste package-to-pallet or waste package-to-waste package impact does not produce tensile strains in the Alloy 22 OCB that exceed the ultimate tensile strain, even after the application of a "knockdown" factor to account for triaxiality of the stress field. This result implies that rupture does not occur from a single kinematic impact. However, a first impact that produces extreme deformation of the OCB could weaken it, potentially resulting in a ruptured OCB from a subsequent impact that also produces extreme deformation. An abstraction for waste package rupture from kinematic impacts, based on multiple impacts with extreme deformation of the OCB, has been included in the seismic scenario class and is described in Sections 6.5.2.1 and 6.6.2.1.

The damage calculations for the waste package surrounded by lithophysal rubble also indicate that a single ground motion does not produce tensile strains in the Alloy 22 OCB that exceed the ultimate tensile strain, even after the application of a "knockdown" factor to account for triaxiality of the stress field. However, extreme deformation of the cylindrical OCB can eliminate the free volume within the OCB, allowing the sharp corners or sharp edges from degraded internal elements to puncture the OCB. An abstraction for puncture of a waste package surrounded by rubble has therefore been included in the seismic scenario class, and is described in Section 6.9.1.

The presence of high residual tensile stress has the potential to result in SCC. This combined mechanical-corrosion failure mechanism is modeled to be a cause of damage to the waste package and drip shield from impact processes caused by vibratory ground motions and by rockfall induced by vibratory ground motions. The areas that exceed the residual tensile stress threshold are referred to as damaged area throughout this document. The abstractions for damaged area on the waste package and drip shield are described in Sections 6.5, 6.6, 6.9, and 6.10.

The damaged or deformed area that exceeds a RST is conceptualized to result in a tightly spaced network of stress corrosion cracks. Application of a residual tensile stress threshold for seismic failures is nonmechanistic in the sense that detailed calculations for potential crack initiation and potential crack propagation are not used to determine the actual failure time after a seismic event. Rather, a network of stress corrosion cracks is considered to immediately form once the residual tensile stress threshold is exceeded, providing potential pathways for radionuclide transport and release. The residual tensile stress threshold is often referred to as the residual stress threshold or RST, with the understanding that the principal residual stress must always be tensile to initiate SCC.

Multiple seismic events may result in impacts to areas on the OCB that have a preexisting network of stress corrosion cracks. In theory, impacts during subsequent seismic events could further deform the preexisting crack network. Alternately, the presence of the crack network could enhance deformation from impact to an adjacent area. These mechanisms have not been included in the damage abstractions for the waste package for two reasons. First, single waste package calculations with very fine finite-element grids indicate that multiple impacts do not enhance damaged areas on the waste package in comparison to the kinematic methodology (see Sections 6.5 and 6.6). The results from the single waste package calculations are expected to be more accurate than the kinematic methodology, as discussed in Sections 6.5.2.2 and 6.6.2.2. These results demonstrate that calculations of multiple impacts at the 0.4 m/s PGV level with a fine finite-element grid result in very low values for deformed area (see Tables 6-8 and 6-23), so there is little apparent “amplification” from multiple hits to the same area during a seismic event. These results also demonstrate that the kinematic approach significantly overestimates damaged areas in comparison to the single waste package calculations at the 0.4 m/s PGV level. It follows that the conservatisms in the kinematic approach are much greater than the potential for multiple impacts to enhance deformation. The second reason relates to the conservatisms inherent in the crack density model for the network: (1) cracks are always in a tight hexagonal array, (2) cracks instantly propagate through the OCB, independent of local stress gradients, (3) the area of the crack opening is maximized, based on a stress difference given by the yield stress, (4) the crack opening is constant throughout the OCB thickness, and (5) there is no stress relief when a crack forms, even though there is no internal pressure to drive the cracks through the OCB.

The RST for Alloy 22 is an uncertain parameter because of the time scales for peak dose assessment and because of the uncertainty in the local chemical environment on the waste package. The RST is represented in TSPA as a uniform distribution with a lower bound of 90% of the yield strength of Alloy 22 and an upper bound of 105% of the yield strength of Alloy 22 (DTN: MO0702PASTRESS.002 [DIRS 180514], Table 8-1 in file *Model Output DTN.doc*). The distribution for RST represents epistemic (i.e., knowledge) uncertainty, so it remains constant for all seismic events in a given realization of the TSPA.

The results from each structural response calculation for the waste package are evaluated for three discrete values of the RST for Alloy 22: 90%, 100%, and 105% of the yield strength of Alloy 22. The intermediate value of 100% has been included because damaged areas may be a nonlinear function of RST. The intermediate value allows for a bilinear fit, if needed, for the damage abstractions. For convenience, these three values are referred to as the 90% RST, 100% RST, and 105% RST, respectively, throughout this document.

In practice, the results from each structural response calculation are postprocessed to determine the elements in the outer barrier of the waste package whose residual stress exceeds the 90% RST, 100% RST, and 105% RST levels. These elements are then converted into an area susceptible to potential SCC. The elements that exceed the 100% RST are always a subset of the elements that exceed 90% RST. In other words, the damaged area for the 100% RST is always less than or equal to the damaged area for the 90% RST. Similarly, the damaged area for the 105% RST is always less than or equal to the damaged area for the 100% RST. The RST levels are three different ways of looking at a single seismic event, not three separate events, consistent with the conceptualization of the distribution for RST as representing epistemic uncertainty.

The RSTs for seismic response are similar to the criteria for initiation of potential SCC on Alloy 22 in the nominal scenario (SNL 2007 [DIRS 181953], Section 6.2). The use of an SCC initiation criterion is appropriate for seismic analysis because regions where the residual stress from mechanical damage exceeds the RST are expected to be extensively cold-worked and, hence, potentially subject to SCC.

The potential for damaged areas on the plates of the drip shield is determined by a similar approach. The RST for determining damaged area in the Titanium Grade 7 plates of the drip shield is a constant value of 80% of its yield strength (DTN: MO0702PASTRESS.002 [DIRS 180514], Table 8-1 in the file *Model Output DTN.doc*).

Figure 6-5 is a simplified illustration of how residual stress is generated by permanent (plastic) deformation in a simple uniaxial strain model. The loading path in Figure 6-5 has three phases: (1) elastic loading until reaching the yield strength, (2) plastic loading above the yield strength, and (3) elastic unloading when the external load reduces the local stress. Figure 6-5 also shows that plastic deformation does not always generate a damaged area because the final residual stress state may be compressive or, if tensile, may be below the tensile threshold to initiate localized corrosion or potential SCC.

The fragility analysis for the drip shield defines its probability of failure as a function of the thickness and plastic load capacity of the drip shield elements, of the static rockfall load on the crown of the drip shield, and of the vertical component of peak ground acceleration for the seismic event. Fragility curves are defined in Section 6.8 for two modes of failure: (1) rupture or tearing of the drip shield plates and (2) buckling or collapse of the sidewalls and/or crown of the drip shield. A third failure mode from waste package impacts to the drip shield is considered but not incorporated into the TSPA, as explained in Section 6.8.5.

Impacts by large rock blocks in unfilled or partly filled drifts in nonlithophysal units may deform the drip shield or fail the plates and axial stiffeners on the crown of the drip shield. Failed plates provide a potential pathway for seepage through the drip shield. Areas that are breached from SCC provide a potential pathway for seepage through the drip shield. The probability of plate failure and the magnitude of damaged areas on the plates from large rock block impacts are defined in Section 6.10.2.

Vibratory ground motion may cause adjacent drip shields to separate if there is large vertical displacement between adjacent drip shields or if the welds holding the drip shield connector guides tear loose from the drip shield plates during the dynamic response. Separation would compromise the capacity of the drip shield to deflect seepage and rockfall away from the waste package. However, a kinematic study of drip shield motion has confirmed that a relatively small amount of rubble can constrain the asynchronous motion of the drip shields and prevent drip shield separation, as explained in Section 6.7.3. Vibratory ground motion may also cause waste package-to-drip shield impacts that could collapse the drip shield or tear interior support bulkheads. As explained in Section 6.8.5, drip shield failure from lateral or longitudinal impacts of the waste package is excluded from the compliance case for the TSPA.

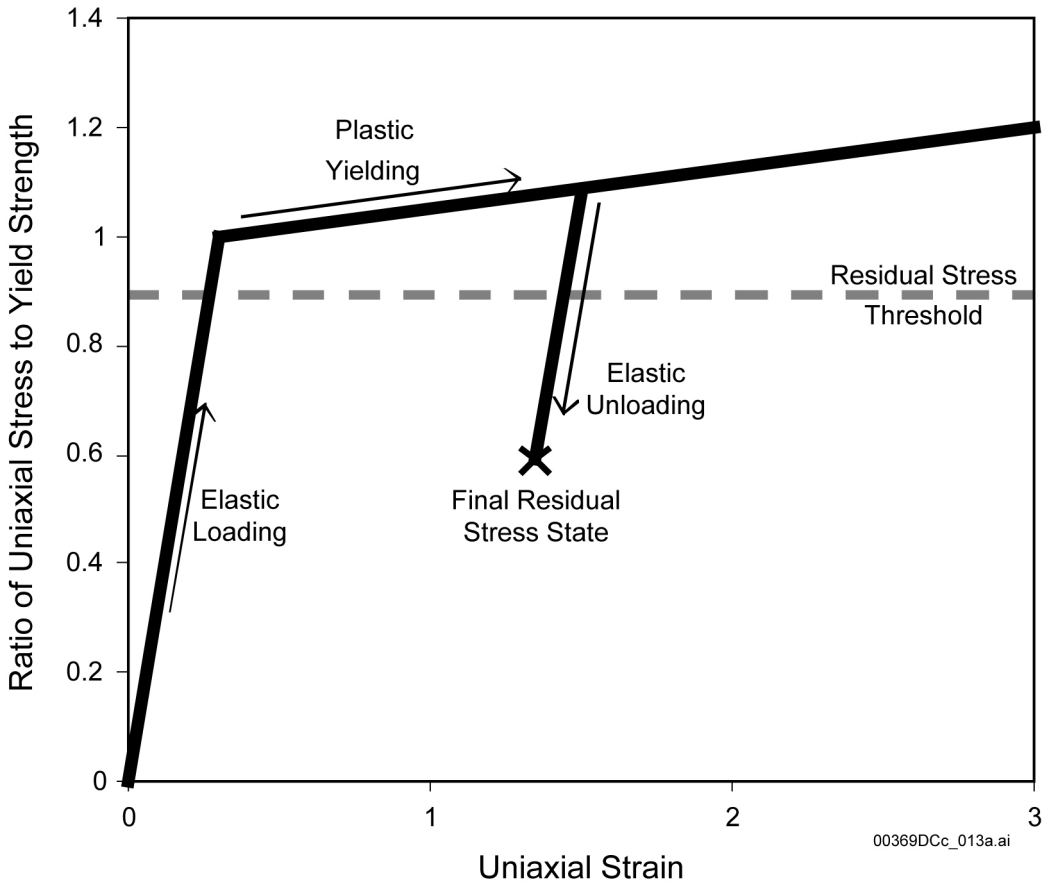

Source: Created for illustrative purposes only.

Figure 6-5. Idealized Stress-Strain Curve Showing How Permanent Deformation from Plastic Yielding Generates Residual Stress

Large displacements on known faults in the repository block have the potential to shear waste packages and drip shields if the EBS components become pinned by the fault response. The response of EBS components to fault displacement is discussed in Section 6.11.

6.1.5 Effective Area for Transport

The damaged or deformed area that exceeds a RST is conceptualized to result in a tightly spaced network of stress corrosion cracks. The network of stress corrosion cracks provides a potential pathway for diffusive transport of radionuclides and possibly for advective transport. The effective area for transport through the network is based on the estimated crack density and crack width for several idealized networks of hexagonal cracks (SNL 2007 [DIRS 181953], Sections 6.7.3 and 6.8.5). The effective area for transport through the network is a small fraction of the damaged area because of the finite number of cracks and the small opening area of individual cracks. The seismic damage abstractions predict the damaged area that exceeds the RST on the surface of the OCB, not the effective transport area through the network of stress corrosion cracks. Further discussion of the RSTs for Alloy 22 and Titanium Grade 7 and of the properties of the crack network can be found in *Stress Corrosion Cracking of Waste Package Outer Barrier and Drip Shield Materials* (SNL 2007 [DIRS 181953], Sections 6.7.3 and 6.8.5).

6.1.6 Methodology for Seismic Damage Abstractions

The seismic damage abstractions for the waste package are based on a three-part approach:

1. The probabilities of incipient rupture, (immediate) rupture, or puncture are defined as a function of horizontal PGV and the thickness of the OCB. If rupture or puncture occurs, the resulting rupture area or puncture area is defined using a bounding, uniform distribution. The probabilities of incipient rupture, (immediate) rupture, or puncture are represented as a power-law function of PGV. The rationale for two types of rupture, incipient and immediate, is explained in Section 6.5.2.1.

2. The probability of nonzero damaged area is defined as a function of PGV, RST, and the thickness of the OCB. Damaged area is defined as the area that exceeds the RST and is thereby susceptible to potential SCC. Damaged area represents the physical area of a dented region with high residual stress. Damaged area is significantly greater than the effective area for transport through a network of stress corrosion cracks, as explained in Section 6.1.5.

   The probability of nonzero damaged area, or more simply the probability of damage, is usually represented as a lookup table that uses PGV and RST as the independent variables. The typical lookup table for probability of damage at a given OCB thickness has 12 entries defined by four values of PGV (0.4 m/s, 1.05 m/s, 2.44 m/s, and 4.07 m/s) and by three values of RST (90% , 100%, and 105% of the yield strength of Alloy 22). A piecewise linear interpolation scheme is used between the points in the lookup table, avoiding the need for a functional fit to a probability surface.

3. When nonzero damaged area occurs, a conditional probability distribution for the magnitude of the conditional damaged area is defined as a function of PGV, RST, and the thickness of the OCB. The conditional damaged areas are always nonzero areas, by definition.

This approach is useful because it eliminates zero values from the conditional probability distributions in Step 3.

When a seismic event occurs within a TSPA realization, the value of PGV is determined from the bounded hazard curve and the probabilities of rupture and puncture are calculated by evaluation of the power-law functions. These probabilities are compared to random numbers between 0 and 1 that are sampled for each seismic event. If the random number is less than or equal to the probability, then the component has failed during this event, and, if the random number is greater than the probability of rupture or puncture, then the component remains intact. This sampling procedure is consistent with the Monte Carlo approach in the TSPA, wherein rupture/puncture does or does not occur during a given event with intensity PGV. A similar procedure is used to determine if nonzero damaged area occurs during a seismic event, based on interpolation (or sometimes extrapolation for small values of PGV) within the lookup table.

The nonzero damaged areas are conditional damaged areas because they are conditional on the occurrence of nonzero damage during an event. The nonzero damaged area is defined by conditional probability distributions whose parameters are functions of PGV and RST. There are potentially 12 separate distributions for each of the four values of PGV and three values of RST, although it is often possible to simplify this representation.

The nonzero damaged area is represented as a conditional probability distribution in each of the seismic damage abstractions. Five types of probability distributions have been considered to represent the conditional damaged areas: gamma, log-normal, normal, Weibull, and log-triangular. In effect, these five types of distributions represent alternate conceptual models for representing the nonzero damaged areas from the structural response calculations. These distributions are defined in *User's Guide, GoldSim Probabilistic Simulation Environment* (GoldSim Technology Group 2003 [DIRS 166226], Appendix B, Mathematical Representation of Probability Distributions) as follows:

The probability density function for the gamma distribution is defined as:

$$f(x) = \frac{\lambda(\lambda x)^{k-1} e^{-\lambda x}}{\Gamma(k)}$$

$$k = \frac{\mu^2}{\sigma^2} \qquad \text{(Eq. 6.1-1)}$$

$$\lambda = \frac{\mu}{\sigma^2}$$

where μ is the mean and σ is the standard deviation of the observations. The gamma distribution in Excel is defined in terms of two parameters, α and β, which are defined as:

$$\alpha = k = \frac{\mu^2}{\sigma^2}$$
$$\beta = \frac{1}{\lambda} = \frac{\sigma^2}{\mu} \qquad \text{(Eq. 6.1-2)}$$

The probability density function for the normal distribution is defined as:

$$f(x) = \frac{1}{\sqrt{2\pi\sigma^2}} e^{-\frac{1}{2}\left(\frac{x-\mu}{\sigma}\right)^2} \qquad \text{(Eq. 6.1-3)}$$

where μ is the mean and σ is the standard deviation of the observations.

The probability density function for the log-normal distribution is defined as:

$$f(x) = \frac{1}{x\beta\sqrt{2\pi}} e^{-0.5\left(\frac{\ln(x)-\lambda}{\beta}\right)^2} \qquad \text{(Eq. 6.1-4)}$$

where λ is the mean and β is the standard deviation of the natural logarithm of the observations. The λ and β in Equation 6.1-4 are unrelated to the quantities in Equation 6.1-2, which are only relevant to Excel calculations. Within this report, λ and β always refer to the parameters for a log-normal distribution, as defined by Equation 6.1-4.

The cumulative distribution function for the Weibull distribution is defined as:

$$F(x) = 1 - \exp\left(-\left(\frac{x-\varepsilon}{\delta-\varepsilon}\right)^{\gamma}\right) \qquad \text{(Eq. 6.1-5)}$$

where γ and δ are constant parameters and ε is the minimum value of the argument for the random variable.

The probability density function for the log-triangular distribution is defined as:

$$f(x) = \frac{\frac{2}{x}\ln\left(\frac{x}{a}\right)}{\ln\left(\frac{b}{a}\right)\ln\left(\frac{c}{a}\right)} \qquad for\ a \le x \le b$$
$$= \frac{\frac{2}{x}\ln\left(\frac{c}{x}\right)}{\ln\left(\frac{c}{a}\right)\ln\left(\frac{c}{b}\right)} \qquad for\ b \le x \le c \qquad \text{(Eq. 6.1-6)}$$

where a, b, and c represent the minimum, most likely, and maximum values, respectively, in linear space.

A similar approach has been used for the rockfall abstractions. A probability of (nonzero) rockfall is defined as a function of PGV and the conditional rockfall volumes are defined as a function of PGV. When a seismic event occurs within a TSPA realization, the value of PGV is determined from the bounded hazard curve and the corresponding probability for rockfall is calculated. This probability is compared to a random number between 0 and 1 that is sampled for each seismic event. If the random number is less than or equal to the probability of rockfall, then rockfall occurs for this event, the conditional rockfall volume is determined by sampling the conditional probability distribution, and the accumulated rockfall for this and all previous events is also determined. If the random number is greater than the probability of rockfall, then there is no rockfall for this event. The conditional rockfall volumes are defined using the same conditional probability distributions identified in Equations 6.1-1 through 6.1-6. Separate damage abstractions have been developed for the lithophysal and nonlithophysal units of the repository.

The statistical analyses for the seismic damage abstractions are documented in Excel spreadsheets that are contained in an output DTN from this model report: DTN: MO0703PASDSTAT.001.

6.1.7 Terminology

The terminology for the seismic hazard curves and for the suite of ground motions corresponding to a given exceedance frequency is explained here. In addition, the difference between a damage abstraction and a fragility curve is briefly explained.

A mean hazard curve defines the relationship between the mean estimate of the mean annual frequency of exceedance and the amplitude of the seismic effect, either for vibratory ground motion (measured by PGV) or for fault displacement (measured by a vertical displacement). The mean annual exceedance frequency represents the mean value of the frequency in any year with which future seismic events will exceed a given value of the PGV or fault displacement. All hazard curves in this report are based on the mean annual exceedance frequency.

The mean annual exceedance frequency spans many orders of magnitude, from a minimum of 10^{-8} per year to a maximum of 1 per year (or greater). The frequency is defined as the number of observed events, divided by the time interval of observation. This calculated value and hence the frequency vary randomly from one observation to the next. We use the mean of this random frequency as a measure of how likely an event is over any future year. When the mean annual exceedance frequency of interest is much less than 1, as it is here, the mean annual exceedance frequency and the annual exceedance probability are essentially equal.[3] This report uses the term exceedance frequency because it is more general, although the annual exceedance frequency and

[3] The probability of one or more events for a Poisson process (Assumption 5.2, Section 5) with annual rate λ over duration T (in years) is given by $(1 - e^{-\lambda T})$. When λ is small enough, the probability that one or more events occur in an interval T becomes $(1 - e^{-\lambda T}) = 1 - (1 - \lambda T + \frac{1}{2}(\lambda T)^2 - \ldots) \approx \lambda T$, so the annual probability for one or more events is given by $(\lambda T)/T = \lambda$, the annual frequency of events. A typical criterion for the accuracy of this expansion is for $\lambda T \leq 0.1$.

annual exceedance probability are interchangeable for the very infrequent seismic hazards considered in this study.

Ground motions are characterized by the value of the first horizontal component of PGV, denoted as PGV-H1 or more simply as PGV in this report. This characterization does not imply that the second horizontal or the vertical velocity components have the same PGV value. In fact, there is substantial variability in the second horizontal and vertical components of PGV, conditional on a given value of PGV-H1. This variability is directly incorporated into the damage abstractions and fragility curves through 17 sets of ground motions at three PGV levels: 1.05 m/s, 2.44 m/s, and 5.35 m/s. These ground motion sets are sometimes referred to as the 10^{-5} per year, the 10^{-6} per year and the 10^{-7} per year ground motions (respectively) because PGV values of 1.05 m/s, 2.44 m/s, and 5.35 m/s correspond to these frequency values on the unbounded hazard curve at the emplacement drifts (DTNs: MO0303DPGVB106.002 [DIRS 162712]; MO0210PGVPB107.000 [DIRS 162713]; and MO0401SEPPGVRL.022 [DIRS 169099]; see Table 4-1 for specific locations within these DTNs).

The use of exceedance frequency to identify ground motion sets is misleading because a given PGV level can be associated with two or more values of the exceedance frequency, as shown in Figure 6-7 (Section 6.4.3). The value of PGV provides a unique and unambiguous identifier for each set of ground motions. The use of exceedance frequency is also misleading because a seismic event with a PGV of 2.44 m/s will not occur with a frequency of 10^{-6} per year. The correspondence of 2.44 m/s with 10^{-6} per year on the hazard curve indicates that ground motion events with a PGV *equal to or greater than* 2.44 m/s occur with a mean annual frequency of 10^{-6} per year. In other words, the ensemble of seismic ground motions with PGV exceeding 2.44 m/s will occur with a mean frequency of 10^{-6} per year. To make an additional point, the probability of encountering an earthquake with a PGV of *exactly* 2.44 m/s is zero and does not occur with a frequency of 10^{-6} per year.

The finite-element and discrete-element calculations for the kinematic response of the waste package (Sections 6.5 and 6.6) and for the waste package surrounded by rubble (Section 6.9) are based on four levels of horizontal PGV: 0.4 m/s, 1.05 m/s, 2.44 m/s, and 4.07 m/s, and each level is represented by 17 sets of three-component ground motions. These PGV levels correspond to exceedance frequencies of 10^{-4} per year, 10^{-5} per year, 4.52×10^{-7} per year, and 10^{-8} per year, respectively, on the bounded hazard curve (see Table 6-3). Rockfall calculations (Sections 6.7 and 6.10) were performed with 15 sets of ground motions at the 1.05 m/s, 2.44 m/s, and 5.35 m/s PGV levels. The 5.35 m/s PGV level was appropriate because 5.35 m/s corresponds to the 10^{-7} annual exceedance frequency on the unbounded hazard curve.

The first horizontal component of the ground motions is oriented in a random direction and may be in the longitudinal direction, parallel with the drift axis, or in the transverse direction, perpendicular to the drift axis but still in the horizontal plane. For the current set of calculations, the first horizontal component has been oriented in the longitudinal direction. The kinematic calculations in *Mechanical Assessment of Degraded Waste Packages and Drip Shields Subject to Vibratory Ground Motion* (SNL 2007 [DIRS 178851]) clearly indicate that waste package-pallet impacts are the major source of damage. This result does not invalidate the structural response calculations, but indicates that calculations based on the vertical component of PGV may generate less spread in damaged area for a given set of 17 ground motions. This latter option has

not been pursued because a bounded hazard curve for the vertical component of PGV is not available.

The seismic damage abstractions for EBS components are based on response surfaces and fragility curves. A typical response surface represents the least-squares fit to the mean damage and a conditional probability distribution for the residuals about the least-squares fit. The damage abstractions for the waste package are similar to a response surface, but represent the data for damaged area directly as a conditional probability distribution whose parameters are a function of PGV and/or RST. This approach is appropriate because the data for damaged area are observed to be heteroskedastic, with a large variation in standard deviation between the individual PGV levels. In general, a gamma distribution provides a very good to excellent fit to the damaged areas at all PGV levels. This approach provides a simple, transparent, and accurate representation of the variability and uncertainty in seismically induced damage based on Monte Carlo sampling for the TSPA.

A fragility curve is defined as the probability of a binary event; for example, a fragility curve can define the probability of drip shield failure as a function of PGV-H1 and other parameters. A family of fragility curves could be used to define the probability that the damaged area exceeds 0.01 m^2, 0.1 m^2, or 1 m^2 on the surface of the waste package or drip shield. However, this is an awkward methodology to incorporate into a Monte Carlo approach, such as the TSPA for the Yucca Mountain Project. Therefore, while fragility curves have been used to define the probability of drip shield failure, they have not been used to represent damaged areas on the waste package or drip shield.

6.2 CORROBORATING INFORMATION

The abstractions for damage to EBS components from seismic hazards are based on the direct input information in Table 4-1 and the corroborating information in Table 6-1. The sixth and seventh entries in Table 6-1 have the results of calculations that were performed with ground motions at the 5.35 m/s PGV level. These calculations were performed before the bounded hazard curve was available, and the 5.35 m/s PGV level corresponds to the 1×10^{-7}-per-year exceedance frequency on the unbounded hazard curve. While the information from these calculations provides corroborating data for the seismic damage abstractions, the compliance case for TSPA-LA will be based on the bounded hazard curve with a maximum PGV of 4.07 m/s.

Table 6-1. Corroborating Input Information for Seismic Consequence Abstractions

Input Information	Value	Source
Kinematic Damage to the Waste Package:		
Damaged areas for the single CDSP waste package calculation for Realization 6 and waste package H at the 1.05 m/s PGV level	0.034 m^2 for 90% RST, 0.004 m^2 for 100% RST, 0.0 m^2 for 105% RST	SNL 2007 [DIRS 178851], Section 7.3.1.1.2 and Table 7-4
Damaged areas for the kinematic calculation for Realization 6 and waste package H at the 1.05 m/s PGV level	0.096 m^2 for 90% RST, 0.046 m^2 for 100% RST, 0.0 m^2 for 105% RST	SNL 2007 [DIRS 178851], Section 7.3.1.1.2 and Table 7-4

Table 6-1. Corroborating Input Information for Seismic Consequence Abstractions (Continued)

Input Information	Value	Source
Seismic Failure Criterion:		
Residual stress threshold for initiation of potential SCC on a smooth surface of Titanium Grade 7	80% of the yield strength of Titanium Grade 7	DTN: MO0702PASTRESS.002 [DIRS 180514], Table 8-1 in the file *Model Output DTN.doc*
Crack Density Model for determining transport area through a network of stress corrosion cracks	General reference to calculation of transport area from damaged area	SNL 2007 [DIRS 181953], Sections 6.7.3 and 6.8.5
Potential for Drip Shield Separation in Response to Vibratory Ground Motion:		
Timing of rockfall within the lithophysal units	Within seconds of the first pulse of the accelerogram	BSC 2004 [DIRS 166107], Section 6.4.2.2.2
Timing of rockfall within the nonlithophysal units	Shortly after the arrival of the ground motion	BSC 2004 [DIRS 166107], Section 6.3.1.6.1
Response of three interlocked drip shields to vibratory ground motion at the 2.44-m/s PGV level	There is no separation of drip shields at the 2.44-m/s PGV level	BSC 2004 [DIRS 169753], Section 5.3.3.2.2
Kinematic studies of drip shield motion for an open drift and for a drift partly or completely filled with rockfall	Drip shields do not separate in response to the 1×10^{-7} per year ground motions (5.35-m/s PGV level) because a small amount of rockfall or frictional forces stabilize drip shield motion and prevent separation	BSC 2004 [DIRS 169753], Sections 5.3.1.1 and 5.3.3.1
Rockfall Induced by Ground Motion in the Nonlithophysal Zone:		
Structural response of the drip shield from impact by the largest rock block generated at the 1×10^{-7} (5.35-m/s PGV level) ground motions	Failure of the axial stiffeners beneath the crown of the drip shield is not predicted to result in rupture of the waste package	SNL 2007 [DIRS 178851], Section 6.4.7.3
Rockfall Induced by Ground Motion in the Lithophysal Zone:		
Swelling factor for caved rock	1.16 for fine fragmentation; 1.12 for medium fragmentation; 1.08 for coarse fragmentation	Laubscher 1994 [DIRS 179773]
Porosity of the rock fill for dams	23% to 36%	Duncan et al. 1980 [DIRS 161776], Table 5
UDEC computational results for the bulking factor for lithophysal rock	0.19 to 0.25	BSC 2004 [DIRS 166107], Table P-9

Table 6-1. Corroborating Input Information for Seismic Consequence Abstractions (Continued)

Input Information	Value	Source
Damage to the Waste Package and Drip Shield from Fault Displacement:		
Fault displacement hazard at Site 2 – on the Solitario Canyon Fault	See Figure 8-3 in source	CRWMS M&O 1998 [DIRS 103731], Figure 8-3
Fault displacement features of the Sever Wash Fault and the Pagany Wash Fault	Similar to Drill Hole Wash Fault	Menges and Whitney 1996 [DIRS 106342], Section 4.2.4.10, and Table 4.2.1.2
Fault displacement hazard at Site 8d—generic repository location, midway between the Solitario Canyon and Ghost Dance Faults. Site 8d has intact rock	Displacement is below 0.1 cm down to 10^{-8} per year	DTN MO0401MWDRPSHA.000 [DIRS 183046], File *\displ\tot_haz\s8d.frac_mean.gz*
Subsurface facility layout and numbering of emplacement drifts	See source for figure with nomenclature	SNL 2007 [DIRS 179466], Item Number 01-02
Alternative conceptual model for probability-weighted number of waste package failures from fault displacement	1.91×10^{-4} to 1.91×10^{-6}	Waiting et al. 2003 [DIRS 164449]
Alternative conceptual model for number of fault intersections with emplacement drifts	191	Waiting et al. 2003 [DIRS 164449]
Typical vertical displacements of the waste package without rupture	9.9 cm over 0.010 seconds and 21.6 cm over 0.025 seconds	DTN MO0403AVTHM107.003 [DIRS 168892], File *MAT09V.dts* in the file *dts.zip*, based on the vertical displacements at points 162 and 164 and at points 163 and 168 in the time history for ground motion 9. The time difference between points 162 and 164 is 0.010 s and between points 163 and 168 is 0.025 s. The vertical displacements for these points are as follows: **Point No. / Row/Column / Value (cm)** 162 / 33/2 / −76.56 164 / 33/4 / −86.48 163 / 33/3 / −81.52 168 / 34/3 / −103.10
Drip Shield Fragility Calculations:		
The distribution for the general corrosion rate ratio between Titanium Grade 29 and Grade 7	Equal to 1 up to the 50th percentile and greater than 1 above the 50th percentile	SNL [DIRS 180778], Table 6-8[a]
Fault Displacement Standoff Analysis:		
Range of friction angles from direct shear testing on tuff core	33.1° to 45.7°	DTN: GS031083114222.002 [DIRS 177299], worksheet "Test Summary," Cell D39 in two files: *gs031083114222_002/65A-657-all-specimens.xls* and *gs031083114222_002/65A-642-all specimens.xls*
Friction angle for quartz-rich rocks	35°	Brady and Brown 1985 [DIRS 126811], p. 117
Typical friction angle for smooth joints	30°	Goodman 1980 [DIRS 101966], p. 158

Table 6-1. Corroborating Input Information for Seismic Consequence Abstractions (Continued)

Input Information	Value	Source
Damage to Cladding from Vibratory Ground Motion:		
Range of axial g-loads for cladding failure due to buckling	82 g's to 252 g's	Chun et al. 1987 [DIRS 144357], Table 4
Range of lateral g-loads for cladding failure from side drops	63 g's to 211 g's	Chun et al. 1987 [DIRS 144357], Table 4

6.3 RELEVANT FEATURES, EVENTS, AND PROCESSES FOR THE SEISMIC SCENARIO CLASS

The development of a comprehensive list of features, events, and processes (FEPs) potentially relevant to postclosure performance of the Yucca Mountain repository is an ongoing, iterative process based on site-specific information, design, and regulations. This report is relevant to the list of seismic-related FEPs extracted from the TSPA-LA FEP list (DTN: MO0706SPAFEPLA.001 [DIRS 181613]). Table 6-2 identifies the TSPA-LA FEPs that are included in the seismic scenario class, the section in this report where each FEP is addressed, and the tables that define the parameters for the TSPA.

FEP 1.2.03.02.0B, Seismic-Induced Rockfall Damages EBS Components, is being excluded from the TSPA compliance case for the license application. The screening argument focuses on the potential impacts on the drip shields and waste packages from rockfalls involving large rock blocks in the nonlithophysal zones. Such impacts may result in damaged areas on the drip shield plates or failure of the drip shield plates or axial stiffeners beneath the crown of the drip shield. A detailed analysis of the magnitude of the damaged areas and the probability of failure of the drip shield plates and axial stiffeners is presented in Section 6.10.2 of this report. However, damaged areas on the drip shield are excluded from the TSPA because advective flow through stress corrosion cracks on the drip shield is excluded in FEP 2.1.03.10.0B, Advection of Liquids and Solids Through Cracks in the Drip Shield, so the presence of a crack network in the damaged areas does not compromise the ability of the drip shield to divert seepage away from the waste package. In addition, failure of the drip shield plates is shown to have low consequence on dose (see FEP 1.2.03.02.0B in DTN: MO0706SPAFEPLA.001 [DIRS 181613]). Finally, failure of the axial stiffeners beneath the crown of the drip shield is considered unrealistic because: (1) it only occurs for the largest rock block with the greatest kinetic energy that is produced by the 5.35-m/s PGV level ground motions, which are beyond the maximum PGV level of 4.07 m/s on the bound hazard curve; (2) the irregular shape of large rock blocks makes it very unlikely that its center of mass is directly above the impact point, mitigating the conservative representation of the impact process in the structural response calculations; and (3) substantial rockfall is expected to fill the drift by the time all drip shield components have a 10-mm thickness reduction, mitigating the impact. It follows that the drip shield is expected to retain its integrity as a physical barrier, able to deflect large rock blocks away from the waste package. The full screening argument for FEP 1.2.03.02.0B can be found in (DTN: MO0706SPAFEPLA.001 [DIRS 181613]). It is important to note that this screening argument does not exclude drip shield failure, which is represented in the TSPA by the fragility curves in Section 6.8.

Table 6-2. FEPs Included in Seismic Consequence Abstractions, Their Disposition in TSPA-LA, and the Relevant Sections of This Report

FEP #	FEP Name	Section Where FEP is Addressed
1.2.02.03.0A	Fault displacement damages EBS components	Sections 6.11.1 through 6.11.5 define the damage abstraction for the waste package, drip shield, and fuel rod cladding in response to fault displacement. Step 21 in Section 6.12.2 provides an algorithmic description for the fault displacement damage abstraction for the EBS components. Table 6-93 defines the TSPA parameters for the fault displacement damage abstraction.
1.2.03.02.0A	Seismic ground motion damages EBS components	Sections 6.5 and 6.6 define the damage abstractions for the waste package and drip shield in response to vibratory ground motion. Sections 6.8, 6.9, and 6.10.1 define the damage abstractions for the waste package and drip shield in response to vibratory ground motion with lithophysal rockfall (see FEP 1.2.03.02.0C below). Steps 9 through 17 in Section 6.12.2 provide an algorithmic description for the damage abstractions for the waste package. Steps 7, 8, and 19 in Section 6.12.2 provide an algorithmic description for the drip shield damage abstractions. Table 6-90 defines the TSPA parameters for the waste package damage abstractions. Table 6-91 defines the TSPA parameters for the drip shield damage abstractions. Table 6-88 defines the TSPA parameters for the drip shield fragility curves.
1.2.03.02.0D	Seismic-induced drift collapse alters in-drift thermohydrology	Analysis of the changes to in-drift thermohydrology after drift collapse is beyond the scope of this report. However, Section 6.7 defines the abstractions for accumulation of rubble in lithophysal units and accumulation of rockfall in nonlithophysal units. This information is useful for defining the degree of partial collapse or complete collapse of the emplacement drifts from multiple seismic events. Step 5 in Section 6.12.2 provides an algorithmic description of rock caving and drift collapse in lithophysal units. Step 6 in Section 6.12.2 provides an algorithmic description of block caving and drift collapse in nonlithophysal units. Table 6-89 defines the TSPA parameters for the abstractions for rubble and rockfall accumulation.
1.2.03.02.0C	Seismic-induced drift collapse damages EBS components	Sections 6.8, 6.9, and 6.10.1 define the damage abstractions for the waste package and drip shield under the combined loads from lithophysal rockfall and vibratory ground motion. Steps 7, 8, 15, 16, 17, and 19 in Section 6.12.2 provide an algorithmic description for the drip shield plate fragility, for the drip shield framework fragility, and for the damage abstractions for the waste package when the waste package and drip shield are loaded by lithophysal rubble. Tables 6-88, 6-90, and 6-91 define the TSPA parameters for the abstractions for the waste package and drip shield surrounded by rubble.

6.4 GROUND MOTIONS AT THE EMPLACEMENT DRIFTS

6.4.1 Probabilistic Seismic Hazard Analysis

A probabilistic seismic hazard analysis (PSHA) was performed to assess the seismic hazards of vibratory ground motion and fault displacement at Yucca Mountain. The PSHA (CRWMS M&O 1998 [DIRS 103731]) provides quantitative hazard results to support an assessment of the repository's postclosure performance and to form the basis for developing seismic design criteria for the license application. Key attributes of the PSHA methodology for Yucca Mountain are: (1) utilization of an extensive geologic and seismologic database developed over a 20-year period in the Yucca Mountain region; (2) explicit consideration and quantification of uncertainties regarding alternative seismic-source, ground-motion, and fault-displacement

models; and (3) use of a formal, structured expert elicitation process to capture the informed scientific community's views of key inputs to the PSHA.

The PSHA methodology for vibratory ground motions has become standard practice for deriving vibratory ground motion hazards for design purposes. Less commonly, probabilistic fault displacement analyses are conducted to provide quantitative assessments of the location and amount of differential ground displacement that might occur. Both analyses provide hazard curves, which express the annual frequency of exceeding various amounts of ground motion (or fault displacement). The resulting seismic hazard curves represent the integration over relevant earthquake sources and over the magnitudes of the frequency of future earthquake occurrence and, given an occurrence, its effect at a site of interest.

The basic elements of a PSHA for vibratory ground motions are:

a) Identification of seismic sources that contribute to the vibratory ground motion hazard at Yucca Mountain and characterization of their geometry

b) Characterization of seismic sources by the mean recurrence rates of earthquakes of various magnitudes and the maximum magnitude

c) Attenuation relations that define the probability distribution of a specified ground motion parameter (such as peak ground velocity) as a function of magnitude, source-to-site distance, local site conditions, and, in some cases, seismic source characteristics

d) Integration of the seismic source characterization and ground motion attenuation evaluations, including associated uncertainties, into a seismic hazard curve and associated uncertainty distribution.

Probabilistic fault displacement hazard analysis follows a similar path:

a) Identification of fault sources of fault displacement (principal faults)

b) Characterization of the frequency, size, and locations of displacements on principal faults

c) Characterization of the amounts and locations of subsidiary displacements as a function of magnitude and distance from principal faults and magnitudes

d) Integration of source characterization and distance distribution, including associated uncertainties, into a fault displacement hazard curve and associated uncertainty distribution.

The PSHA incorporates both variability and uncertainty. Variability, also termed randomness or aleatory uncertainty, is the natural randomness in a process. For discrete variables, the randomness is parameterized by the probability of each possible value. For continuous variables, the randomness is parameterized by the probability density function. An example of variability is the range of amplitudes of ground motions that would occur at a particular location from

repeated earthquakes having exactly the same magnitude at exactly the same distance (e.g., magnitude 6 at 25-km distance). Variations in ground motion amplitude are expected due to unknowable complexities in earthquake-to-earthquake source properties and in the propagation path.

Uncertainty, also termed epistemic uncertainty, is the scientific uncertainty in the model of the process. It is due to limited data and knowledge. The uncertainty is characterized by alternative models and/or parameter values. For discrete random variables, the epistemic uncertainty is modeled by alternative probability distributions. For continuous random variables, the uncertainty is modeled by alternative probability density functions. Examples of uncertainty are alternative ground motion attenuation relations that express the median amplitude of ground motion at a particular site as a function of distance to the source and earthquake magnitude. Unlike variability, uncertainty is potentially reducible with additional knowledge and data.

Given the input evaluations, the hazard calculation method integrates over of the full range of the variables and estimates the annual frequency of exceedance of any ground-shaking amplitude at the site. Because of this integration, the final hazard curve incorporates the variability that is inherent in the earthquake occurrence and ground-shaking attenuation. In addition to the variability of the seismic hazard, however, is uncertainty about the seismotectonic environment of a site. Significant advances in development of methodology to quantify uncertainty in seismic hazard have been made in the past 20 years, as discussed in *Probabilistic Seismic Hazard Analysis: Guidance on the Uncertainty and Use of Experts* (Budnitz et al. 1997 [DIRS 103635]). These advances involve the development of alternative interpretations and representations of the earthquake sources and of the propagation of ground motions from the sources to the site. Evaluations by multiple experts are made within a structured expert elicitation process designed to minimize uncertainty due to uneven or incomplete knowledge and understanding (Budnitz et al. 1997 [DIRS 103635]). The weighted alternative interpretations are expressed by use of logic trees. Each pathway through the logic tree represents a weighted interpretation of the seismotectonic environment of the site for which a seismic hazard curve is computed. The result of computing the hazard for all relevant pathways is a distribution of hazard curves representing the full variability and uncertainty in the hazard at a site.

The seismic scenario class for TSPA-LA uses the mean hazard curves for peak ground velocity and for fault displacement. Each mean hazard curve, which is defined as the mean estimate or average of the distribution of hazard curves referred to in the preceding paragraph, typically lies above the 80th percentile of the distribution for high intensity ground motions (i.e. at low annual exceedance frequencies) because the average is dominated by the larger values of the distribution. The use of the mean hazard curves simplifies the Monte Carlo sampling process for the TSPA, overestimates the intensity of a seismic event relative to the median hazard curve, and provides an appropriate representation for the mean dose to the reasonably maximally exposed individual.

6.4.2 Site-Specific Ground Motions

Site-specific ground motions are needed for the structural response calculations and rockfall analyses supporting postclosure performance assessment. Ground motion results from the PSHA are for a hypothetical reference rock outcrop and do not reflect site-specific soil and rock

properties at the locations for which the ground motions are needed (e.g., the emplacement area level). The PSHA was conducted in this fashion because the site-specific rock and soil properties were not characterized at the time of the PSHA. Thus, further analyses are carried out to modify the PSHA results to reflect the appropriate site-specific conditions for the site of interest. These site-specific analyses are briefly described here, based on the detailed description in *Development of Earthquake Ground Motion Input for Preclosure Seismic Design and Postclosure Performance Assessment of a Geologic Repository at Yucca Mountain, NV* (BSC 2004 [DIRS 170027]).

Postclosure performance assessment requirements determine the location and the annual exceedance probabilities for which site-specific ground motions are needed. For analyses supporting postclosure performance assessment, site-specific ground motions are developed for the waste emplacement level. Selection of annual exceedance probabilities is motivated by the requirement to "*consider only events that have at least one chance in 10,000 of occurring over 10,000 years*" (10 CFR 63.114(d) [DIRS 180319]). To address this requirement, ground motions are developed for PGV levels of 1.05 m/s, 2.44 m/s, and 5.35 m/s. Analyses using the developed ground motions form the basis for evaluating repository performance for seismic events with annual exceedance probabilities from 5×10^{-4} per year to as low as 1×10^{-8} per year.

A detailed site response model provides the basis for development of seismic time histories at the level of the emplacement drifts (BSC 2004 [DIRS 170027]). Different approaches are used for developing time histories depending on how they will be used (e.g., in design or in evaluating postclosure repository performance). For Yucca Mountain, three approaches have been used to develop time histories: spectral matching, scaling to peak ground velocity, and scaling to peak ground velocity preceded by spectral conditioning. The spectral-matching approach is used primarily to develop time histories that will be used in preclosure design analyses and is not discussed further here.

The peak-ground-velocity scaling approaches are used to develop time histories for postclosure analyses. The goal of these analyses is to determine how the EBS components perform under earthquake loads that are significantly beyond their design basis. In addition to determining the consequences of these low-probability ground motions, another goal is to evaluate the variability in the consequences. Because much of the variability in consequences will be driven by random variability in the ground motion, the time histories for postclosure analyses are developed to capture and represent that random variability.

Peak ground velocity is selected as the scaling parameter because damage to underground structures has been correlated with peak ground velocity (McGarr 1984 [DIRS 163996], p. 206). PGV is appropriate for structural damage caused by sliding or impact under earthquake loads (Newmark and Rosenblueth 1971 [DIRS 151246], Sections 11.3.5 and 11.4). Finally, PGV is also appropriate for the response of a rock mass to dynamic loading because the change in stress across a weak compression wave[4] is directly proportional to the particle velocity. The abstractions in this document therefore use the horizontal PGV as the measure of the amplitude of the ground motion.

[4] A compression wave, also known as a p-wave, has particle velocity in the same direction as the direction of wave propagation. The wave is weak if the wave velocity is equal to the acoustic (compressional) velocity in the medium. An acoustic wave in air is an example of a weak compression wave.

In the PGV-scaling approach, the earthquake recordings are scaled such that their peak ground velocity matches the peak ground velocity determined in the site-response analysis for a location of interest. The records may be scaled such that both horizontal components match the target horizontal peak ground velocity and the vertical component matches the target vertical peak ground velocity. Alternatively, one horizontal component may be scaled to the target horizontal peak ground velocity with the scaling of the other components done in a manner to maintain the intercomponent variability of the original recordings. The ground motions for postclosure seismic analyses are based on the latter scaling technique because it maintains intercomponent variability.

For each annual exceedance frequency of interest, 17 sets of time histories are developed. Each set of time histories consists of acceleration, velocity, and displacement in each of two horizontal component directions and in the vertical component direction. The site-specific time histories are based on actual recordings of strong ground motion from earthquakes in the western United States and around the world (McGuire et al. 2001 [DIRS 157510], Appendix B). Recordings are selected to represent those earthquakes that dominate the seismic hazard at a given annual probability of exceedance. In other words, the recordings used as a basis for the time histories are selected to have a range of magnitudes and distances that corresponds to the magnitudes and distances of earthquakes making the dominant contribution to the seismic hazard at the given annual exceedance frequency. By basing the time histories on actual earthquake recordings and choosing records consistent with the seismic hazard, the resulting time histories exhibit realistic frequency content and phase characteristics as well as durations.

A variation of the PGV-scaling approach involves spectrally conditioning the original strong-ground-motion records before using them to develop time histories. Spectral conditioning modifies the original strong motion records such that their response spectra reflect to a greater degree the site conditions at Yucca Mountain. Conditioning can be done with respect to the PSHA reference rock outcrop conditions (referred to as Point A in Figure 6-6) or to the waste emplacement level conditions (referred to as Point B in Figure 6-6) that reflect the site response. Conditioning can be thought of as a weak spectral match. A strong spectral match is not desired in this case because it would tend to reduce the random variability of the original recordings.

For the 2.44-m/s PGV level, a suite of time histories was developed by first spectrally conditioning the records to weakly match Yucca Mountain site conditions based on the response spectra for the PSHA reference rock outcrop. Specifically, the ratios between mean response spectra for average western U.S. conditions and mean response spectra for the PSHA reference rock outcrop at Yucca Mountain were determined. The western U.S. response spectra are considered typical of the strong ground motion records forming the basis for Yucca Mountain time histories. These smooth ratios, or transfer functions, were then applied to the naturally irregular response spectrum for each of the strong ground motion records to be used in generating time histories. Finally, the modified response spectra formed targets for weak spectral matches of the original records. Following this conditioning, the records were scaled to the site-specific peak ground velocity. In this case, only one horizontal component was scaled to the peak ground velocity and the other components were scaled to preserve the intercomponent variability of the original records.

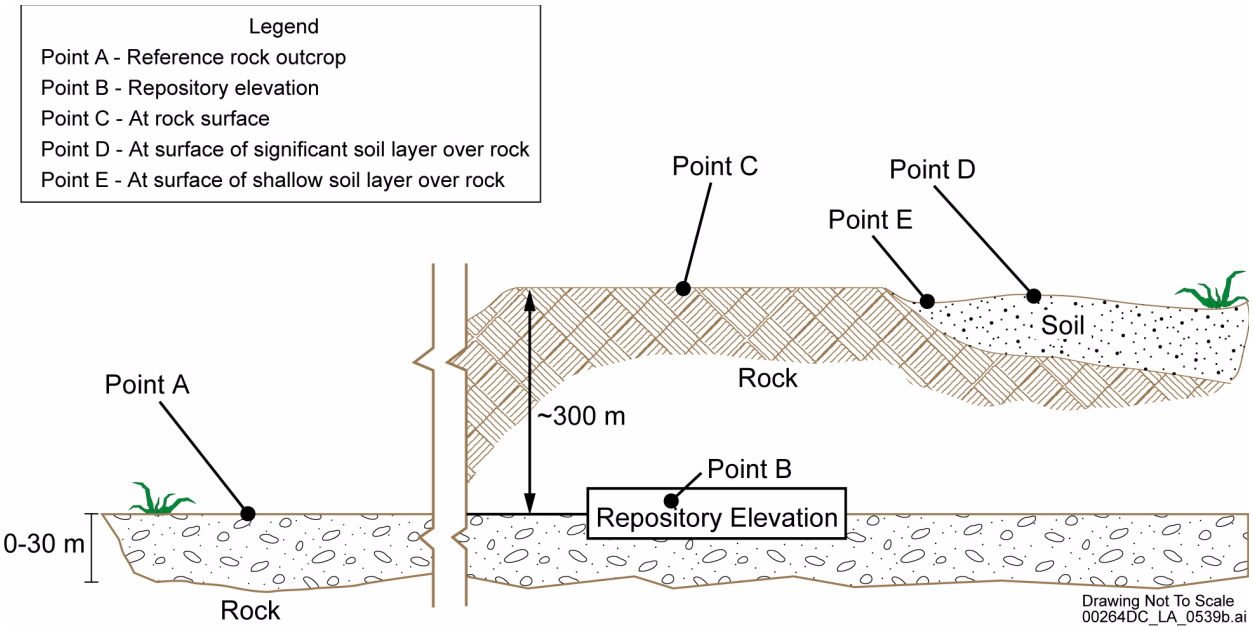

Source: Created for illustrative purposes only.

Figure 6-6. Schematic Diagram Showing Location of Points A and B

A similar approach has been used to develop suites of 17 sets of time histories for the 1.05 m/s and 5.35 m/s PGV levels. For these PGV levels, the suites were developed by first spectrally conditioning the records to weakly match Yucca Mountain site conditions based on the response spectra for the waste emplacement level (Point B in Figure 6-6), rather than for the reference rock outcrop (Point A in Figure 6-6). All suites of ground motions preserve intercomponent variability, which is a major contributor to the aleatory uncertainty in the ground motions.

6.4.3 Bounded PGV Hazard Curve at the Emplacement Drifts

The hazard curve at Point A is unbounded, in the sense that PGV continues to increase (albeit more slowly) with decreasing values of the exceedance frequency. This general behavior leads to PGV values that exceed 5.35 m/s for annual exceedance frequencies below 10^{-7} per year. These PGV values are extremely large and may not be physically realizable for the seismic sources and geologic conditions in and around Yucca Mountain. In particular, the physical properties of the lithophysal rocks at the emplacement drift level are expected to provide physical limits on the PGV experienced at that location (Point B) (BSC 2005 [DIRS 170137]).

A study (BSC 2005 [DIRS 170137]) has estimated the limits for maximum shear strain in the lithophysal rock, based on existing large-core compression testing and on numerical analyses of fracturing limits using field-mapped lithophysae geometries. The maximum shear strain can be related to the in situ response by using the site response model (Section 6.4.2) to determine the dynamic shear strains induced at the repository horizon as a function of the PGV level of the ground motion. The PGV levels equivalent to the maximum shear strains define a distribution of horizontal PGV values that are consistent with the observation that failure or fracturing of the lithophysae has not occurred in approximately 12.8 million years. The final result of this study is a bounded hazard curve for horizontal PGV at the repository waste emplacement level

(DTN: MO0501BPVELEMP.001 [DIRS 172682], worksheet "Bounded Horizontal PGV Hazard" in the file *Bounded Horizontal Peak Ground Velocity Hazard at the Repository Waste Emplacement Level.xls*).

The points on the bounded hazard curve are listed in Table 6-3. The bounded and unbounded hazard curves at Point B are compared in Figure 6-7. With the bounded hazard, the value of PGV never exceeds 4.07 m/s for annual exceedance frequencies greater than or equal to 10^{-8} per year.

Table 6-3. Bounded Hazard Curve for Horizontal PGV at the Emplacement Drifts

Horizontal PGV (m/s)	Mean Annual Exceedance Frequency (1/yr)
0.4019	1.000×10^{-04}
0.60	3.826×10^{-05}
0.80	1.919×10^{-05}
1.05	9.955×10^{-06}
1.20	6.682×10^{-06}
1.40	3.812×10^{-06}
1.60	2.136×10^{-06}
1.80	1.288×10^{-06}
2.00	8.755×10^{-07}
2.20	6.399×10^{-07}
2.44	4.518×10^{-07}
2.60	3.504×10^{-07}
2.80	2.507×10^{-07}
3.00	1.731×10^{-07}
3.20	1.137×10^{-07}
3.40	7.168×10^{-08}
3.60	4.362×10^{-08}
3.80	2.508×10^{-08}
4.00	1.319×10^{-08}
4.20	5.967×10^{-09}

Source: DTN: MO0501BPVELEMP.001 [DIRS 172682], worksheet "Bounded Horizontal PGV Hazard" in the file Bounded Horizontal Peak Ground Velocity Hazard at the Repository Waste Emplacement Level.xls.

NOTE: Horizontal PGV values have been converted from cm/s to m/s by dividing by 100.

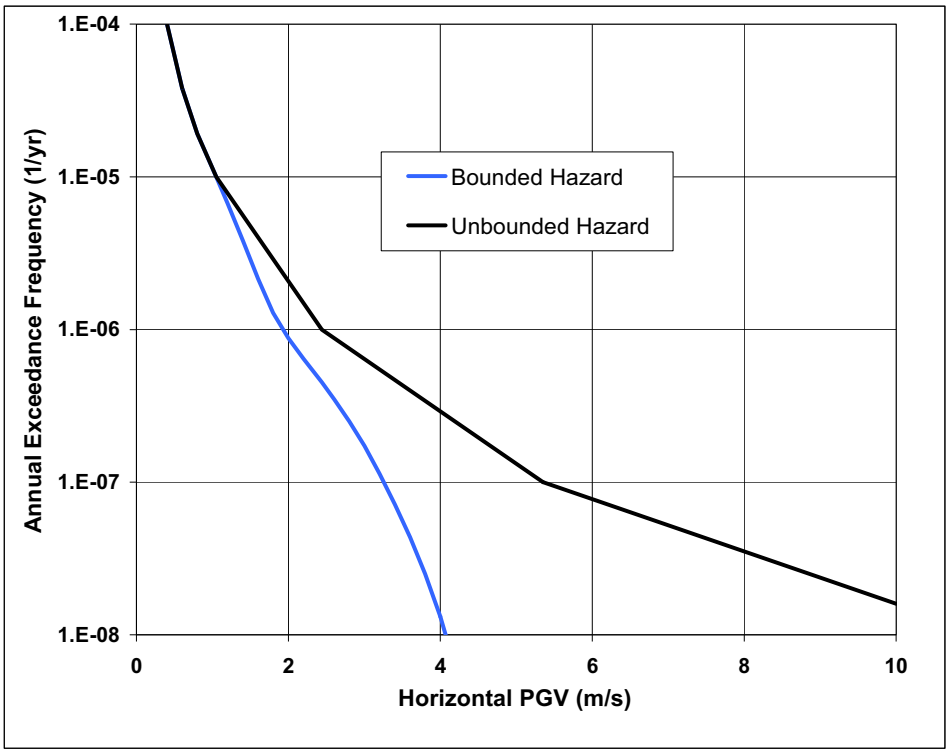

Source: DTN: MO0501BPVELEMP.001 [DIRS 172682], worksheet "Bounded Horizontal PGV Hazard" in the file *Bounded Horizontal Peak Ground Velocity Hazard at the Repository Waste Emplacement Level.xls* for the bounded hazard curve at Point B; Table 4-1 for PGV values on the unbounded hazard curve at Point B with exceedance frequencies greater than or equal to 10^{-7} per year.

NOTE: The exceedance frequency corresponding to 10 m/s on the unbounded hazard curve is based on a power law extrapolation.[5]

Figure 6-7. Bounded and Unbounded Hazard Curves for Horizontal Peak Ground Velocity at Point B, the Repository Waste Emplacement Level

If the TSPA is to represent the full range of mechanical response to seismic events, the lowest value of PGV on the hazard curve must result in no damage and no failures for all future states of the waste package. Based on the information in Tables 6-11 and 6-26, the minimum PGV threshold for the onset of damage during the kinematic response of the waste package is 0.219 m/s. This threshold occurs for kinematic damage to a codisposal waste package with a 17-mm-thick OCB, degraded internals and 90% RST, as discussed in Section 6.6.2.2.

Since this value of PGV is less than 0.4019 m/s, the smallest PGV value in Table 6-3, the annual exceedance frequency corresponding to 0.219 m/s is estimated by extrapolation from the first two points in Table 6-3: (1.0×10^{-4} 1/yr, 0.4019 m/s) and (3.826×10^{-5} 1/yr, 0.6 m/s). Using a power-law fit for the annual exceedance frequency, λ, given by $a(\mathrm{PGV})^b$, the coefficients b and a are calculated as $b = \log(1 \times 10^{-4}/3.826 \times 10^{-5})/\log(0.4019/0.6) = -2.3976$ and

[5] The exceedance frequency at 10 m/s is estimated from a power-law fit to the points at the 10^{-6} and 10^{-7} annual exceedance frequencies on the unbounded hazard curve: (244 cm/s, 10^{-6} 1/yr) and (535 cm/s, 10^{-7} 1/yr). For a power-law fit of $\lambda = a(PGV)^b$ to these data, b and a are calculated to be $b = \log(10^{-6}/10^{-7})/\log(244/535) = -2.9329$, and $a = (10^{-6})/(244)^{-2.9329} = 10.046$. The value of λ at 10 m/s (1,000 cm/s) on the unbounded hazard curve is then given by $\lambda = a(PGV)^b = (10.046)(1{,}000)^{-2.9329} = 1.597 \times 10^{-8}$ 1/yr.

$a = (1 \times 10^{-4})/(0.4019)^{-2.3976} = 1.1242 \times 10^{-5}$. The value of λ at 0.219 m/s is then $\lambda = a(\text{PGV})^b = (1.124 \times 10^{-5})(0.219)^{-2.3976} = 4.287 \times 10^{-4}$ per year. The data in Table 6-3, plus the point (4.287×10^{-4} 1/yr, 0.219 m/s), define the bound hazard curve for vibratory ground motion.

The use of the bounded hazard curve for horizontal PGV does not mean that all three components of a vibratory ground motion are bounded. Only the first horizontal component of the ground motions, denoted as H1, is scaled to a given value of PGV on the bounded hazard curve. The second horizontal component, H2, and the vertical component, V, are scaled to maintain the intercomponent variability in the original accelerogram. This means that the H2 and V components will not have the same value for PGV as the first horizontal component of the ground motion. The resulting PGVs for some of the H2 and V components will exceed the value of PGV for the H1 component and some will exceed the maximum PGV value on the bounded hazard curve, 4.07 m/s.

6.5 ABSTRACTIONS FOR THE KINEMATIC RESPONSE OF THE TAD-BEARING WASTE PACKAGE

Kinematic damage abstractions have been developed for three future states of the TAD-bearing waste package:

- 23-mm-thick OCB with intact internals
- 23-mm-thick OCB with degraded internals
- 17-mm-thick OCB with degraded internals.

Each abstraction defines the probability of rupture, the probability of nonzero damage, and the conditional probability distributions for conditional damaged area, all as functions of PGV and RST. This damaged area is called conditional because it depends on the occurrence of a seismic event that causes nonzero damaged area. The kinematic abstractions are applicable when the drip shield is intact and waste packages are free to move beneath the drip shield, as shown in Figure 6-2(a). The probability of nonzero damaged is referred to as the probability of damage throughout this report.

The results from the kinematic calculations (SNL 2007 [DIRS 178851]) provide the basis for these damage abstractions. The damaged area from each kinematic calculation is defined through a two-step process: first, the kinematic calculation defines the number, velocity, and angle of impacts for each waste package; second, the impact parameters are converted to damaged area. This second step is based on catalogs or lookup tables for damaged area from individual waste package-to-pallet impacts and from individual end-to-end impacts between adjacent waste packages. The second step is necessary because the finite-element grid for the kinematic calculations is designed to accurately represent the gross rigid body motions and interactions of multiple packages but is not fine enough to accurately predict the deformation and residual stress distribution from multiple impacts. This limitation in the kinematic calculations is avoided by using a lookup table that is based on many calculations with a highly refined finite-element grid.

The results from the structural response calculations for kinematic damage to the TAD-bearing waste package have been analyzed two ways: with a damaged area cutoff of 0.0024 m^2, and without a cutoff. Analysis of kinematic results without a cutoff generates extremely small damaged areas, on the order of 10^{-4} m^2. These extremely small values are not physical. They are an artifact of the numerical interpolation scheme that interprets kinematic impacts as damaged area, sometimes resulting in areas that are smaller than a single element in the finite-element mesh. In this situation, a damaged area cutoff of 0.0024 m^2 was selected to ensure that the area exceeding the RST represents the deformation of at least two or three elements of a very fine finite-element mesh, rather than the result of a numerical interpolation. The data for the kinematic damage abstraction incorporate this cutoff by setting damaged area to 0 when it is less than 0.0024 m^2.

The kinematic damage abstractions are derived in three spreadsheets: *Kinematic Damage Abstraction 23-mm Intact.xls*, *Kinematic Damage Abstraction 23-mm Degraded.xls*, and *Kinematic Damage Abstraction 17-mm Degraded.xls*. These spreadsheets contain all of the input data for the kinematic damage abstractions, which are based on DTN: LL0704PA048SPC.023 [DIRS 180735]. These spreadsheets also contain plots for several types of conditional probability distributions and plots comparing computational results at the four PGV levels to the damage abstractions. The abstractions for probability of rupture are derived in the spreadsheet *Rupture and Puncture Abstractions.xls*. Electronic versions of the spreadsheets are provided in output DTN: MO0703PASDSTAT.001.

The response for the 23-mm-thick OCB with intact internals is described in this report. The responses for the 23-mm-thick and 17-mm-thick OCBs with degraded internals are very similar (refer to output DTN: MO0703PASDSTAT.001, Files *Kinematic Damage Abstraction 23-mm Degraded.xls* and *Kinematic Damage Abstraction 17-mm Degraded.xls)*, so only the case for the 17-mm-thick OCB is illustrated in this text.

The potential for damage to the waste package from lateral impacts between the waste package and drip shield is not included in the seismic damage abstractions for the TSPA. The justification for excluding the potential damage from waste package-drip shield impacts is based on the observations that the damaged areas from side-on impacts of the waste package and drip shield are zero or very small. In addition, the damaged areas from side-on impacts are significantly less than from end-to-end impacts which have an insignificant contribution to total damaged area in comparison to waste package-to-pallet impacts. Vertical impacts of the waste package on the drip shield will also produce minimal damage because the three axial stiffeners at the crown of the drip shield will spread the impact load in a similar manner to the side-on impacts. It follows that the damaged areas from waste package-drip shield impacts will have a negligible contribution to total damaged area on the waste package, as discussed in more detail in Section 6.5.6.

Throughout Section 6, damaged area is synonymous with the area that exceeds the RST, resulting in enhanced susceptibility to potential SCC and the formation of pathways for radionuclide transport from the waste package. Permanent structural deformation does not always result in damaged area because the residual stress may be below the stress threshold for Alloy 22, as shown in Figure 6-5.

6.5.1 23-mm-Thick OCB with Intact Internals

6.5.1.1 Probability of Rupture

The probability of rupture for the TAD-bearing waste package with a 23-mm-thick OCB and intact internals for a single impact is zero. The structural response calculations for kinematic response at the 0.4 m/s, 1.05 m/s, 2.44 m/s, and 4.07 m/s PGV levels and the associated damage catalogs demonstrate that the strain in the OCB from a single impact is always below the ultimate tensile strain for Alloy 22 (SNL 2007 [DIRS 178851], Section 6.3.4). Consideration of multiple impacts to a TAD-bearing waste package with intact internals does not change the probability of rupture for intact internals (SNL 2007 [DIRS 178851], Sections 6.3.3 and 6.3.4.2).

6.5.1.2 Probability of Damage

Table 6-4 and Figure 6-8 present the probability of damage for the 23-mm-thick OCB with intact internals. The probability is zero except for a single point with a probability of 0.118 at the 4.07 m/s PGV level and 90% RST. The TAD-bearing waste package with intact internals will remain undamaged for any seismic events at or below the 2.44 m/s PGV level, or for all realizations with a residual stress threshold at or above the 100% RST.

Table 6-4. Probability of Damage for the TAD-Bearing Waste Package with 23-mm-Thick OCB and Intact Internals

PGV Level (m/s)	Residual Stress Threshold (% of Yield Strength)		
	90%	100%	105%
0.40	0	0	0
1.05	0	0	0
2.44	0	0	0
4.07	0.118	0	0

Source: Output DTN: MO0703PASDSTAT.001, worksheet “Probability of Damage” in the file *Kinematic Damage Abstraction 23-mm Intact.xls*.

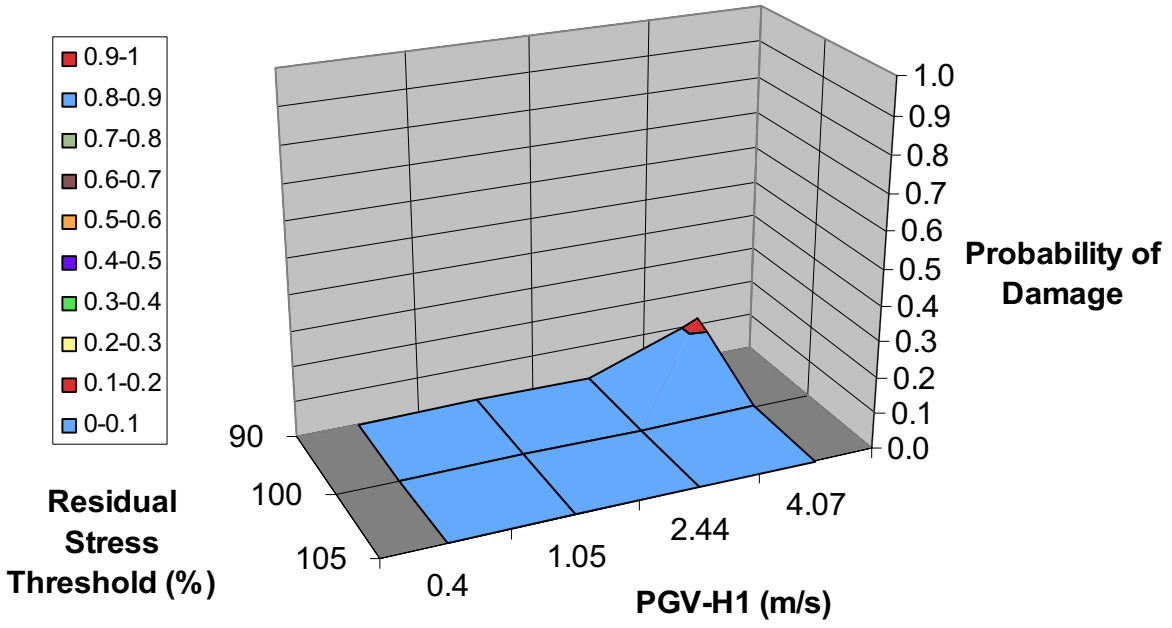

Source: Output DTN: MO0703PASDSTAT.001, worksheet "Probability of Damage" in the file *Kinematic Damage Abstraction 23-mm Intact.xls*.

Figure 6-8. Probability of Damage for the TAD-Bearing Waste Package with 23-mm-Thick OCB and Intact Internals

Seismic events between the 2.44 m/s and 4.07 m/s PGV levels occur with a frequency of $(4.518 \times 10^{-7} - 1 \times 10^{-8}) = 4.418 \times 10^{-7}$ per year, based on the data in Table 6-3. It follows that nonzero damage to the TAD-bearing waste package only occurs for very low probability seismic events and, if those events occur, the probability of damage is less than 0.118. In this situation, the first breach of the OCB on the TAD-bearing waste package with intact internals may occur after drip shield failure (described in Section 6.8) or when stress corrosion cracks form in the lid welds due to general corrosion.

Table 6-4 shows that the probability of damage is based on two independent parameters: the value of *PGV* for the *j*th seismic event and the value of *RST* for a given realization. TSPA requires the probability of damage at intermediate values of *PGV* and *RST,* so a linear interpolation is used to define the variation of the probability of damage as a function of *PGV* and *RST*. Damaged areas are often observed to follow a power law, as illustrated by the quadratic fit for mean damaged area as a function of *PGV* in Figure 6-19. The use of linear interpolation for *PGV* and *RST* is appropriate because it provides results at intermediate values that are greater than those from a power-law fit with a positive and increasing slope.

The spatially averaged thickness of the OCB is a time-dependent parameter that is predicted by other elements of the TSPA calculations. The probability of damage with intact internals is based on a constant OCB thickness of 23 mm, which corresponds to a thickness reduction of 2.4 mm from the initial OCB thickness of 25.4-mm. The abstraction for the 23-mm-thick OCB provides a reasonable representation of the probability of damage for several hundred thousand

years after repository closure. The median corrosion rate of Alloy 22 at 60ºC is 6.35 nm/yr ≈ 7 nm/year, based on a medium uncertainty level in the distributions for general corrosion rate (DTN: MO0612WPOUTERB.000 [DIRS 182035], File *BaseCase GC CDFs2.xls*, worksheet "Data," Cell L71). The value of 60°C is appropriate because it is an upper bound on OCB temperature beyond 10,000 years after repository closure (SNL 2007 [DIRS 178851], Figure 1-3) and because it is consistent with the structural response calculations for the seismic scenario (SNL 2007 [DIRS 178851], Assumption 5.7, Section 5). The time for a 2.4-mm thickness reduction from general corrosion is estimated as $(2.4 \times 10^{-3}$ m$)/(7 \times 10^{-9}$ m/yr$) \approx$ 340,000 years. More detailed probabilistic corrosion calculations must be performed, but this estimate indicates that the probabilities for a 23-mm-thick OCB provide a reasonable representation for seismic response during the first few hundred thousand years after repository closure.

6.5.1.3 Conditional Probability Distribution for Nonzero Damaged Area

When damage does occur at the 4.07 m/s PGV level and 90% RST, a gamma distribution provides a reasonable representation of the conditional probability distribution for nonzero damaged areas. The mean and standard deviation for the gamma distribution, 0.00408 m^2 and 0.00130 m^2, respectively, are defined by the structural response calculations for conditional damaged area (output DTN: MO0703PASDSTAT.001, worksheet "ACM for 90%_i23" in file *Kinematic Damage Abstraction 23-mm Intact.xls*). Figure 6-9 is a plot, called a quantile-quantile (or Q-Q) plot, that shows excellent agreement between the quantiles of the observed values of the nonzero damaged area and the corresponding quantiles on a gamma distribution. (If the agreement were exact, all points would lie on the colored line in Figure 6-9.) Note that the nonzero damaged areas in Figure 6-9 are less than 0.006 m^2, which is a very small fraction of the cylindrical surface area of the TAD-bearing waste package, 33.64 m^2, as calculated in Section 6.5.4.

The abstraction for TSPA must represent the conditional damaged area for the full range of PGV levels and RST values, rather than at the single point (4.07 m/s PGV level, 90% RST) shown in Figure 6-8 and Figure 6-9. It is not possible to extrapolate the conditional damage at this single point to the range of values for the TSPA. In this particular case, the single point results are an upper bound for all values of PGV less than 4.07 m/s and all values of the RST greater than 90%. In addition, the magnitude of the conditional damaged area is extremely small in comparison to the cylindrical surface area of the TAD-bearing waste package. It is then reasonable to use the conditional damage at 4.07 m/s and 90% RST for all values of PGV and RST in TSPA.

Conditional damage only occurs when the probability of damage is greater than zero. The probabilities in Figure 6-8 ensure that the damaged area for the TSPA remains zero for most values of PGV, in spite of the use of an upper bound for the magnitude of the conditional damaged area. This can be demonstrated by plotting the expected damaged area, defined as the product of the probability of damage and the mean conditional damaged area. The expected damaged area is the effective damaged area for the TSPA because it combines the probability of damage with the magnitude of the nonzero damaged area. Figure 6-10 demonstrates that the expected damaged area remains zero over most of the TSPA's range for PGV and RST, even with the upper bound for the magnitude of nonzero damaged area.

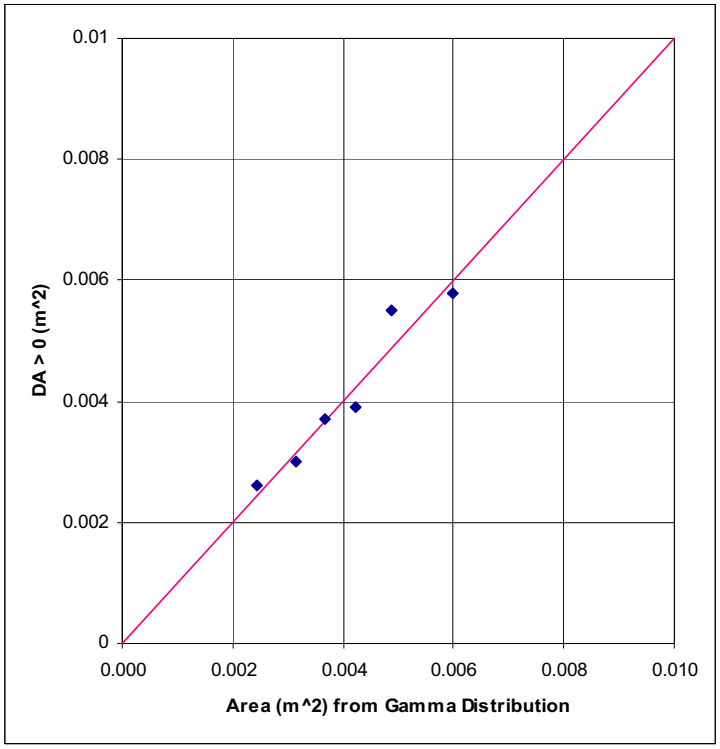

Source: Output DTN: MO0703PASDSTAT.001, worksheet "ACM for 90%_i23" in the file *Kinematic Damage Abstraction 23-mm Intact.xls*.

NOTE: 4.07 m/s PGV level at 90% RST. DA > 0 is the conditional nonzero damaged area.

Figure 6-9. Q-Q Plot for Conditional Nonzero Damaged Areas versus a Gamma Distribution for the TAD-Bearing Waste Package with 23-mm-Thick OCB and Intact Internals

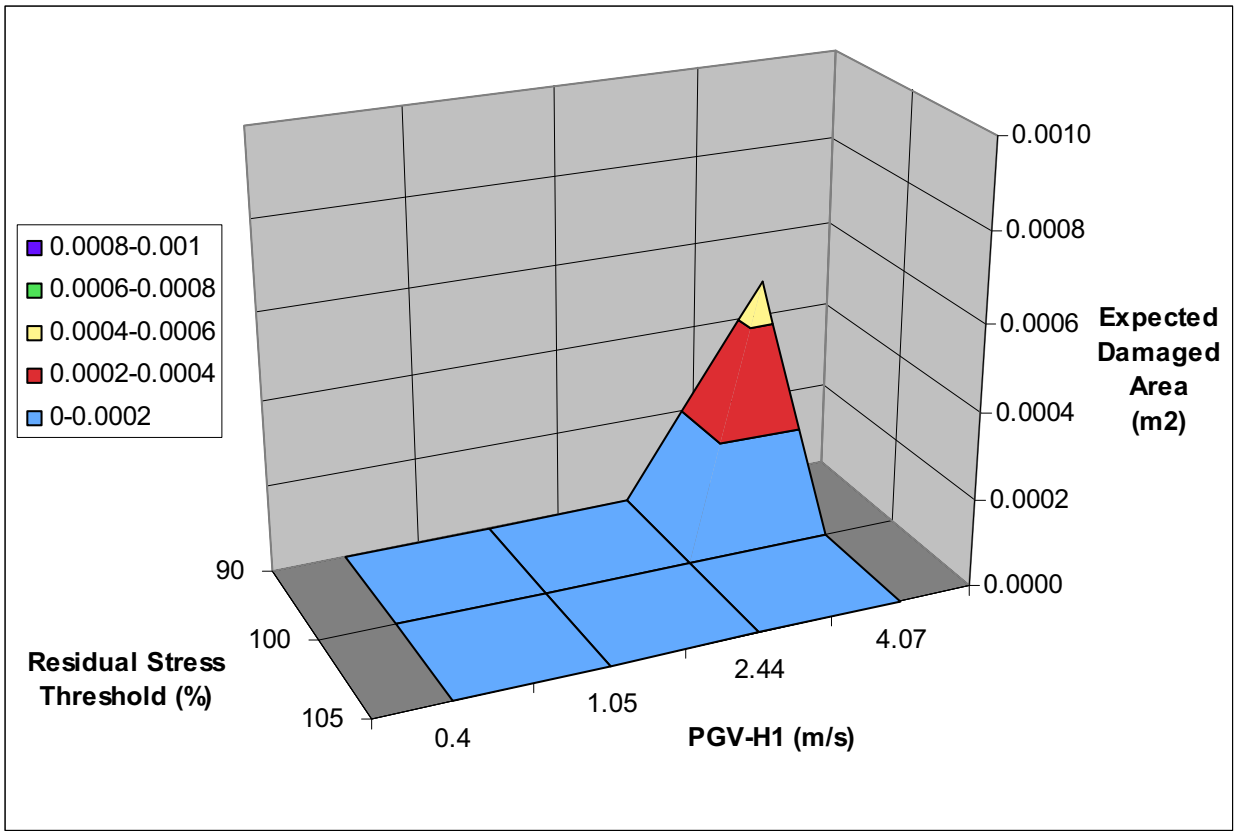

Source: Output DTN: MO0703PASDSTAT.001, worksheet "Expected Damage" in the file *Kinematic Damage Abstraction 23-mm Intact.xls*.

Figure 6-10. Expected Damaged Area for the TAD-Bearing Waste Package with 23-mm-Thick OCB and Intact Internals

6.5.1.4 Alternate Conditional Probability Distributions

Q-Q plots for log-normal and normal probability distributions show similar agreement to that for the gamma distribution in Figure 6-9. Q-Q plots for these distributions are presented in worksheet "ACM 90%_i23" in the file *Kinematic Damage Abstraction 23-mm Intact.xls*, which can be found in output DTN: MO0703PASDSTAT.001. The gamma distribution was selected for the damage abstraction because it is consistent with the other seismic damage abstractions described in this section and in Sections 6.6 and 6.9. A fit to a Weibull distribution was also attempted, but appropriate values for its input parameters could not be determined by the Excel Solver.

6.5.1.5 Dependence on OCB Thickness

The time dependent thickness of the OCB is not incorporated into the damage abstraction for the TAD-bearing waste package with intact internals. The data in Figures 6-8 to 6-10 are for a 23-mm-thick OCB, which corresponds to a thickness reduction of 2.4 mm from the initial OCB thickness of 25.4 mm. The abstraction for the 23-mm-thick OCB provides a reasonable bound for damaged area for several hundred thousand years after repository closure, based on the estimated corrosion time in Section 6.5.1.2.

6.5.2 17-mm-Thick OCB with Degraded Internals

6.5.2.1 Probability of Rupture

The probability of rupture for the TAD-bearing waste package with degraded internals is zero for a single waste package-to-pallet impact or a single waste package-to-waste package impact. The structural response calculations for kinematic response at the 0.4 m/s, 1.05 m/s, 2.44 m/s, and 4.07 m/s PGV levels and the associated damage catalogs demonstrate that the strain in the OCB is always below the ultimate tensile strain for Alloy 22 from a single impact (SNL 2007 [DIRS 178851], Section 6.3.4). However, an impact with severe deformation of the OCB has the potential to weaken the OCB, potentially causing rupture if there is severe deformation from a subsequent impact. The second impact that causes severe deformation could occur during a single ground motion or during subsequent events. The accumulation of extreme deformation in the OCB is conceptualized to have the potential to rupture the OCB from multiple severe impacts.

For the TAD-bearing waste package with degraded internals, the effect of multiple waste package-to-pallet impacts is assessed (SNL 2007 [DIRS 178851], Section 6.3.3, "Applying Damaged Areas and Rupture Condition to the Kinematic Analyses"; SNL 2007 [DIRS 178851], Section 6.3.4, "Damaged Area and Rupture Results") by evaluating the severity of deformation after a single impact. If the deformation is deemed to be large enough, then it is hypothesized that a second large impact can potentially cause rupture of the waste package OCB.

The degree of deformation from waste package-to-pallet impacts during a single ground motion was used to define the probability of no rupture, the probability of incipient rupture, and the probability of (complete) rupture (DTN: LL0703PA029SPC.014 [DIRS 179775]). A minor degree of deformation indicates that no rupture occurs, consistent with the observation that the strain in the OCB is below the ultimate tensile strain for Alloy 22 for individual impacts. A significant degree of deformation is interpreted as causing an incipient rupture, in the sense that a second severe impact has the potential to cause rupture. Finally, if two severe impacts occur, then the accumulation of severe deformation is interpreted as causing a rupture in the OCB.

The seventeen realizations at 0.4 m/s, 1.05 m/s, 2.44 m/s, and 4.07 m/s PGV level used in the kinematic analysis for the TAD-bearing waste package with degraded internals have been assessed for these probabilities. The probability of incipient rupture and probability of rupture are defined by the number of waste packages in each realization that have a single severe impact or more than one severe impact, respectively. The probabilities for each realization are then averaged over all ground motions at a given PGV level to define the data in Table 6-5. Table 6-5 displays the resulting probabilities for the TAD-bearing waste package with 23-mm-thick OCB and with 17-mm-thick OCB.

The probabilities in Table 6-5 are essentially independent of the thickness of the OCB, so the TSPA abstraction is based on the mean of the probabilities for the 23-mm-thick OCB and for the 17-mm-thick OCB, as shown in Table 6-6. The mean probability, as used here, refers to the mean probability for the two OCB thicknesses. In other words, the mean probability in Table 6-6 is the number of average overall ground motions at a given PGV level, as shown by the data in Table 6-5, and a subsequent average for the two OCB thicknesses.

Table 6-5. Probability of Rupture for the TAD-Bearing Waste Package with Degraded Internals

PGV Level (m/s)	Probability of Incipient Rupture		Probability of Rupture	
	23-mm-thick OCB	17-mm-thick OCB	23-mm-thick OCB	17-mm-thick OCB
0.40	0	0	0	0
1.05	0.005	0.007	0	0
2.44	0.035	0.040	0	0
4.07	0.123	0.127	0.174	0.188

Source: DTN: LL0703PA029SPC.014 [DIRS 179775], worksheet "Naval Long TAD Summary" in the file *kinematic_analyses_rupture_summary.xls*.

Table 6-6. Mean Probability Data for Incipient Rupture and Rupture of the TAD-Bearing Waste Package with Degraded Internals

PGV Range (m/s)	Average Probability of Incipient Rupture	Average Probability of Rupture
0.4	0	0
1.05	0.006	0
2.44	0.037	0
4.07	0.125	0.181

Source: Output DTN: MO0703PASDSTAT.001, worksheet "TAD Kinematic Abstraction" in the file *Rupture and Puncture Abstractions.xls*.

The mean probability data for incipient rupture are represented in the TSPA as a power-law function of the form $a(\text{PGV}-0.4)^b$. This function goes to 0 at the 0.40 m/s PGV level, consistent with the data in Table 6-6. The coefficients a and b are determined by a least-squares fit to the natural logarithm of the nonzero data points. This fit, shown in Figure 6-11, demonstrates that the data points follow a power-law dependence because the R^2 of the least-squares fit is 0.9959. This fit also defines the coefficients of the power law: $a = \exp(-4.4204) = 0.0120$ and $b = 1.7449$.

The mean probability of rupture is represented in the TSPA as a power-law function of the form $c(\text{PGV}-2.44)^d$. This functional form goes to 0 at the 2.44 m/s PGV level, consistent with the data in Table 6-6. However, there is only one nonzero data point for the mean probability of rupture, so there is not enough data to define the coefficients c and d. A reasonable simplification is to set the value of d equal to 1.7449, the same value as b. The value of c is then calculated as $c = (0.181)/(4.07 - 2.44)^{1.7449} = 0.0772$. (Numerical values are based on the spreadsheet calculations in output DTN: MO0703PASDSTAT.001, worksheet "TAD Kinematic Abstraction" in file *Rupture and Puncture Abstractions.xls*.)

Figure 6-12 presents comparisons of the power-law functions for incipient rupture and rupture versus the data in Table 6-6. These functions define the probabilities for a three state system: p_{nr}, the probability of no rupture, p_{inc_rup}, the probability of incipient rupture, and p_{rup}, the probability of immediate rupture. The sum of these three probabilities is always 1.

An integer counter tracks the rupture status of the system through multiple events. This counter is initialized to 0 at the start of each realization. For each seismic event, the counter is incremented by sampling a discrete distribution with (value, probability) pairs given by (0, p_{nr}), (1, p_{inc_rup}), and (2, p_{rup}). If the sampled value is zero, then the TAD-bearing waste package does

not sustain significant damage and the counter does not change. If the sampled value is 1, then 1 is added to the counter. If the value of the counter becomes 2 from this addition, then the package is considered to be ruptured. If the value of the counter is 1 after this addition, then the package does not rupture but the counter is saved for subsequent events within the realization. If the sampled value is 2, then 2 is added to the counter and the package is considered to be ruptured.

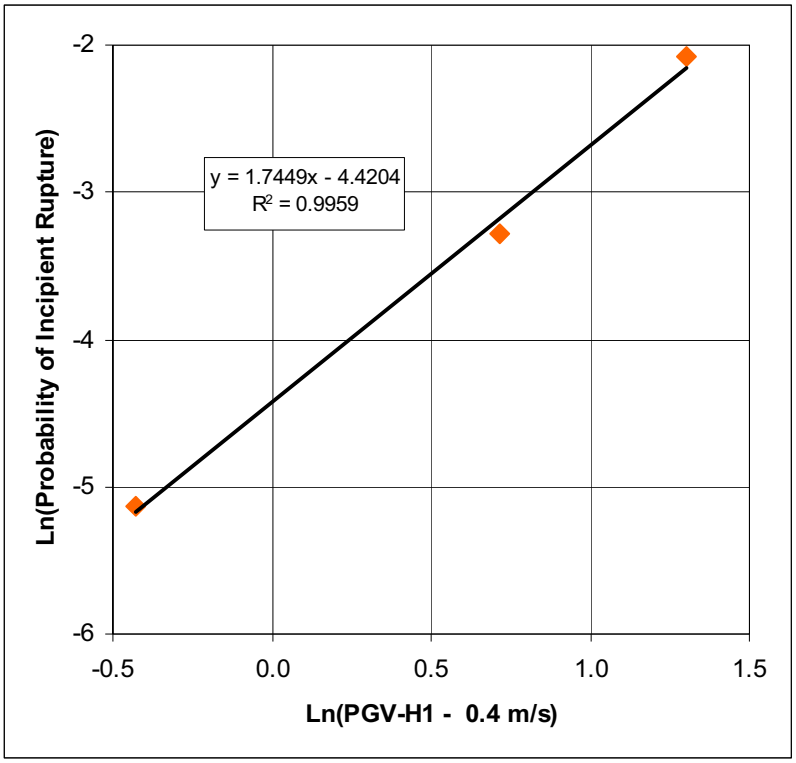

Source: Output DTN: MO0703PASDSTAT.001, worksheet "TAD Kinematic Abstraction" in *Rupture and Puncture Abstractions.xls.*

NOTE: Kinematic response of TAD-bearing waste package with degraded internals, based on average of results for 17-mm-thick and 23-mm-thick OCBs.

Figure 6-11. Least-Squares Fit for Power-Law Dependence for Probability of Incipient Rupture for the TAD-Bearing Waste Package with Degraded Internals

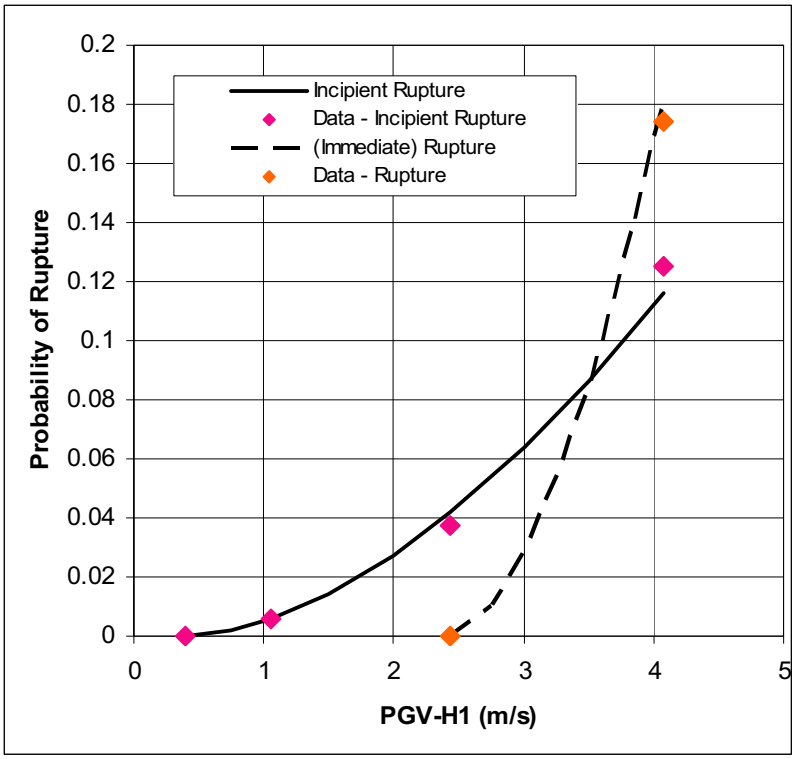

Source: Output DTN: MO0703PASDSTAT.001, worksheet "TAD Kinematic Abstraction" in *Rupture and Puncture Abstractions.xls*.

NOTE: Kinematic response of TAD-bearing waste package with degraded internals, based on average of results for 17-mm-thick and 23-mm-thick OCBs.

Figure 6-12. Comparison of Power-Law Dependence with Probability Data for Incipient Rupture and for Rupture for the TAD-Bearing Waste Package with Degraded Internals

When a waste package is ruptured, the failed area is determined by sampling a uniform distribution with a lower bound of 0 m^2 and an upper bound equal to the cross-sectional area of the waste package OCB. The cross-sectional area for the TAD-bearing waste package is 2.78 m^2, based on an OCB outer diameter of 1881.6 mm for the TAD-bearing waste package (SNL 2007 [DIRS 179394], Table 4-3). This failed area allows advective flow through the ruptured TAD-bearing waste packages and advective and diffusive transport out of the ruptured TAD-bearing waste packages. This failed area is conceptualized to be a tear or rupture along a crease that lies in a plane normal to the central axis of the waste package. The failed area can be represented as a circumferential band around the waste package for transport calculations in the TSPA. Once the TAD-bearing waste package ruptures, there is no further rupture damage on successive events and the TAD-bearing waste packages remain ruptured for the remainder of the realization.

6.5.2.2 Probability of Damage

The approach to defining the probability of damage for the TAD-bearing waste package with 17-mm-thick OCB and degraded internals is more complex than the simple analysis described in Section 6.5.1.2. Table 6-7 and Figure 6-13 present the probability of damage from the kinematic calculations for the 17-mm-thick OCB with degraded internals. Table 6-7 also includes the probability of damage for the 23-mm-thick OCB with degraded internals because these numerical values are used later in this section. The values in Table 6-7 are not the final results for the probability of damage because the results from single waste package calculations are used to refine the values in Table 6-7 for PGV values below 1.05 m/s, as explained next.

Table 6-7. Probability of Damage from the Kinematic Calculations for the TAD-Bearing Waste Package with Degraded Internals

PGV Level (m/s)	Residual Stress Threshold (% of Yield Strength)		
	90%	100%	105%
17-mm-thick OCB:			
0.40	0.412	0.392	0.333
1.05	0.882	0.843	0.804
2.44	1	1	1
4.07	1	1	1
23-mm-thick OCB:			
0.40	0.275	0.255	0.255
1.05	0.804	0.804	0.784
2.44	1	1	1
4.07	1	1	1

Sources: Output DTN: MO0703PASDSTAT.001, worksheet “Prob of Damage – Old” in the file *Kinematic Damage Abstraction 17-mm Degraded.xls* and worksheet “Prob of Damage – Old” in the file *Kinematic Damage Abstraction 23-mm Degraded.xls*.

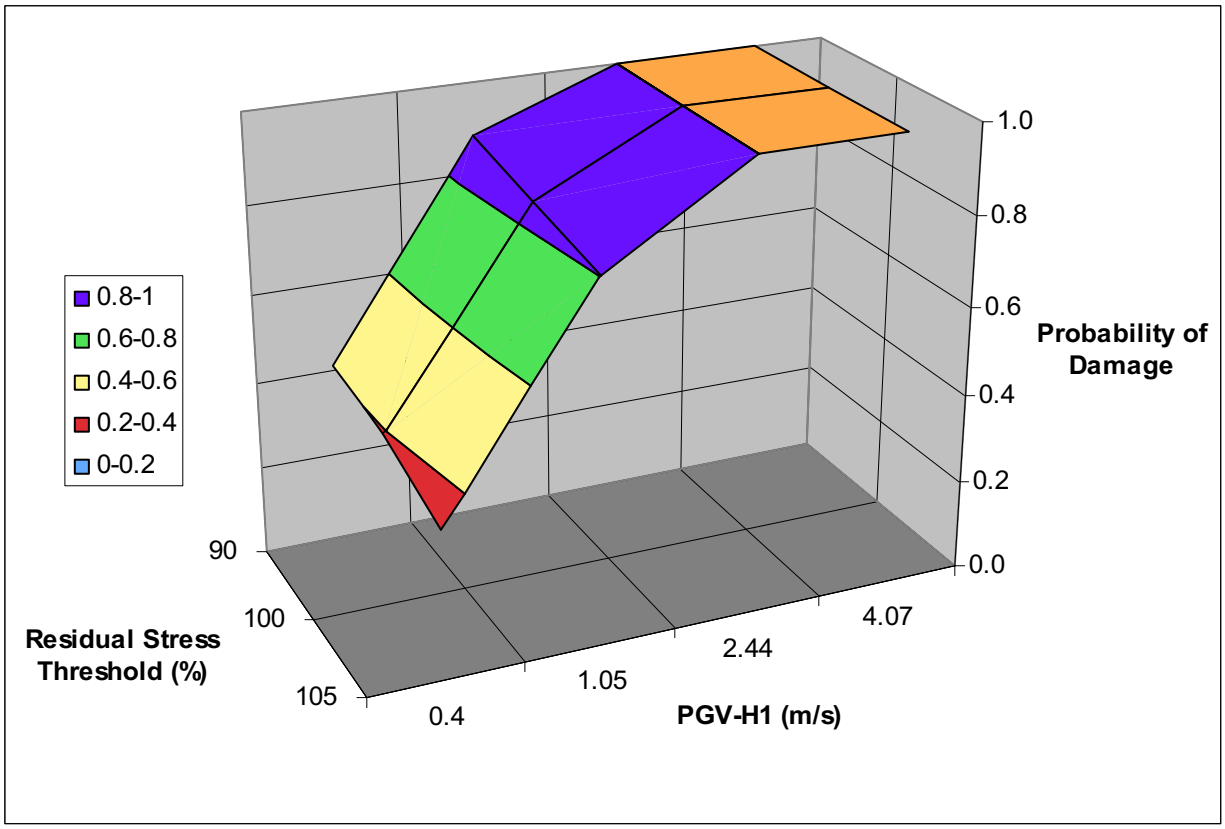

Source: Output DTN: MO0703PASDSTAT.001, worksheet "Prob of Damage – Old" in *Kinematic Damage Abstraction 17-mm Degraded.xls.*

NOTE: Orange area represents a probability of 1.0.

Figure 6-13. Probability of Damage Based on Kinematic Calculations for the TAD-Bearing Waste Package with 17-mm-Thick OCB and Degraded Internals

The methodology for the kinematic calculations is expected to overestimate damaged area and the probability of damage at the 0.4 m/s PGV level. This overestimate is significant for the seismic scenario because the PGV threshold for nonzero damage would be at or below the 0.2 m/s PGV level, greatly expanding the hazard range for the TSPA. A sensitivity study was therefore performed to quantify the overestimate in the probability of damage from the kinematic approach at the 0.4 m/s PGV level.

The results from the kinematic calculations at the 0.4 m/s PGV level demonstrate that end-to-end impacts of adjacent waste packages do not occur for any of the 17 ground motions (output DTN: MO0703PASDSTAT.001, File *Kinematic Damage Abstraction 17-mm Degraded.xls,* worksheet: "WP-WP Data"). With this behavior, the response of an individual waste package is independent of the adjacent packages. It is possible to perform structural response calculations for a single waste package with a fine finite-element mesh, and the damaged area is determined directly from the finite-element mesh.

Three single package calculations were performed for the TAD-bearing waste package with 17-mm-thick OCB and degraded internals. This case was chosen to maximize the damaged area relative to a 23-mm-thick OCB. The three calculations represent the three central waste packages (denoted as I, J, and K) in the kinematic model for Realization 4. The calculations for the three packages are identical, except for the values of the metal-to-metal and metal-to-rock friction coefficients for each package and pallet. Realization 4 was selected because it has the greatest damaged areas without any waste package to drip shield impacts (or end-to-end impacts).

Table 6-8 compares the damaged areas for the kinematic analysis and for the three single waste package calculations. A comparison of these results clearly indicates that the kinematic approach overestimates damaged area for three central waste packages, denoted as I, J, and K in Table 6-8. The single waste package model has zero damage for all kinematic damaged areas less than 0.24 m^2 and very small damaged areas up to kinematic damaged areas of 0.51 m^2.

Table 6-8. Comparison of Damaged Area for the TAD-Bearing Waste Package with 17-mm-Thick OCB and Degraded Internals Using Different Analytical Methods at 0.4 m/s PGV Level

Waste Package ID	Damaged Area (m^2)					
	90% RST		100% RST		105% RST	
	Kinematic	Single Package	Kinematic	Single Package	Kinematic	Single Package
I	0.3873	0.0009	0.1829	0	0.0483	0
J	0.5083	0	0.2358	0	0.0619	0
K	0.4791	0.0034	0.2246	0	0.0600	0

Sources: DTN: LL0702PA055SPC.002 [DIRS 179406], File *NavalLong_TAD_1WP_analyses_DA_summary.xls;* output DTN: MO0703PASDSTAT.001, worksheet "Prob of Damage Anal. 17-mm OCB" in the file *Kinematic Damage Abstraction 17-mm Degraded.xls*.

The calculations with a single waste package are a more accurate approach for calculating damaged area than the kinematic approach for two reasons. First, the detailed finite-element model provides a more realistic representation of the structural stiffness of the waste package in comparison to the coarser kinematic representation. Second, the detailed finite-element model integrates the effects of multiple impacts during a given seismic event through the time-dependent stress and strain in individual finite-elements. This integration with the finite-element grid differs from the kinematic approach, which overestimates the total damaged area from multiple impacts as the sum of the damaged area from the individual impacts (see Section 6.5.3),. Since the single waste package calculations are more accurate, the probability of damage from the kinematic calculations at the 0.4 m/s PGV level has been reinterpreted, based on the results in Table 6-8.

Table 6-9 summarizes the nonzero damaged areas from the kinematic analyses at the 0.4 m/s PGV level and the rationale for reassigning damage states based on the results in Table 6-8. Note that the damaged area in Table 6-8 for waste package I at the 90% RST, 0.0009 m^2, is considered nonzero damage even though it is less than the cutoff area for the kinematic analyses, 0.0024 m^2, discussed in Section 6.5. This approach is appropriate because single waste package calculations have not been performed for all realizations in Table 6-9, and including areas as small as 0.0009 m^2 is appropriate for estimating the revised probability for nonzero damage.

Entries that are positive or ">0" in the sixth through eighth columns of Table 6-9 contribute to the revised probability of damage.

Table 6-9. Reinterpretation of Damage States for a TAD-Bearing Waste Package with 17-mm-Thick OCB and Degraded Internals at the 0.4 m/s PGV Level

Real. No.	WP ID	Kinematic Damaged Area (m^2)			Damaged Area Estimated from Single WP Results (m^2)			Rationale
		90% RST	100% RST	105% RST	90% RST	100% RST	105% RST	
3	I	0.294	0.142	0.036	> 0	0	0	Damaged areas < 0.25 m^2 from kinematic approach are reset to zero based on results in Table 6-8.
	J	0.363	0.169	0.054	> 0	0	0	
	K	0.229	0.112	0.029	0	0	0	
4	I	0.387	0.183	0.048	0.0009	0	0	Calculated results from single package model (see Table 6-8).
	J	0.508	0.236	0.062	0	0	0	
	K	0.479	0.225	0.060	0.0034	0	0	
6	I	0.010	0.006	0	0	0	0	Damaged areas < 0.25 m^2 from kinematic approach are reset to zero based on results in Table 6-8.
	J	0.014	0.004	0	0	0	0	
	K	0	0	0	0	0	0	
8	I	0	0	0	0	0	0	Damaged areas < 0.25 m^2 from kinematic approach are reset to zero based on results in Table 6-8.
	J	0.042	0.030	0.003	0	0	0	
	K	0.061	0.041	0.008	0	0	0	
10	I	1.010	0.420	0.138	> 0	> 0	0	Large damaged areas at 90% and 100% RSTs remain nonzero. Damaged areas < 0.25 m^2 from kinematic approach are reset to 0 based on results in Table 6-8.
	J	0.828	0.362	0.121	> 0	> 0	0	
	K	1.184	0.543	0.208	> 0	> 0	0	
11	I	0.130	0.073	0.020	0	0	0	Damaged areas < 0.25 m^2 from kinematic approach are reset to zero, based on results in Table 6-8.
	J	0.138	0.081	0.024	0	0	0	
	K	0.114	0.066	0.017	0	0	0	
13	I	0	0	0	0	0	0	Damaged areas < 0.25 m^2 from kinematic approach are reset to zero based on results in Table 6-8.
	J	0.003	0	0	0	0	0	
	K	0	0	0	0	0	0	
14	I	0	0	0	0	0	0	Damaged areas < 0.25 m^2 from kinematic approach are reset to zero based on results in Table 6-8.
	J	0.012	0.008	0	0	0	0	
	K	0.199	0.108	0.028	0	0	0	
17	I	0.028	0.013	0.003	0	0	0	Damaged areas < 0.25 m^2 from kinematic approach are reset to zero based on results in Table 6-8.
	J	0	0	0	0	0	0	
	K	0.034	0.022	0.005	0	0	0	

Sources: Output DTN: MO0703PASDSTAT.001, worksheet "Prob of Damage Anal. 17-mm OCB" in the file *Kinematic Damage Abstraction 17-mm Degraded.xls.*

DTN: LL0702PA055SPC.002 [DIRS 179406], File *NavalLong_TAD_1WP_analyses_DA_summary.xls*.

NOTE: Positive values and values greater than 0 in the sixth through eighth columns define the revised probability of damage.

WP = waste package.

Based on the analysis in Table 6-9, the number of observations with nonzero damaged area for the 90%, 100%, and 105% RST are 7, 3, and 0, respectively. The corresponding probabilities of damage for the TAD-bearing waste package at the 0.4 m/s PGV level with 17-mm-thick OCB and degraded internals are 0.137, 0.059, and 0.0 at the 90%, 100%, and 105% RSTs, respectively. These revised probabilities are incorporated into the damage abstraction for the TSPA, as shown in Figure 6-14.

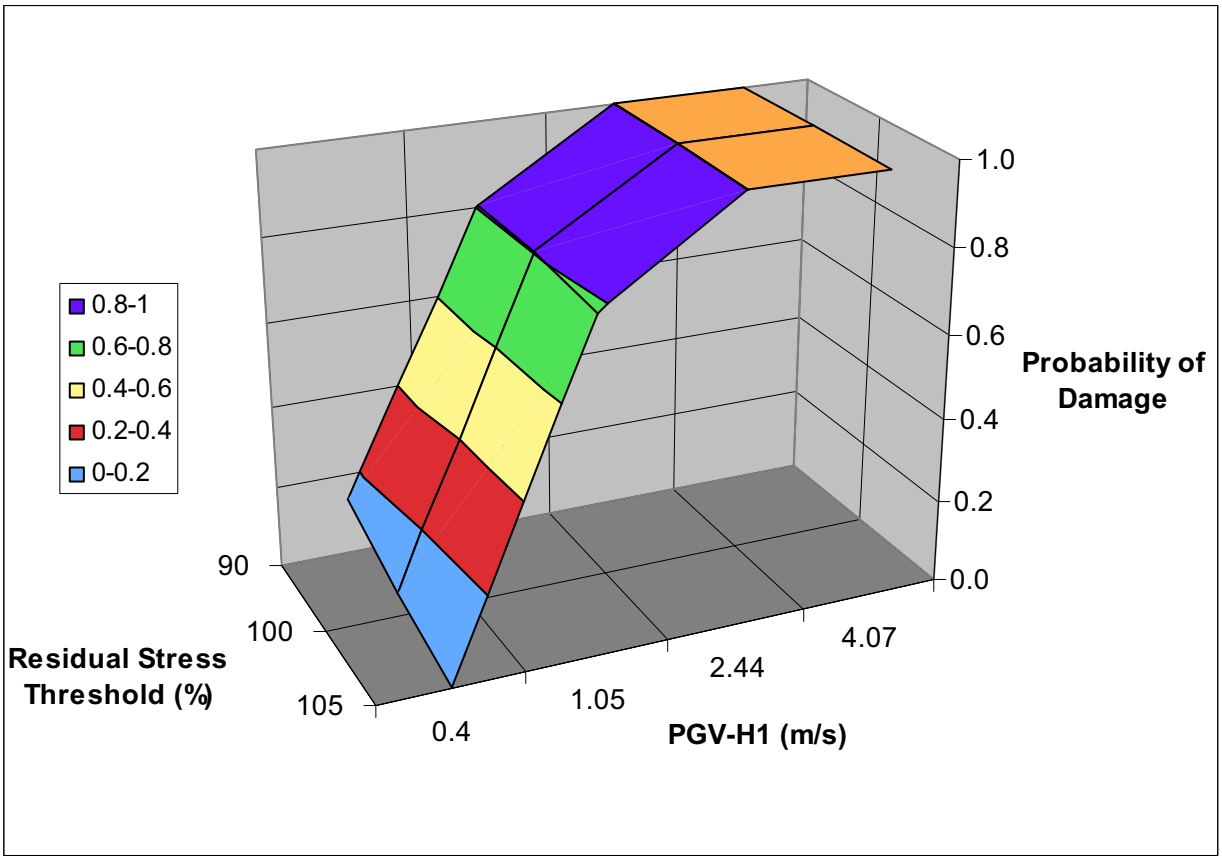

Source: Output DTN: MO0703PASDSTAT.001, worksheet "Prob of Damage – New" in *Kinematic Damage Abstraction 17-mm Degraded.xls.*

NOTE: Orange area represents a probability of 1.0.

Figure 6-14. Revised Probability of Damage with Reinterpreted Damage States for the TAD-Bearing Waste Package with 17-mm-Thick OCB and Degraded Internals

A similar analysis has been performed for the damage states with a 23-mm-thick OCB at the 0.4 m/s PGV level, based on the results in Table 6-8. The results in Table 6-8 are for the 17-mm-thick OCB should provide an upper bound for the 23-mm-thick OCB. The revised damage states, which are derived in worksheet "Prob of Damage Anal. 23-mm OCB" in the file *Kinematic Damage Abstraction 23-mm Degraded.xls* in output DTN: MO0703PASDSTAT.001, are the same as those shown in Table 6-9. The revised probabilities for the 23-mm-thick OCB are identical to those for the 17-mm-thick OCB at the 0.4 m/s PGV level: 0.137, 0.059, and 0.0 at the 90%, 100%, and 105% RSTs, respectively.

The response for the probability of damage at the 0.4 m/s PGV level is extrapolated to define the PGV threshold for zero damage, as discussed in Section 6.4.3. Table 6-10 presents the calculations, which are based on the modified probabilities for nonzero damage at the 0.4 m/s PGV level and the original probabilities for nonzero damage at the 1.05 m/s PGV level. To illustrate the calculations, consider the 17-mm-thick OCB at 90% RST. The PGV/probability data for the extrapolation are (0.4 m/s, 0.137) and (1.05 m/s, 0.882). The resulting slope, m_1, is (0.882 – 0.137)/(1.05 m/s – 0.4 m/s) = 1.146 m/s, and the PGV-intercept is calculated as $\{(0.4 \text{ m/s}) - (0.137)/m_1\}$ = 0.280 m/s. The minimum PGV-intercept in Table 6-10 is 0.266 m/s.

Table 6-10. PGV-Intercepts for the TAD-Bearing Waste Package with Degraded Internals

	Residual Stress Threshold (% of Yield Strength)		
PGV Level or Parameter	**90%**	**100%**	**105%**
17-mm-thick OCB			
0.40 m/s	0.137	0.059	0
1.05 m/s	0.882	0.843	0.804
Slope (s/m)	1.146	1.207	1.237
PGV-Intercept (m/s)	0.280	0.351	0.4
23-mm-thick OCB			
0.40 m/s	0.137	0.059	0
1.05 m/s	0.804	0.804	0.784
Slope (s/m)	1.026	1.146	1.207
PGV-Intercept (m/s)	0.266	0.349	0.4

Sources: Output DTN: MO0703PASDSTAT.001, worksheet "Prob of Damage - New" in the file *Kinematic Damage Abstraction 17-mm Degraded.xls* and worksheet "Prob of Damage - New" in the file *Kinematic Damage Abstraction 23-mm Degraded.xls* for data at the 1.05 m/s PGV level and the analysis based on Table 6-9 for probabilities at the 0.4 m/s PGV level.

Table 6-11 summarizes the final probabilities for nonzero damage for the TAD-bearing waste package with degraded internals. Table 6-11 includes the appropriate PGV intercepts from Table 6-10. Table 6-11 also includes the calculated probabilities for PGV values less than 0.40 m/s, based on the same linear extrapolation that defines the intercepts in Table 6-10.

Table 6-11. Revised Probability of Damage for the TAD-Bearing Waste Package with Degraded Internals

	Residual Stress Threshold (% of Yield Strength)		
PGV Level (m/s)	**90%**	**100%**	**105%**
17-mm-thick OCB:			
0.280	0	0	0
0.351	0.081	0	0
0.40	0.137	0.059	0
1.05	0.882	0.843	0.804
2.44	1	1	1
4.07	1	1	1

Table 6-11. Revised Probability of Damage for the TAD-Bearing Waste Package with Degraded Internals (Continued)

PGV Level (m/s)	Residual Stress Threshold (% of Yield Strength)		
	90%	100%	105%
23-mm-thick OCB:			
0.266	0	0	0
0.349	0.085	0	0
0.40	0.137	0.059	0
1.05	0.804	0.804	0.784
2.44	1	1	1
4.07	1	1	1

Sources: Output DTN: MO0703PASDSTAT.001, worksheet "Prob of Damage – New" in the file *Kinematic Damage Abstraction 17-mm Degraded.xls* and worksheet "Prob of Damage - New" in the file *Kinematic Damage Abstraction 23-mm Degraded.xls*.

The probability of damage in Table 6-11 has three independent parameters: the value of *PGV* for the *j*th seismic event, the value of *RST* for a given realization, and the time-dependent thickness of the OCB. Linear interpolation is used to define the variation of the probability of damage as a function of *PGV* and *RST*. Damaged areas are often observed to follow a power law whose slope is positive and increasing with increasing values of PGV. A typical functional dependence is illustrated by the quadratic fit for mean damaged area as a function of *PGV* in Figure 6-19. The use of linear interpolation for *PGV* and *RST* is appropriate because it provides results at intermediate values that are greater than those from a power-law fit with a positive, increasing slope.

The spatially averaged thickness of the OCB is a time-dependent parameter that is predicted by other elements of the TSPA. The probability of damage corresponding to the average OCB thickness at the time of the *j*th seismic event is calculated by linear interpolation if the OCB thickness is between 17 mm and 23 mm. The probability of damage is set to the value at 23 mm if the average OCB thickness is greater than 23 mm. The probability is set to the value at 17 mm if the average OCB thickness is less than 17 mm. The abstraction for the 17-mm-thick OCB is anticipated to provide a reasonable lower bound to damaged area until the drip shield fails, after which the kinematic response is not applicable. The logic for the dependence of damaged area on OCB thickness is illustrated in Equation 6.5-1:

$$PD_{TAD,j} = \text{If } t \geq 23 \text{ mm}, PD_{TAD,j,23\text{-}mm} \quad \text{(Eq. 6.5-1)}$$

$$\text{Or if } t \leq 17 \text{ mm}, PD_{TAD,j,17\text{-}mm}$$

$$\text{else}, PD_{TAD,j,17\text{-}mm} + (PD_{TAD,j,23\text{-}mm} - PD_{TAD,j,17\text{-}mm})*(\text{t} - 17 \text{ mm})/(6 \text{ mm})$$

where t is the spatially averaged thickness (in mm) of the OCB at the time of the jth event and $PD_{TAD,j,17\text{-}mm}$ and $PD_{TAD,j,23\text{-}mm}$ are the probabilities of damage for the 17-mm-thick and 23-mm-thick OCBs, respectively, at the values of *PGV* for the jth seismic event and of *RST*.

The probabilities for the 23-mm-thick OCB provide a reasonable representation for several hundred thousand years after repository closure, as explained in Section 6.5.1.2. The probabilities for the 17-mm-thick OCB provide a reasonable representation at the end of the time period for peak dose assessment. The median corrosion rate of Alloy 22 at 60ºC is 6.35 nm/yr ≈ 7 nm/yr, based on a medium uncertainty level in the distributions for general corrosion rate (DTN: MO0612WPOUTERB.000 [DIRS 182035], File *BaseCase GC CDFs2.xls*, worksheet "Data," Cell L71). The value of 60ºC is appropriate because it is an upper bound on OCB temperature beyond 10,000 years after repository closure (SNL 2007 [DIRS 178851], Figure 1-3) and because it is consistent with the structural response calculations for the seismic scenario (SNL 2007 [DIRS 178851], Assumption 5.7, Section 5). The 17-mm-thick OCB, which corresponds to an 8.4-mm ≈ 8-mm thickness reduction, will occur at a time of $(8 \times 10^{-3}$ m)/ $(7 \times 10^{-9}$ m/yr) ≈ 1,100,000 years. More detailed corrosion calculations must be performed probabilistically, but this estimate indicates that the probabilities for a 17-mm-thick OCB provide a reasonable representation for seismic response at the end of the period for peak dose assessment.

6.5.2.3 Conditional Probability Distributions for Nonzero Damaged Area

Figures 6-15 to 6-18 present the Q-Q plots for gamma distributions versus the conditional damaged areas at the 0.4 m/s, 1.05 m/s, 2.44 m/s, and 4.07 m/s PGV levels for 90% RST. The values of the mean and standard deviation of the conditional damaged areas, which are the input to the gamma distributions, are shown in Table 6-12. Gamma distributions provide an excellent fit to the conditional (nonzero) damaged areas at the 0.4 m/s, 1.05 m/s, and 2.44 m/s PGV levels and an acceptable fit at the 4.07 m/s PGV level.

Q-Q plots for gamma distributions versus the conditional damaged areas for the 17-mm-thick and 23-mm-thick OCBs at all RST levels show similar comparisons as Figure 6-15 through Figure 6-18. These plots are documented in output DTN: MO0703PASDSTAT.001, worksheets "Gamma for 100%_d17" and "Gamma for 105%_d17" in the file *Kinematic Damage Abstraction 17-mm Degraded.xls*. Q-Q plots for 23-mm-thick OCB with degraded internals are documented in the file *Kinematic Damage Abstraction 23-mm Degraded.xls* in output DTN: MO0703PASDSTAT.001. Based on these results, gamma distributions are selected as the probability distribution for conditional damaged areas on the TAD-bearing waste package with degraded internals.

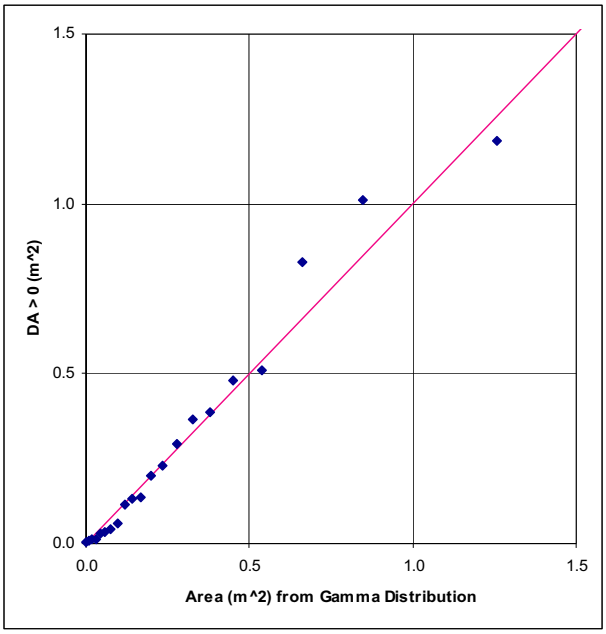

Source: Output DTN: MO0703PASDSTAT.001, worksheet "Gamma for 90%_d17" in the file *Kinematic Damage Abstraction 17-mm Degraded.xls*.

NOTE: 0.4 m/s PGV level at 90% RST. DA > 0 is the conditional nonzero damaged area.

Figure 6-15. Q-Q Plot for Conditional Damaged Areas versus a Gamma Distribution for the TAD-Bearing Waste Package with 17-mm-Thick OCB and Degraded Internals

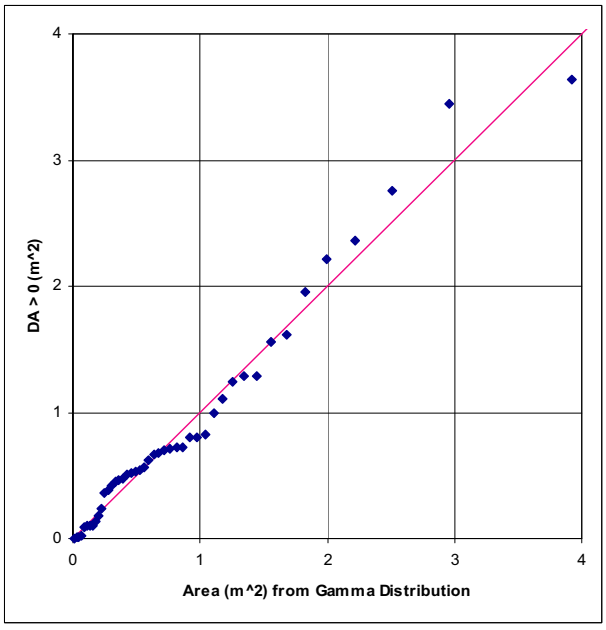

Source: Output DTN: MO0703PASDSTAT.001, worksheet "Gamma for 90%_d17" in the file *Kinematic Damage Abstraction 17-mm Degraded.xls.*

NOTE: 1.05 m/s PGV level at 90% RST. DA > 0 is the conditional nonzero damaged area.

Figure 6-16. Q-Q Plot for Conditional Damaged Areas versus a Gamma Distribution for the TAD-Bearing Waste Package with 17-mm-Thick OCB and Degraded Internals

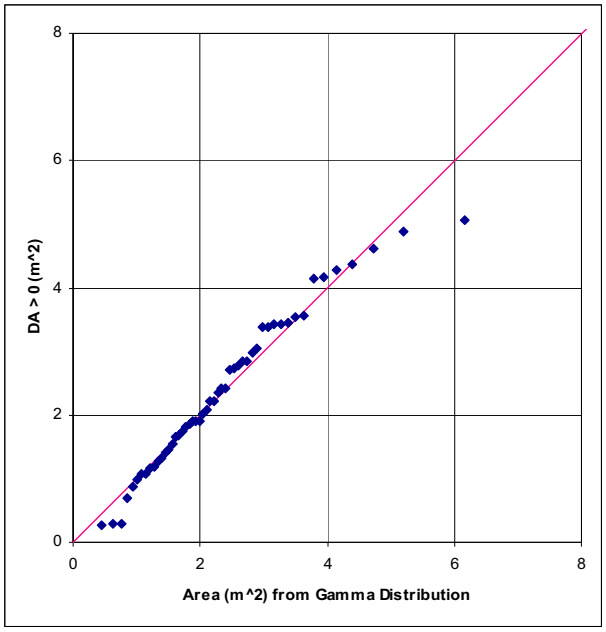

Source: Output DTN: MO0703PASDSTAT.001, worksheet "Gamma for 90%_d17" in the file *Kinematic Damage Abstraction 17-mm Degraded.xls*.

NOTE: 2.44 m/s PGV level at 90% RST. DA > 0 is the conditional nonzero damaged area.

Figure 6-17. Q-Q Plot for Conditional Damaged Areas versus a Gamma Distribution for the TAD-Bearing Waste Package with 17-mm-Thick OCB and Degraded Internals

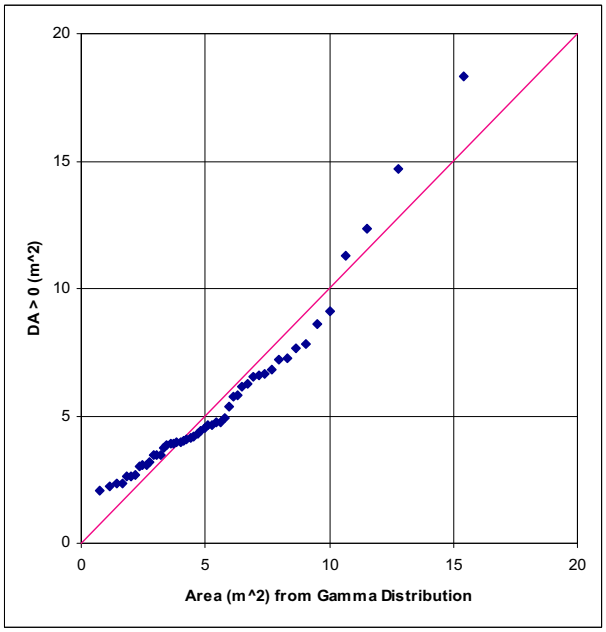

Source: Output DTN: MO0703PASDSTAT.001, worksheet "Gamma for 90%_d17" in the file *Kinematic Damage Abstraction 17-mm Degraded.xls*.

NOTE: 4.07 m/s PGV level at 90% RST. DA > 0 is the conditional nonzero damaged area.

Figure 6-18. Q-Q Plot for Conditional Damaged Areas versus a Gamma Distribution for the TAD-Bearing Waste Package with 17-mm-Thick OCB and Degraded Internals

Table 6-12. Mean and Standard Deviations of the Conditional Damaged Areas for the 17-mm-Thick OCB with Degraded Internals

PGV Level (m/s)	Residual Stress Threshold (% of Yield Strength)					
	90%		100%		105%	
	Mean (m^2)	Standard Deviation (m^2)	Mean (m^2)	Standard Deviation (m^2)	Mean (m^2)	Standard Deviation (m^2)
0.4	0.289	0.343	0.142	0.151	0.0508	0.0560
1.05	0.865	0.872	0.444	0.425	0.198	0.228
2.44	2.37	1.24	1.29	0.704	0.620	0.391
4.07	5.42	3.18	3.06	1.77	1.62	1.03

Source: Output DTN: MO0703PASDSTAT.001, worksheets "Gamma for 90%_d17," "Gamma for 100%_d17," and "Gamma for 105%_d17" in the file *Kinematic Damage Abstraction 17-mm Degraded.xls.*

The abstraction for the TSPA must represent the response for intermediate values of PGV between the four PGV levels in Figures 6-15 to 6-18. Quadratic fits to the mean and standard deviation of the data at the four PGV levels provide a convenient way to represent the input parameters for the gamma distribution as a function of PGV. Figure 6-19 shows the quadratic fits for the mean and standard deviation of damaged area data at the 90% RST for the 17-mm-thick OCB with degraded internals.

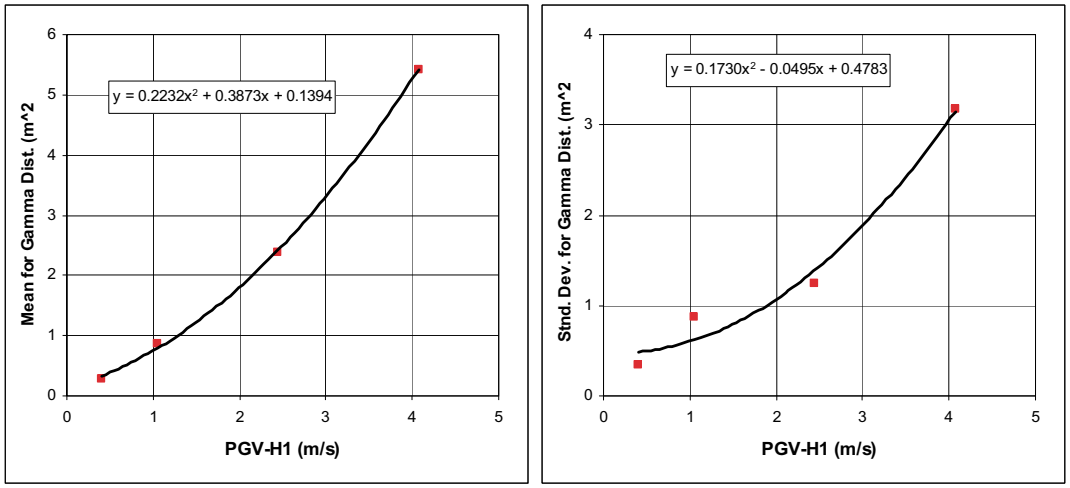

Source: Output DTN: MO0703PASDSTAT.001, worksheet "Gamma for 90%_d17" in the file *Kinematic Damage Abstraction 17-mm Degraded.xls*.

NOTE: 90% RST.

Figure 6-19. Quadratic Fits to the Mean and Standard Deviation of Conditional Damaged Areas for the TAD-Bearing Waste Package with 17-mm-Thick OCB and Degraded Internals

Figure 6-20 plots the 1st, 5th, 50th, 95th, and 99th percentiles of the resulting gamma distributions against the conditional damaged areas as a function of PGV. The gamma distributions, with the quadratic fits defined in Figure 6-19, provide an excellent representation of the conditional damaged areas over the PGV range of 0.4 m/s to 4.07 m/s.

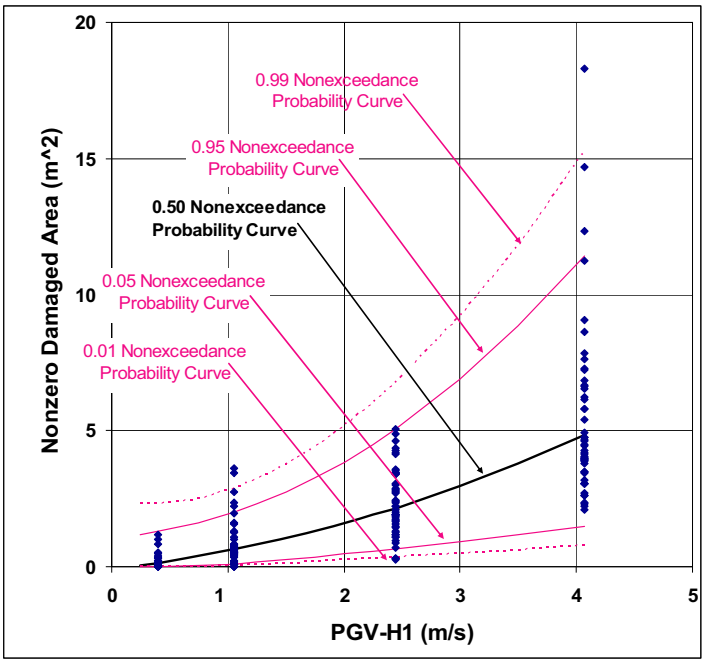

Source: Output DTN: MO0703PASDSTAT.001, worksheet "Gamma for 90%_d17" in the file *Kinematic Damage Abstraction 17-mm Degraded.xls.*

NOTE: 90% RST.

Figure 6-20. Comparison of Percentiles on the Gamma Distributions to Conditional Damaged Areas for the TAD-Bearing Waste Package with 17-mm-Thick OCB and Degraded Internals

The abstraction for the TSPA must also represent the response for the full range of the RST, from 90% to 105%. Figures 6-21 and 6-22 demonstrate that the mean value of the conditional damaged area varies approximately linearly over this RST range. More specifically, a linear fit to the data at 90% and 100% provides a piecewise linear fit that slightly overestimates the mean value of the conditional damaged area at the 105% RST over the full range of PGV. A similar result holds for the standard deviation of the conditional damaged area.

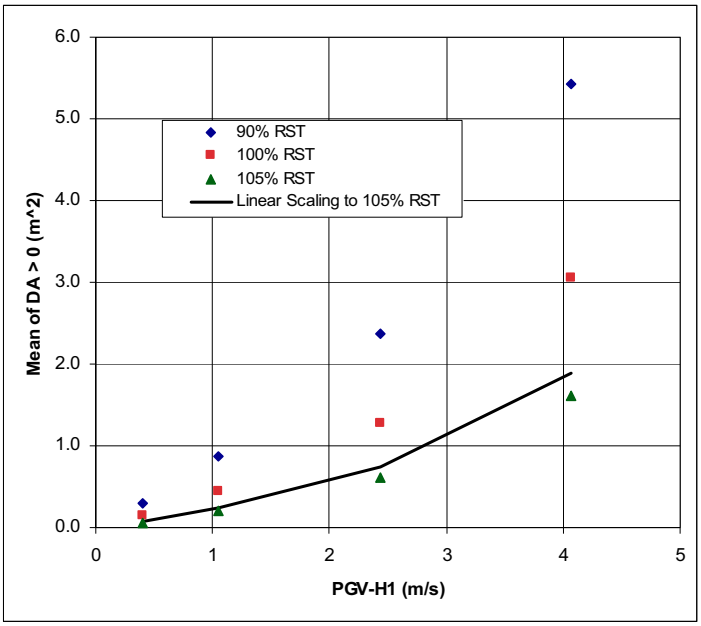

Source: Output DTN: MO0703PASDSTAT.001, worksheet "Dependence on RST" in the file *Kinematic Damage Abstraction 17-mm Degraded.xls.*

Figure 6-21. Overestimation of the Mean Conditional Damaged Area at 105% RST for the TAD-Bearing Waste Package with 17-mm-Thick OCB and Degraded Internals

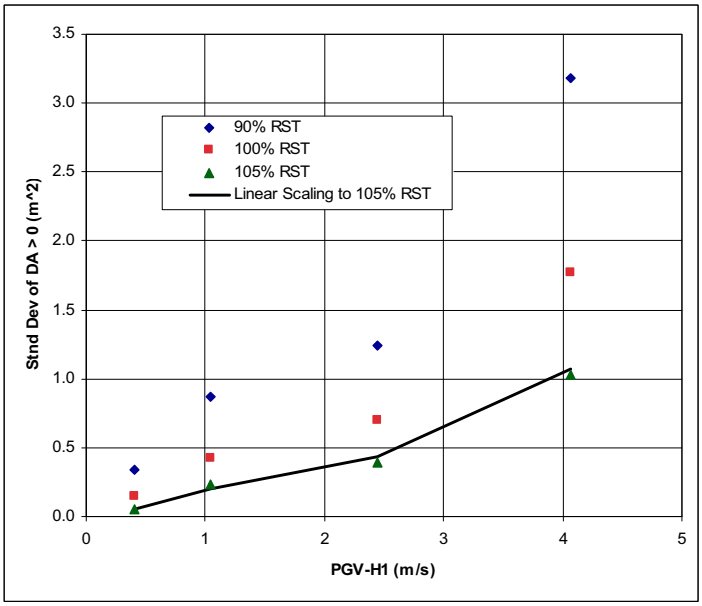

Source: Output DTN: MO0703PASDSTAT.001, worksheet "Dependence on RST" in the file *Kinematic Damage Abstraction 17-mm Degraded.xls.*

Figure 6-22. Overestimation of the Standard Deviation of Conditional Damaged Area at 105% RST for the TAD-Bearing Waste Package with 17-mm-Thick OCB and Degraded Internals

Given the results in Figures 6-21 and 6-22, it is reasonable to extend the quadratic equations in Figure 6-19 by defining coefficients that are linear in RST, based on the values at 90% RST and 100% RST in Table 6-12. The resulting equations for the mean, μ, and standard deviation, σ, are:

$$\mu = (-0.00838*(RST - 100) + 0.1394)*PGV^2 + (-0.02224*(RST - 100) + 0.1649)*PGV + (-0.00628*(RST - 100) + 0.0766), \quad \text{(Eq. 6.5-2)}$$

$$\sigma = (-0.00828*(RST - 100) + 0.0902)*PGV^2 + (0.00665*(RST - 100) + 0.0170)*PGV + (-0.02851*(RST - 100) + 0.1932). \quad \text{(Eq. 6.5-3)}$$

The numerical parameters for these quadratic fits are derived in output DTN: MO0703PASDSTAT.001, in the file *Kinematic Damage Abstraction 17-mm Degraded.xls*, worksheet "Dependence on RST." Note that RST is expressed as an integer value (i.e., 95, rather than 0.95) in these equations.

Figures 6-23 and 6-24 compare Equations 6.5-2 and 6.5-3 to the mean and standard deviation for the conditional damaged areas from Table 6-12. This comparison demonstrates that Equations 6.5-2 and 6.5-3 provide an excellent representation of parameters defining the gamma distribution over the PGV range of 0.4 m/s to 4.07 m/s and RST range of 90% to 105%.

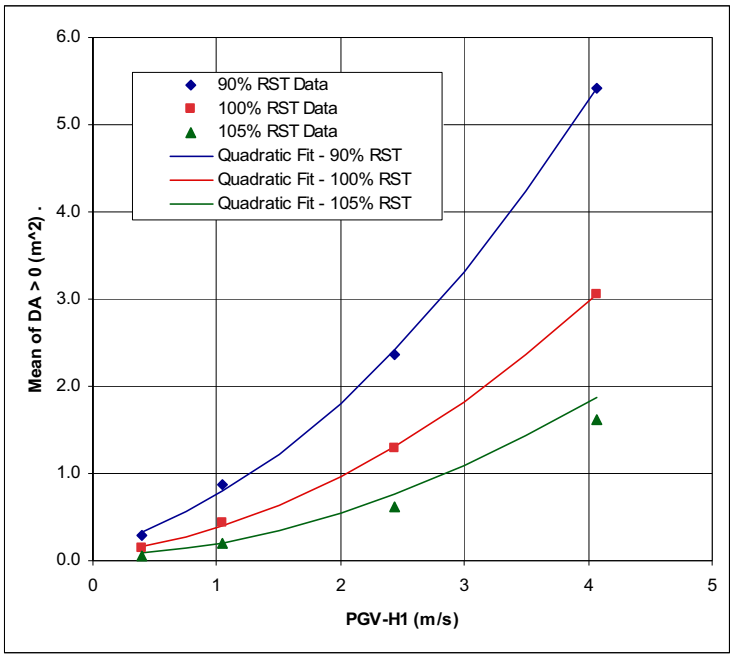

Source: Output DTN: MO0703PASDSTAT.001, worksheet "Dependence on RST" in the file *Kinematic Damage Abstraction 17-mm Degraded.xls.*

Figure 6-23. Comparison of Equation 6.5-2 to the Mean of the Conditional Damaged Areas for the TAD-Bearing Waste Package with 17-mm-Thick OCB and Degraded Internals

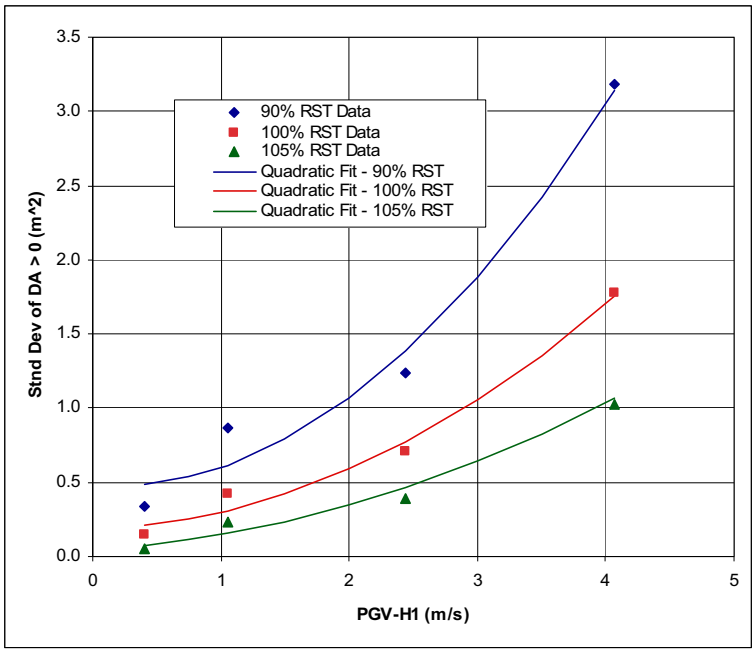

Source: Output DTN: MO0703PASDSTAT.001, worksheet "Dependence on RST" in the file *Kinematic Damage Abstraction 17-mm Degraded.xls.*

Figure 6-24. Comparison of Equation 6.5-3 to the Standard Deviation of the Conditional Damaged Areas for the TAD-Bearing Waste Package with 17-mm-Thick OCB and Degraded Internals

6.5.2.4 Alternate Conditional Probability Distributions

Q-Q plots were prepared for the damaged area data versus gamma, log-normal, and Weibull distributions for 90% RST at the 0.4 m/s, 1.05 m/s, and 2.44 m/s PGV levels. The gamma distribution provides a reasonable representation of the damaged area data at all PGV levels, as shown by Figures 6-15 to 6-18. The log-normal distribution provides a poor representation of the conditional damaged areas at the 1.05 m/s and 2.44 m/s PGV levels and was not considered further. Figure 6-25 presents the Q-Q plot for the conditional damaged areas versus a log-normal distribution at the 1.05 m/s PGV level. A normal distribution was eliminated from consideration because the standard deviation of the conditional damaged area is often greater than its mean, as shown in Table 6-12. In this situation, a normal distribution will predict conditional damaged areas that are less than zero, which is unacceptable.

The Weibull distribution provides a good representation of the damaged area data at all three PGV levels. However, defining the parameters for the Weibull distribution is not straightforward. For the present analysis, the Weibull parameters are defined numerically by using the Excel Solver to minimize the sum of the squared differences between the observations and the corresponding points on a Weibull distribution. In some cases, the minimum value for the distribution (ε) is negative or is greater than the smallest value of the data. This is not acceptable, so the value of ε is reset to a reasonable value and the remaining parameters are readjusted to minimize the sum of the squared differences. This procedure is successful in defining Weibull parameters that provide a good fit to the data. However, the need to adjust the

value of ε is less desirable than using a gamma distribution, which has no free parameters. The gamma distribution is the preferred approach for the abstractions for the TSPA.

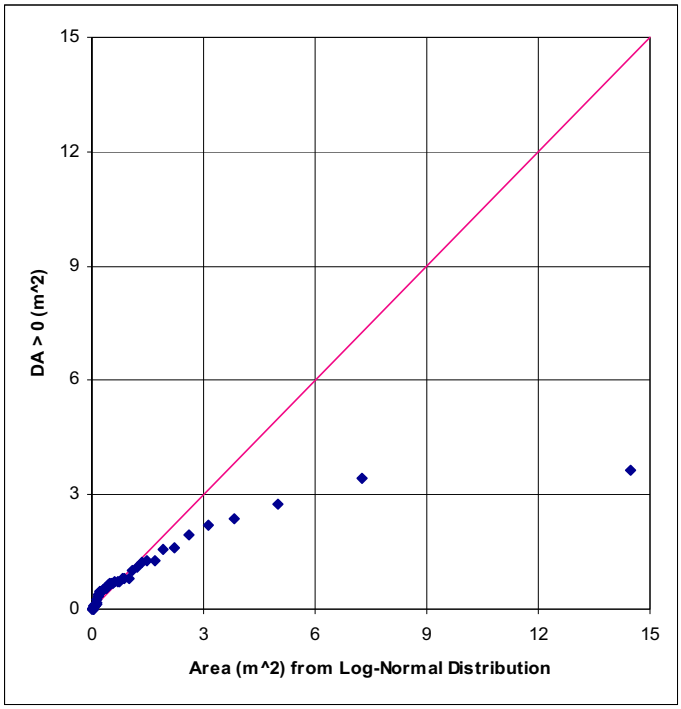

Source: Output DTN: MO0703PASDSTAT.001, worksheet "Log-Normal for 90%_d17" in the file *Kinematic Damage Abstraction 17-mm Degraded.xls.*

NOTE: 1.05 m/s PGV level at 90% RST. DA > 0 is the conditional nonzero damaged area.

Figure 6-25. Q-Q Plot for Conditional Damaged Areas versus a Log-Normal Distribution for the TAD-Bearing Waste Package with 17-mm-Thick OCB and Degraded Internals

6.5.2.5 Dependence on OCB Thickness

The conditional probability distributions described in previous sections represent the variation of damaged area as a function of PGV and RST. The time-dependent thickness of the OCB must also be incorporated into the damage abstraction. The spatially averaged thickness of the OCB is a time-dependent parameter that is predicted by other elements of the TSPA. The conditional damaged area corresponding to the average OCB thickness at the time of the *j*th seismic event is calculated by linear interpolation if the OCB thickness is between 17 mm and 23 mm. Damaged areas are often observed to follow a power law, as illustrated by the quadratic fit for mean damaged area as a function of PGV in Figure 6-19. The use of linear interpolation is appropriate because it provides results at intermediate values that are greater than those from a power-law fit with a positive and increasing slope. The logic for the dependence on damaged area on OCB thickness is illustrated in Equation 6.5-4:

$$DA_{TAD\_Degraded} = \text{If } t \geq 23 \text{ mm}, DA_{TAD\_Degraded,23\text{-}mm} \quad \text{(Eq. 6.5-4)}$$

$$\text{Or if } t \leq 17 \text{ mm}, DA_{TAD\_Degraded,17\text{-}mm}$$

$$\text{else, } DA_{TAD\_Degraded,17\text{-}mm} + (DA_{TAD\_Degraded,23\text{-}mm} - DA_{TAD\_Degraded,17\text{-}mm})*(t - 17 \text{ mm})/(6 \text{ mm})$$

where t is the spatially averaged thickness of the OCB (in mm) at the time of the jth event, $DA_{TAD\_Degraded}$ is the final damaged area at the current average OCB thickness, $DA_{TAD\_Degraded,17\text{-}mm}$ is the value of the conditional damaged area from the 17-mm damage abstraction, and $DA_{TAD\_Degraded,23\text{-}mm}$ is the value of the conditional damaged area from the 23-mm damage abstraction. Based on Equation 6.5-4, the damaged area is set to the value at 23 mm if the average OCB thickness is greater than 23 mm. This is reasonable because the damaged area abstraction for the 23-mm-thick OCB bounds the waste package response for several hundred thousand years after repository closure, based on the estimated corrosion time in Section 6.5.1.2. The damaged area is set to the value for the 17 mm thickness if the average OCB thickness is less than 17 mm. This is a reasonable approach because the damaged area abstraction for the 17-mm-thick OCB provides a reasonable representation at the end of the peak dose period (approximately 1,000,000 years), based on the estimated corrosion time in Section 6.5.2.2. In addition, the drip shield is expected to fail from general corrosion before the OCB thickness is reduced to 17 mm because the general corrosion rate for titanium is greater than for Alloy 22 (SNL 2007 [DIRS 178851], Section 1.2). This kinematic damage abstraction is not applicable after the drip shield fails, which should occur before the thickness of the OCB is reduced to 17 mm.

6.5.3 Damage from Multiple Events

The damaged area from multiple seismic events is defined as the sum of the damaged areas from the individual seismic events. This approach provides an upper bound for damaged area because work hardening of dented or deformed areas on the surface of the waste package makes it more difficult to damage these areas during a subsequent event, and because the summation of damaged areas from individual events ignores impact location entirely. This viewpoint is confirmed by the results for the single waste package calculations with a fine finite-element grid at 0.4 m/s PGV level, which demonstrate that there is little apparent "amplification" from multiple hits to the same area during a seismic event, judging by the very small magnitude of the damaged areas in Table 6-8. In this situation, linear summation of damaged area overestimates the accumulation of residual stress.

6.5.4 Location of Damaged Area

The damaged areas from end-to-end impacts of the TAD-bearing waste package are always zero at the 0.4 m/s, 1.05 m/s, and 2.44 m/s PGV levels. At the 4.07 m/s PGV level, most damaged areas have zero values except for a few very small, nonzero values (DTN: LL0704PA048SPC.023 [DIRS 180735], File *NavalLong_TAD_kinematic_ analyses_ DA_summary.xls*, worksheet "WP-WP"). Damaged areas are therefore almost exclusively due to waste package-to-pallet impacts. This conclusion is applicable to any of the three future states of the waste package.

In this situation, the damaged areas from the kinematic response of the TAD-bearing waste package occur on the cylindrical surface of the OCB, rather than on the lids of the waste package. The damaged areas are conceptualized to be randomly located on the cylindrical surface. That is, any location on the surface is equally likely to sustain damage. This is a reasonable approach because the orientation of individual waste packages will change through translation and rotation during the multiple kinematic events that are expected to occur during

the peak dose period. The surface area of the OCB for the TAD-bearing waste package is 33.64 m^2, based on an outer diameter of the OCB of 1,881.6 mm and a nominal length of the OCB of 5,691.38 mm (SNL 2007 [DIRS 179394], Table 4-3).

6.5.5 Spatial Variability

Damage to or rupture of the waste package from vibratory ground motion is constant throughout the repository for each seismic event in the TSPA. That is, there is no spatial variability of damage or rupture for the waste package groups within the TSPA. Spatial variability is represented in the kinematic calculations through the variability of friction factors on a package-by-package basis and in the abstraction of damaged areas for the three central TAD-bearing waste packages in the kinematic model (SNL 2007 [DIRS 178851], Section 6.3.2).

Lack of spatial variability is not important for predicting the mean dose in the TSPA. The mean dose is independent of spatial variability because the sum of the mean doses from groups of waste packages with different damage levels is equal to the mean of the sum of the doses from the individual groups. On the other hand, the coefficient of variation (i.e., the variability about the mean) of the total dose over all realizations is overestimated without spatial variability because lack of spatial variability makes an extreme response for all waste package groups more likely than for a model with spatial variability.

6.5.6 Damaged Area from Waste Package-to-Drip Shield Impacts

The potential for damage from impacts between the waste package and drip shield is not included in the seismic damage abstractions for the TSPA. The rationale for not including damage from waste package-drip shield impacts is based on the observation that the damaged areas from side-on impacts of a waste package on a flat elastic surface are zero or very small, and are significantly less than the damaged areas from end-on impacts on a flat elastic surface. The side-on impact on a flat, elastic surface is a good representation for the lateral impact of the waste package on the drip shield because the inside surface of the drip shield side walls is a smooth surface, with no protruding bulkheads.

Table 6-13 summarizes the damaged areas from end-on impacts of the waste package versus side-on impacts of the waste package for representative values of impact velocity and angle of impact (BSC 2004 [DIRS 162293], Table 5). Table 6-13 is based on an RST level of 90% with material properties for Alloy 22 at 150ºC. The temperature difference between 150ºC and 60ºC, which is the standard temperature for material properties for structural response calculations during the peak dose period, is not considered significant because damaged areas are insensitive to this range of temperature differences (SNL 2007 [DIRS 178851], Section 6.3.2.2.2).

Table 6-13 demonstrates that there is zero or very little side-on damage for impact velocities up to 4 m/s, which encompasses most of the waste package-drip shield impacts. In addition, the ratio of damaged areas for end-on to side-on impacts varies between 1.7 and 61.2 (or infinite in three cases), implying that damage from end-on impacts is typically much greater than damage from side-on impacts throughout the ranges of impact velocities (1 m/s to 10 m/s) and impact angles (1° to 8°) that are relevant to damaged areas. As noted in Section 6.5.4, damaged areas are almost exclusively due to waste package-to-pallet impacts, with only a few small nonzero

values from end-to-end impacts. Since the damaged areas from side-on impacts are zero or very small for impact velocities below 4 m/s and since the damaged areas from side-on impacts are significantly less than from end-to-end impacts, it follows that the damaged areas from lateral impacts between the waste package and drip shield will make a negligible contribution to total damaged area on the waste package.

Vertical impacts between the waste package and drip shield will also have a small contribution to total damaged area on the waste package. The framework on the underside of the drip shield plates includes three axial stiffeners that run along the crown for the full length of the drip shield. These axial stiffeners are perpendicular to the interior bulkheads that are 1 m apart axially and provide cross-bracing for the plates. The large diameter of the waste package and the limited clearances between the waste package and drip shield constrain the vertical motion of the waste package. Most vertical impacts will involve contact between the waste package and the axial stiffeners at the crown, plus possibly a portion of an interior bulkhead. The impact loads on the waste package are then spread over a significant contact area, similar to the side-on impact on a flat, elastic surface. It follows that the damage from vertical impacts should also be zero or very small, based on the data in Table 6-13 for a side-on impact. This assessment is an engineering judgment because vertical impact calculations for waste package-to-drip shield impacts have not been performed; however, this is a reasonable assessment of damage level based on the data in Table 6-13.

This discussion has focused on the situation where rubble surrounds the drip shield, restricting its movement during the impact. In an unfilled drift, the drip shield is not pinned to the invert and will cause no damage to the waste package because it is free to move once the waste package makes contact with the drip shield.

Based on these arguments, the potential for damage to the waste package from lateral or vertical impacts between the waste package and drip shield is not included in the seismic damage abstractions for the TSPA.

Table 6-13. Comparison of Damaged Areas (m^2) From End-On and Side-On Impacts of a Waste Package on a Flat, Elastic Surface for a RST of 90%

		1° End-On Impact Area	1° Side-On Impact Area	Ratio: End-On to Side-On	8° End-On Impact Area	8° Side-On Impact Area	Ratio: End-On to Side-On
Impact Velocity (m/s)	1	0.0018	0	∞	0.0009	0	∞
	2	0.0112	0.0011	10.2	0.0066	0	∞
	4	0.0212	0.0015	14.1	0.0367	0.0006	61.2
	6	0.0549	0.0092	6.0	0.0501	0.0081	6.2
	10	0.0264	0.0157	1.7	0.0379	0.0160	2.4

Source: BSC 2003 [DIRS 162293], Table 5.

6.6 ABSTRACTIONS FOR THE KINEMATIC RESPONSE OF THE CODISPOSAL WASTE PACKAGE

Kinematic damage abstractions have been developed for three future states of the codisposal waste package:

- 23-mm-thick OCB with intact internals
- 23-mm-thick OCB with degraded internals
- 17-mm-thick OCB with degraded internals.

Each abstraction defines the probability of rupture, probability of damage, and the conditional probability distributions for conditional damaged area, all as functions of PGV and RST. The response for the 23-mm-thick OCB with intact internals is described in this report. The responses for the 23-mm-thick and 17-mm-thick OCBs with degraded internals are very similar, so only the case for the 17-mm-thick OCB is illustrated in the text.

The design of the 5-DHLW/DOE SNF Long waste package has been used to represent the codisposal waste packages in all structural response calculations. This particular design is a reasonable choice because the 5-DHLW/DOE SNF Long waste package is the most common type of codisposal waste package, accounting for over 60% of the inventory of 5-DHLW/DOE SNF Long, 5-DHLW/DOE SNF Short, and 2-MCO/2-DHLW waste packages in the design basis inventory (see Table 6-62). The 5-DHLW/DOE SNF Long waste package is simply referred to as the codisposal waste package throughout this report.

The results from the structural response calculations for kinematic damage to the codisposal waste package have been analyzed with a damaged area cutoff of 0.0024 m^2. This cutoff was determined for the TAD-bearing waste package (Section 3.4) and applied to the codisposal waste package. The damaged area cutoff of 0.0024 m^2 ensures that the area exceeding the RST represents the deformation of at least two or three elements of a very fine finite-element mesh, rather than the result of a numerical interpolation. This cutoff is incorporated by setting the damaged area to 0 when it is less than 0.0024 m^2.

The kinematic damage abstractions are derived in three spreadsheets: *CDSP Kinematic Damage Abstraction 23-mm Intact.xls*, *CDSP Kinematic Damage Abstraction 23-mm Degraded.xls*, and *CDSP Kinematic Damage Abstraction 17-mm Degraded.xls*; electronic versions of these spreadsheets are provided in output DTN: MO0703PASDSTAT.001. These spreadsheets contain all of the input data for the kinematic damage abstractions, which are based on DTN: LL0704PA049SPC.024 [DIRS 180736]. These spreadsheets also contain Q-Q plots for several types of conditional probability distributions and plots comparing computational results at the four PGV levels to the damage abstractions. The abstractions for probability of rupture are derived in the spreadsheet *Rupture and Puncture Abstractions.xls.*

6.6.1 23-mm-Thick OCB with Intact Internals

6.6.1.1 Probability of Rupture

The probability of rupture for the codisposal waste package with a 23-mm-thick OCB and intact internals in response to a single impact is zero. The structural response calculations for kinematic response at the 0.4 m/s, 1.05 m/s, 2.44 m/s, and 4.07 m/s PGV levels demonstrate that the strain in the OCB is always below the ultimate tensile strain for Alloy 22 (SNL 2007 [DIRS 178851], Section 6.3.4). Consideration of multiple impacts to a codisposal waste package does not change the zero probability of rupture with intact internals (SNL 2007 [DIRS 178851], Sections 6.3.3 and 6.3.4).

6.6.1.2 Probability of Damage

Table 6-14 and Figure 6-26 present the probability of damage for the 23-mm-thick OCB with intact internals. The probability is zero for all PGV levels at 105% RST, and for PGV levels at or below 1.05 m/s at 100% RST. The codisposal waste package will remain undamaged for the zero probability states.

Table 6-14. Probability of Damage from the Kinematic Calculations for the Codisposal Waste Package with 23-mm-Thick OCB and Intact Internals

	Residual Stress Threshold (% of Yield Strength)		
PGV Level (m/s)	90%	100%	105%
0.40	0.176	0	0
1.05	0.559	0	0
2.44	0.941	0.147	0
4.07	1	0.412	0

Source: Output DTN: MO0703PASDSTAT.001, worksheet “Prob of Damage - Old” in the file *CDSP Kinematic Damage Abstraction 23-mm Intact.xls.*

The methodology for the kinematic calculations is expected to overestimate damaged areas. If this is true, it is likely that the kinematic methodology will overestimate the probability of damage at the 0.4 m/s PGV level. Such an overestimate is significant for the seismic scenario because the PGV threshold for nonzero damage would be at or below the 0.2 m/s PGV level, greatly expanding the hazard range for the TSPA. The approach discussed in Section 6.6.2.2 for the codisposal waste package with 17-mm-thick OCB and degraded internals has been applied to the codisposal waste package with intact internals. Table 6-23 presents the damaged areas for the single codisposal waste package calculations with 17-mm-thick OCB and degraded internals. These results are applied to the codisposal waste package with 23-mm-thick OCB and intact internals because the results for the 17-mm-thick OCB with degraded internals should overestimate the probability of damage in comparison to calculations for a 23-mm-thick OCB with intact internals.

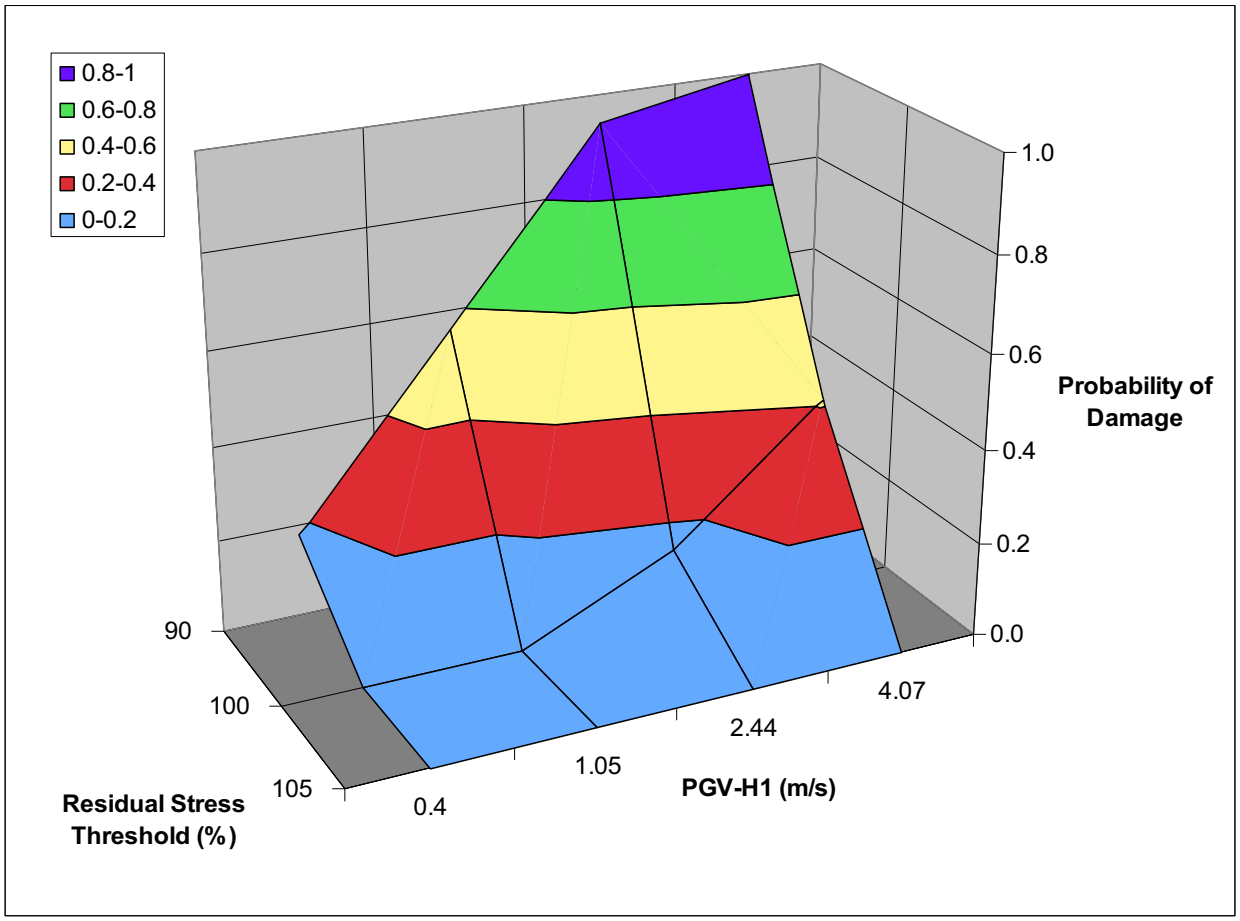

Source: Output DTN: MO0703PASDSTAT.001, worksheet "Prob of Damage - Old" in the file *CDSP Kinematic Damage Abstraction 23-mm Intact.xls.*

Figure 6-26. Probability of Damage Based on Kinematic Calculations for the Codisposal Waste Package with 23-mm-Thick OCB and Intact Internals

Table 6-15 summarizes the nonzero damaged areas from the kinematic analyses at the 0.4 m/s PGV level and the rationale for reassigning damage states based on the results in Table 6-23. Entries that are positive or ">0" in the sixth through eighth columns of Table 6-15 contribute to the revised probability of damage.

Based on the analysis in Table 6-15, the number of observations with nonzero damaged area for the 90%, 100%, and 105% RST are 1, 0, and 0, respectively. The corresponding probabilities of damage for the codisposal waste package at the 0.4 m/s PGV level with 23-mm-thick OCB and intact internals are 0.029, 0, and 0 at the 90%, 100%, and 105% RSTs, respectively. These revised probabilities are incorporated into the damage abstraction for the TSPA, as shown in Table 6-16 and Figure 6-27. The PGV intercept for 90% RST is 0.364, based on the linear extrapolation of the probabilities at the 0.40 m/s and 1.05 m/s PGV levels, as documented in output DTN: MO0703PASDSTAT.001, worksheet "Prob of Damage – New" in the file *CDSP Kinematic Damage Abstraction 23-mm Intact.xls*.

Table 6-15. Reinterpretation of Damage States for a Codisposal Waste Package with 23-mm-Thick OCB and Intact Internals at the 0.4 m/s PGV Level

Real. No.	WP ID	Kinematic Damaged Area (m^2)			Damage State Estimated from the Single WP Results (m^2)			Rationale
		90% RST	100% RST	105% RST	90% RST	100% RST	105% RST	
3	H	0.0028	0	0	0	0	0	Damaged areas < 0.057 m^2 from kinematic approach are reset to zero based on results in Table 6-23
	L	0.0053	0	0	0	0	0	
4	H	0.0223	0	0	0	0	0	Damaged areas < 0.057 m^2 from kinematic approach are reset to zero based on results in Table 6-23
	L	0.0072	0	0	0	0	0	
10	H	0.0376	0	0	0	0	0	Damaged areas < 0.057 m^2 from kinematic approach are reset to zero based on results in Table 6-23
	L	0.1088	0	0	> 0	0	0	

Source: Output DTN: MO0703PASDSTAT.001, worksheet "Prob of Damage Anal. 23-mm OCB" in the file *CDSP Kinematic Damage Abstraction 23-mm Intact.xls.*

NOTES: Positive values and values greater than 0 in the sixth through eighth columns define the revised probability of damage.

WP = waste package.

Table 6-16. Revised Probability of Damage for the Codisposal Waste Package with 23-mm-Thick OCB and Intact Internals

PGV Level (m/s)	Residual Stress Threshold (% of Yield Strength)		
	90%	100%	105%
0.364	0	0	0
0.40	0.029	0	0
1.05	0.559	0	0
2.44	0.941	0.147	0
4.07	1	0.412	0

Source: Output DTN: MO0703PASDSTAT.001, worksheet "Prob of Damage – New" in the file *CDSP Kinematic Damage Abstraction 23-mm Intact.xls.*

Figure 6-27 shows that the probability of damage is based on two independent parameters: the value of *PGV* for the *j*th seismic event and the value of *RST* for a given realization. Linear interpolation is used to define the variation of the probability of damage as a function of *PGV* and *RST*. Damaged areas are often observed to follow a power law whose slope is positive and increasing with increasing values of PGV. A typical functional dependence is illustrated by the quadratic fit for mean damaged area as a function of *PGV* in Figure 6-32. The use of linear interpolation for *PGV* and *RST* is appropriate because it provides results at intermediate values that are greater than those from a power-law fit with a positive, increasing slope.

The spatially averaged thickness of the OCB is a time-dependent parameter that is predicted by other elements of the TSPA. The probability of damage with intact internals is based on a constant OCB thickness of 23 mm, which corresponds to a thickness reduction of 2.4 mm from the initial OCB thickness of 25.4 mm. The abstraction for the 23-mm-thick OCB is anticipated to provide a reasonable approximation to the probability of damage for a few hundred thousand years after repository closure, as discussed in Section 6.5.1.2.

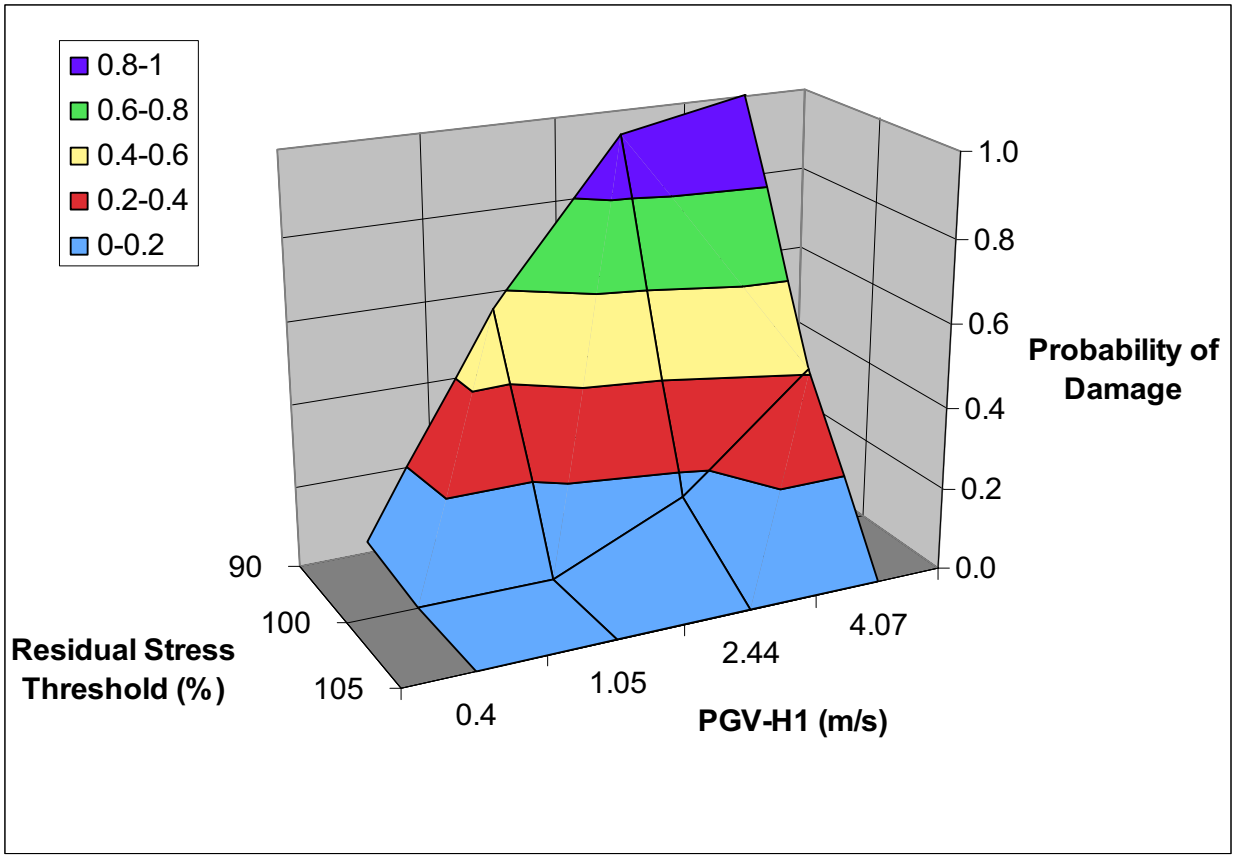

Source: Output DTN: MO0703PASDSTAT.001, worksheet "Prob of Damage – New" in *CDSP Kinematic Damage Abstraction 23-mm Intact.xls.*

Figure 6-27. Revised Probability of Damage with Reinterpreted Damage States for the Codisposal Waste Package with 23-mm-Thick OCB and Intact Internals

6.6.1.3 Conditional Probability Distribution for Nonzero Damaged Area

When damage does occur at 90% and 100% RST, a gamma distribution provides a reasonable representation of the conditional probability distribution for nonzero damaged areas. The values of the mean and standard deviation of the conditional damaged areas, which are the input to the gamma distributions, are shown in Table 6-17. These values are defined by the structural response calculations for conditional damaged area (output DTN: MO0703PASDSTAT.001, worksheets "Gamma for 90%_i23" and "Gamma for 100%_i23" in the file *CDSP Kinematic Damage Abstraction 23-mm Intact.xls*).

For 100% RST, there was zero damage to the codisposal waste package at the 0.4 m/s and 1.05 m/s PGV levels. At the 2.44 m/s PGV level and 100% RST, five instances of nonzero damage were recorded. The results from the 4.07 m/s PGV level at 100% RST provide more observations, with 14 instances of nonzero damage. Despite the larger number of observations, the number of nonzero observations at 100% RST is still relatively small when compared with the data for 90% RST.

Table 6-17. Mean and Standard Deviations of the Conditional Damaged Areas for the 23-mm-Thick OCB with Intact Internals

PGV Level (m/s)	Residual Stress Threshold (% of Yield Strength)					
	90%		100%		105%	
	Mean (m^2)	Standard Deviation (m^2)	Mean (m^2)	Standard Deviation (m^2)	Mean (m^2)	Standard Deviation (m^2)
0.4	0.031	0.040	0	0	0	0
1.05	0.120	0.144	0	0	0	0
2.44	0.338	0.314	0.005	0.004	0	0
4.07	0.792	0.533	0.006	0.004	0	0

Source: Output DTN: MO0703PASDSTAT.001, worksheets "Gamma for 90%_i23," "Gamma for 100%_i23," and "WP Total" in the file *CDSP Kinematic Damage Abstraction 23-mm Intact.xls.*

In order to ensure a reasonable value for the standard deviation at 100% RST, the coefficient of variation[6] at 90% RST is used as a check on the value of the standard deviation at the 100% RST and 4.07 m/s PGV level. The coefficient of variation at 90% RST is (0.533/0.792) = 0.673. If the coefficient of variation is constant, then the standard deviation at 100% RST is estimated as (0.006)(0.673) = 0.004, consistent with the limited data at the 100% RST. The mean and estimated standard deviation at the 4.07 m/s PGV level are then conservatively extended to all PGV levels at 100% RST. The rationale for this extension is that there are relatively few observations with nonzero damaged area at 100% RST and that this approach avoids the potential for negative values of the standard deviation with the typical quadratic fits in PGV. Table 6-18 presents the modified values of the mean and standard deviation at 100% RST.

Table 6-18. Revised Mean and Standard Deviations of the Conditional Damaged Areas for the 23-mm-Thick OCB with Intact Internals

PGV Level (m/s)	Residual Stress Threshold (% of Yield Strength)					
	90%		100%		105%	
	Mean (m^2)	Standard Deviation (m^2)	Mean (m^2)	Standard Deviation (m^2)	Mean (m^2)	Standard Deviation (m^2)
0.4	0.031	0.040	0.006	0.004	0	0
1.05	0.120	0.144	0.006	0.004	0	0
2.44	0.338	0.314	0.006	0.004	0	0
4.07	0.792	0.533	0.006	0.004	0	0

Source: Table 6-17 with modified values for the mean and standard deviation at 100% RST as explained in the text.

[6] The coefficient of variation is the ratio of the standard deviation to the mean.

Figures 6-28 to 6-31 present the Q-Q plots for gamma distributions versus the conditional damaged areas at the 0.4 m/s, 1.05 m/s, 2.44 m/s, and 4.07 m/s PGV levels for 90% RST. Gamma distributions provide a very good fit to the conditional (nonzero) damaged areas at each of the PGV levels. Based on these results, gamma distributions are selected as the probability distribution for conditional damaged areas on the codisposal waste package with intact internals.

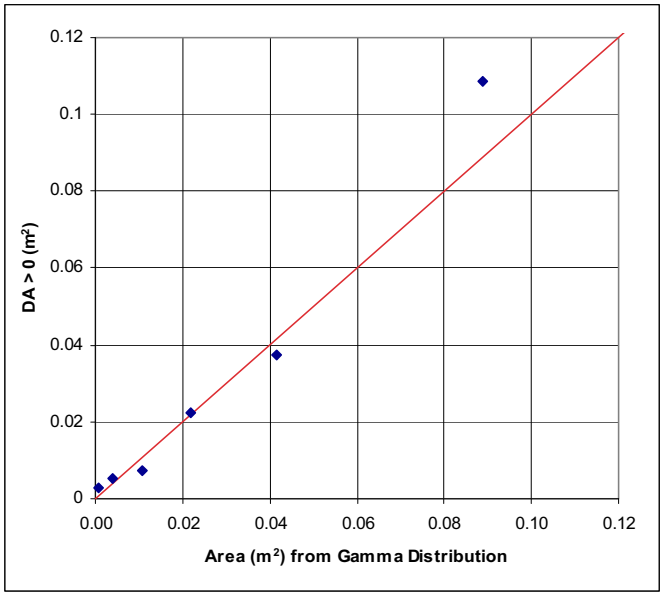

Source: Output DTN: MO0703PASDSTAT.001, worksheet "Gamma for 90%_i23" in the file *CDSP Kinematic Damage Abstraction 23-mm Intact.xls.*

NOTE: Plot shows 0.4 m/s PGV level at 90% RST. "DA > 0(m^2)" is the conditional nonzero damaged area.

Figure 6-28. Q-Q Plot for Conditional Nonzero Damaged Areas versus a Gamma Distribution for the Codisposal Waste Package with 23-mm-Thick OCB and Intact Internals

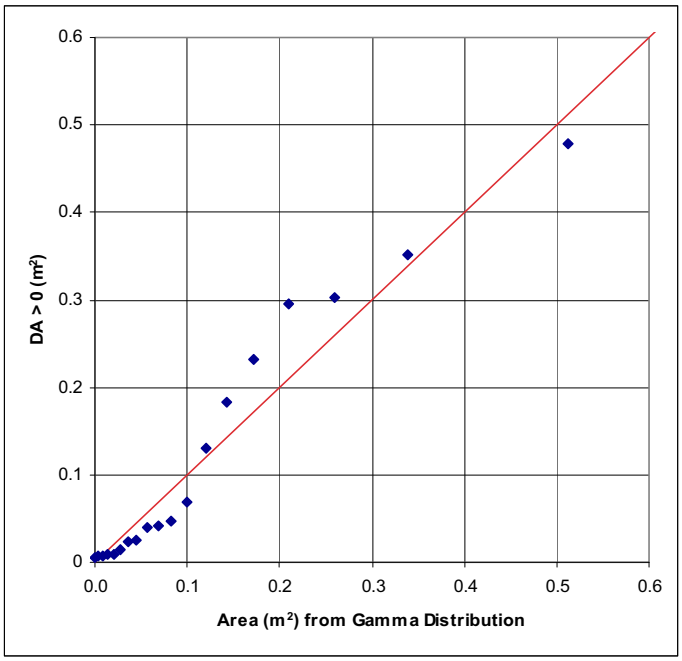

Source: Output DTN: MO0703PASDSTAT.001, worksheet "Gamma for 90%_i23" in the file *CDSP Kinematic Damage Abstraction 23-mm Intact.xls.*

NOTE: Plot shows 1.05 m/s PGV level at 90% RST. "DA > 0 (m^2)" is the conditional nonzero damaged area.

Figure 6-29. Q-Q Plot for Conditional Nonzero Damaged Areas versus a Gamma Distribution for the Codisposal Waste Package with 23-mm-Thick OCB and Intact Internals

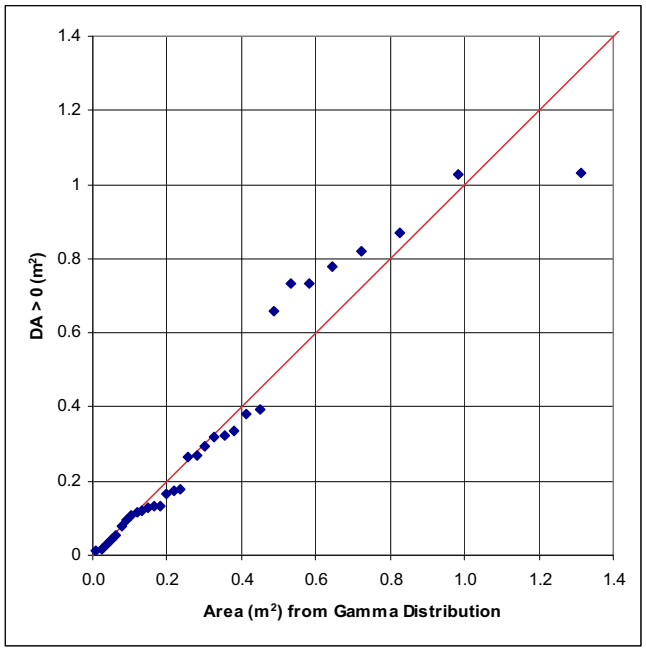

Source: Output DTN: MO0703PASDSTAT.001, worksheet "Gamma for 90%_i23" in the file *CDSP Kinematic Damage Abstraction 23-mm Intact.xls.*

NOTE: Plot shows 2.44 m/s PGV level at 90% RST. "DA > 0 (m^2)" is the conditional nonzero damaged area.

Figure 6-30. Q-Q Plot for Conditional Nonzero Damaged Areas versus a Gamma Distribution for the Codisposal Waste Package with 23-mm-Thick OCB and Intact Internals

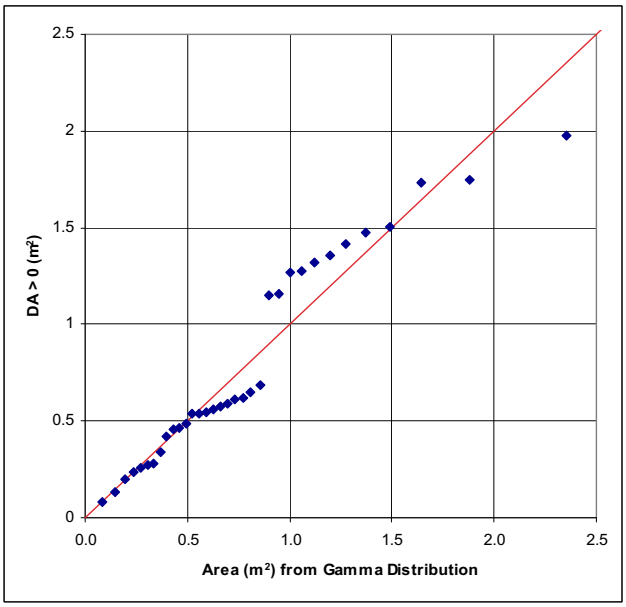

Source: Output DTN: MO0703PASDSTAT.001, worksheet "Gamma for 90%_i23" in the file *CDSP Kinematic Damage Abstraction 23-mm Intact.xls.*

NOTE: Plot shows 4.07 m/s PGV level at 90% RST. "DA > 0 (m^2)" is the conditional nonzero damaged area.

Figure 6-31. Q-Q Plot for Conditional Nonzero Damaged Areas versus a Gamma Distribution for the Codisposal Waste Package with 23-mm-Thick OCB and Intact Internals

Q-Q plots for gamma distributions versus the conditional damaged areas for the 90% RST and 100% RST show similar comparisons to Figures 6-28 to 6-31. These plots are documented in output DTN: MO0703PASDSTAT.001, worksheets "Gamma for 90%_i23" and "Gamma for 100%_i23" in file *CDSP Kinematic Damage Abstraction 23-mm Intact.xls*.

The abstraction for the TSPA must represent the response for intermediate values of PGV between the four PGV levels in Figures 6-28 to 6-31. Simple quadratic fits to the mean and standard deviation of the data at the four PGV levels provide a convenient way to represent the input parameters for the gamma distribution as a function of PGV. Figure 6-32 shows the quadratic fits for the mean and standard deviation of damaged area data at the 90% RST for the 23-mm-thick OCB with intact internals.

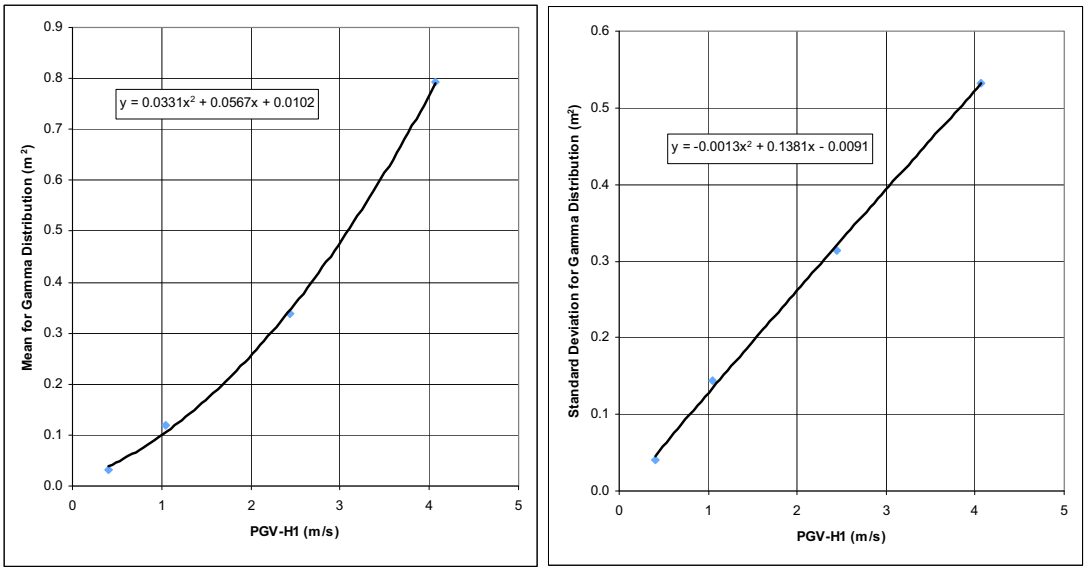

Source: Output DTN: MO0703PASDSTAT.001, worksheet "Gamma for 90%_i23" in the file *CDSP Kinematic Damage Abstraction 23-mm Intact.xls.*

NOTE: 90% RST.

Figure 6-32. Quadratic Fits to the Mean and Standard Deviation of Conditional Damaged Areas for the Codisposal Waste Package with 23-mm-Thick OCB and Intact Internals

Figure 6-33 plots the 1st, 5th, 50th, 95th, and 99th percentiles of the resulting gamma distributions against the conditional damaged areas as a function of PGV. The gamma distributions, with the quadratic fits defined in Figure 6-33, provide an excellent representation of the conditional damaged areas over the PGV range of 0.4 m/s to 4.07 m/s.

The abstraction for the TSPA must also represent the response for the full range of the RST, from 90% to 105%. Because there was close to zero damage at 100% RST and zero damage at 105% RST, a bilinear fit was used. Using a bilinear fit provides an exact representation of the data at the 90%, 100%, and 105% and a reasonable fit that slightly overestimates the mean value of the conditional damaged area at intermediate RST values. When combined with the steps taken in assigning the standard deviation at 100% RST, the bilinear fit ensures a similar result for the standard deviation of the conditional damaged area at all RST values.

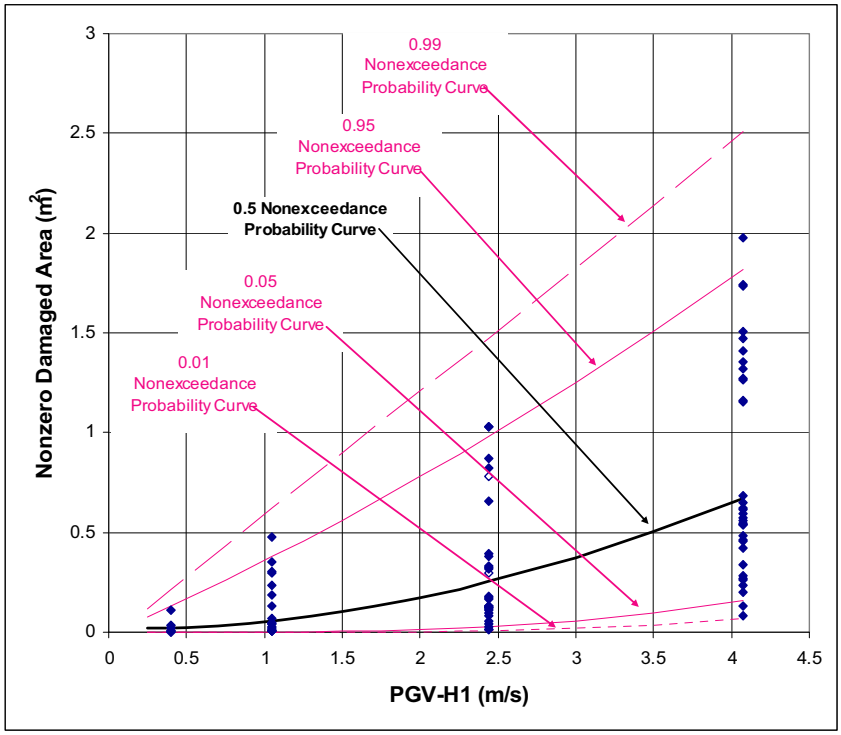

Source: Output DTN: MO0703PASDSTAT.001, worksheet "Gamma for 90%_i23" in the file *CDSP Kinematic Damage Abstraction 23-mm Intact.xls.*

Figure 6-33. Comparison of Percentiles on the Gamma Distributions to Conditional Damaged Areas for the Codisposal Waste Package with 23-mm-Thick OCB, Intact Internals and 90% RST

Table 6-19 presents the resulting equations for the mean, μ, and the standard deviation, σ, as a function of PGV and RST. RST is expressed as an integer value (i.e., 95, rather than 0.95) in these equations. Figures 6-34 and 6-35 compare the results from using these equations to the mean and standard deviation for the conditional damaged areas from Table 6-18. This comparison demonstrates that the equations in Table 6-19 provide an excellent representation of the parameters defining the gamma distribution over the PGV range of 0.4 m/s to 4.07 m/s and over the RST range of 90% to 105% are relevant for the TSPA.

Table 6-19. Gamma Distribution Parameters for the Conditional Damaged Areas on the Codisposal Waste Package with 23-mm-Thick OCB and Intact Internals

RST Range (%)	Parameter μ	Parameter σ
90-100	$(-0.0033*(RST_I - 100))PGV^2 + (-0.00567*(RST_I - 100))PGV + 0.0061 - 0.0004*(RST_I - 100)$	$(0.0001*(RST_I - 100))PGV^2 + (-0.0138*(RST_I - 100))PGV + 0.0041 + 0.0013*(RST_I - 100)$
100-105	$-0.0012*(RST_I - 105)$	$-0.0008*(RST_I - 105)$

Source: Output DTN: MO0703PASDSTAT.001, worksheet "Dependence on RST" in the file *CDSP Kinematic Damage Abstraction 23-mm Intact.xls.*

NOTE: Minor errors in the coefficients for σ were discovered after this parameter was defined in the TSPA database. This table presents the correct values, while the TSPA database has 0.0048 in place of 0.0041, 0.0014 in place of 0.0013, and −0.0010 in place of −0.0008. These minor errors produce insignificant changes in Figure 6-35 and have no impact on TSPA.

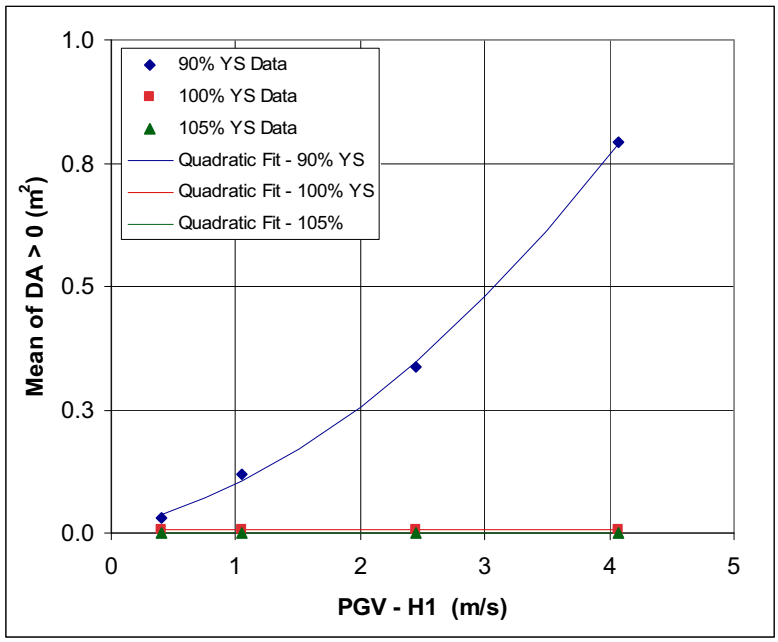

Source: Output DTN: MO0703PASDSTAT.001, worksheet "Dependence on RST" in the file *CDSP Kinematic Damage Abstraction 23-mm Intact.xls.*

Figure 6-34. Comparison of Equations in Table 6-18 to the Mean of the Conditional Damaged Areas for the Codisposal Waste Package with 23-mm-Thick OCB and Intact Internals

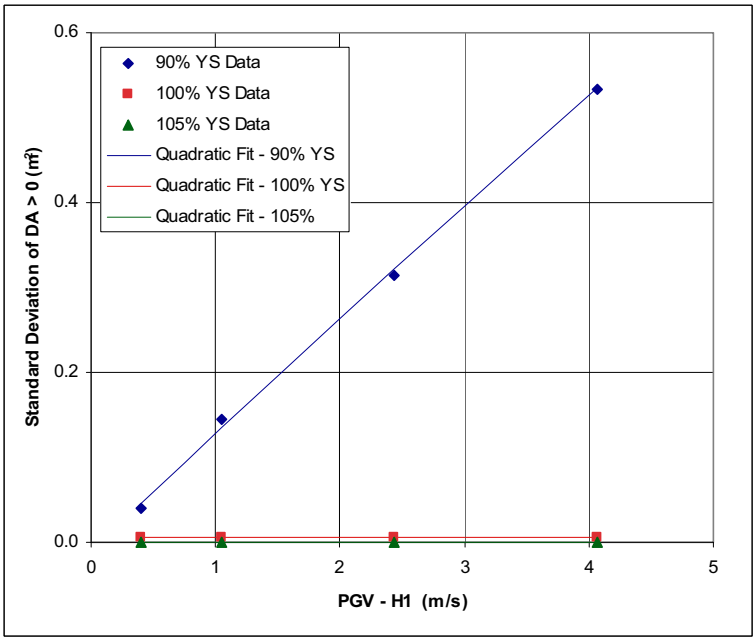

Source: Output DTN: MO0703PASDSTAT.001, worksheet "Dependence on RST" in the file *CDSP Kinematic Damage Abstraction 23-mm Intact.xls.*

Figure 6-35. Comparison of Equations in Table 6-18 to the Standard Deviation of the Conditional Damaged Areas for the Codisposal Waste Package with 23-mm-Thick OCB and Intact Internals

The conditional damage can only occur when the probability of damage is greater than zero, as shown in Figure 6-26. The probabilities in Figure 6-26 ensure that the damaged area for the TSPA remains zero for most values of PGV, in spite of the bounding approach for the magnitude of the conditional damaged area. This can be demonstrated by plotting the expected damaged area, which is defined as the product of the probability of damage and the mean conditional damaged area. The expected damaged area is the effective damaged area for the TSPA because it combines the probability of damage with the magnitude of the nonzero damaged area. Figure 6-36 demonstrates that the expected damaged area remains zero over most of the TSPA range for PGV and RST.

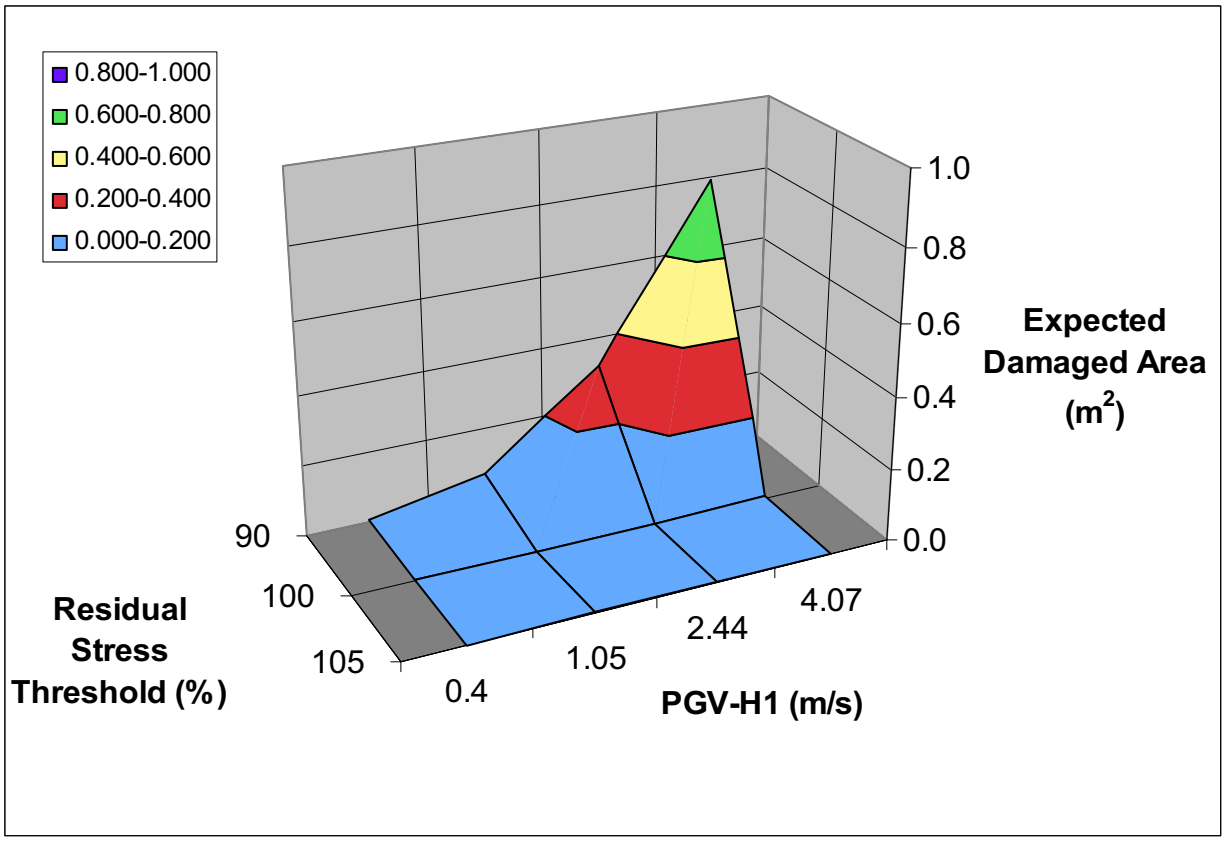

Source: Output DTN: MO0703PASDSTAT.001, worksheet "Expected Damage" in the file *CDSP Kinematic Damage Abstraction 23-mm Intact.xls.*

Figure 6-36. Expected Damaged Area for the Codisposal Waste Package with 23-mm-Thick OCB and Intact Internals

6.6.1.4 Alternate Conditional Probability Distributions

Q-Q plots were prepared for the conditional damaged area versus gamma and log-normal distributions for 90% RST at the 0.4 m/s, 1.05 m/s, 2.44 m/s, and 4.07 m/s PGV levels. The gamma distribution provides a reasonable representation of the damaged area data at all PGV levels, as shown by Figures 6-28 to 6-31. The log-normal distribution provides a poor representation of the conditional damaged areas at the 1.05 m/s, 2.44 m/s, and 4.07 m/s PGV levels, and was not considered further. Figure 6-37 presents the Q-Q plot for the log-normal

distribution versus the conditional damaged areas at the 1.05 m/s PGV level. A normal distribution was eliminated from consideration because the standard deviation of the conditional damaged area is often greater than its mean, as shown in Table 6-18. In this situation, a normal distribution will predict damaged areas that are less than zero, which is unacceptable. The Weibull distribution was not attempted for the codisposal waste package because of its rejection for the TAD-bearing waste package (see Sections 6.5.1.4 and 6.5.2.4).

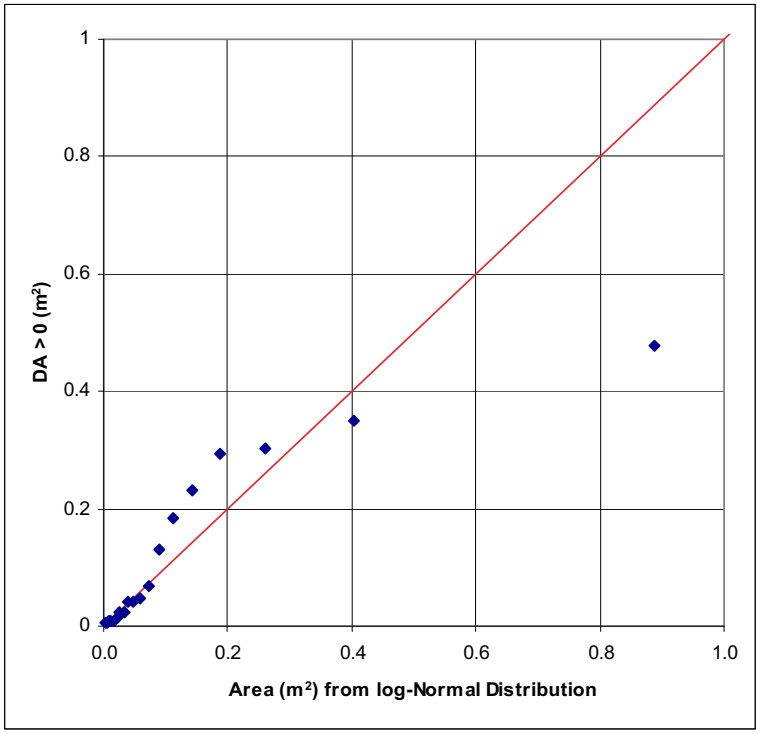

Source: Output DTN: MO0703PASDSTAT.001, worksheet "Log-Normal for 90%_i23" in the file *CDSP Kinematic Damage Abstraction 23-mm Intact.xls.*

NOTE: 1.05 m/s PGV level at 90% RST. DA > 0 is the conditional nonzero damaged area.

Figure 6-37. Q-Q Plot for Conditional Damaged Areas versus a Log-Normal Distribution for the Codisposal Waste Package with 23-mm-Thick OCB and Intact Internals

6.6.1.5 Dependence on OCB Thickness

The time-dependent thickness of the OCB is not incorporated into the damage abstraction for the codisposal waste package with intact internals. The data in Figures 6-26 to 6-36 are for a 23-mm-thick OCB, which corresponds to a thickness reduction of 2.4 mm from the initial OCB thickness of 25.4 mm. The abstraction for the 23-mm-thick OCB provides a reasonable approximation to damaged area for the first few hundred thousand years after repository closure, based on the estimated corrosion time in Section 6.5.1.2.

6.6.2 17-mm-Thick OCB with Degraded Internals

6.6.2.1 Probability of Rupture

The probability of rupture for the codisposal waste package with degraded internals is zero for a single waste package-to-pallet impact or a single waste package-to-waste package impact. The structural response calculations for kinematic response at the 0.4 m/s, 1.05 m/s, 2.44 m/s, and 4.07 m/s PGV levels and the associated damage catalogs demonstrate that strain in the OCB is always below the ultimate tensile strain for Alloy 22 from a single impact (SNL 2007 [DIRS 178851], Section 6.3.4). However, an impact with severe deformation of the OCB has the potential to weaken the OCB, potentially causing rupture if there is severe deformation from a subsequent impact. The second impact that causes severe deformation could occur during a single ground motion or during subsequent events. The accumulation of extreme deformation in the OCB is conceptualized to have the potential to weaken the OCB, leading to rupture from multiple impacts.

For the codisposal waste package with degraded internals, the effect of multiple waste package-to pallet impacts is assessed in *Mechanical Assessment of Degraded TAD Canisters and Degraded Drip Shields Subject to Vibratory Ground Motion* (SNL 2007 [DIRS 178851], Sections 6.3.3 and 6.3.4) by evaluating the severity of deformation after a single impact. If the deformation is large enough, then it is hypothesized that a second large impact can potentially cause rupture of the waste package OCB.

The degree of deformation from waste package-to-pallet impacts during a single ground motion was used to define the probabilities of no rupture, incipient rupture, and immediate rupture (DTN: LL0703PA029SPC.014 [DIRS 179775]). A minor degree of deformation indicates that no rupture occurs, consistent with the observation that the strain in the OCB is below the ultimate tensile strain for Alloy 22 for individual impacts. A significant degree of deformation is interpreted as causing a condition of incipient rupture, in the sense that a second severe impact has the potential to cause rupture. Finally, if two severe impacts occur during a given ground motion, each of which causes severe deformation to the OCB, then the accumulation of severe deformation is interpreted as causing rupture.

The 17 realizations at 0.4 m/s, 1.05 m/s, 2.44 m/s, and 4.07 m/s PGV level used in the kinematic analysis for the codisposal waste package with degraded internals have been assessed for these probabilities. The probability of incipient rupture and probability of rupture are defined by the number of waste packages in each realization that have a single severe impact or more than one severe impact, respectively. The probabilities for each realization are then averaged over all ground motions at a given PGV level to define the data in Table 6-21. Table 6-20 displays the resulting probabilities for the codisposal waste package with 23-mm-thick OCB and 17-mm-thick OCB.

The probabilities in Table 6-20 for incipient rupture or rupture are essentially identical for the 23-mm OCB and 17-mm OCB, so the TSPA abstraction is based on the mean value of the probabilities for the 23-mm-thick OCB and for the 17-mm-thick OCB, as shown in Table 6-21. The mean probability, as used here, refers to the mean probability for the two OCB thicknesses. In other words, the mean probability in Table 6-21 is the average overall ground motions at a given PGV level, given by the data in Table 6-20, and a subsequent average for the two OCB thicknesses.

Table 6-20. Probability of Rupture for the Codisposal Waste Package with Degraded Internals

PGV Level (m/s)	Probability of Incipient Rupture		Probability of Rupture	
	23-mm-thick OCB	17-mm-thick OCB	23-mm-thick OCB	17-mm-thick OCB
0.40	0	0	0	0
1.05	0	0	0	0
2.44	0.028	0.030	0	0
4.07	0.122	0.124	0.115	0.120

Source: DTN: LL0703PA029SPC.014 [DIRS 179775], worksheet "CDSP Summary" in the file *kinematic_analyses_rupture_summary.xls*.

Table 6-21. Mean Probability Data for Incipient Rupture and Rupture for the Codisposal Waste Package with Degraded Internals

PGV Range (m/s)	Average Probability of Incipient Rupture	Average Probability of Rupture
0.4	0	0
1.05	0	0
2.44	0.029	0
4.07	0.123	0.118

Source: Output DTN: MO0703PASDSTAT.001, worksheet "CDSP Kinematic Abstraction" in the file *Rupture and Puncture Abstractions.xls*.

The mean probability data for incipient rupture are represented in the TSPA as a power-law function of the form $a(\text{PGV} - 1.05)^b$. This function goes to 0 at the 1.05 m/s PGV level, consistent with the data in Table 6-21. The coefficients a and b are calculated from the two nonzero data points in Table 6-21: $b = \log(0.123/0.029)/\log((4.07 - 1.05)/(2.44 - 1.05)) = 1.8586$ and $a = (0.123)/(4.07 - 1.05)^{1.8586} = 0.0158$ (numerical values are based on the spreadsheet calculations in output DTN: MO0703PASDSTAT.001, worksheet "CDSP Kinematic Abstraction" in the file *Rupture and Puncture Abstractions.xls*).

The mean probability of rupture is represented in the TSPA as a power-law function of the form $c(\text{PGV}-2.44)^d$. This functional form goes to 0 at the 2.44 m/s PGV level, consistent with the data in Table 6-21. However, there is only one nonzero data point for the mean probability of rupture, so there is not enough data to define the coefficients c and d. A reasonable simplification is to set the value of d equal to 1.8586, the same value as b. The value of c is then calculated as $c = (0.118)/(4.07 - 2.44)^{1.8586} = 0.0474$. (Numerical values are based on the spreadsheet calculations in output DTN: MO0703PASDSTAT.001, worksheet "CDSP Kinematic Abstraction" in file *Rupture and Puncture Abstrations.xls*.)

Figure 6-38 presents comparisons of the power-law functions for incipient rupture and rupture against the data in Table 6-21. These power-law functions define the probabilities for a three-state system: p_{nr}, the probability of no rupture, p_{inc_rup}, the probability of incipient rupture, and p_{rup}, the probability of rupture. The sum of these three probabilities is always 1.

An integer counter tracks the rupture status of the system through multiple events. This counter is initialized to 0 at the start of each realization. For each seismic event, the counter is incremented by sampling a discrete distribution with (value, probability) pairs given by (0, p_{nr}), (1, p_{inc_rup}), and (2, p_{rup}). If the sampled value is zero, then the codisposal waste package does not sustain significant damage and the counter does not change. If the sampled value is 1, then 1 is added to the counter. If the value of the counter becomes 2 from this addition, then the package is considered to be ruptured. If the value of the counter is 1 after this addition, then the package does not rupture but the counter is saved for subsequent events within the realization. If the sampled value is 2, then 2 is added to the counter and the package is considered to be ruptured.

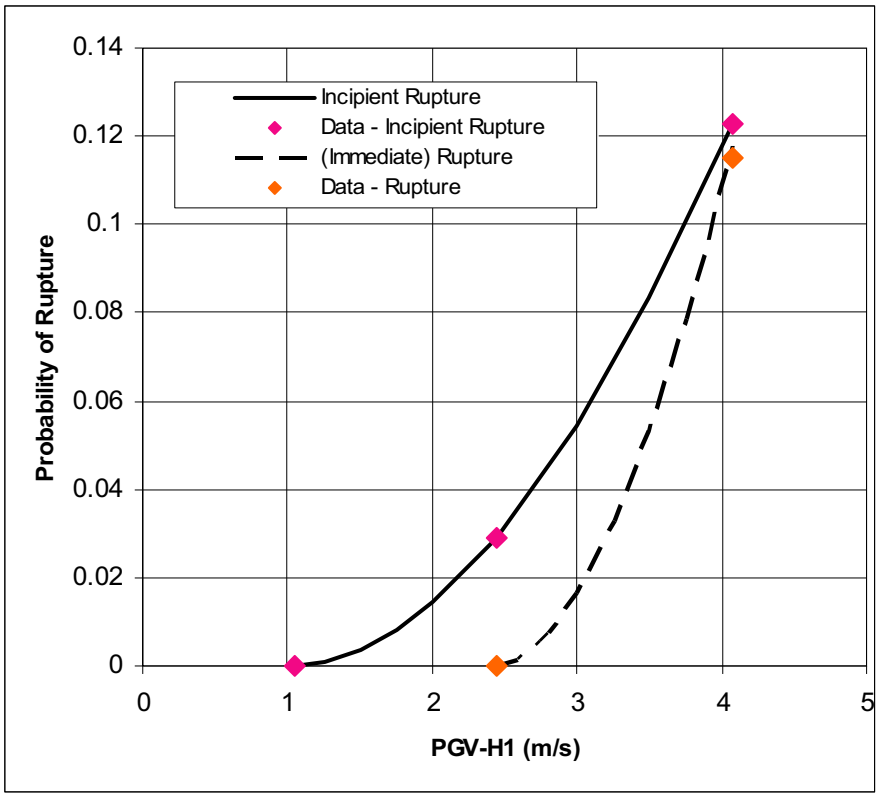

Source: Output DTN: MO0703PASDSTAT.001, worksheet "CDSP Kinematic Abstraction" in the file *Rupture and Puncture Abstractions.xls.*

NOTE: Kinematic response of codisposal waste package with degraded internals, based on the average of results for 17-mm-thick and 23-mm-thick OCBs.

Figure 6-38. Comparison of Power-Law Dependence with Probability Data for Incipient Rupture and for Rupture of the Codisposal Waste Package with Degraded Internals

When a waste package is ruptured, the failed area is determined by sampling a uniform distribution with a lower bound of 0 m^2 and an upper bound equal to the cross-sectional area of the waste package OCB. The cross-sectional area for the codisposal waste package is 3.28 m^2, based on an OCB outer diameter of 2,044.7-mm for the 5-DHLW/DOE SNF Long waste package (SNL 2007 [DIRS 179567], Table 4-9). This failed area allows advective flow through the ruptured codisposal waste packages and advective and diffusive transport out of the ruptured codisposal waste packages. This failed area is conceptualized to be a tear or rupture along a crease that lies in a plane normal to the central axis of the waste package. The failed area can be represented as a circumferential band around the waste package for transport calculations in the TSPA. Once the codisposal waste package ruptures, there is no further rupture damage on successive events, and the codisposal waste packages remain ruptured for the remainder of the realization.

6.6.2.2 Probability of Damage

Table 6-22 and Figure 6-39 present the probability of damage from the kinematic calculations for the 17-mm-thick OCB with degraded internals. Table 6-22 also includes the probability of damage for the 23-mm-thick OCB with degraded internals because these numerical values are used later in this section.

Table 6-22. Probability of Damage from the Kinematic Calculations for the Codisposal Waste Package with Degraded Internals

PGV Level (m/s)	Residual Stress Threshold (% of Yield Strength)		
	90%	100%	105%
17-mm-thick OCB:			
0.40	0.235	0.235	0.088
1.05	0.676	0.676	0.382
2.44	0.941	0.941	0.882
4.07	1	1	1
23-mm-thick OCB:			
0.40	0.206	0.206	0.147
1.05	0.588	0.588	0.559
2.44	0.941	0.941	0.941
4.07	1	1	1

Sources: Output DTN: MO0703PASDSTAT.001, worksheet "Prob of Damage – Old" in the file *CDSP Kinematic Damage Abstraction 17-mm Degraded.xls* and worksheet "Prob of Damage – Old" in the file *CDSP Kinematic Damage Abstraction 23-mm Degraded.xls*.

The methodology for the kinematic calculations is expected to overestimate damaged areas. If this is true, it is likely that the kinematic methodology will overestimate the probability of damage at the 0.4 m/s PGV level. Such an overestimate is significant for the seismic scenario because the PGV threshold for nonzero damage would be at or below the 0.2 m/s PGV level, greatly expanding the hazard range for the TSPA. A sensitivity study was therefore performed to quantify the overestimate in the probability of damage from the kinematic approach at the 0.4 m/s PGV level.

The results from the kinematic calculations at the 0.4 m/s PGV level demonstrate that end-to-end impacts of adjacent waste packages do not occur for 16 of the 17 ground motions (worksheet "WP-WP Data" in *CDSP Kinematic Damage Abstraction 17-mm Degraded.xls*, in output DTN: MO0703PASDSTAT.001). The response of an individual waste package is independent of the adjacent packages for 16 of the 17 ground motions. It is possible to perform structural response calculations for a single waste package with a fine finite-element mesh for these ground motions, and the damaged area is determined directly from the finite-element mesh.

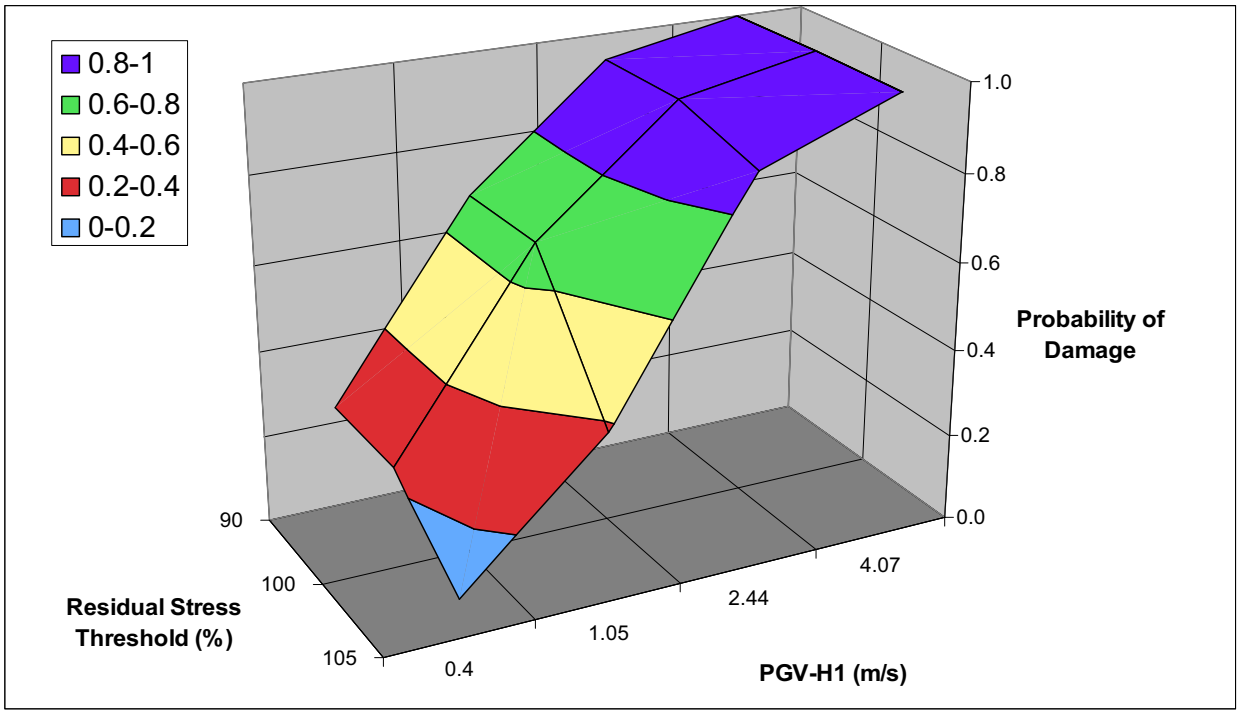

Source: Output DTN: MO0703PASDSTAT.001, worksheet "Prob of Damage – Old" in *CDSP Kinematic Damage Abstraction 17-mm Degraded.xls.*

Figure 6-39. Probability of Damage Based on Kinematic Calculations for the Codisposal Waste Package with 17-mm-Thick OCB and Degraded Internals

Four single package calculations were performed for the codisposal waste package with 17-mm-thick OCB and degraded internals. The four calculations represent two packages independent of boundary effects in the repository (denoted as H and L) in the kinematic model for Realizations 3 and 4 (worksheet "Prob of Damage Anal. 17-mm OCB" in *CDSP Kinematic Damage Abstraction 17-mm Degraded.xls* in output DTN: MO0703PASDSTAT.001). The calculations for the two packages in each realization are identical, except for the values of the metal-to-metal and metal-to-rock friction coefficients for each package and pallet, respectively. Realizations 3 and 4 were selected because they have the greatest damaged areas without any waste package-to-drip shield impacts or waste package-to-waste package impacts.

Table 6-23 compares the damaged areas for the kinematic analysis and for the four single waste package calculations. A comparison of these results clearly indicates that the kinematic approach for the waste packages overestimates the damaged areas relative to the single waste package model.

The calculations with a single waste package are a more accurate approach for calculating damaged area than the kinematic approach because the finite-element model provides a more realistic representation of the structural stiffness of the waste package in comparison to the coarser kinematic representation and because the finite-element model integrates the effects of multiple impacts through the stress and strain in individual elements, rather than by linear addition of damage from separate impacts in the kinematic approach. Since the single waste package calculations are more accurate, the probability of damage from the kinematic calculations at the 0.4 m/s PGV level has been reinterpreted, based on the results in Table 6-23.

Table 6-23. Comparison of Damaged Area for the Codisposal Waste Package with 17-mm-Thick OCB and Degraded Internals Using Different Analytic Methods at the 0.4 m/s PGV level

	Damaged Area (m^2)					
	90% RST		100% RST		105% RST	
WP ID / Rlz	Kinematic	Single Package	Kinematic	Single Package	Kinematic	Single Package
H / 3	0.059	0.0222	0.030	0	0	0
L / 3	0.061	0.0154	0.018	0	0	0
H / 4	0.192	0	0.057	0	0.003	0
L / 4	0.099	0.0026	0.038	0	0	0

Sources: DTN: LL0703PA007SPC.005 [DIRS 179644], File *CDSP_1WP_analyses_DA_summary.xls* and output DTN: MO0703PASDSTAT.001, worksheet "Prob of Damage Anal. 17-mm OCB" in the file *CDSP Kinematic Damage Abstraction 17-mm Degraded.xls*.

NOTES: WP = waste package; H and L identify specific waste packages; Rlz = realization.

As shown in Table 6-23, the single waste package model has zero damage for all kinematic damaged areas less than 0.057 m^2 at the 100% RST level. This statement is also true for the data at the 90% RST level, although the kinematic damaged areas of 0.059 m^2 and 0.061 m^2 are reduced significantly but remain greater than zero. On the other hand, the largest kinematic damaged area in Table 6-23, 0.192 m^2, has zero damage for the single package calculation. These results probably reflect the statistical variability introduced by the ground motions and possibly a numerical sensitivity in calculating relatively small damaged areas on the codisposal waste package. In either case, there is uncertainty in using 0.057 m^2 as a cutoff for zero damage, and some kinematic damaged areas less than 0.057 m^2 may remain nonzero at the 0.4 m/s PGV level. This potential nonconservatism in using 0.057 m^2 as a cutoff for determining the probability of damage appears minor compared to the demonstrated conservatism in the kinematic model, which overestimates damaged area by a factor of between 2.7 (case H/3) to 38 (case L/4) at 90% RST for the 0.4 m/s PGV level, as shown in Table 6-23. Since the abstraction for conditional damaged area is based exclusively on the damaged areas from the kinematic calculations (see the next section), TSPA retains the overestimated damaged areas from the kinematic approach at the 0.4 m/s PGV level. Given these considerations, the use of 0.057 m^2 as a cutoff for determining the probability of damage of a codisposal waste package is a reasonable approximation for the seismic damage abstractions.

The results in Table 6-23 are for the two ground motions at the 0.4 m/s PGV level that cause the greatest damaged areas without impacts between the waste package and the drip shield or adjacent waste packages. A single waste package calculation was also performed for codisposal waste package H based on realization 6 at the 1.05 m/s PGV level, predicting damaged areas of

0.034 m^2 for 90% RST, 0.004 m^2 for 100% RST, and 0.0 m^2 for 105% RST. The corresponding values from the kinematic analyses are 0.096 m^2, 0.046 m^2, and 0.0 m^2, respectively (SNL 2007 [DIRS 178851], Section 7.3.1.1.2 and Table 7-4). The results from this calculation are not included in Table 6-23 because the focus here is to provide better estimates of the PGV intercepts for zero probability by reinterpreting the cases with zero damaged area at the 0.4 m/s PGV level. Even though the kinematic analysis damaged area for 100% RST of 0.046 m^2 was not reduced to zero in the single waste package analysis at the 1.05 m/s PGV level, the 0.057 m^2 cutoff remains a reasonable approximation for the seismic damage abstractions because of the conservatism described above.

Table 6-24 summarizes the nonzero damaged areas from the kinematic analyses at the 0.4 m/s PGV level and the rationale for reassigning damage states based on the results in Table 3-18. Based on the analysis in Table 6-24, the number of observations with nonzero damaged area for the 90%, 100%, and 105% RST are 5, 2, and 0, respectively. The corresponding probabilities of damage for the codisposal waste package at the 0.4 m/s PGV level with 17-mm-thick OCB and degraded internals are 0.147, 0.059, and 0 at the 90%, 100%, and 105% RSTs, respectively. These revised probabilities are incorporated into the damage abstraction for the TSPA, as shown in Figure 6-40.

A similar analysis has been performed for the damage states with a 23-mm-thick OCB at the 0.4 m/s PGV level, based on the results in Table 6-23. The results in Table 6-23 are for the 17-mm-thick OCB, which should be an upper bound for the 23-mm-thick OCB with degraded internals. The revised damage states, which are derived in worksheet "Prob of Damage Anal. 23-mm OCB" in the file *CDSP Kinematic Damage Abstraction 23-mm Degraded.xls* (from output DTN: MO0703PASDSTAT.001), are the same as those shown in Table 6-25. It follows that the revised probabilities are identical to those for the 17-mm-thick OCB: 0.147, 0.059, and 0.059 at the 90%, 100%, and 105% RSTs, respectively.

Table 6-24. Reinterpretation of Nonzero Damage for a Codisposal Waste Package with 17-mm-Thick OCB and Degraded Internals at the 0.4 m/s PGV Level

Real. No.	WP ID	Kinematic Damaged Area (m^2)			Damage State Based on Single WP Results			Rationale
		90% RST	100% RST	105% RST	90% RST	100% RST	105% RST	
3	H	0.059	0.030	0	0.0222	0	0	Calculated results from single package model (see Table 6-23)
	L	0.061	0.018	0	0.0154	0	0	
4	H	0.192	0.057	0.003	0	0	0	Calculated results from single package model (see Table 6-23)
	L	0.099	0.038	0	0.0026	0	0	
8	H	0.022	0.007	0	0	0	0	Damaged areas < 0.057 m^2 from kinematic approach are reset to zero based on results in Table 6-23
	L	0.013	0.006	0	0	0	0	
10	H	0.251	0.064	0.007	> 0	> 0	0	Damaged areas < 0.057 m^2 from kinematic approach are reset to zero based on results in Table 6-23
	L	0.7	0.251	0.0589	> 0	> 0	0	

Source: Output DTN: MO0703PASDSTAT.001, worksheet "Prob of Damage Anal. 17-mm OCB" in the file *CDSP Kinematic Damage Abstraction 17-mm Degraded.xls.* Kinematic data have been rounded to three decimal places.

NOTE: WP = waste package; H and L identify specific waste packages.

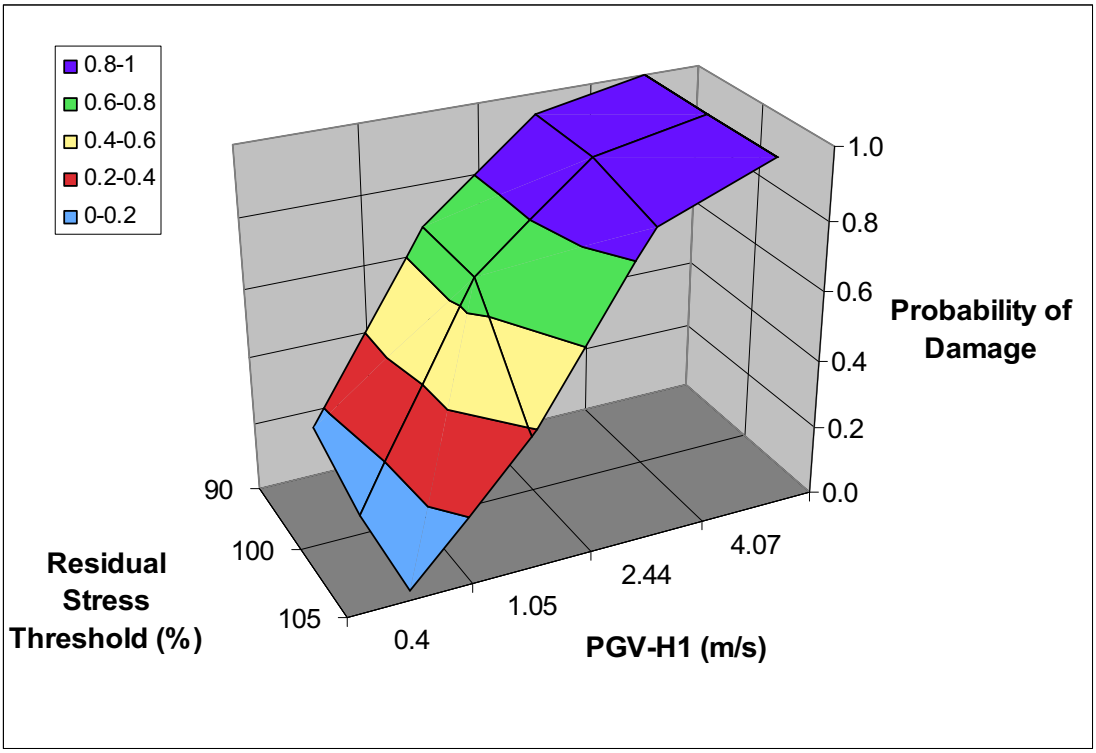

Source: Output DTN: MO0703PASDSTAT.001, worksheet "Prob of Damage – New" in *CDSP Kinematic Damage Abstraction 17-mm Degraded.xls.*

Figure 6-40. Revised Probability of Damage with Reinterpreted Damage States for the Codisposal Waste Package with 17-mm-Thick OCB and Degraded Internals

Table 6-25. PGV-Intercepts for the Codisposal Waste Package with Degraded Internals

PGV Level or Parameter	Residual Stress Threshold (% of Yield Strength)		
	90%	100%	105%
17-mm-thick OCB:			
0.40 m/s	0.147	0.059	0.029
1.05 m/s	0.676	0.676	0.382
Slope (s/m)	0.814	0.950	0.543
PGV-Intercept (m/s)	0.219	0.338	0.346
23-mm-thick OCB:			
0.40 m/s	0.088	0.088	0.029
1.05 m/s	0.588	0.588	0.559
Slope (s/m)	0.769	0.769	0.814
PGV-Intercept (m/s)	0.285	0.285	0.364

Sources: Output DTN: MO0703PASDSTAT.001, worksheet "Prob of Damage - New" in the file *CDSP Kinematic Damage Abstraction 17-mm Degraded.xls*, worksheet "Prob of Damage - New" in the file *CDSP Kinematic Damage Abstraction 23-mm Degraded.xls* for data at the 1.05 m/s PGV level, and the results from Table 6-24 for probabilities at the 0.4 m/s PGV level.

Table 6-26. Revised Probability of Damage for the Codisposal Waste Package with Degraded Internals

PGV Level (m/s)	Residual Stress Threshold (% of Yield Strength)		
	90%	100%	105%
17-mm-thick OCB:			
0.219	0	0	0
0.338	0.097	0	0
0.346	0.103	0.007	0
0.40	0.147	0.059	0.029
1.05	0.676	0.676	0.382
2.44	0.941	0.941	0.882
4.07	1	1	1
23-mm-thick OCB:			
0.285	0	0	0
0.364	0.060	0.060	0
0.40	0.088	0.088	0.029
1.05	0.588	0.588	0.559
2.44	0.941	0.941	0.941
4.07	1	1	1

Sources: Output DTN: MO0703PASDSTAT.001, worksheet "Prob of Damage – New" in the file *CDSP Kinematic Damage Abstraction 17-mm Degraded.xls* and worksheet "Prob of Damage – New" in the file *CDSP Kinematic Damage Abstraction 23-mm Degraded.xls.*

NOTE: The probability of damage at the 0.4 m/s PGV level and 105% RST level for the 17-mm-thick OCB with degraded internals was revised after these data were defined in the TSPA database. This table presents the corrected values. The probability at 0.4 m/s PGV level and 105% RST for the 17-mm-thick OCB with degraded internals changed from 0 in the TSPA database to 0.029. This value moves the PGV-intercept for zero probability at 105% RST from 0.40 m/s to 0.346 m/s, adding an additional row that is very similar to the existing row at 0.338 m/s in the TSPA database. This minor change to the probability of damage will not produce significant changes in the expected damaged areas (i.e., the product of the probability of damage and the mean conditional damaged area) on codisposal waste packages for TSPA.

Finally, the probability of damage is extrapolated to define the PGV threshold for zero damage, as discussed in Section 6.4.3. Table 6-25 presents the calculations, which are based on the modified probabilities for nonzero damage at the 0.4 m/s PGV level and the original probabilities for nonzero damage from the kinematic analyses at the 1.05 m/s PGV level. To illustrate the calculations, consider the 17-mm-thick OCB at 90% RST. The PGV/probability data for the extrapolation are (0.4 m/s, 0.147) and (1.05 m/s, 0.676). The resulting slope, m_1, is given by (0.676 − 0.147)/(1.05 m/s – 0.4 m/s) = 0.814 s/m and the PGV intercept is calculated as (0.4 m/s) – (0.147)/m_1) = 0.219 m/s. The minimum PGV-intercept in Table 6-25 is 0.219 m/s, which defines the PGV threshold for nonzero damage in Section 6.4.3. Table 6-26 summarizes the final probabilities for nonzero damage for the codisposal waste package with degraded internals. Table 6-26 includes the appropriate PGV intercepts from Table 6-25. Table 6-26 also includes the calculated probabilities for PGV values less than 0.40 m/s, based on the linear extrapolation that defines the intercepts in Table 6-25.

The probability of damage is based on three independent parameters: the value of *PGV* for the *j*th seismic event, the value of *RST* for a given realization, and the time-dependent thickness of the OCB. Linear interpolation is used to define the variation of the probability of damage as a function of *PGV* and *RST*. Damaged areas are often observed to follow a power law whose slope is positive and increasing with increasing values of PGV. A typical functional dependence is illustrated by the quadratic fit for mean damaged area as a function of *PGV* in Figure 6-45. The use of linear interpolation for *PGV* and *RST* is appropriate because it provides results at intermediate values that are greater than those from a power-law fit with a positive and increasing slope.

The spatially averaged thickness of the OCB is a time-dependent parameter that is predicted by other elements of the TSPA. The probability of damage corresponding to the average OCB thickness at the time of the *j*th seismic event is calculated by linear interpolation if the OCB thickness is between 17 mm and 23 mm. The probability of damage is set to the value at 23 mm if the average OCB thickness is greater than 23 mm. The probability is set to the value at 17 mm if the average OCB thickness is less than 17 mm. The abstraction for the 17-mm-thick OCB is anticipated to provide a reasonable lower bound to damaged area until the drip shield fails, after which the kinematic response is not applicable. The logic for the dependence of damaged area on OCB thickness is illustrated in Equation 6.6-1:

$$PD_{CDSP,j} = \text{If } t \geq 23 \text{ mm}, PD_{CDSP,j,23\text{-}mm} \quad \text{(Eq. 6.6-1)}$$

$$\text{Or if } t \leq 17 \text{ mm}, PD_{CDSP,j,17\text{-}mm}$$

$$\text{else}, PD_{CDSP,j,17\text{-}mm} + (PD_{CDSP,j,23\text{-}mm} - PD_{CDSP,j,17\text{-}mm})*(\text{t} - 17 \text{ mm})/(6 \text{ mm})$$

where t is the spatially averaged thickness (in mm) of the OCB at the time of the *j*th event, and $PD_{CDSP,j,17\text{-}mm}$ and $PD_{CDSP,j,23\text{-}mm}$ are the probabilities of damage for the 17-mm-thick and 23-mm-thick OCBs, respectively, at the value of *PGV* for the *j*th seismic event and of RST. Based on Equation 6.6-1, the probability is set to the value at 23 mm if the average OCB thickness is greater than 23 mm. This is reasonable because the probability for the 23-mm-thick OCB bounds the waste package response for several hundred thousand years after repository closure, based on the estimated corrosion time in Section 6.5.1.2. The probability is set to the value for the 17 mm thickness if the average OCB thickness is less than 17 mm. This is a reasonable approach because the probability for the 17-mm-thick OCB provides a reasonable representation at the end of the peak dose period (approximately 1,000,000 years), based on the estimated corrosion time in Section 6.5.2.2. In addition, the drip shield is expected to fail from general corrosion before the OCB thickness is reduced to 17 mm because the general corrosion rate for titanium is greater than for Alloy 22 (SNL 2007 [DIRS 178851], Section 1.2). This abstraction is not applicable after the drip shield fails, which should occur before the thickness of the OCB is reduced to 17 mm.

6.6.2.3 Conditional Probability Distributions for Nonzero Damaged Area

Figures 6-41 to 6-44 present the Q-Q plots for gamma distributions versus the conditional damaged areas at the 0.4 m/s, 1.05 m/s, 2.44 m/s, and 4.07 m/s PGV levels for 90% RST. The values of the mean and standard deviation of the conditional damaged areas, which are the input to the gamma distributions, are shown in Table 6-27 for all RST levels. Gamma distributions provide a very good fit to the conditional (nonzero) damaged areas. Q-Q plots for gamma distributions versus the conditional damaged areas for the 17-mm-thick and 23-mm-thick OCBs at all RST levels show similar comparisons as Figures 6-41 to 6-44. These plots are documented in output DTN: MO0703PASDSTAT.001, worksheets "Gamma for 100%_d17" and "Gamma for 105%_d17" in file *CDSP Kinematic Damage Abstraction 17-mm Degraded.xls*. Q-Q plots for 23-mm-thick OCB with degraded internals are documented in the file *CDSP Kinematic Damage Abstraction 23-mm Degraded.xls* in output DTN: MO0703PASDSTAT.001. Based on these results, gamma distributions are selected as the probability distribution for conditional damaged areas on the codisposal waste package with degraded internals.

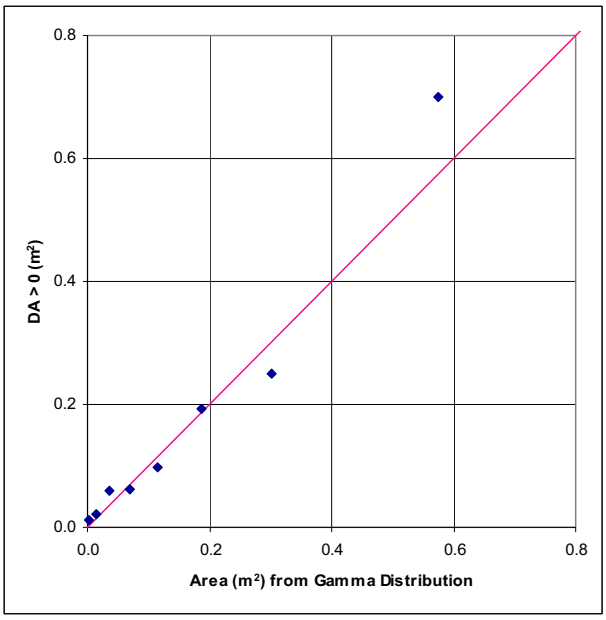

Source: Output DTN: MO0703PASDSTAT.001, worksheet "Gamma for 90%_d17" in the file *CDSP Kinematic Damage Abstraction 17-mm Degraded.xls.*

NOTE: 0.4 m/s PGV level at 90% RST. DA > 0 is the conditional nonzero damaged area.

Figure 6-41. Q-Q Plot for Conditional Damaged Areas versus a Gamma Distribution for the Codisposal Waste Package with 17-mm-Thick OCB and Degraded Internals

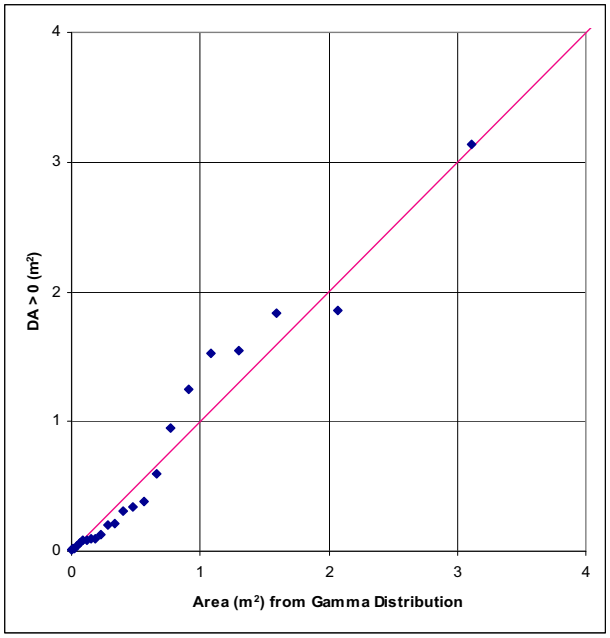

Source: Output DTN: MO0703PASDSTAT.001, worksheet "Gamma for 90%_d17" in the file *CDSP Kinematic Damage Abstraction 17-mm Degraded.xls.*

NOTE: 1.05 m/s PGV level at 90% RST. DA > 0 is the conditional nonzero damaged area.

Figure 6-42. Q-Q Plot for Conditional Damaged Areas versus a Gamma Distribution for the Codisposal Waste Package with 17-mm-Thick OCB and Degraded Internals

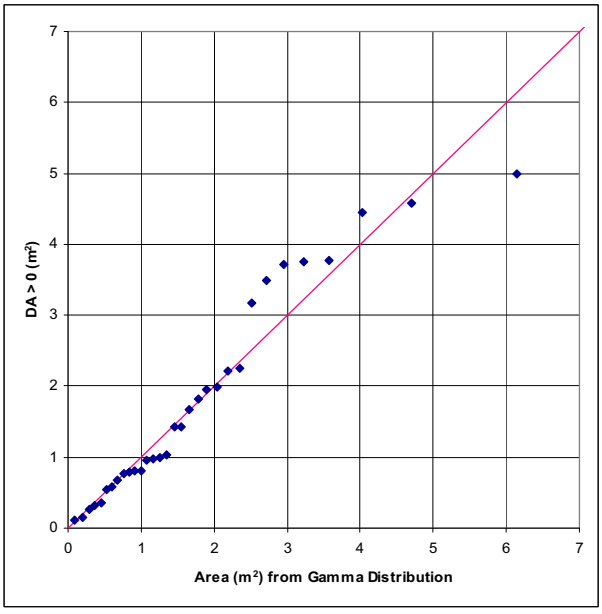

Source: Output DTN: MO0703PASDSTAT.001, worksheet "Gamma for 90%_d17" in the file *CDSP Kinematic Damage Abstraction 17-mm Degraded.xls.*

NOTE: 2.44 m/s PGV level at 90% RST. DA > 0 is the conditional nonzero damaged area.

Figure 6-43. Q-Q Plot for Conditional Damaged Areas versus a Gamma Distribution for the Codisposal Waste Package with 17-mm-Thick OCB and Degraded Internals

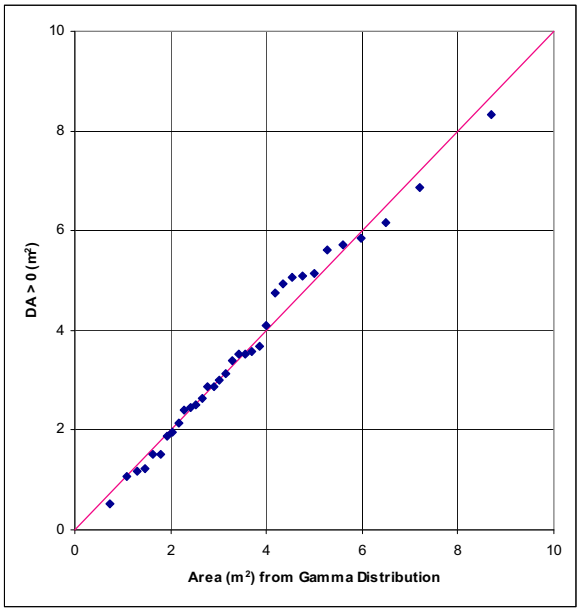

Source: Output DTN: MO0703PASDSTAT.001, worksheet "Gamma for 90%_d17" in the file *CDSP Kinematic Damage Abstraction 17-mm Degraded.xls.*

NOTE: 4.07 m/s PGV level at 90% RST. DA > 0 is the conditional nonzero damaged area.

Figure 6-44. Q-Q Plot for Conditional Damaged Areas versus a Gamma Distribution for the Codisposal Waste Package with 17-mm-Thick OCB and Degraded Internals

Table 6-27. Mean and Standard Deviations of the Conditional Damaged Areas for the 17-mm-Thick OCB with Degraded Internals

PGV Level (m/s)	Residual Stress Threshold (% of Yield Strength)					
	90%		100%		105%	
	Mean (m^2)	Standard Deviation (m^2)	Mean (m^2)	Standard Deviation (m^2)	Mean (m^2)	Standard Deviation (m^2)
0.4	0.174	0.228	0.059	0.080	0.023	0.031
1.05	0.643	0.830	0.268	0.369	0.196	0.197
2.44	1.775	1.449	0.830	0.755	0.407	0.403
4.07	3.535	1.858	1.858	1.159	0.973	0.717

Sources: Output DTN: MO0703PASDSTAT.001, worksheets "Gamma for 90%_d17," "Gamma for 100%_d17," and "Gamma for 105%_d17" in the file *CDSP Kinematic Damage Abstraction 17-mm Degraded.xls.*

The abstraction for the TSPA must represent the response for intermediate values of PGV between the four PGV levels in Figures 6-41 to 6-44. Simple quadratic fits to the mean and standard deviation of the data at the four PGV levels provide a convenient way to represent the input parameters for the gamma distribution as a function of PGV. Figure 6-45 shows the quadratic fits for the mean and standard deviation of conditional damaged area data at the 90% RST for the 17-mm-thick OCB with degraded internals.

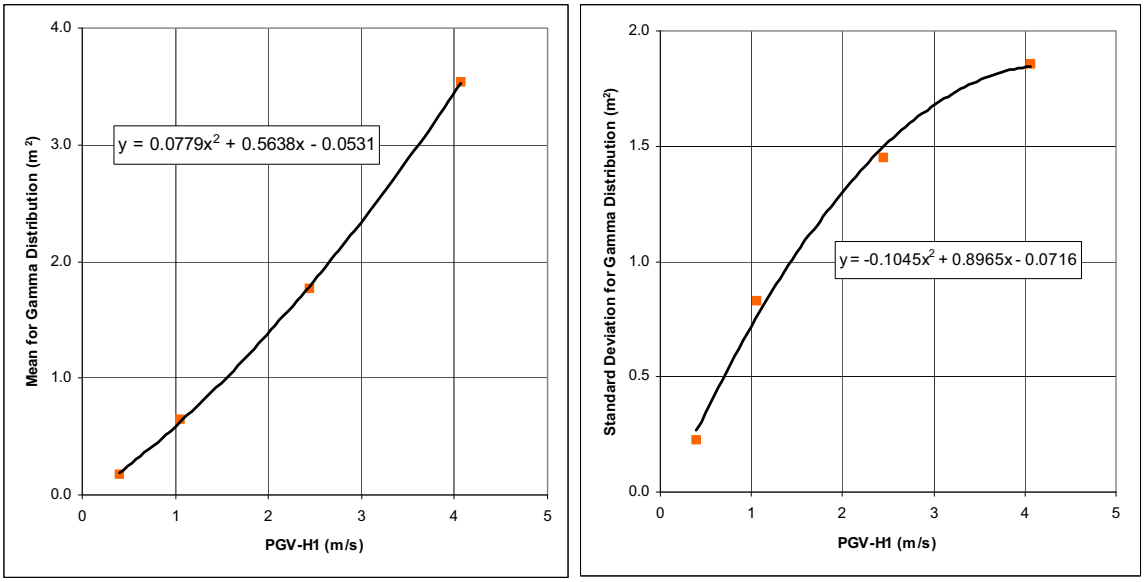

Source: Output DTN: MO0703PASDSTAT.001, worksheet "Gamma for 90%_d17" in the file *CDSP Kinematic Damage Abstraction 17-mm Degraded.xls.*

NOTE: 90% RST.

Figure 6-45. Quadratic Fits to the Mean and Standard Deviation of Conditional Damaged Areas for the Codisposal Waste Package with 17-mm-Thick OCB and Degraded Internals

Figure 6-46 plots the 1st, 5th, 50th, 95th, and 99th percentiles of the resulting gamma distributions against the conditional damaged areas as a function of PGV. The gamma distributions, with the quadratic fits defined in Figure 6-45, provide an excellent representation of the conditional damaged areas over the PGV range of 0.4 m/s to 4.07 m/s.

The abstraction for the TSPA must also represent the response for the full range of the RST, from 90% to 105%. Figure 6-47 and Figure 6-48 demonstrate that the mean value of the conditional damaged area and the standard deviation of the conditional damaged area vary approximately linearly over this RST range. This is, a linear fit to the data at 90% and 100% provides a reasonable fit to the conditional damaged area at the 105% RST over the full range of PGV.

Given the results in Figure 6-47 and Figure 6-48, it is reasonable to extend the quadratic equations in Figure 6-45 by defining coefficients that are linear in RST, based on the values at 90% RST and 100% RST in Table 6-27. The resulting equations for the mean, μ, and standard deviation, σ, are:

$$\mu = (-0.0011*(\mathrm{RST} - 100) + 0.0670)*\mathrm{PGV}^2 + (-0.0376*(\mathrm{RST} - 100) + 0.1879)*\mathrm{PGV} + (0.0034*(\mathrm{RST} - 100) - 0.0187) \quad \text{(Eq. 6.6-2)}$$

$$\sigma = (0.0078*(\mathrm{RST} - 100) - 0.0266)*\mathrm{PGV}^2 + (-0.0490*(\mathrm{RST} - 100) + 0.4066)*\mathrm{PGV} + (0.0011*(\mathrm{RST} - 100) - 0.0605) \quad \text{(Eq. 6.6-3)}$$

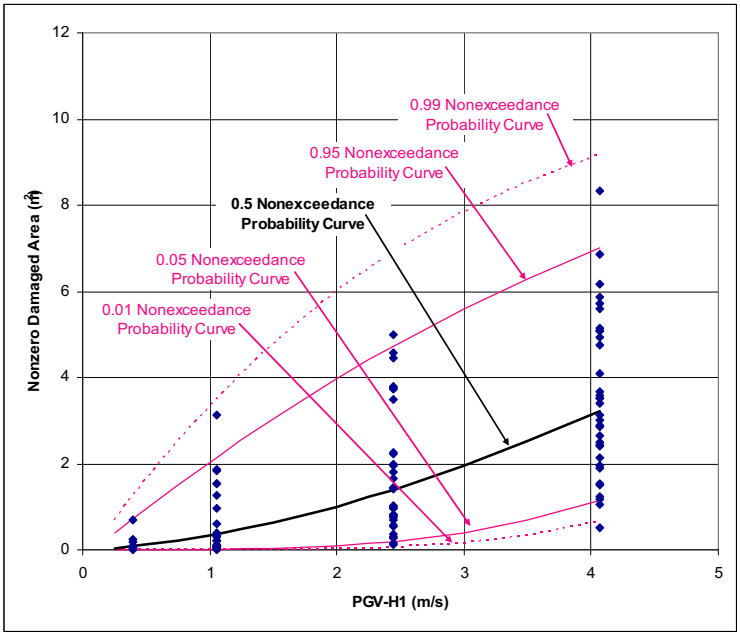

Source: Output DTN: MO0703PASDSTAT.001, worksheet "Gamma for 90%_d17" in the file *CDSP Kinematic Damage Abstraction 17-mm Degraded.xls.*

NOTE: 90% RST.

Figure 6-46. Comparison of Percentiles on the Gamma Distributions to Conditional Damaged Areas for the Codisposal Waste Package with 17-mm-Thick OCB and Degraded Internals

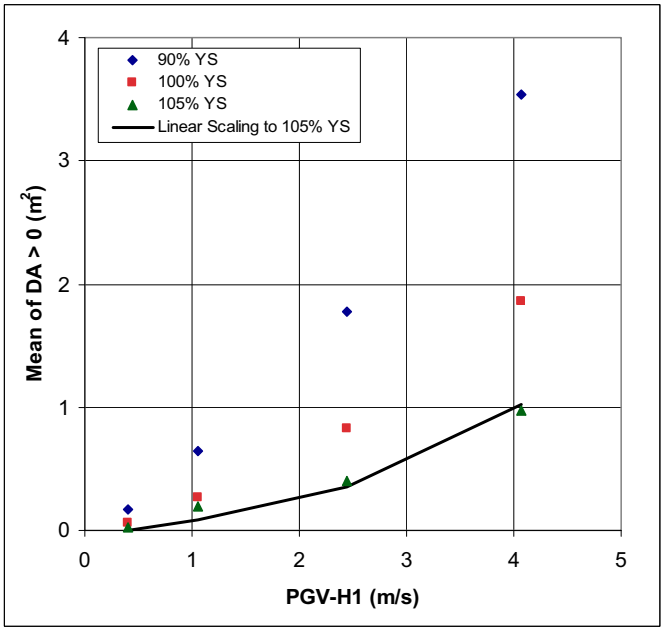

Source: Output DTN: MO0703PASDSTAT.001, worksheet "Dependence on RST" in the file *CDSP Kinematic Damage Abstraction 17-mm Degraded.xls.*

Figure 6-47. Linear Estimate of the Mean Conditional Damaged Area at 105% RST for the Codisposal Waste Package with 17-mm-Thick OCB and Degraded Internals

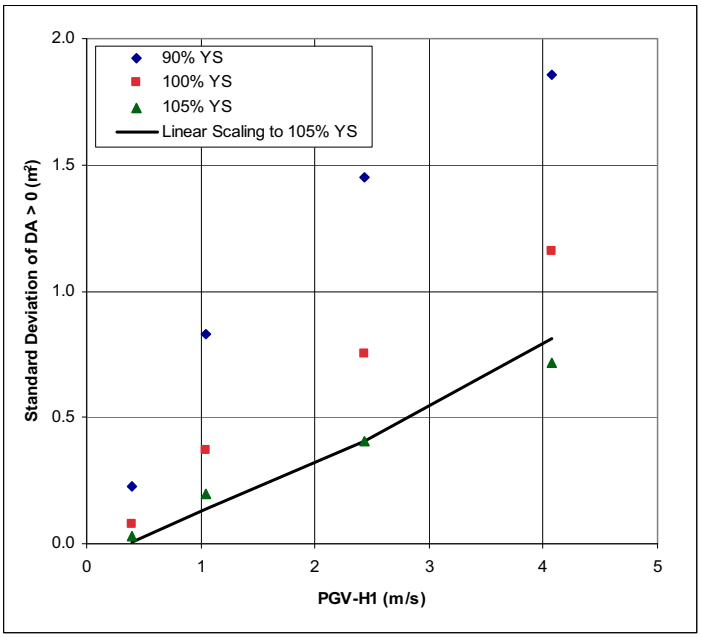

Source: Output DTN: MO0703PASDSTAT.001, worksheet "Dependence on RST" in the file *CDSP Kinematic Damage Abstraction 17-mm Degraded.xls.*

Figure 6-48. Linear Estimate of the Standard Deviation of Conditional Damaged Area at 105% RST for the Codisposal Waste Package with 17-mm-Thick OCB and Degraded Internals

These equations are derived in the worksheet "Dependence on RST" in the file *CDSP Kinematic Damage 17-mm Degraded.xls* (output DTN: MO0703PASDSTAT.001). Note that RST is expressed as an integer value (i.e., 95, rather than 0.95) in these equations. If the RST is between 102% and 105% of yield strength and the PGV is less than 0.4 m/s, the standard deviation needs to be set to the calculated value at 0.4 m/s. This will avoid negative values being calculated for the standard deviation.

Figures 6-49 and 6-50 compare Equations 6.6-2 and 6.6-3 to data in Table 6-27 for the mean and standard deviation for the conditional damaged areas. This comparison demonstrates that Equations 6.6-2 and 6.6-3 provide a reasonable representation of the parameters defining the gamma distribution over the PGV range of 0.4 m/s to 4.07 m/s and over the RST range of 90% to 105% that are relevant for the TSPA.

6.6.2.4 Alternate Conditional Probability Distributions

Q-Q plots were prepared for the damaged area data versus gamma and log-normal distributions for 90% RST at the 0.4 m/s, 1.05 m/s, 2.44 m/s, and 4.07 m/s PGV levels. The gamma distribution provides a reasonable representation of the damaged area data at all PGV levels, as shown by Figures 6-41 to 6-44.

The log-normal distribution provides a poor representation of the conditional damaged areas at the 1.05 m/s, 2.44 m/s, and 4.07 m/s PGV levels and was not considered further. Figure 6-51 presents the Q-Q plot for the log-normal distribution versus the conditional damaged areas at the 1.05 m/s PGV level. A normal distribution was eliminated from consideration because the

standard deviation of the conditional damaged area is often greater than its mean, as shown in Table 6-27. In this situation, a normal distribution will predict conditional damaged areas that are less than zero, which is unacceptable. The Weibull distribution was not attempted for the codisposal waste package because of its rejection for the TAD-bearing waste package (see Sections 6.5.1.4 and 6.5.2.4).

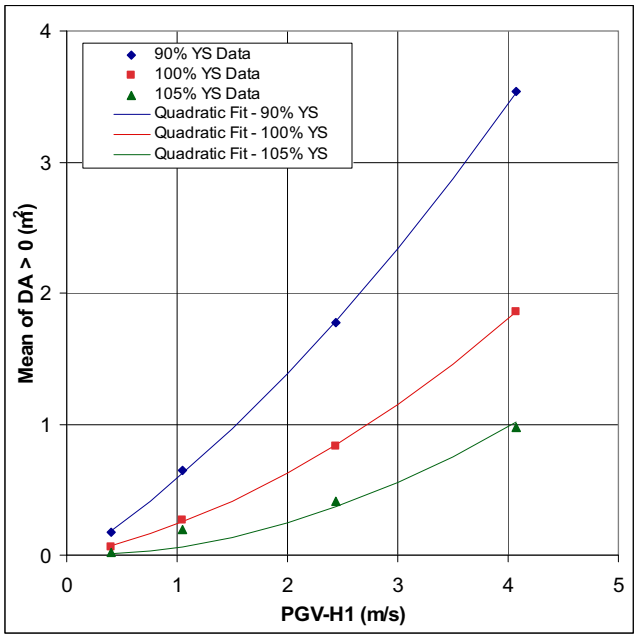

Source: Output DTN: MO0703PASDSTAT.001, worksheet "Dependence on RST" in the file *CDSP Kinematic Damage Abstraction 17-mm Degraded.xls.*

Figure 6-49. Comparison of Equation 6.6-2 to the Mean of the Conditional Damaged Areas for the Codisposal Waste Package with 17-mm-Thick OCB and Degraded Internals

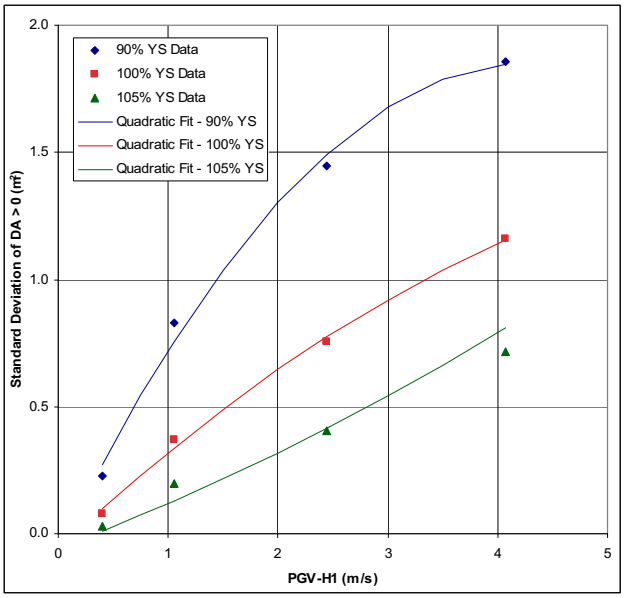

Source: Output DTN: MO0703PASDSTAT.001, worksheet "Dependence on RST" in the file *CDSP Kinematic Damage Abstraction 17-mm Degraded.xls.*

Figure 6-50. Comparison of Equation 6.6-3 to the Standard Deviation of the Conditional Damaged Areas for the Codisposal Waste Package with 17-mm-Thick OCB and Degraded Internals

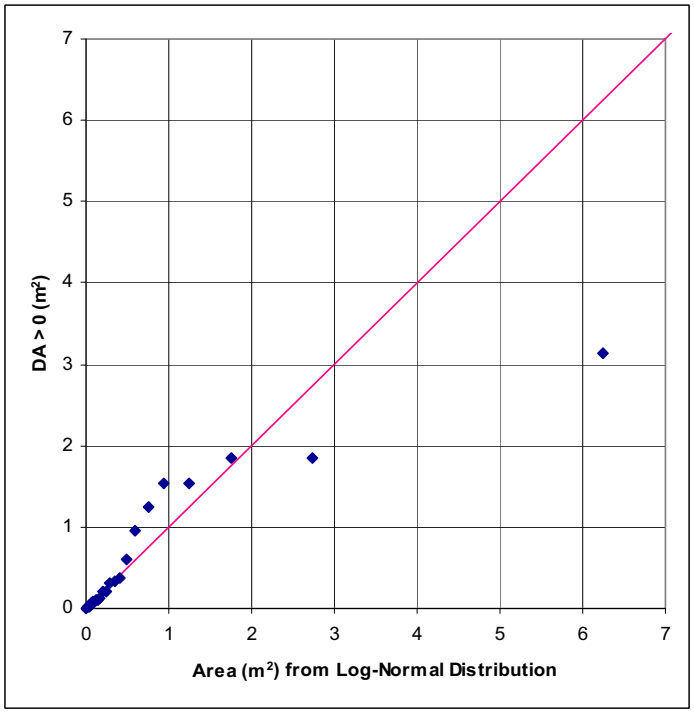

Source: Output DTN: MO0703PASDSTAT.001, worksheet "Log-Normal for 90%_d17" in the file *CDSP Kinematic Damage Abstraction 17-mm Degraded.xls.*

NOTE: Plot shows 1.05 m/s PGV level at 90% RST. "DA > 0 (m^2)" is the conditional nonzero damaged area.

Figure 6-51. Q-Q Plot for Conditional Damaged Areas versus a Log-Normal Distribution for the Codisposal Waste Package with 17-mm-Thick OCB and Degraded Internals

6.6.2.5 Dependence on OCB Thickness

The conditional probability distributions described in previous sections represent the variation of damaged area as a function of PGV and RST. The time-dependent thickness of the OCB must also be incorporated into the damage abstraction for the codisposal waste package with degraded internals.

The spatially averaged thickness of the OCB is a time-dependent parameter that is predicted by other elements of the TSPA. The conditional damaged area corresponding to the average OCB thickness at the time of the seismic event is calculated by linear interpolation if the OCB thickness is between 17 mm and 23 mm. Damaged areas are often observed to follow a power law, as illustrated by the quadratic fit for mean damaged area as a function of PGV in Figure 6-45. The use of linear interpolation for *PGV* and *RST* is appropriate because it provides results at intermediate values that are greater than those from a power-law fit with a positive and increasing slope. The logic for the dependence on damaged area on OCB thickness is illustrated in Equation 6.6-4:

$$DA_{CDSP\_Degraded} = \text{If } t \geq 23 \text{ mm}, DA_{CDSP\_Degraded,23\text{-}mm} \quad \text{(Eq. 6.6-4)}$$

$$\text{Or if } t \leq 17 \text{ mm}, DA_{CDSP\_Degraded,17\text{-}mm}$$

$$\text{else, } DA_{CDSP\_Degraded,17\text{-}mm} + (DA_{CDSP\_Degraded,23\text{-}mm} - DA_{CDSP\_Degraded,17\text{-}mm})*(t - 17 \text{ mm})/(6 \text{ mm})$$

where t is the spatially averaged thickness of the OCB (in mm) at the time of the jth event, $DA_{CDSP\_Degraded}$ is the final damaged area at the current average OCB thickness, $DA_{CDSP\_Degraded,17\text{-}mm}$ is the value of the conditional damaged area from the 17 mm damage abstraction, and $DA_{CDSP\_Degraded,23\text{-}mm}$ is the value of the conditional damaged area from the 23 mm damage abstraction. Based on Equation 6.6-4, the damaged area is set to the value at 23 mm if the average OCB thickness is greater than 23 mm. This is reasonable because the damaged area abstraction for the 23-mm-thick OCB bounds the waste package response for several hundred thousand years after repository closure, based on the estimated corrosion time in Section 6.5.1.2. The damaged area is set to the value for the 17-mm thickness if the average OCB thickness is less than 17 mm. This is a reasonable approach because the damaged area abstraction for the 17-mm-thick OCB provides a reasonable representation at the end of the peak dose period (approximately 1,000,000 years), based on the estimated corrosion time in Section 6.5.2.2. In addition, the drip shield is expected to fail from general corrosion before the OCB thickness is reduced to 17 mm because the general corrosion rate for titanium is greater than for Alloy 22 (SNL 2007 [DIRS 178851], Section 1.2). This kinematic damage abstraction is not applicable after the drip shield fails, which should occur before the thickness of the OCB is reduced to 17 mm.

6.6.3 Damage from Multiple Events

The damaged area from multiple seismic events is defined as the sum of the damaged areas from the individual seismic events. This approach is an upper bound for total damaged area because work-hardening of dented or deformed areas on the surface of the waste package makes it more difficult to damage these areas during a subsequent event and because the summation of damaged areas from individual events ignores impact location entirely. This viewpoint is

confirmed by the results for the single waste package calculations with a fine finite-element grid at 0.4 m/s PGV level, which demonstrate that there is little apparent "amplification" from multiple hits to the same area during a seismic event, judging by the small magnitude of the damaged areas in Table 6-23. In this situation, linear summation of damaged area overestimates the accumulation of residual stress.

6.6.4 Location of Damaged Area

The damaged areas from end-to-end impacts of the codisposal waste package are always zero at the 0.4 m/s, 1.05 m/s, and 2.44 m/s PGV levels. At the 4.07 m/s PGV level, almost all damaged areas are zero except for two observations with very small, nonzero values (DTN: LL0704PA049SPC.024 [DIRS 180736], File *CDSP_kinematic_analyses_DA_summary.xls*, worksheet "WP-WP"). Damaged areas are therefore almost exclusively due to waste package-to-pallet impacts. This conclusion is applicable to any of the three future states of the waste package.

In this situation, the damaged areas from the kinematic response of the codisposal waste package occur on the cylindrical surface of the OCB, rather than on the lids of the waste package. The damaged areas are conceptualized to be randomly located on the cylindrical surface. That is, any location on the cylindrical surface is equally likely to sustain damage. This is a reasonable approach because the orientation of individual waste packages will change through translation and rotation during the multiple kinematic events that are expected to occur during the peak dose period. The surface area of the OCB for the 5 DHLW/1 DOE SNF Long waste package, which is representative of the codisposal waste packages, is 33.05 m^2, based on an outer diameter of the OCB of 2,044.7 mm and a nominal length of the OCB of 5,145.38 mm (SNL 2007 [DIRS 179567], Table 4-9).

6.6.5 Spatial Variability

Damage to or rupture of the waste package from vibratory ground motion is constant throughout the repository for each seismic event in the TSPA. That is, there is no spatial variability of damage or rupture for the waste package groups within the TSPA. Spatial variability is represented in the kinematic calculations through the variability of friction factors on a package-by-package basis and in the abstraction of damaged areas for the two codisposal waste packages in the kinematic model (SNL 2007 [DIRS 178851], Section 6.3.2).

Lack of spatial variability is not important for predicting the mean dose in the TSPA. The mean dose is independent of spatial variability because the sum of the mean doses from groups of waste packages with different damage levels is equal to the mean of the sum of the doses from the individual groups. On the other hand, the coefficient of variation (i.e., the variability about the mean) of the total dose over all realizations is overestimated without spatial variability because lack of spatial variability makes an extreme response for all waste package groups more likely than for a model with spatial variability.

6.7 ABSTRACTIONS FOR ROCKFALL VOLUME

Rockfall induced by vibratory ground motion has the potential to fill the emplacement drifts during the time scale for peak dose assessment. Rockfall refers to the large rock blocks that may be ejected from the nonlithophysal units of the repository during vibratory ground motion. Rockfall also refers to the fractured and rubblized material that may surround the drip shield and fill the drifts during partial or complete collapse of drifts in lithophysal units of the repository. Detailed rockfall analyses have been performed for both of these rock types under vibratory ground motion. These rockfall analyses are documented in *Drift Degradation Analysis* (BSC 2004 [DIRS 166107]).

The abstractions for rockfall volume in the lithophysal and nonlithophysal units are defined in the following sections. The abstraction for rockfall in the lithophysal zone is a central element of the seismic algorithm for the TSPA because 80% to 85% of the emplacement drifts lie in the lithophysal zones (SNL 2007 [DIRS 179466], Table 4-1, Item Number 01-03) and because rockfall volume accumulates much faster in the lithophysal than in the nonlithophysal zone (see Section 6.7.2.1). The abstraction for the nonlithophysal zone is also presented here because it may be used as part of the seepage abstraction for the TSPA.

6.7.1 Rubble Accumulation in the Lithophysal Zones

In the lithophysal zones, the rock mass has very low compressive strength and is permeated with void spaces of varying size. Average joint spacing is less than 1 meter, and at certain locations this spacing is much smaller, on the order of 0.1 meters (BSC 2004 [DIRS 166107], Section 6.4.1.1). The drifts in the lithophysal zone are predicted to collapse into small fragments with particle sizes of centimeters to decimeters (BSC 2004 [DIRS 166107], Section 8.1) under the loads imposed by vibratory ground motion. *Drift Degradation Analysis* (BSC 2004 [DIRS 166107], Section 6.4) provides a detailed description of the lithophysal rockfall analyses. The rubble volumes at the 0.4 m/s, 1.05 m/s, and 2.44 m/s PGV levels are defined in DTN: MO0611ROCKFALL.000 [DIRS 178831]. Rockfall calculations were not performed at the 5.35 m/s PGV level because complete drift collapse was observed at the 2.44 m/s PGV level.

6.7.1.1 Probability of Rockfall in the Lithophysal Zones

The probability of nonzero lithophysal rockfall volume from a seismic event, or more simply the probability of rockfall, is based on computational results for 15 ground motions at the 0.4 m/s, 1.05 m/s, and 2.44 m/s PGV levels. The volume of rockfall per meter of drift is presented in Table 6-28. The volumes in Table 6-28 are the volumes of intact lithophysal rock that cave into the drift during the seismic event. These volumes do not include the effect of bulking in the rubble, as discussed in Section 6.7.1.5. The ground motion number and rock mass category for each realization in Table 6-28 are defined in DTN: MO0301SPASIP27.004 [DIRS 161869], Table I-3 in the file *Sampling_ Description.doc*.

The ground motion numbers and rock mass categories in Table 6-28 are based on a Latin Hypercube sampling for these two parameters (see *Sampling of Stochastic Input Parameters for Rockfall Calculations and for Structural Response Calculations Under Vibratory Ground Motion* (BSC 2004 [DIRS 169999])). Instead of simulating all possible combinations of the 15 sets of

ground motion with the five rock-mass categories, only the 15 realizations shown in Table 6-28 were simulated (BSC 2004 [DIRS 166107], Section 6.4.2.2 and Table 6-44). Note that the 15 ground motions are numbered sequentially 1 through 14 and 16 and are considered equally probable.

Rock mass categories 1 through 5 represent approximately 3%, 7%, 25%, 35%, and 30% of the lithophysal rock mass, respectively (output DTN: MO0705ROCKMASS.000, File *Rock Mass Category Percentages.xls*, worksheet "Sheet1"). Since the rock mass categories are not equally probable, it is appropriate to define the probability of rockfall based on a weighted average of the results for each rock mass category. The calculations for the weighted probability of rockfall at the 0.4 m/s, 1.05 m/s, and 2.44 m/s PGV levels are documented in Table 6-29.

Table 6-28. Data for Rubble Volume in the Lithophysal Zones

Realization Number	Ground Motion Number	Rock Mass Category Number	Rubble Volume (m^3/m) by PGV Level		
			0.4 m/s	1.05 m/s	2.44 m/s
1	4	3	0.06	2.26	104.75
2	8	5	0	7.63	67.92
3	16	4	0	3.22	69.3
4	12	1	2.13	5.62	109.77
5	2	3	0	3.62	84.2
6	8	1	2.46	3.11	109.85
7	14	2	0.06	5.52	76.59
8	4	4	0	3.42	94.52
9	10	2	0.03	0.58	94.28
10	6	3	0	11.84	60.83
11	9	1	7.16	21.95	82.53
12	1	1	2.12	4.35	111.21
13	1	3	0	0.79	103.52
14	7	4	0	28.96	62.22
15	11	4	0	14.38	72.16

Sources: Rubble volumes from DTN: MO0611ROCKFALL.000 [DIRS 178831], File *summary.xls*, worksheet "Sheet1." Ground motion numbers and rock mass category numbers from DTN: MO0301SPASIP27.004 [DIRS 161869], Table I-3 in the file *Sampling_Description.doc*.

The weighted probabilities at the 0.4 m/s and 1.05 m/s PGV levels define (1) the slope of a straight line between these two points: (1 − 0.1625)/(1.05 m/s − 0.4 m/s) = 1.288 s/m, (2) the PGV-intercept: 0.4 m/s − (0.1625/1.288 s/m) = 0.274 m/s, and (3) the y-intercept: 0.1625 − (1.288 s/m)(0.4 m/s) = −0.353. Note that the PGV intercept is slightly larger than the minimum PGV intercept for zero kinematic damage, 0.219 m/s, derived in Table 6-25. This result means that the PGV range for the TSPA, as defined in Section 6.4.3, encompasses the threshold for nonzero rockfall in the lithophysal units. The resulting piecewise linear definition for the probability of rockfall is given by:

$$P(Rockfall > 0) = Min(1.0, Max(0.0, (1.288)PGV - 0.353)) \qquad \text{(Eq. 6.7-1)}$$

which is plotted in Figure 6-52.

Table 6-29. Probability of Rockfall Weighted by Rock Mass Category

Rock Mass Category Number	Weight (%)	Probability of Rockfall for each Rock Mass Category (Unweighted)		
		0.4 m/s	1.05 m/s	2.44 m/s
1	3	1	1	1
2	7	1	1	1
3	25	0.25	1	1
4	35	0	1	1
5	30	0	1	1
Weighted Probability		0.1625	1	1

Sources: Unweighted probabilities calculated from data in Table 6-28; weighting defined in output DTN: MO0705ROCKMASS.000, File *Rock Mass Category Percentages.xls*, worksheet "Sheet1."

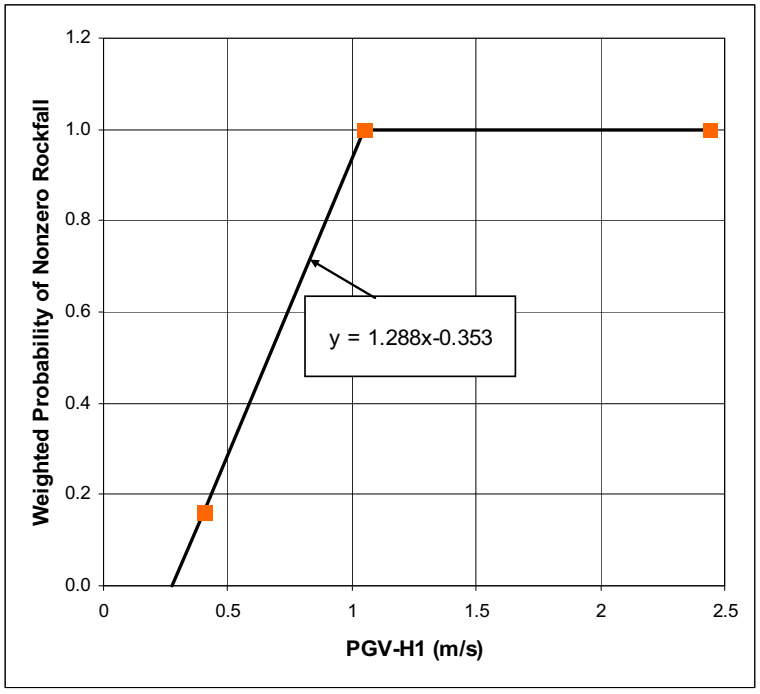

Source: Output DTN: MO0703PASDSTAT.001, worksheet "Probability of Rockfall" in the file *Lith Rubble Abstraction.xls.*

Figure 6-52. Weighted Probability of Lithophysal Rockfall into the Drifts

6.7.1.2 Conditional Probability Distributions for Lithophysal Rockfall

Figures 6-53 to 6-55 present the Q-Q plots for gamma distributions versus the conditional (nonzero) lithophysal rock volume that caves into the drifts in response to ground motions at the 0.4 m/s, 1.05 m/s, and 2.44 m/s PGV levels. The volume of lithophysal rock that caves during the event is based on the results for rock mass categories 2 through 5. Rock mass categories 2 through 5 represent 97% of the emplacement drifts in the repository and generally produce similar rubble volumes at the 0.4 m/s, 1.05 m/s, and 2.44 m/s PGV levels (see Table 6-28). More specifically, there are very small rubble volumes at the 0.4 m/s PGV level, intermediate rubble volumes at the 1.05 m/s PGV level, and large rubble volumes at the 2.44 m/s PGV level for all of

the realizations with rock mass categories 2 through 5. This "uniform" behavior is consistent with TSPA, which does not represent spatial variability by rock mass category.

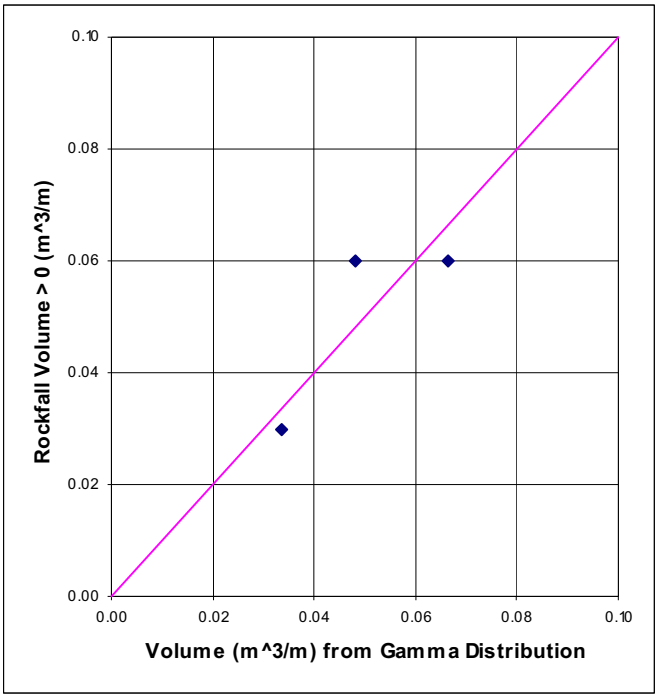

Source: Output DTN: MO0703PASDSTAT.001, worksheet "Gamma Abstraction" in the file *Lith Rubble Abstraction.xls.*

NOTE: Rockfall Volume > 0 is the conditional lithophysal rock volume that caves into the drift for rock mass categories 2 through 5.

Figure 6-53. Q-Q Plot for Conditional Lithophysal Rock Volume versus a Gamma Distribution at the 0.4 m/s PGV Level

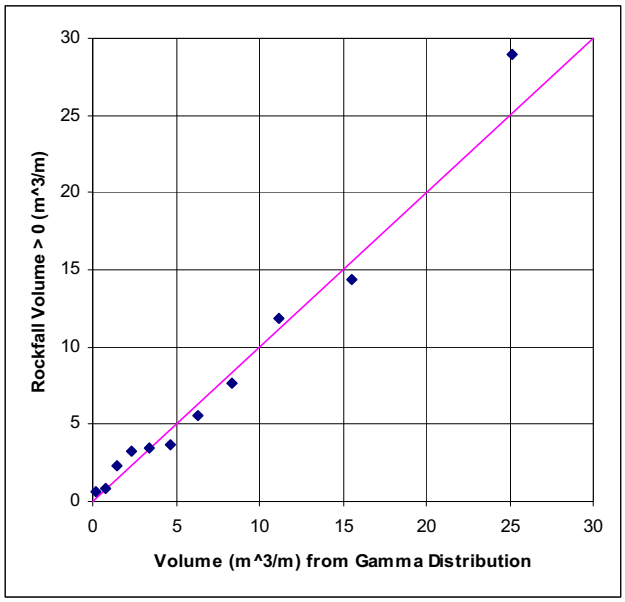

Source: Output DTN: MO0703PASDSTAT.001, worksheet "Gamma Abstraction" in the file *Lith Rubble Abstraction.xls.*

NOTE: Rockfall Volume > 0 is the conditional lithophysal rock volume that caves into the drift for rock mass categories 2 through 5.

Figure 6-54. Q-Q Plot for Conditional Lithophysal Rock Volume versus a Gamma Distribution at the 1.05 m/s PGV Level

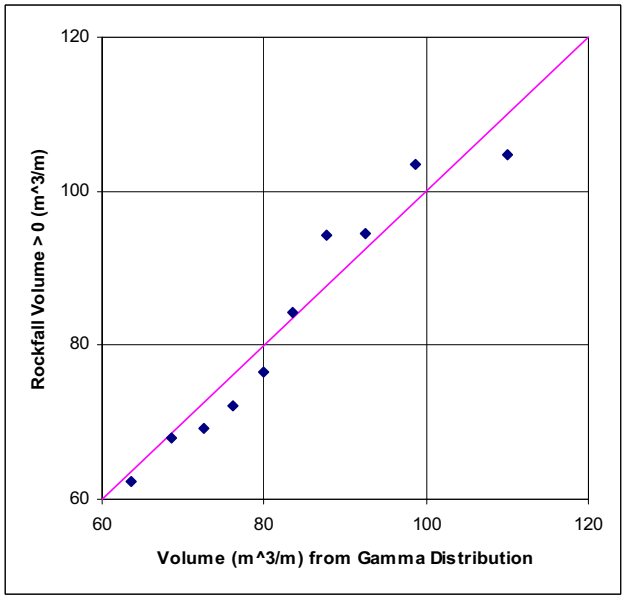

Source: Output DTN: MO0703PASDSTAT.001, worksheet "Gamma Abstraction" in the file *Lith Rubble Abstraction.xls.*

NOTE: Rockfall volume > 0 is the conditional nonzero lithophysal rock volume that caves into the drift for rock mass categories 2 through 5.

Figure 6-55. Q-Q Plot for Conditional Lithophysal Rock Volume versus a Gamma Distribution at the 2.44 m/s PGV Level

The results for rock mass category 1 have not been included in the conditional rubble volumes. Rock mass category 1 produces significantly greater rubble volume at the 0.4 m/s PGV level than rock mass categories 2 through 5. However, rock mass category 1 represents only 3% of the emplacement drifts in the lithophysal zones. This 3% represents a small spatial variability in the rock mass. TSPA does not represent this variability, but applies a single value for rubble volume from a seismic event throughout the lithophysal units. The data for rock-mass category 1 has therefore not been included in the abstraction because the large rubble volumes in 3% of the lithophysal zones would be applied throughout the repository (for 3% of the realizations). An alternative is to perform a weighted regression analysis across the five rock-mass categories, but the uniformity of results for rock categories 2 through 5 provides a simple and adequate solution. The values of the mean and standard deviation of the conditional lithophysal rock volumes for rock mass categories 2 through 5, which are the input parameters for the gamma distributions, are listed in Table 6-30.

Table 6-30. Mean and Standard Deviations of the Conditional Lithophysal Rock Volumes

PGV Level (m/s)	Nonzero Rubble Volume	
	Mean (m^3/m)	Standard Deviation (m^3/m)
0.4	0.050	0.017
1.05	7.47	8.37
2.44	80.94	16.14

Source: Output DTN: MO0703PASDSTAT.001, worksheet “Gamma Abstraction” in the file *Lith Rubble Abstraction.xls.*

Gamma distributions provide a very good fit to the conditional (nonzero) lithophysal rock volumes at the three PGV levels, as shown in Figures 6-53 to 6-55. Based on these results, gamma distributions are selected as the probability distribution for conditional lithophysal rock volume that collapses during the seismic event.

The abstraction for the TSPA must represent the response for intermediate values of PGV. Quadratic fits to the mean and standard deviation of the rock volumes at the three PGV levels provide a convenient way to represent the input parameters for the gamma distribution as a function of PGV, as shown in Figure 6-56. Figure 6-57 plots the 1st, 5th, 50th, 95th, and 99th percentiles of the resulting gamma distributions against the conditional lithophysal rock volume as a function of PGV. Figure 6-56 shows that extrapolation of the quadratic fit for the standard deviation below 0.4 m/s PGV level would produce negative values, which is not acceptable. The curves in Figure 6-57 avoid this problem by using the conditional distribution for rubble volume at the 0.4 m/s PGV level as an upper bound for all values of PGV less than 0.4 m/s. The gamma distributions, with the quadratic fits defined in Figure 6-56, provide an excellent representation of the conditional lithophysal rock volume over the full range of PGV values relevant to the TSPA.

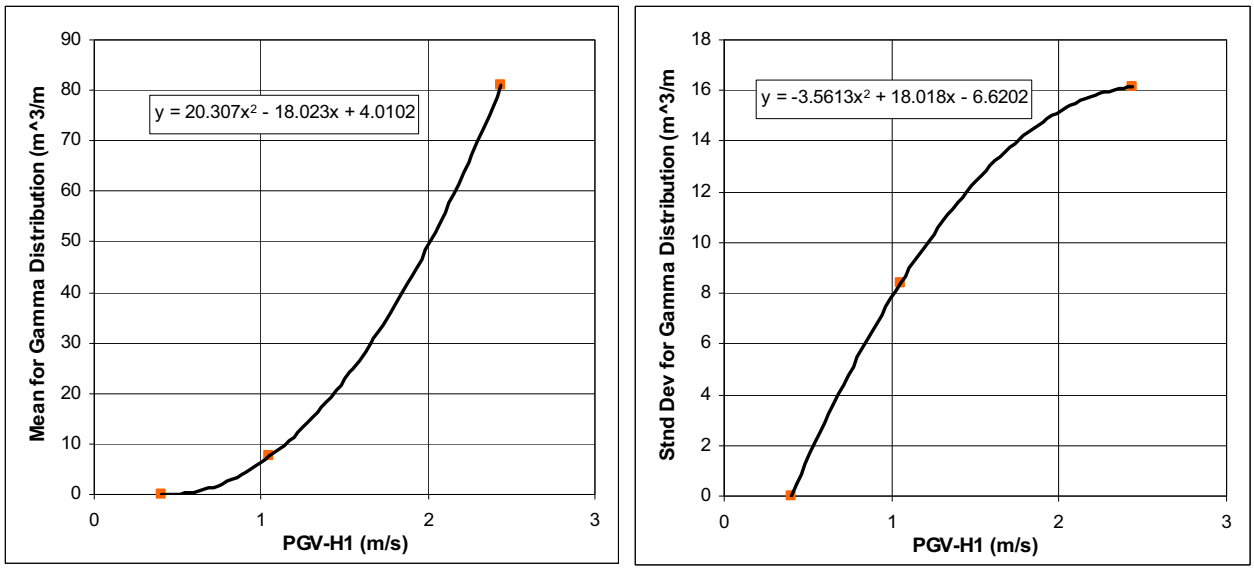

Source: Output DTN: MO0703PASDSTAT.001, worksheet "Gamma Abstraction" in the file *Lith Rubble Abstraction.xls.*

Figure 6-56. Quadratic Fits to the Mean and Standard Deviation of Conditional Lithophysal Rock Volume

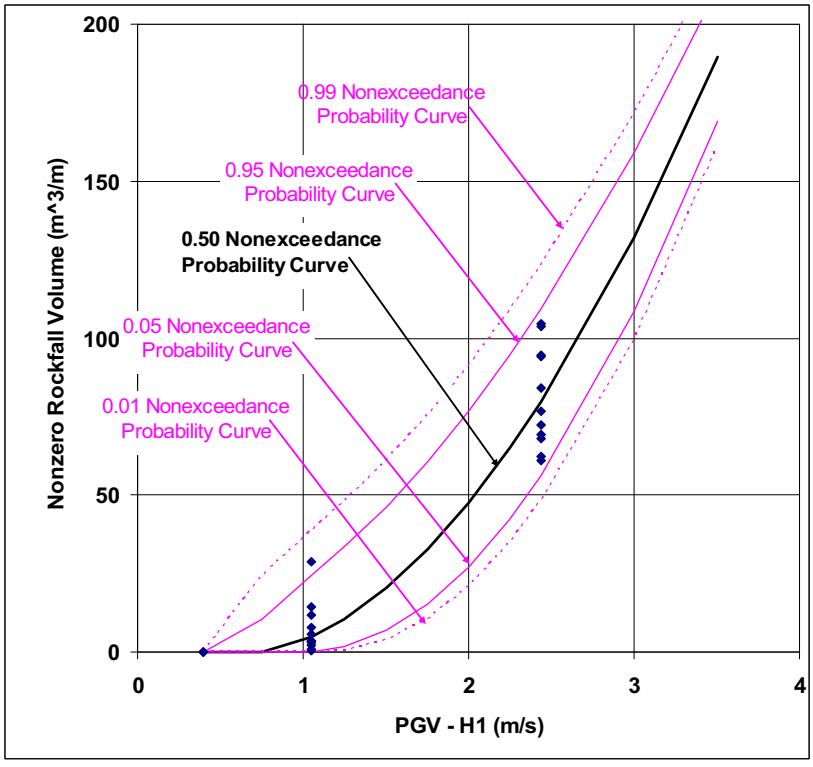

Source: Output DTN: MO0703PASDSTAT.001, worksheet "Gamma Abstraction" in the file *Lith Rubble Abstraction.xls.*

Figure 6-57. Comparison of Percentiles on the Gamma Distributions for Conditional Lithophysal Rock Volumes

6.7.1.3 Alternate Conditional Probability Distributions

Q-Q plots were also prepared for the conditional lithophysal rock volumes versus log-normal distributions at the 0.4 m/s, 1.05 m/s, and 2.44 m/s PGV levels (see worksheet "Log-Normal Abstraction" in the file *Lith Rubble Abstraction.xls* in output DTN: MO0703PASDSTAT.001). The log-normal distribution provides a reasonable representation of the data for the three PGV levels, but quadratic fits to the mean and standard deviation of the natural logarithm of the conditional rockfall volumes produced highly anomalous behavior at intermediate values of PGV, so this approach was not considered further.

6.7.1.4 Damage from Multiple Events

There is no spatial variability in the lithophysal rockfall volume from a seismic event, and the lithophysal rock volume from multiple seismic events is defined as the sum of the volumes from the individual seismic events. This approach provides a reasonable representation for the accumulation of failed rock over time. It is possible that the host rock might become weakened after a seismic event that causes partial collapse of the drift. This effect has not been directly included in the calculations of lithophysal response. However, the rapid filling of drifts in lithophysal units mitigates concerns about numerous seismic events slowly weakening the rock mass. To understand this point, compare the range of lithophysal rock volumes, as presented in Figure 6-57, to the rubble volume needed to fill a drift, which is estimated to be 30 m^3/m to 120 m^3/m (see Section 6.7.1.5). Based on this comparison, individual seismic events with PGV greater than 2 m/s often completely fill the drifts, while individual seismic events with PGV between 1 m/s and 2 m/s fill a substantial fraction of the free space in a drift. The rapid filling of the drifts for seismic events with PGV greater than 1 m/s mitigates concerns about multiple events weakening the rock mass.

6.7.1.5 Fraction of Filled Drift

The total rock volume from multiple seismic events must be related to the static load of rubble on the drip shield (required for the drip shield fragility curves described in Section 6.8). Since static rockfall loads have been calculated for fully collapsed drifts in the lithophysal zones (BSC 2004 [DIRS 166107], Section 6.4.2.5), it is reasonable to associate rockfall load for a partially collapsed drift with the fraction of the drift that is filled with rubble. This fraction is defined as the total rubble volume (from multiple seismic events) divided by the effective drift volume after collapse. The effective drift volume after collapse may be significantly greater than the initial drift volume because the solid drift walls move outward as the rubble falls into the drift.

The rockfall load in a drift that is partly filled with rubble is defined as the product of the fraction of drift filled with rubble and the rockfall load for a fully collapsed drift. This is a reasonable approach that tends to overestimate the vertical loads on the drip shield for small rubble volumes. Small amounts of rubble will tend to settle around the sides of the drip shield, leaving the crown bare, with no static rockfall load. However, the definition of rockfall load in a partly filled drift produces a small static load on the crown of the drip shield, providing a slight overestimate of rockfall load for the abstraction.

The initial cross-sectional volume of the 216-inch-diameter emplacement drift (SNL 2007 [DIRS 179354], Table 4-1, Item Number 01-10) is 254 ft^3/ft or 23.6 m^3/m of emplacement drift. Part of this volume is unavailable because of the presence of the invert and drip shield. On the other hand, the drift walls expand outward and upward as the host rock caves into the drift. Both of these factors need to be considered in defining the effective drift volume after collapse.

The unavailable volume is estimated from the volumes of the invert and drip shield. The volume of the invert is 47 ft^3/ft[7] or 4.4 m^3/m of emplacement drift. The cross-sectional area of the drip shield is estimated with a simple approximation. The nominal width and nominal height of the drip shield are 2,535 mm and 2,886 mm, respectively (SNL 2007 [DIRS 179354], Table 4-2, Item Number 07-01). Based on these dimensions, the volume excluded by the drip shield is less than (2.535 m)(2.886 m) = 7.3 m^3/m of drift. The actual volume of the drip shield is somewhat less than this value because of its "mailbox" shape. The open volume is then greater than (23.6 − 4.4 − 7.3) = 11.9 m^3/m of emplacement drift. The open volume is rounded up to 12 m^3/m of drift for the TSPA.

The shape of the collapsed drift varies with the local fracture pattern in the host rock and the competency of the rock mass. There is significant uncertainty in the appropriate volume of intact lithophysal rock that, through caving, can generate enough rubble to fill the open volume (12 m^3/m) in the drift. This uncertainty is represented as a range of bulking factors for the rubble from the intact rock (BSC 2004 [DIRS 166107], Section 6.4.2.5.2). The bulking factor, B, is defined as the rubble volume, V_r, relative to its initial volume as intact rock, V_i (BSC 2004 [DIRS 166107], Section 6.4.2.5.2, Equation 6-11):

$$V_r = (1 + B)V_i \qquad \text{(Eq. 6.7-2)}$$

An equivalent definition of the bulking factor is $\phi/(1-\phi)$, where ϕ is the porosity of the caved rock.

Laubscher (1994 [DIRS 179773]) recommends values of the swelling factor for caved rock as 1.16 for fine fragmentation, 1.12 for medium fragmentation and 1.08 for coarse fragmentation. The size scales for the lithophysal rubble and for the nonlithophysal rock blocks fit into the fine to medium category of fragmentation. The swelling factor is defined as (1 + B), which implies bulking factors between 0.12 and 0.16 for caved rock. As a second example, Duncan et al. (1980 [DIRS 161776], Table 5) reported that porosity of the graded rock fill for dams is between 23% and 36%, which is equivalent to a bulking factor between 0.30 and 0.56.

An alternate approach is to evaluate the calculated bulking factors for lithophysal rock with the UDEC code. Using rock fragments with a characteristic length scale of 0.2 m, as is expected to occur in the lithophysal zones, the calculated bulking factor with UDEC varies between 0.19 and 0.25 (BSC 2004 [DIRS 166107], Table P-9).

[7] The diameter of the cross section of the drift is 216 in (SNL 2007 [DIRS 179354], Table 4-1, Item 01-10), so the drift radius is 108 in. The invert is 52 in high at its center (SNL 2007 [DIRS 179354], Table 4-1, Item 01-10A), so the top of the invert is (108 − 52) = 56 in from the center of the drift cross section. The central half-angle subtended by the top of the invert is then given by $\cos^{-1}(56/108)$ = 58.767 degrees. The area of the circular sector containing the full invert is then $(2*58.767^o/360^o)\pi(108)^2$ = 11,964 in^2. The triangular area formed by the extreme end points of the invert and the center of the circle is given by: $(56)(108)\sin(58.767^o)$ = 5,171 in^2. The cross-sectional area of the invert is then 11,964 in^2 − 5,171 in^2 = 6,793 in^2, which converts to 47 ft^2. This area corresponds to an invert volume of 47 ft^3 per foot of drift length.

The range of bulking factors for the caved rock is assumed to be 0.1 to 0.4 (see Assumption 5.3, Section 5). This range of values encompasses the derived bulking factors from (Laubscher 1994 [DIRS 179773]). This range of values encompasses the calculated bulking factors for lithophysal rock with the UDEC code. Finally, this range of values encompasses part of the data from Duncan et al. (1980 [DIRS 161776]) for graded rock fill for dams. The extreme bulking factors for a graded rock fill are less applicable to the properties of ungraded caved rock than the other citations.

Equation 6.7-2 shows that the increase in volume for the mass of rubble, $V_b - V_i$, is given by BV_i. This increase in volume must equal the unfilled drift volume, 12 m^3/m of drift, for complete drift collapse (i.e., when rubble completely fills the drift). It follows that the volume of intact rock corresponding to complete drift collapse is (12 m^3/0.4) = 30 m^3 to (12 m^3/0.1) = 120 m^3 of intact rock per meter of emplacement drift. These volumes are applicable to both the lithophysal and nonlithophysal units in the repository because the range of bulking factors is designed to represent a wide range of in situ response for caved rock.

It is useful to compare this range of volumes for complete collapse to the results from rockfall calculations. At the 2.44 m/s PGV level, the volume of intact rock that caves into the drift varies between 61 m^3/m and 111 m^3/m (Table 6-28). Since these volumes are on the same order as the estimated volumes to fill the open volume within a drift (30 m^3/m to 120 m^3/m of emplacement drift), it follows that complete drift collapse occurs for many ground motions at the 2.44-m/s PGV level. At the 1.05-m/s PGV level, the volume of intact rock that caves into the drift varies between 0.8 m^3/m and 29 m^3/m of emplacement drift, so complete collapse is very unlikely for a single seismic event, but there can be substantial rockfall relative to the volume for drift collapse. These results are consistent with previous analyses that determined that the 2-m/s PGV level is an approximate threshold for drift collapse in the lithophysal zones of the repository (BSC 2004 [DIRS 166107], Section 6.4.2.2.2, 4th bullet under subheading “Discussion”).

The uncertainty in the volume of intact lithophysal rock corresponding to complete drift collapse is represented as a uniform distribution between 30 m^3/m and 120 m^3/m of emplacement drift. A uniform distribution is appropriate for this volume because the upper and low bounds for the bulking factor have been estimated, but there is limited information about the distribution of values within the range. This distribution is sampled once per realization to determine the volume of intact lithophysal or nonlithophysal rock corresponding to complete drift collapse.

6.7.1.6 Fraction of Filled Drift After Multiple Events

The lithophysal rock volume from multiple seismic events is defined as the sum of the volumes from the individual seismic events (see Section 6.7.1.4). The fraction of drift that is filled with rubble or rockfall after multiple events is defined as the accumulated volume of rubble/rockfall from the current and all previous seismic events divided by the sampled value of the volume corresponding to complete drift collapse.

6.7.1.7 Probability of Drift Collapse in Lithophysal Zones

The Navy has requested that the Yucca Mountain Project provide an analysis of the probability of drift collapse within the first 80 years after repository closure. This analysis is based, in part, on the abstraction for lithophysal rubble volume defined in Sections 6.7.1.1 and 6.7.1.2. It is appropriate to use the lithophysal rubble abstraction because 80% to 85% of the emplacement drifts are in lithophysal units (SNL 2007 [DIRS 179466], Table 4-1, Item Number 01-03) and because the rubble volume in the lithophysal units is significantly greater than the rockfall volume in the nonlithphysal units, as discussed in Section 6.7.2.1. This analysis begins by considering the probability of 1 versus 2 seismic events during the 80-year period, followed by the definition of drift collapse in Section 6.7.1.7.2 and the mathematical formulation for the numerical calculations in Section 6.7.1.7.3.

6.7.1.7.1 Probability of Exactly One or Exactly Two Seismic Events

A simple probability calculation demonstrates that the probability of exactly two seismic events during the first 80 years after repository closure is a factor of 58 less than the probability of exactly one seismic event during this time period. The probabilities of exactly one or exactly two seismic events are based on the standard (Poisson) formulation (Hahn and Shapiro 1967 [DIRS 146529], Equation 4-9) for events that occur randomly over T years with a given rate, $\Delta\lambda$ per year:

$$P(1 \mid \Delta\lambda, T) = T\Delta\lambda e^{-T\Delta\lambda} \quad \text{(Eq. 6.7-3)}$$

and

$$P(2 \mid \Delta\lambda, T) = \frac{(T\Delta\lambda)^2}{2} e^{-T\Delta\lambda} \quad \text{(Eq. 6.7-4)}$$

respectively.

The value, $\Delta\lambda$, is defined as ($\lambda_{max} - \lambda_{min}$) on the bounded hazard curve. The value, λ_{max}, corresponds to the PGV threshold of 0.219 m/s that can cause damage to the waste package. The exceedance frequency corresponding to 0.219 m/s on the bounded hazard curve is 4.287×10^{-4} per year (see Section 6.4.3). The value of λ_{min} is 1×10^{-8} per year (10 CFR 63.114(d) [DIRS 180319]). The numerical value of $\Delta\lambda$ is 4.2869×10^{-4} per year for the TSPA compliance case, and the probabilities of exactly one or exactly two events for $T = 80$ years are:

$$P(1 \mid \Delta\lambda, T) = 3.3 \times 10^{-2} \quad \text{(Eq. 6.7-5)}$$

$$P(2 \mid \Delta\lambda, T) = 5.7 \times 10^{-4} \quad \text{(Eq. 6.7-6)}$$

Given the low probability of exactly two events relative to the probability of exactly one event, the occurrence of two events is likely to have a minor effect on the probability of drift collapse. The probability analysis therefore focuses on a single seismic event during the first 80 years.

6.7.1.7.2 Definition of Drift Collapse

Drift collapse is defined as complete drift collapse, with lithophysal rubble completely filling the volume of the collapsed drift. Based on the analysis in Section 6.7.1.5, the volume of intact rock that must collapse to completely fill a drift is a random variable with a uniform distribution of 30 m^3/m of drift to 120 m^3/m of drift. Rather than incorporate this distribution into the probability analysis, the minimum value of 30 m^3/m of drift, the mean value of 75 m^3/m of drift, and the maximum value of 120 m^3/m of drift have been used as representative rock volumes that define complete drift collapse.

6.7.1.7.3 Mathematical Formulation for Probability Analysis

The incremental probability that the volume of rockfall from seismic events with horizontal peak ground velocity centered on a small interval around v exceeds the volume for drift collapse is the product of four factors:

1. The probability that a single seismic event occurs during the first 80 years after repository closure (Equation 6.7-5)

2. The conditional probability that seismic events with PGV centered on v have nonzero rockfall (defined in Section 6.7.1.1)

3. The conditional probability that the rockfall volume from the seismic events with PGV centered on v equals or exceeds the volume for drift collapse (based on the gamma distributions defined in Section 6.7.1.2)

4. The conditional probability that a seismic event with peak ground velocity centered on v is sampled from the bounded hazard curve.

The probabilities in steps 2 through 4 are conditional because they are based on a single seismic event occurring during the first 80 years after repository closure.

Mathematically, the incremental probability is defined as:

$$dG(V > V_C) = P(1 \mid \Delta\lambda, T) P(V_{rock} > 0 \mid v) G(V_{lith} > V_C \mid v) \frac{-1}{\Delta\lambda} \frac{d\lambda(v)}{dv} dv \qquad \text{(Eq. 6.7-7)}$$

where

v	is the horizontal peak ground velocity
$\lambda = \lambda(v)$	is the annual exceedance frequency on the bounded hazard curve for v
V	is the rockfall volume from the seismic event
V_C	is the volume for drift collapse
$V_{lith}(v)$	is the conditional probability distribution for nonzero lithophysal rockfall

$G(V > V_C)$	is the probability that V exceeds V_C for all possible seismic events
$P(1 \mid \Delta\lambda, T)$	is the probability of a single seismic event with Poisson rate $\Delta\lambda$ during the period of T = 80 years (this is the first factor)
$P(V_{rock} > 0 \mid v)$	is the conditional probability of having nonzero rockfall volume for a seismic event of intensity v (this is the second factor)
$G(V_{lith} > V_C \mid v)$	is the exceedance probability that the conditional probability distribution for nonzero lithophysal rockfall exceeds V_C, the volume for drift collapse, for a seismic event of intensity v (this is the third factor)
$\frac{-1}{\Delta\lambda}\frac{d\lambda(v)}{dv}dv$	is the conditional probability that the value of the horizontal peak ground velocity, v, lies within the interval [v - ½dv, v + ½dv] on the bounded hazard curve (this is the fourth factor).

The first factor is defined by Equation 6.7-3. The second factor is defined by Equation 6.7-1. The third factor is based on a gamma distribution, with the quadratic fits in Figure 6-56. The fourth factor is derived as follows. The probability of v being within a small interval (v - ½dv, v + ½dv) is calculated from the bound hazard curve, based on the difference in annual exceedance frequency:

$$\lambda(v - 0.5dv) - \lambda(v + 0.5dv) = -d\lambda(v) = -\frac{d\lambda(v)}{dv}dv \qquad \text{(Eq. 6.7-8)}$$

Equation 6.7-8 defines the absolute probability of v being within the small interval dv. However, Equation 6.7-7 already includes the factor $P(1 \mid \Delta\lambda, T)$, so Equation 6.7-8 must be modified to represent the conditional probability of sampling (v-dv/2, v+dv/2) within the range of $\Delta\lambda = \lambda_{max} - \lambda_{min}$. This is achieved by adding a term $1/\Delta\lambda$ to the product, which normalizes the conditional probabilities over $\Delta\lambda$ to 1.

The total probability that the volume of rockfall from all relevant seismic events exceeds the volume for drift collapse is then given by:

$$G(V > V_C) = P(1 \mid \Delta\lambda, T)\int_{v_{min}}^{v_{max}} P(V_{rock} > 0 \mid v)G(V_{lith} > V_C \mid v)\frac{-1}{\Delta\lambda}\frac{d\lambda(v)}{dv}dv \qquad \text{(Eq. 6.7-9)}$$

where v_{min} is 0.219 m/s (see Section 6.7.1.7.1). The value of v_{max} is 4.07 m/s, based on Table 6-3 in Section 6.4.3.

6.7.1.7.4 Numerical Results

Equation 6.7-9 has been numerically evaluated for three volumes for drift collapse: 30 m^3/m of drift, 75 m^3/m of drift, and 120 m^3/m (output DTN: MO0703PASDSTAT.001, worksheet "Exceed Prob for V>V0" in the file *Lith Rubble Abstraction.xls*). The resulting probabilities that the volume of rockfall from all relevant seismic events exceeds the volume for drift collapse are given by 1.96×10^{-4}, 4.17×10^{-5}, and 1.70×10^{-5} for the 30, 75, and 120 m^3/m collapse volumes, respectively.)

6.7.2 Rubble Accumulation in the Nonlithophysal Zones

In the nonlithophysal zones, large rock blocks may be shaken loose from the drift walls and fall onto the drip shield in response to vibratory ground motion. *Drift Degradation Analysis* (BSC 2004 [DIRS 166107], Section 6.3) provides a detailed description of the nonlithophysal rockfall analyses. The rockfall calculations evaluate the response of a 25-meter long section of drift in nonlithophysal rock with randomly selected fracture patterns (BSC 2004 [DIRS 166107], Section 6.3). The total volume of rockfall in the 25-meter-long section is summarized in Table 6-31 for the 1.05 m/s, 2.44 m/s, and 5.35 m/s PGV levels (DTN: MO0703SUMM3DEC.000 [DIRS 179895], worksheet "rockfall per simulation" in each of the files *nonlith rockfall characteristics in emplacement drifts with 1e-5 gm.xls, nonlith rockfall characteristics in emplacement drifts with 1e-6 gm.xls,* and *nonlith rockfall characteristics in emplacement drifts with 1e-7 gm.xls*). The correspondence between PGV level and annual exceedance frequency on the unbounded hazard curve is defined by DTNs: MO0303DPGVB106.002 [DIRS 162712], MO0210PGVPB107.000 [DIRS 162713], and MO0401SEPPGVRL.022 [DIRS 169099]; see Table 4-1 for specific locations within these DTNs.

The corresponding volume of rockfall per meter of drift is also presented in Table 6-31 to provide an equivalent basis for comparison to lithophysal rockfall volumes. The rockfall per meter is based on the effective drift length in the 3DEC model that can experience rockfall. The 3DEC model is 25 meters long (BSC 2004 [DIRS 166107], Section 6.3.1) with a 2-m-thick layer of solid continuum at the ends of the drift (BSC 2004 [DIRS 166107], scaled from Figure 6-34(f)). This solid continuum does not generate rockfall. In addition, the azimuthal angle of the drift is 75 degrees (BSC 2004 [DIRS 166107], Section 6.3.1.1). The effective drift length for rockfall is then (25 m − 2 m − 2 m)/sin(75°) = 21.74 meters, and the rockfall volume per meter of drift is calculated by dividing the total volume in Table 6-31 by 21.74 meters.

Table 6-31. Data for Rockfall Volume in Nonlithophysal Rock

1.05 m/s PGV Level			2.44 m/s PGV Level			5.35 m/s PGV Level		
Case	Total Vol. (m^3)	Vol. per m (m^3/m)	Case	Total Vol. (m^3)	Vol. per m (m^3/m)	Case	Total Vol. (m^3)	Vol. per m (m^3/m)
14	1.844	0.085	14	2.118	0.097	14	2.347	0.108
15	7.067	0.325	15	16.514	0.760	15	38.033	1.749
16	4.264	0.196	16	10.652	0.490	16	23.029	1.059
17	0.045	0.002	17	0.647	0.030	17	2.828	0.130
18	0.544	0.025	18	1.417	0.065	18	5.632	0.259
19	7.375	0.339	19	15.123	0.696	19	–	–
20	0.417	0.019	20	0.602	0.028	20	1.456	0.067
21	1.041	0.048	21	1.445	0.066	21	3.532	0.162
22	1.846	0.085	22	2.055	0.095	22	2.260	0.104
23	5.217	0.240	23	8.316	0.383	23	33.630	1.547
24	1.308	0.060	24	1.620	0.075	24	–	–

Table 6-31. Data for Rockfall Volume in Nonlithophysal Rock (Continued)

1.05 m/s PGV Level			2.44 m/s PGV Level			5.35 m/s PGV Level		
Case	Total Vol. (m^3)	Vol. per m (m^3/m)	Case	Total Vol. (m^3)	Vol. per m (m^3/m)	Case	Total Vol. (m^3)	Vol. per m (m^3/m)
25	14.296	0.658	25	12.913	0.594	25	–	–
27	5.661	0.260	27	6.512	0.300	27	13.322	0.613
28	3.520	0.162	28	5.974	0.275	28	–	–
29	1.386	0.064	29	2.919	0.134	29	8.469	0.390
31	0.149	0.007	31	0.221	0.010	31	0.981	0.045
32	0.193	0.009	32	2.404	0.111	32	6.058	0.279
33	0.725	0.033	33	13.741	0.632	33	19.501	0.897
34	2.845	0.131	34	5.374	0.247	34	13.436	0.618
35	1.449	0.067	35	1.753	0.081	35	1.421	0.065
36	2.697	0.124	36	2.954	0.136	36	6.543	0.301
38	42.030	1.933	38	58.486	2.690	38	–	–
39	8.179	0.376	39	17.014	0.783	39	36.451	1.677
40	21.902	1.007	40	35.204	1.619	40	51.291	2.359
41	2.145	0.099	41	5.194	0.239	41	8.866	0.408
42	0.111	0.005	42	1.820	0.084	42	21.141	0.972
43	6.232	0.287	43	18.513	0.852	43	26.606	1.224
44	8.815	0.405	44	21.158	0.973	44	36.713	1.689
45	2.489	0.114	45	4.188	0.193	45	14.267	0.656
46	0.891	0.041	46	1.891	0.087	46	25.590	1.177
48	0.276	0.013	48	4.445	0.204	48	14.942	0.687
49	24.099	1.109	49	9.695	0.446	49	36.387	1.647
50	5.812	0.267	50	6.449	0.297	50	7.720	0.355
51	1.056	0.049	51	4.173	0.192	51	13.863	0.638
52	15.880	0.730	52	63.335	2.913	52	–	–
53	4.525	0.208	53	25.427	1.170	53	36.445	1.676
54	6.371	0.293	54	11.759	0.541	54	17.647	0.812
55	1.285	0.059	55	2.377	0.109	55	3.057	0.141
56	6.056	0.279	56	10.011	0.460	56	7.132	0.328
57	1.435	0.066	57	3.893	0.179	57	10.432	0.480
58	0.133	0.006	58	0.323	0.015	58	4.505	0.207
59	2.130	0.098	59	4.972	0.229	59	9.584	0.441
60	0.526	0.024	60	8.221	0.378	60	9.565	0.440
61	0.299	0.014	61	7.074	0.325	61	8.212	0.378
62	1.807	0.083	62	4.921	0.226	62	8.736	0.402
63	0	0	63	0.480	0.022	63	9.204	0.423
64	13.611	0.626	64	25.130	1.156	64	58.927	2.711

Table 6-31. Data for Rockfall Volume in Nonlithophysal Rock (Continued)

1.05 m/s PGV Level			2.44 m/s PGV Level			5.35 m/s PGV Level		
Case	Total Vol. (m^3)	Vol. per m (m^3/m)	Case	Total Vol. (m^3)	Vol. per m (m^3/m)	Case	Total Vol. (m^3)	Vol. per m (m^3/m)
65	3.020	0.139	65	3.034	0.140	65	6.050	0.278
66	2.776	0.128	66	8.815	0.405	66	22.520	1.036
67	7.601	0.350	67	14.415	0.663	67	16.889	0.777
Mean	5.108	0.235	**Mean**	9.954	0.458	**Mean**	16.028	0.737
Std Dev	7.563	0.348	**Std Dev**	12.944	0.595	**Std Dev**	14.062	0.647

Sources: Total rockfall volume from DTN: MO0703SUMM3DEC.000 [DIRS 179895], worksheet "rockfall per simulation" in each of the files *nonlith rockfall characteristics in emplacement drifts with 1e-5 gm.xls, nonlith rockfall characteristics in emplacement drifts with 1e-6 gm.xls*, and *nonlith rockfall characteristics in emplacement drifts with 1e-7 gm.xls*. Values for the mean, standard deviation, and rockfall per meter of drift are calculated in output DTN: MO0703PASDSTAT.001, worksheet "Lith Versus Nonlith" in the file *Nonlith Rockfall Abstraction.*xls. The correspondence between annual exceedance frequency and PGV level is defined by DTNs: MO0303DPGVB106.002 [DIRS 162712], MO0210PGVPB107.000 [DIRS 162713], and MO0401SEPPGVRL.022 [DIRS 169099]; see Table 4-1 for specific locations within these DTNs.

NOTES: Volume per meter defined by dividing the Total Volume by the effective length of the drift in the 3DEC calculations, 21.74 m.

Std Dev is standard deviation.

6.7.2.1 Comparison of Lithophysal versus Nonlithophysal Rockfall Volumes

The rockfall volume in the nonlithophysal zones is significantly less than in the lithophysal zones at the same PGV level. Table 6-32 compares the mean and standard deviation of the conditional (nonzero) rockfall volumes in the lithophysal and nonlithophysal zones for the 1.05 m/s and 2.44 m/s PGV levels. The data in Table 6-32 indicate that the mean rockfall volume in the lithophysal rock is a factor of 32 to 188 greater than the mean rockfall volume in the nonlithophysal rock for the 1.05 m/s and 2.44 m/s PGV levels, respectively. This situation is likely to persist at higher PGV levels, although lithophysal calculations were not performed beyond 2.44 m/s PGV level. Figure 6-58 presents the rockfall volumes for lithophysal and nonlithophysal rock at the 1.05 m/s and 2.44 m/s PGV levels. This figure confirms the conclusion that the rockfall volume in the nonlithophysal rock is significantly less than the volume in lithophysal rock.

Table 6-32. Comparison of Statistical Parameters for Conditional Rock Volumes in Lithophysal and Nonlithophysal Rock

	Conditional Rock Volumes (m^3/m of emplacement drift)					
	1.05 m/s PGV Level		2.44 m/s PGV Level		5.35 m/s PGV Level	
	Lith	Nonlith	Lith	Nonlith	Lith	Nonlith
Mean	7.8	0.24	86.9	0.46	NA	0.74
Std. Dev.	8.2	0.35	18.2	0.60	NA	0.65

Source: Output DTN: MO0703PASDSTAT.001, worksheet "Lith Versus Nonlith" in the file *Nonlith Rockfall Abstraction.xls*.

NOTE: NA = "Not Available," Std. Dev. = standard deviation.

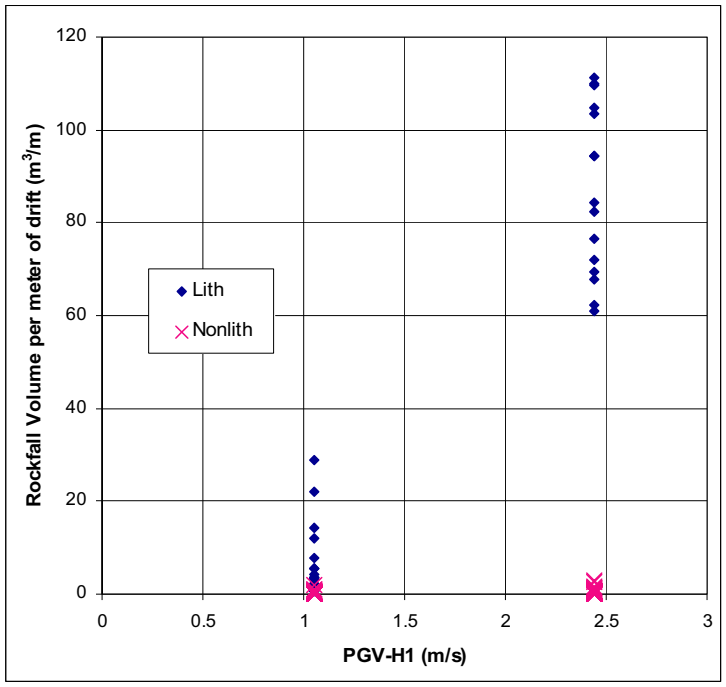

Source: Output DTN: MO0703PASDSTAT.001, worksheet "Lith Versus Nonlith" in the file *Nonlith Rockfall Abstraction.xls*.

Figure 6-58. Comparison of Rockfall Volumes in Lithophysal and Nonlithophysal Rock

6.7.2.2 Probability of Rockfall in the Nonlithophysal Zones

Based on the data in Table 6-31, the probability of rockfall in nonlithophysal rock is 0.98, 1, and 1 for the 1.05 m/s, 2.44 m/s, and 5.35 m/s PGV levels. These results are almost identical to the probabilities of rockfall in lithophysal rock, which are 1 at the 1.05 m/s and 2.44 m/s PGV levels (see Table 6-29).

3DEC calculations were performed for the nonlithophysal rock at the 0.4 m/s PGV level (BSC 2004 [DIRS 166107], Tables 6-19 and 6-26). These simulations use a single preclosure ground motion, rather than 15 postclosure ground motions for the simulations at the 1.05 m/s and 2.44 m/s PGV levels. The 3DEC results at the 0.4 m/s PGV level do not include the aleatory uncertainty associated with multiple ground motions, which is generally a significant factor in all seismic analyses, so these 3DEC results are not used to define the probability of rockfall in the nonlithophysal zones at the 0.4 m/s PGV level. As an alternative, the probability of rockfall for the lithophysal rock is expected to be greater than the probability of rockfall for the nonlithophysal rock at the 0.4 m/s PGV level. The lithophysal rock is generally weaker than nonlithophysal rock and generally has greater rockfall volumes than the nonlithophysal rock, as shown in Table 6-32 and Figure 6-58. Lithophysal rock will usually fail before nonlithophysal rock, so the results for lithophysal rock define an upper bound for the probability of rockfall in the nonlithophysal zones. This probability is defined by Equation 6.7-1 in Section 6.7.1.1.

6.7.2.3 Conditional Probability Distributions for Nonlithophysal Rockfall

Figures 6-59 to 6-61 present the Q-Q plots for gamma distributions versus the conditional nonlithophysal rock volume that caves into the drifts in response to ground motions at the 1.05 m/s, 2.44 m/s, and 5.35 m/s PGV levels. The values of the input parameters for the gamma distributions are the mean and standard deviation of the conditional (nonzero) rockfall volumes in Table 6-32. Gamma distributions provide a very good fit to the conditional nonlithophysal rock volumes at the three PGV levels. Based on these results, gamma distributions are selected as the probability distribution for conditional nonlithophysal rock volume that caves into the drift.

The abstraction for the TSPA must represent the response for intermediate values of PGV. Quadratic fits to the mean and standard deviation of the rock volumes at the three PGV levels provide a convenient way to represent the input parameters for the gamma distribution as a function of PGV, as shown in Figure 6-62.

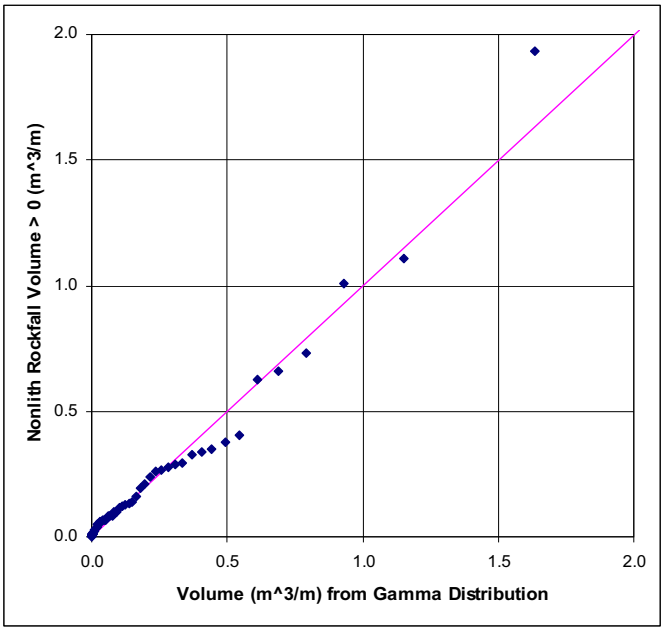

Source: Output DTN: MO0703PASDSTAT.001, worksheet "Gamma Abstractions" in the file *Nonlith Rockfall Abstraction.xls*.

NOTE: Rockfall Volume > 0 is the conditional nonlithophysal rock volume that caves into the drift.

Figure 6-59. Q-Q Plot for Conditional Nonlithophysal Rock Volume versus a Gamma Distribution at the 1.05 m/s PGV Level

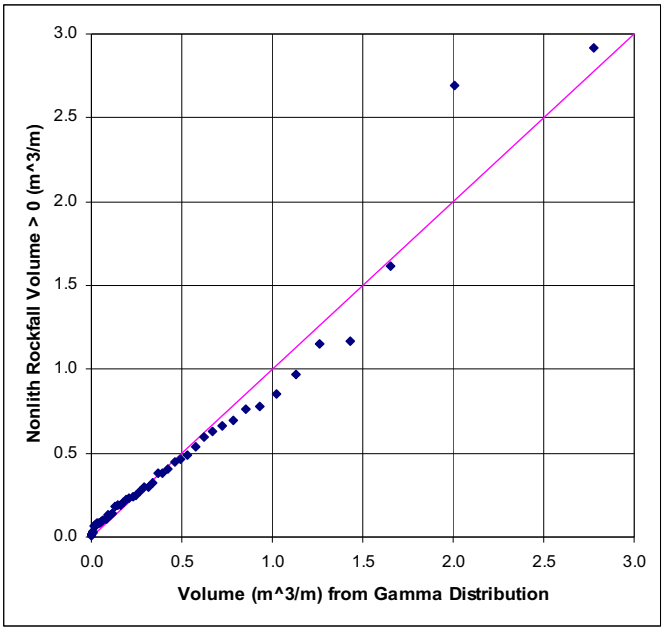

Source: Output DTN: MO0703PASDSTAT.001, worksheet "Gamma Abstractions" in the file *Nonlith Rockfall Abstraction.xls*.

NOTE: Rockfall Volume > 0 is the conditional nonlithophysal rock volume that caves into the drift.

Figure 6-60. Q-Q Plot for Conditional Nonlithophysal Rock Volume versus a Gamma Distribution at the 2.44 m/s PGV Level

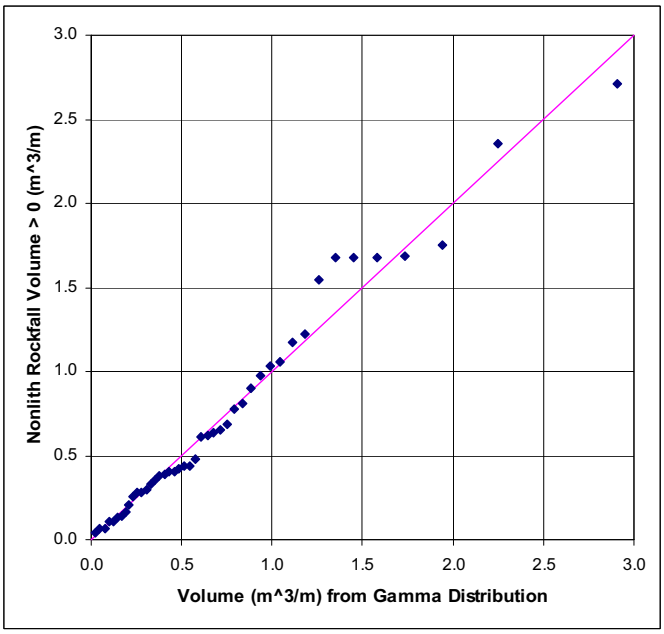

Source: Output DTN: MO0703PASDSTAT.001, worksheet "Gamma Abstractions" in the file *Nonlith Rockfall Abstraction.xls*.

NOTE: Rockfall Volume > 0 is the conditional nonlithophysal rock volume that caves into the drift.

Figure 6-61. Q-Q Plot for Conditional Nonlithophysal Rock Volume versus a Gamma Distribution at the 5.35 m/s PGV Level

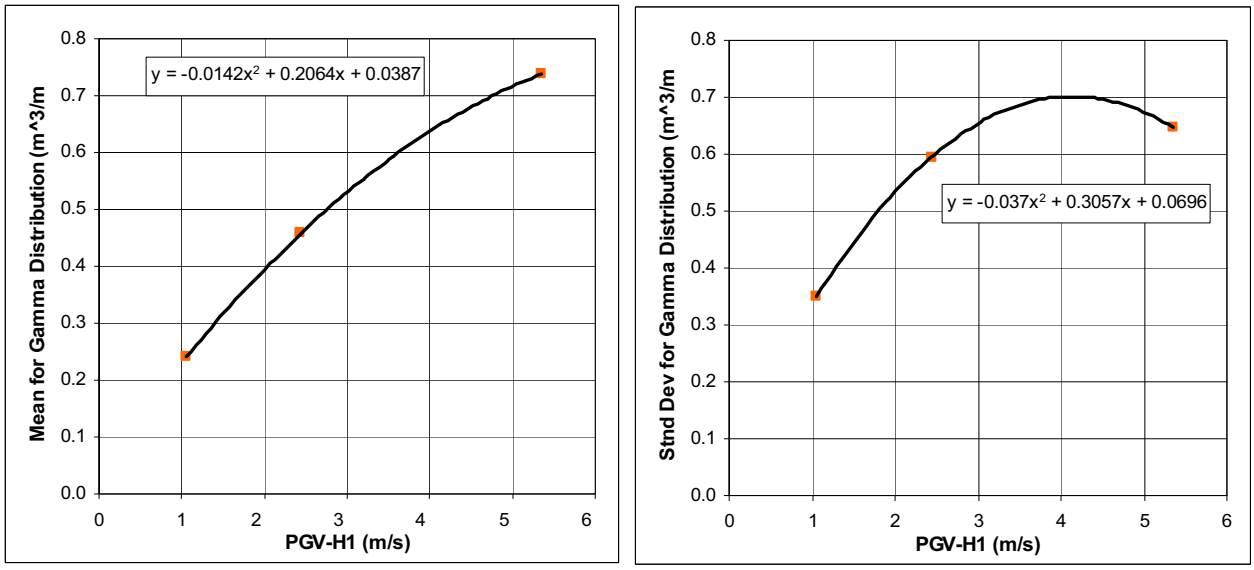

Source: Output DTN: MO0703PASDSTAT.001, worksheet "Gamma Abstractions" in the file *Nonlith Rockfall Abstraction.xls.*

Figure 6-62. Quadratic Fits to the Mean and Standard Deviation of Conditional Nonlithophysal Rock Volume

Figure 6-63 plots the 1st, 5th, 50th, 95th, and 99th percentiles of the resulting gamma distributions against the conditional nonlithophysal rock volumes as a function of PGV. The gamma distributions, with the quadratic fits defined in Figure 6-62, provide an excellent representation of the conditional nonlithophysal rock volume over the 0.2 m/s to 4.07 m/s PGV levels that are relevant to the TSPA.

6.7.2.4 Alternate Conditional Probability Distributions

Q-Q plots were also prepared for the conditional nonlithophysal rock volumes versus log-normal distributions at the 1.05 m/s, 2.44 m/s, and 5.35 m/s PGV levels (see worksheet "Log-Normal Distributions" in the file *Nonlith Rockfall Abstraction.xls* in output DTN: MO0703PASDSTAT.001). The log-normal distribution significantly overestimates the rockfall volumes for the realizations with the highest values of rockfall volume in comparison to the gamma distributions, so this approach was not considered further.

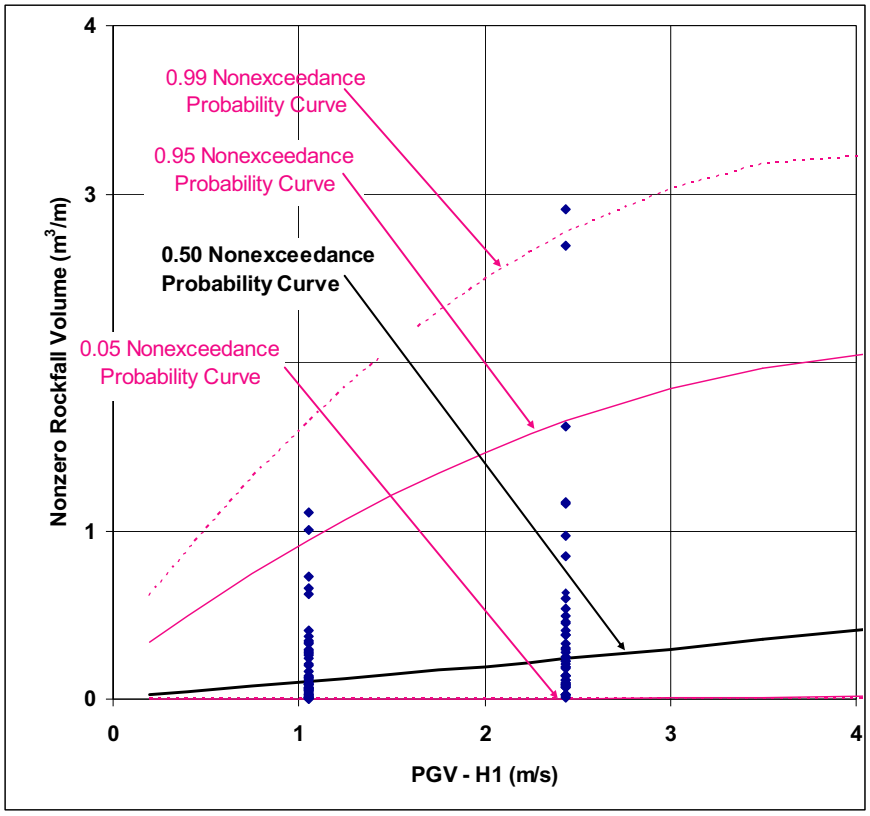

Source: Output DTN: MO0703PASDSTAT.001, worksheet "Gamma Abstractions" in the file *Nonlith Rockfall Abstraction.xls.*

Figure 6-63. Comparison of Percentiles on the Gamma Distributions for Conditional Nonlithophysal Rock Volumes

6.7.2.5 Damage from Multiple Events

Nonlithophysal rockfall volume from a seismic event is constant throughout the nonlithophysal units of the repository. That is, there is no spatial variability in the rockfall volume. The nonlithophysal rock volume from multiple seismic events is defined as the sum of the volumes from the individual seismic events. This approach provides a reasonable representation for the accumulation of failed rock over time. It is possible that the host rock might become weakened after a seismic event that causes partial collapse of the drift. However, a study of drift stability due to the effect of time-dependent rock joint degradation concluded that joint strength degradation has a minor impact on drift stability and produces only a slight increase in rockfall volume (BSC 2004 [DIRS 166107], Section 6.3.1.5 and p. ix in the Executive Summary). It is then reasonable to expect that weakening of rock joints from prior seismic events does not have a significant impact on rockfall volumes in nonlithophysal units.

6.7.2.6 Fraction of Filled Drift

The fraction of a drift that is filled with nonlithophysal rockfall is defined as the total rockfall volume (from multiple seismic events) divided by the effective drift volume after collapse. The recommended range of bulking factors for the nonlithophysal rock is 0.1 to 0.4 (see

Assumption 5.3, Section 5), identical to the range for lithophysal rock. The volume of intact nonlithophysal rock blocks that can fill the open volume within the drift is (12 m^3/0.4) = 30 m^3 to (12 m^3/0.1) = 120 m^3 of intact nonlithophysal rock blocks per meter of emplacement drift. The uncertainty in the volume of intact nonlithophysal rock corresponding to complete drift collapse is represented as a uniform distribution between 30 m^3 to 120 m^3 per meter of emplacement drift, identical with the distribution for lithophysal rockfall.

6.7.3 Analysis of Drip Shield Separation

6.7.3.1 Axial Separation of Adjacent Drip Shields

Drip shield separation is defined as an axial gap or space between two adjacent drip shields that allows in-drift seepage to flow directly onto a waste package. Axial separation is important because it negates the functionality of the drip shield as a barrier to seepage and rockfall for the waste package. Axial separation could occur during a ground motion because of high plastic deformation in the drip shield's connector subassemblies or because of large relative vertical displacements between adjacent drip shields. For example, drip shields could separate if the connector guides securing adjacent drip shields are torn loose from the drip shield plates. Alternately, a large relative vertical displacement between adjacent drip shields would disconnect the connector guides, allowing axial displacement to separate the drip shields.

Axial separation of adjacent drip shields is excluded from the compliance case for the TSPA-LA because: (1) ground motion amplitudes that are sufficient to cause axial separation are also large enough to partially or completely collapse drifts in the repository, (2) rockfall occurs within the first second or two of the arrival of these large amplitude ground motions, and (3) a kinematic study indicates that small static loads from rubble or frictional loads between EBS components are sufficient to eliminate axial separation of drip shields. In this situation, rockfall provides restraints on the motion of the drip shields, preventing differential motion that could lead to separation.

Ground motion amplitudes near and above the 2.44-m/s PGV level are large enough to cause large rockfall volumes in both the lithophysal and nonlithophysal zones. In the lithophysal zones, Table 6-30 indicates that the mean rubble volume at the 1.05 m/s and 2.44 m/s PGV levels is 7.47 m^3/m and 80.94 m^3/m of drift, respectively. Graphically, Figure 6-57 indicates large lithophysal rubble volumes starting at the 1 m/s PGV level. These rubble volumes provide a constraint on the sidewalls of the drip shield and may also cover to crown of the drip shield. In the nonlithophysal zones, Table 6-31 indicates that the mean rockfall volumes are smaller: 0.235 m^3/m and 0.458 m^3/m of drift at the 1.05 m/s and 2.44 m/s PGV levels, respectively. While the rockfall volumes in the nonlithophysal units are smaller than in the lithophysal units, they will still provide a constraint on the sidewalls of the drip shield.

Smaller, more frequent seismic events will also provide rockfall around the drip shield (see Figures 6-57 and 6-63). These smaller events can contribute to the buildup of rockfall around the drip shield from multiple seismic events, as described in Sections 6.7.1 and 6.7.2. It is reasonable to expect that some rubble would exist in the drift and provide some confinement for the drip shield prior to the occurrence of a high amplitude, very low probability ground motion that could potentially result in axial separation of adjacent drip shields.

The caving in the lithophysal rock is coincident with the arrival of the first strong ground motion (i.e., collapse occurs within seconds of the arrival of the first pulse of the accelerogram (BSC 2004 [DIRS 166107], Section 6.4.2.2.2)). Large blocks also start to fall from the drift walls in the nonlithophysal zones shortly after the arrival of the ground motion (BSC 2004 [DIRS 166107], Section 6.3.1.6.1).

Structural response calculations for the drip shield in response to vibratory ground motion have been performed with a detailed three-dimensional finite-element representation of the drip shield geometry that takes into account elastic and inelastic deformation of the structural components of the drip shield, and drip shield interaction with the waste package and the emplacement pallet. Three interlocked drip shields are included in the analysis with rigid longitudinal boundaries (moving synchronously with the far-field) on each end of the drip shield chain. The analyses have demonstrated that the drip shields do not separate for the 2.44 m/s ground motions; identified as the 1×10^{-6} ground motions in *Mechanical Assessment of the Drip Shield Subject to Vibratory Motion and Dynamic and Static Rock Loading* (BSC 2004 [DIRS 169753], Section 5.3.3.2.2).

It follows that the drip shield is partly surrounded by rockfall at PGV levels that are below the levels with the potential for causing separation, and this rockfall occurs within the first few seconds of the ground motion. The larger rock blocks or the lithophysal rubble provide normal and shear confinement to the sidewalls and possibly the crown of the drip shield. The horizontal acceleration imparted to the drip shield by the ground motion will be resisted by the weight of the rockfall and by the frictional forces between the rock and the drip shield plates and between the footings and the invert. The exterior bulkheads on the sidewalls of the drip shield provide an additional physical restraint or "locking" mechanism between the drip shield and rubble that will constrain axial movement. Thus, the presence of rockfall around the drip shields will restrict the relative displacements that are required to separate adjacent drip shields, so that separation is not expected to occur, even for extreme ground motions.

A kinematic study of drip shield motion (BSC 2004 [DIRS 169753], Sections 5.3.1.1 and 5.3.3.1) has confirmed that a relatively small amount of rubble can constrain the asynchronous motion of the drip shields and prevent drip shield separation. This study considers the kinematic response of multiple drip shields in a single emplacement drift under vibratory ground motion. Analyses were conducted for emplacement drifts that are open, partly filled with collapsed rock, and completely filled with collapsed rock. The drip shields remain connected for almost all cases, even for open drifts with ground motions at the 5.35-m/s PGV level, beyond the maximum PGV level on the bounded hazard curve. Separation is only observed in the very unrealistic case that there is no metal-to-metal friction, an open drift, and the 5.35-m/s PGV ground motion. However, the kinematic calculations demonstrate that a small weight of rock or a small amount of friction force is sufficient to stabilize the motion of the drip shields and prevent drip shield separation. Since rockfall in the lithophysal or nonlithophysal zones occurs at PGV levels substantially lower than the 5.35-m/s PGV level that results in drip shield separation, and since smaller, more frequent seismic events may also provide rockfall around the drip shield, the weight of the rockfall and the associated friction forces will prevent drip shield separation.

6.7.3.2 Vertical Displacements between Adjacent Drip Shields

Small relative vertical displacements between adjacent drip shields may also occur during vibratory ground motion. Vertical separation of adjacent drip shields is excluded from the compliance case for the TSPA-LA because it will be limited by the same physical mechanisms discussed in Section 6.7.3.1: (1) ground motion amplitudes above the 1 m/s PGV level are sufficient to generate rubble and rockfall volumes that provide a constraint on the sidewalls of the drip shield, (2) rockfall occurs within the first second or two of the arrival of the ground motions, and (3) a kinematic study indicates that small static loads from rubble or frictional loads between EBS components are sufficient to eliminate significant relative displacements between adjacent drip shields. In addition, the drip shield connector subassembly provides a 320-mm-long (12.6-inch-long) overlap at the joint between adjacent drip shields (SNL 2007 [DIRS 179354], Table 4-2, Item Number 07-01). This overlap will protect the waste package from direct seepage and direct rockfall that might result from a vertical displacement of a few inches between adjacent drip shields.

The buckling of the sidewalls of the drip shield, discussed in Section 6.8.3, provides an alternate mechanism with the potential to generate a vertical displacement between adjacent drip shields. Buckling occurs when the static load from rockfall is amplified by the dynamic load from vibratory ground motion. As shown in Figure 6-73, the probability of sidewall buckling is essentially zero with 10% rockfall load until the drip shield components have been thinned to a 2-mm thickness. On the other hand, the probability of sidewall buckling is much greater with 50% and 100% rockfall loads (compare Figure 6-74 with Figures 6-75 and 6-76). It follows that buckling will occur when drifts are filled with a significant volume of rubble or rockfall, and that this rubble and rockfall will again restrict the relative vertical displacements between adjacent drip shields for the reasons discussed above. Two additional considerations are as follows:

- The drip shield connector plate and drip shield connector guide (see Figure 6-3) provide a mechanical connection that transmits the load from one drip shield onto its overlapped neighbor. While this is a one-sided connection, it tends to spread the dynamic load, thereby reducing shield-to-shield variability in mechanical response.

- If the drip shield becomes tilted after the sidewalls buckle, the drip shield connector plate and the connector guide on the top of the drip shield (see Figure 6-3) provide a physical barrier that will divert seepage away from the center of the crown and towards the sidewalls of the drip shield.

The combined effects of a significant volume of rubble and rockfall for buckling and the presence of the drip shield connector plate and connector guides make it reasonable to exclude vertical displacement of adjacent drip shields from the compliance case for the TSPA-LA.

6.8 DRIP SHIELD FRAGILITY

The fragility analysis for the drip shield defines its probability of failure as a function of the thickness and plastic load capacity of the drip shield components, the static rockfall load on the drip shield, and the vertical component of peak ground acceleration (PGA) for the seismic event. Fragility curves are developed for two modes of failure: (1) rupture or tearing of the drip shield

plates and (2) buckling or collapse of the sidewalls and/or crown of the drip shield. A third failure mode from waste package impacts to the drip shield is considered but not incorporated into the TSPA, as explained in Section 6.8.5.

6.8.1 Mathematical Formulation for Fragility Analysis

The key parameters for the fragility analysis are the vertical component of PGA from a seismic event, the static load of rockfall on the crown of the drip shield, and the plastic load capacity of the drip shield plate or framework. This section describes the approach to representing each of these key parameters, followed by the mathematical formulation for the fragility analysis.

The fragility analysis is based on the vertical component of PGA because the peak vertical acceleration is expected to be directly correlated with buckling of the legs or rupture of the plates forming the crown of the drip shield. This viewpoint is confirmed by calculations for lithophysal rockfall loads on the drip shield. These calculations demonstrate that the average loads on the crown are significantly greater than the average loads on the sidewalls of the drip shield (BSC 2004 [DIRS 166107], Table P-9), indicating that vertical loads are likely to be the critical loads for failure.

The bounded hazard curve (see Section 6.4) defines the value of horizontal PGV for each seismic event, rather than the vertical component of PGA. The vertical component of PGA must be defined by a probability distribution that is conditional on the PGV level for a seismic event. The vertical component of PGA is referred to as the peak vertical acceleration in this section. It is denoted as the variable A in the following analysis and has the unit of "g's." The conditional probability distribution for peak vertical acceleration is defined in Section 6.8.1.1.

The static load from rockfall is based on lithophysal rubble because the static lithophysal load is an upper bound relative to the static load from nonlithophysal rockfall. Rockfall in lithophysal rock has significantly greater volume (see Figure 6-58 and Section 6.7.2.1) than rockfall in nonlithophysal rock, resulting in greater static loads from lithophysal rockfall at a given point in time. The load from lithophysal rubble is treated as uniform on the crown of the drip shield because the typical particulate sizes in the lithophysal rubble, on the order of 0.2 meters, are less than the typical dimensions of the drip shield plates. For example, the half-span across the drip shield is ½ (2,535 mm) or approximately 1.3 m (SNL 2007 [DIRS 179354], Table 4-2, Item Number 07-01 for external width at base of drip shield), much greater than the typical dimensions of rubble particulates. The probability distribution for the static load from lithophysal rubble, denoted as P_{STAT}, is defined in Section 6.8.1.2.

The plastic load capacity is the vertical load on the top of the drip shield that causes plastic failure. Failure can occur if the vertical load pushes individual plates through the framework beneath the top of the drip shield, causing ultimate tensile failure of the plates. Failure can also occur if the vertical load causes the sidewalls or framework of the drip shield to buckle. The vertical load is conceptualized to be a uniform load on the top of the drip shield, as explained in the preceding paragraph. The plastic load capacity of the drip shield plates and of the drip shield framework is defined in Sections 6.8.2.1 and 6.8.3.2, respectively.

The fragility analysis is based on a comparison of the dynamic vertical load on the drip shield with the plastic load capacity. The dynamic vertical load is the sum of two factors: the static load from rockfall and the dynamic amplification of the static load. The static load from rockfall on top of the drip shield is represented as L_{STAT}. The dynamic amplification is defined by the vertical component of peak ground acceleration during the ground motion, denoted as *PGA-V*. *PGA-V* is in the unit of "g's" of acceleration for this analysis, where *g* is the acceleration of gravity. The total dynamic load is approximated as the sum of the static rockfall load and the dynamic amplification of the static load: $L_{STAT} + L_{STAT}\ (PGA\text{-}V)/g = L_{STAT}(1 + (PGA\text{-}V)/g)$. The plastic load capacity is denoted as L_{CAP}.

When the dynamic vertical load is greater than the plastic load capacity, the drip shield will fail by plate rupture or buckling. When the dynamic vertical load is less than the plastic load capacity, the drip shield may deform plastically but will not fail by plate rupture or buckling. The failure criterion for the fragility analysis can then be written as:

$$L_{STAT}\left(1+\frac{(PGA-V)}{g}\right) > L_{CAP} \qquad \text{(Eq. 6.8-1)}$$

Defining *A* as the nondimensional acceleration (*PGA-V*)/*g*, Equation 8.6-1 can be rewritten as:

$$(1+A) > \frac{L_{CAP}}{L_{STAT}} = \frac{P_{CAP}}{P_{STAT}} \qquad \text{(Eq.6.8-2)}$$

where P_{CAP} represents the pressure on top of the drip shield that results in the equivalent plastic load at capacity, and P_{STAT} represents the pressure on top of the drip shield that is equivalent to the static rockfall load. The use of P_{CAP} and P_{STAT} is appropriate in Equation 6.8-2 because the computational results for plastic load capacity and for static rockfall load are generally reported as a pressure on the top of the drip shield, rather than a load. The parameters *A*, P_{CAP}, and P_{STAT} are represented as random variables with log-normal probability distributions, as explained later in this section. The cumulative distribution functions for these random variables can then be written as:

$$\begin{aligned} p_{ne}(A) &= cdf_N\left(\ln(A), \lambda_A, \beta_A\right) \\ p_{ne}(P_{CAP}) &= cdf_N\left(\ln(P_{CAP}), \lambda_{CAP}, \beta_{CAP}\right) \\ p_{ne}(P_{STAT}) &= cdf_N\left(\ln(P_{STAT}), \lambda_{STAT}, \beta_{STAT}\right) \end{aligned} \qquad \text{(Eq. 6.8-3)}$$

where p_{ne} is the nonexceedance probability, cdf_N is the cumulative distribution function for a normal distribution, λ_x is the expected value of $ln(x)$, and β_x is the standard deviation of $ln(x)$, where *x* denotes *A*, *CAP*, or *STAT*. $p_{ne}(A)$ is conditional on the value of *PGV* because λ_A is defined as a least-squares fit with a linear function of $ln(PGV)$, as shown in Section 6.8.1.1. $p_{ne}(P_{STAT})$ is a function of the fraction of drift filled with lithophysal rubble, as discussed in Section 6.8.1.2. $p_{ne}(P_{CAP})$ is conditional on the thickness of the drip shield components because λ_{CAP} and β_{CAP} are dependent on the thickness, as shown in Sections 6.8.2.1 and 6.8.3.2.

The failure criterion in Equation 6.8-2 is based on the ratio of P_{CAP} to P_{STAT}. The quotient of two log-normally distributed random variables is also log-normally distributed because the sum (or difference) of independent normally distributed random variables is also normally distributed with a mean equal to the sum of the means and a variance equal to the sum of the individual variances (Hahn and Shapiro 1967 [DIRS 146529], p. 186). Applying this theorem to the ratio of P_{CAP} to P_{STAT}, the mean, λ, and standard deviation, β, for the ratio of P_{CAP} to P_{STAT} are defined as:

$$\lambda = \lambda_{CAP} - \lambda_{STAT} \quad \text{(Eq. 6.8-4)}$$

and

$$\beta = \sqrt{\beta_{CAP}^2 + \beta_{STAT}^2} \quad \text{(Eq. 6.8-5)}$$

The probability of the criterion in Equation 6.8-2 being satisfied (and resulting in failure) during a seismic event with a given value of PGV is evaluated as follows. First, the probability of the peak vertical acceleration being within a small interval dA centered on the value of A is given by:

$$p_{ne}(A + 0.5dA) - p_{ne}(A - 0.5dA) = \frac{dp_{ne}(A)}{dA} dA \quad \text{(Eq. 6.8-6)}$$

This value of A results in failure whenever P_{CAP}/P_{STAT} is less than $(1+A)$. The cumulative probability of P_{CAP}/P_{STAT} being less than $(1+A)$ is given by:

$$p_{ne}(1 + A) = cdf_N\left(\ln(1 + A), \lambda, \beta\right) \quad \text{(Eq. 6.8-7)}$$

which incorporates the mean and standard deviation from Equations 6.8-4 and 6.8-5. The probability that the peak vertical acceleration has the value A within the interval dA and that this value of A results in failure is given by the product of the probabilities in Equations 6.8-6 and 6.8-7:

$$cdf_N\left(\ln(1 + A), \lambda, \beta\right)\frac{dp_{ne}(A)}{dA} dA \quad \text{(Eq. 6.8-8)}$$

The total probability of failure, P_{TOT}, is then the integral of Equation 6.8-8 over all possible values of A during a seismic event with a given value of PGV:

$$P_{TOT} = \int_0^\infty cdf_N\left(\ln(1 + A), \lambda, \beta\right)\frac{dp_{ne}(A)}{dA} dA \quad \text{(Eq. 6.8-9)}$$

P_{TOT} is evaluated numerically by defining finite intervals for the peak vertical acceleration based on the points $\{A_i\}$, i = 0, 1, 2, …., n. The probability that the peak vertical acceleration has a value within the ith interval, $[A_{i-1}, A_i]$, is given by:

$$p_{ne}(A_i) - p_{ne}(A_{i-1}) = cdf_N\left(\ln(A_i), \lambda_A, \beta_A\right) - cdf_N\left(\ln(A_{i-1}), \lambda_A, \beta_A\right) \quad \text{(Eq. 6.8-10)}$$

and the probability that the mean value of A in this interval, $\overline{A}_i$, causes failure is given by:

$$cdf_N\left(\ln(1+\overline{A}_i),\lambda,\beta\right) \quad \text{(Eq. 6.8-11)}$$

The total probability of failure, P_{TOT}, is then approximated by:

$$P_{TOT} \approx \sum_{i=1}^{n}\left(\left(p_{ne}(A_i)-p_{ne}(A_{i-1})\right)cdf_N\left(\ln(1+\overline{A}_i),\lambda,\beta\right)\right) \quad \text{(Eq. 6.8-12)}$$

6.8.1.1 Conditional Probability Distribution for Peak Vertical Acceleration

The PGA is defined by a conditional probability distribution that is a function of horizontal PGV, denoted as PGV-H1 in the tables and plots. Table 6-33 presents the peak vertical acceleration, denoted as *A*, for 17 ground motions at the 1.05 m/s, 2.44 m/s, and 5.35 m/s PGV levels. Table 6-33 also lists the standard deviation of *ln*(*A*), as calculated in worksheet "PGV-H1 to PGA-V Correlation" in the file *Plate Fragility Analysis.xls* in output DTN: MO0703PASDSTAT.001. The standard deviation of *ln*(*A*) varies between 0.66 and 0.80, indicating that there is a wide range of values for the PGA at a given PGV level. These values also indicate that the correlation is homoskedastic (i.e., the standard deviation is approximately constant as a function of PGV) because the standard deviation of *ln*(*A*) is approximately constant with PGV. The homoskedastic behavior allows a more classic approach than some of the other abstractions.

Figure 6-64 presents the least-squares fit to the values of *ln*(*A*) as a function of *ln*(PGV-H1). The equation for the least-squares fit in Figure 6-64 defines λ_A as a function of *PGV-H1*:

$$\lambda_A = 1.1079 ln(PGV\text{-}H1) + 0.3514 \quad \text{(Eq. 6.8-13)}$$

The value of β_A, which is defined as the standard deviation of the residuals of *ln*(*A*) with respect to the least-squares fit at the three PGV levels, is constant:

$$\beta_A = 0.700 \quad \text{(Eq. 6.8-14)}$$

(numerical calculation in worksheet "PGV-H1 to A Correlation" in the file *Plate Fragility Analysis.xls* in output DTN: MO0703PASDSTAT.001).

Figure 6-65 is a Q-Q plot for a normal distribution versus the residuals of *ln*(*A*) relative to Equation 6.8-13. Figure 6-65 demonstrates that a normal distribution provides an excellent representation for the conditional probability distribution of *ln*(*A*) relative to the least squares fit in Equation 6.8-13 with the constant value of β_A defined in Equation 6.8-14. This result confirms that the conditional probability distribution for *A* as a function of PGV-H1 is log-normal, as stated in Section 6.8.1. Figure 6-66 confirms that this log-normal distribution provides a reasonable representation for the peak vertical acceleration in physical space.

Table 6-33. Data for Peak Vertical Acceleration as a Function of Horizontal PGV

Ground Motion No.	PGV-H1 (m/s)	*A* (g's)	PGV-H1 (m/s)	*A* (g's)	PGV-H1 (m/s)	*A* (g's)
1	1.046	2.630	2.441	4.903	5.353	13.148
2	1.046	4.146	2.441	7.296	5.353	19.563
3	1.046	3.615	2.441	6.528	5.353	17.504
4	1.046	1.451	2.441	4.489	5.353	12.038
5	1.046	2.009	2.441	3.086	5.353	8.276
6	1.045	1.603	2.441	3.180	5.353	8.528
7	1.045	2.609	2.447	7.808	5.362	20.936
8	1.046	1.756	2.441	3.760	5.351	10.081
9	1.046	6.812	2.442	12.875	5.352	34.524
10	1.046	1.650	2.440	3.554	5.352	9.530
11	1.046	1.635	2.441	3.002	5.352	8.050
12	1.045	0.554	2.441	1.461	5.354	3.918
13	1.046	1.398	2.441	3.145	5.353	8.434
14	1.046	0.818	2.442	3.385	5.353	9.077
15	1.046	0.243	2.441	0.859	5.353	2.303
16	1.046	1.049	2.441	2.570	5.353	6.892
17	1.046	0.683	2.445	1.511	5.353	4.001
Standard Deviation of *ln*(*A*) (-)		0.801		0.664		0.665

Sources: DTN: MO0402AVDTM105.001 [DIRS 168890], PGV-H1 from file *matxh1.vts* in *vts.zip*, where x = 01, 02, 03, …, 16, and 17.

DTN: MO0403AVDSC106.001 [DIRS 168891], PGV-H1 from file *matxh1.vts* in *vts.zip*, where x = 01, 02, 03, …, 16, and 17.

DTN: MO0403AVTMH107.003 [DIRS 168892], PGV-H1 from file *matxh1.vts* in *vts.zip*, where x = 01, 02, 03, …, 16, and 17.

Output DTN: MO0702PAFRAGIL.000, *A* (*PGA-V)* from files *MATxV_105.xls*, *MATxV_244.xls*, and *MATxV_535.xls*, where x = 01, 02, 03, …., 16, and 17.

Logarithmic standard deviation at each PGV-H1 level is calculated in output DTN: MO0703PASDSTAT.001, cells K49:K51, in worksheet "PGV-H1 to A Correlation" in *Plate Fragility Analysis.xls.*

NOTES: Values for PGV have been converted from cm/s to m/s by dividing by 100.
"*A*" denotes the vertical component of the peak ground acceleration.

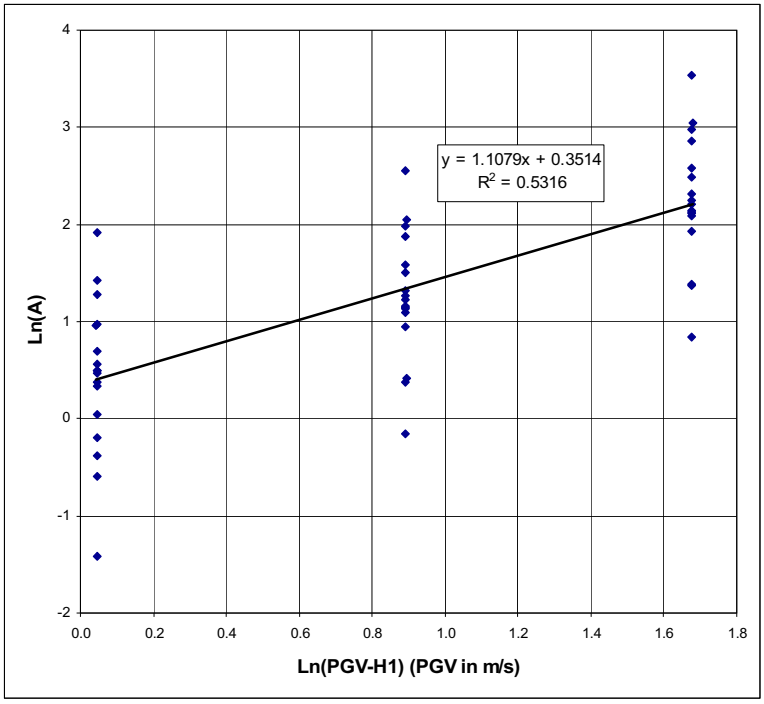

Source: Output DTN: MO0703PASDSTAT.001, worksheet "PGV-H1 to A Correlation" in the file *Plate Fragility Analysis.xls*.

NOTE: *A* is defined as (*PGA-V*)/*g*, where *PGA-V* is the vertical component of PGA and *g* is the acceleration of gravity.

Figure 6-64. Correlation of Peak Vertical Acceleration with PGV-H1

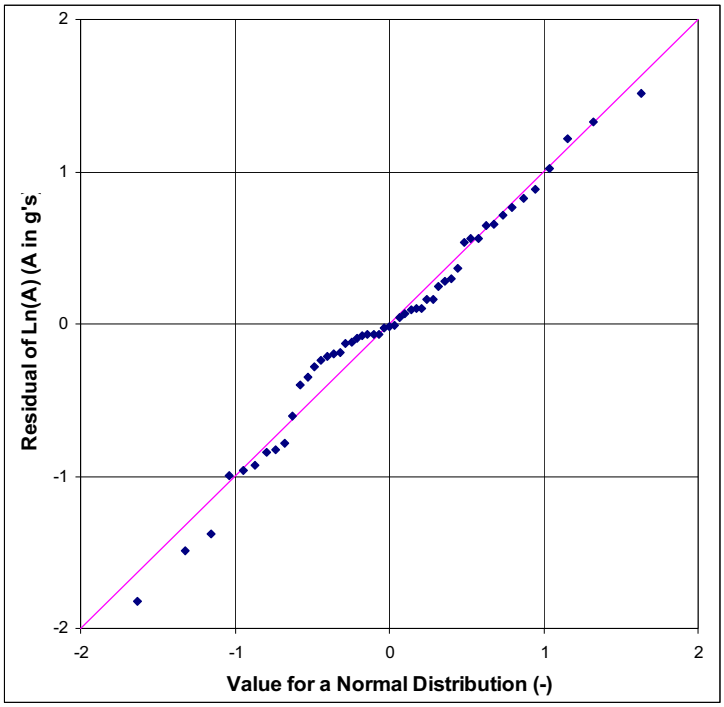

Source: Output DTN: MO0703PASDSTAT.001, worksheet "PGV-H1 to A Correlation" in the file *Plate Fragility Analysis.xls*.

Figure 6-65. Q-Q Plot for a Normal Distribution versus the Residuals of $ln(A)$ with Respect to the Least-Squares Fit, λ_A

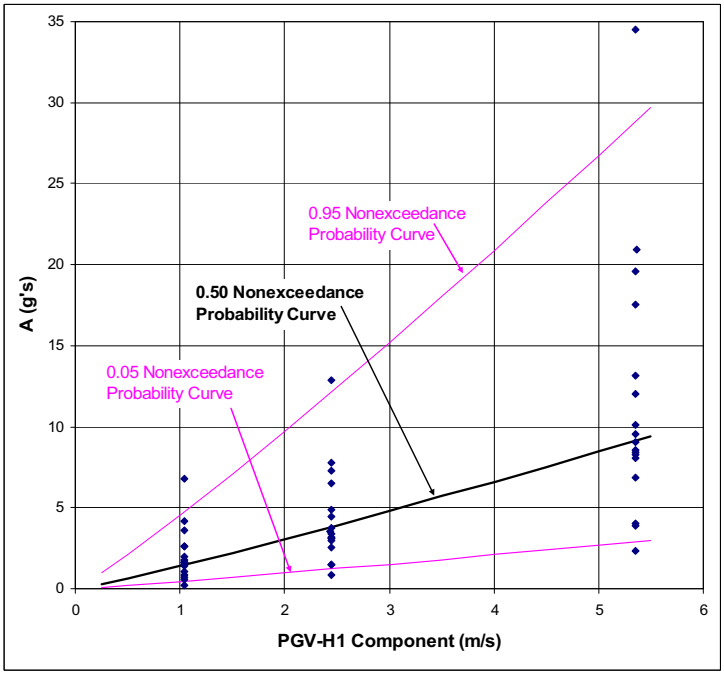

Source: Output DTN: MO0703PASDSTAT.001, worksheet "PGV-H1 to A Correlation" in the file *Plate Fragility Analysis.xls*.

Figure 6-66. Comparison of Percentiles on the Log-Normal Distributions with Peak Vertical Acceleration

6.8.1.2 Probability Distribution for Lithophysal Rubble Load

Lithophysal rockfall is expected to vary significantly because of the variability in mechanical properties in the host rock at the repository horizon and because of the variability in the fracture pattern and fracture spacing in the host rock. As the lithophysal rock mass fails, pre-existing and new fractures will break, forming block sizes of relatively small volume. The falling rubble will come to rest on the invert of the drift and the drip shield. A two-dimensional discontinuum numerical approach has been applied to represent the fractured rock mass and to determine the ultimate load on the drip shield from the lithophysal rubble (BSC 2004 [DIRS 166107], Section 6.4.2.5.1). The rock mass is represented as an assembly of polygonal blocks of random shape but with a defined average dimension (approximately 0.2 m). The resulting rockfall loads on the drip shield from lithophysal rubble have been evaluated with six quasi-static realizations for drift collapse in lithophysal rock (BSC 2004 [DIRS 166107], Section 6.4.2.5.1, Numerical Discontinuum Approach). Each of the six realizations is based on a different random block geometry.

The drip shield is represented as an elastic structure in which the contact between its footings and the invert are free to slide (frictional) or to separate from the invert if forces dictate. The elastic stiffness of the two-dimensional drip shield has been calibrated to be equivalent to the deformability of a three-dimensional representation for the drip shield framework. The drip shield is represented by 30 segments (i.e., finite elements), starting at segment number 1 at the right-hand footing. Segments number 11 through 20 represent the curved crown of the drip shield. A full description of the structural model for the drip shield is provided in *Drift Degradation Analysis* (BSC 2004 [DIRS 166107], Section 6.4.2.5.1, Numerical Discontinuum Approach).

The resultant pressure on segments 11 through 20 at quasi-static equilibrium for these six realizations is presented in Table 6-34 (DTN: MO0407MWDDSLCR.000 [DIRS 170873], File *final drip shield quasi-static pressures.xls*). The mean and standard deviation of the natural logarithm of the average pressure on the crown of the drip shield in a collapsed drift are:

$$\lambda_{STAT} = 11.749 \qquad \text{(Eq. 6.8-15)}$$

and

$$\beta_{STAT} = 0.149 \qquad \text{(Eq. 6.8-16)}$$

Table 6-34. Data for Average Rockfall Pressure on the Crown of the Drip Shield

Segment No. (-)	Pressure Real 1 (Pa)	Pressure Real 2 (Pa)	Pressure Real 3 (Pa)	Pressure Real 4 (Pa)	Pressure Real 5 (Pa)	Pressure Real 6 (Pa)
11	2.466×10^{03}	7.790×10^{04}	5.219×10^{05}	2.549×10^{03}	2.389×10^{04}	0.000×10^{00}
12	1.373×10^{05}	9.381×10^{04}	6.983×10^{03}	2.280×10^{05}	6.474×10^{03}	1.463×10^{05}
13	1.850×10^{03}	2.755×10^{05}	1.369×10^{03}	6.830×10^{04}	1.966×10^{05}	1.513×10^{05}
14	2.339×10^{05}	1.037×10^{05}	1.984×10^{05}	6.566×10^{04}	1.438×10^{05}	1.293×10^{05}
15	3.072×10^{03}	4.556×10^{04}	3.396×10^{05}	0.000×10^{00}	5.439×10^{04}	1.788×10^{05}
16	3.033×10^{04}	7.905×10^{02}	5.462×10^{03}	3.252×10^{05}	5.622×10^{05}	2.543×10^{04}
17	6.782×10^{05}	1.258×10^{05}	1.987×10^{05}	1.138×10^{05}	0.000×10^{00}	2.776×10^{03}

Table 6-34. Data for Average Rockfall Pressure on the Crown of the Drip Shield (Continued)

Segment No. (-)	Pressure Real 1 (Pa)	Pressure Real 2 (Pa)	Pressure Real 3 (Pa)	Pressure Real 4 (Pa)	Pressure Real 5 (Pa)	Pressure Real 6 (Pa)
18	0.000×10^{00}	1.696×10^{05}	9.350×10^{04}	3.015×10^{04}	4.419×10^{03}	1.591×10^{05}
19	2.018×10^{03}	0.000×10^{00}	1.802×10^{05}	4.638×10^{05}	1.355×10^{05}	3.457×10^{05}
20	0.000×10^{00}	5.780×10^{05}	2.002×10^{03}	0.000×10^{00}	0.000×10^{00}	0.000×10^{00}
Avg. Crown Pressure[1]	1.089×10^{05}	1.471×10^{05}	1.548×10^{05}	1.297×10^{05}	1.127×10^{05}	1.139×10^{05}
Ln(Avg. Crown Pressure)	11.60	11.90	11.95	11.77	11.63	11.64
Mean of Ln(Avg. Crown Pressure), λ_{STAT}			11.749			
Standard Deviation of Ln(Avg. Crown Pressure), β_{STAT}			0.149			

[1] Sample average crown pressure calculation for Realization 1:
(2,466 + 137,300 + 1,850 + 233,900 + 3,072 + 30,330 + 678,200 + 0 + 2,018 + 0)/10 = 108,900.

Source: MO0407MWDDSLCR.000 [DIRS 170873], Rows 14 through 23 in worksheet "data" in file *final drip shield quasi-static pressures.xls*.

NOTES: Average crown pressure is the average for segments 11 through 20 on the crown of the drip shield. Average crown pressure has been rounded to four significant digits. The mean and standard deviation of the natural logarithm of the average crown pressures are calculated in worksheet "Load and Capacity" in the file *Plate Fragility Analysis.xls* in output DTN: MO0703PASDSTAT.001.

(-) = dimensionless.

Figure 6-67 is a Q-Q plot for a normal distribution versus the residuals of the logarithm of the average rockfall pressure relative to λ_{STAT}. Figure 6-67 demonstrates that a normal distribution provides a reasonable representation for the probability distribution of *ln*(*Average Crown Pressure*) for a fully collapsed drift, confirming that P_{STAT} follows a log-normal distribution.

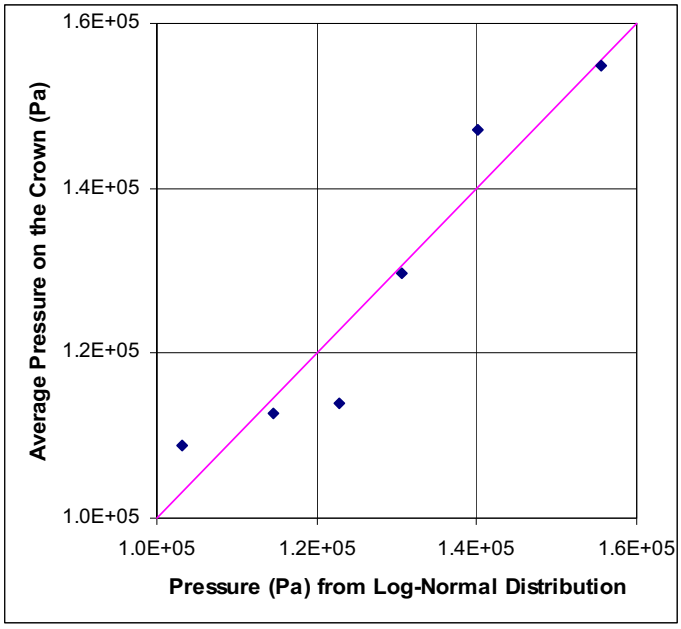

Source: Output DTN: MO0703PASDSTAT.001, worksheet "Load and Capacity" in the file *Plate Fragility Analysis.xls*.

Figure 6-67. Q-Q Plot for a Log-Normal Distribution versus the Residuals of the Logarithm of Average Pressure with λ_{STAT}

The accumulated volume from multiple seismic events is defined as the sum of the rockfall volumes from the individual events, as discussed in Section 6.7.1.4. This accumulated rubble may partly or completely fill the free volume in the drift, as discussed in Section 6.7.1.5. The fraction of the drift that is filled with rubble is defined as the ratio of the accumulated rubble volume to the volume of rubble that is required to completely fill the free volume in the drift. This latter quantity is a function of the bulking factor of the rubble, and is an uncertain parameter for the TSPA.

The rockfall load in a drift that is partly filled with rubble is defined as the product of the fraction of drift filled with rubble and the rockfall load for a fully collapsed drift. This is a reasonable approach that tends to overestimate the vertical loads on the drip shield for small rubble volumes. Small amounts of rubble will tend to settle around the sides of the drip shield, leaving the crown uncovered with no static rockfall load. However, the definition for load in a partly-filled drift always has a static rockfall load on the crown of the drip shield, providing a slight overestimate of the rockfall load. The numerical calculations in Section 6.8.2.2 for the fragility analysis consider three fractions of a filled drift: 10%, 50%, and 100%.

6.8.2 Fragility of the Drip Shield Plates

6.8.2.1 Ultimate Plastic Capacity of the Plates

Finite-element calculations have been performed to define the plastic (nonlinear) load-bearing capacity of the curved plates on the crown of the drip shield (SNL 2007 [DIRS 178851], Section 6.4.4). These calculations define the magnitude of the uniform load that causes an element of the plate to exceed the ultimate tensile strain of Titanium Grade 7. The plates are initially 15 mm thick. Calculations were performed for 15-mm-, 10-mm-, and 5-mm-thick plates to represent degraded states of the system.

The boundary conditions on the plate are a major uncertainty in the analysis. The rockfall loads on the plates may be nonuniform, producing an asymmetric response between the sides of the plate. The welds between the plates and the underlying framework may also constrain displacement and rotation of the plates to varying degrees. The resulting response of a plate may not match typical boundary conditions, such as fixed or simply supported, because of these effects. The range of potential boundary conditions is represented by considering two options that represent the extremes of the response: (1) a plate that is fixed to maximize the load-bearing capacity, and (2) a plate that is free to move laterally, which tends to minimize the load-bearing capacity. The resulting ultimate plastic loads as a function of plate thickness and boundary condition are presented in Table 6-35 and in Figure 6-68, based on the calculations documented in *Mechanical Assessment of Degraded Waste Packages and Drip Shields Subject to Vibratory Ground Motion* (SNL 2007 [DIRS 178851], Section 6.4.4).

Table 6-35. Data for Plastic Load Capacity of the Drip Shield Plates

Thickness (mm)	Plastic Load Capacity for a Laterally Free BC (Pa)	Plastic Load Capacity for a Fixed BC (Pa)	λ_{CAP} (-)	β_{CAP} (-)
2	236,800	622,700	12.86	0.377
5	739,600	1,086,000	13.71	0.150
10	1,609,000	1,911,000	14.38	0.067
15	2,438,000	2,668,000	14.75	0.035

Source: DTN: MO0701DRIPSHLD.000 [DIRS 182334], File *summary DS plate fragility.xls*, worksheet "limit load."

NOTES: BC = boundary condition.

The values for λ_{CAP} and β_{CAP} at the 5-mm, 10-mm, and 15-mm thicknesses are calculated in worksheet "Load and Capacity" in the file *Plate Fragility Analysis.xls* in output DTN: MO0703PASDSTAT.001. The methodology for these calculations is explained in the last paragraph in this section. The ultimate load at the 2-mm thickness is based on the least-squares fits in Figure 6-68.

(-) = dimensionless.

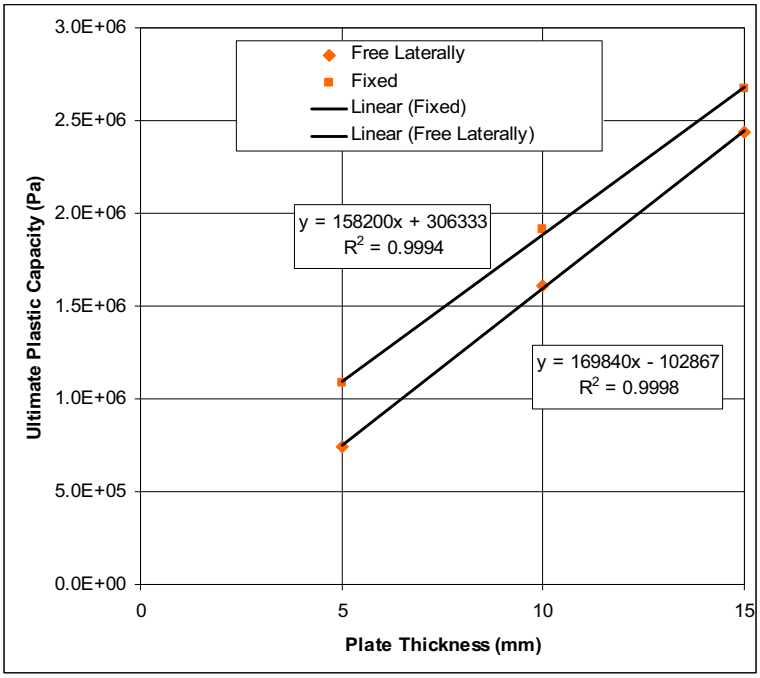

Source: Output DTN: MO0703PASDSTAT.001, worksheet "Load and Capacity" in the file *Plate Fragility Analysis.xls.*

Figure 6-68. Plastic Load Capacity as a Function of Plate Thickness and Boundary Conditions

The results for the fixed and laterally free boundary conditions represent the extremes of the response, corresponding to the 90th and 10th percentiles of a log-normal distribution, respectively. The value of λ_{CAP} is then the average of the natural log of the ultimate plastic capacities for the two boundary conditions at a given thickness. The value of β_{CAP} is given by the difference of the natural log of the ultimate plastic capacities at a given thickness divided by 2(1.2816). The value of 1.2816 is the standard normal variate that corresponds to a cumulative probability of 0.90 on a normal distribution, as calculated by Excel's NORMSINV function. By symmetry, −1.2816 is the standard normal variate that corresponds to a cumulative probability of

0.10 on a normal distribution. The difference in parameter values for the 10th and 90th percentiles is then equal to $2(1.2816)\beta_{CAP}$ for a normal distribution. The calculated values of λ_{CAP} and β_{CAP} are shown in Table 6-35.

6.8.2.2 Numerical Calculations

Numerical integration of Equation 6.8-12 for the total probability of failure has been performed for the following cases:

- PGV levels of 0.2 m/s, 0.4 m/s, 1.05 m/s, 2.44 m/s, and 4.07 m/s, with the values of λ_A and β_A defined by Equations 6.8-13 and 6.8-14
- Plate thicknesses of 2 mm, 5 mm, 10 mm, and 15 mm, with the values of λ_{CAP} and β_{CAP} defined by Table 6-35
- Static rockfall loads for drifts that are 10%, 50%, and 100% filled with lithophysal rock. The values of λ_{STAT} and β_{STAT} for the fully collapsed drift are defined by Equations 6.8-15 and 6.8-16. The value of λ_{STAT} is reduced by $ln(2)$ and $ln(10)$ for drifts that are 50% and 10% filled with lithophysal rubble, respectively. The value of β_{STAT} remains constant at 0.149 for partly or completely filled drifts.

The results of the numerical integrations, which are documented in the file *Plate Fragility Analysis.xls* (output DTN: MO0703PASDSTAT.001), are presented in Table 6-36 and Figures 6-69 to 6-71. Table 6-36 also includes a column for a 0-mm-thick plate in order to encompass the full range of thicknesses for the TSPA. The 0-mm-thick plate is assigned a probability of failure of 1 at any PGV level. The probabilities of failure in Table 6-36 are applied to the lithophysal and nonlithophysal zones throughout the repository (i.e., there is no spatial variability in drip shield failure).

Table 6-36. Probability of Failure for the Drip Shield Plates

	Plate Thickness				
PGV Level (m/s)	**0 mm**	**2 mm**	**5 mm**	**10 mm**	**15 mm**
Probability of Failure with 0% Rockfall Load:					
All	1	0	0	0	0
Probability of Failure with 10% Rockfall Load:					
0.2	1	0	0	0	0
0.4	1	0	0	0	0
1.05	1	0	0	0	0
2.44	1	0.006	0	0	0
4.07	1	0.036	0	0	0
Probability of Failure with 50% Rockfall Load:					
0.2	1	0	0	0	0
0.4	1	0.005	0	0	0
1.05	1	0.083	0.002	0	0
2.44	1	0.377	0.047	0.004	0
4.07	1	0.637	0.182	0.028	0.007

Table 6-36. Probability of Failure for the Drip Shield Plates (Continued)

PGV Level (m/s)	Plate Thickness				
	0 mm	2 mm	5 mm	10 mm	15 mm
Probability of Failure with 100% Rockfall Load:					
0.2	1	0.027	0	0	0
0.4	1	0.093	0	0	0
1.05	1	0.390	0.030	0.001	0
2.44	1	0.765	0.268	0.047	0.013
4.07	1	0.912	0.557	0.186	0.073

Source: Output DTN: MO0703PASDSTAT.001, File *Plate Fragility Analysis.xls*, worksheet "Summary."

NOTE: Probabilities below 0.001 have been rounded down to 0.

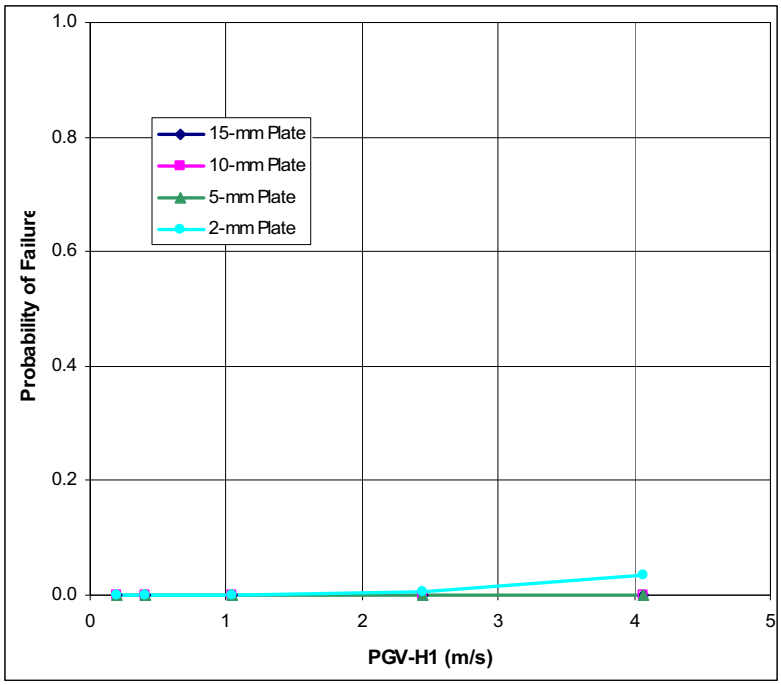

Source: Output DTN: MO0703PASDSTAT.001, worksheet "Summary" in the file *Plate Fragility Analysis.xls.*

NOTE: The probabilities for the 15-mm-thick and 10-mm-thick plates are 0. These data points are hidden by the probabilities for the 5-mm-thick plate.

Figure 6-69. Probability of Failure of the Drip Shield Plates for 10% Rockfall Load

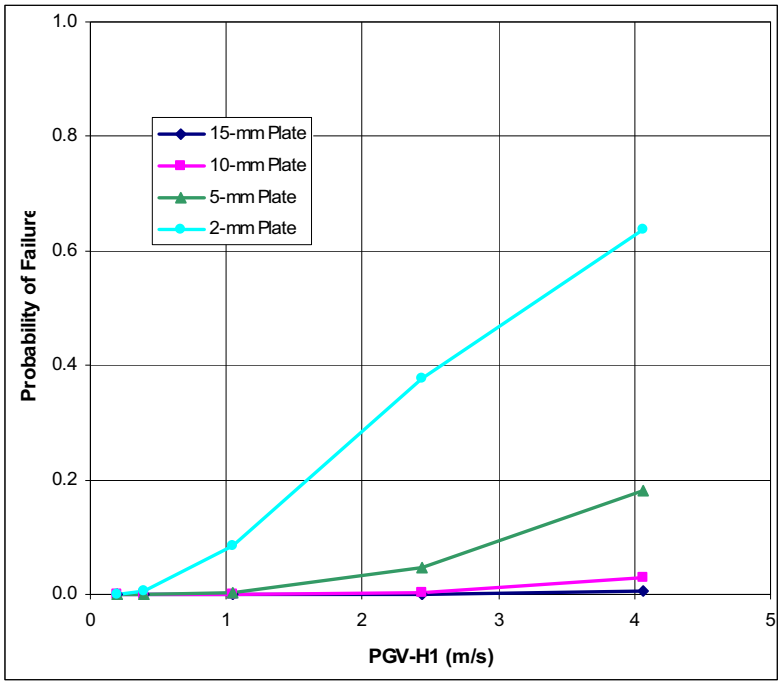

Source: Output DTN: MO0703PASDSTAT.001, worksheet "Summary" in the file *Plate Fragility Analysis.xls.*

Figure 6-70. Probability of Failure of the Drip Shield Plates for 50% Rockfall Load

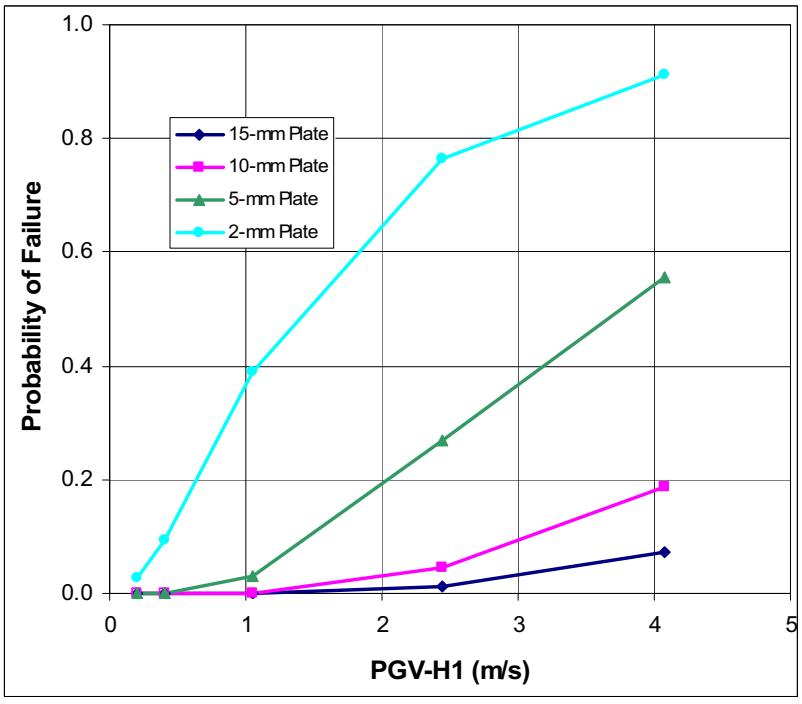

Source: Output DTN: MO0703PASDSTAT.001, worksheet "Summary" in the file *Plate Fragility Analysis.xls.*

Figure 6-71. Probability of Failure of the Drip Shield Plates for 100% Rockfall Load

6.8.3 Fragility of the Drip Shield Framework

6.8.3.1 Failure Mode of the Framework

Quasi-static calculations have been performed to define the failure modes of the drip shield framework (SNL 2007 [DIRS 178851], Section 6.4.4). The failure mode is important for defining the configuration of the drip shield and its relationship to the waste package after failure. Two failure modes were observed in the quasi-static calculations. For the intact drip shield, with no thickness reduction from general corrosion, the observed failure mode is a snap-through of the crown of the drip shield. For degraded states of the drip shield, with 5-mm or 10-mm thickness reductions to all structural elements, the observed failure mode is buckling of the sidewalls of the framework.

It seemed likely that the snap-through failure could be caused by the quasi-static methodology, which tends to intensify loads relative to a dynamic simulation by making them constant in time. In this situation, the snap-through of the crown might not happen for the dynamic response with time-varying ground motions. A series of dynamic calculations were performed using ground motions for the 2.44 m/s and 4.07 m/s PGV levels. Three ground motions were selected for each PGV level because a full suite of 17 ground motions is very computationally intensive. The selected ground motions generally produce significant or maximal response at the given PGV level. Thickness reductions of 0 mm, 5 mm, and 10 mm in the plates and framework of the drip shield were considered.

The dynamic calculations demonstrate that failure occurs through buckling of the sidewalls of the drip shield, rather than snap-through of the crown, in each of the calculations. Based on these results, the failure mode for the fragility analysis for the drip shield framework is buckling or collapse of the sidewalls of the drip shield.

6.8.3.2 Ultimate Plastic Capacity of the Framework

Finite-element calculations have been performed to define the plastic (nonlinear) load-bearing capacity of the drip shield framework with intact plates. These calculations define the magnitude of the load on the crown that causes the side or “leg” of the drip shield to buckle. The thickness of all drip shield components, including the plates and the individual structural members in the framework, is reduced by a constant value of 0 mm, 5 mm, or 10 mm for these calculations. The thickness reduction is taken in the smaller dimension for each structural member in the framework to simplify the changes to the computational model. This approach is appropriate because the smaller dimension generally determines the load-bearing capacity of the framework.

The drip shield plates are fabricated from Titanium Grade 7, and the framework is fabricated from Titanium Grade 29. The physical/chemical mechanisms for the general corrosion processes on Titanium Grades 7 and 29 are expected to be similar, although the absolute corrosion rates can be somewhat different (SNL 2007 [DIRS 180778], Section 6.2[a], third paragraph). The general corrosion rate of Titanium Grade 29 is characterized as a distribution for the ratio of the Titanium Grade 29 rate to the sampled value of the general corrosion rate for Titanium Grade 7 (SNL 2007 [DIRS 180778], Section 6.2[a], fourth paragraph). If the general corrosion rate ratio is less than 1, it is conservatively reset to 1 (SNL 2007 [DIRS 180778], Section 6.2.2[a]). The

resulting distribution for the general corrosion rate ratio is 1 below the 50th percentile and greater than 1 above the 50th percentile (SNL 2007 [DIRS 180778], Table 6-8[a]).

The structural response calculations for the drip shield have equal thickness reduction in all structural elements of the drip shield. Equal thickness reduction is a reasonable approach because the physical/chemical mechanisms for the general corrosion processes are similar and because the data for the general corrosion rate ratio are less than 1 approximately 50% of the time and greater than 1 approximately 50% of the time.

The plastic load capacity of the framework has been evaluated for two nonuniform load patterns. The nonuniform load pattern is important because an asymmetric load pattern has the potential to cause the sidewalls of the drip shield to buckle before a uniform load. The UDEC calculations evaluate lithophysal loads for 30 segments on the surface of the drip shield, with 10 segments on each of the sidewalls and 10 segments on the crown of the drip shield (BSC 2004 [DIRS 166107], pp. 6-224 through 6-229; DTN: MO0407MWDDSLCR.000 [DIRS 170873], worksheet "data" in *final drip shield quasi-static pressures.xls*). The loads on the individual segments are highly nonuniform within a given lithophysal realization, as illustrated by the data in Table 6-37 for the segments on the crown of the drip shield and by *Drift Degradation Analysis* (BSC 2004 [DIRS 166107], Figure 6-174) for all segments of the drip shield.

The first load pattern for determining plastic load capacity is based on averaging the results from the six UDEC lithophysal realizations on a segment-by-segment basis. *Drift Degradation Analysis* (BSC 2004 [DIRS 166107], Figure 6-175, base case) defines the averaged pressure on all segments of the drip shield. Table 6-37 presents the average loads for segments 11 through 20 on the crown of the drip shield. These average loads retain the nonuniform character of the loads from the six UDEC realizations.

Table 6-37. Data for Average Rockfall Pressure on the Segments on the Crown of the Drip Shield

Segment No.	Pressure Real 1 (Pa)	Pressure Real 2 (Pa)	Pressure Real 3 (Pa)	Pressure Real 4 (Pa)	Pressure Real 5 (Pa)	Pressure Real 6 (Pa)	Average Pressure (Pa)
11	2.466×10^{03}	7.790×10^{04}	5.219×10^{05}	2.549×10^{03}	2.389×10^{04}	0.000×10^{00}	1.05×10^{05}
12	1.373×10^{05}	9.381×10^{04}	6.983×10^{03}	2.280×10^{05}	6.474×10^{03}	1.463×10^{05}	1.03×10^{05}
13	1.850×10^{03}	2.755×10^{05}	1.369×10^{03}	6.830×10^{04}	1.966×10^{05}	1.513×10^{05}	1.16×10^{05}
14	2.339×10^{05}	1.037×10^{05}	1.984×10^{05}	6.566×10^{04}	1.438×10^{05}	1.293×10^{05}	1.46×10^{05}
15	3.072×10^{03}	4.556×10^{04}	3.369×10^{05}	0.000×10^{00}	5.439×10^{04}	1.788×10^{05}	1.04×10^{05}
16	3.033×10^{04}	7.905×10^{02}	5.462×10^{03}	3.252×10^{05}	5.622×10^{05}	2.543×10^{04}	1.58×10^{05}
17	6.782×10^{05}	1.258×10^{05}	1.987×10^{05}	1.138×10^{05}	0.000×10^{00}	2.776×10^{03}	1.87×10^{05}
18	0.000×10^{00}	1.696×10^{05}	9.350×10^{04}	3.015×10^{04}	4.419×10^{03}	1.591×10^{05}	7.61×10^{04}
19	2.018×10^{03}	0.000×10^{00}	1.802×10^{05}	4.638×10^{05}	1.355×10^{05}	3.457×10^{05}	1.88×10^{05}
20	0.000×10^{00}	5.780×10^{05}	2.002×10^{03}	0.000×10^{00}	0.000×10^{00}	0.000×10^{00}	9.67×10^{04}

Source: DTN: MO0407MWDDSLCR.000 [DIRS 170873], columns C, F, I, L, O, R, and U and rows 14 through 23 in worksheet "data" in file *final drip shield quasi-static pressures.xls.*

NOTE: Pressure is shown to four significant figures, and average pressure is shown to three significant figures.

This averaging process is appropriate because the UDEC calculations are based on a two-dimensional model that does not represent spatial variability along the axial length of the drip shield. This spatial variability will be significant because the typical rubble size of 0.1 m to 0.3 m (BSC 2004 [DIRS 166107], Section 6.4.1.1) is much less than the 5.805-m nominal length of the drip shield (SNL 2007 [DIRS 179354], Table 4-2, Item Number 07-01). In this situation, the rockfall load will vary between axial locations on the drip shield, and the average load on each segment provides a reasonable estimate of the effective load on the drip shield with axial variability. This averaged nonuniform load pattern is referred to as the mean load pattern.

The second load pattern is based on Realization 3, which has the maximum average load on the 10 segments on the crown of the drip shield (see Table 6-34). This second load pattern provides a nonuniform load that is biased toward the highest total load on the crown of the drip shield, but is not envisioned to represent an extreme load for determining plastic load capacity.

The ultimate plastic capacity has been evaluated for thickness reductions of 0 mm, 5 mm, and 10 mm in the structural elements of the framework, corresponding to plate thicknesses of 15 mm, 10 mm, and 5 mm, respectively (SNL 2007 [DIRS 178851], Section 6.4.3). Figure 6-72 and Table 6-38 present the plastic load capacity for three thicknesses and two load patterns.

Figure 6-72 presents these results as a function of plate thickness to simplify comparison with the plastic load capacity of the plates. The loads for buckling, as shown in Figure 6-72, are always less than the plastic load capacity of the plates, as shown in Figure 6-68. This result confirms that the plastic load capacity of the plates is greater than the plastic load capacity of the framework, as stated above.

Table 6-38. Data for Ultimate Load Capacity of the Drip Shield Framework

Thickness Reduction (mm)	Plate Thickness (mm)	Plastic Load Capacity for Mean Load Pattern (Pa)	Plastic Load Capacity for Realization 3 Pattern (Pa)
10	5	500,800	606,200
5	10	1,094,000	1,183,000
0	15	1,698,000	1,622,000

Source: DTN: MO0701DRIPSHLD.000 [DIRS 182334], File *summary DS framework fragility.xls*, worksheet “limit load.”

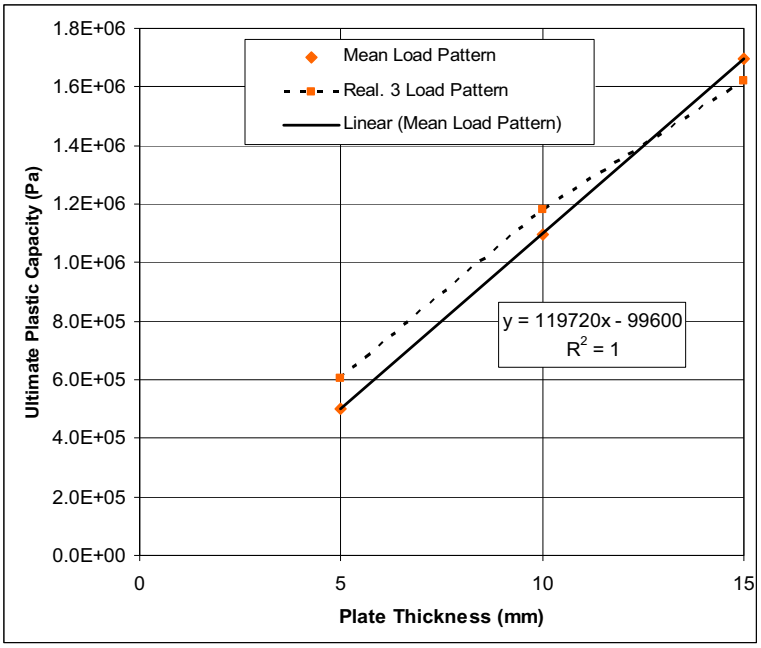

Source: Output DTN: MO0703PASDSTAT.001, worksheet "Load and Capacity" in file *Frame Fragility Analysis.xls.*

Figure 6-72. Plastic Load Capacity of the Drip Shield Framework as a Function of Plate Thickness and Boundary Conditions

Figure 6-72 indicates that there is complexity in the plastic load capacity, judging by the reversal in capacity between plate thicknesses of 10 mm and 15 mm for the two load patterns. The data in Figure 6-72 are based on quasi-static calculations, which have a different failure mode for the 15-mm-thick plate than for the 5-mm-thick and 10-mm-thick plates, as discussed in Section 6.8.3.1. This may explain the change in character in Figure 6-72.

This uncertainty in the ultimate load capacity is represented as a probability distribution whose mean is defined by a least-squares fit to the load capacity for the mean load pattern (see Figure 6-72). This is appropriate because the mean load pattern provides a reasonable estimate of the effective uniform load on the drip shield. The standard deviation of the probability distribution is defined by the maximum capacity difference for the two load patterns. Realization 3, which is biased toward the highest total load on the crown of the drip shield, provides a reasonable estimate for +1 standard deviation in the load capacity because it is not envisioned as an extreme load. The resulting values for λ_{CAP} and $(\beta_{CAP})^2$ for a log-normal probability distribution are given in Table 6-39. The value for $(\beta_{CAP})^2$ has been evaluated at the three plate thicknesses in Figure 6-72, and the largest value for β_{CAP}, 0.208, has been used to represent uncertainty about the mean for all plate thicknesses.

Figure 6-71 compares a log-normal probability distribution with the parameters in Table 6-39 with the calculated values of plastic load capacity. The mean of the log-normal distribution exactly matches the response for the mean load pattern. In addition, the data point for the Realization 3 load pattern at the 5-mm plate thickness is at $+1\sigma$, as expected. The log-normal fit provides a reasonable representation for the plastic load capacity of the framework.

Table 6-39. Log-Normal Parameters for the Ultimate Load Capacity of the Drip Shield Framework

Thickness Reduction (mm)	Thickness (mm)	Plastic Load Capacity for Mean Load Pattern (Pa)	Plastic Load Capacity for Realization 3 Pattern (Pa)	$(\beta_{CAP})^2$ (-)	Maximum Value of β_{CAP} (-)	λ_{CAP} (-)
10	5	500,800	606,200	0.0433	0.208	13.10
5	10	1,094,000	1,183,000	0.0066	0.208	13.88
0	15	1,698,000	1,622,000	0.0020	0.208	14.32

Sources: DTN: MO0701DRIPSHLD.000 [DIRS 182334], File *summary DS framework fragility.xls,* worksheet "limit load," defines the plastic load capacities. Calculations of λ_{CAP} and β_{CAP} documented in output DTN: MO0703PASDSTAT.001, worksheet "Load and Capacity" in the file *Frame Fragility Analysis.xls*.

NOTES: The mean value of the data is defined by $\mu = (119720)t - 99600$, where t is plate thickness (see Figure 6-73). The log-normal parameter β^2 is defined as $\beta^2 = ln(1+(\sigma/\mu)^2)$, where σ is the standard deviation. The value for β_{CAP} is based on the maximum value of β^2 at 5-mm, 10-mm, and 15-mm plate thicknesses. The log-normal parameter λ_{CAP} is defined by $\lambda_{CAP} = ln(\mu) - 0.5\beta^2_{CAP}$. The equations for β^2 and λ are defined in (GoldSim Technology Group 2003 [DIRS 166226], Appendix B, Mathematical Representation of Probability Distributions).

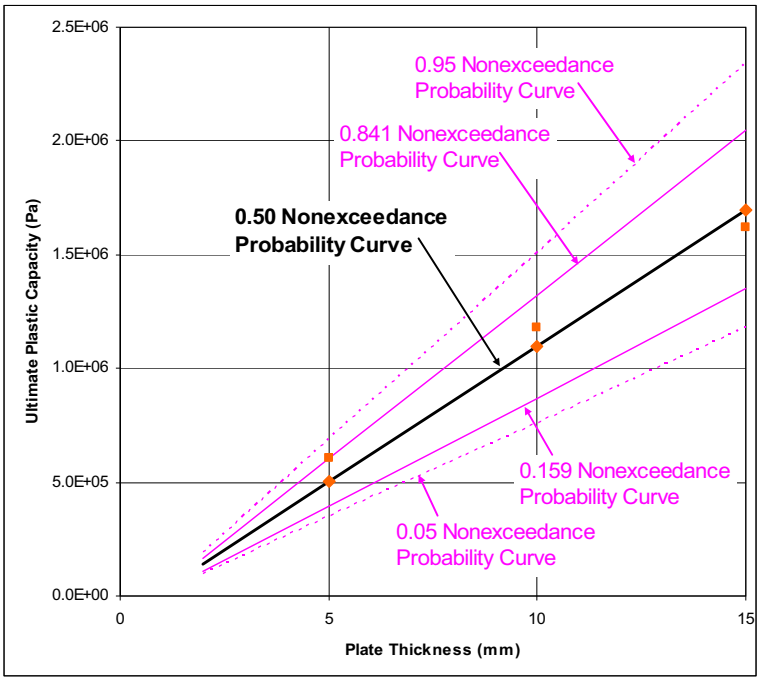

Source: Output DTN: MO0703PASDSTAT.001, worksheet "Load and Capacity" in file *Frame Fragility Analysis.xls*.

NOTE: Squares for realization 3 load pattern, diamonds for mean load pattern. The 0.841 and 0.159 percentiles represent ±1 standard deviation.

Figure 6-73. Comparison of Percentiles on the Log-Normal Distributions with Plastic Load Capacity of the Drip Shield Framework

6.8.3.3 Numerical Calculations

Numerical integration of Equation 6.8-12 for the total probability of framework failure (i.e., buckling of the sidewalls) has been performed for the following cases:

- PGV levels of 0.2 m/s, 0.4 m/s, 1.05 m/s, 2.44 m/s, and 4.07 m/s, with the values of λ_A and β_A defined by Equations 6.8-13 and 6.8-14
- Thickness reductions of 0 mm, 5 mm, 10 mm, and 13 mm for the plates and structural elements of the framework (reductions correspond to plate thicknesses of 15 mm, 10 mm, 5 mm, and 2 mm, with the values of λ_{CAP} and β_{CAP} defined by Table 6-39)
- Static rockfall loads for drifts that are 10%, 50%, and 100% filled with lithophysal rock. The values of λ_{STAT} and β_{STAT} for the fully collapsed drift are defined by Equations 6.8-15 and 6.8-16. The value of λ_{STAT} is reduced by $ln(2)$ and $ln(10)$ for drifts that are 50% and 10% filled with lithophysal rubble, respectively. The value of β_{STAT} remains constant at 0.149 for partly or completely filled drifts.

The results of the numerical integrations, which are documented in the file *Frame Fragility Analysis.xls* (output DTN: MO0703PASDSTAT.001), are presented in Table 6-40 and Figures 6-74 to 6-76. Table 6-40 also includes a column for a 15-mm thickness reduction (0-mm-thick plate) in order to encompass the full range of thickness reductions for the TSPA. The 0-mm-thick plate is assigned a probability of failure of 1 at any PGV level. The probabilities of failure in Table 6-40 are applied to all drip shields in the repository (i.e., there is no spatial variability in drip shield failure).

Within the TSPA model, the time-dependent reduction in thickness of the framework components should incorporate double-sided corrosion for the sides of the bulkheads and stiffeners. The width of the bulkheads and stiffeners in the axial direction of the drip shield is usually less than the depth of the bulkheads and stiffeners, normal to the plates. In this geometry, the thickness reduction of the width is the important parameter for buckling of the legs, and both sides of the bulkhead or stiffener that are perpendicular to the width will be exposed to the in-drift environment and experience general corrosion.

Table 6-40. Probability of Failure for the Drip Shield Framework

PGV Level (m/s)	Thicknesses of Drip Shield Components[a]				
	Frame: Reduced by 15 mm	Frame: Reduced by 13 mm	Frame: Reduced by 10 mm	Frame: Reduced by 5 mm	Frame: Intact
Probability of Failure with 0% Rockfall Load:					
All	1	0	0	0	0
Probability[b] of Failure with 10% Rockfall Load:					
0.2	1	0	0	0	0
0.4	1	0	0	0	0
1.05	1	0.007	0	0	0
2.44	1	0.107	0.001	0	0
4.07	1	0.311	0.011	0	0

Table 6-40. Probability of Failure for the Drip Shield Framework (Continued)

PGV Level (m/s)	Thicknesses of Drip Shield Components[a]				
	Frame: Reduced by 15 mm	Frame: Reduced by 13 mm	Frame: Reduced by 10 mm	Frame: Reduced by 5 mm	Frame: Intact
Probability of Failure with 50% Rockfall Load:					
0.2	1	0.048	0	0	0
0.4	1	0.192	0	0	0
1.05	1	0.635	0.025	0	0
2.44	1	0.929	0.230	0.029	0.006
4.07	1	0.985	0.502	0.127	0.039
Probability of Failure with 100% Rockfall Load:					
0.2	1	0.716	0.001	0	0
0.4	1	0.867	0.016	0	0
1.05	1	0.981	0.210	0.018	0.003
2.44	1	0.999	0.649	0.191	0.063
4.07	1	1.000	0.867	0.449	0.219

[a] The second through sixth columns correspond to plate thicknesses of 0 mm, 2,mm, 5 mm, 10 mm, and 15 mm, respectively.

[b] Probabilities below 0.001 have been rounded down to 0. The failure mode of the drip shield framework is buckling of the sidewalls.

Source: Output DTN: MO0703PASDSTAT.001, worksheet "Summary" in the file *Frame Fragility Analysis.xls.*

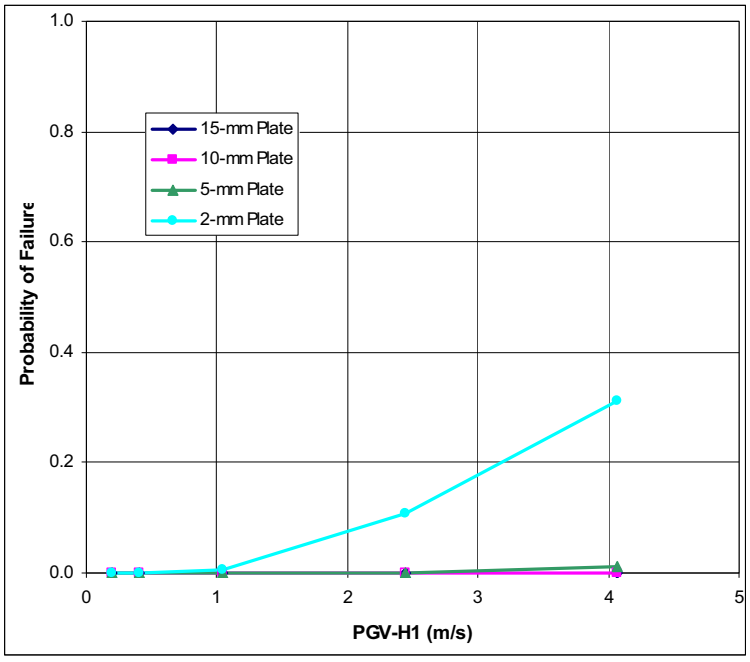

Source: Output DTN: MO0703PASDSTAT.001, worksheet "Summary" in the file *Frame Fragility Analysis.xls.*

NOTE: The probabilities for the intact frame and for the frame with a 5 mm thickness reduction are 0. These data points are partly hidden by the probabilities for the frame with a 10 mm thickness reduction.

Figure 6-74. Probability of Collapse of the Drip Shield Framework for 10% Rockfall Load

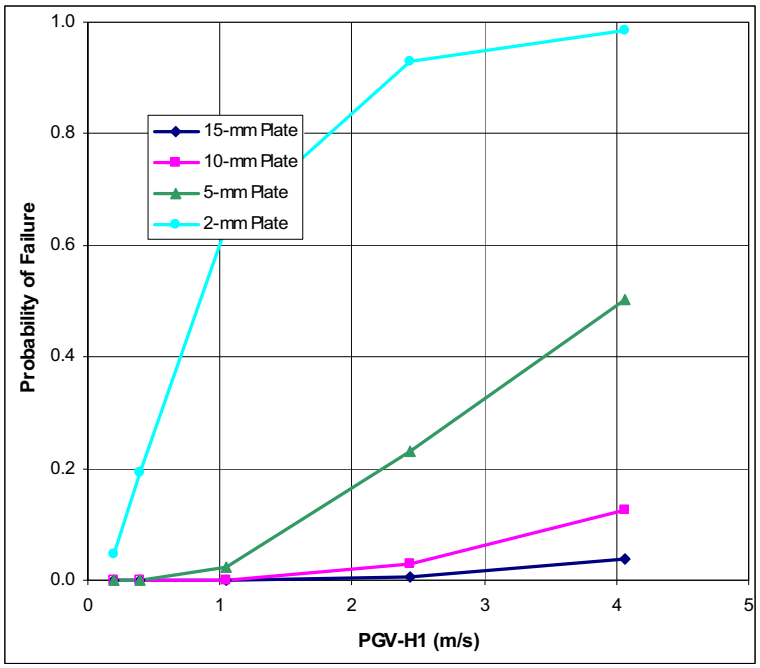

Source: Output DTN: MO0703PASDSTAT.001, worksheet "Summary" in the file *Frame Fragility Analysis.xls.*

Figure 6-75. Probability of Collapse of the Drip Shield Framework for 50% Rockfall Load

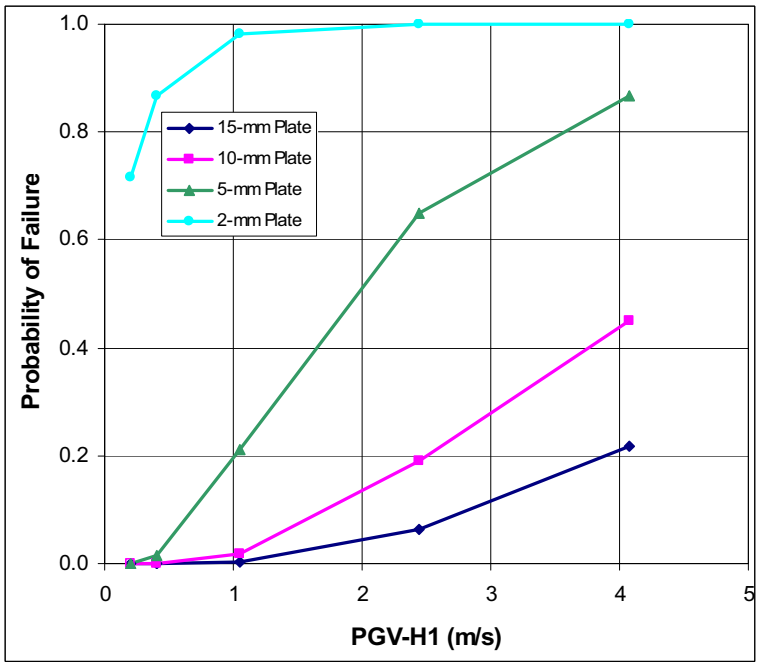

Source: Output DTN: MO0703PASDSTAT.001, worksheet "Summary" in the file *Frame Fragility Analysis.xls.*

Figure 6-76. Probability of Collapse of the Drip Shield Framework for 100% Rockfall Load

6.8.4 Waste Package Response after Drip Shield Failure

Failure of the drip shield changes the configuration of the EBS components, as discussed in Section 6.1.1. The configuration of the EBS and the mechanical response of the waste packages to seismic events must be defined for three states of the system: (1) the initial state, with an intact drip shield, (2) the final state, with the waste packages surrounded by rubble after failure of the drip shield plates, and (3) an intermediate state, where the legs of the drip shield have buckled, but the plates remain intact. This intermediate state can occur because the plastic load capacity of the plates is significantly greater than the plastic load capacity of the drip shield framework for a given reduction in thickness of the drip shield components from general corrosion. The plastic load capacities of the plates and framework are presented in Figures 6-68 and 6-72, respectively, and are also discussed in Section 6.8.3.2.

While the drip shield is intact, the waste packages are free to move and interact in response to vibratory ground motion. In this condition, end-to-end impacts between adjacent waste packages and impacts between a waste package and its emplacement pallet may occur. The response of the waste package for this initial state is defined by the kinematic damage abstractions in Sections 6.5 and 6.6 for the TAD-bearing and codisposal waste packages, respectively.

After the drip shield plates fail, rockfall can pass through the drip shield and surround the waste package. The response for a waste package surrounded by rubble (i.e., the final state of the EBS) is defined in Section 6.9 for both the TAD-bearing and codisposal waste packages.

After the drip shield framework buckles or collapses, the drip shield may be resting on top of the waste package. The deformation and stresses in the OCB of a TAD-bearing waste package that is loaded by a collapsed drip shield has been investigated with three-dimensional finite-difference models (SNL 2007 [DIRS 178851], Section 6.5.2). The entire drip shield is not explicitly represented in the model, only the bulkhead flanges that are expected to contact the waste package after collapse of the framework. The structural response of the OCB is calculated by moving the bulkhead flanges downward at a velocity that is sufficiently small to maintain quasi-static response in the OCB.

Separate models represent the response of the TAD-bearing waste package with intact or degraded internals. For intact internals, the finite-element representation includes the inner vessel, the TAD canister, and the fuel baskets and plates inside the canister. For degraded internals, all internal components inside the OCB are represented as a very weak continuum that fills 50% of the interior volume of the OCB; the continuum has minimal friction angle and cohesion.

OCB thicknesses of 17 mm and 23 mm were analyzed for the intact and degraded internals. The percentage of the OCB surface area with stresses greater than 90% of the yield strength of Alloy 22 is the primary output from the calculations. In determining this surface area, the damage to interior and exterior surfaces are added and then divided by the surface area of the cylinder. The load on the waste package is expressed as a spatially averaged vertical pressure (i.e., the total vertical force between the flanges and the waste package divided by the area of the horizontal cross section through the center of the waste package).

Figure 6-77 presents the resulting damaged areas as a function of the effective vertical load. For reference, the average vertical pressure from lithophysal rockfall on the crown of the drip shield is given by $e^{11.749}$ = 127 kPa (see Table 6-34).

The results for intact internals for the 17-mm-thick or 23-mm-thick OCBs indicate very small damage, less than 0.025%, up to an average vertical pressure of 1,200 kPa. This vertical pressure is equivalent to the initial lithophysal rockfall load with a vertical acceleration of about 8 g's. In addition, the quasi-static analysis generally overestimates strain and deformation relative to dynamic analysis with individual ground motions because the peak ground velocity or peak ground acceleration only persists for a very short period of time in a ground motion, while the quasi-static load is effectively constant in time. With these considerations, the expected damaged area for the waste package surrounded by rubble provides an upper bound for the damage shown in Figure 6-77 for the case of intact internals. For example, the maximum expected damaged area for a waste package surrounded by rubble with a 17-mm-thick OCB is 0.9% of the surface area, as discussed in the last paragraph of Section 6.9.3. This result is greater than the maximum value of damaged area for the drip shield resting on a waste package, which is 0.3% at 1,500 kPa (see Figure 6-77).

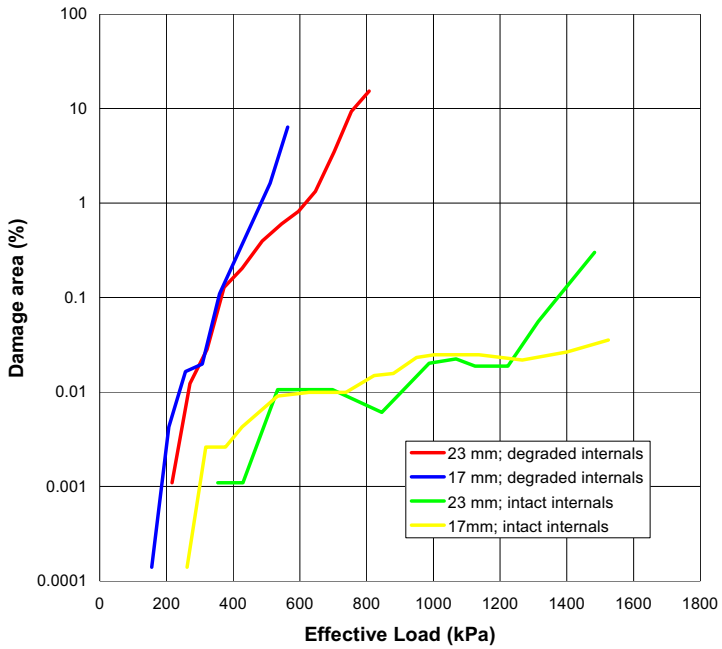

Source: DTN: MO0701DRIPSHLD.000 [DIRS 182334], File *summary WP loaded by DS.xls.*

NOTE: 90% RST.

Figure 6-77. Damaged Areas for a Collapsed Drip Shield on Top of the TAD-Bearing Waste Package

The results for degraded internals with 17-mm-thick or 23-mm-thick OCBs rise rapidly to damaged areas in the 1% to 10% range for average vertical pressure of 500 kPa or greater (see Figure 6-77). This higher level of damage with degraded internals is consistent with the kinematic damage abstractions with intact versus degraded internals. For example, the TAD-bearing waste package with 17-mm-thick OCB and degraded internals has damaged areas

between 2 m^2 and 10 m^2 over a wide range of PGV levels (see Figure 6-20). These damaged areas are equivalent to approximately 6% to 30% of the surface area of the TAD-bearing waste package, thereby providing an upper bound to the damaged area for the drip shield resting on the waste package.

Separate calculations were not performed for a codisposal waste package loaded by a collapsed drip shield. The calculations for the TAD-bearing waste package were performed quasi-statically, and it is anticipated that the response of the codisposal waste packages would be very similar. With intact internals, the OCB and the 2-in-thick inner liner of stainless steel are the main load-bearing components. The thickness of the OCB is identical for both package types and the outer diameter of the OCBs differs by about 9%, as shown in Table 6-48. Similarly, the thickness of the inner stainless steel liner is identical, and the outer diameters of the inner liners also differ by about 9% because the inner liner fits tightly within the OCB. With quasi-static loading, the two waste packages will respond in a similar fashion because the thicknesses of the key structural components are identical and the outer diameters of the key structural components are quite similar. With degraded internals the response will also be similar, although the OCB is the only load-bearing component.

In summary, the damage abstraction for a waste package surrounded by rubble provides an upper bound for the damage shown in Figure 6-77 for the case of intact internals, and the kinematic damage abstractions for the TAD-bearing waste package with degraded internals provide an upper bound for the damage shown in Figure 6-77 for the case of degraded internals. These abstractions should be used to represent the response of the waste package after the drip shield framework has collapsed.

6.8.5 Response of the Drip Shield to Waste Package Impacts

Fragility curves have been defined for two failure modes of the drip shield: (1) rupture or tearing of the drip shield plates (see Section 6.8.2), and (2) buckling or collapse of the sidewalls of the drip shield (see Section 6.8.3). A third failure mode of the drip shield could occur from waste package impacts to the sidewalls and top of the drip shield. This failure mode has been analyzed with structural response calculations and with kinematic analyses for waste package-to-drip shield impacts. As used in this section, a lateral impact is one with its primary velocity components in a two-dimensional cross section that is perpendicular to the drift axis, and a longitudinal impact is one with its primary velocity along the drift axis.

This third failure mode is not represented in the TSPA for two reasons. First, lateral impact of the waste package on the drip shield does not cause catastrophic failure of the drip shield, as discussed later in this section. Second, high-velocity longitudinal impacts of the waste package on the bulkhead support beams exposed on the underside of the crown of the drip shield occur infrequently, even at the 4.07 m/s PGV level (see Table 6-41). The high-velocity longitudinal impacts with the potential to damage the bulkhead support beams occur with much lower probability than the probability of buckling the sidewalls of the drip shield, as shown in Figures 6-75 and 6-76 at the 4.07 m/s PGV level for various drip shield thicknesses. It follows that the drip shield sidewalls are likely to buckle before longitudinal impacts damage the bulkhead support beams and, after the sidewalls buckle, high-velocity longitudinal impacts are eliminated because the waste package can no longer move freely beneath the drip shield.

The analysis for the third failure mode is based on an intact drip shield that is surrounded by rubble. The drip shield must be intact to allow significant relative motion between the waste package and the drip shield. In other words, relative velocity between the waste package and drip shield will be restricted after collapse of the sidewalls of the drip shield or after failure of the drip shield plates, when rubble surrounds the waste package. The drip shield must also be surrounded by rubble for a significant impact force to be generated. The drip shield is a free-standing structure that will move with the heavier waste package in an unfilled drift, thereby mitigating the forces on impact.

The structural stability of the drip shield subjected to lateral impacts by a waste package has been investigated with three-dimensional finite-element calculations (BSC 2005 [DIRS 173172], Section 5.6.2). The impact parameters for these calculations included waste package orientation, magnitude and direction of the impact velocity, and location of impact, based on the results of two-dimensional kinematic analyses with multiple waste packages. The drip shield is surrounded by rubble for these calculations. The waste package is based on the 21-PWR design, but the results are also applicable to other waste package designs because the waste package is represented as a simplified cylindrical shell, without details of the internal structures or end lids (BSC 2005 [DIRS 173172], Figure 5-26).

The magnitude of the lateral impact velocity for most calculations is 6 m/s (BSC 2005 [DIRS 173172], p. 5-49). This is a bounding value at the 2.44 m/s PGV level because it is greater than the maximum observed impact velocities from the kinematic analyses (BSC 2005 [DIRS 173172], Table 5-7). Three additional calculations were performed with a lateral impact velocity of 11 m/s to demonstrate the robustness of the drip shield under extreme impact velocities.

The results from these calculations demonstrate that none of the lateral impacts cause catastrophic failure and the drip shield component materials remain within their true ultimate strengths for the sidewall impacts, even under the extreme impact velocity of 11 m/s (BSC 2005 [DIRS 173172], Section VI-3.3). Based on these results, drip shield failure from lateral impacts of the waste package is excluded from the TSPA compliance case for the license application.

A set of three-dimensional kinematic calculations were performed for two ground motions at the 1.05 m/s PGV level, for five ground motions at the 2.44 m/s PGV level, and for 17 ground motions at the 4.07 m/s PGV level to define the frequency and magnitude of the longitudinal impacts between the waste package and the bulkhead support beams on the underside of the crown of the drip shield (DTN: LL0704PA050SPC.025 [DIRS 180819], File *WPDS_kinematic_analyses_ summary.xls*, worksheets "NLTAD Impacts Summary" and "CDSP Impacts Summary"). The maximum longitudinal impact velocities at the 1.05 m/s and 2.44 m/s PGV levels are 0.501 m/s and 0.994 m/s, respectively, and occur with the codisposal waste packages. The frequency and maximum longitudinal impact velocities at the 4.07 m/s PGV level are summarized in Table 6-41 for the TAD-bearing and codisposal waste packages. The maximum longitudinal impact velocity in Table 6-41 is less than 6 m/s for all realizations, providing confirmation that lateral impact velocities of 6 m/s and 11 m/s represent bounding velocities for the evaluation of structural stability of the drip shield, as discussed above.

Table 6-41. Kinematic Results for Longitudinal Impacts of a Waste Package on the Bulkhead Support Beams of the Drip Shield at the 4.07 m/s PGV Level

Rlz. No	Total No. of Impacts	No. of Impacts > 2 m/s	No. of Impacts > 3 m/s	No. of Impacts > 4 m/s	Max. Impact Velocity (m/s)
Impacts for the TAD-bearing Waste Packages I, J, and K:					
1	0	0	0	0	–
2	0	0	0	0	–
3	1	0	0	0	0.305
4	1	1	1	0	3.071
5	0	0	0	0	–
6	2	0	0	0	1.615
7	0	0	0	0	–
8	0	0	0	0	–
9	0	0	0	0	–
10	8	1	0	0	2.186
Impacts for the TAD-bearing Waste Packages I, J, and K:					
11	0	0	0	0	–
12	2	0	0	0	1.024
13	0	0	0	0	–
14	0	0	0	0	–
15	1	0	0	0	1.554
16	1	1	1	1	4.782
17	1	1	0	0	2.802
Totals	17	4	2	1	–
Impacts for the Codisposal Waste Packages H and L:					
1	0	0	0	0	–
2	0	0	0	0	–
3	1	1	0	0	2.614
4	6	0	0	0	1.978
5	1	1	1	0	3.315
6	0	0	0	0	–
7	0	0	0	0	–
8	0	0	0	0	–
9	0	0	0	0	–
10	5	1	0	0	2.694
11	0	0	0	0	–
12	3	1	1	1	4.301
13	0	0	0	0	–
14	4	1	1	0	3.419
15	10	0	0	0	1.958
16	0	0	0	0	–
17	1	0	0	0	1.957
Totals	31	5	3	1	–

Sources: DTN: LL0704PA050SPC.025 [DIRS 180819], worksheets "NLTAD Impacts Summary" and "CDSP Impacts Summary" in the file *WPDS_kinematic_ analyses_summary.xls*.

NOTE: Rlz. = realization.

Three-dimensional finite-element calculations have been performed for a waste package that "clips" a bulkhead support beam on the underside of the crown of the drip shield (BSC 2005 [DIRS 173172], Figure 5-21 and Section VI-3.4). The drip shield response is analyzed for longitudinal impact velocities of 1 m/s and 2.25 m/s. The longitudinal impact at 1 m/s does not result in failure of the drip shield components. At 2.25 m/s, the maximum stress occurs at the juncture where an axial stiffener beneath the crown of the drip shield meets the bulkhead (BSC 2005 [DIRS 173172], Figure VI-40). This is also the location where the waste package makes contact with the bulkhead flange. The combination of a locally stiff area from the bulkhead support beam and the impact by the edge of the waste package generates shearing forces on the bulkhead and flange. The maximum Von Mises stress in the bulkhead is just within the true ultimate strength of this material, but, with the flange exceeding its true ultimate strength, the load would likely transfer to the bulkhead, causing it to fail. Although detrimental to the bulkhead, the drip shield is predicted to remain structurally stable even if it is missing a section of one bulkhead (BSC 2005 [DIRS 173172], Section VI-3.4.1).

The results from these calculations demonstrate that longitudinal impact at 2.25 m/s is likely to damage the drip shield, but it still remains structurally stable. Based on these results, drip shield failure from longitudinal impacts at 2.25 m/s or less is excluded from the TSPA compliance case for the license application.

The results for the 1.05 m/s and 2.44 m/s PGV levels indicate that the maximum longitudinal impact velocity is less than 1 m/s. Table 6-41 demonstrates that there are a very limited number of impacts at the 4.07 m/s PGV level with longitudinal velocity greater than 2 m/s. Based on these results, there are two longitudinal impacts with velocity greater than 3 m/s at the 4.07 m/s PGV level. Since Table 6-41 tabulates the impacts for 17 realizations and three TAD-bearing waste packages (denoted as I, J, and K), the conditional probability of a longitudinal impact greater than 3 m/s from a single TAD-bearing waste package is (2/3/17) = 0.039 at the 4.07 m/s PGV level and 0 at the 1.05 m/s and 2.44 m/s PGV levels. Since each drip shield covers approximately one waste package, the conditional probability for a longitudinal impact greater than 3 m/s is also 0.039 at the 4.07 m/s PGV level for each drip shield surrounding a TAD-bearing waste package. The equivalent conditional probability for the codisposal waste package is (3/2/17) = 0.088 because there are three longitudinal impacts with velocity greater than 3 m/s at the 4.07 m/s PGV level and because Table 6-41 tabulates the impacts for 17 realizations and 2 codisposal waste packages (denoted as H and L). These probabilities are conditional because they are based on the occurrence of a seismic event at the 4.07 m/s PGV level.

These probabilities are significantly less than the (conditional) probability of collapse of the drip shield sidewalls at the 4.07 m/s PGV level (see Table 6-40). For example, the probabilities of sidewall collapse at the 4.07 m/s PGV level are 0.219 and 0.449 for the intact drip shield and for a drip shield with a 5-mm reduction in the thickness of its components, respectively. These probabilities are based on the 100% rockfall load because drift collapse is predicted to occur for all ground motions beyond the 2.44 m/s PGV level. These results make it very likely that the drip shield will collapse before an impact with longitudinal velocity greater than 3 m/s occurs, and free motion of the waste package is restricted or eliminated after collapse of the sidewalls of the drip shield.

In addition, the current round of kinematic calculations will tend to over-predict the high-velocity longitudinal impacts in Table 6-41 because the 17 ground motions at the 4.07 m/s PGV level have not been bounded. While the first horizontal component is scaled to 4.07 m/s PGV, the PGV magnitudes for the second horizontal and vertical components are not scaled to this PGV level, and each component will be greater than 4.07 m/s in approximately one-half of the ground motions. The high PGV levels of the second horizontal and vertical components will tend to increase the high velocity longitudinal impacts.

In summary, drip shield failure from lateral impacts of the waste package is excluded from the TSPA compliance case for the license application because lateral impacts at 6 m/s and 11 m./s do not cause catastrophic failure of the drip shield. Drip shield failure from longitudinal impacts of the waste package on the bulkhead support beams is also excluded because: (1) longitudinal impacts do not cause failure up to 2.25 m/s impact velocity; (2) the drip shield remains structurally stable even when it is missing one section of a bulkhead support beam; and (3) the estimated conditional probabilities for a longitudinal impact velocity greater than 3 m/s are significantly less than the conditional probabilities for collapse of the drip shield sidewalls.

6.9 ABSTRACTIONS FOR THE WASTE PACKAGE SURROUNDED BY RUBBLE

Two damage abstractions have been developed for a waste package with degraded internals that is surrounded by lithophysal rubble:

- 23-mm-thick OCB with degraded internals
- 17-mm-thick OCB with degraded internals.

A case with intact internals was not performed for the waste package surrounded by rubble. The waste package becomes surrounded by rubble after the drip shield framework and drip shield plates have failed during a seismic event. This is expected to occur at late times after repository closure, when the OCB is modeled as being breached by SCC, resulting in degraded internals inside the waste package (see Assumption 5.4, Section 5). Regardless of the time scale, the damage abstractions for degraded internals will define damaged areas that are greater than the response with intact internals (see Sections 6.5 and 6.6), so this is a bounding approach.

Lithophysal rubble was selected for the dynamic load on the waste package. Rockfall in lithophysal rock has significantly greater volume (see Figure 6-58) than rockfall in nonlithophysal rock, resulting in greater static loads from lithophysal rockfall at a given point in time. Lithophysal rubble also has smaller particle sizes than rockfall in the nonlithophysal zones, which is dominated by large rock blocks. Smaller particle sizes minimize load bridging in the rock mass, resulting in higher loads from lithophysal rubble than from rock blocks in the nonlithophysal zones. It is acknowledged that large rock blocks would tend to have point contacts in localized areas on the waste package, but the cumulative loading from the lithophysal rubble is expected to be significantly greater because the volume of lithophysal rubble is much greater than the volume of nonlithophysal rockfall, as demonstrated in Table 6-32 and Figure 6-58.

The abstractions for the mechanical response of a waste package surrounded by rubble to a seismic event are based on the TAD-bearing waste package with degraded internals. When the internals are degraded, the damaged areas for the TAD-bearing waste package are expected to be similar to but greater than the response of the codisposal waste package, so a single damage abstraction has been developed for both types of waste packages. The rationale for the similarity of response is explained in Section 6.9.10.

The damage abstractions are documented in two spreadsheets: *WP-Rubble Damage Abstraction 23-mm Degraded.xls* and *WP-Rubble Damage Abstraction 17-mm Degraded.xls*, in output DTN: MO0703PASDSTAT.001. These spreadsheets also contain the analyses for various types of distributions and the final comparisons for conditional probability distributions versus the input data.

6.9.1 Probability of Rupture/Puncture

The probability of rupture for the TAD-bearing waste package surrounded by rubble for the 17-mm-thick and 23-mm-thick OCBs with degraded internals is zero. The structural response calculations for the waste package surrounded by rubble at the 0.4 m/s, 1.05 m/s, 2.44 m/s, and 4.07 m/s PGV levels demonstrate that the strain in the OCB is always below the ultimate tensile strain for Alloy 22 (SNL 2007 [DIRS 178851], Section 6.5.1). However, a severely deformed OCB may be punctured by the sharp edges of fractured or partly degraded internal components. In this conceptualization, the volume reduction in a severely deformed OCB is hypothesized to have the potential to puncture the OCB.

The deformation of the OCB is assessed by calculating the ratio of the volume within the deformed OCB, at the end of the ground motion, to the initial volume within the OCB (DTN: MO0704PUNCTURE.000 [DIRS 180634], File *Puncture Probability Data – WP Surrounded by Rubble.xls*). As this ratio is reduced from 1.0 to 0.50, which corresponds to the porosity in the OCB, the probability of puncture increases monotonically from 0 to 1. Table 6-42 displays the resulting probabilities for the 17-mm-thick OCB, based on calculations at the 0.4 m/s, 1.05 m/s, 2.44 m/s, and 4.07 m/s PGV levels. Each calculation is based on 1 of 17 ground motions at each PGV level and on a random block geometry for the lithophysal rock.

The average probability for puncture of the waste package surrounded by rubble is represented in the TSPA as a power-law function of the form a(PGV–0.4)b. This function goes to 0 at the 0.40 m/s PGV level, consistent with the data in Table 6-42. The coefficients a and b are determined by a least squares fit to the natural logarithm of the nonzero data points. This fit, shown in Figure 6-78, demonstrates that the data points follow a power-law dependence because the R2 of the least-squares fit is 0.9958. This fit also defines the coefficients of the power law: a = exp(−3.8656) = 0.0210 and b = 1.6971.

Table 6-42. Probabilities of Puncture for the Waste Package with 17-mm OCB and Degraded Internals Surrounded by Rubble

Realization Number	Probability of Puncture by PGV Level			
	0.4 m/s	1.05 m/s	2.44 m/s	4.07 m/s
1	0	0	0	0.567
2	0	0	0	0
3	0	0	0	0.107
4	0	0.050	0.250	0.171
5	0	0	0	0.432
6	0	0	0	0
7	0	0.128	0	0.128
8	0	0	0	0.065
9	0	0	0	0.175
10	0	0	0	0
11	0	0	0	0.490
12	0	0	0	0
13	0	0	0.820	1.000
14	0	0	0	0
15	0	0	0	0.152
16	0	0	0	0
17	0	0	0	0.194
Average	0	0.010	0.063	0.205

Source: DTN: MO0704PUNCTURE [DIRS 180634], worksheet “TAD Rubble Data” in the file *Puncture Probability Data – WP Surrounded by Rubble.xls.*

NOTE: Probabilities have been rounded to three significant digits.

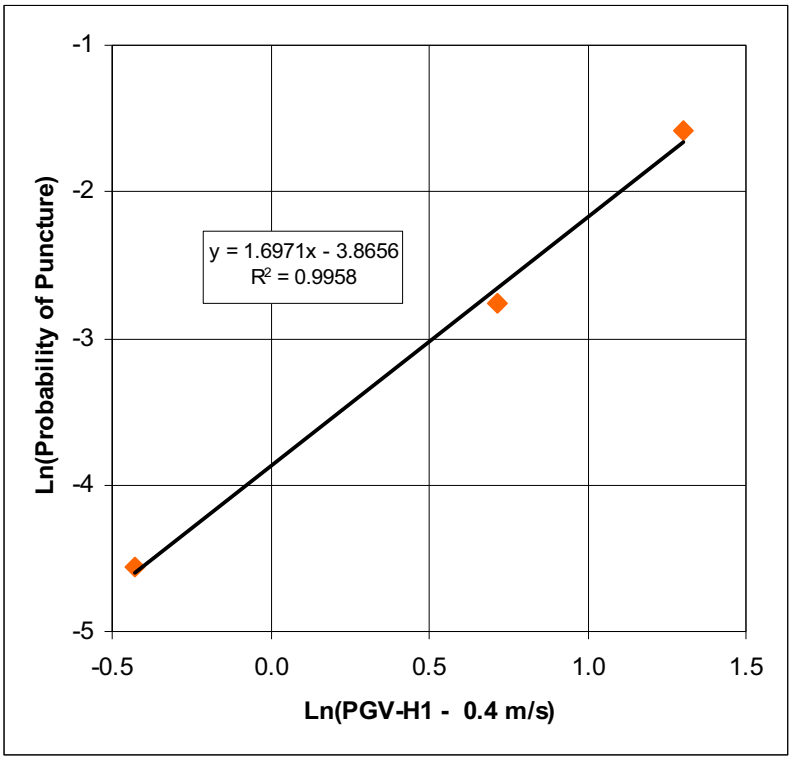

Source: Output DTN: MO0703PASDSTAT.001, worksheet "TAD Rubble Abstraction" in *Rupture and Puncture Abstractions.xls.*

NOTE: TAD-bearing waste package surrounded by rubble with 17-mm-thick OCB and degraded internals.

Figure 6-78. Least-Squares Fit for Power-Law Dependence for Probability of Puncture

Table 6-43 displays the corresponding probabilities for the 23-mm-thick OCB, based on calculations with 17 ground motions at each of the 0.4 m/s, 1.05 m/s, 2.44 m/s, and 4.07 m/s PGV levels. The average probability of rupture is represented in the TSPA as a power-law function of the form $c(\text{PGV} - 1.05)^d$. This functional form goes to 0 at the 1.05 m/s PGV level, consistent with the data in Table 6-43. The coefficients c and d are calculated from the two nonzero data points in Table 6-43: $d = \log(0.070/0.007)/\log((4.07-1.05)/(2.44-1.05)) = 2.9007$ and $c = (0.070)/(4.07 - 1.05)^{2.9007} = 0.0028$. (Numerical values are based on the spreadsheet calculations in output DTN: MO0703PASDSTAT.001, worksheet "TAD Rubble Abstraction" in the file *Rupture and Puncture Abstractions.xls.*) Figure 6-79 presents the two power-law representations for the average probability of puncture for the waste package surrounded by rubble.

Table 6-43. Probabilities of Puncture for the Waste Package with 23-mm OCB and Degraded Internals Surrounded by Rubble

Realization Number	Probability of Puncture by PGV Level			
	0.4 m/s	1.05 m/s	2.44 m/s	4.07 m/s
1	0	0	0	0.070
2	0	0	0	0
3	0	0	0	0
4	0	0	0.020	0.052
5	0	0	0	0.009
6	0	0	0	0
7	0	0	0	0
8	0	0	0	0
9	0	0	0	0
10	0	0	0	0
11	0	0	0	0.239
12	0	0	0	0
13	0	0	0	0.817
14	0	0	0	0
15	0	0	0	0
16	0	0	0	0
17	0	0	0.105	0
Average	0	0	0.007	0.070

Source: DTN: MO0704PUNCTURE [DIRS 180634], worksheet "TAD Rubble Data" in the file *Puncture Probability Data – WP Surrounded by Rubble.xls.*

NOTE: Probabilities have been rounded to three significant digits.

The time-dependent thickness of the OCB must also be incorporated into the average probability of puncture for the waste package surrounded by rubble. The spatially averaged thickness of the OCB is a time-dependent parameter that is predicted by other elements of the TSPA. The probability of puncture corresponding to the average OCB thickness at the time of the seismic event is calculated by linear interpolation if the OCB thickness is between 17 mm and 23 mm. The use of linear interpolation is appropriate because it provides results at intermediate values that are greater than those from a power-law fit with a positive and increasing slope. This calculation is defined in Equation 6.9-1:

$$PP = \text{If } t \geq 23 \text{ mm}, PP\_23 \quad \text{(Eq. 6.9-1)}$$

$$\text{Or if } t \leq 17 \text{ mm}, PP\_17$$

$$\text{Else } PP\_17 + (PP\_23 - PP\_17)*(t - 17 \text{ mm})/(6 \text{ mm})$$

where t is the spatially averaged thickness of the OCB (in mm) at the time of the seismic event, PP is the final probability of puncture at the current average OCB thickness, PP_17 is the value of the probability from the power-law representation for the 17-mm-thick OCB, and PP_23 is the value of the probability from the power-law representation for the 23-mm-thick OCB. Based on Equation 6.9-1, the probability is set to the value at 23 mm if the average OCB thickness is greater than 23 mm. This is reasonable because the probability for the 23-mm-thick OCB bounds the waste package response for several hundred thousand years after repository closure, based on the estimated corrosion time in Section 6.5.1.2. The probability is set to the value for

the 17-mm thickness if the average OCB thickness is less than 17 mm. This is a reasonable approach because the probability for the 17-mm-thick OCB provides a reasonable representation at the end of the peak dose period (approximately 1,000,000 years), based on the estimated corrosion time in Section 6.5.2.2.

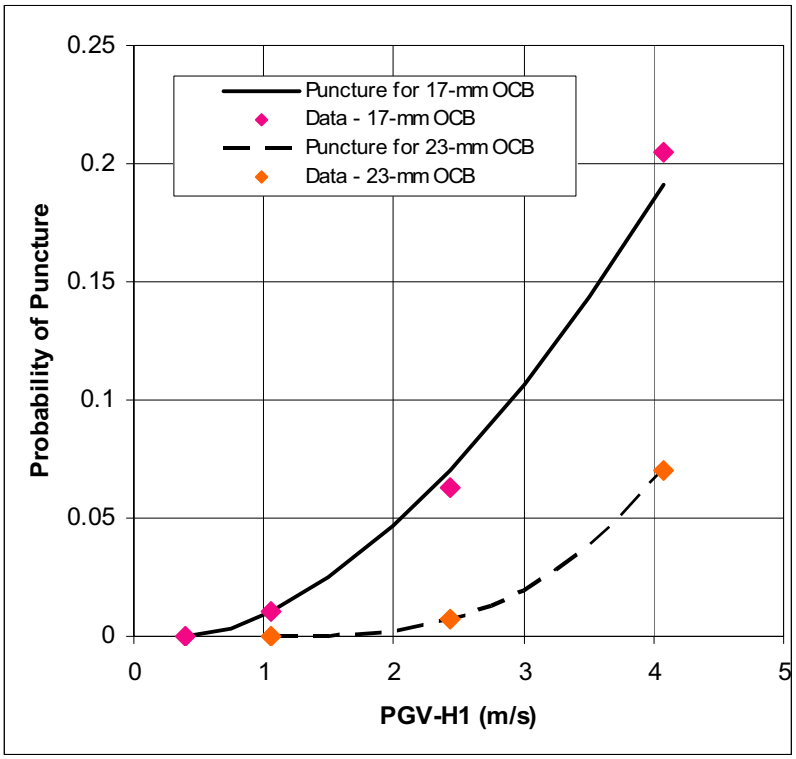

Source: Output DTN: MO0703PASDSTAT.001, worksheet "TAD Rubble Abstraction" in *Rupture and Puncture Abstractions.xls.*

NOTE: TAD-bearing waste package surrounded by rubble with 23 mm and 17 mm OCB and degraded internals.

Figure 6-79. Power-Law Dependence for Probability of Puncture

When the waste packages are punctured, the failed area is determined by sampling a uniform distribution with a lower bound of 0 m^2 and an upper bound of 0.10 m^2. This failed area allows advective flow through the punctured waste package and advective and diffusive transport out of the punctured waste package. This failed area is conceptualized to be a small patch that is randomly located on the surface of the OCB. Once the waste package is penetrated, there is no further damage from penetrations in successive events, and the packages remain punctured for the remainder of the realization.

The upper bound of the uniform distribution is based on two estimates for the area of a hypothetical puncture. If the puncture occurs from a sharp fragment of a fuel rod, the corresponding hole is likely to be quite small, with a size scale on the order of 1 to 2 inches. As an upper bound, a fragment of the inner vessel could form a "hole" that is 1 foot-by-1 foot, or (0.3048 m)(0.3048 m) = 0.092 m^2. This latter value allows for the possibility that multiple fragments may puncture the OCB. In the second estimate, one of the fuel basket plates is conceptualized to form a lengthwise slice through the OCB. The length of this slice is less than

the length of the waste package because the end lids provide support for the OCB at both ends of the waste package. As a first approximation, each end lid provides support for a length equal to one-half of its diameter. The resulting length of the slice is then the nominal length of the waste package minus the diameter of the OCB. For the TAD-bearing waste package, the length of the slice is calculated as 5,850.1 mm – 1,881.6 mm = 3,968.5 mm (SNL 2007 [DIRS 179394], Table 4-3). If the width of the slice is 1 inch, then the area of the slice is (3,968.5 mm)(25.4 mm) = 100,800 mm^2 or 0.10 m^2. The area of the slice, which is slightly greater than the first estimate, is used for the upper bound of the distribution.

6.9.2 Probability of Damage

Figures 6-80 and 6-81 present the probability of damage from the calculations for the TAD-bearing waste package surrounded by rubble. Table 6-44 provides the numerical values for the probability of damage. With the 23-mm-thick OCB, the probability of damage is 0 except at the 4.07 m/s PGV level. With the 17-mm-thick OCB, the probability of damage is 0 at the 0.4 m/s and 1.05 m/s PGV levels, and nonzero at the 2.44 m/s and 4.07 m/s PGV levels.

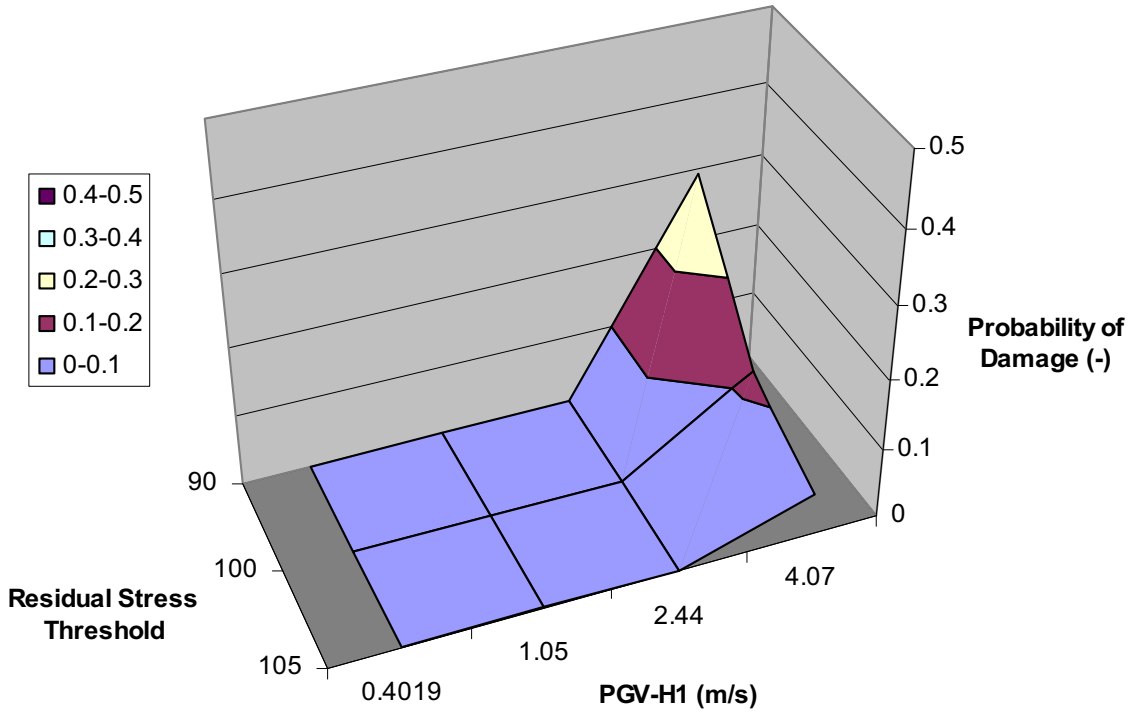

Source: Output DTN: MO0703PASDSTAT.001, worksheet "Probability of Damage" in the file *WP-Rubble Damage Abstraction 23mm Degraded.xls.*

NOTE: 23-mm-thick OCB with degraded internals.

Figure 6-80. Probability of Damage for the TAD-Bearing Waste Package Surrounded by Rubble

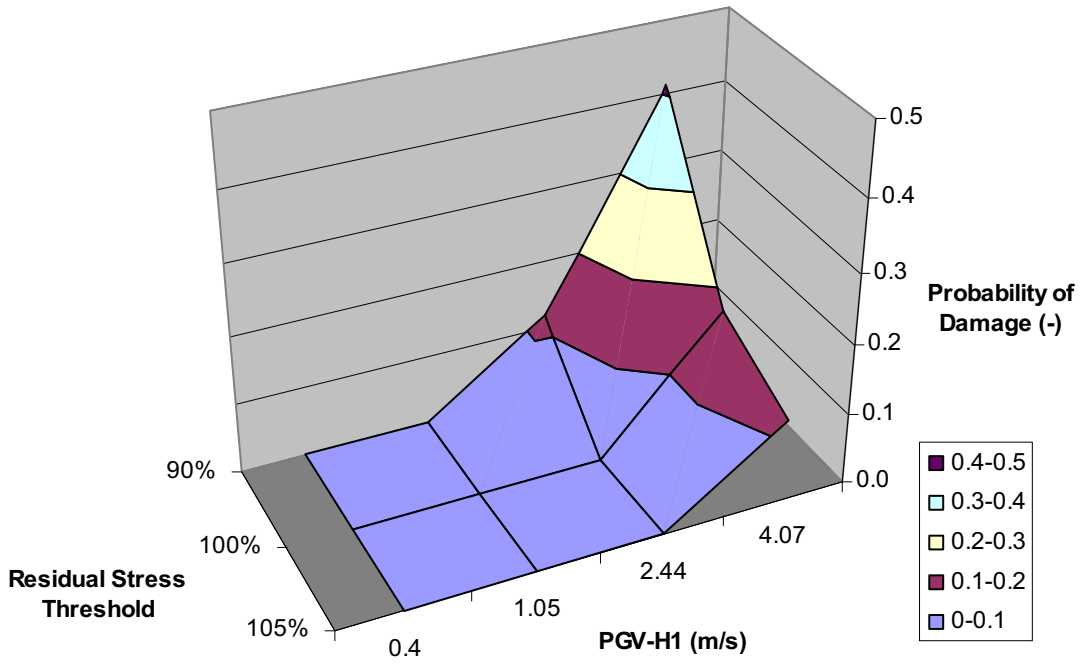

Source: Output DTN: MO0703PASDSTAT.001, worksheet "Probability of Damage" in the file *WP-Rubble Damage Abstraction 17-mm Degraded.xls.*

NOTE: 17-mm-thick OCB with degraded internals.

Figure 6-81. Probability of Damage for the TAD-Bearing Waste Package Surrounded by Rubble

Table 6-44. Probability of Damage for the Waste Package Surrounded by Rubble

	Residual Stress Threshold (% of Yield Strength)		
PGV Level (m/s)	**90%**	**100%**	**105%**
23-mm-thick OCB with Degraded Internals:			
0.40	0	0	0
1.05	0	0	0
2.44	0	0	0
4.07	0.294	0.118	0.059
17-mm-thick OCB with Degraded Internals:			
0.40	0	0	0
1.05	0	0	0
2.44	0.118	0	0
4.07	0.412	0.176	0.118

Sources: Output DTN: MO0703PASDSTAT.001, worksheet "Probability of Damage" in the file *WP-Rubble Damage Abstraction 23-mm Degraded.xls*, and worksheet "Probability of Damage" in the file *WP-Rubble Damage Abstraction 17-mm Degraded.xls.*

The probability of damage in Table 6-44 is based on three independent parameters: the value of *PGV* for the *j*th seismic event, the value of *RST* for a given realization, and the time-dependent thickness of the OCB. Linear interpolation is used to define the variation of the probability of damage as a function of *PGV* and *RST*. Damaged areas are often observed to follow a power law, as illustrated by the quadratic fit for mean damaged area as a function of *RST* in Figure 6-19

and Figure 6-45. The use of linear interpolation for *PGV* and *RST* is appropriate because it provides greater probability values at intermediate points relative to a power-law fit with positive and increasing slope.

The spatially averaged thickness of the OCB is a time-dependent parameter that is predicted by other elements of the TSPA calculations. The probability of damage corresponding to the average OCB thickness at the time of the *j*th seismic event is calculated by linear interpolation if the OCB thickness is between 17 mm and 23 mm. The use of linear interpolation is appropriate because it provides results at intermediate values that are greater than those from a power-law fit with a positive and increasing slope. The logic for this calculation is illustrated in Equation 6.9-2:

$$PD_{RUB,j} = \text{If } t \geq 23 \text{ mm}, PD_{RUB,j,23\text{-}mm} \quad \text{(Eq. 6.9-2)}$$

$$\text{Or if } t \leq 17 \text{ mm}, PD_{RUB,j,17\text{-}mm}$$

$$\text{else}, PD_{RUB,j,17\text{-}mm} + (PD_{RUB,j,23\text{-}mm} - PD_{RUB,j,17\text{-}mm})*(\text{t} - 17 \text{ mm})/(6 \text{ mm})$$

where $PD_{RUB,j}$ is the probability of damage, t is the spatially averaged thickness of the OCB (in mm) at the time of the *j*th event, and $PD_{RUB,j,17\text{-}mm}$ and $PD_{RUB,j,23\text{-}mm}$ are the probabilities of damage for the 17-mm-thick and 23-mm-thick OCBs, respectively, at the value of *PGV* for the *j*th seismic event and the value of *RST* for a given realization. Based on Equation 6.9-1, the probability is set to the value at 23 mm if the average OCB thickness is greater than 23 mm. This is reasonable because the probability for the 23-mm-thick OCB bounds the waste package response for several hundred thousand years after repository closure, based on the estimated corrosion time in Section 6.5.1.2. The probability is set to the value for the 17-mm thickness if the average OCB thickness is less than 17 mm. This is a reasonable approach because the probability for the 17-mm-thick OCB provides a reasonable representation at the end of the peak dose period (approximately 1,000,000 years), based on the estimated corrosion time in Section 6.5.2.2.

6.9.3 Conditional Probability Distributions for Nonzero Damaged Area with 17-mm-Thick OCB

Relatively few data points have nonzero damaged area for the 17-mm-thick OCB. There are only seven points, three points, and two points with nonzero damaged areas at the 90%, 100%, and 105% RSTs, respectively, for the 4.07 m/s PGV level. There are only two points with nonzero damaged area for the 90% RST at the 2.44 m/s PGV level. Since most of the nonzero observations occur at the 4.07 m/s PGV level, a reasonable approach is to abstract these data as a function of RST at this PGV level.

Figure 6-82 is a Q-Q plot for a gamma distribution versus the conditional damaged areas at the 90% RST and the 4.07 m/s PGV level. The values of the mean and standard deviation of the conditional damaged areas, which are the input to the gamma distributions, are shown in Table 6-45 for all RST levels. Figure 6-83 demonstrates that the gamma distribution provides a very good fit to the damaged area data. Note that these conditional damaged areas are expressed as a percent of outside surface area, rather than as an absolute area (square meters), because the calculations for the waste package surrounded by rubble analyze the response of a

two-dimensional cross section of the waste package, perpendicular to its center line. The output from the two-dimensional model is more directly interpreted as a percent of surface area, rather than as an area per meter of package length.

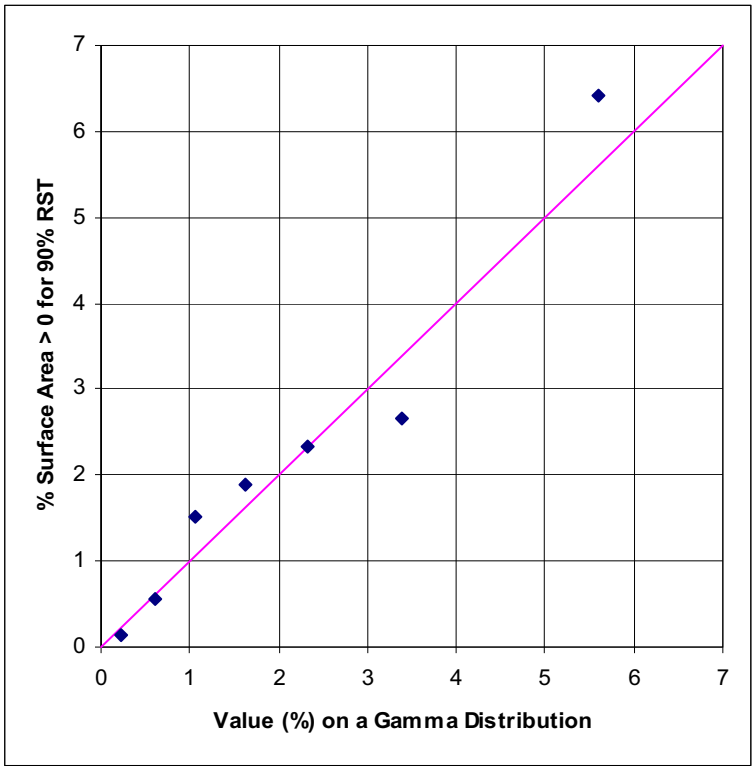

Source: Output DTN: MO0703PASDSTAT.001, worksheet "ACMs at 4.07 PGV" in the file *WP-Rubble Damage Abstraction 17-mm Degraded.xls.*

NOTE: 17-mm-thick OCB with degraded internals. 90% RST at the 4.07 m/s PGV level.

Figure 6-82. Q-Q Plot for Conditional Damaged Areas versus a Gamma Distribution for the TAD-Bearing Waste Package Surrounded by Rubble

Table 6-45. Mean and Standard Deviations of the Conditional Damaged Areas for the 17-mm-Thick OCB with Degraded Internals

PGV Level (m/s)	Residual Stress Threshold (% of Yield Strength)					
	90%		100%		105%	
	Mean (% Surface Area)	Standard Deviation (% Surface Area)	Mean (% Surface Area)	Standard Deviation (% Surface Area)	Mean (% Surface Area)	Standard Deviation (% Surface Area)
2.44	1.396	1.003	–	–	–	–
4.07	2.214	2.064	0.409	0.134	0.136	0.008

Source: Output DTN: MO0703PASDSTAT.001, worksheets "Gamma Abstraction" and "Data at 2.44 mps PGV" in the file *WP-Rubble Damage Abstraction 17-mm Degraded.xls.*

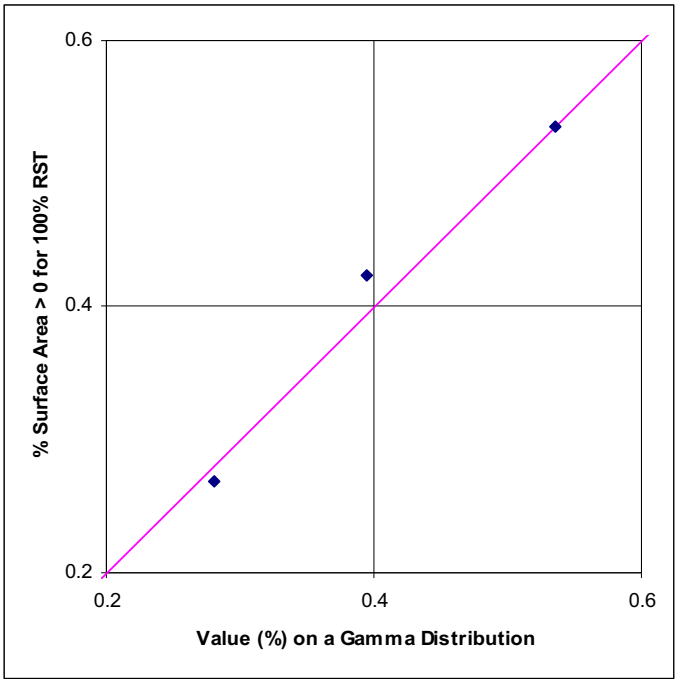

Source: Output DTN: MO0703PASDSTAT.001, worksheet "ACMs at 4.07 PGV" in the file *WP-Rubble Damage Abstraction 17-mm Degraded.xls.*

NOTE: 17-mm-thick OCB with degraded internals. 100% RST at the 4.07 m/s PGV level.

Figure 6-83. Q-Q Plot for Conditional Damaged Areas versus a Gamma Distribution for the TAD-Bearing Waste Package Surrounded by Rubble

Figure 6-83 is a Q-Q plot for a gamma distribution versus the conditional damaged areas at the 100% RST and the 4.07 m/s PGV level. Figure 6-83 demonstrates that the gamma distribution again provides a very good fit to the damaged area data for the 100% RST.

The standard deviations in Table 6-45 are quite small at the 100% and 105% RST levels. This behavior is probably due to the small sample size at 100% RST and 105% RST, three points and two points, respectively. Since there are seven data points at the 90% RST level, it seems reasonable to use the coefficient of variation at the 90% RST level to estimate the standard deviations at 100% and 105% RST. The coefficient of variation is the ratio of the standard deviation to the mean. Table 6-46 presents the data set with modified values of the standard deviation at 100% RST and 105% RST.

The abstraction for the TSPA must represent the response for intermediate values of RST, between 90% and 105%. Simple quadratic fits to the mean and modified standard deviations of the data sets at the three values of RST shown in Table 6-46 provide a convenient way to represent the input parameters for the gamma distribution as a function of RST. Figure 6-84 shows the quadratic fits for the mean and standard deviation at the 4.07 m/s PGV level as a function of RST.

Table 6-46. Mean and Modified Standard Deviations of the Conditional Damaged Areas for the 17-mm-Thick OCB with Degraded Internals

PGV Level (m/s)	Residual Stress Threshold (% of Yield Strength)					
	90%		100%		105%	
	Mean (% Surface Area)	Standard Deviation (% Surface Area)	Mean (% Surface Area)	Modified Standard Deviation (% Surface Area)	Mean (% Surface Area)	Modified Standard Deviation (% Surface Area)
2.44	1.396	1.003	–	–	–	–
4.07	2.214	2.064	0.409	0.381	0.136	0.127

Source: Output DTN: MO0703PASDSTAT.001, worksheets "Gamma Abstraction - Modified" and "Data at 2.44 mps PGV" in the file *WP-Rubble Damage Abstraction 17-mm Degraded.xls.*

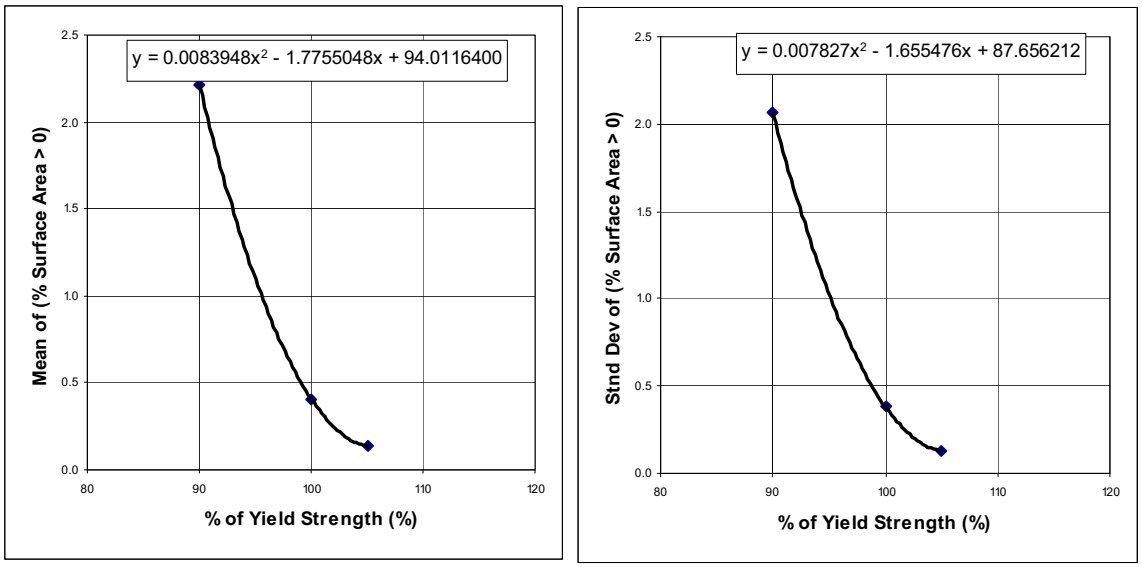

Source: Output DTN: MO0703PASDSTAT.001, worksheet "Gamma Abstraction - Modified" in the file *WP-Rubble Damage Abstraction 17-mm Degraded.xls.*

NOTE: 17-mm-thick OCB with degraded internals at the 4.07 m/s PGV level.

Figure 6-84. Quadratic Fits to the Mean and Standard Deviation of Conditional Damaged Areas for the TAD-Bearing Waste Package Surrounded by Rubble

Figure 6-85 plots the 1st, 5th, 50th, 95th, and 99th percentiles of the resulting gamma distributions against the conditional damaged areas. The gamma distributions, with the quadratic fits defined in Figure 6-84, provide a reasonable representation of the conditional damaged areas over the complete RST range, from 90% to 105%.

The abstraction for the TSPA must represent the response for a range of PGV levels, rather than the damage at the single 4.07 m/s PGV level shown in Figures 6-82 to 6-85. It is difficult to extrapolate the conditional damage at the 4.07 m/s PGV level to the range of PGV values for the TSPA. In this particular case, the damaged areas for the 4.07 m/s PGV level are greater than the damaged areas for all values of PGV less than 4.07 m/s, so the conditional damage at the 4.07 m/s PGV level is an upper bound for all values of PGV in the TSPA.

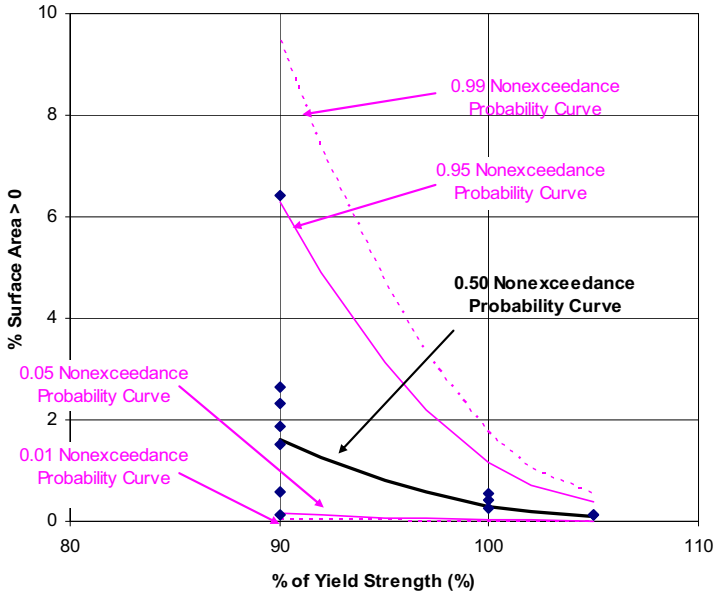

Source: Output DTN: MO0703PASDSTAT.001, worksheet "Gamma Abstraction - Modified" in the file *WP-Rubble Damage Abstraction 17-mm Degraded.xls.*

NOTE: 17-mm-thick OCB with degraded internals at the 4.07 m/s PGV level.

Figure 6-85. Comparison of Percentiles on the Gamma Distributions to Conditional Damaged Areas for the TAD-Bearing Waste Package Surrounded by Rubble

Conditional damage can only occur when the probability of damage is greater than zero. The probabilities in Figure 6-81 ensure that the damaged area for the TSPA remains zero for small values of PGV, in spite of the bounding approach for the conditional damaged area. This can be demonstrated by plotting the expected damaged area, defined as the product of the probability of damage and the mean conditional damaged area. The expected damaged area is the effective damaged area for the TSPA because it is the product of the probability of damage and the magnitude of the conditional damaged area. Figure 6-86 demonstrates that the expected damaged area remains zero for small values of PGV, even with the bounding approach for the magnitude of the conditional damaged area. Figure 6-86 also demonstrates that the magnitude of the expected damaged area is always less than 1% of the surface area of the waste package at all PGV levels.

6.9.4 Alternate Conditional Probability Distributions for the 17-mm-Thick OCB

The gamma distribution produces a better match to the sum of the squared differences than a log-normal distribution and approximately the same match as a Weibull distribution for this data set (see numerical calculations in output DTN: MO0703PASDSTAT.001, worksheet "ACMs for 4.07 ms PGV Data" in the file *WP-Rubble Damage Abstraction 17-mm Degraded.xls*). The gamma distribution is the preferred approach because it is straightforward and does not involve the adjustment of parameters for the Weibull distribution.

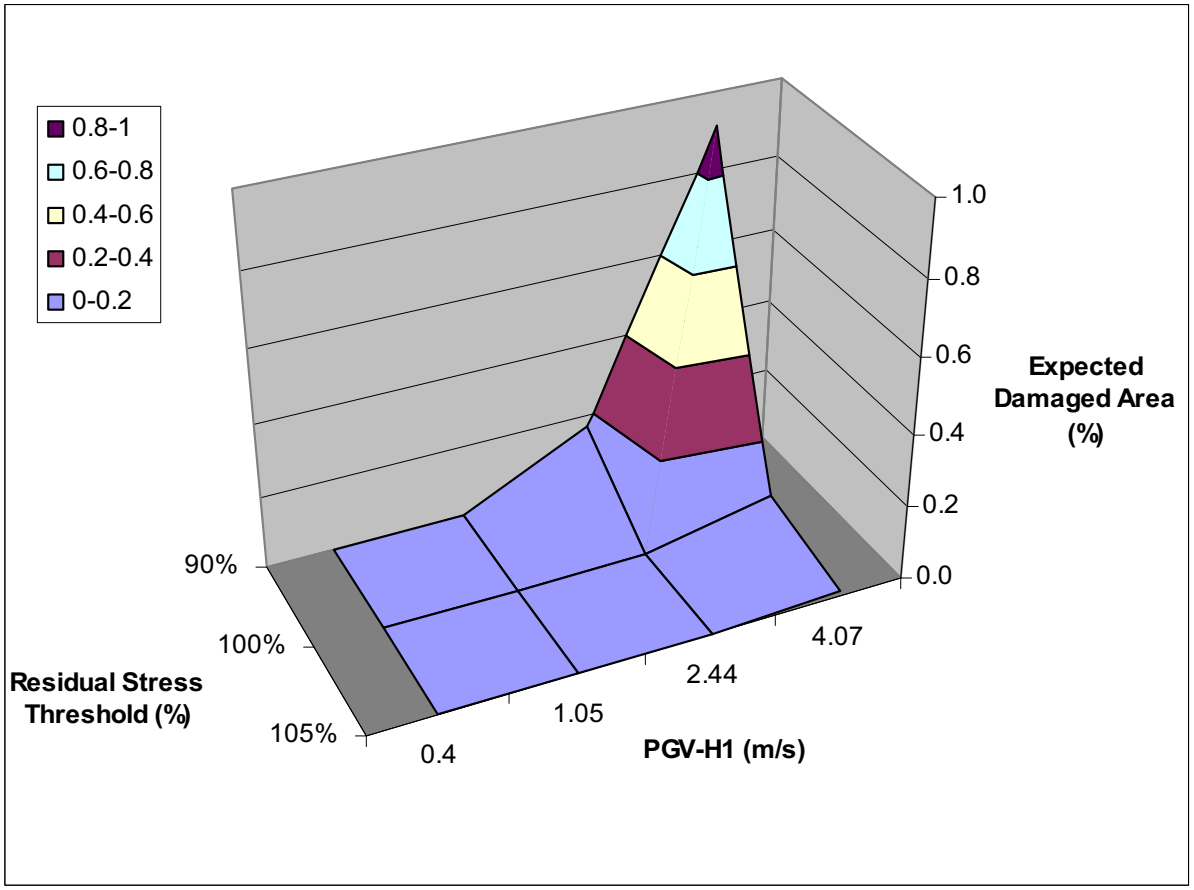

Source: Output DTN: MO0703PASDSTAT.001, worksheet "Expected Damage" in the file *WP-Rubble Damage Abstraction 17-mm Degraded.xls.*

NOTE: 17-mm-thick OCB with degraded internals at the 4.07 m/s PGV level.

Figure 6-86. Expected Damaged Area for the TAD-Bearing Waste Package Surrounded by Rubble

6.9.5 Conditional Probability Distributions for Nonzero Damaged Area with 23-mm-Thick OCB

Relatively few data points have nonzero damaged areas for the 23-mm-thick OCB. There are only five points, two points, and one point with nonzero damaged areas at the 90%, 100%, and 105% RSTs, respectively, for the 4.07 m/s PGV level. There are no points with nonzero damaged areas at the 0.4 m/s, 1.05 m/s, and 2.44 m/s PGV levels. With few nonzero damaged area data points, the fact that gamma distributions provide a reasonable representation of the damaged areas for the 17-mm-thick OCB is used to guide the approach for the 23-mm-thick OCB.

Figure 6-87 is a Q-Q plot for a gamma distribution versus the conditional damaged areas at 90% RST and the 4.07 m/s PGV level. Figure 6-87 demonstrates that the gamma distribution provides an acceptable fit to the conditional damaged areas data at 90% RST and the 4.07 m/s PGV level.

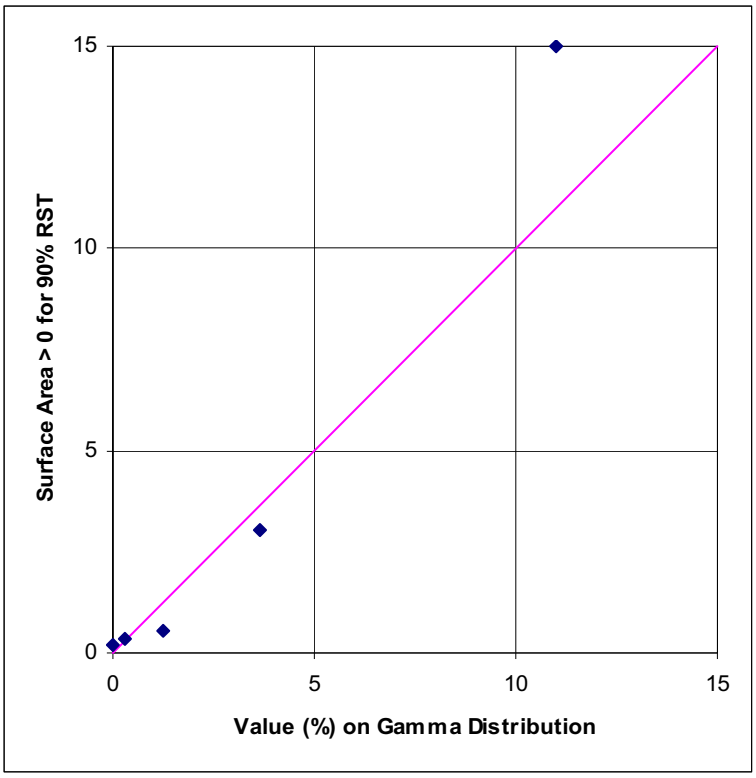

Source: Output DTN: MO0703PASDSTAT.001, worksheet "ACMs at 4.07 PGV" in the file *WP-Rubble Damage Abstraction 23-mm Degraded.xls.*

NOTE: 23-mm-thick OCB with degraded internals. 90% RST at the 4.07 m/s PGV level.

Figure 6-87. Q-Q Plot for Conditional Damaged Areas versus a Gamma Distribution for the TAD-Bearing Waste Package Surrounded by Rubble

The 100% RST and 105% RST data have so few points that it is difficult to estimate the standard deviation. In this situation, the standard deviations at 100% RST and 105% RST have been estimated based on the coefficient of variation for the 90% RST where there are more samples. The mean values and the modified values for the standard deviation are shown in Table 6-47.

Quadratic fits to the mean and standard deviation of the data sets at the three values of RST, based on the data in Table 6-47, provide a convenient way to represent the input parameters for the gamma distribution as a function of RST (see Figure 6-88). Using these quadratic fits, Figure 6-89 plots the 1st, 5th, 50th, 95th, and 99th percentiles of the resulting gamma distributions against the conditional damaged areas. The gamma distributions provide a reasonable representation of the conditional damaged areas over the complete RST range, from 90% to 105%, at the 4.07 m/s PGV level.

Table 6-47. Mean and Standard Deviations of the Conditional Damaged Areas for the 23-mm-Thick OCB with Degraded Internals

PGV Level (m/s)	Residual Stress Threshold (% of Yield Strength)					
	90%		100%		105%	
	Mean (% Surface Area)	Standard Deviation (% Surface Area)	Mean (% Surface Area)	Modified Standard Deviation (% Surface Area)	Mean (% Surface Area)	Modified Standard Deviation (% Surface Area)
4.07	3.836	6.344	1.186	1.961	1.012	1.673

Source: Output DTN: MO0703PASDSTAT.001, worksheet "Gamma Abstraction - Modified" in the file *WP-Rubble Damage Abstraction 23-mm Degraded.xls.*

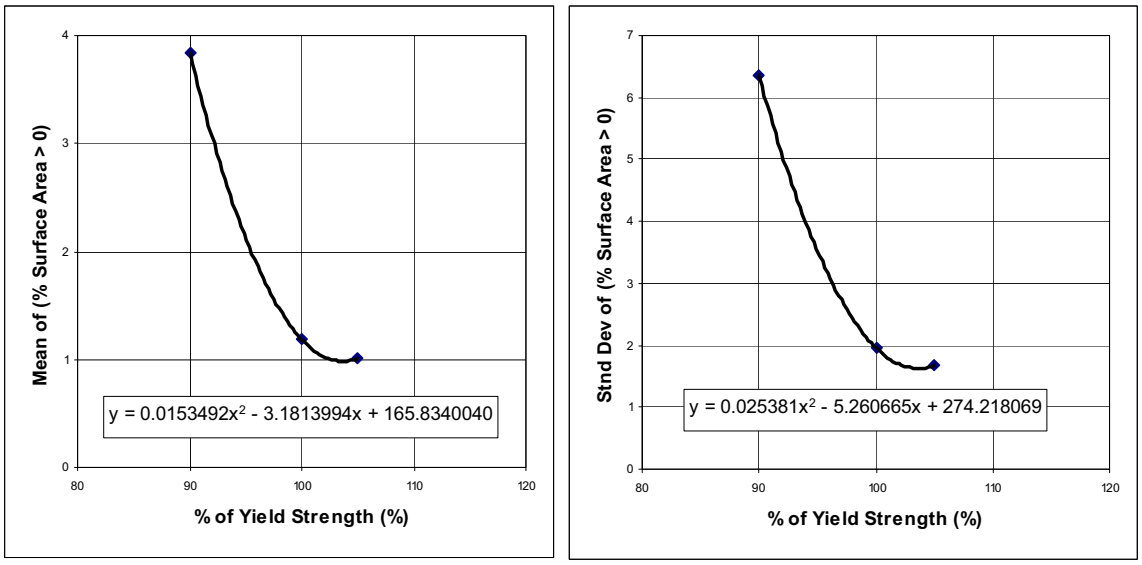

Source: Output DTN: MO0703PASDSTAT.001, worksheet "Gamma Abstraction - Modified" in the file *WP-Rubble Damage Abstraction 23-mm Degraded.xls.*

NOTE: 23-mm-thick OCB with degraded internals at the 4.07 m/s PGV level.

Figure 6-88. Quadratic Fits to the Mean and Standard Deviation of Conditional Damaged Areas for the TAD-Bearing Waste Package Surrounded by Rubble

The abstraction for the TSPA must represent the response for a range of PGV levels, rather than the damage at the single PGV level of 4.07 m/s shown in Figures 6-87 to 6-89. It is not possible to extrapolate the conditional damage at the 4.07 m/s PGV level to the range of PGV values for the TSPA. In this particular case, the results for the 4.07 m/s PGV level are applied at all PGV levels because the conditional damage at the 4.07 m/s PGV level is an upper bound for the damage for all values of PGV less than 4.07 m/s in the TSPA.

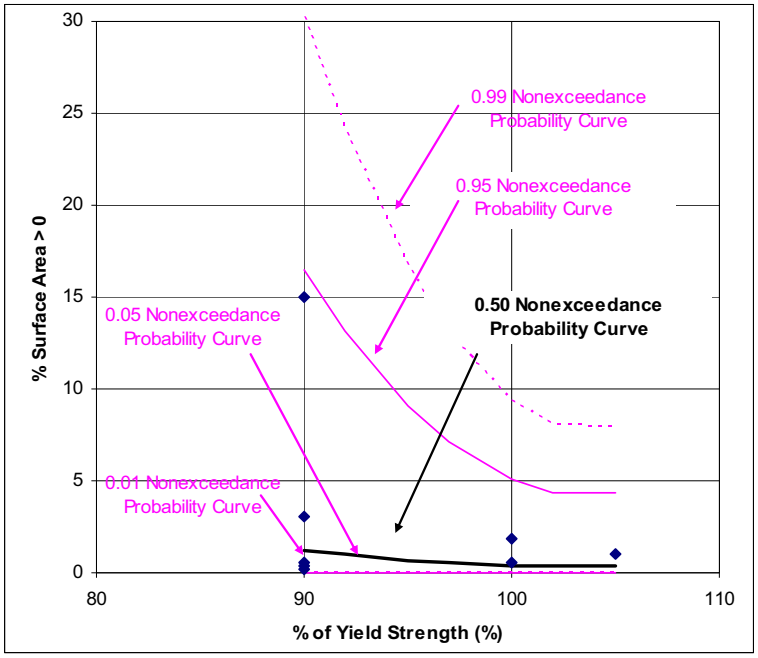

Source: Output DTN: MO0703PASDSTAT.001, worksheet "Gamma Abstraction - Modified" in the file *WP-Rubble Damage Abstraction 23-mm Degraded.xls.*

NOTE: 23-mm-thick OCB with degraded internals at the 4.07 m/s PGV level.

Figure 6-89. Comparison of Percentiles on the Gamma Distributions to Conditional Damaged Areas for the TAD-Bearing Waste Package Surrounded by Rubble

6.9.6 Dependence on OCB Thickness and State of the Internals

The conditional probability distributions described in previous sections represent the variation of damaged area as a function of PGV and RST for a waste package surrounded by rubble. The time-dependent thickness of the OCB must also be incorporated into the damage abstraction for the waste package surrounded by rubble.

The spatially averaged thickness of the OCB is a time-dependent parameter that is predicted by other elements of the TSPA. The conditional damaged area corresponding to this average OCB thickness is calculated by linear interpolation if the OCB thickness is between 17 mm and 23 mm. Damaged areas are often observed to follow a power law, as illustrated by the quadratic fit for mean damaged area as a function of RST in Figure 6-84. But since data are only available at two thicknesses (17 mm and 23 mm), the use of linear interpolation is appropriate because it provides greater probabilities at intermediate values relative to a power-law fit whose slope is positive and increasing as a function of PGV between the two thicknesses. The logic for the dependence on damaged area on OCB thickness is illustrated in Equation 6.9-3:

$$DA_{WP\_Rubble} = \text{If } t \geq 23 \text{ mm}, DA_{WP\_Rubble,23\text{-}mm} \quad \text{(Eq. 6.9-3)}$$

$$\text{Or if } t \leq 17 \text{ mm}, DA_{WP\_Rubble,17\text{-}mm}$$

$$\text{else, } DA_{WP\_Rubble,17\text{-}mm} + (DA_{WP\_Rubble,23\text{-}mm} - DA_{WP\_Rubble,17\text{-}mm})*(t - 17 \text{ mm})/(6 \text{ mm})$$

where t is the spatially averaged thickness of the OCB (in mm) at the time of the seismic event, DA_{WP_Rubble} is the final damaged area at the current average OCB thickness, $DA_{WP\_Rubble,17\text{-}mm}$ is the value of the conditional damaged area from the 17-mm damage abstraction, and $DA_{WP\_Rubble,23\text{-}mm}$ is the value of the conditional damaged area from the 23-mm damage abstraction. Based on Equation 6.9-3, the damaged area is set to the value at 23 mm if the average OCB thickness is greater than 23 mm. This is reasonable because the damaged area abstraction for the 23-mm-thick OCB bounds the waste package response for several hundred thousand years after repository closure, based on the estimated corrosion time in Section 6.5.1.2. The damaged area is set to the value for the 17 mm thickness if the average OCB thickness is less than 17 mm. This is a reasonable approach because the damaged area abstraction for the 17-mm-thick OCB provides a reasonable representation at the end of the peak dose period (approximately 1,000,000 years), based on the estimated corrosion time in Section 6.5.2.2.

Finally, it is possible that the drip shield will fail before the OCB is breached, resulting in a waste package that has intact internals and is surrounded by rubble. The damage abstraction for degraded internals provides an upper bound for the damage to a waste package with intact internals that is surrounded by rubble. The damage abstractions defined in this section should be used regardless of the state of the internals.

6.9.7 Damage from Multiple Events

The damaged area from multiple seismic events is defined as the sum of the damaged areas from the individual seismic events. This approach overestimates total damaged area because work hardening of dented or deformed areas on the surface of the waste package makes it more difficult to damage these areas during a subsequent event, and because the summation of damaged areas from individual events ignores impact location entirely. This viewpoint is confirmed by the results for the single waste package calculations with a fine finite-element grid at 0.4 m/s PGV level, which demonstrate that there is little apparent "amplification" from multiple hits to the same area during a seismic event, judging by the very small magnitude of the damaged areas in Tables 6-8 and 6-23. In this situation, linear summation of damaged area overestimates the accumulation of residual stress.

6.9.8 Location of Damaged Area

The damaged areas on the waste package surrounded by rubble are represented as randomly located on the cylindrical surface of the OCB. The damaged areas for the waste package surrounded by rubble are based on two-dimensional calculations for a cross section through the waste package, in the plate perpendicular to its axis of symmetry. Given this computational model, the calculated damaged areas on waste package always occur on the cylindrical surface of the OCB, rather than on the lids of the waste package. But this representation is reasonable because the cylindrical surface has a large area that directly bears the dynamic loads from the surrounding rockfall during vibratory ground motion. In addition, the pattern of rock fragments and their contact with the cylindrical surface is expected to be highly random, consistent with damaged areas that are randomly located on the surface of the OCB. The cylindrical surface area of the OCB for the TAD-bearing waste package is 33.64 m^2, based on an outer diameter of the OCB of 1,881.6 mm and a nominal length of the OCB of 5,691.38 mm (SNL 2007 [DIRS 179394], Table 4-3).

6.9.9 Spatial Variability

Damage to or puncture of the waste package surrounded by rubble is constant throughout the repository, for each seismic event in the TSPA. That is, there is no spatial variability of damage or rupture for the waste package groups within the TSPA. Lack of spatial variability is not important for predicting the mean dose in the TSPA. The mean dose is independent of spatial variability because the sum of the mean doses from groups of waste packages with different damage levels is equal to the mean of the sum of the doses from the individual groups. On the other hand, the coefficient of variation (i.e., the variability about the mean) of the total dose over all realizations, is overestimated without spatial variability because lack of spatial variability makes an extreme response for all waste package groups more likely than for a model with spatial variability.

6.9.10 Response of TAD-Bearing versus Codisposal Waste Packages with Degraded Internals

Separate models are not being developed for the TAD-bearing and codisposal waste packages surrounded by rubble because the results from the TAD-bearing waste package provide a reasonable estimate of damage for the codisposal waste package. With degraded internals, the computational model for the TAD-bearing waste package has a 23-mm-thick or 17-mm-thick OCB, and all internal components (inner vessel, TAD canister, fuel baskets, and fuel assemblies) are represented as a material that is similar to sand, with no significant strength and with very limited cohesion (SNL 2007 [DIRS 178851], Section 6.5.1). The computational model for the codisposal waste package with degraded internals is similar to the model for the TAD-bearing waste package because the initial OCB thicknesses of both waste packages are the same and because the outer diameter and total loaded mass of both waste packages are similar.

Table 6-48 shows the numerical comparisons for these parameters. The outer diameter of the OCB for the codisposal waste package is 8.7% greater than the corresponding quantity for the TAD-bearing waste package, and the mass of the fully loaded codisposal waste package is 21.1% less than the weight of the TAD-bearing waste package. The structural response of the TAD-bearing and codisposal waste packages with degraded internals is expected to be quite similar because the load-bearing structural component, the cylindrical OCB, has the same thickness for either waste package, and because the differences in outer diameter of the OCB and fully loaded weight are modest.

The concept that the TAD-bearing and codisposal packages will have similar structural response with degraded internals can be confirmed by comparing the damaged areas in Sections 6.5.2 and 6.6.2 for the kinematic response of the TAD-bearing and codisposal waste packages with degraded internals and a 17-mm-thick OCB. Figures 6-90 and 6-91 compare the mean and standard deviations of the damaged areas at four PGV levels and three values of RST. Results for the 23-mm-thick OCB with degraded internals are very similar to the results for the 17-mm-thick OCB, so they are not repeated here. The results for the 23-mm-thick OCB can be found in output DTN: MO0703PASDSTAT.001, worksheet “CDSP-TAD Comparison” in the file *CDSP Kinematic Damage Abstraction 23-mm Degraded.xls*.

Table 6-48. Structural Parameters for the TAD-Bearing and Codisposal Waste Packages

Parameter	TAD-Bearing Waste Package	Codisposal Waste Package	Difference
OCB Thickness	25.4 mm	25.4 mm	0%
Outer Diameter of OCB	1,881.6 mm (74.08 in)	2,044.7 mm (80.50 in)	+8.7%
Fully Loaded Mass	162,055 lbm	127,870 lbm	−21.1%

Sources: SNL 2007 [DIRS 179394], Table 4-3 for the TAD-bearing waste package.
SNL 2007 [DIRS 179567], Table 4-9 for the 5 DHLW/DOE SNF-Long codisposal waste package.

Figure 6-90 demonstrates that the mean conditional damaged areas for the TAD-bearing and codisposal waste packages have similar magnitudes up to the 2.44 m/s PGV level, with the damaged area for the TAD-bearing waste package always equal to or greater than the damaged area for the codisposal waste package. The increase in damaged area for the TAD-bearing waste package is probably caused by its greater mass. Figure 6-91 demonstrates that the standard deviations of the conditional damaged areas for the TAD-bearing and codisposal waste packages generally have very similar magnitudes up to the 2.44 m/s PGV levels.

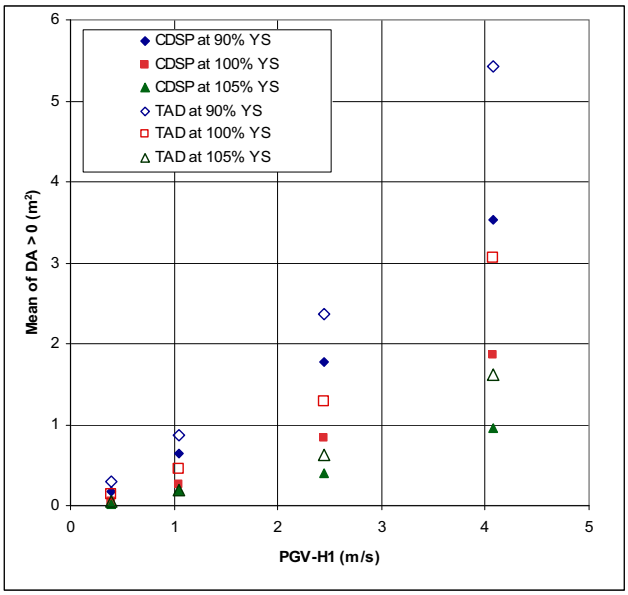

Source: Output DTN: MO0703PASDSTAT.001, worksheet “CDSP-TAD Comparison” in the file *CDSP Kinematic Damage Abstraction 17-mm Degraded.xls.*

NOTE: Kinematic response, 17-mm-thick OCB.

Figure 6-90. Comparison of Mean Conditional Damaged Areas for the Kinematic Response of the TAD-Bearing and Codisposal Waste Packages with Degraded Internals

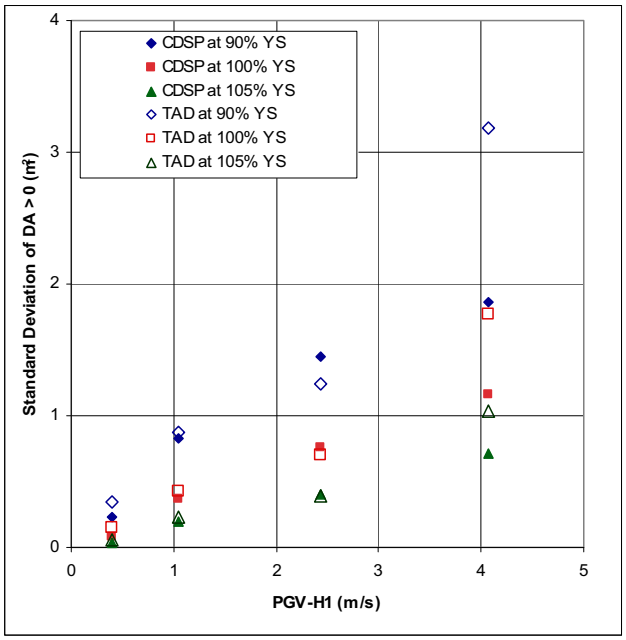

Source: Output DTN: MO0703PASDSTAT.001, worksheet "CDSP-TAD Comparison" in the file *CDSP Kinematic Damage Abstraction 17-mm Degraded.xls.*

NOTE: Kinematic response, 17-mm-thick OCB.

Figure 6-91. Comparison of Standard Deviations for the Conditional Damaged Areas from the Kinematic Response of the TAD-Bearing and Codisposal Waste Packages with Degraded Internals

The potential differences in mean damaged areas for a TAD-bearing or codisposal waste package surrounded by rubble are expected to be less than the differences in Figure 6-90. Damage in the kinematic models arises from waste package-to-pallet impacts, which are sensitive to the mass differences between the packages. Damage for a waste package surrounded by rubble is caused by the deformation of the OCB under dynamic rockfall loads and not by discrete impacts between components. In this situation, the damaged areas for a waste package surrounded by rubble should be less sensitive to the mass difference between the waste packages, and the damaged areas for the TAD-bearing waste package are a reasonable representation for the damaged areas for the codisposal waste package surrounded by rubble.

6.10 ABSTRACTIONS FOR DAMAGE TO THE DRIP SHIELD

The drip shields may accumulate damage from vibratory ground motion and from rockfall induced by vibratory ground motion from repository closure until the drip shield plates fail. In the lithophysal units, the accumulation of rubble from multiple seismic events and the dynamic motion during a seismic event may generate damaged areas on the drip shield. These damaged areas are regions that exceed the residual (tensile) stress threshold for the drip shield plates, potentially leading to a network of stress corrosion cracks that could allow seepage to flow through the cracks. The focus here is on the drip shield plates because the plates are located on the crown of the drip shield and are the main barrier to seepage. The plates are fabricated from Titanium Grade 7, which has a RST of 80% of the yield strength of this alloy. The damaged areas in the lithophysal zones are analyzed as a function of the thickness of the drip shield plate,

the rockfall load on the drip shield, and the vertical component of peak ground acceleration for the seismic event.

In the nonlithophysal units, rock blocks can impact the drip shield in an unfilled or partly filled drift. Block impacts may result in damaged areas on the drip shield plates and, in more extreme cases, may result in tearing or rupture of the plates and failure of the axial stiffeners beneath the crown of the drip shield. The damaged areas and potential for plate or stiffener failure are analyzed as a function of the thickness of the drip shield plates and framework, the rockfall load on the drip shield, and the vertical component of peak ground acceleration for the seismic event.

Section 6.10.1 discusses the abstraction for damaged area on the drip shields in the lithophysal zones. Section 6.10.2 discusses the abstraction for damaged area and plate failures for drip shields in unfilled or partly filled drifts in the nonlithophysal units of the repository. Section 6.10.1.6 discusses the potential for damage to the waste package from lithophysal rubble and Section 6.10.2.11 discusses the potential for damage to the waste package from large rock blocks in the nonlithophysal units.

FEP 1.2.03.02.0B, Seismic-Induced Rockfall Damages EBS Components, is being excluded from the TSPA compliance case for the license application. The screening argument focuses on the potential impacts on the drip shields and waste packages from rockfalls involving large rock blocks in the nonlithophysal zones. The seismic damage abstractions for the drip shield, as derived in this section, support the screening arguments for excluding FEP 1.2.03.02.0B. However, these seismic damage abstractions are not included in the compliance case for the TSPA-LA because of the exclusion of FEP 1.2.03.02.0B. The damage abstractions in this section are independent of the drip shield fragility curves in Section 6.8, which depend on the loads from lithophysal rubble rather than large rock blocks in the nonlithophysal zone. The drip shield fragility curves are included in the compliance case for the TSPA-LA.

6.10.1 Drip Shield Damaged Area in the Lithophysal Zone

The key parameters for the damaged area analysis are the rockfall load on the crown of the drip shield, the peak ground velocity from a seismic event, and the thickness of the drip shield plate.

6.10.1.1 Static Load on the Drip Shield

The static rockfall load in a drift that is partly filled with rubble is defined as the product of the fraction of drift filled with rubble and the static rockfall load for a fully collapsed drift (see Section 6.8.1.2). Mathematically:

$$P_{Eff} = FD_j \times P_{STAT} \qquad \text{(Eq. 6.10-1)}$$

where P_{Eff} is the effective pressure on the drip shield for a partially filled drift, FD_j is the fraction of the drift that is filled with lithophysal rubble after the jth seismic event, and P_{STAT} is the static pressure from rockfall on the drip shield for a fully collapsed drift. This is a reasonable approach that tends to overestimate the vertical loads on the drip shield for small rubble volumes, as discussed in Section 6.7.2.1.

The static load from lithophysal rubble is expected to be much greater than the static load from nonlithophysal rockfall because the rockfall volume in the lithophysal units is much greater than that in the nonlithophysal units at a given PGV level (as discussed in Section 6.7.2.1). The damaged area analysis for the drip shield is based on the upper bound provided by the static load from lithophysal rubble and is applied throughout the repository.

6.10.1.2 Dynamic Load on the Drip Shield

Based on Equation 6.8-2, the dynamic pressure is approximated as $P_{Eff}(A+1)$ where A is the nondimensional peak ground acceleration in the vertical direction. The representations of both components of the dynamic load, P_{Eff} and $(A+1)$, are defined here. The representation for P_{STAT} is identical to the discussion in Section 6.8.1.2. The representation for $(A+1)$ follows a similar approach to the analysis in Section 6.8.1.1, except the regression analysis is performed for $(A+1)$ rather than A.

Lithophysal rockfall is expected to vary significantly because of the variability in mechanical properties in the host rock at the repository horizon and because of the variability in the fracture pattern and fracture spacing in the host rock. The resulting variability of rockfall loads from lithophysal rubble has been evaluated with six quasi-static calculations for degradation of drifts in lithophysal rock (BSC 2004 [DIRS 166107], Appendix P). The results for the average loads on the crown of the drip shield are presented in Table 6-34 (DTN: MO0407MWDDSLCR.000 [DIRS 170873], File *final drip shield quasi-static pressures.xls*). The mean and standard deviation of the natural logarithm of the average pressure for a fully collapsed drift are defined by Equations 6.8-15 and 6.8-16, repeated here from Section 6.8.1.2:

$$\lambda_{STAT} = 11.749 \qquad \text{(Eq. 6.8-15)}$$

and

$$\beta_{STAT} = 0.149 \qquad \text{(Eq. 6.8-16)}$$

For a partly filled drift, the static load is defined by Equation 6.10-1. The mean of the natural logarithm of the static load for a partly collapsed drift, λ_{pSTAT}, is then given by:

$$\lambda_{pSTAT} = \ln(f) + \lambda_{STAT} \qquad \text{(Eq. 6.10-2)}$$

where f is defined as:

$$f = Max(FD_j, 10^{-4}) \qquad \text{(Eq. 6.10-3)}$$

The lower limit for f of 10^{-4} avoids undefined values for the natural log of FD_j when FD_j is equal to zero. The resulting minimum value of P_{Static} is approximately 13 Pascals, small enough to be negligible in this analysis.

A regression analysis determines the relationship between the horizontal peak ground velocity (PGV-H1) and the quantity $(A+1)$. Figure 6-92 plots the least-squares fit for the natural logarithm of $(A+1)$ versus the natural logarithm of PGV-H1. Figure 6-93 evaluates the appropriateness of using a normal distribution to represent the residuals of $ln(A+1)$ relative to the least-squares fit in Figure 6-92. Figure 6-93 demonstrates an excellent fit for a normal

distribution, confirming the validity of a log-normal distribution for (A+1). Figure 6-94 confirms that the log-normal distribution provides a reasonable representation for (A+1) in physical space.

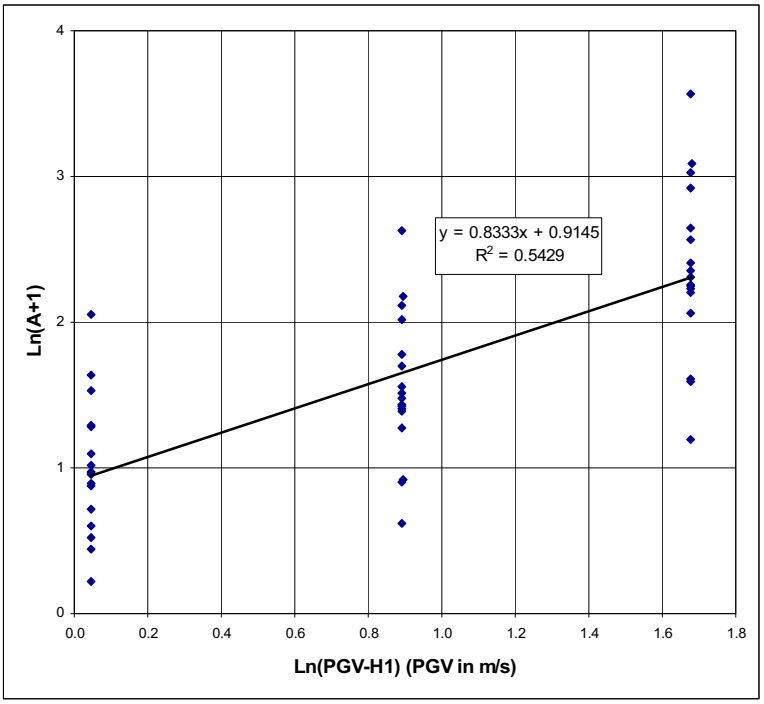

Source: Output DTN: MO0703PASDSTAT.001, worksheet "PGV-H1 to (A+1) Regression" in the file *DS Damaged Areas with Rubble.xls*.

NOTE: *A* is defined as (*PGA-V*)/*g*, where *PGA-V* is the vertical component of peak ground acceleration and *g* is the acceleration of gravity.

Figure 6-92. Least Squares Fit for *ln*(*A*+1) versus *ln*(PGV-H1)

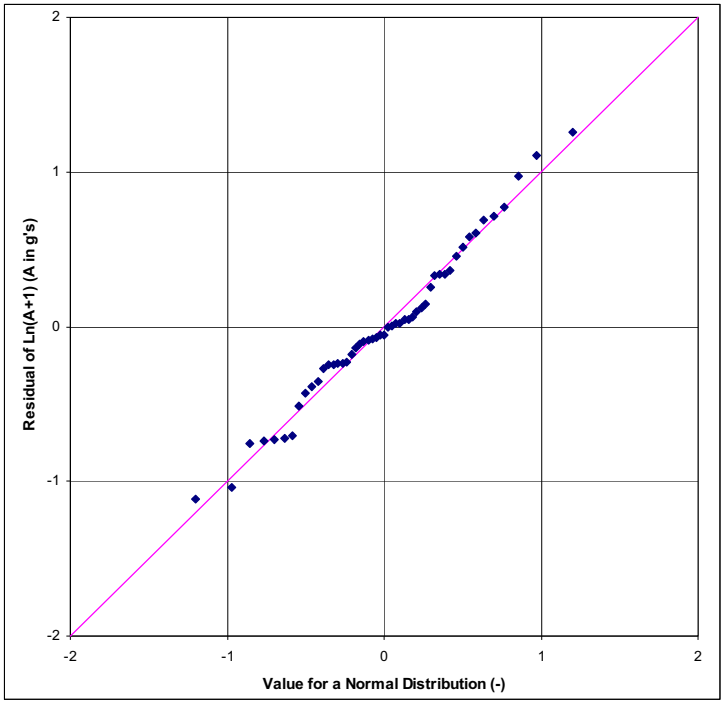

Source: Output DTN: MO0703PASDSTAT.001, worksheet "PGV-H1 to (A+1) Regression" in the file *DS Damaged Areas with Rubble.xls*.

Figure 6-93. Q-Q Plot for the Residuals of *ln*(A+1) versus a Normal Distribution

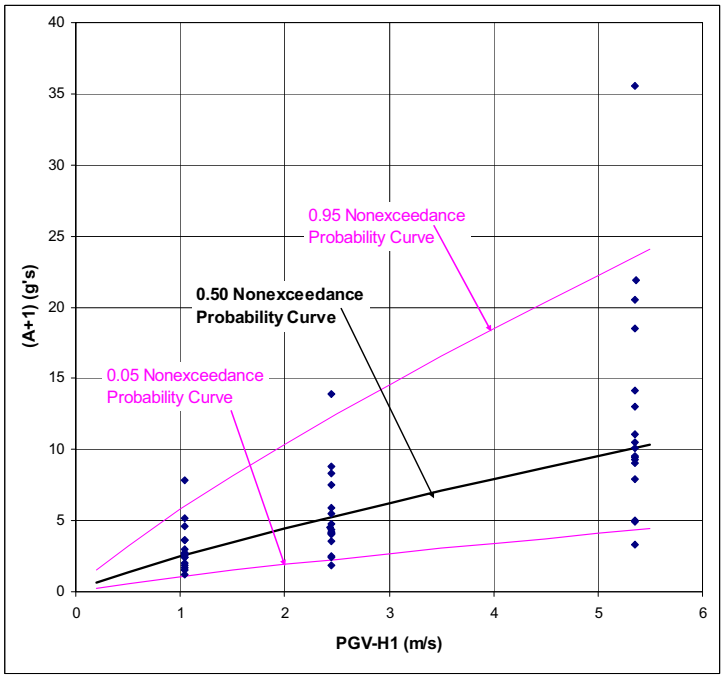

Source: Output DTN: MO0703PASDSTAT.001, worksheet "PGV-H1 to (A+1) Regression" in the file *DS Damaged Areas with Rubble.xls.*

Figure 6-94. Comparison of Percentiles on the Log-Normal Distributions with Observations for (*A*+1)

Equations 6.10-4 and 6.10-5 define the mean and standard deviation of the natural logarithm of (A+1). Equation 6.10-4 is based on the least-squares fit in Figure 6-92. Equation 6.10-5 is based on the calculated standard deviation in output DTN: MO0703PASDSTAT.001, worksheet "PGV-H1 to (A+1) Regression" in the file *DS Damaged Areas with Rubble.xls.*

$$\lambda_{(A+1)} = 0.8333 \times ln(PGV\text{-}H1) + 0.9145 \quad \text{(Eq. 6.10-4)}$$

and

$$\beta_{(A+1)} = 0.515 \quad \text{(Eq. 6.10-5)}$$

where *PGV-H1* represents the peak ground velocity for the first horizontal component of the ground motion. The total dynamic load is then the product of two independent parameters with log-normal distributions; it also has a log-normal distribution with parameters given by Hahn and Shapiro (1967 [DIRS 146529], p. 186):

$$\lambda_{dynamic} = \lambda_{(A+1)} + \lambda_{pSTAT} = \lambda_{(A+1)} + \ln(f) + \lambda_{STAT} \quad \text{(Eq. 6.10-6)}$$

$$\beta_{dynamic} = (\beta^2_{\ln(A+1)} + \beta^2_{pSTAT})^{\frac{1}{2}} \quad \text{(Eq. 6.10-7)}$$

Substituting the appropriate numerical values from Figure 6-92 and from Equations 6.8-15, 6.8-16, and 6.10-5 gives:

$$\lambda_{dynamic} = (0.8333 \times ln(PGV\text{-}H1) + 0.9145) + 11.749 + ln(f) \quad \text{(Eq. 6.10-8)}$$

$$\beta_{dynamic} = \sqrt{(0.149)^2 + (0.515)^2} = 0.536 \quad \text{(Eq. 6.10-9)}$$

6.10.1.3 Damaged Area as a Function of Total Dynamic Load

Quasi-static analyses were performed to determine damaged area as a function of total dynamic load for three plate thicknesses: 15 mm, 10 mm, and 5 mm. The calculations were carried out for uniformly distributed loads over a segment of the drip shield crown plate (SNL 2007 [DIRS 178851], Section 6.4.3.1). The analyzed segment includes the crown plate between two bulkheads, the middle stiffener and the shoulder (or legs) of the drip shield. Using symmetry of the segment geometry with respect to the vertical plane perpendicular to the drip shield axis, located half-way between the stiffeners, and symmetry of loading, only half of the segment was analyzed (SNL 2007 [DIRS 178851], Section 6.4.3.1.2 and Figures 6-38 and 6-39). This half of the segment between the bulkheads, middle stiffener, and the shoulder represents one twentieth of the crown of the drip shield. To obtain the damaged area for the entire drip shield, the reported results should be multiplied by 20.

The analyses were carried out for two sets of boundary conditions because of uncertainty in the distribution of rubble load along the drip shield and because only a single segment was considered in the plate fragility analysis. For the first boundary condition (Case 1), the plate boundaries along the middle stiffener and the bulkhead are considered fixed (for both translation and rotation). For the other boundary condition (Case 2), those boundaries are allowed to move laterally, but the rotation is fixed.

The damaged area is determined as the total area of elements on the inner and outer surfaces of the drip shield crown plate with the major principal stress greater than the RST for Titanium Grade 7, which is 80% of the yield strength of the Titanium Grade 7 at 60°C (SNL 2007 [DIRS 178851], Section 6.4.2, "Mechanical Properties of Titanium").

The overlapping damaged areas on the inner and outer surfaces should not be counted twice. However, the procedure for calculating the damaged areas is based on the sum of the areas on the inner and outer surfaces, irrespective of their relative geometrical position. Although the reported damaged area overestimates the actual damaged area, the overestimate is not significant for a significant portion of the load range while bending is the dominant mode of deformation. Bending causes tension on one side and compression on the other side, so the overlap does not occur with bending because damaged area only occurs for a tensile stress that exceeds the residual stress threshold.

Figures 6-95 to 6-97 summarize the cumulative distribution functions for damaged area at 1.05 m/s, 2.44 m/s, and 4.07 m/s PGV levels with 100% rockfall load, respectively. The results for Case 1 and Case 2 are generally very close, except near failure. In this situation, the case with the greatest damaged area has been selected for each plate thickness. Table 6-49 summarizes the numerical values for damaged areas for a single drip shield plate at plate thicknesses of 5 mm, 10 mm, and 15 mm. The data for the 10-mm- and 15-mm-thick plates are for the Case 2 boundary condition. The data for the 5-mm-thick plate are from the Case 1 boundary condition.

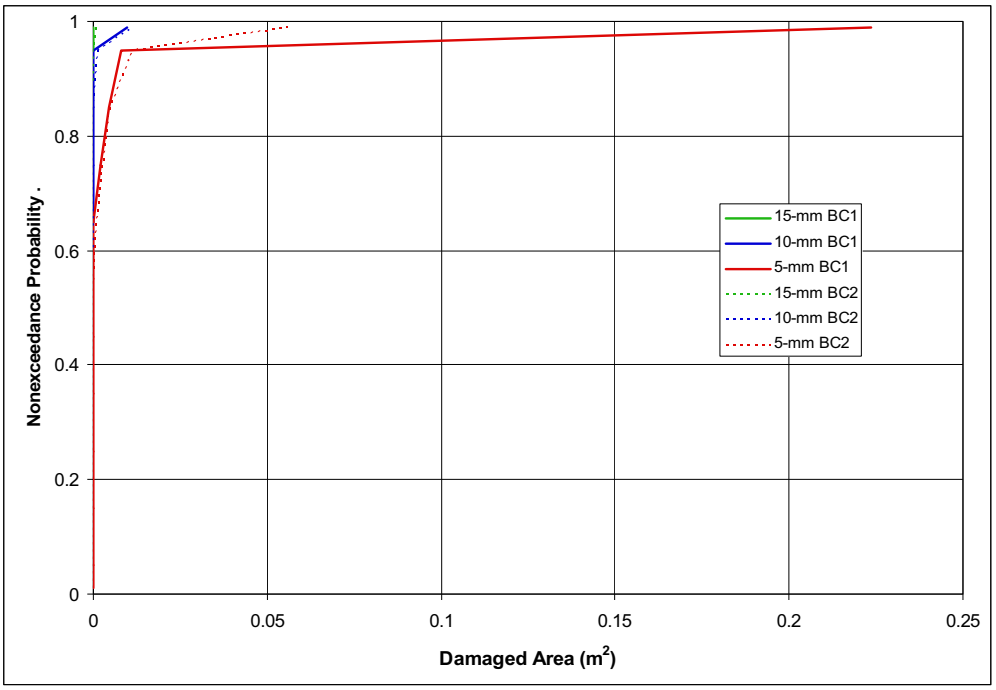

Source: Output DTN: MO0703PASDSTAT.001, worksheet "Summary" in the file *DS Damaged Areas with Rubble.xls*.

Figure 6-95. Cumulative Distribution Function for Damaged Area at 1.05 m/s PGV Level with 100% Rockfall Load

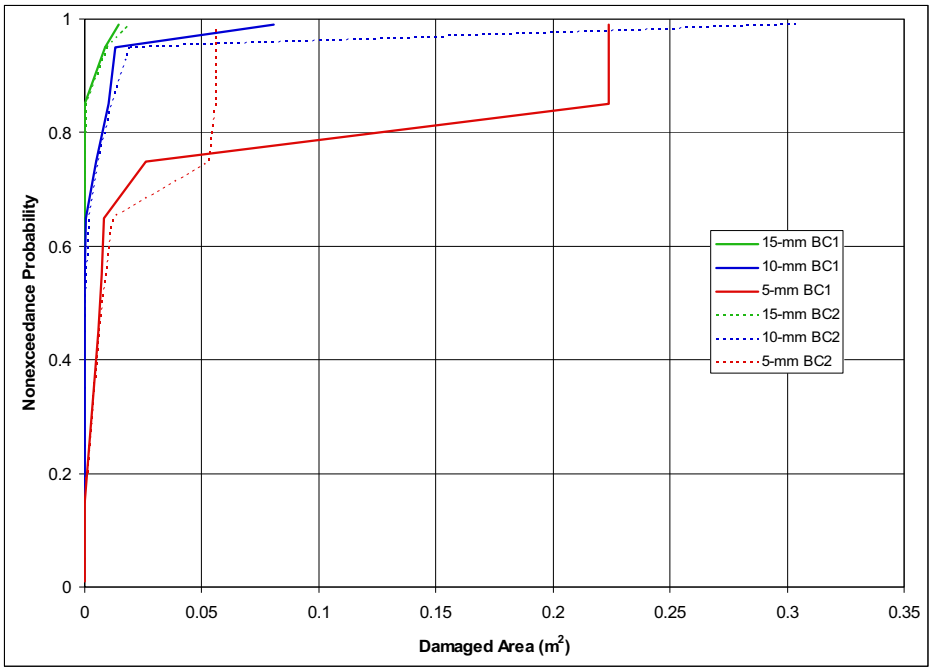

Source: Output DTN: MO0703PASDSTAT.001, worksheet "Summary" in the file *DS Damaged Areas with Rubble.xls.*

Figure 6-96. Cumulative Distribution Function for Damaged Area at 2.44 m/s PGV Level with 100% Rockfall Load

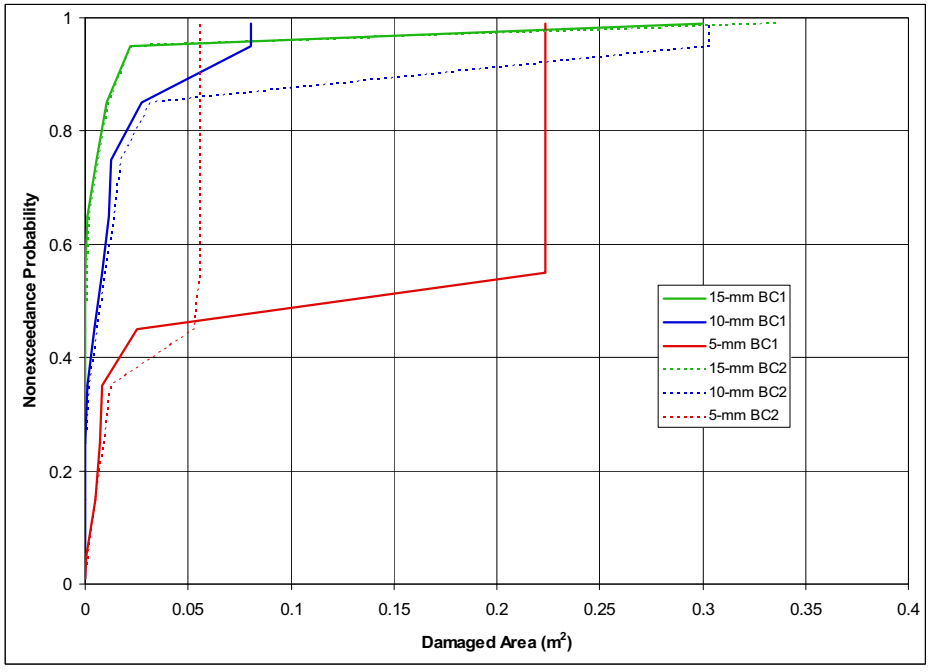

Source: Output DTN: MO0703PASDSTAT.001, worksheet "Summary" in the file *DS Damaged Areas with Rubble.xls.*

Figure 6-97. Cumulative Distribution Function for Damaged Area at 4.07 m/s PGV Level with 100% Rockfall Load

Table 6-49. Damaged Plate Areas as a Function of Total Dynamic Load

5-mm Plate Thickness		10-mm Plate Thickness		15-mm Plate Thickness	
Dynamic Load (Pa)	Damaged Plate Area (m^2)	Dynamic Load (Pa)	Damaged Plate Area (m^2)	Dynamic Load (Pa)	Damaged Plate Area (m^2)
1.00×10^{05}	0.00×10^{00}	2.00×10^{05}	0.00×10^{00}	4.00×10^{05}	0.00×10^{00}
2.00×10^{05}	0.00×10^{00}	4.00×10^{05}	0.00×10^{00}	8.00×10^{05}	0.00×10^{00}
3.00×10^{05}	0.00×10^{00}	6.00×10^{05}	0.00×10^{00}	1.20×10^{06}	1.24×10^{-03}
4.00×10^{05}	0.00×10^{00}	8.00×10^{05}	1.33×10^{-03}	1.60×10^{06}	9.43×10^{-03}
5.00×10^{05}	2.79×10^{-03}	1.00×10^{06}	7.39×10^{-03}	2.00×10^{06}	1.38×10^{-02}
6.00×10^{05}	5.34×10^{-03}	1.20×10^{06}	1.29×10^{-02}	2.40×10^{06}	2.09×10^{-02}
7.00×10^{05}	7.01×10^{-03}	1.40×10^{06}	1.71×10^{-02}	2.42×10^{06}	2.14×10^{-02}
8.00×10^{05}	8.03×10^{-03}	1.60×10^{06}	1.94×10^{-02}	2.44×10^{06}	2.22×10^{-02}
8.20×10^{05}	8.21×10^{-03}	1.62×10^{06}	1.97×10^{-02}	2.46×10^{06}	2.24×10^{-02}
8.40×10^{05}	8.38×10^{-03}	1.64×10^{06}	2.02×10^{-02}	2.48×10^{06}	2.29×10^{-02}
8.60×10^{05}	9.64×10^{-03}	1.66×10^{06}	2.04×10^{-02}	2.50×10^{06}	2.31×10^{-02}
8.80×10^{05}	1.11×10^{-02}	1.68×10^{06}	2.06×10^{-02}	2.52×10^{06}	2.39×10^{-02}
9.00×10^{05}	1.38×10^{-02}	1.70×10^{06}	2.07×10^{-02}	2.54×10^{06}	2.52×10^{-02}
9.20×10^{05}	1.78×10^{-02}	1.72×10^{06}	2.14×10^{-02}	2.56×10^{06}	2.55×10^{-02}
9.40×10^{05}	2.19×10^{-02}	1.74×10^{06}	2.27×10^{-02}	2.58×10^{06}	2.61×10^{-02}
9.60×10^{05}	2.80×10^{-02}	1.76×10^{06}	2.53×10^{-02}	2.60×10^{06}	2.64×10^{-02}
9.80×10^{05}	3.86×10^{-02}	1.78×10^{06}	3.44×10^{-02}	2.62×10^{06}	2.67×10^{-02}
1.00×10^{06}	1.64×10^{-01}	1.80×10^{06}	2.53×10^{-01}	2.64×10^{06}	2.70×10^{-02}
1.02×10^{06}	1.74×10^{-01}	1.82×10^{06}	2.71×10^{-01}	2.66×10^{06}	2.72×10^{-02}
1.04×10^{06}	1.96×10^{-01}	1.84×10^{06}	2.73×10^{-01}	2.68×10^{06}	2.83×10^{-02}
1.06×10^{06}	2.11×10^{-01}	1.86×10^{06}	2.79×10^{-01}	2.70×10^{06}	2.90×10^{-02}
1.08×10^{06}	2.23×10^{-01}	1.88×10^{06}	2.89×10^{-01}	2.72×10^{06}	3.11×10^{-02}
1.10×10^{06}	2.24×10^{-01}	1.90×10^{06}	2.91×10^{-01}	2.74×10^{06}	3.47×10^{-02}
–	–	1.92×10^{06}	2.95×10^{-01}	2.76×10^{06}	3.71×10^{-02}
–	–	1.94×10^{06}	3.04×10^{-01}	2.78×10^{06}	4.24×10^{-02}
–	–	–	–	2.80×10^{06}	4.71×10^{-02}
–	–	–	–	2.82×10^{06}	3.36×10^{-01}

Source: DTN: MO0703PADSBLOC.000 [DIRS 179662], File *DS plate damage due to distributed loads.xls*. The data for the 10-mm and 15-mm plate thicknesses are based on worksheet "Case 2 boundary condition." The data for the 5-mm plate thickness are based on worksheet "Case 1 boundary condition."

NOTE: An entry of "–" indicates that data are not available because of plate failure.

Within the TSPA, the damaged plate area on the drip shield is calculated from Table 6-49 and the total dynamic load. The total dynamic load for a seismic event with intensity *PGV-H1* is determined by sampling a log-normal distribution with parameter values $\lambda_{dynamic}$ and $\beta_{dynamic}$ defined by Equations 6.10-8 and 6.10-9. Once the dynamic load is determined for the seismic event, the entries in Table 6-49 provide a lookup table for calculating the damaged plate area. Two linear interpolations are required to calculate the damaged plate area. First, the damaged plate areas at thicknesses of 5 mm, 10 mm, and 15 mm are calculated with the sampled value of the total dynamic load. This first step produces three values of damaged plate area that provide the basis for a second interpolation that determines the damaged area at the current drip shield plate thickness, t, at the time of the seismic event. If t is less than 5 mm, then the value at 5 mm

is used to define the final damaged area. The use of the value for 5 mm is not expected to be a significant factor in the TSPA because the plates become increasingly likely to fail for plate thicknesses less than 5 mm, as defined in Section 6.8.2.

6.10.1.4 Damage from Multiple Events

The damaged area from multiple seismic events is defined as the sum of the damaged areas on the drip shield from the individual seismic events. This approach is an upper bound for total damaged area because work hardening of dented or deformed areas on the drip shield plates makes it more difficult to damage these areas during a subsequent event, and because the summation of damaged areas from individual events ignores the potential for the physical overlap of damage from multiple events. This viewpoint is confirmed by the results for the single waste package calculations with a fine finite-element grid at 0.4 m/s PGV level, which demonstrate that there is little apparent "amplification" from multiple hits to the same area during a seismic event, judging by the very small magnitude of the damaged areas in Tables 6-8 and 6-23. In this situation, linear summation of damaged area overestimates the accumulation of residual stress.

6.10.1.5 Location of Damaged Area

The damaged areas for the drip shield plates should be represented as randomly located on the crown on the drip shield. No damaged areas on the sides of the drip shield are considered because any seepage that passes through the sides is likely to flow down the sides and not make contact with the waste packages.

6.10.1.6 Waste Package Damage from Lithophysal Rubble

Rockfall in the lithophysal units can cause damaged areas on the drip shield, as defined by the damage abstraction in Section 6.10.1.3, and can cause buckling of the drip shield sidewalls and failure of the drip shield plates, as defined by the fragility curves in Sections 6.8.2.2 and 6.8.3.3. The response of the waste package after the sidewalls buckle is defined in Section 6.8.4, and the response of the waste package after failure of the drip shield plates is defined by the damaged abstractions for the waste package surrounded by rubble (see Section 6.9). These abstractions encompass the full range of response for the drip shield and waste package to seismically induced rockfall in the lithophysal units.

6.10.2 Drip Shield Damage in Nonlithophysal Units

Vibratory ground motions have the potential to eject large rock blocks in the nonlithophysal units. The mechanical response of the drip shield in response to impact by a large rock block could impair the functionality of the drip shield as a barrier to flow and as a barrier to rockfall on the waste package. This section describes the structural response calculations that have been performed to evaluate the mechanical response of intact and degraded drip shields to these impacts, and the damage abstractions that have been prepared for the seismic scenario class.

The technical approach for developing the damage abstraction for the drip shield due to large block impacts in the nonlithophysal units is summarized in the following steps. Figure 6-98 presents a flowchart of these steps. Additional details of the technical approach are provided in the subsections to this section.

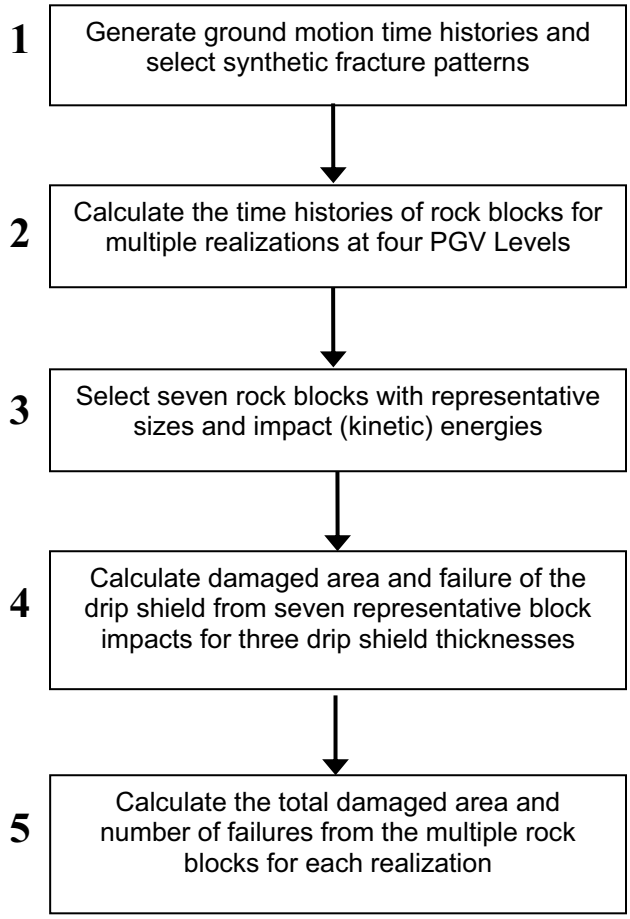

Source: Created for illustrative purposes only.

NOTE: The rockfall calculations for Box #1 and Box #2 are documented in (BSC 2004 [DIRS 166107]).

Figure 6-98. Methodology for Drip Shield Damage Abstraction from Rock Block Impacts

- Rockfall calculations for the nonlithophysal units (BSC 2004 [DIRS 166107]) have been performed for ground motions at the 0.4 m/s, 1.05 m/s, 2.44 m/s, and 5.35 m/s PGV levels. The nonlithophysal units are represented by a suite of 105 synthetic fracture patterns (see Box #1 above). Within the rockfall calculations, the drip shield is represented as a simplified, rectangular structure for the purposes of determining block impacts. Each rockfall calculation defines the sequence of rock blocks that strike the sides or top of the drip shield. The output parameters for each calculation include the mass, relative impact velocity, impact location, impact angle, and impact energy associated with each block that strikes the drip shield (see Box #2 above). Further details of the rockfall calculations are provided in Section 6.10.2.1.

- Based on the block output parameters, a set of seven representative blocks that span the full range of impact energies are selected to optimize the structural response calculations (see Box #3 above). The seven representative blocks include blocks with small impact energies that do minimal damage to the drip shield and the block with the maximum impact energy. The properties of the seven representative blocks are described in Section 6.10.2.2.

- Structural response calculations determine the dynamic response of the drip shield to impact by the seven blocks (see Box #4 above). Three states of the drip shield are considered. The intact state has no thickness reduction to drip shield components from general corrosion. There are two degraded states: one with a 5-mm thickness reduction from general corrosion and a second with a 10-mm thickness reduction from general corrosion. These thickness reductions are uniformly applied to the smallest dimensions of the drip shield plates and the drip shield framework. For example, these three states correspond to drip shield plate thicknesses of 15 mm, 10 mm, and 5 mm, respectively, because the drip shield plates are initially 15 mm thick. The structural response calculations for individual rock blocks impacting the drip shield are described in Section 6.10.2.2.

  The structural response calculations determine the plate area that exceeds the RST of 80% of the yield strength for Titanium Grade 7. This area is referred to as damaged area throughout Section 6.10. The structural response calculations also determine the maximum plastic strain in the plates, the maximum plastic strain in the axial stiffeners beneath the crown of the drip shield, and the final deflection of the crown of the drip shield. A comparison of the maximum plastic strains with the ultimate plastic strain determines the potential for tearing or rupture of the drip shield plates and axial stiffeners, as discussed in Section 6.10.2.2. Tearing or rupture of the drip shield plates and axial stiffeners is referred to as drip shield failure throughout Section 6.10. The results for damaged area, maximum plastic strains, and final deflection are collated into four catalogs, as shown in Section 6.10.2.2. Each catalog represents the drip shield response as a function of block kinetic energy and plate thickness (i.e., drip shield condition).

- For each realization, the catalogs provide the basis for estimating the response of the drip shield to multiple block impacts at intermediate values of the kinetic energy. The damaged area from multiple block impacts is estimated as the sum of the damaged areas from the individual impacts (see Box #5 above). The potential for failure of the drip shield plates or axial stiffeners is also evaluated for each realization. The calculations for multiple rock blocks are described in Section 6.10.2.3.

  The damage abstraction is structured as a probability of damage/plate failure with conditional probabilities for five different failed states and conditional probability distributions for damaged areas. Each of these quantities is defined for four PGV levels and three degraded states of the drip shield. The probability of damage/plate failure is defined in Section 6.10.2.4. The conditional probabilities for different damage states are defined in Section 6.10.2.5. The conditional probability distributions for damaged areas are represented as 12 gamma distributions for each of the four PGV levels and three

degraded states of the drip shield. The final value for damaged area is based on interpolation to the PGV value for a given seismic event and to the thickness of the drip shield components at the time of the seismic event. Typical Q-Q plots for the gamma distributions are presented in Section 6.10.2.6.

6.10.2.1 Rockfall Calculations

Rockfall calculations for the nonlithophysal units were performed for ground motions at the 0.4 m/s, 1.05 m/s, 2.44 m/s, and 5.35 m/s PGV levels. There were a total of 50 rockfall calculations at each of the 1.05 m/s, 2.44 m/s, and 5.35 m/s PGV levels. Each of these PGV levels was represented by 15 sets of ground motion time histories. There were a total of 32 rockfall calculations at the 0.4 m/s PGV level, based on a single preclosure ground motion time history. Within the rockfall calculations, the drip shield was represented as a simplified, rectangular structure for the purposes of determining block impacts. The rockfall calculations are described in detail in *Drift Degradation Analysis* (BSC 2004 [DIRS 166107], Sections 6.3.1.2.3 through 6.3.1.2.6).

Analysis of rockfall in the nonlithophysal zone required ground motion time histories, fracture geometries, and fracture properties as input parameters or boundary conditions for the calculations. To ensure adequate representation of uncertainty and variability, the input for the individual rockfall calculations was based on a pairing of a ground motion and a synthetic fracture pattern (BSC 2004 [DIRS 166107], Section 6.3.1.2.2). The ground motion was sampled from 15 ground motions at each of the 1.05 m/s, 2.44 m/s, and 5.35 m/s PGV levels. The synthetic fracture pattern was based on a random sampling of 105 centroid locations within a cube of rock that is 100 meters on a side (BSC 2004 [DIRS 166107], Sections 6.1.6 and 6.3.1.2.2). A simple Latin Hypercube sampling scheme was used for pairing ground motion number and the centroid location for the synthetic fracture pattern (DTN: MO0301SPASIP27.004 [DIRS 161869], Table I-2 in the file *Sampling Description.doc*). The rockfall calculations for the 0.4 m/s PGV level used a single preclosure ground motion with the sampled values for the synthetic fracture patterns.

Each rockfall calculation defined the sequence of rock blocks that strike the sides or top of the drip shield. The output parameters for each calculation included the mass, relative impact velocity, impact location, impact angle, and impact energy associated with each block that strikes the drip shield. The data for the block output parameters at the 0.4 m/s, 1.05 m/s, 2.44 m/s, and 5.35 m/s PGV levels are documented in DTN: MO0703SUMM3DEC.000 [DIRS 179895], worksheet "block information" in each of the files *nonlith rockfall characteristics in emplacement drifts with 1e-4 gm.xls*, *nonlith rockfall characteristics in emplacement drifts with 1e-5 gm.xls*, *nonlith rockfall characteristics in emplacement drifts with 1e-6 gm.xls*, *nonlith rockfall characteristics in emplacement drifts with 1e-7 gm.xls*. The 1e-4, 1e-5, 1e-6, and 1e-7 identifiers on the files correspond to the 0.4019 m/s, 1.05 m/s, 2.44 m/s, and 5.35 m/s PGV levels, respectively. The correspondence between annual exceedance frequency and PGV level is defined by DTNs: MO0303DPGVB106.002 [DIRS 162712], MO0210PGVPB107.000 [DIRS 162713], MO0401SEPPGVRL.022 [DIRS 169099], and MO0404PGVRL104.000 [DIRS 170437]; see Table 4-1 for specific locations within these DTNs.

6.10.2.2 Drip Shield Damage—Single Block Impact

In order to minimize the number of structural response calculations, a set of seven representative impacts are selected to span the range of block energies. The idea behind this approach is to perform a limited set of calculations that span the range of rock sizes and rock velocities on the drip shield. This limited set of calculations then provides the basis for estimating the response of the drip shield when multiple blocks are ejected from drift walls in response to vibratory ground motion. This limited set of calculations is referred to as a "catalog of results" or simply a "catalog."

The selection of representative rocks is based on their kinetic energy since the impact energy of a rock block should provide a direct correlation with damaged area or failure of the drip shield plates from tearing. The impact energies associated with the selected rocks correspond to the 99.9th, 99th, 90th, 70th, 40th, and 20th percentiles of block impact energies for the 1.05 m/s PGV level (output DTN: MO0703PASDSTAT.001, File *Nonlith Damage Abstraction for DS.xls*, worksheet "Data Catalogs"). A seventh block that corresponds to the maximum impact energy at the 5.35 m/s PGV level has been added to ensure that the selected rocks encompass all significant impacts from the 0.4 m/s to 5.35 m/s PGV levels. Other characteristics of these rock blocks are given in Table 6-50. Note that the variability in ground velocity and rock ejection velocity sometimes leads to blocks with approximately equal mass having different kinetic energies.

Damage to the drip shield from impact of the representative rock blocks is determined by structural response calculations (SNL 2007 [DIRS 178851], Section 6.4.7). The objective of these calculations is to determine the areas on the drip shield where the residual stress exceeds the threshold value (80% of yield strength for Titanium Grade 7) for initiation of potential SCC and to determine potential failures of the drip shield by evaluating the maximum plastic strains in the drip shield plates and axial stiffeners.

Table 6-50. Characteristics of Representative Rock Blocks

Block Number	Rock Block Mass (Metric Tons)	Rock Block Volume (m^3)	Total Velocity (m/s)	Kinetic Energy (J)
1	28.29	11.7	7.07	706,914
2	7.49	3.11	4.81	86,559
3	1.86	0.771	4.50	18,846
4	0.38	0.157	4.24	3,412
5	0.15	0.0615	3.58	949
6	0.14	0.0562	1.83	228
7	0.13	0.0537	1.14	84

Source: Output DTN: MO0703PASDSTAT.001, File *Nonlith Damage Abstraction for DS.xls*, worksheet "Data Catalogs" for the identification of the percentiles and properties of the seven individual rock blocks.

NOTES: Rock block 1 has the maximum kinetic energy for all calculations. Rock blocks 2 through 7 are based on the 99.9th, 99th, 90th, 70th, 40th, and 20th percentiles of impact kinetic energy for the 1.05 m/s PGV level.

Rock block impact is represented as an edge-on impact at the center of the drip shield, with the center of mass of the block directly above the impact point. These choices are reasonable for several reasons. First, seepage through a dented or failed plate at the center of the drip shield is more likely to allow seepage to drip onto the waste package than a dent for failed plate at the "shoulder" (where the crown meets the vertical side) or side of the drip shield. Second, a corner or side impact will generally create a crease that diverts the flow of seepage toward the side(s) of the drip shield, rather than forming a central depression that could collect seepage. The collection of seepage in a depression is potentially important because the resulting hydrostatic head from the pooled seepage could facilitate advective flow through stress corrosion cracks. (FEP 2.1.03.10.0B, Advection of Liquids and Solids Through Cracks in the Drip Shield, is being excluded from the TSPA (see Section 6.3), so the potential impacts from pooled seepage are not included in the compliance case for the TSPA-LA.) Finally, the cubic shape of the block and the alignment of the block's center of mass with the impact point maximizes deformation for a given kinetic energy, which maximizes the damaged area and failures from rupture for the damage catalogs.

Table 6-51 summarize the results for damaged area, maximum plastic strain in the plates, maximum plastic strain in the axial stiffeners (beneath the crown), and maximum stiffener displacement. Damaged area is the area on the plate that exceeds the RST for Titanium Grade 7, which is 80% of its yield strength. The strain for Titanium Grade 7 that results in tearing is taken to be 0.11, based on the ultimate plastic strain of 0.22 from uniaxial testing and a knockdown factor of 2 for triaxiality effects (SNL 2007 [DIRS 178851], Sections 6.4.2 and 6.4.7). Drip shield failure corresponds to those cases where the plates tear or rupture because the maximum plastic strain exceeds 0.11.

The data in Table 6-51 shows a decrease in the damaged areas between plate thicknesses of 10-mm and 5-mm for rock block numbers 3 and 4. This decrease is probably caused by the distribution of load between the plate itself and the axial stiffeners and support bulkheads beneath the plate. The minor decreases in damaged areas that are observed for the 5-mm-thick plate would occur if the axial stiffeners and support bulkheads bear more of the load for rock block numbers 3 and 4 than the plate itself.

Table 6-51. Catalogs for Damaged Area, Maximum Plastic Strain, and Maximum Stiffener Displacement for the Seven Representative Rock Blocks

Block Number	Kinetic Energy (J)	15-mm-Thick Plate (0-mm Reduction)	10-mm-Thick Plate (5-mm Reduction)	5-mm-Thick Plate (10-mm Reduction)
Damaged Area[a] (m^2):				
1	706,914	2.30×10^{-02}	2.72×10^{-02}	NA[b]
2	86,559	1.59×10^{-02}	8.27×10^{-03}	3.61×10^{-02}
3	18,846	1.15×10^{-03}	3.32×10^{-03}	3.27×10^{-03}
4	3,412	2.79×10^{-04}	6.17×10^{-04}	4.80×10^{-04}
5	949	0	0	8.08×10^{-05}
6	228	0	0	0
7	84	0	0	0

Table 6-51. Catalogs for Damaged Area, Maximum Plastic Strain, and Maximum Stiffener Displacement for the Seven Representative Rock Blocks (Continued)

Block Number	Kinetic Energy (J)	15-mm-Thick Plate (0-mm Reduction)	10-mm-Thick Plate (5-mm Reduction)	5-mm-Thick Plate (10-mm Reduction)
Maximum Plastic Strain in Plates (-):				
1	706,914	6.55×10^{-01}	7.53×10^{-01}	NA[b]
2	86,559	1.14×10^{-01}	2.12×10^{-01}	2.56×10^{-01}
3	18,846	4.11×10^{-02}	6.77×10^{-02}	1.64×10^{-01}
4	3,412	5.00×10^{-03}	2.41×10^{-02}	9.63×10^{-02}
5	949	1.14×10^{-04}	4.88×10^{-03}	3.89×10^{-02}
6	228	0	0	8.16×10^{-04}
7	84	0	0	0
Maximum Plastic Strain in Axial Stiffeners (-):				
1	706,914	2.47×10^{-01}	2.74×10^{-01}	NA[b]
2	86,559	4.37×10^{-02}	6.69×10^{-02}	8.41×10^{-02}
3	18,846	≤ 0.01	≤ 0.01	4.92×10^{-03}
4	3,412	≤ 0.01	≤ 0.01	≤ 0.01
5	949	≤ 0.01	≤ 0.01	≤ 0.01
6	228	≤ 0.01	≤ 0.01	≤ 0.01
7	84	≤ 0.01	≤ 0.01	≤ 0.01
Maximum Stiffener Displacement (m):				
1	706,914	1.71×10^{-01}	2.04×10^{-01}	NA[b]
2	86,559	1.50×10^{-02}	2.52×10^{-02}	4.17×10^{-02}
3	18,846	≤ 0.01	≤ 0.01	8.15×10^{-03}
4	3,412	≤ 0.01	≤ 0.01	≤ 0.01
5	949	≤ 0.01	≤ 0.01	≤ 0.01
6	228	≤ 0.01	≤ 0.01	≤ 0.01
7	84	≤ 0.01	≤ 0.01	≤ 0.01

[a] Damaged area represents damage to one-quarter of the drip shield because the structural response model uses quarter symmetry. Damaged area per drip shield is four times greater.

[b] NA = Not applicable because calculation stopped with illegal geometry in an element. It was not continued because the plates are expected to fail based on the computational results for the 10-mm-thick plate.

Source: DTN: MO0703PADSBLOC.000 [DIRS 179662], File *DS damage due to large block impacts.xls*, worksheets "damage area," "max plate plastic strains," "max stiffener plastic strains," and "stiffener displacements." Kinetic energy for block numbers 1 through 7 are defined in Table 6-50.

6.10.2.3 Drip Shield Damage—Multiple Block Impacts

Each rockfall calculation with UDEC, as described in Section 6.10.2.1, defines the sequence of rock blocks that impact the drip shield during a ground motion. This sequence of rock blocks and the "catalogs" in Table 6-51 for the damage from individual block impacts provide the basis for defining the total damaged area and total number of failed drip shield plates for each UDEC realization.

Only rockfall impacts to the crown and shoulders are considered because damage or tearing on the vertical sides of the drip shield is very unlikely to result in seepage that can drip onto the waste package. Seepage that passes through stress corrosion cracks or tears on the vertical sides is expected to flow down the sides of the drip shield, with minimal potential for dripping onto the waste package.

The blocks that impact the crown and shoulders of the drip shield versus the sides of the drip shield are identified by impact angle. The drip shield is represented as a rectangular structure in the rockfall analyses, and the origin of the coordinate system for impact parameters is located at the center of the rectangle. The nominal height and the nominal width of the drip shield are 2,886 mm and 2,535 mm, respectively (SNL 2007 [DIRS 179354], Table 4-2, Item Number 07-01). The angle from the center of the rectangle to the right-hand corner is then given by $\tan^{-1}(1443/1267.5) = 48.7$ degrees. The half-width and half-height are used in this calculation because the origin is located at the center of the rectangle. Based on this calculation, all impact angles greater than or equal to 47 degrees and less than or equal to $(180 – 47) = 133$ degrees are used to define the blocks which strike the crown or corners of the drip shield. The value of 47 degrees is less than 48.7 degrees to ensure than all shoulder impacts are considered in the damage abstraction.

It might be reasonable to exclude shoulder impacts that cause only damaged area from the abstraction. Seepage leaking through stress corrosion cracks at the shoulder is likely to flow down the sides of the drip shield rather than drip onto the waste package. However, the shoulder impacts are being included because a plate tear can potentially propagate toward the center of the drip shield. In this situation, it is reasonable to also include the damaged area from shoulder impacts in the abstraction.

Once the blocks that impact the crown and shoulders of the drip shield are identified, the information in Table 6-51 is used to estimate the damaged areas from the individual impacts. Damaged area is the area on the plate that exceeds the RST for Titanium Grade 7, which is 80% of its yield strength. Interpolation within the catalog for damaged areas is based on a log-linear interpolation. That is, the natural logarithm of the impact energy is used as the interpolation parameter in Table 6-51. This is appropriate because of the large variation in magnitude for the impact energies for blocks 1 through 7. The total damaged area from a UDEC realization with multiple block impacts is estimated as the sum of the damaged areas from the individual impacts.

A similar approach is used to define the plastic strain in the plates. The catalog for maximum plastic plate strain from Table 6-51 is used with a log-linear interpolation to calculate the plastic plate strain for each block impact on the crown or corners of the drip shield. If the interpolated strain exceeds 0.11, then the drip shield fails as a barrier to advective flow from this impact. The catalog for maximum plastic strain in the stiffeners has not been used because the plates are expected to fail before the stiffeners, because the drip shield deformation will dissipate much of the kinetic energy from the rock block impact, and because an impact by even the largest rock block (Block 1) is not expected to rupture the waste package (SNL 2007 [DIRS 178851], Section 6.4.7.3). Note that Block 1 is produced by the 5.35 m/s PGV level ground motions, which are beyond the maximum PGV level of 4.07 m/s on the bound hazard curve.

The model for the nonlithophysal rockfall calculations has an effective drift length of 21.74-meters, as explained in Section 6.7.2. There are approximately 4 drip shields within this effective length because the nominal axial length of each drip shield is 5,805 mm (SNL 2007 [DIRS 179354], Table 4-2, Item Number 07-01) and the axial length of the connector subassembly that overlaps the adjacent drip shield is 320 mm (SNL 2007 [DIRS 179354], Table 4-2, Item Number 07-01), so the effective length of each drip shield is approximately 5,805 mm – 320 mm = 5,485 mm ~ 5.5 m. It follows that there are approximately four drip shields within the effective drift length for the calculations, so up to four drip shields could fail from multiple block impacts during a given realization.

The number of failed drip shields is determined from the following methodology. If two blocks in a given realization are predicted to cause plate failure (i.e., result in plate strains above 0.11), then one or two drip shields may fail. If the distance between the block impact points is more than 5.5 m, then two drip shields will always fail. If the distance between the block impact points is less than 5.5 m, the number of failed drip shields will depend on the location of the joint between drip shields versus the block impact points. If the joint between drip shields is located randomly relative to the block impact locations, a reasonable simplification is as follows: if the distance between two blocks is less than one-half the effective length of the drip shield (2.75 m), then one drip shield fails, or if the distance between block impact points is greater than 2.75 m, then two drip shields fail. This simplification is reasonable because blocks that cause failure tend to be larger blocks whose presence prevents multiple impacts at the same impact location. However, the rockfall calculations remove a block as soon as it contacts the drip shield, rather than allowing the accumulation of blocks and rubble to build up around the drip shield, thereby protect it from further direct impacts. In other words, the potential for interference between large blocks at the same location to eliminate a subsequent impact is ignored in the rockfall calculations.

A similar approach is appropriate if three blocks are predicted to cause plate failure. These three blocks can cause one, two, or three drip shields to fail. If the maximum distance between block impact points is greater than 11 meters (two drip shield lengths), then two or three drip shields will always fail. If the joints between drip shields are randomly located relative to the block impact locations, a reasonable simplification is as follows: if the maximum distance between the three block impact points is less than 2.75 meters, then one drip shield fails, or if the maximum distance between the three block impact points is between 2.75 meters and 8.25 meters (1.5 drip shield lengths), then two drip shields fail, or if the maximum impact distance between 3 block impact points is greater than 8.25 meters, then three drip shields fail. This logic leads to the following decision tree:

Two block impacts cause failure if $\Delta x < 2.75$ meters $\Rightarrow$ 1 drip shield fails,
if $\Delta x > 2.75$ meters $\Rightarrow$ 2 drip shields fail;

Three block impacts cause failure if $\Delta x < 2.75$ meters $\Rightarrow$ 1 drip shield fails,
if 2.75 meters $< \Delta x < 8.25$ meters $\Rightarrow$ 2 drip shields fail,
if $\Delta x > 8.25$ meters $\Rightarrow$ 3 drip shields fail;

Four or more block impacts cause failure if $\Delta x < 2.75$ meters $\Rightarrow$ 1 drip shield fails,
if 2.75 meters $< \Delta x < 8.25$ meters $\Rightarrow$ 2 drip shields fail,
if 8.25 meters $< \Delta x < 13.75$ meters $\Rightarrow$ 3 drip shields fail,
if $\Delta x > 13.75$ meters $\Rightarrow$ 4 drip shields fail.

As an illustration of the results with this methodology, Table 6-52 presents the damaged areas and number of failed drip shields for the 2.44 m/s PGV level with a 10-mm-thick plate (i.e., 5-mm thickness reduction in all drip shield components). The first column is the case or realization number for each of the 50 rockfall calculations. The realizations are not numbered sequentially because some of the realizations did not cause drip shield damage. The second column is the damaged area from multiple block impacts on all four drip shields. This damaged area includes a factor of 4 to compensate for the quarter symmetry in the structural response model that is incorporated in Table 6-52. A blank in the second column indicates that there is no damaged area for the realization. The third column defines the number of drip shields with failed plates, based on the logic outlined above, for each realization. Similar results are documented for each of the four PGV levels (0.4 m/s, 1.05 m/s, 2.44 m/s, and 5.35 m/s) and three plate thicknesses (15 mm, 10 mm, and 5 mm) in output DTN: MO0703PASDSTAT.001, File *Nonlith Damage Abstraction for DS.xls*.

Table 6-52. Damaged Areas and Plate Failures for the 2.44 m/s PGV Level with 10-mm-Thick Plates (5-mm Thickness Reduction)

Case No.	Damaged Area Per Case* (m^2)	Drip Shields with Failed Plates
14	1.60×10^{-02}	0
15	5.04×10^{-02}	0
16	6.01×10^{-02}	0
17	5.46×10^{-04}	0
18	4.99×10^{-03}	0
19	1.14×10^{-01}	1
20	2.79×10^{-03}	0
21	1.84×10^{-02}	0
22	2.10×10^{-02}	0
23	2.91×10^{-02}	0
24	2.59×10^{-02}	0
25	1.05×10^{-01}	0
27	2.06×10^{-02}	0
28	6.18×10^{-02}	0
29	1.53×10^{-02}	0
31	NDA	0
32	Drip shield failure	1
33	8.07×10^{-02}	1
34	2.85×10^{-02}	0
35	8.12×10^{-03}	0
36	1.24×10^{-02}	0
38	4.30×10^{-01}	3
39	1.05×10^{-01}	2

Table 6-52. Damaged Areas and Plate Failures for the 2.44 m/s PGV Level with 10-mm-Thick Plates (5-mm Thickness Reduction) (Continued)

Case No.	Damaged Area Per Case* (m^2)	Drip Shields with Failed Plates
40	1.33×10^{-01}	1
41	1.36×10^{-02}	0
42	1.82×10^{-02}	0
43	5.91×10^{-02}	0
44	4.04×10^{-02}	0
45	4.06×10^{-02}	0
46	4.28×10^{-03}	0
48	5.02×10^{-03}	0
49	3.80×10^{-02}	0
50	6.07×10^{-02}	0
51	4.67×10^{-02}	0
52	1.28×10^{-01}	1
53	1.44×10^{-01}	1
54	2.95×10^{-02}	1
55	9.74×10^{-03}	0
56	8.56×10^{-02}	0
57	4.37×10^{-02}	0
58	8.05×10^{-04}	0
59	6.87×10^{-03}	0
60	1.49×10^{-03}	1
61	1.20×10^{-02}	1
62	5.95×10^{-02}	0
63	NDA	0
64	1.84×10^{-01}	1
65	3.29×10^{-02}	0
66	1.35×10^{-01}	0
67	1.14×10^{-01}	1

Source: Output DTN: MO0703PASDSTAT.001, File *Nonlith Damage Abstraction for DS.xls*," worksheet "2.44 ms PGV 10-mm Plate," columns AF, AG, and AD.

NOTE: Damaged area is the damaged area per rockfall realization, and includes a factor of 4 to compensate for the quarter symmetry in the structural response model as discussed in footnote a in Table 6-51.

NDA = no damaged area for realization.

6.10.2.4 Probability of Damage/Plate Failure

Table 6-53 presents the probability of damage/plate failure. There is a high probability of damage or plate failure at and above the 1.05 m/s PGV level. The probability of damage/plate failure in Table 6-53 are applicable to drip shields in the nonlithophysal units of the repository.

Table 6-53. Probability of Damage/Plate Failures from Rock Block Impacts

PGV Level (m/s)	Probability of Damage/Failure			
	Plate Thickness (mm)			
	15	10	5	0
0.40	0.5	0.5	0.56	1
1.05	0.78	0.78	0.88	1
2.44	0.96	0.96	0.98	1
5.35	0.86	0.86	0.86	1

Source: Output DTN: MO0703PASDSTAT.001, File *Nonlith Damage Abstraction for DS.xls,* worksheet "Summary."

NOTE: Probability of damage/failure for the 0-mm plate thickness has been set to 1. See discussion of the probability of damage/failure at the 1.05 m/s PGV level with 15-mm- and 10-mm-thick plates below.

The abstraction for the TSPA must represent the response for intermediate values of PGV and of the plate thickness. Linear interpolation between the values in Table 6-53 provides a reasonable method to represent the probability of damage/plate failure as a function of PGV and plate thickness. If PGV is less than 0.40 m/s, then the probability of damage/plate failure at 0.4 m/s PGV level is used as an upper bound.

6.10.2.5 Conditional Probabilities for Damaged States

If the drip shield is damaged by multiple block impacts, then each realization may experience one of five states:

- State 1: Damaged areas with no drip shield failures
- State 2: Damaged areas on three drip shields and one drip shield failure
- State 3: Damaged areas on two drip shields and two drip shield failures
- State 4: Damaged areas on one drip shield and three drip shield failures
- State 5: Four drip shield failures.

A sixth state, with one drip shield failure and no damaged area, is also encountered. Four realizations have a single rock block that causes one drip shield failure with no damage to the other drip shields. These four cases are combined into State 2 for the conditional probability calculations for the abstraction. Table 6-54 presents the conditional probabilities of States 1 through 5 as a function of PGV level and plate thickness. These are conditional probabilities because they depend on the probability of having nonzero damage or failure as determined by the probabilities in Table 6-53. The conditional probabilities in Table 6-54 are applicable to drip shields in the nonlithophysal units of the repository.

Table 6-54. Conditional Probabilities of Damage States 1 through 5

PGV Level (m/s)	15-mm-Thick Plate (0-mm Reduction)	10-mm-Thick Plate (5-mm Reduction)	5-mm-Thick Plate (10-mm Reduction)
State 1: Damaged Area with No Drip Shield Failures:			
0.4	1	1	0.56
1.05	0.95	0.87	0.34
2.44	0.94	0.73	0.18
5.35	0.81	0.33	0.05
State 2: Damaged Area with 1 Drip Shield Failure:			
0.4	0	0	0.28
1.05	0.05	0.13	0.36
2.44	0.06	0.23	0.31
5.35	0.16	0.42	0.16
State 3: Damaged Area with 2 Drip Shield Failures:			
0.4	0	0	0.11
1.05	0	0	0.20
2.44	0	0.02	0.22
5.35	0.02	0.21	0.23
State 4: Damaged Area with 3 Drip Shield Failures:			
0.4	0	0	0
1.05	0	0	0.05
2.44	0	0.02	0.20
5.35	0	0.05	0.28
State 5: 4 Drip Shield Failures:			
0.4	0	0	0.06
1.05	0	0	0.05
2.44	0	0	0.08
5.35	0	0	0.28

Source: Output DTN: MO0703PASDSTAT.001, File *Nonlith Damage Abstraction for DS.xls*, worksheet "Summary."

NOTE: Minor errors were identified in the conditional probabilities for States 1 and 2 after this table had been defined in the TSPA database. For the 15-mm-thick plate at the 5.35 m/s PGV level, the conditional probabilities for State 1 and State 2 changed from 0.79 and 0.19 to 0.81 and 0.16, respectively. For the 5-mm-thick plate at the 2.44 m/s PGV level, the conditional probability for State 1 increased from 0.16 to 0.18. These errors will have no impact on the compliance case for the TSPA-LA because FEP 1.2.03.02.0B has been screened out of TSPA (see Section 6.3). These minor errors will also not have a significant impact on the low-consequence argument that supports the screening decision for FEP 1.2.03.02.0B.

The abstraction for the TSPA must represent the response for intermediate values of PGV and of the plate thickness. Linear interpolation between the values in Table 6-54 provides a reasonable method to define the conditional probability for the drip shield states as a function of PGV and plate thickness. If the PGV value is less than 0.40 m/s, the probability is set to the value at the 0.4 m/s PGV level as an upper bound. If the plate thickness is less than 5 mm, then the probability is set to the value for the 5-mm-thick plate. The use of the value for 5 mm is not expected to be a significant factor in the TSPA because the plates become increasingly likely to fail for plate thicknesses less than 5 mm, as defined in Section 6.8.2.

6.10.2.6 Conditional Probability Distributions for Nonzero Damaged Areas on Intact Plates

Figures 6-99 to 6-101 present the Q-Q plots for the gamma distribution versus the conditional damaged area on intact plates at the 2.44 m/s PGV level for 15-mm-, 10-mm-, and 5-mm-thick plates. These damaged areas are the damaged area per rockfall realization and include a factor of 4 to compensate for the quarter symmetry in the structural response model. The values of the mean and standard deviation of the conditional damaged areas, which are the input to the gamma distributions, are shown in Table 6-55. The data in Table 6-55 show a decrease in the mean and standard deviation of the damaged areas between plate thicknesses of 10 mm and 5 mm. This decrease is caused by the increased number of ruptured plates at the 5-mm thickness. Once a plate is ruptured, the associated damaged area is not included in the calculation of the mean and standard deviation for the intact plates. This approach tends to drop the largest damaged areas from the calculated mean and standard deviation, leading to the decrease observed in Table 6-55. Gamma distributions provide a very good fit to the conditional (nonzero) damaged areas.

Table 6-55. Mean and Standard Deviations of the Conditional Damaged Areas for Realizations of Rock Block Impacts on the Drip Shield

PGV Level (m/s)	Plate Thickness (mm)					
	15		10		5	
	Mean (m^2)	Standard Deviation (m^2)	Mean (m^2)	Standard Deviation (m^2)	Mean (m^2)	Standard Deviation (m^2)
0.4	0.0052	0.0064	0.013	0.016	0.0029	0.0025
1.05	0.018	0.031	0.031	0.046	0.0079	0.010
2.44	0.037	0.054	0.056	0.072	0.013	0.012
5.35	0.093	0.088	0.105	0.085	0.020	0.018

Source: Output DTN: MO0703PASDSTAT.001, File Nonlith Damage Abstraction for DS.xls, worksheet "Summary."

Q-Q plots for the gamma distributions versus the conditional damaged areas for the 0.4 m/s, 1.05 m/s, and 5.35 m/s PGV levels with 15-mm, 10-mm, and 5-mm thick plates show similar comparisons to Figure 6-99 through Figure 6-101. These plots are documented in output DTN: MO0703PASDSTAT.001, File *Nonlith Damage Abstraction for DS.xls,* worksheets "0.4 ms PGV 15-mm Plate," "0.4 ms PGV 10-mm Plate," "0.4 ms PGV 5-mm Plate," "1.05 ms PGV 15-mm Plate," "1.05 ms PGV 10-mm Plate," "1.05 ms PGV 5-mm Plate," "2.44 ms PGV 15-mm Plate," "2.44 ms PGV 10-mm Plate," "2.44 ms PGV 5-mm Plate," "5.35 ms PGV 15-mm Plate," "5.35 ms PGV 10-mm Plate," and "5.35 ms PGV 5-mm Plate." Based on these results, gamma distributions are selected as the probability distribution for conditional damaged areas on the drip shield in response to block impacts in the nonlithophysal units.

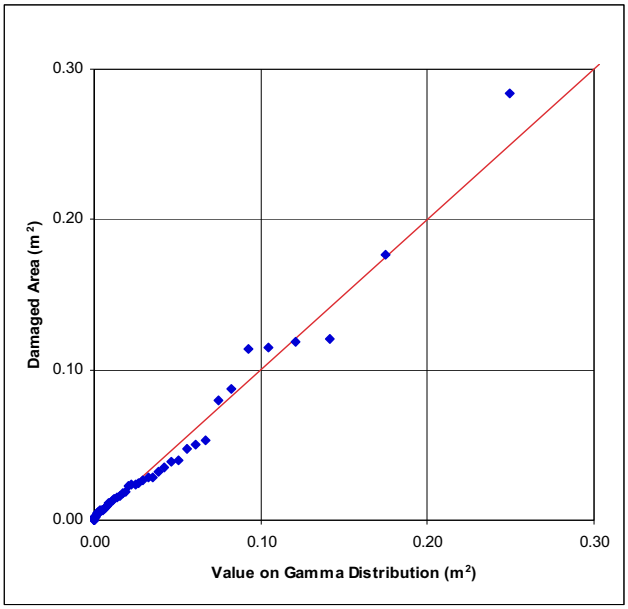

Source: Output DTN: MO0703PASDSTAT.001, worksheet "2.44 ms PGV 15-mm Plate" in the file *Nonlith Damage Abstraction for DS.xls*.

NOTE: 2.44 m/s PGV level with 15-mm plate thickness. Damaged area is the conditional nonzero damaged area for each rockfall realization.

Figure 6-99. Q-Q Plot for Conditional Nonzero Damaged Area from Rock Block Impacts versus a Gamma Distribution

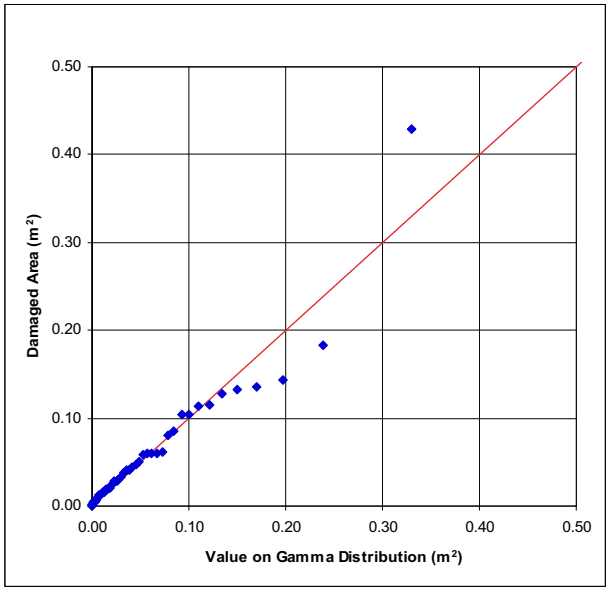

Source: Output DTN: MO0703PASDSTAT.001, worksheet "2.44 ms PGV 10-mm Plate" in the file *Nonlith Damage Abstraction for DS.xls*.

NOTE: 2.44 m/s PGV level with 10-mm plate thickness. Damaged area is the conditional nonzero damaged area for each rockfall realization.

Figure 6-100. Q-Q Plot for Conditional Nonzero Damaged Area from Rock Block Impacts versus a Gamma Distribution

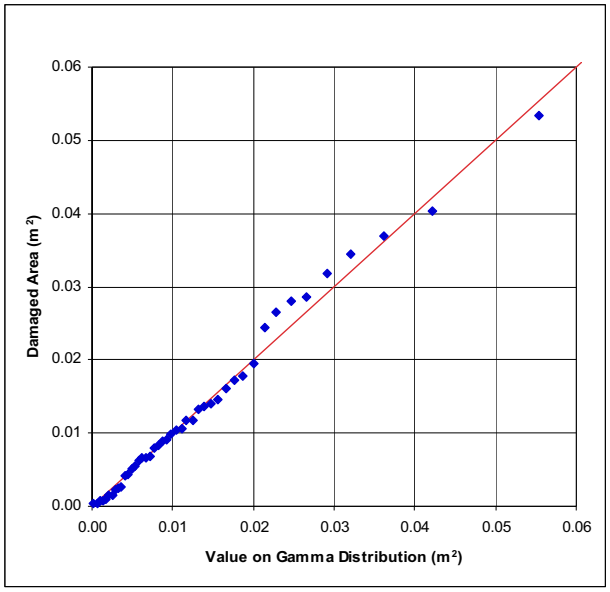

Source: Output DTN: MO0703PASDSTAT.001, worksheet "2.44 ms PGV 5-mm Plate" in the file *Nonlith Damage Abstraction for DS.xls*.

NOTE: 2.44 m/s PGV level with 5-mm plate thickness. Damaged area is the conditional nonzero damaged area for each rockfall realization.

Figure 6-101. Q-Q Plot for Conditional Nonzero Damaged Area from Rock Block Impacts versus a Gamma Distribution

6.10.2.7 Dependence of Conditional Damaged Area on PGV and Plate Thickness

The abstraction for the TSPA must represent the response for values of PGV between the four PGV levels of 0.4 m/s, 1.05 m/s, 2.44 m/s, and 5.35 m/s. Linear interpolation between the values of the mean and standard deviation of the data in Table 6-55 provides a convenient way to represent the input parameters for the gamma distribution as a function of PGV. Figures 6-102 to 6-104 compare the damaged area data across the full range of PGV at the 15-mm, 10-mm, and 5-mm plate thicknesses. These figures indicate that linear interpolation in PGV for the mean and standard deviation provides a reasonable representation for the TSPA.

The abstraction for the TSPA must also represent the response for the full range of values for the plate thickness, from 15 mm to 0 mm. The data in Figure 6-102 through Figure 6-104 indicate that linear interpolation between the responses at 15 mm, 10 mm, and 5 mm will provide a reasonable representation of conditional damaged area as a function of plate thickness. If the plate thickness is less then 5 mm, then the conditional damaged area is set to the value for the 5-mm-thick plate. The use of the value for 5 mm is not expected to be a significant factor in the TSPA because the plates become increasingly likely to fail for plate thicknesses less than 5 mm, as defined in Section 6.8.2.

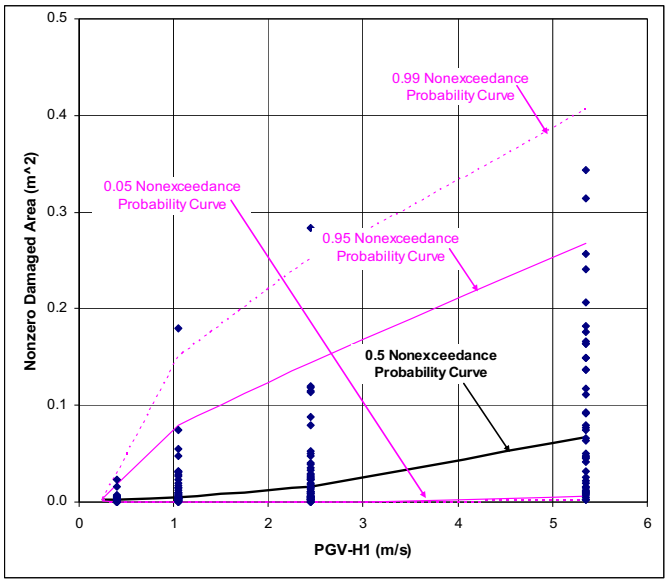

Source: Output DTN: MO0703PASDSTAT.001, worksheet "Plot 15-mm" in the file *Nonlith Damage Abstraction for DS.xls*.

NOTE: The conditional nonzero damaged area is for each rockfall realization.

Figure 6-102. Comparison of Percentiles on the Gamma Distributions to Conditional Damaged Areas for the 15-mm-Thick Plate

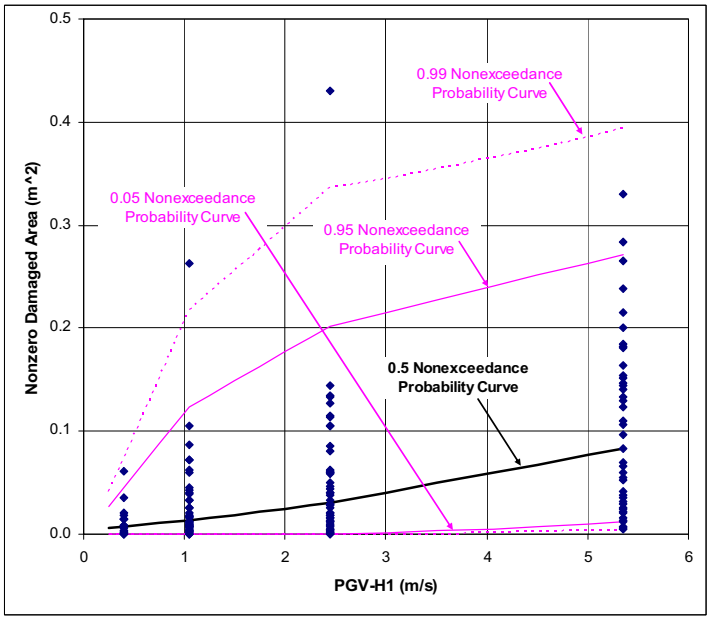

Source: Output DTN: MO0703PASDSTAT.001, worksheet "Plot 10-mm" in the file *Nonlith Damage Abstraction for DS.xls*.

NOTE: The conditional nonzero damaged area is for each rockfall realization.

Figure 6-103. Comparison of Percentiles on the Gamma Distributions to Conditional Damaged Areas for the 10-mm-Thick Plate

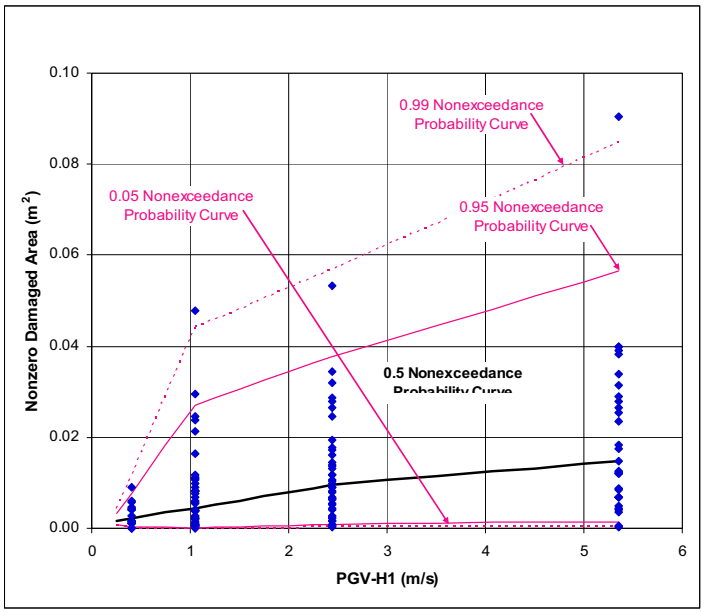

Source: Output DTN: MO0703PASDSTAT.001, worksheet "Plot 5-mm" in the file *Nonlith Damage Abstraction for DS.xls*.

NOTE: The conditional nonzero damaged area is for each rockfall realization.

Figure 6-104. Comparison of Percentiles on the Gamma Distributions to Conditional Damaged Areas for the 5-mm-Thick Plate

6.10.2.8 Alternate Conditional Probability Distributions for Nonzero Damaged Areas

The gamma distribution provides an excellent representation of the damaged area data, as shown by Figures 6-99 to 6-101. Q-Q plots were also prepared for log-normal and log-triangular distributions. The log-normal distribution provides a poor representation of the conditional damaged areas at higher values, as shown in Figure 6-105. The log-triangular distribution provides a similar representation to the gamma distribution for the conditional damaged areas at the 2.44 m/s PGV level with 10-mm-thick plate, as shown by comparing Figure 6-106 with Figure 6-100. However, the log-triangular distribution involves selection of minimum and maximum values (which may not be obvious from the data set) and then defining the mode by minimizing the sum of the squared differences between the data points and the values on a log-triangular distribution. The gamma distribution is selected to represent the conditional probability distributions because it is consistent with the other damage abstractions, because it provides an excellent representation of the data with only two parameters that are determined directly from the underlying observations, and because it avoids a numerical fit for the distribution parameters.

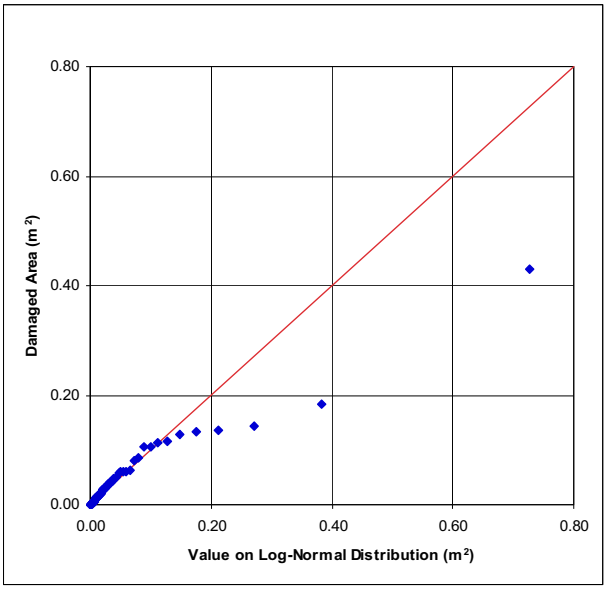

Source: Output DTN: MO0703PASDSTAT.001, worksheet "2.44 ms PGV 10-mm Plate" in the file *Nonlith Damage Abstraction for DS.xls*.

NOTE: 2.44 m/s PGV level with 10-mm plate thickness. Damaged area is the conditional nonzero damaged area for each rockfall realization.

Figure 6-105. Q-Q Plot for Conditional Nonzero Damaged Area from Rock Block Impacts versus a Log-Normal Distribution

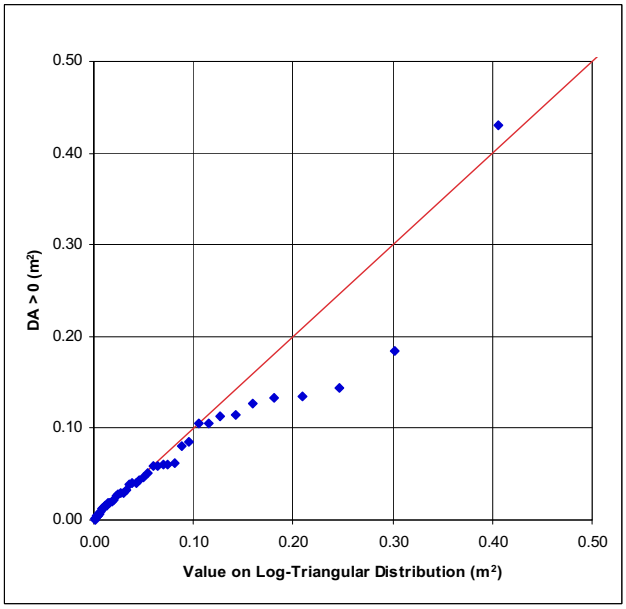

Source: Output DTN: MO0703PASDSTAT.001, worksheet "2.44 ms PGV 10-mm Plate" in the file *Nonlith Damage Abstraction for DS.xls*.

NOTE: 2.44 m/s PGV level with 10-mm plate thickness. Damaged area is the conditional nonzero damaged area for each rockfall realization.

Figure 6-106. Q-Q Plot for Conditional Nonzero Damaged Area from Rock Block Impacts versus a Log-Triangular Distribution

6.10.2.9 Damage from Multiple Events

The damaged areas on the drip shield from rock block impacts are applicable to all drip shields in the nonlithophysal units of the repository. Similarly, zero, one, two, three, or four out of four drip shields in the nonlithophysal units may fail, depending on the state determined from the probabilities in Table 6-54. There is no spatial variability for drip shield damage in the nonlithophysal units.

Damage to the drip shield from rock block impacts in nonlithophysal units will continue until the drip shield plates fail, as described in Section 6.8.2, or until the drifts in the nonlithophysal units become 50% filled with rubble.

The damaged area from multiple seismic events is defined as the sum of the damaged areas from the individual seismic events. The number of failed drip shields in the nonlithophysal units from multiple seismic events is defined as the sum of the failed drip shields from the individual seismic events. The linear summation of damaged area overestimates the accumulation of residual stress, as discussed in Section 6.10.1.4.

6.10.2.10 Location of Damaged Area

The damaged areas for the drip shield plates should be represented as randomly located on the crown on the drip shield. No damaged areas on the sides of the drip shield are considered because any seepage that passes through the sides is likely to flow down the sides and not make contact with the waste packages.

6.10.2.11 Waste Package Damage in Nonlithophysal Units

Damage to the waste package from rockfall in nonlithophysal units is not included in the abstractions for the TSPA-LA. Impacts by Blocks 2 through 7 (see Tables 6-50 and 6-51) do not fail the drip shield as a barrier to rockfall. For example, the maximum plastic strain is 0.0841 and the maximum stiffener displacement is 0.0417 meters, or less than 2 inches, even for an impact by Block 2 (second highest kinetic energy in Table 6-50) with a 10-mm reduction in the thickness of the drip shield components. The waste package is therefore not damaged by impacts for Blocks 2 through 7 because the drip shield remains structurally intact and does not come into contact with the waste package.

The axial stiffeners are predicted to fail only for an impact by Block 1 on a drip shield with a 10-mm thickness reduction for all components (see Table 6-51). Block 1 is a 28.3 metric ton rock block with the maximum kinetic energy of 706,914 Joules (see Table 6-50). The 10-mm thickness reduction corresponds a 5-mm-thick plate, and is the most degraded state considered by the structural response calculations. The following observations are relevant here:

- This rock block occurs at only the 5.35 m/s PGV level, which is beyond the maximum PGV level of 4.07 m/s considered by TSPA.

- The simplified representation of this block in the structural response calculation is not realistic. For the calculation, the block has a cubic shape with its center of mass directly over the edge that impacts the drip shield. However, large rock blocks are expected to have a highly irregular shape, with a center of mass that is far from the impact point. In this situation, the block will rotate upon impact, providing a larger contact surface that distributes its load over one or more drip shields.

- The 10-mm thickness reduction is a highly degraded state of the drip shield, and, when it occurs, rockfall is likely to have filled the drift, thereby mitigating the damage from rock block impacts. The mean corrosion rates for Titanium Grade 7 under benign conditions, 5.15 nm/yr (SNL 2007 [DIRS 180778], Table 8-1[a]), is appropriate for the underside of the drip shield plates. The mean corrosion rate for Titanium Grade 7 under aggressive conditions, 46.1 nm/yr (SNL 2007 [DIRS 180778], Table 8-1[a]), is appropriate for the top side of the drip shield plates. A 10-mm thickness reduction from general corrosion on the top and bottom of the plates occurs at $(10 \times 10^{-3}$ m)/$(5.15 \times 10^{-9}$ m/yr + 46.1×10^{-9} m/yr) $\approx$ 195,000 years. A large volume of rockfall is likely to have accumulated in the drifts by this time, mitigating the damage from direct impact of any rock blocks on the drip shield.

The prediction of failure of the axial stiffeners is therefore not realistic even for the maximum rock block with a 10-mm thickness reduction and does not occur for the other representative rock blocks in Table 6-50. The 10-mm thickness reduction corresponds a 5-mm-thick plate, and is the most degraded state considered by the structural response calculations. It follows that the drip shield is expected to retain its integrity as a physical barrier, able to deflect large rock blocks away from the waste package. Seismic-induced damage to the waste package and its internals from rock block impacts in nonlithophysal units is therefore screened out of TSPA.

6.11 FAULT DISPLACEMENT DAMAGE ABSTRACTION

Fault displacement could impact key EBS components by causing mechanical damage to the waste packages, drip shields, and fuel rod cladding. Potential faulting within the emplacement drifts is expected to result in small displacements along the faults. With the exception of the Solitario Canyon and Ghost Dance Faults, which are immediately outside the western and eastern boundaries of the emplacement drifts, a fault displacement of greater than 0.1 cm is associated with a mean annual exceedance frequency of less than 10^{-5} per year (see Table 6-61). In addition, only the small number of waste packages located directly on a fault is subject to damage from fault displacement, as shown in Appendix D. It follows that the dose related to fault displacement is expected to be a small fraction of the total dose for the seismic scenario class because damage from fault displacement affects at most a small fraction of the inventory and because this damage occurs only for events with very low exceedance frequencies.

Given that the dose related to fault displacement is expected to be a small fraction of total dose, detailed calculations of the structural response of EBS components to fault displacement are not warranted for TSPA. Instead, the focus is on the potential for the waste package to be damaged when fault displacement exceeds the available clearance around the waste package. A fault displacement that occurs in an emplacement drift may cause a sudden discontinuity in the profile of the drift. This could result in one portion of the drift being displaced vertically or horizontally

relative to the adjacent section. Such a discontinuity in the drift could cause shearing of the waste package, its cladding, and the drip shield if the fault displacement exceeds the available clearance in the EBS. The comparison of fault displacements with available clearances provides an analysis that can define the potential for damage to EBS components from fault displacement.

Detailed calculations for the response of EBS components during a fault displacement are expected to reduce the predicted damage to EBS components. First, the rubble surrounding a drip shield or waste package is a highly porous medium that will respond dynamically during a fault displacement, as discussed in Section 6.11.1.2 and as calculated in Appendix D. This dynamic response is expected to allow significant displacement of EBS components, thereby providing more clearance than the estimates in Section 6.11.1. In addition, a waste package surrounded by rubble is able to rotate in the direction of the fault displacement. This rotation can reduce or eliminate crimping or shearing of a waste package, given that the maximum fault displacement is 2.2 m at the 10^{-8} annual exceedance frequency for Sites 4 through 8 (see Table 6-61) and the initial tunnel diameter, 5.5 m (see Figure 6-107), is significantly greater than the maximum fault displacement. These considerations are not important for TSPA, as noted above, but may be useful for criticality-related issues.

The DOE does not intend to emplace Naval waste packages on faults that intersect the emplacement drifts. This decision is not represented in the damage abstraction for TSPA because the Naval waste packages are a minor part of the TAD canister group, as explained in Section 6.11.4, and because the dose related to fault displacement is expected to be a small fraction of the total dose. This decision is represented in the fault displacement analyses in Section 6.11.7.

6.11.1 Clearances for EBS Components

Two distinct cases are considered in analyzing the clearances between EBS components: (1) an intact drip shield and (2) a drip shield that has failed. The first case represents the as-emplaced configuration of the EBS, shortly after repository closure, and is expected to be applicable to the first 10,000 years after repository closure. The second case represents the late time response of the EBS after the drip shield framework and drip shield plates have failed and rockfall has partly filled the emplacement drifts and surrounded the waste packages with rubble. Each of these cases is considered separately in this section.

6.11.1.1 Clearances with an Intact Drip Shield

To determine the response of EBS components to fault displacement with an intact drip shield, consider the emplacement drift layout, shown schematically in Figure 6-107. The emplacement drift has a nominal diameter of 216 inches or 18 feet (5,490-mm) (SNL 2007 [DIRS 179354], Table 4-1, Item Number 01-10). Within the drift, the steel support beams and associated ballast form a level invert whose top surface is 52 inches (1,320.8 mm) above the lowest part of the drift (SNL 2007 [DIRS 179354], Table 4-1, Item Number 01-10A). The waste package sits on an emplacement pallet that raises the bottom of the waste package above the invert. While the elevation difference between the top of the invert and the bottom of the waste package varies depending on the waste package diameter, the exact value is not important for this analysis because this elevation difference is not actually used in the analysis.

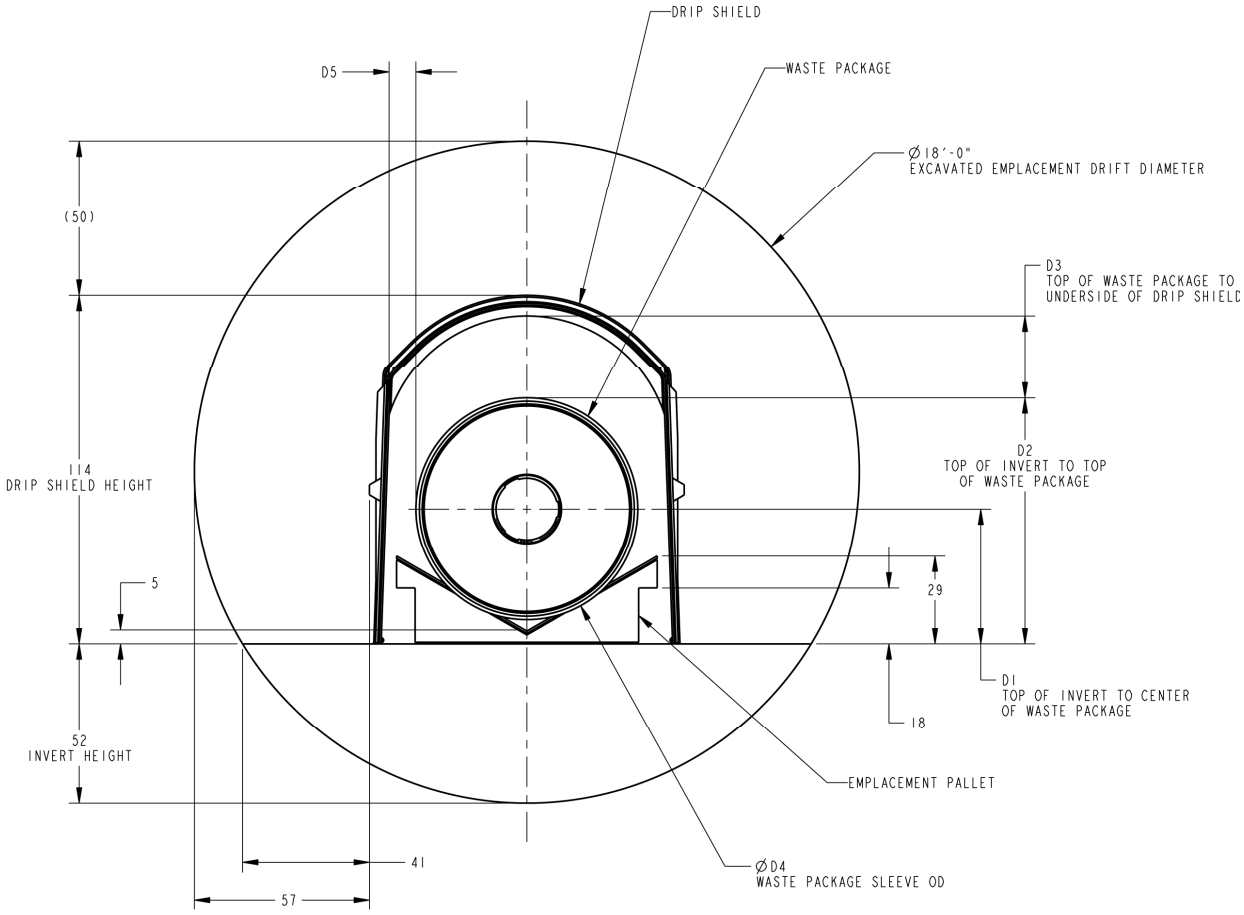

WASTE PACKAGE TYPE	D1	D2	D3	D4	D5
2-MCO/2-DHLW	44	80	27	72	9
NAVAL SHORT/LONG	47	86	21	77	6
TAD	47	86	21	77	6
5-DHLW/DOE SNF SHORT/LONG	51	92	14	84	3

00431DR

NOTE: DIMENSIONS ARE ROUNDED TO THE NEAREST INCH FROM THOSE SHOWN IN 800-M00-WIS0-00101-000

Source: SNL 2007 [DIRS 179354], Figure 4-1.

Figure 6-107. Emplacement Drift Cross Section

The drip shield is a free-standing structure that sits on the invert. The drip shield has an external height of 2,886 mm (SNL 2007 [DIRS 179354], Table 4-2, Item Number 07-01), rounded up to 2,890 mm for this analysis. The internal height of the drip shield, defined as the distance from the invert floor to the lowest point on the underside of the top of the drip shield, is 107 inches (2,717.8 mm) (SNL 2007 [DIRS 179354], Table 4-2, Item Number 07-01). The clearance between the crown (top) of the drip shield and the drift roof is 50 inches (SNL 2007 [DIRS 179354], Table 4-2, Item Number 07-01) or 1,270 mm. These parameters, which are independent of waste package design, are summarized in Table 6-56.

Table 6-56. Emplacement Drift Configuration Dimensions that are Independent of the Waste Package

Description	Value	Source
Emplacement drift diameter	216 inches (5,486.4 mm)	SNL 2007 [DIRS 179354], Table 4-1 Item Number 01-10
Invert height (maximum)	52 inches (1,320.8 mm)	SNL 2007 [DIRS 179354], Table 4-1 Item Number 01-10A
Drip shield height - exterior	2,886 mm	SNL 2007 [DIRS 179354], Table 4-2 Item Number 07-01
Drip shield height - interior	107 inches (2,717.8 mm)	SNL 2007 [DIRS 179354], Table 4-2 Item Number 07-01
Clearance from crown of drip shield to roof of drift	50 inches (1,270 mm)	SNL 2007 [DIRS 179354], Table 4-2 Item Number 07-01

Table 6-57 summarizes the exterior dimensions of the various waste package designs. The most important parameter for the analyses presented herein is the outside diameter of the waste package OCB, which is seen to vary between 1,749 mm to 2,045 mm. Also shown in Table 6-57 is the calculated clearance between the top of the waste package and the underside of the drip shield, without the pallet. This clearance is defined as the interior height of the drip shield less the outside diameter of the waste package OCB. The elevation of the package above the invert is not included in calculating the clearance, as explained below. This clearance varies between 673 mm and 969 mm, depending on waste package type. Table 6-57 also shows the clearance between the top of the waste package and underside of the drip shield for selected packages with the pallet in place. The presence of the pallet reduces the clearance by 283 mm to 317 mm.

Table 6-57. Waste Package Dimensions and Clearance between Drip Shield and Waste Package

Package Type	Outside Diameter of OCB (mm)	Nominal Length (mm)	Clearance Without Pallet (mm)	Clearance With Pallet (mm)	Difference in Clearances (mm)
TAD	1,881.6	5,850.1	836	533	303
Naval Fuel - Long	1,881.6	5,850.1	836	533	303
Naval Fuel - Short	1,881.6	5,215.10	836	533	303
5-DHLW/DOE SNF Short	2,044.7	3,697.4	673	356	317
5-DHLW/DOE SNF Long	2,044.7	5,303.9	673	356	317
2-MCO/2-DHLW	1,749.3	5,278.6	969	686	283

Sources: SNL 2007 [DIRS 179394], Table 4-3, for outside diameter of OCB and for nominal length of the TAD waste package; SNL 2007 [DIRS 179567], Tables 4-6 through 4-10, for the outside diameter of OCB and nominal length of the other waste package types.

Clearance with pallet based on SNL 2007 [DIRS 179354], Table 4-1, Item Number 02-02, rounded to the nearest inch and then converted to millimeters with three significant figures.

NOTES: Clearance without the pallet is calculated as the interior height of the drip shield (2,717.8 mm) minus the outside diameter of the waste package OCB, rounded to three significant digits.

TAD = transportation, aging, and disposal (canister); DHLW = defense high-level radioactive waste; DOE = U.S. Department of Energy; SNF = spent nuclear fuel; MCO = multi-canister overpack.

The clearance between the crown of the drip shield and the roof of the drift (1,270 mm from Table 6-56) and the clearance between the top of the waste package and the bottom of the drip shield (see Table 6-57) are measures of how much fault displacement could occur before the waste packages are potentially degraded through a shearing mechanism. At the start of a seismic event, the clearance above the drip shield will depend on the amount of rockfall that has accumulated during previous seismic events. Once a drift collapses, the space surrounding the drip shield will be almost filled or completely filled with loosely packed rock fragments. This loosely packed material still allows significant motion of the drip shield during the fault displacement even for a collapsed drift, as explained below. For those drifts in the lower lithophysal zone of the repository, drift collapse is calculated to occur for ground motions with PGV values greater than or equal to 2.0 m/s (BSC 2004 [DIRS 166107], Section 6.4.2.2.2). For drifts in the nonlithophysal zones, rockfall accumulates more slowly than in the lithophysal zones (see discussion in Section 6.7.2.1). However, the beneficial effect from unfilled emplacement drifts in the nonlithophysal zones is ignored in the analysis of clearances for fault displacement.

The actual response of the EBS components to a fault displacement scenario is complicated. The fault displacement analysis is simplified by considering:

- The fault is perpendicular to the drift axis with the displacement being purely vertical
- The fault displacement occurs at a discrete plane, creating a sharp discontinuity
- The temporal evolution of rockfall in the emplacement drifts is ignored. Clearances are minimized by considering emplacement drifts in the lithophysal and nonlithophysal zones that are filled with rockfall at the time of the seismic event.

Vertical faulting is consistent with the faults investigated at the site. As part of the exploratory studies of the site, the Enhanced Characterization of the Repository Block (ECRB) Cross Drift was excavated through a representative part of the repository footprint to obtain visual evidence of both rock stratigraphy and faulting. This investigation (Mongano et al. 1999 [DIRS 149850], pp. 51 to 59) found evidence for four faults along the length of the ECRB Cross Drift between the Ghost Dance and Solitario Canyon Faults that lie outside the location of the emplacement drifts. One of these was the Sundance Fault; the other three are unnamed faults that showed between one and a few meters of cumulative faulting from multiple seismic events. In each of these cases, the measured displacements were characterized as vertical, which is consistent with this approach. By treating the faults as perpendicular to the drift axis, no credit is taken for sideways movement of the waste packages that could lessen the degree to which fault displacement could cause damage.

An actual fault zone has a finite width over which the displacement could occur. However, based on the observations reported in the investigation of the ECRB Cross-Drift (Mongano et al. 1999 [DIRS 149850], pp. 51 to 59), the width of the fault disturbed zone varied between just under a meter to a little over 2 meters. Thus, the width of the zone is less than the length of any waste package type. If the total displacement from a single seismic faulting event were to be distributed over a sufficiently wide zone, a single waste package could potentially see less than the total fault displacement, resulting in a decreased probability of failure. By treating fault

displacement as a sharp discontinuity in the drift floor/roof, the likelihood of damage to the waste package on the fault is increased. Thus, the overall treatment increases the likelihood of waste package failure.

A sudden discontinuity in the drift floor would tend to raise one end of a drip shield and waste package. However, the other EBS components, specifically the invert and emplacement pallet, would also be affected. Fault displacement may collapse any remaining steel supports in the invert at the plane of displacement, and a significant amount of the invert ballast from the elevated portion of the drift may fall into the lower drift segment (if rockfall only partly fills the drifts). A degraded emplacement pallet may collapse during the fault displacement. The potential for the dynamic response of the invert or emplacement pallet to provide additional clearance for the waste package and drip shield is not directly considered in this analysis.

Movement along a sudden discontinuity will affect the rubble surrounding the drip shield after drift collapse. The lithophysal rubble is a loosely packed material with bulking factors in the 0.1 to 0.4 range, which are equivalent to porosities between 0.09 and 0.29 (see Section 6.7.1.5 for definition of the bulking factor and the relationship between bulking factor and porosity). With this free space, the rubble has substantial movement in the plane of discontinuity and longitudinally along the drift axis during the fault displacement. The movement of the rubble will allow the drip shield to move with the fault displacement, rather than being rigidly pinned to the invert. In this situation, the effective clearance around the drip shield is expected to be significantly larger than space between the top of the waste package and bottom of the drip shield. The porosity of rockfall in the nonlithophysal units is similar because the range of bulking factors is similar in the lithophysal and nonlithophysal units (see Section 6.7.2.6).

The potential for substantial movement of the drip shield after drift collapse has been confirmed in ground motion analyses for the 1.05 m/s PGV level (BSC 2004 [DIRS 166107], Appendix P2.1). The rockfall loads from lithophysal rubble have the capability to move the entire drip shield both by sliding it along the invert and by lifting it from the invert. The inertial forces during seismic shaking can also cause movement of the drip shield. Substantial displacement of the drip shield must be accompanied by similar displacements in the rubble. Additional calculations were performed at the 2.44 m/s and 5.35 m/s PGV levels to determine if the drip shield could be overturned by strong ground motions (BSC 2004 [DIRS 166107], Appendix P3). These simulations demonstrate that the rubble particles undergo large dynamic motion in response to displacements of the drip shield, similar to what would occur during a vertical fault displacement. It follows that the clearance between the top of the drip shield and the roof of the drift will be partly available, but the exact value is difficult to quantify.

The dynamic response of the rubble, invert and emplacement pallet during a fault displacement is difficult to predict. As a simplification, the approximation is made that the clearance between the top of the waste package and the bottom of the drip shield is determined without the pallet. This is a reasonable approximation because the clearance between the top of the drip shield and the roof of the drift, 1,270 mm (Table 6-56), is more than four times greater than the differences in clearance with or without the pallet, 283 mm to 317 mm (Table 6-57). In other words, the height of rubble above the drip shield is much greater than the difference in clearance due to the pallet. Since the porosity and dynamic motion of the rubble allows the drip shield to displace horizontally and vertically during the ground motion, the difference in clearance due to the pallet

can be accommodated by drip shield displacements that are a small percentage of the height of the rubble. It follows that the potential for upward displacements of the drip shield into the large rubble-filled space between the top of drip shield and roof of the drift allows for vertical motions that can exceed the maximum difference (317 mm) in clearance due to the pallet. It is then reasonable to exclude the presence of the pallet in defining clearance between components because of the potential for upward displacement of the drip shield. No credit is taken for any shifting of the ballast in the invert.

The maximum allowable displacement of the waste package before it is pinned also depends on the condition and dynamic response of the drift after the seismic event. For collapsed drifts, the loosely packed rubble can still allow substantial dynamic movement of the drip shield. The maximum allowable fault displacement prior to waste package damage is determined without including the potential for upward displacement of the drip shield to provide additional clearance.

The calculated clearances are summarized in Table 6-58. The values in Table 6-58 represent the failure criteria for waste packages and drip shields under fault displacement when the drip shield is intact at the time of the seismic event. These clearances are appropriate during the first 10,000 years after repository closure. The clearances in Table 6-58 exclude the presence of the pallet, and no credit is taken for the downward collapse of the invert. Fault displacement in excess of these values is considered to fail the waste package and the overlying drip shield through direct shearing.

Table 6-58. Maximum Allowable Displacement with Drift Collapse for an Intact Drip Shield

Package Type	Maximum Allowable Displacement With Drift Collapse (mm)
TAD	836
Naval Fuel - Long	836
Naval Fuel - Short	836
5-DHLW/DOE SNF Short	673
5-DHLW/DOE SNF Long	673
2-MCO/2-DHLW	969

Source: Output DTN: MO0703PASDSTAT.001, worksheet “Tables” in the file *Fault Displacement Abstraction.xls*.

NOTES: Maximum allowable displacement with drift collapse = clearance without pallet in Table 6-57.

TAD = transportation, aging, and disposal (canister); DHLW = defense high-level radioactive waste; SNF = spent nuclear fuel; MCO = multi-canister overpack.

Failure of the drip shields could also occur without direct waste package damage. One mechanism for this is lifting of one drip shield relative to its neighbor. However, drip shield separation in the axial or vertical directions during a high intensity seismic event has been screened out, based on the discussion in Section 6.7.3, and is not considered further.

6.11.1.2 Clearances with a Failed Drip Shield

At late times after closure, the waste package can become surrounded by rubble after the drip shield plates rupture (see the plate fragility analysis in Section 6.8.2), allowing the accumulated rubble and rockfall in the drifts to fall through the drip shield. The presence of the rubble eliminates the free space between the top of the waste package and the bottom of the drip shield shown in Figure 6-107. The potential for fault displacement to cause rupture of the waste package in the presence of rockfall needs to be evaluated for this system configuration.

Movement along a sudden discontinuity will affect the rubble surrounding the drip shield after drift collapse. The lithophysal rubble is a loosely packed material with a typical porosity range of 0.09 to 0.29 (see previous section). With this free space, the rubble has substantial movement in the plane of discontinuity and longitudinally along the drift axis during the fault displacement. The movement of the rubble will allow the waste package to move with the fault displacement, rather than being rigidly fixed. A similar range of porosities should exist for the rockfall in the nonlithophysal zones because its range of bulking factors is similar to those for the lithophysal rubble (see Section 6.7.2.6).

The potential for substantial movement of rubble after drift collapse has been confirmed in ground motion analyses at the 1.05 m/s, 2.44 m/s, and 5.35 m/s PGV levels. These analyses are based on calculations for an intact drip shield surrounded by rubble, but they serve to illustrate the point that the rubble is not rigidly locked in place. For example, the inertial forces for a drip shield surrounded by rubble during seismic shaking at the 1.05 m/s PGV level can cause movement of the drip shield (BSC 2004 [DIRS 166107], Appendix P2.1). The inertial forces for a drip shield surrounded by rubble at higher PGV levels have the capability to move the entire drip shield by sliding it along the invert and by lifting it from the invert. In each of these cases, substantial displacement of the drip shield must be accompanied by similar displacements in the rubble. Calculations with ground motions at the 2.44 m/s and 5.35 m/s PGV levels investigated if the drip shield could be overturned by strong ground motions (BSC 2004 [DIRS 166107], Appendix P3). These simulations demonstrate that the rubble particles undergo large dynamic motion in response to displacements of the drip shield and drift walls, similar to what would occur during a vertical fault displacement. It follows that the clearance between the waste package and the sides of the collapsed drift will be partly available, but the exact value is difficult to quantify.

As a reasonable simplification, the approximation is made that fault displacement has to exceed one-quarter of the outer diameter of the OCB in order to cause failure of the waste package. One quarter of the OCB outer diameter is between 437 mm to 511 mm, or about 0.4 meters to 0.5 meters, based on the waste package outer diameters in Table 6-57. The rationale for this simplification is as follows:

- The typical size of lithophysal rubble fragments is between 0.1 meter to 0.3 meters (BSC 2004 [DIRS 166107], Section 6.4.1.1, second paragraph). A displacement of one-quarter of the waste package diameter, about 0.4 m to 0.5 m, corresponds to between 2 and 5 rubble fragments in the lithophysal zones. This displacement should not generate extreme forces on the waste package, because this displacement corresponds to a small number of rubble fragments, because this displacement represents a small fraction of the

characteristic length scale of the waste package and because of the potential for substantial movement of the rubble after drift collapse (as discussed above).

- If the drift has not completely collapsed, then there will be free space above the rubble that allows movement during the fault displacement. If the drift has completely collapsed, then the roof of the drift expands upward to approximately twice its initial height in the lithophysal zones, as shown in (BSC 2004 [DIRS 166107], Figures 6-132 and 6-137). In this situation, the distance from the waste package to the top of the drift increases by 5.5 meters during the collapse process. With the minimum rubble porosity of 0.09 for the lithophysal rubble, the "free space" within the rubble is greater than (0.09)(5.5 meters) = 0.5 meters, which is on the order of one quarter of the waste package diameter (0.4 meters to 0.5 meters). With the maximum rubble porosity of 0.29, the "free space" is greater than (0.29)(5.5 meters) = 1.6 meters. The presence of this "free space" provides room for displacement of the waste package without generating significant stresses on the waste package.

- The calculations for a waste package surrounded by rubble in response to vibratory ground motion confirm the idea that substantial waste package displacement can occur without rupture. Using the vertical component of ground motion number 9 at the 5.35 m/s PGV level as an example, a vertical displacement of 9.9 cm occurs over a time interval of 0.010 seconds and a vertical displacement of 21.6 cm occurs over a time interval of 0.025 seconds in this ground motion (DTN: MO0403AVTHM107.003 [DIRS 168892], File *MAT09V.DTS* in dts.zip, points 162 (displacement of −76.56 cm) and 164 (displacement of −86.48 cm) and points 163 (displacement of −81.52 cm) and 168 (displacement of −103.10 cm), respectively, in the ground motion time history). While this ground motion is scaled down by 24% to represent ground motions at 4.07 m/s PGV level, the fact that the waste package with degraded internals is not ruptured by ground motion 9 at the 4.07 m/s PGV level provides confirmation that significant displacements can occur without failing the waste package.

This reasoned argument provides an estimate of the minimum fault displacement that could rupture the waste package. The simplified analysis is based on a characteristic length scale for the waste package. A more complete representation of the minimum fault displacement that can rupture the waste package could depend on the size distribution of the rock fragments, the state of the waste package internals, the fraction of the drift that is filled with rockfall at the time of the fault displacement, the state of the pallet (intact or failed) and the exact positioning of the waste package and drip shield relative to the fault. In this situation, there is clearly significant uncertainty in the value of the minimum fault displacement. This uncertainty is not being included in the TSPA because the current analysis provides an estimated lower bound for the minimum fault displacement that could rupture the waste package. The uncertainty is also not included in the TSPA because damage from fault displacement affects only a small fraction of the inventory and then only for very low probability seismic events, with the result that fault displacement is expected to have a small impact on total dose. This expectation will be confirmed by the TSPA calculations for the compliance case for the TSPA-LA. The fraction of affected waste packages and the exceedance frequencies of the seismic events that can cause damage from fault displacement are quantified in Section 6.11.5.

The displacements corresponding to one-quarter of the outer diameter of the OCB are summarized in Table 6-59. The values in Table 6-59 represent the failure criteria for the waste package under fault displacement after the drip shields have failed and the waste package is surrounded by rubble. These values are also appropriate for the EBS configuration with a failed drip shield framework sitting on top of the waste package because its characteristic length scale is very similar to that for a waste package surrounded by rubble and because the dynamics of displacement in a rubble-filled drift are identical. Fault displacement in excess of these values is considered to fail the waste package (and its associated drip shield) through direct shearing.

Table 6-59. Maximum Allowable Displacement after Drip Shield Failure

Package Type	Maximum Allowable Displacement (mm)
TAD	470
Naval Fuel - Long	470
Naval Fuel - Short	470
5-DHLW/DOE SNF Short	511
5-DHLW/DOE SNF Long	511
2-MCO/2-DHLW	437

Source: Output DTN: MO0703PASDSTAT.001, worksheet "Tables" in the file *Fault Displacement Abstraction.xls*.

NOTES: Maximum allowable displacement with drift collapse = one-quarter of outer diameter of OCB in Table 6-57 rounded to three significant figures.

TAD = transportation, aging, and disposal (canister); DHLW = defense high-level radioactive waste; SNF = spent nuclear fuel; MCO = multi-canister overpack.

6.11.1.3 Failure Criteria for EBS Components in Response to Fault Displacement

The values in Tables 6-58 and 6-59 represent the failure criteria for waste packages and drip shields in response to fault displacement for two possible states of the EBS: a case for intact drip shields (Table 6-58) and a case for a failed drip shield (Table 6-59). Fault displacement in excess of these values is considered to fail the waste package and the overlying drip shield through direct shearing, allowing advective flow through the sheared components. The cladding within the affected waste package(s) would also be failed but is not considered here because the compliance case for the TSPA-LA is not taking credit for the cladding.

The values from Table 6-59 should be used for the TSPA. This is reasonable because the seismic fault displacement modeling case for TSPA may not determine the time-dependent state of the drip shield, so it is appropriate to use the smaller, more conservative values in Table 6-59 because they are valid for all times after repository closure. The resulting damage abstraction for TSPA is summarized in Section 6.11.5 and in Table 6-67.

The values in Table 6-58 may be used for criticality evaluations, which are based on the first 10,000 years after repository closure. This is an appropriate choice because the drip shields are expected to remain intact during the first 10,000 years after repository closure. The resulting damage abstraction for criticality is summarized in Section 6.11.7 and in Table 6-73.

6.11.2 Faults Intersecting Emplacement Drifts

The location, frequency, and magnitude of potential fault displacements within the footprint of the emplacement drifts must be analyzed to determine the potential impacts of fault displacement on the Yucca Mountain repository. Fault displacements are considered to occur at known faults that intersect the emplacement drifts (based on surface mapping), and to occur at generic locations within the repository.

6.11.2.1 Location of Known Faults

Information on known faults intersecting the emplacement drifts is obtained from several sources. The traces for the Sever Wash Fault, Drill Hole Wash Fault, Pagany Wash Fault, and the western splay off the main Ghost Dance Fault relative to the repository are provided in *Total System Performance Assessment Data Input Package for Requirements Analysis for Subsurface Facilities* (SNL 2007 [DIRS 179466], Table 4-1, Item Number 01-03). The intersection of these traces with individual emplacement drifts, as well as the intersections for the Sundance fault with the emplacement drifts, are defined in DTN: MO0707FAULTEMP.000 [DIRS 182092].

The intersections of known faults with the emplacement drifts have been determined using this information. The intersections are summarized in Table 6-60, where drifts are identified by panel number and drift number, plus a designation for east or west when appropriate (SNL 2007 [DIRS 179466], Table 4-1, Item Number 01-02, for the drift nomenclature). As can be seen from Table 6-60, there are a total of 43 locations where a known fault intersects an emplacement drift. The local rock type (lithophysal versus nonlithophysal) at the point of intersection is not presented in Table 6-60 because the clearances in Table 6-58 and Table 6-59 ignore the beneficial effects from drifts that might not be completely filled with rubble or rockfall at the time of the fault displacement.

Table 6-60. Intersections of Known Faults with Emplacement Drifts

Fault Designator	Drift Intersections	Number of Intersections
Sundance Fault	1-2, 1-3, 1-4, 1-5, 1-6, and 2-1	6
Drill Hole Wash Fault	4-1, 4-2, 3-4W, 3-5W, 3-6W, 3-7W, 3-8W, 3-9W, 3-9E1, 3-10E1, 3-11E1, 3-12E1, 3-13E1, 3-14E, 3-15E1, 3-16E1, and 3-17E1	17
Pagany Wash Fault	3-1W, 3-1E, 3-2E, 3-3E, 3-4E, 3-5E, 3-6E1, and 3-7E1	8
Sever Wash Fault	3-2E	1
West Ghost Dance Fault	2-17, 2-18, 2-19, 2-20, 2-21, 2-22, 2-23, 2-24, 2-25, 2-26, and 2-27	11

Sources: DTN: MO0707FAULTEMP.000 [DIRS 182092], File *Output.xls*, with results summarized in the *README* file.

SNL 2007 [DIRS 179466], Table 4-1, Item Number 01-02 for panel and drift nomenclature.

6.11.2.2 Faulting at Generic Locations

During a major seismic event, faulting could occur not only coincident with the location of well-characterized, known faults but also elsewhere in the repository. In characterizing the potential for fault displacement elsewhere in the repository, rock conditions ranging from intact rock to the presence of existing small faults with about 2 m of cumulative offset have been considered by *Probabilistic Seismic Hazard Analysis for Fault Displacement and Vibratory Ground Motion at Yucca Mountain, Nevada* (CRWMS M&O 1998 [DIRS 103731]). As discussed in Section 3.10.3 of that document, only locations with an existing fault with a cumulative offset of about 2 m have the capacity to produce significant fault displacements for exceedance frequencies greater than 10^{-8} per year. The exact number or location of these small faults is not known because they are not readily identified through surface mapping. Thus, it is necessary to estimate the density of such small faults based on either site data or natural analogues.

One means of quantifying the likelihood of such smaller faults is through use of the data obtained from the characterization of the ECRB Cross Drift (Mongano et al. 1999 [DIRS 149850], pp. 51 to 59). The ECRB Cross Drift extends through the repository footprint near its north/south midpoint and spans the approximate east/west extent of the repository. Over the length of this drift, three small faults were identified with cumulative displacement of between about one meter and a few meters. This is thought to be generally representative of the density of small faults throughout the repository, so one can make an estimate of the number of such small faults that might intersect the emplacement drifts. In reviewing the repository layout (BSC 2007 [DIRS 179466], Table 4-1, Item Number 01-02), it can be seen that there are 57 emplacement drifts that span the entire north to south extent of the repository (designated 3-1W through 3-22W, 1-1 through 1-8, and 2-1 through 2-27). Some of these drifts are much shorter than the ECRB Cross Drift. However, for abstraction purposes, the three unknown small faults in the ECRB Cross Drift are taken to intersect the repository footprint along its entire north to south extent. There are then 57 drifts, each of which has three unknown small faults, for a total of 3×57 or 171 locations where small faults have the potential to intersect the emplacement drifts.

6.11.3 Fault Displacement Hazards

Magnitudes of fault displacement along two of the known faults (Sundance and Drill Hole Wash) as a function of probability are obtained from *Probabilistic Seismic Hazard Analyses for Fault Displacement and Vibratory Ground Motion at Yucca Mountain, Nevada* (CRWMS M&O 1998 [DIRS 103731]; DTN: MO0401MWDRPSHA.000 [DIRS 183046]). In Section 8 of that document, the DOE has developed fault displacement hazard curves for fifteen faulting conditions mapped within the immediate vicinity of Yucca Mountain. Mean fault displacement hazard curves are used in the following analyses. The faulting conditions relevant to this abstraction are as follows:

- Site 2 - Solitario Canyon Fault.
- Site 3 - Drill Hole Wash Fault.

- Site 4 - Ghost Dance Fault.
- Site 5 - Sundance Fault.
- Site 7 - A generic location within the repository, approximately 100 meters east of the Solitario Canyon Fault. The ground conditions at the generic location include intact rock (7d), a hypothetical fracture with no cumulative displacement (7c), a hypothetical shear with 10 cm of offset (7b), and a hypothetical small fault with a 2-m offset (7a).
- Site 8 - A generic location within the repository, midway between the Solitario Canyon Fault and the Ghost Dance Fault. The ground conditions at the generic location include intact rock (8d), a hypothetical fracture with no cumulative displacement (8c), a hypothetical shear with 10 cm of offset (8b), and a hypothetical small fault with a 2-m offset (8a).

Five known faults intersect the emplacement areas of the repository. These five faults are the Drill Hole Wash Fault, the Sundance Fault, the Pagany Wash Fault, the Sever Wash Fault and the western splay of the Ghost Dance Fault (called the West Ghost Dance Fault). It is assumed that displacements on the Pagany Wash and Sever Wash Faults are identical to those on the Drill Hole Wash Fault (see Assumption 5.1, Section 5). The hazard curve for the main Ghost Dance Fault provides an upper bound for the fault displacement on the West Ghost Dance Fault. Generic locations identified as Site 7 and Site 8 may also exist in the repository. Locations 7a and 8a correspond to small hypothetical faults with about a 2-m offset. There are 171 intersections of these small faults with the emplacement drifts, based on the estimate in Section 6.11.2.2.

Table 6-61 provides the displacement values from the mean hazard curves as a function of the mean annual exceedance frequency (or probability) (DTN: MO0401MWDRPSHA.000 [DIRS 183046]; data files associated with Sites 2, 3, 4, 5, 7a-7d, and 8a-8c are identified in Table 4-1 of this report).

The Solitario Canyon Fault is adjacent to the repository block and is not considered further because no waste packages lie on this fault. The Ghost Dance Fault is adjacent to the repository block and no waste packages lie directly on this fault, but it is used as an upper bound for displacements on the West Ghost Dance Fault which does intersect drifts in Panel 2. Locations 7 and 8 have essentially the same estimated hazard curves and fault displacements relative to the accuracy of the results in DTN: MO0401MWDRPSHA.000 [DIRS 183046], as demonstrated by the values in Table 6-61. Thus, this analysis does not distinguish between Sites 7a and 8a for estimating the consequences to waste packages.

Table 6-61. Fault Displacement from Mean Hazard Curves

	Mean Annual Exceedance Frequency (1/yr)				
	10^{-4}	10^{-5}	10^{-6}	10^{-7}	10^{-8}
Site Number and Fault Name	**Displacement (cm)**				
2 - Solitario Canyon	<0.1	32	180	490	1300
3 - Drill Hole Wash [a]	<0.1	<0.1	15	75	240
4 - Ghost Dance [b]	<0.1	<0.1	15	69	220
5 - Sundance	<0.1	<0.1	6	40	140
7a - Small fault with 2-m offset	<0.1	<0.1	2	18	73
7b - Shear with 10-cm offset	<0.1	<0.1	1	6	9
7c - Fracture with no displacement	<0.1	<0.1	0.1	0.5	0.6
7d - Intact rock	<0.1	<0.1	<0.1	<0.1	<0.1
8a - Small fault with 2-m offset	<0.1	<0.1	2	18	78
8b - Shear with 10-cm offset	<0.1	<0.1	0.9	6	9
8c - Fracture with no displacement	<0.1	<0.1	0.1	0.5	0.6
8d - Intact rock [c]	<0.1	<0.1	<0.1	<0.1	<0.1

[a] Also representative of Pagany Wash and Sever Wash Faults.
[b] Representative of West Ghost Dance Fault.
[c] Data for Site 8d are based on the observation that the fault displacements for Sites 7a, 7b, and 7c are essentially identical with the fault displacements for Sites 8a, 8b, and 8c, respectively. In this situation, the fault displacements at Site 8d are anticipated to be very similar to the fault displacements at Site 7d considering that both generic locations involve intact rock within the repository block. This observation is corroborated by information in *Probabilistic Seismic Hazard Analyses for Fault Displacement and Vibratory Ground Motion at Yucca Mountain, Nevada* (CRWMS M&O 1998 [DIRS 103731], Section 8.2.1, first paragraph), which indicates that displacements at Site 8d are below 0.1 cm down to 10^{-8} per year annual exceedance frequency.

Sources: DTN: MO0401MWDRPSHA.000 [DIRS 183046]; data files associated with Sites 2, 3, 4, 5, 7a-7d, and 8a-8c are listed in Table 4-1 of this report. Displacements are calculated in the output
DTN: MO0703PASDSTAT.001, worksheet "Hazard Calcs" in the file *Fault Displacement Abstraction.xls*.

NOTE: Displacements between 1 cm and 10 cm are rounded to one significant figure, and displacements above 10 cm are rounded to two significant figures.

The fault displacement hazard curves for Sites 4 and 5 are being modified as this document is being completed. The fault displacement damage abstraction is based on the data in the existing DTN.

6.11.4 Consequence for the Waste Packages

A comparison of Table 6-61 with Table 6-59 shows that no waste package would be damaged by even the most extreme events with exceedance frequency of 10^{-8} per year at locations 7b, 7c, 7d, 8b, 8c, and 8d. The waste packages will survive these events because the maximum displacement at these sites, 9 cm (90 mm), is less than the minimum clearances in Table 6-59. However, several of the waste package designs could potentially fail due to fault displacement for hazards near the 10^{-7}- to 10^{-8}-per-year level if they are directly over one of the known faults (Drill Hole Wash, Sundance, Pagany Wash, Sever Wash, and West Ghost Dance) intersecting the emplacement drifts. Further, the waste packages could potentially fail when placed over the small hypothetical faults at Sites 7a and 8a. The frequency of waste package failure at a given location is a function of the clearance for the specific type of waste package emplaced there.

Waste package distribution by type is available in the design basis inventory (MO0702PASTREAM.001 [DIRS 179925], File *DTN-Inventory-Rev00.xls*, worksheet "UNIT CELL," cells B14:L15). This inventory is presented in Table 6-62, along with the waste package dimensions. The TAD-bearing waste package in Table 6-62 includes all medium and small TAD-bearing waste packages in the design basis inventory. The 5-DHLW/DOE SNF Long waste package includes the 1S/5L and the 1D/4L codisposal waste packages in the design basis inventory. The nominal quantity is the expected number of waste packages in the TSPA inventory.

Table 6-62. Waste Package Dimensions and Design Basis Inventory

Waste Package Configuration	Nominal Length (mm)	Outer Diameter of OCB (mm)	Nominal Quantity
TAD	5,850.1	1,881.6	7,483
Naval Fuel - Long	5,850.1	1,881.6	310
Naval Fuel - Short	5,215.1	1,881.6	90
5-DHLW/DOE SNF Short	3,697.4	2,044.7	1,207
5-DHLW/DOE SNF Long	5,303.9	2,044.7	1,862
2-MCO/2-DHLW	5,278.6	1,749.3	210

Sources: SNL 2007 [DIRS 179394], Table 4-3, for outside diameter of OCB and for nominal length of the TAD waste package; SNL 2007 [DIRS 179567], Tables 4-6 through 4-10, for outside diameter of OCB and nominal length of the other waste package types.

DTN: MO0702PASTREAM.001 [DIRS 179925], File *DTN-Inventory-Rev00.xls*, worksheet "UNIT CELL," cells B14:L15, for nominal quantity in design basis inventory.

NOTES: The nominal quantity is the most likely or expected number of waste packages in the inventory. The nominal quantity of TAD-bearing waste packages includes all medium and small TAD-bearing waste packages in the design basis inventory.

The 5-DHLW/DOE SNF Long waste package includes the 1S/5L and the 1D/4L codisposal waste packages in the design basis inventory.

TAD = transportation, aging, and disposal (canister); DHLW = defense high-level radioactive waste; DOE = U.S. Department of Energy; SNF = spent nuclear fuel; MCO = multi-canister overpack.

To simplify the analysis, the inventory of waste packages is split into two groups with similar design and similar waste type. The two groups are defined as follows:

- **TAD**: includes the TAD-bearing, Naval Fuel-Long, and Naval Fuel-Short waste packages
- **Codisposal**: includes the 5-DHLW/DOE SNF Short, the 5-DHLW/DOE SNF Long, and the 2-MCO/2-DHLW waste packages.

The waste package designs with the smallest diameter in the group are chosen to minimize the allowable displacement for all packages in that group. For the TAD group, all waste packages have the same outer diameter. For the codisposal group, the 2-MCO/2-DHLW waste package has the smallest outer diameter, as shown in Table 6-62. This abstraction uses the allowable displacement for the 2-MCO/2-DHLW waste package, even though this package constitutes less than 7% of the inventory in the codisposal group (see data in Table 6-62). The allowable fault displacements for each waste package group are summarized in Table 6-63.

Table 6-63. Maximum Allowable Fault Displacements Before a Waste Package Group Is Pinned

Waste Package Group	Maximum Allowable Displacement
TAD	470 mm (47.0 cm)
Codisposal	437 mm (43.7 cm)

Source: Output DTN: MO0703PASDSTAT.001, cells B31 and B36 for the TAD-bearing and codisposal waste packages, respectively, in the worksheet "Tables" in the file *Fault Displacement Abstraction.xls*.

NOTE: TAD = transportation, aging, and disposal (canister).

The fraction of waste packages in each group is calculated based on the total length of the waste package types in the group versus the total length of all emplaced waste packages. Length is the appropriate parameter here because it more accurately represents the probability that a waste package is directly on a fault. These results are shown in Table 6-64. The effective length for each package type is shown because it is used to calculate the surface area for the package type.

The DOE does not intend to emplace Naval waste packages on known secondary faults or generic faults with greater than a 2 meter cumulative offset that intersect the emplacement drifts. There are a total of 400 Naval-Long and Naval-Short waste packages, which constitute less than 4% of the total inventory of waste packages. Removal of the 400 Naval waste packages from the inventory for fault displacement produces insignificant changes to the relative fraction of the TAD-bearing and codisposal groups shown in the last column of Table 6-64, and in the number of failed waste packages in Tables 6-66 and 6-67. Given that the changes are very small and that damage from fault displacement is a minor contributor to dose, the inventory of Naval waste packages is not excluded from the damage abstraction for fault displacement for TSPA.

Waste package failure occurs when displacements on the fault displacement hazard curve(s) exceed the maximum allowable displacement. By comparing the displacements in Table 6-63 with the points on the hazard curve in Table 6-61, it can be seen that waste package failures occur for exceedance frequencies between 10^{-7} per year and 10^{-8} per year for waste packages emplaced on the five known faults (Drill Hole Wash, Sundance, Pagany Wash, Sever Wash, and West Ghost Dance Faults). Waste package failures can also occur for waste packages emplaced on the small generic faults (locations 7a and 8a in Table 6-61), although these failures occur for exceedance frequencies close to 10^{-8} per year. As a reminder, the Solitario Canyon and main Ghost Dance Faults are not included in this discussion because these faults lie outside the emplacement areas of the repository.

The fault displacement hazard curves from *Probabilistic Seismic Hazard Analyses for Fault Displacement and Vibratory Ground Motion at Yucca Mountain, Nevada* (DTN: MO0401MWDRPSHA.000 [DIRS 183046]) define which fault displacement events are severe enough to cause waste package failure. The relevant hazard curves are provided in File ./displ/tot-haz/s3.frac_mean.gz of the DTN for the Drill Hole Wash Fault, in File ./displ/tot_haz/s5rev.frac_mean.gz for the Sundance Fault, in Files ./displ/tot-haz/s7a.frac_mean.gz and ./displ/tot-haz/s8a.frac_mean.gz of the DTN for locations 7a and 8a, and in File /displ/tot_haz/s4rev.frac_mean.gz of the DTN for the West Ghost Dance Fault. A comparison of the allowable displacements (see Table 6-63) with the individual hazard curves defines the range of exceedance frequencies that can cause waste package failure. The ranges of exceedance frequencies are listed in Table 6-65 for each fault and each waste package group.

There are four locations where the Sundance Fault intersects the emplacement drifts, 26 locations where the Drill Hole Wash, Pagany Wash, or Sever Wash Faults intersect the emplacement drifts, 11 locations where the West Ghost Dance Fault intersects the emplacement drifts, and 171 locations where additional small faults intersect the emplacement drifts (Table 6-60 and Section 6.11.2.2). Combining this information with the probability of finding a particular waste package group at a given point in the repository (last column in Table 6-64), an estimate can be made of the expected number of each type of waste package at the five known faults. This result is shown in Table 6-66. Note that the number of waste packages is not an integral number because it represents an average expectation of finding a particular waste package along a particular fault. The Pagany Wash, Sever Wash and Drill Hole Wash Faults have been combined in Table 6-66 because they have the same fault-displacement hazard curves.

Table 6-64. Parameters for Simplified Groups of Waste Packages

Waste Package Group	Effective Waste Package Length[c], L_{eff} (mm)	Effective Waste Package Diameter[d], D (mm)	Effective Waste Package Surface Area[a] (m^2)	Nominal Quantity (-)	Total Waste Package Length for Group [b] (mm)	Fraction of Waste Packages (% of Total Length)[e]
TAD	5,843	1,881.6	40.10	7,883	4.606×10^{07}	74.9
Codisposal	4,711	2,044.7	36.83	3,279	1.545×10^{07}	25.1

[a] Effective surface area = $(\pi/2)(D)^2 + \pi D L_{eff}$.

[b] Total waste package length for group= $\Sigma(\text{length})_i \times (\text{nominal quantity})_i$ summed over the package types in each group, based on the lengths and nominal quantities in Table 6-62.

[c] Effective waste package length = L_{eff} = total length / nominal quantity.

[d] Outer diameter of the OCB is 1,881.6 mm for all waste package types in the TAD group. Outer diameter of the OCB for the codisposal group is based on the 5-DHLW/DOE SNF packages because they constitute more than 90% of the inventory in this group, based on the quantities in Table 6-62.

[e] This fraction includes the Naval waste packages, as explained in a previous paragraph.

Source: Output DTN: MO0703PASDSTAT.001, worksheet "Tables" in the file *Fault Displacement Abstraction.xls*. Formulas for total length, effective length, and effective surface area of each waste package group are defined in footnotes a, b, and c above.

NOTES: The nominal quantity is the most likely or expected number of waste packages in the inventory.
(-) = dimensionless; TAD = transportation, aging, and disposal (canister).

Table 6-65. Mean Annual Exceedance Frequencies That Cause Waste Package Failure

Fault	TAD Group	Codisposal Group
3—Drill Hole Wash	$< 2.2 \times 10^{-7}$	$< 2.5 \times 10^{-7}$
Pagany Wash	$< 2.2 \times 10^{-7}$	$< 2.5 \times 10^{-7}$
Sever Wash	$< 2.2 \times 10^{-7}$	$< 2.5 \times 10^{-7}$
4—West Ghost Dance	$< 2.0 \times 10^{-7}$	$< 2.2 \times 10^{-7}$
5—Sundance	$< 7.8 \times 10^{-8}$	$< 8.6 \times 10^{-8}$
Sites 7a/8a[a]	$< 2.6 \times 10^{-8}$	$< 2.9 \times 10^{-8}$

[a] The hazard curves for Sites 7a and 8a are very similar, as shown by the data in Table 6-61. The maximum exceedance frequency for Sites 7a or 8a is presented here.

Source: Output DTN: MO0703PASDSTAT.001, Cells B169:B174 for the TAD-bearing waste package group and cells C169:C174 codisposal waste package group, respectively, in worksheet "Tables" in the file *Fault Displacement Abstraction.xls*. The codisposal waste package group is represented by the 2-MCO/2-DHLW waste package because it has the smallest allowable displacement of the package types in this group.

NOTE: TAD = transportation, aging, and disposal (canister).

Table 6-66. Expected Number of Waste Packages Emplaced on Each Fault

Fault	TAD-Bearing Waste Package Group	Codisposal Waste Package Group	Total
3—Drill Hole Wash	19.5	6.5	26
4—West Ghost Dance	8.2	2.8	11
5—Sundance	4.5	1.5	6
Sites 7a/8a	128.1	42.9	171

Source: Output DTN: MO0703PASDSTAT.001, worksheet "Tables," cells B185:D188 in the file *Fault Displacement Abstraction.xls*.

NOTES: Values for the TAD group includes the Naval waste packages.
TAD = transportation, aging, and disposal (canister).

6.11.5 Damage Abstraction for Fault Displacement

The expected number of waste package failures as a function of annual exceedance frequency is calculated by combining the data in Tables 6-65 and 6-66. For a given waste package group, Table 6-65 defines the range of annual exceedance frequencies that can cause the number of waste packages identified in Table 6-66 to fail. The results are summarized in Table 6-67. Smaller values of the exceedance frequency result in sequential failures on the West Ghost Dance Fault, the Sundance Fault, and finally at Sites 7a/8a, producing incremental increases in the number of package failures. In other words, lower values of exceedance frequency cause additional waste package failures on multiple faults within the repository.

Table 6-67. Expected Number of Waste Package Failures versus Annual Exceedance Frequency

Annual Exceedance Frequency (1/yr)	Expected Number of Failures—TAD-Bearing Waste Package Group	Annual Exceedance Frequency (1/yr)	Expected Number of Failures—Codisposal Waste Package Group
$> 2.2 \times 10^{-7}$	0	$> 2.5 \times 10^{-7}$	0
2.0×10^{-7} to 2.2×10^{-7}	19.5	2.2×10^{-7} to 2.5×10^{-7}	6.5
7.8×10^{-8} to 2.0×10^{-7}	27.7	8.6×10^{-8} to 2.2×10^{-7}	9.3
2.6×10^{-8} to 7.8×10^{-8}	32.2	2.9×10^{-8} to 8.6×10^{-8}	10.8
1×10^{-8} to 2.6×10^{-8}	160.3	1×10^{-8} to 2.9×10^{-8}	53.7

Source: Output DTN: MO0703PASDSTAT.001, worksheet "Tables", cells B196:B200 and cells D196:D200 in the file *Fault Displacement Abstraction.xls*.

NOTES: Fault intersections and the hazard curves at Sites 4 and 5 were revised after the data for the fault displacement damage abstraction were defined in the TSPA database. This table presents the corrected values. With regard to annual exceedance frequencies, the TSPA data base has 1.4×10^{-7} in place of 2.0×10^{-7} for the TAD-bearing waste package group and 1.6×10^{-7} in place of 2.2×10^{-7} for the codisposal group. With regard to expected number of failures, the TSPA database has 30.7 in place of 32.2, 10.3 in place of 10.8, 158.8 in place of 160.3, and 53.2 in place of 53.7. These minor errors at very low values of the annual exceedance frequency will produce insignificant changes in TSPA predictions of total dose to the reasonably maximally exposed individual.

Values for the TAD group include the Naval waste packages.

TAD = transportation, aging, and disposal (canister).

When a waste package fails by fault displacement, the failed area on the waste package is determined by sampling a uniform distribution with a lower bound of 0 m^2 and an upper bound equal to the area of the waste package lid. The lower bound is appropriate for annual exceedance frequencies near 10^{-7} per year because a waste package that is minimally pinned from fault displacement is expected to have only minor crimping and is unlikely to rupture. The upper bound is appropriate for a large fault displacement that shears a waste package near its lid. In this case, the lid welds have the potential to fracture, separating the lid from the package and potentially exposing the entire waste form to seepage and release. The use of a uniform distribution for failed area is appropriate here because reasonable upper and lower bounds can be defined and because the use of this type of distribution maintains the uncertainty in the damaged area for this abstraction. The area of the lid for the TAD-bearing and codisposal waste package groups is 2.78 m^2 and 3.28 m^2, respectively, based on the diameters of 1.8816 m, and 2.0447 m shown in Table 6-64.

This failed area is conceptualized to be a shear that lies in a plane normal to the central axis of the waste package. The failed area can be represented as a circumferential band around the waste package for advective transport calculations in the TSPA. Once a waste package fails in shear, there is no further damage on successive events and the waste package remains failed for the remainder of the realization.

When a waste package fails from fault displacement, the associated drip shield fails as a barrier to flow and transport (if it has not already failed from the fragility model in Section 6.8). A sheared drip shield will allow all seepage to pass through it for the TSPA; that is, there is no flux splitting (diversion of seepage) on the drip shield. TSPA is not taking credit for the fuel rod cladding as a barrier to radionuclide release for the TSPA-LA. However, if analyses are performed with the fuel rod cladding as a barrier, then the fuel rod cladding becomes 100% perforated in response to a fault displacement that can shear a waste package. These damage abstractions for the drip shield and fuel rod cladding represent bounding approximations, particularly for annual exceedance frequencies near 10^{-7} per year where there is only minor crimping of the EBS components.

Fault displacement can only fail waste packages that are emplaced directly on faults, so multiple events should not fail the same package twice. If multiple events with damage from fault displacement occur in a given realization, then the number of failed waste packages and the magnitude of the failed area should be determined by the highest intensity seismic event. The highest-intensity seismic event corresponds to the event with the greatest value of PGV or the lowest exceedance frequency.

6.11.6 Alternative Conceptual Model for Damage from Fault Displacement

The analysis of waste package failure due to fault displacement presented in Sections 6.11.1 through 6.11.5 provides a basis for estimating the number of potentially damage-inducing faults that intersect the emplacement drifts. This analysis uses the known location of larger faults (e.g., Sundance Fault, Drill Hole Wash Fault) relative to the planned location of the emplacement drifts, as well as an estimate of the density of smaller-displacement faults based on the observed fault density along the exploratory tunnel. The maximum allowable fault displacement before waste package damage occurs was shown to vary between 437 mm and 470 mm, depending on

waste package type (Table 6-63). Using this site-specific information, it is shown that there are 43 locations where known faults intersected the planned emplacement drifts (Table 6-60), plus an estimated 171 locations where unmapped faults could intersect the drifts (Section 6.11.2.2), for a total of 214 fault intersections.

As an alternative conceptual model, a paper titled "Methodologies for the Evaluation of Faulting at Yucca Mountain, Nevada" (Waiting et al. 2003 [DIRS 164449]) was considered. This paper presents an assessment of the consequences of fault displacement at Yucca Mountain based on historical earthquake activity in the Western United States. Four historic rupture events were considered, to arrive at a median value for fault rupture density (length of faulting per unit area of surface). A conservative median value of 20 km/km^2 was obtained from this analysis of the four events considered. Using this value, along with a representative angle of 50 degrees between the typical drift orientation and the orientation of the faults and an 80-m drift spacing, the authors determined that there would be 191 waste package locations where a fault would intersect an emplacement drift at Yucca Mountain. This result compares favorably to the 214 fault intersections calculated in this report.

The specific analog event considered by Waiting et al. (2003 [DIRS 164449]), for purposes of quantification, was the 1983 Borah Peak earthquake in the Lost River Range in Idaho. Prior analysis of this event had shown that the maximum displacement for the Borah Peak earthquake was 2.7 meters, with an average displacement of approximately 1 meter. Given the fact that the mean annual exceedance frequency for 1 meter of displacement at Yucca Mountain ranges from approximately 10^{-6}/yr for the Solitario Canyon Fault to approximately 10^{-8}/yr for the Sundance Fault, the probability-weighted number of waste package failures is calculated to be between 1.91×10^{-4} to 1.91×10^{-6}. Note that the upper end of this range applies only to the Solitario Canyon Fault. As discussed in Section 6.11.3, no drifts intersect the Solitario Canyon Fault or the main Ghost Dance Fault for the current repository footprint. The largest fault displacement would be expected to correspond to the Drill Hole Wash Fault. The mean annual exceedance frequency for one meter of displacement for this fault is on the order of 10^{-7}/yr. Thus, the probability-weighted number of waste package failures would be between 1.91×10^{-5} and 1.91×10^{-6}.

The results presented in Table 6-67 are not stated in terms of probability-weighted number of waste package failures. Thus, an immediate comparison with the results of the alternate model is not possible. However, it is straightforward to calculate the probability-weighted number of waste package failures from the data in Table 6-67. The probability-weighted or expected number of waste package failures is defined as the product of two terms that are summed over all relevant exceedance frequencies. The two terms are: (1) the number of waste package failures for a given range of exceedance frequency and (2) the probability that a fault displacement will occur within the given range of exceedance frequency. For example, using data in the first row of Table 6-67, there are 19.5 failures of the TAD-bearing waste package group over the exceedance frequency interval (1.4×10^{-7}, 2.2×10^{-7}). The probability-weighted failures in this interval are calculated as $(19.5)(2.2 \times 10^{-7} - 1.4 \times 10^{-7}) = 1.56 \times 10^{-6} \sim 1.6 \times 10^{-6}$. The difference of exceedance frequencies is appropriate in this calculation because the probability of an event within the interval (1.4×10^{-7}, 2.2×10^{-7}) is defined by the difference of exceedance

frequencies. The total probability-weighted failures are summed over all relevant intervals in Table 6-67. Mathematically, the sum over all relevant intervals can be written as:

$$E(n) = \sum_{i=1}^{n} n_i \left(\lambda_{i+1} - \lambda_i \right) \qquad \text{(Eq. 6.11-1)}$$

where $E(n)$ is the expected number of waste package failures and n_i is the number of waste package failures in the ith internal $[\lambda_i, \lambda_{i+1}]$. The values for $[\lambda_i, \lambda_{i+1}]$ are based on the data in the first or third columns of Table 6-67. There are four intervals with nonzero failures in Table 6-67, so $n = 4$ in Equation 6.11-1. Table 6-68 summarizes the numerical calculations for both types of waste packages.

The probability-weighted number of waste package failures for the abstraction in this report is 1.1×10^{-5}, as shown in Table 6-68. This value is within the range of results provided by the alternative conceptual model, 1.91×10^{-6} to 1.91×10^{-5}. Thus, the alternative conceptual model based on the use of analog data provides results that are consistent with the results of the model presented in this report for the probability-weighted number of waste package failures. The number of fault intersections is also similar: 214 intersections for this report versus 191 fault intersections for the alternative conceptual model. This comparison provides added confidence in the validity of the fault displacement damage abstraction in this report.

Table 6-68. Calculation of Probability-Weighted Waste Package Failures

Exceedance Frequency Range (Per Year)	Number Failures in TAD Group	Product of Columns 1 and 2	Exceedance Frequency Range (Per Year)	Number Failures in Codisposal Group	Product of Columns 4 and 5
2.0×10^{-7} to 2.2×10^{-7}	19.5	3.9×10^{-7}	2.2×10^{-7} to 2.5×10^{-7}	6.5	2.0×10^{-7}
7.8×10^{-8} to 2.0×10^{-7}	27.7	3.4×10^{-6}	8.6×10^{-8} to 2.2×10^{-7}	9.3	1.2×10^{-6}
2.6×10^{-8} to 7.8×10^{-8}	32.2	1.7×10^{-6}	2.9×10^{-8} to 8.6×10^{-8}	10.8	6.2×10^{-7}
1×10^{-8} to 2.6×10^{-8}	160.3	2.6×10^{-6}	1×10^{-8} to 2.9×10^{-8}	53.7	1.0×10^{-6}
Total for TAD Group		8.1×10^{-6}	**Total for Codisposal Group**		3.0×10^{-6}
Total for Both Groups		1.1×10^{-5}			

Sources: Data in Table 6-67 for number of waste package failures as a function of the exceedance frequency range. Equation 6.11-1 provides the basis for the numerical calculations.

NOTE: TAD = transportation, aging, and disposal (canister).

6.11.7 Damage from Fault Displacement for Criticality Studies

As noted in Section 6.11.1.3, the clearances in Table 6-59 are being used for the TSPA because drip shield failure is expected to occur during the long time scale for peak dose assessment. On the other hand, the clearances in Table 6-58 are appropriate for criticality evaluations, which are based on the first 10,000 years after repository closure when the drip shields are expected to remain intact. In addition, the damage abstraction for the TSPA is based on two waste package groups: the TAD group and the codisposal group. While this grouping is consistent with the representation of waste package groups in the TSPA, criticality studies may require a more detailed analysis of waste package failures by individual waste package type. Finally, Naval

waste packages will not be emplaced on known secondary faults or generic faults at Sites 7a/8a and are therefore excluded from this analyses.

This section applies the same methodology that is used for the fault damage abstraction (see Sections 6.11.1 through 6.11.5) to individual waste package types with the clearances for intact drip shields in Table 6-58. The information for this analysis is consistent with the methodology for the damage abstraction for fault displacement in the TSPA-LA, but represents a finer level of detail. The calculations for this analysis are documented in output DTN: MO0705FAULTABS.000 from this report. Table 6-57, Table 6-58, Table 6-60, Table 6-61, and Table 6-62 remain unchanged for this analysis. The data in Table 6-58 provide the maximum allowable fault displacements for this analysis. Table 6-69 presents the calculated fraction of individual waste package types in the inventory. This table differs from Table 6-64 because Table 6-64 has data for two waste package groups (TAD and codisposal), rather than by individual waste package type as in Table 6-69. Table 6-70 presents the mean annual exceedance frequencies that result in fault displacements that are greater than the maximum allowable fault displacements in Table 6-58. Table 6-71 presents the expected number of waste packages by type that are emplaced on each fault. Tables 6-72 and 6-73 combine the exceedance frequencies that cause failure in Table 6-70 and the number of packages emplaced on faults in Table 6-71 to determine the expected number of failed packages by type as a function of annual exceedance frequency. Naval waste packages are not included in Tables 6-69 through 6-71, as noted above. If a Naval waste package is erroneously placed on a secondary fault or generic fault, it will be damaged at the same exceedance frequencies as the TAD-bearing waste package (see Table 6-70) because the outer diameter and hence the clearance for the TAD-bearing and Naval waste packages are identical.

6.11.8 Standoff Distance Analysis

Appendix D presents an analysis of the potential damage zone resulting from displacement on a known secondary fault that intersects an emplacement drift in lithophysal rock at the Yucca Mountain site. The results of this analysis may be used to define the standoff distance for Naval-Long and Naval-Short waste packages relative to known secondary or generic (Sites 7a/8a) faults.

Table 6-69. Fraction of Waste Packages By Waste Package Type

Waste Package Type	Nominal Waste Package Length by Type (mm)	Waste Package Diameter by Type (mm)	Waste Package Surface Area[a] by Type (m^2)	Nominal Quantity (-)	Total Waste Package Length by Type[b] (mm)	Fraction of Waste Packages (% of Total Length)
TAD	5,850.1	1,881.6	40.14	7,483	4.378×10^{07}	73.9
5-DHLW/DOE SNF Short	3,697.4	2,044.7	30.32	1,207	4.463×10^{06}	7.5
5-DHLW/DOE SNF Long	5,303.9	2,044.7	40.64	1,862	9.876×10^{06}	16.7
2-MCO/2-DHLW	5,278.6	1,749.3	33.82	210	1.109×10^{06}	1.9

[a] Surface area = $(\pi/2)(D)^2 + \pi DL$, where L is the nominal length and D is the diameter.

[b] Total waste package length by type = (L) × (nominal quantity).

Source: Output DTN: MO0705FAULTABS.000, rows 120 to 128 and rows 135 to 143 in worksheet "Tables by WP Type" in the file *Fault Displacement Abstraction for Criticality.xls*. Formulas for total length, and surface area of each waste package type are defined in footnotes a, and b, above,

NOTES: (-) = dimensionless; TAD = transportation, aging, and disposal (canister).

Table 6-70. Mean Annual Exceedance Frequencies That Cause Waste Package Failure

Fault	TAD	5-DHLW/DOE SNF Short	5-DHLW/DOE SNF Long	2-MCO/2-DHLW
3 - Drill Hole Wash	$< 8.2 \times 10^{-8}$	$< 1.2 \times 10^{-7}$	$< 1.2 \times 10^{-7}$	$< 6.3 \times 10^{-8}$
Pagany Wash	$< 8.2 \times 10^{-8}$	$< 1.2 \times 10^{-7}$	$< 1.2 \times 10^{-7}$	$< 6.3 \times 10^{-8}$
Sever Wash	$< 8.2 \times 10^{-8}$	$< 1.2 \times 10^{-7}$	$< 1.2 \times 10^{-7}$	$< 6.3 \times 10^{-8}$
4 - West Ghost Dance	$< 7.0 \times 10^{-8}$	$< 1.1 \times 10^{-7}$	$< 1.1 \times 10^{-7}$	$< 5.4 \times 10^{-8}$
5 - Sundance	$< 2.7 \times 10^{-8}$	$< 4.1 \times 10^{-8}$	$< 4.1 \times 10^{-8}$	$< 2.1 \times 10^{-8}$
Sites 7a/8a[a]	$< 8.7 \times 10^{-9}$	$< 1.3 \times 10^{-8}$	$< 1.3 \times 10^{-8}$	$< 6.6 \times 10^{-9}$

[a] The hazard curves for Sites 7a and 8a are very similar, as shown in Table 6-61. The maximum exceedance frequency for Sites 7a or 8a is presented here.

Source: Output DTN: MO0705FAULTABS.000, rows 164 to 172 in worksheet "Tables by WP Type" in the file *Fault Displacement Abstraction for Criticality.xls*.

NOTE: TAD = transportation, aging, and disposal (canister).

Table 6-71. Expected Number of Waste Packages by Type Emplaced on Faults

Fault	TAD	5-DHLW/DOE SNF Short	5-DHLW/DOE SNF Long	2-MCO/2-DHLW
3 - Drill Hole Wash, Pagany Wash, & Sever Wash	19.2	2.0	4.3	0.5
4 - West Ghost Dance	8.1	0.8	1.8	0.2
5 - Sundance	4.4	0.5	1.0	0.1
Sites 7a/8a	126.4	12.9	28.5	3.2
Totals	158.2	16.1	35.7	4.0

Source: Output DTN: MO0705FAULTABS.000, rows 180 to 185 in worksheet "Tables by WP Type" in the file *Fault Displacement Abstraction for Criticality.xls*.

NOTE: TAD = transportation, aging, and disposal (canister).

Table 6-72. Expected Number of Failed TAD Waste Packages as a Function of Annual Exceedance Frequency

Annual Exceedance Frequency (1/yr)	Expected Number of Failures – TAD
$> 8.2 \times 10^{-8}$	0
7.0×10^{-8} to 8.2×10^{-8}	19.2
2.7×10^{-8} to 7.0×10^{-8}	27.3
1.0×10^{-8} to 2.7×10^{-8}	31.8

Source: Output DTN: MO0705FAULTABS.000, rows 191 to 195 in worksheet "Tables by WP Type" in the file *Fault Displacement Abstraction for Criticality.xls*.

NOTE: TAD = transportation, aging, and disposal (canister).

Table 6-73. Expected Number of Failed DHLW Short, DHLW Long, and 2-MCO/2-DHLW Waste Packages as a Function of Annual Exceedance Frequency

Annual Exceedance Frequency (1/yr)	Expected Number of Failures—DHLW Short	Expected Number of Failures—DHLW Long	Annual Exceedance Frequency (1/yr)	Expected Number of Failures—2-MCO/2-DHLW
$> 1.2 \times 10^{-7}$	0	0	$> 6.3 \times 10^{-8}$	0
1.1×10^{-7} to 1.2×10^{-7}	2.0	4.3	5.4×10^{-8} to 6.3×10^{-8}	0.5
4.1×10^{-8} to 1.1×10^{-7}	2.8	6.2	2.1×10^{-8} to 5.4×10^{-8}	0.7
1.3×10^{-8} to 4.1×10^{-8}	3.2	7.2	1.0×10^{-8} to 2.1×10^{-8}	0.8
1.0×10^{-8} to 1.3×10^{-8}	16.1	35.7		

Source: Output DTN: MO0705FAULTABS.000, rows 191 to 196 in worksheet "Tables by WP Type" in the file *Fault Displacement Abstraction for Criticality.xls*.

NOTES: DHLW Short = 5-DHLW/DOE SNF Short; DHLW Long = 5-DHLW/DOE SNF Long.

6.12 SEISMIC SCENARIO CLASS

6.12.1 Computational Approach

The dose calculation for the seismic scenario class is based on a set of R realizations that have robust sampling of all levels of seismic events (i.e., for the full ranges of PGV levels and fault displacement amplitudes) with the potential to generate releases from the EBS. The following discussion explains how these R realizations are generated using a Monte Carlo computational procedure in the TSPA.

The R realizations represent the future performance of the repository for the seismic hazards of ground motion and fault displacement. These realizations represent the combined epistemic and aleatory uncertainty in the compliance case for the seismic scenario class. Epistemic uncertainty is captured by those stochastic parameters that represent the "lack of knowledge" uncertainty in various processes. Aleatory uncertainty is captured by the stochastic parameters that represent the randomness of processes, such as the uncertainty in the timing and amplitude of seismic events.

The compliance case for the seismic scenario class is very similar to the compliance case for the nominal scenario class, with the following notable differences: (1) failure of the waste package can occur from rupture and puncture, in addition to general corrosion processes; (2) failure of the drip shield can occur from rupture in addition to general corrosion processes; (3) damaged area on the waste package and drip shield is determined by sampling stochastic parameters in the seismic damage abstractions, rather than by general corrosion processes; and (4) the damaged area on the waste package and drip shield is represented as a network of stress corrosion cracks, rather than as large breaches on the waste package or drip shield. The primary output from each of these R realizations is a time history of dose to the reasonably maximally exposed individual.

Seismic events occur randomly in time (see Assumption 5.2, Section 5). For each seismic event, the value of the horizontal peak ground velocity, PGV_j, and its associated annual exceedance frequency, λ_j, are determined by a Monte Carlo process that samples appropriate distributions for these parameters for the jth event. Since PGV and λ are functionally related, it is sufficient to sample one parameter or the other; λ is sampled for the TSPA-LA.

The annual exceedance frequency, λ_j, is determined by sampling a uniform distribution with lower bound λ_{min} and upper bound λ_{max}. The bounds of the uniform distribution must be chosen to encompass the seismic events with the potential to release significant radionuclides from the EBS. Values of λ_{max} and λ_{min} for the seismic scenario class are 4.287×10^{-4} per year and 10^{-8} per year, respectively, because this range spans the response of the system, from no damage to the waste package at 4.287×10^{-4} per year to the regulatory probability limit at 10^{-8} per year. The basis for these limits is discussed in Section 6.4.3.

Once the value of the annual exceedance frequency (λ_j) is determined for the jth event, the corresponding value of the peak ground velocity (PGV_j) is calculated. The relationship between PGV and λ is defined by the mean bounded hazard curve, and is site-specific and location-specific (see Section 6.4).

The mean bounded hazard curve for vibratory ground motion and the mean hazard curves for fault displacements are central to the seismic scenario class. These mean hazard curves represent both aleatory and epistemic uncertainties in the hazards (Sections 6.4.1 and 6.4.2). The seismic scenario class is based on the mean hazard, considering the range of epistemic uncertainty for a given value of PGV. This is a reasonable approach because the mean (epistemic) estimate of the (aleatory) mean dose is linear in the exceedance frequency, λ, for a given value of PGV. The derivation of the mean bounded hazard curve is described in *Peak Ground Velocities for Seismic Events at Yucca Mountain, Nevada* (BSC 2005 [DIRS 170137]). Analysis of the geologic conditions at Yucca Mountain and other corroborating evidence provides a basis for estimating the maximum feasible or bounding value of PGV at the emplacement drifts. The numerical values for the bounded hazard curve are defined in Table 6-3.

Once the value for PGV_j is known, the seismic damage abstractions for the waste package and drip shield are evaluated and sampled for each seismic event. This evaluation also requires (1) the RST for Alloy 22 in the ith realization, denoted as RST_i, (2) the spatially averaged thickness of the OCB at the time of the seismic event, and (3) the accumulated volume of lithophysal rubble in the emplacement drifts. This approach explicitly propagates the variability from the structural response calculations and rockfall calculations into the compliance case for the TSPA-LA through the sampling process.

Damage from fault displacement occurs simultaneously with damage from vibratory ground motion. The sampled value of λ_j determines the number of damaged waste packages by type, based on the abstraction in Table 6-67 (Section 6.11.5). Simultaneous damage from fault displacement and vibratory ground motion is a reasonable approach for the seismic scenario class. A significant nearby earthquake simultaneously induces both ground motions and fault displacements. For the compliance case, all the known on-site faults and small generic (hypothetical) faults with a 2-meter cumulative offset (Sites 7a/8a in the PSHA) move simultaneously. The potential correlations for displacements on different faults were not considered during the expert elicitation for the PSHA, and little information is available to support development of correlations for dependent or independent displacement along the known faults.

6.12.2 Computational Algorithm

The potential for deformation and rupture/puncture of EBS components from multiple seismic events within a given realization of the TSPA model is described in the following computational steps that are aligned with the separate elements of the seismic damage abstractions. As used in this section, a realization of the TSPA model represents one of many future potential histories of the repository. Each realization has a unique value for each random variable that represents epistemic (knowledge) uncertainty, such as friction coefficients or the RST for initiation of potential SCC. Each realization also has a unique sequence of seismic events whose timing and intensity capture the aleatory uncertainty (i.e., the randomness) in the seismic process. Note that the notation for some parameters in the following equations has been modified for clarity in comparison to the notation in Tables 6-88 to 6-93.

Determine the RST for Alloy 22 for the *i*th realization.

The RST for Alloy 22 is a random variable that is sampled once per realization from a uniform distribution between 90 and 105 (DTN: MO0702PASTRESS.002 [DIRS 180514], Table 8-1 in the file *Model Output DTN.doc*). This random variable is sampled once per realization because it represents the epistemic uncertainty in the RST. The sampled value for the *i*th realization is denoted as RST_i.

Determine the time of the *j*th event in this realization.

Seismic events occur randomly in time (see Assumption 5.2, Section 5). The time of the *j*th event is determined by a random time interval (Poisson) event generator (GoldSim Technology Group 2003 [DIRS 166226], Chapter 9, under Simulating Discrete Events) using a Poisson frequency of (λ_{max} - λ_{min}). The values of λ_{min} and λ_{max} are tentatively set to 1×10^{-8} per year and 4.287×10^{-4} per year, respectively. The Poisson frequency is then given by (4.287×10^{-4} per year – 1×10^{-8} per year) = 4.287×10^{-4} per year.

Determine the annual exceedance frequency, λ_j, for the *j*th event in this realization.[8]

The value of λ_j is sampled from a uniform distribution between λ_{min} and λ_{max}.

Determine the corresponding value of the horizontal peak ground velocity, PGV_j, on the bounded hazard curve, $\lambda = \lambda(PGV)$, for the *j*th seismic event in this realization.

The value of PGV_j is determined by the mean bounded hazard curve for the horizontal component of peak ground velocity at the emplacement drifts. The points on the mean bounded hazard curve are defined in Table 6-74. Interpolation between points on the hazard curve is based on a piecewise linear interpolation with the values of log(λ) and log(PGV) at the individual points. This interpolation is equivalent to a power-law fit,

[8] The results from Steps 2 and 4 determine the answers to two questions: "When does an event occur?" and "What is the intensity of the seismic event?" The sampled value of λ_j in Step 3 is an intermediate step in determining the value of PGV_j on the bounded hazard curve. λ_j is not used directly in the damage abstractions for EBS components in response to vibratory ground motion or rockfall induced by vibratory ground motion; these damage abstractions are only a function of PGV_j and are therefore independent of λ_j and independent of the hazard curve.

$\lambda = a\,(PGV_j)^b$, where $b = (\log(\lambda_1/\lambda_2))/(\log(PGV_1/PGV_2))$ and $a = \lambda_1/(PGV_1)^b$. The resulting value of PGV_j is denoted simply as PGV in subsequent text and equations.

A general discussion of the basis for the site-specific ground motions and of the bounded hazard curve is presented in Section 6.4.

Table 6-74. Bounded Hazard Curve for Horizontal PGV at the Emplacement Drifts

λ (1/yr)	PGV (m/s)
4.287×10^{-4}	0.219[a]
1.000×10^{-4}	0.4019
3.826×10^{-5}	0.6
1.919×10^{-5}	0.8
9.955×10^{-6}	1.05
6.682×10^{-6}	1.2
3.812×10^{-6}	1.4
2.136×10^{-6}	1.6
1.288×10^{-6}	1.8
8.755×10^{-7}	2.0
6.399×10^{-7}	2.2
4.518×10^{-7}	2.44
3.504×10^{-7}	2.6
2.507×10^{-7}	2.8
1.731×10^{-7}	3.0
1.137×10^{-7}	3.2
7.168×10^{-8}	3.4
4.362×10^{-8}	3.6
2.508×10^{-8}	3.8
1.319×10^{-8}	4.0
5.967×10^{-9}	4.20

[a] The exceedance frequency corresponding to 0.219 m/s is extrapolated from the points (1.0×10^{-4} 1/yr, 0.4019 m/s) and (3.826×10^{-5} 1/yr, 0.6 m/s) on the bounded hazard curve. For a power-law fit of $\lambda = a(PGV)^b$ between points, the coefficients b and a are defined as $b = \log(1 \times 10^{-4}/3.826 \times 10^{-5})/\log(0.4019/0.6) = -2.398$ and $a = (1 \times 10^{-4})/(0.4019)^{-2.398} = 1.124 \times 10^{-5}$. The corresponding value of λ at 0.219 m/s is then $\lambda = a(PGV)^b = (1.124 \times 10^{-5})(0.219)^{-2.398} = 4.287 \times 10^{-4}$ 1/yr.

Sources: DTN: MO0501BPVELEMP.001 [DIRS 172682], worksheet "Bounded Horizontal PGV Hazard" in the file *Bounded Horizontal Peak Ground Velocity Hazard at the Repository Waste Emplacement Level.xls*. The exceedance frequency for the first point in this table is calculated in the footnote above.

NOTE: Horizontal PGV values have been converted from cm/s to m/s by dividing by 100.

Determine the volume of lithophysal rock that collapses due to the *j*th seismic event, $RV_{LITH,j}$, and calculate the fraction of drift filled with lithophysal rubble from the first through *j*th seismic events.

a. For each seismic event, first determine the probability of rockfall in the lithophysal zones. The probability of lithophysal rockfall is defined by Equation 6.7-1 in Section 6.7.1.1:

$$P_{rockfall} = MIN(1.0, MAX(0.0, (1.288)PGV - 0.353)) \quad \text{(Eq. 6.12-1)}$$

b. Sample a random number between 0 and 1. If the random number is less than or equal to $P_{rockfall}$, then $RV_{LITH,j}$ is calculated in Steps 5(c) and 5(d). If the random number is greater than $P_{rockfall}$, then $RV_{LITH,j}$ is set to zero, and Steps 5(c) and 5(d) can be skipped. This random number should be resampled for each event because the uncertainty in the probability of rockfall is primarily caused by the aleatory uncertainty in the 17 ground motions, rather than the epistemic uncertainties due to the fracture pattern in the lithophysal zones.

   This draw of a random number will be used in subsequent computational steps to determine the occurrence of nonzero rockfall, the occurrence of nonzero damaged areas, and the occurrence of drip shield failure (fragility). A more intense ground motion is likely to simultaneously cause nonzero rockfall, nonzero damage, and drip shield failure because the intensity of the ground motion for a given PGV level is the major driver of system response, as discussed in Step 7(c) and Step 8(c). The occurrence of nonzero rockfall, nonzero damage, and drip shield failure are then expected to be highly correlated, rather than independent random variables. The degree of correlation is difficult to quantify but is represented in TSPA as perfectly correlated, in the sense that the same random draw is used to determine the occurrence of nonzero rockfall, nonzero damage, and drip shield failure during a given event.

   This random number is not correlated with the conditional probability distributions for rockfall volume or the damaged areas. Once nonzero rockfall or nonzero damage occurs, the conditional probability distributions must be sampled independently of the common random number to properly represent the full range of nonzero response for the TSPA.

c. For each seismic event, the volume of lithophysal rock that collapses per meter of drift length is a random variable represented by a gamma distribution that is defined in Section 6.7.1.2. A gamma distribution is defined in terms of two parameters: the mean, μ, and the standard deviation, σ. The values of μ and σ are defined as functions of PGV:

$$PGV_{rf} = MAX(PGV, 0.4\,m/s) \quad \text{(Eq. 6.12-2)}$$

$$\mu = (20.307)\left(PGV_{rf}\right)^2 - (18.023)PGV_{rf} + 4.0102 \quad \text{(Eq. 6.12-3)}$$

and

$$\sigma = -(3.5613)\left(PGV_{rf}\right)^2 + (18.018)PGV_{rf} - 6.6202 \quad \text{(Eq. 6.12-4)}$$

   Equation 6.12-2 uses the values of μ and σ at the 0.4 m/s PGV level to provide an upper bound for all values of PGV less than 0.4 m/s. This approach is necessary because extrapolation of Equations 6.12-3 and 6.12-4 to PGV values below 0.4 m/s produces unrealistic behavior, such as a standard deviation that is less than 0, as explained in Section 6.7.1.2. Equations 6.12-3 and 6.12-4 are defined by the quadratic fits in Figure 6-56.

The volume of lithophysal rock that collapses per meter of drift length for the *j*th seismic event, $RV_{LITH,j}$, is determined by sampling the gamma distribution with the parameter values in Equations 6.12-3 and 6.12-4.

d. The total volume of lithophysal rock that collapses per meter of drift length after the *j*th seismic event, $TV_{LITH,j}$ is defined in Section 6.7.1.4 as the sum of the volumes for the first *j* seismic events:

$$TV_{LITH,j} = \sum_{k=1}^{j} RV_{LITH,k} \qquad \text{(Eq. 6.12-5)}$$

where $RV_{LITH,k}$ is the volume of lithophysal rockfall for the *k*th seismic event.

e. The volume of lithophysal rock that must collapse to fill the drift is defined in Section 6.7.1.5 as a uniform distribution between 30 m^3 per meter to 120 m^3/m of drift length. This parameter represents epistemic uncertainty and spatial variability within the lithophysal zones. It should be sampled once per realization.

f. The fraction of the drift that is filled after the *j*th seismic event is defined in Section 6.7.1.5 as the ratio of the total volume of collapsed lithophysal rock after the *j*th seismic event to the volume that is required to fill the drift:

$$FD_{LITH,j} = MAX\left(0.0001, MIN\left(\frac{TV_{LITH,j}}{V_{L,i}}, 1.0\right)\right) \qquad \text{(Eq. 6.12-6)}$$

where $V_{L,i}$ is the sampled value for the volume of intact lithophysal rock that must collapse to completely fill the drift in this realization. Equation 6.12-6 provides a minimum value for $FD_{LITH,j}$ of 0.0001 to maintain finite values in Equation 6.12-27 in Step 19(a). Equation 6.12-6 also has a maximum value for $FD_{LITH,j}$ of 1.

The value for $FD_{LITH,j}$ is applied to all lithophysal zones in the repository.

Determine the volume of nonlithophysal rockfall from the *j*th seismic event, $RV_{NL,j}$, and calculate the fraction of drift filled with nonlithophysal rubble from the first through *j*th seismic events.

a. The probability of rockfall in the nonlithophysal zones is set to be the same as the probability of rockfall in the lithophysal zones, Equation 6.7-1, as discussed in Section 6.7.2.2:

$$P_{rockfall} = MIN(1.0, MAX(0.0, (1.288)PGV - 0.353)) \qquad \text{(Eq. 6.12-7)}$$

b. If the random number sampled in Step 5(b) is less than or equal to $P_{rockfall}$ then $RV_{NL,j}$ is calculated in Steps 6(c) and 6(d). If the random number is greater than $P_{rockfall}$, then $RV_{NL,j}$ is set to zero and Steps 6(c) and 6(d) can be skipped.

c. For each seismic event, the volume of nonlithophysal rockfall that caves into the drift per meter of drift length is a random variable represented by a gamma distribution that is defined in Section 6.7.2.3. The values of μ and σ for this gamma distribution are defined as functions of *PGV*:

$$\mu = (-0.0142)(PGV)^2 + (0.2064)PGV + 0.0387 \quad \text{(Eq. 6.12-8)}$$

and $$\sigma = (-0.037)(PGV)^2 + (0.3057)PGV + 0.0696 \quad \text{(Eq. 6.12-9)}$$

The volume of nonlithophysal rock that collapses per meter of drift length for the *j*th seismic event, $RV_{NL,j}$, is determined by sampling the gamma distribution with the parameter values in Equations 6.12-8 and 6.12-9. Equations 6.12-8 and 6.12-9 are defined by the quadratic fits in Figure 6-62.

d. The total volume of nonlithophysal rockfall that caves per meter of drift length after the *j*th seismic event, $TV_{NL,j}$, is defined in Section 6.7.2.5 as the sum of the volumes for the first *j* seismic events:

$$TV_{NL,j} = \sum_{k=1}^{j} RV_{NL,k}, \quad \text{(Eq. 6.12-10)}$$

where $RV_{NL,k}$ is the volume of nonlithophysal rockfall for the *k*th seismic event.

e. The volume of nonlithophysal rockfall that must cave to fill the drift is defined in Section 6.7.1.5 as a uniform distribution between 30 m^3/m to 120 m^3/m of drift length. This parameter represents epistemic uncertainty and spatial variability within the nonlithophysal zones. It should be sampled once per realization.

f. The fraction of the drift that is filled after the *j*th seismic event is defined in Section 6.7.2.6 as the ratio of the total volume of collapsed nonlithophysal rock after the *j*th seismic event to the volume that is required to fill the drift:

$$FD_{NL,j} = MIN\left(\frac{TV_{NL,j}}{V_{NL,i}}, 1.0\right) \quad \text{(Eq. 6.12-11)}$$

where $V_{NL,i}$ is the sampled value for the volume of nonlithophysal rockfall that must collapse to fill the drift in this realization.

The value for $FD_{NL,j}$ is applied to all nonlithophysal zones in the repository.

Determine drip shield plate fragility in response to the peak vertical acceleration for the *j*th seismic event. The plate fragility is defined as the probability of rupturing the plate during a seismic event. Plate fragility is a function of *PGV*, of the thickness of the drip shield plate, and of the static load on the plates from rockfall, as discussed in Sections 6.8.1 and 6.8.2. The *PGV* level for the *j*th seismic event is determined in Step 4. The thickness of the drip shield plates is calculated by other components within the TSPA model, based on the time of the event, the top-side and bottom-side corrosion rates for Titanium Grade 7, and the initial plate thickness.

The static load is defined by the fraction of the drift that is filled with lithophysal rubble, based on the parameter $FD_{LITH,j}$ determined by Equation 6.12-6 in Step 5(f). The rockfall load in a drift that is partly filled with rubble is defined as the product of the fraction of drift filled with rubble and the rockfall load for a fully collapsed drift (see Section 6.7.1.5). This is a reasonable approach that tends to overestimate the vertical loads on the drip shield for small rubble volumes, as discussed in Section 6.7.1.5.

The static load from lithophysal rubble is expected to be much greater than the static load from nonlithophysal rockfall because the rockfall volume in the lithophysal units is much greater than that in the nonlithophysal units at a given PGV level (as discussed in Section 6.7.2.1). The plate fragility analysis is based on the static load from lithophysal rubble as an upper bound for the rockfall load and the resulting probability of failure is applied throughout the repository.

a. The plate fragility is defined by Table 6-75 for drifts that are 0%, 10%, 50%, and 100% filled with rubble. These rubble levels correspond to values of 0.0, 0.1, 0.5, and 1.0, respectively, for $FD_{LITH,j}$.

Table 6-75. Probability of Failure for the Drip Shield Plates

	Thickness of the Drip Shield Plate (mm):				
	0	**2**	**5**	**10**	**15**
***PGV* (m/s)**	**Probability of Failure for 0% Rockfall Load ($FD_{LITH,j}$ = 0.0):**				
All Values	**1**	**0**	**0**	**0**	**0**
***PGV* (m/s)**	**Probability of Failure for 10% Rockfall Load ($FD_{LITH,j}$ = 0.10):**				
0.2	1	0	0	0	0
0.4	1	0	0	0	0
1.05	1	0	0	0	0
2.44	1	0.006	0	0	0
4.07	1	0.036	0	0	0
***PGV* (m/s)**	**Probability of Failure for 50% Rockfall Load ($FD_{LITH,j}$ = 0.50):**				
0.2	1	0	0	0	0
0.4	1	0.005	0	0	0
1.05	1	0.083	0.002	0	0
2.44	1	0.377	0.047	0.004	0
4.07	1	0.637	0.182	0.028	0.007

Table 6-75. Probability of Failure for the Drip Shield Plates (Continued)

PGV (m/s)	Probability of Failure for 100% Rockfall Load ($FD_{LITH,j}$ = 1.0):				
0.2	1	0.027	0	0	0
0.4	1	0.093	0	0	0
1.05	1	0.390	0.030	0.001	0
2.44	1	0.765	0.268	0.047	0.013
4.07	1	0.912	0.557	0.186	0.073

Source: Output DTN: MO0703PASDSTAT.001, worksheet "Summary" in the file *Plate Fragility Analysis.xls.*

b. A piecewise linear interpolation defines the probability of plate rupture based on the value of *PGV* for the *j*th event, the current plate thickness, and $FD_{LITH,j}$. The first step in this interpolation is to linearly interpolate within each of the four "subtables" using the values of *PGV* for the *j*th event and of the plate thickness at the time of the *j*th event. This first interpolation produces four failure probabilities for drifts that are 0%, 10%, 50%, and 100% filled with rubble. A second piecewise linear interpolation determines the final probability of failure using the value of $FD_{LITH,j}$ for the *j*th event versus the failure probabilities at these four points.

c. If the random number drawn in Step 5(b) is less than or equal to the final probability of rupture then the plates fail. If the random number is greater than the final probability of rupture then the plates do not fail. The random number drawn in Step 5(b) is resampled for each event because the uncertainty in failure probability is primarily caused by the aleatory uncertainty in the peak ground acceleration from the 17 ground motions, rather than by the epistemic uncertainties due to rockfall load and mechanical boundary conditions on the plates. For example, the standard deviation in *ln* space, denoted as β, for the peak vertical acceleration conditional on the value of PGV is on the order of 0.7 (see Table 6-33), while the values of β for the rubble load and plastic load capacity are 0.149 (see Table 6-34) and less than or equal to 0.377 (see Table 6-35), respectively. These results demonstrate that the primary uncertainty is aleatory uncertainty from the peak vertical acceleration (conditional on the value of PGV), rather than the epistemic uncertainties from rubble load or plastic load capacity.

d. If the plates fail in this event, then:

   i. All drip shields fail as a barrier to seepage

   ii. There is no spatial variability for drip shield failure

   iii. The plates of the drip shield remain failed for the remainder of the realization

   iv. The failure of the drip shields as a barrier to seepage is a permanent change for the remainder of the realization

   v. The mechanical response of the waste package is determined from the abstractions in Steps 15 through 17 for a waste package surrounded by rubble.

e. If the plates do not fail, the drip shields do not fail as a barrier to seepage and the mechanical response of the codisposal and TAD-bearing waste packages is determined in Step 8 (as a function of the potential failure of the drip shield framework).

The fragility of the drip shield framework in response to the peak vertical acceleration is determined for the *j*th seismic event. The framework fragility is defined as the probability of collapsing the sides of the drip shield during a seismic event. Framework fragility is a function of *PGV*, of the thickness of the drip shield framework, and of the static load on the crown of the drip shield from rockfall, as discussed in Sections 6.8.1 and 6.8.3. The *PGV* level for the *j*th seismic event is determined in Step 4.

The thickness of the drip shield framework is calculated by other components within the TSPA model, based on the time of the event, the corrosion rate for Titanium Grade 29, and the initial thicknesses of the exterior bulkheads, interior bulkheads, and axial stiffeners that comprise the framework. The time dependent reduction in thickness of the framework components should be based on the exterior corrosion rate of Titanium Grade 29 with double sided corrosion. The external corrosion rate is appropriate because the predicted failure mode for the drip shield framework is collapse of the legs, and the supporting bulkheads on the sides of the drip shield are located on the exterior side of the drip shield plates. Double-sided corrosion is appropriate because the opposite surfaces of each bulkhead, perpendicular to the axis of the drip shield, are exposed to the in-drift environment and general corrosion. A similar approach can also be applied to the axial stiffeners, with double-sided corrosion on the opposite sides of the stiffener that are exposed to the environment underneath the drip shield plates.

The static load is defined by the fraction of the drift that is filled with lithophysal rubble, based on the parameter $FD_{LITH,j}$ determined by Equation 6.12-6 in Step 5(f). The rockfall load in a drift that is partly filled with rubble is defined as the product of the fraction of drift filled with rubble and the rockfall load for a fully collapsed drift. This is a reasonable approach that tends to overestimate the vertical loads on the drip shield for small rubble volumes, as explained in Section 6.7.1.5.

The static load from lithophysal rubble is expected to be much greater than the static load from nonlithophysal rockfall because the rockfall volume in the lithophysal units is much greater than that in the nonlithophysal units for a given PGV level (as discussed in Section 6.7.2.1). The framework fragility analysis is based on the static load from lithophysal rubble as an upper bound for the rockfall load and the resulting probability of failure is applied throughout the repository.

a. The framework fragility is defined by Table 6-76 for drifts that are 0%, 10%, 50%, and 100% filled with rubble. These rubble levels correspond to values of 0.0, 0.1, 0.5, and 1.0, respectively, for $FD_{LITH,j}$.

Table 6-76. Probability of Failure for the Drip Shield Framework

	Reduction in Thickness of Framework Components (mm):				
	15	**13**	**10**	**5**	**0**
***PGV* (m/s)**	**Probability of Failure for 0% Rockfall Load (FD_j = 0.0):**				
All Values	**1**	**0**	**0**	**0**	**0**
***PGV* (m/s)**	**Probability of Failure for 10% Rockfall Load (FD_j = 0.10):**				
0.2	1	0	0	0	0
0.4	1	0	0	0	0
1.05	1	0.007	0	0	0
2.44	1	0.107	0.001	0	0
4.07	1	0.311	0.011	0	0
***PGV* (m/s)**	**Probability of Failure for 50% Rockfall Load (FD_j = 0.50):**				
0.2	1	0.048	0	0	0
0.4	1	0.192	0	0	0
1.05	1	0.635	0.025	0	0
2.44	1	0.929	0.230	0.029	0.006
4.07	1	0.985	0.502	0.127	0.039
***PGV* (m/s)**	**Probability of Failure for 100% Rockfall Load (FD_j = 1.0):**				
0.2	1	0.716	0.001	0	0
0.4	1	0.867	0.016	0	0
1.05	1	0.981	0.210	0.018	0.003
2.44	1	0.999	0.649	0.191	0.063
4.07	1	1.000	0.867	0.449	0.219

Source: Output DTN: MO0703PASDSTAT.001, worksheet "Summary" in the file *Frame Fragility Analysis.xls*.

NOTE: Probabilities below 0.001 have been rounded down to 0.

b. A piecewise linear interpolation defines the probability of collapse based on the value of *PGV* for the *j*th event, the current plate thickness, and $FD_{LITH,j}$. The first step in this interpolation is to linearly interpolate within each of the four "subtables" using the values of *PGV* for the *j*th event and of the plate thickness at the time of the *j*th event. This first interpolation produces four failure probabilities for drifts that are 0%, 10%, 50%, and 100% filled with rubble. A second linear interpolation using the value of $FD_{LITH,j}$ for the *j*th event versus the failure probabilities at these four points determines the final probability of collapse.

c. Compare the random number in Step 5(b) to the final probability of collapse. It is appropriate to use the same random number because the dominant uncertainty in the fragility analysis is the aleatory (random) uncertainty in the correlation between PGV and the vertical component of peak ground acceleration, as can be seen by comparing the values of β in Tables 6-33 to 6-35. If the random number is less than or equal to the final probability of rupture, then the framework collapses. If the random number is greater than the final probability of collapse, then the framework remains intact. The framework always collapses before the plates rupture because

the same random number is used in Steps 7 and 8 and because the probability of framework collapse is always greater than the probability of plate rupture for given values of PGV and plate thickness.

d. If the framework does not collapse (in which case the plates do not rupture), determine the mechanical response of the codisposal and TAD-bearing waste packages in Steps 9 through 11 and Steps 12 through 14, respectively. The abstractions in Steps 9 through 14 are based on kinematic calculations with an intact drip shield.

e. If the framework collapses in this event and the plates remain intact, then:

   i. The drip shields do not fail as a barrier to seepage

   ii. There is no spatial variability for drip shield collapse

   iii. The framework remains collapsed for the remainder of the realization

   iv. The mechanical response of the waste package is a function of the state of the internals. If the internals are intact, the abstraction for a waste package surrounded by rubble (Steps 15 through 17) is used to determine damaged areas on the waste package. If the internals are degraded, the kinematic damage abstraction for degraded internals (Steps 9 through 14) is used to determine damaged areas on the waste package. The rationale for this approach is explained in Section 6.8.4.

f. If the plates have ruptured (in which case the framework has also collapsed), Step 7(d) is used to determine the seismic response of EBS components.

The rupture of a codisposal waste package that can move freely beneath the drip shield is conceptualized to occur from the accumulation of severe deformation due to multiple impacts. Multiple impacts to a codisposal waste package are considered as follows:

a. The codisposal waste package with intact internals and a 23-mm-thick OCB is not ruptured by multiple impacts.

b. For the codisposal waste package with degraded internals, the effect of multiple waste package-to-pallet impacts is assessed by evaluating the severity of accumulated deformation. The degree of deformation from waste package-to-pallet impacts during a single ground motion was used to define the probabilities of no rupture, incipient rupture, and immediate rupture. A minor degree of deformation indicates that no rupture occurs, consistent with the observation that the strain in the OCB is below the ultimate tensile strain for Alloy 22 for individual impacts. A significant degree of deformation is interpreted as causing a condition of incipient rupture, in the sense that a second severe impact has the potential to cause rupture. Finally, if two severe impacts occur during a given ground motion, each of which causes severe deformation to the OCB, then the accumulation of severe deformation is interpreted as causing rupture.

The accumulated deformation is tracked through a counter that is initialized to zero at the start of each realization, before any seismic events occur. A counter value of 1 indicates an incipient condition for rupture after a single severe impact. A counter value of 2 indicates that rupture has occurred, with advective flow through the ruptured area on the waste package.

The probability of incipient rupture and the probability of (immediate) rupture for the codisposal waste package with degraded internals are derived in Section 6.6.2.1, based on power law fits to the probabilities of incipient rupture and (immediate) rupture (output DTN: MO0703PASDSTAT.001, File *Rupture and Puncture Abstractions.xls*, worksheet "CDSP Kinematic Abstraction:"

$$PRinc\_CDSPd = \text{If } (PGV \geq 1.05 \text{ m/s}) \ (0.0158)(PGV - 1.05)^{1.8586}, \text{ else } 0.0 \quad \text{(Eq. 6.12-12)}$$

$$PRimmed\_CDSPd = \text{If } (PGV \geq 2.44 \text{ m/s}) \ (0.0474)(PGV - 2.44)^{1.8586}, \text{ else } 0.0 \quad \text{(Eq. 6.12-13)}$$

$$Pno\_rupture\_CDSPd = 1 - PRinc\_CDSPd - PRimmed\_CDSPd \quad \text{(Eq. 6.12-14)}$$

Equation 6.12-14 is based on the requirement that the sum of the probability of the three outcomes (no rupture, incipient rupture, and rupture) must be 1.

The counter is incremented by sampling a discrete distribution with (value, probability) pairs given by (0, Pno_rupture_CDSPd), (1, PRinc_CDSPd), and (2, PRimmed_CDSPd). If the sampled value is zero, then the codisposal package does not sustain significant damage and the counter does not change. If the sampled value is 1, then 1 is added to the counter. If the value of the counter becomes 2 from this addition, then the package is considered to be ruptured. If the value of the counter is 1 after this addition, then the package does not rupture but the counter is saved for subsequent events within the realization. If the sampled value is 2, then 2 is added to the counter and the package is considered to be ruptured.

c. When a waste package is ruptured, the failed area is determined by sampling a uniform distribution with a lower bound of 0 m^2 and an upper bound equal to the cross-sectional area of the waste package OCB. The cross-sectional area for the codisposal waste package is 3.28 m^2, based on an OCB outer diameter of 2,044.7 mm for the 5-DHLW/DOE SNF Long waste package (SNL 2007 [DIRS 179567], Table 4-9). This failed area allows advective flow through the ruptured codisposal waste packages and advective and diffusive transport out of the ruptured codisposal waste packages. This failed area is conceptualized to be a tear or rupture along a crease that lies in a plane normal to the central axis of the waste package. The failed area can be represented as a circumferential band around the waste package for transport calculations in the TSPA. Once the codisposal waste package ruptures, there is no further rupture damage on successive events and the codisposal waste packages remain ruptured for the remainder of the realization.

Determine the probability of damage for a codisposal waste package that can move freely beneath a drip shield. The probability of damage for the *j*th seismic event, $PD_{CDSP,j}$, is defined in Sections 6.6.1.2 and 6.6.2.2 as a function of the state of the internals (intact or degraded)[9], of the value of *PGV* for the *j*th seismic event, of the value of *RST* for the *i*th realization, and of the OCB thickness at the time of the *j*th seismic event.

a. The probability of damage is defined by Table 6-77:

Table 6-77. Probability of Damage for the Codisposal Waste Package

	Residual Stress Threshold (%):		
	90	**100**	**105**
***PGV* (m/s)**	**Probability of Damage for 23-mm-Thick OCB with Intact Internals:**		
0.364	0	0	0
0.4	0.029	0	0
1.05	0.559	0	0
2.44	0.941	0.147	0
4.07	1	0.412	0
***PGV* (m/s)**	**Probability of Damage for 23-mm-Thick OCB with Degraded Internals:**		
0.285	0	0	0
0.364	0.060	0.060	0
0.4	0.088	0.088	0.029
1.05	0.588	0.588	0.559
2.44	0.941	0.941	0.941
4.07	1	1	1
***PGV* (m/s)**	**Probability of Damage for 17-mm-Thick OCB with Degraded Internals:**		
0.219	0	0	0
0.338	0.097	0	0
0.346	0.103	0.007	0
0.4	0.147	0.059	0.029

[9] Waste package internals are assumed to degrade as structural elements after the OCB is first damaged by a seismic event (see Assumption 5.4, Section 5).

Table 6-77. Probability of Damage for the Codisposal Waste Package (Continued)

PGV (m/s)	Probability of Damage for 17-mm-Thick OCB with Degraded Internals (Continued):		
1.05	0.676	0.676	0.382
2.44	0.941	0.941	0.882
4.07	1	1	1

Source: Output DTN: MO0703PASDSTAT.001, worksheet "Prob of Damage – New" in each of the files *CDSP Kinematic Damage Abstraction 23-mm Intact.xls*, *CDSP Kinematic Damage Abstraction 23-mm Degraded.xls*, and *CDSP Kinematic Damage Abstraction 17-mm Degraded.xls*.

NOTES: Probabilities below 0.001 have been rounded down to 0.

The probability of damage at the 0.4 m/s PGV level and 105% RST level for the 17-mm-thick OCB with degraded internals was revised after these data were defined in the TSPA database. This table presents the corrected values. The probability at 0.4 m/s PGV level and 105% RST for the 17-mm-thick OCB with degraded internals changed from 0 in the TSPA database to 0.029. This value moves the PGV-intercept for zero probability at 105% RST from 0.40 m/s to 0.346 m/s, adding an additional row that is very similar to the existing row at 0.338 m/s in the TSPA database. This minor change to the probability of damage will not produce significant changes in the expected damaged areas (i.e., the product of the probability of damage and the mean conditional damaged area) on codisposal waste packages for TSPA.

b. A piecewise linear interpolation defines the probability of damage based on the value of *PGV* for the *j*th event, the current OCB thickness, and the value of RST_i. The first step in this interpolation is to linearly interpolate within each subtable of Table 6-77 using the values of *PGV* for the *j*th event and of RST_i for the *i*th realization. This first step produces three probabilities of damage, one of which applies to intact internals and two of which apply to degraded internals. If the internals are intact, the single value defines the probability of damage for the codisposal waste package. If the internals are degraded, the probability of damage corresponding to the average OCB thickness at the time of the *j*th seismic event is calculated by linear interpolation if the OCB thickness is between 17 mm and 23 mm. The probability of damage is set to the value at 23 mm if the average OCB thickness is greater than 23 mm. The probability is set to the value at 17 mm if the average OCB thickness is less than 17 mm:

$$PD_{CDSP,j} = \text{If } t \geq 23\text{-mm}, PD_{CDSP,j,23\text{-}mm} \quad \text{(Eq. 6.12-15)}$$

$$\text{Or if t} \leq 17 \text{ mm}, PD_{CDSP,j,17\text{-}mm}$$

$$\text{else}, PD_{CDSP,j,17\text{-}mm} + (PD_{CDSP,j,23\text{-}mm} - PD_{CDSP,j,17\text{-}mm})(t - 17\text{-mm})/(6\text{-mm})$$

where t is the spatially averaged thickness (in mm) of the OCB at the time of the *j*th event and $PD_{CDSP,j,17\text{-}mm}$ and $PD_{CDSP,j,23\text{-}mm}$ are the two probabilities for degraded internals from Table 6-77. The rationale for this approach is explained in Section 6.5.2.2 and Equation 6.5-1.

c. Compare the random number sampled in Step 5(b) to the value of $PD_{CDSP,j}$ computed in Equation 6.12-15 for degraded internals or to the single value of $PD_{CDSP,j}$ for intact internals. If the random number is less than or equal to $PD_{CDSP,j}$ then:

i. All codisposal waste packages are damaged by this seismic event

ii. The damaged area is computed in Step 11

iii. The internals of the codisposal waste packages are degraded for all subsequent seismic events.

If the random number is greater than $PD_{CDSP,j}$, then the damaged area can be set to zero for the *j*th seismic event and it is not necessary to complete Step 11.

If the codisposal waste packages are damaged by the *j*th seismic event (see Step 10), then damaged area (in units of m^2) is defined by gamma distributions whose parameters are functions of *PGV* and *RST*. Separate gamma distributions are defined for three states of the codisposal waste package: (1) 23-mm thick OCB with intact internals, (2) 23-mm thick OCB with degraded internals, and (3) 17-mm thick OCB with degraded internals. There are a total of three gamma distributions. The equations for the parameters μ and σ for these distributions are listed in Table 6-78 where μ is the mean and σ is the standard deviation. The values of μ and σ for the 23-mm-thick OCB with intact internals is discussed in Section 6.6.1.3. The values of μ and σ for the 17-mm-thick OCB with degraded internals are defined by Equations 6.6-2 and 6.6-3 in Section 6.6.2.3. The sources identified for Table 6-78 document all the analyses for μ and σ.

Table 6-78. Gamma Distribution Parameters for the Conditional Damaged Areas on the Codisposal Waste Package

OCB Thick. (mm)	State of Internals	Parameter μ	Parameter σ
23	Intact	If (RST ≤ 100) − (0.0033)*(RST_i − 100)PGV^2 − (0.00567)*(RST_i – 100)*PGV* − (0.0004)* (RST_i – 100) + (0.0061) Else (-0.0012)(RST-105)	If (RST ≤ 100) + (0.0001)*(RST_i - 100)PGV^2 – (0.0138)*(RST_i – 100)PGV + (0.0013)*(RST_i – 100) + (0.0041) Else (-0.0008)(RST-105)
23	Degraded	(0.0637 – 0.0016*(RST_i – 100))PGV^2 + (0.2274 – 0.0277*(RST_i – 100))*PGV* + (–0.0144 + 0.0029*(RST_i – 100))	(–0.0383 + 0.0059*(RST_i – 100))PGV^2 + (0.4623 – 0.0420*(RST_i – 100))PGV + (–0.0601 + 0.0034*(RST_i – 100))

17	Degraded	(0.0670 – 0.0011*(RST_i – 100))PGV^2 +
		(0.1879 – 0.0376*(RST_i – 100))*PGV* +
		(–0.0187 + 0.0034*(RST_i – 100))
			If ((PGV > 0.4 m/s) OR (RST < 102))
			(–0.0266 + 0.0078*(RST_i – 100))PGV^2 +
			(0.4066 – 0.0490*(RST_i – 100))PGV +
			(–0.0605 + 0.0011*(RST_i – 100))
			Else
			Set *PGV* to 0.4 m/s and use above equation

Source: Output DTN: MO0703PASDSTAT.001, worksheet "Dependence on RST" in each of the files *CDSP Kinematic Damage Abstraction 23-mm Intact.xls*, *CDSP Kinematic Damage Abstraction 23-mm Degraded.xls*, and *CDSP Kinematic Damage Abstraction 17-mm Degraded.xls*.

NOTE: Minor errors in the coefficients for σ with the 23-mm-thick OCB and intact internals were discovered after this parameter had been defined in the TSPA database. This table presents the correct values while the TSPA database has 0.0048 in place of 0.0041, 0.0014 in place of 0.0013, and -0.0010 in place of -0.0008. These errors produce insignificant changes in Figure 6-35 and have no impact on the TSPA.

Calculation of the damaged area (m^2) for the *j*th seismic event involves a two-step process: (1) sampling the distributions for damaged area, and (2) interpolation for the spatially averaged thickness of the OCB (determined by other elements of the TSPA). The two-step process for a codisposal waste package with degraded internals is as follows:

a. There are four parameters that define the damaged area on the codisposal waste package with degraded internals: two values for μ and two values for σ. Each of these parameters is a function of the *PGV* value for the *j*th event and of the RST for the *i*th realization. These parameters define two gamma distributions that can be sampled for the damaged areas at 17-mm- and 23-mm-thick OCBs. The sampled values from the two distributions should be fully correlated to provide a consistent basis for interpolation to the specific value of the OCB thickness at the time of the seismic event. The two distributions should be resampled for each event. This sampling should be independent of the sampling for damaged areas on the TAD-bearing waste packages under intact drip shields (in Step 14b). This sampling can also be independent of the sampling for damaged areas on a waste package surrounded by rubble (in Step 17a), although the intact drip shield and the waste package surrounded by rubble never coexist at the same time.

b. Other elements of the TSPA determine the spatially averaged OCB thickness at the time of the *j*th seismic event. The damaged area corresponding to this average OCB thickness is calculated by linear interpolation if the OCB thickness is between 17 mm and 23 mm. The damaged area is set to the value at 23 mm if the average OCB thickness is greater than 23 mm.[10] The damaged area is set to the value at 17 mm if the average OCB thickness is less than 17 mm. The abstraction for the 17-mm-thick OCB is anticipated to provide a reasonable lower bound to damaged area until the drip shield fails, after which the kinematic response is not applicable. The logic for the dependence of damaged area on OCB thickness is illustrated in Equation 6.12-16:

$$DA_{CDSP\_Degraded} = \text{If } t \geq 23 \text{ mm, } DA_{CDSP\_Degraded,23\text{-}mm} \quad \text{(Eq. 6.12-16)}$$

$$\text{Or if } t \leq 17 \text{ mm, } DA_{CDSP\_Degraded,17\text{-}mm}$$

$$\text{else, } DA_{CDSP\_Degraded,17\text{-}mm} + (DA_{CDSP\_Degraded,23\text{-}mm} - DA_{CDSP\_Degraded,17\text{-}mm})*(t - 17 \text{ mm})/(6 \text{ mm})$$

where *t* is the spatially averaged thickness of the OCB (in mm) at the time of the *j*th event, $DA_{CDSP\_Degraded}$ is the final damaged area at the current average OCB thickness, $DA_{CDSP\_Degraded,17\text{-}mm}$ is the value of the conditional damaged area from the 17 mm damage abstraction, and $DA_{CDSP\_Degraded,23\text{-}mm}$ is the value of the conditional damaged area from the 23-mm damage abstraction. The rationale for this approach is explained further in Section 6.5.2.5 and Equation 6.5-4.

[10] The initial OCB thickness of the codisposal waste package is 25.4 mm. The damaged area for the 23-mm-thick OCB provides an upper bound for damaged area at OCB thicknesses between 23 mm and 25.4 mm.

c. There is no spatial variability for the damaged area (i.e., it is applied to all codisposal waste packages) because the average thickness of the codisposal waste package OCB is expected to be constant within each percolation subregion. Damaged area is randomly located on the cylindrical surface of the OCB. The cylindrical surface area of the OCB for the codisposal waste package is 33.05 m^2 (see Section 6.6.4).

d. A similar approach is applied for a waste package with intact internals. In this case, there are two parameters that define the distribution of conditional damaged area on the waste package (see Table 2-5). Step 11(b) is not applicable because there is a single distribution for a single OCB thickness of 23 mm.[11] There is no spatial variability for the damaged area with intact internals, because the average thickness of the waste package OCB is expected to be constant within each percolation subregion for a given package type. Damaged area is randomly located on the cylindrical surface of the OCB.

e. The damaged area (m^2) increases with each seismic event that causes damage to the OCB. Total damaged area (m^2) for the codisposal waste packages is the sum of the damaged areas on the codisposal waste packages for the first through *j*th seismic events. Damaged area cannot exceed the total surface area of a codisposal waste package.

   The effective transport area for the waste package is much smaller than the damaged area because advection and diffusion occurs through a network of stress corrosion cracks, rather than through the total damaged area that exceeds the RST. The effective area for flow and transport is based on the crack density model and associated scaling factor for Alloy 22 defined in *Stress Corrosion Cracking of Waste Package Outer Barrier and Drip Shield Materials* (SNL 2007 [DIRS 181953], Section 6.7.3). The scaling factor for Alloy 22 should be sampled once per realization because it represents epistemic rather than aleatory uncertainty. Further details of the crack-density model and scaling factor are beyond the scope of this report.

The rupture of a TAD-bearing waste package that can move freely beneath the drip shield is conceptualized to occur from the accumulation of severe deformation due to multiple impacts. Multiple impacts to a TAD-bearing waste package are considered as follows:

a. The TAD-bearing waste package with 23-mm-thick OCB and intact internals is not ruptured by multiple impacts.

b. For the TAD-bearing waste package with degraded internals, the effect of multiple waste package-to-pallet impacts is assessed by evaluating the severity of accumulated deformation. The degree of deformation from waste package-to-pallet

[11] A single thickness, 23 mm, is used for determining the damaged area for a codisposal waste package with intact internals. The abstraction for the 23-mm-thick OCB is anticipated to provide a reasonable approximation to damaged area until the OCB is damaged or until the drip shield fails, after which the kinematic response with intact internals is not applicable. This expectation must be confirmed by the TSPA results for the license application.

impacts during a single ground motion was used to define the probabilities of no rupture, incipient rupture, and immediate rupture. A minor degree of deformation indicates that no rupture occurs, consistent with the observation that the strain in the OCB is below the ultimate tensile strain for Alloy 22 for individual impacts. A significant degree of deformation is interpreted as causing a condition of incipient rupture, in the sense that a second severe impact has the potential to cause rupture. Finally, if two severe impacts occur during a given ground motion, each of which causes severe deformation to the OCB, then the accumulation of severe deformation is interpreted as causing rupture.

The accumulated deformation is tracked through a counter that is initialized to zero at the start of each realization, before any seismic events occur. A counter value of 1 indicates an incipient condition for rupture after a single severe impact. A counter value of 2 indicates that rupture has occurred, with advective flow through the ruptured area on the waste package.

The probability of incipient rupture and the probability of (immediate) rupture for the TAD-bearing waste package with degraded internals are derived in Section 6.5.2.1, based on power-law fits to the probabilities of incipient rupture and rupture (output DTN: MO0703PASDSTAT.001, File *Rupture and Puncture Abstractions.xls*, worksheet "TAD Kinematic Abstraction"):

$$\text{PRinc\_TADd} = \text{If (PGV} \geq 0.40 \text{ m/s)} \ (0.0120)(\text{PGV}-0.40)^{1.7449}\text{, else } 0.0 \qquad \text{(Eq. 6.12-17)}$$

$$\text{PRimmed\_TADd} = \text{If (PGV} \geq 2.44 \text{ m/s)} \ (0.0772)(\text{PGV}-2.44)^{1.7449}\text{, else } 0.0 \qquad \text{(Eq. 6.12-18)}$$

$$\text{Pno\_rupture\_TADd} = 1 - \text{PRinc\_TADd} - \text{PRimmed\_TADd} \qquad \text{(Eq. 6.12-19)}$$

Equation 6.12-18 is based on the requirement that the sum of the probability of the three outcomes (no rupture, incipient rupture, and rupture) must be 1.

The counter is incremented by sampling a discrete distribution with (value, probability) pairs given by (0, Pno_rupture_TADd), (1, PRinc_TADd), and (2, PRimmed_TADd). If the sampled value is zero, then the TAD-bearing waste package does not sustain significant damage and the counter does not change. If the sampled value is 1, then 1 is added to the counter. If the value of the counter becomes 2 from this addition, then the package is considered to be ruptured. If the value of the counter is 1 after this addition, then the package does not rupture but the counter is saved for subsequent events within the realization. If the sampled value is 2, then 2 is added to the counter and the package is considered to be ruptured.

c. When a waste package is ruptured, the failed area is determined by sampling a uniform distribution with a lower bound of 0 m^2 and an upper bound equal to the cross-sectional area of the waste package OCB. The cross-sectional area for the TAD-bearing waste package is 2.78 m^2, based on an OCB outer diameter of 1881.6 mm for the TAD-bearing waste package (SNL 2007 [DIRS 179394], Table 4-3). This failed area allows advective flow through the ruptured TAD-bearing waste packages and advective and diffusive transport out of the ruptured TAD-bearing waste packages. The failed area is conceptualized to be a tear or rupture along a crease that lies in a plane normal to the central axis of the waste package. The failed area can be represented as a circumferential band around the waste package for transport calculations in the TSPA. Once the TAD-bearing waste package ruptures, there is no further rupture damage on successive events and the TAD-bearing waste packages remain ruptured for the remainder of the realization.

The probability of damage is determined for a TAD-bearing waste package that can move freely beneath a drip shield. The probability of damage for the *j*th seismic event, $PD_{TAD,j}$, is defined in Sections 6.5.1.2 and 6.5.2.2 as a function of the state of the internals (intact or degraded)[12], of the value of *PGV* for the *j*th seismic event, of the value of *RST* for the *i*th realization, and of the OCB thickness.

a. The probability of damage is defined by Table 6-79.

Table 6-79. Probability of Damage for the TAD-Bearing Waste Package

	Residual Stress Threshold (%):		
***PGV* (m/s)**	**90**	**100**	**105**
	Probability of Damage for 23-mm-Thick OCB with Intact Internals:		
0.2	0	0	0
0.4	0	0	0
1.05	0	0	0
2.44	0	0	0
4.07	0.118	0	0
Probability of Damage for 23-mm-Thick OCB with Degraded Internals:			
0.266	0	0	0
0.349	0.085	0	0
0.4	0.137	0.059	0
1.05	0.804	0.804	0.784
2.44	1	1	1
4.07	1	1	1
Probability of Damage for 17-mm-Thick OCB with Degraded Internals:			
0.280	0	0	0
0.351	0.081	0	0
0.4	0.137	0.059	0

[12] Waste package internals are assumed to degrade as structural elements after the OCB is first damaged by a seismic event (see Assumption 5.4, Section 5).

Table 6-79. Probability of Damage for the TAD-Bearing Waste Package (Continued)

PGV (m/s)	Residual Stress Threshold (%): 90	100	105
Probability of Damage for 17-mm-Thick OCB with Degraded Internals (Continued):			
1.05	0.882	0.843	0.804
2.44	1	1	1
4.07	1	1	1

Source: Output DTN: MO0703PASDSTAT.001, worksheet "Probability of Damage" in file *Kinematic Damage Abstraction 23-mm Intact.xls*, and worksheet "Prob of Damage – New" in each of the files *Kinematic Damage Abstraction 23-mm Degraded.xls*, and *Kinematic Damage Abstraction 17-mm Degraded.xls*.

b. A piecewise linear interpolation defines the probability of damage based on the value of *PGV* for the *j*th event, the current plate thickness, and the value of RST_i. The first step in this interpolation is to linearly interpolate within Table 6-79 using the values of *PGV* for the *j*th event and of RST_i for the *i*th realization. This first step produces two probabilities of damage, one for the 23-mm-thick OCB and a second for the 17-mm-thick OCB. The probability of damage corresponding to the spatially averaged OCB thickness at the time of the *j*th seismic event is calculated by linear interpolation if the OCB thickness is between 17 mm and 23 mm. The probability of damage is set to the value at 23 mm if the average OCB thickness is greater than 23 mm. The probability is set to the value at 17 mm if the average OCB thickness is less than 17 mm. The abstraction for the 17-mm-thick OCB is anticipated to provide a reasonable lower bound to the damaged area until the drip shield fails, after which the kinematic response is not applicable. This calculation is illustrated in Equation 6.12-20:

$$PD_{TAD,j} = \text{If } t \geq 23 \text{ mm}, PD_{TAD,j,23\text{-}mm} \quad \text{(Eq. 6.12-20)}$$

$$\text{Or if } t \leq 17 \text{ mm}, PD_{TAD,j,17\text{-}mm}$$

$$\text{else}, PD_{TAD,j,17\text{-}mm} + (PD_{TAD,j,23\text{-}mm} - PD_{TAD,j,17\text{-}mm})*(t - 17 \text{ mm})/(6 \text{ mm})$$

where *t* is the spatially averaged thickness (in mm) of the OCB at the time of the *j*th event and $PD_{TAD,j,17\text{-}mm}$ and $PD_{TAD,j,23\text{-}mm}$ are the probabilities of damage for the 17-mm-thick and 23-mm-thick OCBs, respectively, at the values of *PGV* for the *j*th seismic event and *RST* for a given realization. The rationale for this approach is explained in Section 6.5.2.2 and Equation 6.5-1.

c. Compare the random number sampled in Step 5(b) to the value of $PD_{TAD,j}$ computed in Equation 6.12-20 for degraded internals or to the single value of $PD_{TAD,j}$ for intact internals. If the random number from Step 5(b) is less than or equal to $PD_{TAD,j}$ then:

   i. All TAD-bearing waste packages are damaged by this seismic event

   ii. The damaged area is computed in Step 14

iii. The internals of the TAD-bearing waste packages are degraded for all subsequent seismic events.

If the random number is greater than $PD_{TAD,j}$ then the damaged area can be set to zero for the *j*th seismic event and it is not necessary to complete Step 14.

If the TAD-bearing waste packages are damaged by the *j*th seismic event (see Step 13), then the conditional damaged area (in units of m^2) is represented by gamma distributions that are defined in Sections 6.5.1.3 and 6.5.2.3. Separate gamma distributions are defined for three states of the TAD-bearing waste package: (1) 23-mm-thick OCB with intact internals, (2) 23-mm-thick OCB with degraded internals, and (3) 17-mm-thick OCB with degraded internals. There are a total of three gamma distributions. The equations for the parameters μ and σ for these distributions are listed in the Table 6-80, where μ is the mean and σ is the standard deviation. The values of μ and σ for the 23-mm-thick OCB with intact internals is discussed in Section 6.5.1.3. The values of μ and σ for the 17-mm-thick OCB with degraded internals is defined by Equations 6.5-2 and 6.5-3 in Section 6.5.2.3. The source identified for Table 6-80 documents all the analyses for μ and σ.

Table 6-80. Gamma Distribution Parameters for the Conditional Damaged Areas on the TAD-Bearing Waste Package

OCB Thick. (mm)	State of Internals	Parameter μ	Parameter σ
23	Intact	0.00408 m^2	0.00130 m^2
23	Degraded	$(0.1096 - 0.00664*(RST_i - 100))PGV^2 + (0.1722 - 0.01701*(RST_i - 100))PGV + 0.0828 - 0.00661*(RST_i - 100)$	$(0.0105 - 0.00098*(RST_i - 100))PGV^2 + (0.2310 - 0.01373*(RST_i - 100))PGV + 0.0829 - 0.01319*(RST_i - 100)$
17	Degraded	$(0.1394 - 0.00838*(RST_i - 100))PGV^2 + (0.1649 - 0.02224*(RST_i - 100))PGV + 0.0766 - 0.00628*(RST_i - 100)$	$(0.0902 - 0.00828*(RST_i - 100))PGV^2 + (0.0170 + 0.00665*(RST_i - 100))PGV + 0.1932 - 0.02851*(RST_i - 100)$

Source: Output DTN: MO0703PASDSTAT.001, worksheet "Dependence on RST" in each of the files *Kinematic Damage Abstraction 23-mm Degraded.xls* and *Kinematic Damage Abstraction 17-mm Degraded.xls,* and worksheet "ACM for 90%_i23" for the file *Kinematic Damage Abstraction 23-mm Intact.xls*.

a. The conditional damaged area (m^2) with intact internals is calculated by sampling a single gamma distribution[13] with mean and standard deviation of 0.00408 m^2 and 0.00130 m^2, respectively, at all values of *PGV* and of RST_i. This approach provides an upper bound for damage because the parameters for the gamma distribution are based on computational results at *PGV* = 4.07 m/s and *RST* = 90%, which will have the maximum damaged area. In spite of using an upper bound, damage will still be zero at most values of *PGV* and *RST* because the damage is conditional on the probability of damage, and this probability is 0 except for a single point in the first five lines of Table 6-79 in Step 13(a). Figure 6-10, which is a plot of the expected

[13] The initial OCB thickness of the TAD-bearing waste package is 25.4 mm. The damaged area for the 23-mm-thick OCB conservatively bounds the damaged area for OCB thicknesses between 23 mm and 25.4 mm. The abstraction for the 23-mm-thick OCB is anticipated to provide a reasonable approximation to damaged area until the OCB is damaged or until the drip shield fails, after which the kinematic response with intact internals is not applicable. This expectation must be confirmed by the TSPA calculations for the license application.

damaged area, confirms this statement. The expected damaged area is defined as the product of the probability of damage and the conditional (nonzero) damaged area.

b. Calculation of conditional damaged area (m^2) with degraded internals is a two step process: (1) sampling the distributions for damaged area (described in step 14(b)), and (2) interpolation for the average thickness of the OCB (determined by other elements of the TSPA) (described in step 14(c)). Four parameters define the damaged area on the TAD-bearing waste package with degraded internals: two values for μ and two values for σ. Each of these parameters is a function of the *PGV* value for the *j*th event and of the RST for the *i*th realization. These parameters define two gamma distributions that can be sampled for the conditional damaged areas for 17-mm-thick and 23-mm-thick OCBs. The sampled values from the two distributions should be fully correlated to provide a consistent basis for interpolation to the specific value of the OCB thickness at the time of the seismic event. The two gamma distributions should be resampled for each event because the aleatory uncertainty from the ground motions is a major contributor to the uncertainty in the gamma distributions.

c. Other elements of the TSPA determine the spatially averaged OCB thickness at the time of the *j*th seismic event for the degraded case. The conditional damaged area corresponding to this average OCB thickness is calculated by linear interpolation if the OCB thickness is between 17 mm and 23 mm. The damaged area is set to the value at 23-mm if the average OCB thickness is greater than 23 mm[14]. The damaged area is set to the value at 17 mm if the average OCB thickness is less than 17 mm. The abstraction for the 17-mm-thick OCB is anticipated to provide a reasonable lower bound to damaged area until the drip shield fails, after which the kinematic response is not applicable. The logic for the dependence on damaged area on OCB thickness is illustrated in Equation 6.12-21:

$$DA_{TAD\_Degraded} = \text{If } t \geq 23 \text{ mm}, DA_{TAD\_Degraded,23\text{-}mm} \quad \text{(Eq. 6.12-21)}$$

$$\text{Or if } t \leq 17 \text{ mm}, DA_{TAD\_Degraded,17\text{-}mm}$$

$$\text{else, } DA_{TAD\_Degraded,17\text{-}mm} + (DA_{TAD\_Degraded,23\text{-}mm} - DA_{TAD\_Degraded,17\text{-}mm})*(t - 17 \text{ mm})/(6 \text{ mm})$$

where $DA_{TAD\_Degraded}$ is the final damaged area at the current average OCB thickness, $DA_{TAD\_Degraded,17\text{-}mm}$ is the value of the conditional damaged area for the 17-mm damage abstraction, and $DA_{TAD\_Degraded,23\text{-}mm}$ is the value of the conditional damaged area from the 23-mm damage abstraction. These two latter values are calculated in Step 14(b). The rationale for this approach is explained in Section 6.5.2.5 and Equation 6.5-4.

[14] The initial OCB thickness for the TAD-bearing waste package is 25.4 mm. The damaged area for the 23-mm-thick OCB conservatively bounds the damaged area for OCB thicknesses between 23 mm and 25.4 mm.

d. For intact or degraded internals, there is no spatial variability for the conditional damaged area (i.e., it is applied to all TAD-bearing waste packages), because the average thickness of the TAD-bearing waste package OCB is expected to be constant within each percolation subregion. Damaged area is randomly located on the cylindrical surface of the OCB. The surface area of the OCB for the TAD-bearing waste package is 33.64 m^2 (see Section 6.5.4).

e. The total damaged area (m^2) increases with each seismic event that causes damage to the OCB. Total damaged area (m^2) for the TAD-bearing waste packages is the sum of the damaged areas to the TAD-bearing waste packages for the first through *j*th seismic events. Damaged area cannot exceed the total surface area of a TAD-bearing waste package.

   The effective flow and transport area for the waste package is much smaller than the damaged area because diffusion and advection occurs through a network of stress corrosion cracks, rather than through the total damaged area that exceeds the RST. The effective area for flow and transport is based on the crack-density model and associated scaling factor for Alloy 22 defined in *Stress Corrosion Cracking of Waste Package Outer Barrier and Drip Shield Materials* (SNL 2007 [DIRS 181953], Section 6.7.3). The scaling factor for Alloy 22 should be sampled once per realization because it represents epistemic, rather than aleatory uncertainty.

The probability of rupture for a waste package surrounded by rubble[15] is conceptualized to occur from puncture by sharp internal fragments when there is severe deformation of the OCB. The probability of puncture for the 23-mm-thick and 17-mm-thick OCBs are derived in Section 6.9.1, based on power law fits to the probability of puncture as a power law function of *PGV* from Step 4 (output DTN: MO0703PASDSTAT.001, File *Rupture and Puncture Abstractions.xls*, worksheet "TAD Rubble Abstraction"):

$$PP\_23 = \text{If } (PGV \geq 1.05 \text{ m/s}) \ (0.0028)(PGV - 1.05)^{2.9007}, \text{ else } 0.0 \quad \text{(Eq. 6.12-22)}$$

$$PP\_17 = \text{If } (PGV \geq 0.40 \text{ m/s}) \ (0.0210)(PGV - 0.40)^{1.6971}, \text{ else } 0.0 \quad \text{(Eq. 6.12-23)}$$

a. Other elements of the TSPA determine the spatially averaged OCB thickness at the time of the *j*th seismic event. The probability of puncture corresponding to the average OCB thickness is calculated by linear interpolation if the OCB thickness is between 17 mm and 23 mm. The probability is set to the value at 23 mm if the average OCB thickness is greater than 23 mm. The probability is set to the value at 17 mm if the average OCB thickness is less than 17 mm. This calculation is defined in Equation 6.12-24:

[15] The damage abstractions for a waste package surrounded by rubble (i.e., after the drip shield plates have failed in Step 7) are based on the damaged areas for the TAD-bearing waste package with degraded internals. The damage abstractions for the TAD-bearing waste package are applicable to the codisposal waste package because the two-dimensional computation models for either package with degraded internals are very similar. Each computational model has a cylindrical shell representing the OCB and a mass of granular material that represents the degraded internals, so the computational models are very similar for either package type. The damaged areas for intact internals are not represented by separate damage abstractions. Rather, the response with degraded internals is used to conservatively bound the response for intact internals.

$$PP = \text{If } t \geq 23 \text{ mm}, PP\_23 \quad \text{(Eq. 6.12-24)}$$

$$\text{Or if } t \leq 17 \text{ mm}, PP\_17$$

$$\text{Else } PP\_17 + (PP\_23 - PP\_17)*(t - 17 \text{ mm})/(6 \text{ mm})$$

where t is the spatially averaged OCB thickness (in mm) at the time of the seismic event, and *PP_23* and *PP_17* are the probabilities of puncture for the 23-mm-thick and 17-mm-thick OCBs, respectively. The rationale for this approach is explained in Section 6.9.1 and Equation 6.9-1.

b. Compare an independently sampled random number with the value of *PP* from Equation 6.12-24. This random number should be sampled independently from the random numbers in Steps 9(b) and 12(b) because of limited correlation between the realizations that cause puncture and those that cause incipient rupture and (immediate) rupture for the TAD-bearing and codisposal waste packages. If the random number is less than or equal to *PP*, then the waste package is punctured. If the random number is greater than *PP,* then the package is not punctured.

c. When the waste packages are punctured, the failed area is determined by sampling a uniform distribution with a lower bound of 0 m^2 and an upper bound of 0.1 m^2. This failed area allows advective flow through the punctured waste package and advective and diffusive transport out of the punctured waste package. This failed area is conceptualized to be a small patch on the surface of the OCB. Once the waste package is penetrated, there is no further damage from penetrations in successive events and the packages remain punctured for the remainder of the realization.

Determine the probability of damage for a waste package that is surrounded by rubble for the *j*th seismic event. The probability of damage for the *j*th seismic event, $PD_{RUB,j}$, is defined in Section 6.9.2 as a function of the value of *PGV* for the *j*th seismic event and of the OCB thickness.

a. The probability of damage is defined in Table 6-81.

Table 6-81. Probability of Damage for the TAD-Bearing Waste Package Surrounded by Rubble

	Residual Stress Threshold (%)		
	90	**100**	**105**
***PGV* (m/s)**	**Probability of Damage for 23-mm-Thick OCB with Degraded Internals:**		
0.4	0	0	0
1.05	0	0	0
2.44	0	0	0
4.07	0.294	0.118	0.059

Table 6-81. Probability of Damage for the TAD-Bearing Waste Package Surrounded by Rubble (Continued)

PGV (m/s)	Probability of Damage for 17-mm-Thick OCB with Degraded Internals:		
0.4	0	0	0
1.05	0	0	0
2.44	0.118	0	0
4.07	0.412	0.176	0.118

Source: Output DTN: MO0703PASDSTAT.001, worksheet "Probability of Damage" in each of the files *WP-Rubble Damage Abstraction 23-mm Degraded.xls* and *WP-Rubble Damage Abstraction 17-mm Degraded.xls*.

b. A piecewise linear interpolation defines the probability of damage based on the value of *PGV* for the *j*th event, the current plate thickness, and the value of RST_i. The first step in this interpolation is to linearly interpolate within each subtable using the values of *PGV* for the *j*th event and of RST_i for the *i*th realization. This first step produces two probabilities of damage, one for a 23-mm-thick OCB and a second for a 17-mm-thick OCB, that are denoted as $PD_{RUB,23\text{-}mm}$ and $PD_{RUB,17\text{-}mm}$, respectively. The probability of damage corresponding to the average OCB thickness is calculated by linear interpolation if the OCB thickness is between 17 mm and 23 mm. The probability is set to the value at 23 mm if the average OCB thickness is greater than 23 mm. The probability is set to the value at 17 mm if the average OCB thickness is less than 17 mm. This calculation is defined in Equation 6.12-25:

$$PD_{RUB,j} = \text{If } t \geq 23\text{mm}, PD_{RUB,23\text{-}mm} \quad \text{(Eq. 6.12-25)}$$

$$\text{Or if } t \leq 17 \text{ mm}, PD_{RUB,17\text{-}mm}$$

$$\text{else, } PD_{RUB,17\text{-}mm} + (PD_{RUB,23\text{-}mm} - PD_{RUB,17\text{-}mm})(t - 17 \text{ mm})/(6 \text{ mm})$$

where t is the spatially averaged thickness (in mm) of the OCB at the time of the *j*th event and $PD_{RUB,17\text{-}mm}$ and $PD_{RUB,23\text{-}mm}$ are the two probabilities for degraded internals. The rationale for this approach is explained in Section 6.9.2 and Equation 6.9-2.

c. Compare the random number from Step 5(b) to the value of $PD_{RUB,j}$ computed in Equation 6.12-25. If the random number from Step 5(b) is less than or equal to $PD_{RUB,j}$ then:

   i. All waste packages are damaged by this seismic event

   ii. The damaged area is computed in Step 17

   iii. The internals of all waste packages are degraded for all subsequent seismic events.

d. If the random number is greater than $PD_{RUB,j}$ then the damaged area can be set to zero for the *j*th seismic event, and it is not necessary to complete Step 17.

If the waste package surrounded by rubble is damaged by the *j*th seismic event (see Step 16), then the conditional damaged area is represented by gamma distributions that are defined in Section 6.9.3. The parameters for these gamma distributions are functions of RST_i as explained in Section 6.9.3. Separate gamma distributions are defined for two states of the waste package: (1) 23-mm-thick OCB with degraded internals and (2) 17-mm-thick OCB with degraded internals. The parameters μ and σ for these two distributions are listed in Table 6-82. Figure 6-84 defines the quadratic fit for the 17-mm-thick OCB. The sources identified for Table 6-82 document all the analyses for μ and σ.

Table 6-82. Gamma Distribution Parameters for Conditional Damaged Areas on the TAD-Bearing Waste Package Surrounded by Rubble

OCB Thick. (mm)	State of Internals	Parameter μ	Parameter σ
23	Degraded	$(0.0153492)(RST_i)^2 - 3.1814*RST_i + 165.834$	$(0.025381)(RST_i)^2 - 5.26067*RST_i + 274.218$
17	Degraded	$(0.0083948)(RST_i)^2 - 1.7755*RST_i + 94.0116$	$(0.007827)(RST_i)^2 - 1.6555*RST_i + 87.656$

Source: Output DTN: MO0703PASDSTAT.001, worksheet "Gamma Abstraction - Modified" in the file *WP-Rubble Damage Abstraction 17-mm Degraded.xls* and worksheet "Gamma Abstraction - Modified" in the file *WP-Rubble Damage Abstraction 23-mm Degraded.xls*.

a. Calculation of conditional damaged area (percentage of outside surface area) with degraded internals is a two-step process: (1) sampling the distributions for damaged area and (2) interpolation for the spatially averaged thickness of the OCB (determined by other elements of the TSPA). Four parameters define the damaged area on the waste package surrounded by rubble: two values for μ and two values for σ. Each of these parameters is a function of the RST for the *i*th realization[16]. These parameters define two gamma distributions that can be sampled for the damaged areas for 17-mm and 23-mm thick OCBs. The sampled values from the two distributions should be fully correlated to provide a consistent basis for interpolation to the specific value of the OCB thickness at the time of the seismic event. The two distributions should be resampled for each event.

b. Other elements of the TSPA determine the spatially averaged OCB thickness for the TAD-bearing and codisposal waste packages at the time of the *j*th seismic event. The damaged area corresponding to the average OCB thickness for each package type is calculated by linear interpolation if the OCB thickness is between 17 mm and 23 mm. The damaged area is equal to the value at 23 mm if the average OCB thickness is greater than 23 mm[17]. The damaged area is set to the value at 17 mm if

[16] The parameters are not a function of *PGV*. Damage for the TAD-bearing waste package surrounded by rubble only occurs at the maximum PGV level of 4.07 m/s. The conditional probability distributions for damaged areas at the 4.07 m/s PGV level are conservatively applied to all values of PGV in the seismic scenario, as explained in Section 6.9.3. This approach does not result in nonzero damaged areas at *PGV* values less than or equal to 2.44 m/s because the probability of damage is always zero, as illustrated in Figure 6-86.

[17] The initial OCB thickness for the TAD-bearing or codisposal waste packages is 25.4-mm. The conditional damaged area for the 23-mm-thick OCB conservatively bounds the conditional damaged areas for OCB thicknesses between 23 mm and 25.4 mm.

the average OCB thickness is less than 17 mm. This calculation is illustrated in Equation 6.12-26:

$$DA_{WP\text{-}rubble} = \text{If } t \geq 23 \text{ mm}, DA_{WP\text{-}rubble,23\text{-}mm} \quad \text{(Eq. 6.12-26)}$$

$$\text{Or if } t \leq 17 \text{ mm}, DA_{WP\text{-}rubble,17\text{-}mm}$$

$$\text{else, } DA_{WP\text{-}rubble,17\text{-}mm} + (DA_{WP\text{-}rubble,23\text{-}mm} - DA_{WP\text{-}rubble,17\text{-}mm})*(t - 17 \text{ mm})/(6 \text{ mm})$$

The rationale for this approach is explained in Section 6.9.6 and Equation 6.9-3.

c. There is no spatial variability for the damaged area (i.e., it is applied to all waste packages), unless the average OCB thicknesses of the TAD-bearing or codisposal waste packages vary within each percolation subregion. Damaged area is randomly located on the cylindrical surface of the OCB, as explained in Section 6.9.8. The cylindrical surface areas of the OCB are 33.64 m^2 and 33.05 m^2 for the TAD-bearing and codisposal waste packages, respectively.

d. The total damaged area (% of outside surface area) increases with each seismic event that causes damage to the OCB. Total damaged area (% of outside surface area) for the TAD-bearing or the codisposal waste packages is the sum of the conditional damaged areas for the first through *j*th seismic events. Total damaged area cannot exceed the total surface area of the TAD-bearing or codisposal waste package, respectively.

Two determinations are required: (1) the damaged area on drip shield plates and (2) the probability of plate failure in response to rock block impacts in an unfilled or partly filled drift in the nonlithophysal units. The damaged area and plate failures are a function of *PGV*, of the thickness of the drip shield plate, and of the kinetic energy of rock blocks that fall from the drift walls during a seismic event, as discussed in Section 6.10.2. This abstraction is applied from repository closure until failure of the drip shield plates, determined by the method described in Step 7, or until the drifts in the nonlithophysal units become half filled with rubble, using the method described in Step 6.

a. The probability of damage/plate failure is defined by Table 6-83, based on Table 6-53.

Table 6-83. Probability of Damage/Plate Failure for Drip Shields in Nonlithophysal Units

	Plate Thickness (mm)			
PGV Level (m/s)	**15**	**10**	**5**	**0**
0.4	0.5	0.5	0.56	1
1.05	0.78	0.78	0.88	1
2.44	0.96	0.96	0.98	1
5.35	0.86	0.86	0.86	1

Source: Output DTN: MO0703PASDSTAT.001, File *Nonlith Damage Abstraction for DS.xls*, worksheet "Summary."

NOTE: Probability of damage/failure for the 0-mm thick plate is set to 1.

A piecewise linear interpolation defines the probability of damage based on the value of *PGV* for the *j*th event and the current plate thickness. If PGV is less than 0.4 m/s, then the probability at the 0.4 m/s PGV level should be used as an upper bound for the probability of damage/plate failure.

b. Compare the random number sampled in Step 5(b) to the probability of damage/plate failure determined in Step 18(a). If the random number is less than or equal to the probability of damage/plate failure then:

   ii. All drip shields in the nonlithophysal units are damaged by this seismic event
   iii. The damage state of the drip shield is determined in Steps 18(c) and 18(d)
   iv. The damaged area is determined in Step 18(e).

   If the random number is greater than the probability of damage/plate failure computed in Step 18(a) then the damaged area can be set to zero for the *j*th seismic event, there are no plate failures for the *j*th seismic event, and it is not necessary to complete Steps 18(c) through 18(e).

c. If the drip shield is damaged by multiple block impacts, then each realization may experience one of five states:

   State 1: Damaged areas on intact drip shields with no drip shield failures
   State 2: Damaged areas on intact drip shields with 1 out of 4 drip shields failing
   State 3: Damaged areas on intact drip shields with 2 out of 4 drip shields failing
   State 4: Damaged areas on intact drip shields with 3 out of 4 drip shields failing
   State 5: Four drip shield failures.

   Table 6-84 presents the conditional probabilities of States 1 through 5 as a function of PGV level and plate thickness. The data in Table 6-84 are based on Table 6-54.

   Piecewise linear interpolations define the conditional probabilities for States 1 through 5 based on the value of *PGV* for the *j*th event and the current plate thickness. If *PGV* is less than 0.4 m/s, then the values in Table 6-84 for the 0.4 m/s PGV level should be used as an upper bound for the conditional probability. Similarly, if the plate thickness is less than 5 mm, then the values in Table 6-84 for the 5-mm thick plates should be used to define the conditional probabilities. There are five conditional probabilities for each of the five damage states, and these probabilities should be readjusted to sum to 1 if necessary after the piecewise linear interpolations. (The values in Table 6-84 do sum to 1 for States 1 through 5 for each value of PGV and thickness reduction in the table.)

Table 6-84. Conditional Probabilities of Damage States 1 through 5

PGV Level (m/s)	15-mm-Thick Plate (0-mm Reduction)	10-mm-Thick Plate (5-mm Reduction)	5-mm-Thick Plate (10-mm Reduction)
State 1: Damaged Area with No Drip Shield Failures:			
0.4	1	1	0.56
1.05	0.95	0.87	0.34
2.44	0.94	0.73	0.18
5.35	0.81	0.33	0.05
State 2: Damaged Area with 1 Drip Shield Failures:			
0.4	0	0	0.28
1.05	0.05	0.13	0.36
2.44	0.06	0.23	0.31
5.35	0.16	0.42	0.16
State 3: Damaged Area with 2 Drip Shield Failures:			
0.4	0	0	0.11
1.05	0	0	0.20
2.44	0	0.02	0.22
5.35	0.02	0.21	0.23
State 4: Damaged Area with 3 Drip Shield Failures:			
0.4	0	0	0
1.05	0	0	0.05
2.44	0	0.02	0.20
5.35	0	0.05	0.28
State 5: Damaged Area with 4 Drip Shield Failures:			
0.4	0	0	0.06
1.05	0	0	0.05
2.44	0	0	0.08
5.35	0	0	0.28

Source: Output DTN: MO0703PASDSTAT.001, File *Nonlith Damage Abstraction for DS.xls*, worksheet "Summary."

NOTE: During the checking process, minor errors were identified in the conditional probabilities for States 1 and 2 after this table had been defined in the TSPA database. For the 15-mm-thick plate at the 5.35 m/s PGV level, the conditional probabilities for State 1 and State 2 changed from 0.79 and 0.19 to 0.81 and 0.16, respectively. For the 5-mm-thick plate at the 2.44 m/s PGV level, the conditional probability for State 1 increased from 0.16 to 0.18. These minor errors will have no impact on the compliance case for the TSPA-LA because FEP 1.2.03.02.0B has been screened out of TSPA (see Section 6.3). These minor errors will also not have a significant impact on the low-consequence argument that supports the screening decision for FEP 1.2.03.02.0B.

d. A discrete distribution for the drip shield damage state is sampled. The probabilities for States 1 through 5 are based on the five conditional probabilities, one for each of the five damage states, determined by the piecewise linear interpolations in Step 18(c):

    i. If State 1 is sampled, then there is damaged area on the drip shields and no plate failures.

ii. If State 2 is sampled, then there is damaged area on the intact drip shields and 1 out of 4 drip shields fail as a barrier to advective flow in the nonlithophysal units. The failed drip shields remain failed for the remainder of the realization.

iii. If State 3 is sampled, then there is damaged area on the intact drip shields and 2 out of 4 drip shields fail as a barrier to advective flow in the nonlithophysal units. The failed drip shields remain failed for the remainder of the realization.

iv. If State 4 is sampled, then there is damaged area on the intact drip shield and 3 out of 4 drip shields fail as a barrier to advective flow in the nonlithophysal units. The failed drip shields remain failed for the remainder of the realization.

v. If State 5 is sampled, then all drip shields fail as a barrier to advective flow in the nonlithophysal units. The failed drip shields remain failed for the remainder of the realization.

e. If the drip shields in the nonlithophysal units are damaged from rock block impacts by the *j*th seismic event, then the conditional damaged area (in units of m^2) is represented by a gamma distribution. The gamma distribution is defined by its mean value and its standard deviation, as derived in Section 6.10.2.6. The values for these parameters are defined in Table 6-85.

Table 6-85. Mean and Standard Deviations of the Conditional Damaged Areas for Realizations of Rock Block Impacts on the Drip Shield

	Plate Thickness (mm)					
	15		10		5	
PGV Level (m/s)	Mean (m^2)	Standard Deviation (m^2)	Mean (m^2)	Standard Deviation (m^2)	Mean (m^2)	Standard Deviation (m^2)
0.4	0.0052	0.0064	0.013	0.016	0.0029	0.0025
1.05	0.018	0.031	0.031	0.046	0.0079	0.010
2.44	0.037	0.054	0.056	0.072	0.013	0.012
5.35	0.093	0.088	0.105	0.085	0.020	0.018

Source: Output DTN: MO0703PASDSTAT.001, File *Nonlith Damage Abstraction for DS.xls*, worksheet "Summary."

Piecewise linear interpolations define the value of the mean and standard deviation for the value of *PGV* for the *j*th event and for the current plate thickness. If *PGV* is less than 0.4 m/s, then the values in Table 6-83 for the 0.4 m/s PGV level should be used as an upper bound. Similarly, if the plate thickness is less than 5 mm, then the values in Table 6-85 for the 5-mm-thick plates should be used to define the conditional probabilities. This approach avoids extrapolations to potentially unphysical values for the mean and standard deviation.

f. The conditional damaged area is determined by sampling a gamma distribution whose mean value and standard deviation are determined in Step 18(e). This conditional damaged area represents the damaged area on four drip shields and must be reduced by a factor of 4 to represent the conditional damaged area per drip shield in the nonlithophysal units.

g. There is no spatial variability for the conditional damaged area or for the number of failed drip shield. That is, it is applied to all drip shields in the nonlithophysal units. Damaged area is randomly located on the crown of the drip shield.

h. The total damaged area increases with each seismic event. Total conditional damaged area is the sum of the conditional damaged areas for the first through *j*th seismic events. Total damaged area cannot exceed the total surface area on the crown of the drip shield. Similarly, the number of failed drip shields increases with each seismic event. The total number of failed drip shields is the sum of the failures for the first through *j*th seismic events.

The damaged area on the drip shield is determined in response to the static rockfall load from lithophysal rubble and the dynamic vertical load for the *j*th seismic event. The damaged area occurs on the crown of the drip shield; damage to the sides has not been abstracted because any seepage through the sides is unlikely to drip onto the waste package. The damaged area is a function of *PGV*, of the thickness of the drip shield plate, and of the static load on the plates from lithophysal rubble, as discussed in Section 6.10.1. The *PGV* level for the *j*th seismic event is determined in Step 4. The thickness of the drip shield plates is calculated by other components within the TSPA model, based on the time of the event, the top-side and bottom-side corrosion rates for Titanium Grade 7, and the initial plate thickness. Damaged area on drip shields in lithophysal units continue to accumulate from multiple events until the drip shield plates fail in Step 7.

The static load is defined by the fraction of the drift that is filled with lithophysal rubble, based on the parameter $FD_{LITH,j}$ determined by Equation 6.12-6 in Step 5(f). The rockfall load in a drift that is partly filled with rubble is defined as the product of the fraction of drift filled with rubble and the rockfall load for a fully collapsed drift (see Section 6.8.1.2). This is a reasonable approach that tends to overestimate the vertical loads on the drip shield for small rubble volumes, as discussed in Section 6.8.1.2.

a. The total dynamic load on the drip shield is defined as a log-normal distribution with the following parameters. The derivation of this distribution and the parameter values is presented in Section 6.10.1.2 and Equations 6.10-8 and 6.10-9.

$$\lambda_{dynamic} = (0.8333)\ln(PGV) + 0.9145 + 11.749 + \ln(FD_{LITH,j}) \qquad \text{(Eq. 6.12-27)}$$

and $$\beta_{dynamic} = 0.536 \qquad \text{(Eq. 6.12-28)}$$

where $\lambda_{dynamic}$ is the expected value of the natural logarithm of the total dynamic load and $\beta_{dynamic}$ is the standard deviation of the natural logarithm of the total dynamic load. The quantity $FD_{LITH,j}$ is defined by Equation 6.12-6 in Step 5(f) and is assigned a minimum value of 0.0001 to maintain a finite value for the *ln* function.

b. The log-normal distribution should be sampled for each seismic event to determine the magnitude of the total dynamic load for this event. This sampling should be perfectly correlated with the random number in Step 5(b) for the fragility of the drip shield plates because high intensity seismic events that have the potential to produce large damaged areas on the drip shield also have the potential to fail the drip shield plates.

c. The damaged areas for a single drip shield plate are defined by Table 6-86 for plate thicknesses of 5 mm, 10 mm, and 15 mm.

Table 6-86. Damaged Plate Areas as a Function of Total Dynamic Load

5-mm Plate Thickness		10-mm Plate Thickness		15-mm Plate Thickness	
Dynamic Load (Pa)	Damaged Plate Area (m^2)	Dynamic Load (Pa)	Damaged Plate Area (m^2)	Dynamic Load (Pa)	Damaged Plate Area (m^2)
1.00×10^{05}	0.00×10^{00}	2.00×10^{05}	0.00×10^{00}	4.00×10^{05}	0.00×10^{00}
2.00×10^{05}	0.00×10^{00}	4.00×10^{05}	0.00×10^{00}	8.00×10^{05}	0.00×10^{00}
3.00×10^{05}	0.00×10^{00}	6.00×10^{05}	0.00×10^{00}	1.20×10^{06}	1.24×10^{-03}
4.00×10^{05}	0.00×10^{00}	8.00×10^{05}	1.33×10^{-03}	1.60×10^{06}	9.43×10^{-03}
5.00×10^{05}	2.79×10^{-03}	1.00×10^{06}	7.39×10^{-03}	2.00×10^{06}	1.38×10^{-02}
6.00×10^{05}	5.34×10^{-03}	1.20×10^{06}	1.29×10^{-02}	2.40×10^{06}	2.09×10^{-02}
7.00×10^{05}	7.01×10^{-03}	1.40×10^{06}	1.71×10^{-02}	2.42×10^{06}	2.14×10^{-02}
8.00×10^{05}	8.03×10^{-03}	1.60×10^{06}	1.94×10^{-02}	2.44×10^{06}	2.22×10^{-02}
8.20×10^{05}	8.21×10^{-03}	1.62×10^{06}	1.97×10^{-02}	2.46×10^{06}	2.24×10^{-02}
8.40×10^{05}	8.38×10^{-03}	1.64×10^{06}	2.02×10^{-02}	2.48×10^{06}	2.29×10^{-02}
8.60×10^{05}	9.64×10^{-03}	1.66×10^{06}	2.04×10^{-02}	2.50×10^{06}	2.31×10^{-02}
8.80×10^{05}	1.11×10^{-02}	1.68×10^{06}	2.06×10^{-02}	2.52×10^{06}	2.39×10^{-02}
9.00×10^{05}	1.38×10^{-02}	1.70×10^{06}	2.07×10^{-02}	2.54×10^{06}	2.52×10^{-02}
9.20×10^{05}	1.78×10^{-02}	1.72×10^{06}	2.14×10^{-02}	2.56×10^{06}	2.55×10^{-02}
9.40×10^{05}	2.19×10^{-02}	1.74×10^{06}	2.27×10^{-02}	2.58×10^{06}	2.61×10^{-02}
9.60×10^{05}	2.80×10^{-02}	1.76×10^{06}	2.53×10^{-02}	2.60×10^{06}	2.64×10^{-02}
9.80×10^{05}	3.86×10^{-02}	1.78×10^{06}	3.44×10^{-02}	2.62×10^{06}	2.67×10^{-02}
1.00×10^{06}	1.64×10^{-01}	1.80×10^{06}	2.53×10^{-01}	2.64×10^{06}	2.70×10^{-02}
1.02×10^{06}	1.74×10^{-01}	1.82×10^{06}	2.71×10^{-01}	2.66×10^{06}	2.72×10^{-02}
1.04×10^{06}	1.96×10^{-01}	1.84×10^{06}	2.73×10^{-01}	2.6×10^{06}	2.83×10^{-02}
1.06×10^{06}	2.11×10^{-01}	1.86×10^{06}	2.79×10^{-01}	2.70×10^{06}	2.90×10^{-02}
1.08×10^{06}	2.23×10^{-01}	1.88×10^{06}	2.89×10^{-01}	2.72×10^{06}	3.11×10^{-02}
1.10×10^{06}	2.24×10^{-01}	1.90×10^{06}	2.91×10^{-01}	2.74×10^{06}	3.47×10^{-02}

Table 6-86. Damaged Plate Areas as a Function of Total Dynamic Load (Continued)

5-mm Plate Thickness		10-mm Plate Thickness		15-mm Plate Thickness	
Dynamic Load (Pa)	Damaged Plate Area (m^2)	Dynamic Load (Pa)	Damaged Plate Area (m^2)	Dynamic Load (Pa)	Damaged Plate Area (m^2)
–	–	1.92×10^{06}	2.95×10^{-01}	2.76×10^{06}	3.71×10^{-02}
–	–	1.94×10^{06}	3.04×10^{-01}	2.78×10^{06}	4.24×10^{-02}
–	–	–	–	2.80×10^{06}	4.71×10^{-02}
–	–	–	–	2.82×10^{06}	3.36×10^{-01}

Source: DTN: MO0703PADSBLOC.000 [DIRS 179662], File *DS plate damage due to distributed loads.xls*. The data for the 10 mm and 15 mm plate thicknesses are based on worksheet "Case 2 boundary condition." The data for the 5-mm plate thickness are based on worksheet "Case 1 boundary condition."

NOTE: An entry of "–" indicates that no data are available because of plate failure.

d. Two linear interpolations define the damaged plate area for the *j*th seismic event. First, the damaged plate areas at thicknesses of 5 mm, 10 mm, and 15 mm are determined for the total dynamic load determined in Step 19(b). This first step provides three values of damaged plate area that provide the basis for the second interpolation that determines the damaged area at the current drip shield plate thickness, *t,* at the time of the seismic event. If *t* is less than 5 mm, then the value at 5 mm should be used to define the final damaged area. The use of the 5-mm values is not expected to be a significant factor in the TSPA because the plates become increasingly likely to fail for plate thicknesses less than 5 mm (see Step 7).

e. The total damaged area on the crown of the drip shield is defined by multiplying the damaged area for a single plate by 20.

f. The damaged area from Step 19(d) is applied to all drip shields in the lithophysal units. There is no spatial variability for the damaged area.

g. The damaged area (m^2) for drip shields in the lithophysal units increases with each seismic event that causes damage to the drip shield while the drip shield plates are intact. Total damaged area (m^2) for the drip shield is the sum of the damaged areas on the drip shield for the first through *j*th seismic events. Damaged area cannot exceed the total surface area of a drip shield.

   The effective flow area for the drip shield is much smaller than the damaged area because diffusion or advection occurs through a network of stress corrosion cracks, rather than through the total damaged area that exceeds the RST. The effective flow area is based on the crack-density model and associated scaling factor for Titanium Grade 7 defined in *Stress Corrosion Cracking of Waste Package Outer Barrier and Drip Shield Materials* (SNL 2007 [DIRS 181953], Section 6.8.5). The scaling factor for Titanium Grade 7 should be sampled once per realization because it represents epistemic rather than aleatory uncertainty.

There is no damage abstraction for cladding failure because the compliance case for the license application is not taking credit for the cladding as a barrier to radionuclide release.

The percent failed area on the waste packages due to fault displacement is determined. This damage abstraction is appropriate for the TSPA because it is based on waste package clearances after drip shields fail, which is expected to occur more than 10,000 years after repository closure. This damage abstraction is not appropriate for criticality studies, which are concerned with the first 10,000 years after repository closure. A separate output DTN is being created by this report to define the frequency and number of failed waste packages for criticality studies.

The expected number of waste packages that fail from fault displacement is small because the number of waste packages lying on known and generic faults is estimated to be 214, which is a small fraction of the approximately 11,000 packages in the repository. In this situation, a special waste package group(s) or bin(s) should be used to represent the waste package failures from fault displacement.

The following logic defines the damage to the waste packages and drip shield while the drip shields remain intact (i.e., before the plates rupture):

- The thermohydrologic and seepage environment for the special group(s) or bin(s) should be chosen independently and randomly. If the fault-failed packages are binned into two groups for the TAD-bearing and codisposal packages, then two randomly chosen environments are used for each of the two groups.

- When a waste package group fails by fault displacement, the failed area for each waste package in the group is determined by sampling a uniform distribution with a lower bound of 0 m^2 and an upper bound equal to the cross-sectional area of the waste package OCB.

- The cross-sectional areas for the TAD-bearing and codisposal waste package groups are 2.78 m^2 and 3.28 m^2, respectively. These areas are calculated from OCB outer diameters of 1,881.6 mm and 2,044.7 mm for the TAD-bearing and 5-DHLW/DOE SNF Long waste packages, respectively (SNL 2007 [DIRS 179394], Table 4-3; [DIRS 179567], Table 4-9).

- The fraction of failed area for the TAD-bearing waste package group is calculated as the ratio of the sampled value of the failed area divided by the total surface area of the waste package. The total surface area of the average waste package in the TAD-bearing group and in the codisposal group is 40.10 m^2 and 36.83 m^2, respectively (Table 6-64, Section 6.11.4). These areas, which include the cylindrical surface and end lids of the waste package, are calculated from the OCB outer diameter and the average length of the waste packages in the TAD-bearing and codisposal groups. The average nominal lengths are 5,843 mm and 4,711 mm for the TAD-bearing and the codisposal groups, respectively (Table 6-64, Section 6.11.4). These failed areas allow advective flow through the damaged waste packages and advective and diffusive transport out of the waste packages.

- The number of package failures for the two waste package groups is defined in Table 6-87, based on Table 6-67. Fractional values for failed waste packages should be

rounded to the nearest integer. The annual exceedance frequency in Table 6-87 is the mean annual exceedance frequency for the fault displacement hazard curves. The mean exceedance frequency for fault displacement could be different from the exceedance frequency in Steps 3 and 4 for the bounded hazard curve. However, in the absence of a correlation between the mean exceedance frequencies for ground motion and fault displacement, it is recommended that the same exceedance frequency determined in Step 3 be used to determine the expected number of waste package failures in Table 6-87.

– If a waste package is damaged by fault displacement, the associated drip shield is taken to be 100% damaged. There is no flux splitting (i.e., diversion of seepage) for these failed drip shields. The number of impacted drip shields is identical to the total number of waste packages that will be damaged by the fault displacement.

– Fuel rod cladding is already 100% perforated because the TSPA compliance case for the license application is not taking credit for the cladding. However, if sensitivity calculations investigate the effect of cladding as a barrier, then the cladding in any waste package that is failed by fault displacement should be 100% perforated.

Table 6-87. Expected Number of Waste Package Failures as a Function of Mean Annual Exceedance Frequency

Annual Exceedance Frequency (1/yr)	Expected Number of Failures—TAD-Bearing Waste Package Group	Annual Exceedance Frequency (1/yr)	Expected Number of Failures—Codisposal Waste Package Group
$> 2.2 \times 10^{-7}$	0	$> 2.5 \times 10^{-7}$	0
2.0×10^{-7} to 2.2×10^{-7}	19.5	2.2×10^{-7} to 2.5×10^{-7}	6.5
7.8×10^{-8} to 2.0×10^{-7}	27.7	8.6×10^{-8} to 2.2×10^{-7}	9.3
2.6×10^{-8} to 7.8×10^{-8}	32.2	2.9×10^{-8} to 8.6×10^{-8}	10.8
1×10^{-8} to 2.6×10^{-8}	160.3	1×10^{-8} to 2.9×10^{-8}	53.7

Source: Output DTN: MO0703PASDSTAT.001, worksheet "Tables," cells B196:B200 and cells D196:D200 in the file *Fault Displacement Abstraction.xls*.

NOTES: Fault intersections and the hazard curves at Sites 4 and 5 were revised after the data for the fault displacement damage abstraction were defined in the TSPA database. This table presents the corrected values. With regard to annual exceedance frequencies, the TSPA data base has 1.4×10^{-7} in place of 2.0×10^{-7} for the TAD-bearing waste package group and 1.6×10^{-7} in place of 2.2×10^{-7} for the codisposal group. With regard to expected number of failures, the TSPA database has 30.7 in place of 32.2, 10.3 in place of 10.8, 158.8 in place of 160.3, and 53.2 in place of 53.7. These minor errors at very low values of the annual exceedance frequency will produce insignificant changes in TSPA predictions of total dose to the reasonably maximally exposed individual.

Values for the TAD group include the Naval waste packages.

TAD = transportation, aging, and disposal (canister).

– If multiple events with failures from fault displacement occur in a given realization, then the number of failed waste packages and their damaged areas should be determined by the most intense seismic event causing failure from fault displacement. This is a reasonable approach because only the waste packages lying on a fault can be damaged, and once damaged they remain in this state. The most intense seismic event has the largest value for PGV or the smallest value of exceedance frequency.

6.12.3 TSPA Parameter Name, Definition/Description, Type, and Value

Tables 6-88 to 6-93 list the name, definition/description, type, and values for the TSPA parameters for the seismic scenario class. These parameters are documented in output DTN: MO0703PASEISDA.002, Seismic Damage Abstractions for the TSPA Compliance Case. Tables 6-88 to 6-93 provide a parametric representation of the computational algorithm defined in Section 6.12.2.

Table 6-88. Definition of Hazard Parameters and Drip Shield Fragility for the Seismic Damage Abstractions

Parameter Name	Description/Definition	Type	Parameter Value
RST	RST for Alloy 22 Units: unitless	Random variable sampled once per realization	Uniform Distribution: Minimum Value: 90 Maximum Value: 105
LAMBDA	Distribution of annual exceedance frequency for the seismic scenario class Units: 1/yr	Random variable sampled each seismic event	Uniform Distribution: Minimum Value: LAMBDA_MIN Maximum Value: LAMBDA_MAX
LAMBDA_MIN	Minimum annual exceedance frequency Units: 1/yr	Constant	1×10^{-8} per year
LAMBDA_MAX	Maximum annual exceedance frequency Units: 1/yr	Constant	4.287×10^{-4} per year
PGV	Value of the horizontal peak ground velocity for this realization Units: m/s	Table lookup	Function of the value of LAMBDA for each seismic event. Use a power law (log) interpolation between points in the table. **λ (1/yr) — PGV (m/s)** 4.287×10^{-4} — 0.219 1.000×10^{-4} — 0.4019 3.826×10^{-5} — 0.6 1.919×10^{-5} — 0.8 9.955×10^{-6} — 1.05 6.682×10^{-6} — 1.2 3.812×10^{-6} — 1.4 2.136×10^{-6} — 1.6 1.288×10^{-6} — 1.8 8.755×10^{-7} — 2.0 6.399×10^{-7} — 2.2 4.518×10^{-7} — 2.44 3.504×10^{-7} — 2.6 2.507×10^{-7} — 2.8 1.731×10^{-7} — 3.0 1.137×10^{-7} — 3.2 7.168×10^{-8} — 3.4 4.362×10^{-8} — 3.6 2.508×10^{-8} — 3.8 1.319×10^{-8} — 4.0 5.967×10^{-9} — 4.2

Table 6-88. Definition of Hazard Parameters and Drip Shield Fragility for the Seismic Damage Abstractions (Continued)

Parameter Name	Description/Definition	Type	Parameter Value
PLATE_FRAGILITY	Fragility (i.e., probability of failure) of the drip shield plates Units: unitless	Lookup table	See Table 6-75 for numerical values, which are a function of PGV, plate thickness, and the rockfall load.
PLATE_FAILURE	Indicator for drip shield plate failure (0 = intact, 1 = failed) Units: unitless	Function	If RN_DSF ≤ PLATE_FRAGILITY, then 1, else 0, where RN_DSF is a random number between 0 and 1.
FRAME_FRAGILITY	Fragility (i.e., probability of failure) of the drip shield framework Units: unitless	Lookup table	See Table 6-76 for numerical values, which are a function of PGV, plate thickness, and the rockfall load.
FRAME_FAILURE	Indicator for drip shield framework failure (0 = intact, 1 = failed) Units: unitless	Function	If RN_DSF ≤ FRAME_FRAGILITY then 1, else 0, where RN_DSF is a random number between 0 and 1.

Table 6-89. Definition of Parameters for the Rockfall Abstractions

Parameter Name	Description/Definition	Type	Parameter Value
PRF	Probability of rockfall in the lithophysal and nonlithophysal zones Units: unitless	Function	MIN(1.0,MAX(0.0,1.288* PGV − 0.353))
PGV_RF	Minimum value of PGV for calculation of intact lithophysal rock volume that caves into the drift during this seismic event Units: m/s	Function	MAX(0.4 m/s, PGV)
LITH_MU	Mean volume of intact lithophysal rock that caves into the drift during this seismic event Units: volume per length of drift, m^3/m	Function	$20.307*(PGV\_RF)^2 - 18.023*(PGV\_RF) + 4.0102$
LITH_SIGMA	Standard deviation of intact lithophysal rock volume that caves into the drift during this seismic event Units: m^3/m	Function	$-3.5613*(PGV\_RF)^2 + 18.018*(PGV\_RF) - 6.6202$
LITH_VOL	Conditional volume of intact lithophysal rock that caves into the drift during this seismic event Units: volume per meter of drift, m^3/m	Random variable sampled each seismic event	Gamma Distribution: Mean: LITH_MU, Standard Deviation: LITH_SIGMA
LITH_RV	Final volume of intact lithophysal rock that caves into the drift during this seismic event, including probability of rockfall Units: m^3/m	Function	If (RN_DSF ≤ PRF) then LITH_VOL, else 0, where RN_DSF is the same random number between 0 and 1 that is identified in Table 6-88

Table 6-89. Definition of Parameters for the Rockfall Abstractions (Continued)

Parameter Name	Description/Definition	Type	Parameter Value
LITH_VOL_ACCUM	Accumulated volume of intact lithophysal rock that has collapsed from this and all previous seismic events Units: volume per meter of drift, m^3/m	Function	Sum of LITH_RV for the first through the current seismic event
MAX_RUBBLE_VOLUME	Volume of intact rock that must collapse to fill the free space in the emplacement drifts Units: volume per meter of drift, m^3/m	Random variable sampled each seismic event	Uniform Distribution: Minimum Value: 30 m^3/m of drift Maximum Value: 120 m^3/m of drift
FRAC_DRIFT_LITH	Fraction of the drift that is filled with lithophysal rock Units: unitless	Function	MAX(0.0001,MIN(1.0, LITH_VOL_ACCUM/ MAX_RUBBLE_VOLUME))
NONLITH_MU	Mean volume of nonlith rock blocks that cave into the drift during this seismic event Units: volume per length of drift, m^3/m	Function	$-0.0142*(PGV)^2 + 0.2064*(PGV) + 0.0387$
NONLITH_SIGMA	Standard deviation of nonlith rock block volume that caves into the drift during this seismic event Units: m^3/m	Function	$-0.037*(PGV)^2 + 0.3057*(PGV) + 0.0696$
NONLITH_VOL	Conditional volume of nonlith rock blocks that cave into the drift during this seismic event Units: volume per meter of drift, m^3/m	Random variable sampled each seismic event	Gamma Distribution: Mean: NONLITH_MU, Standard Deviation: NONLITH_SIGMA
NONLITH_RV	Final volume of nonlith rock blocks that cave into the drift during this seismic event, including probability of rockfall Units: m^3/m	Function	If ($RN\_DSF \leq PRF$), then NONLITH_VOL, else 0, where RN_DSF is the same random number between 0 and 1 that is identified in Table 6-88
NONLITH_VOL_ACCUM	Accumulated volume of nonlith rock blocks that have caved in the drift from this and all previous seismic events Units: volume per meter of drift, m^3/m	Function	Sum of NONLITH_RV for the first through the current seismic event
MAX_BLOCK_VOLUME	Volume of nonlith rock blocks that must cave into the drift to fill the free space in the emplacement drifts Units: volume per meter of drift, m^3/m	Random variable sampled each seismic event	Uniform Distribution: Minimum Value: 30 m^3/m of drift Maximum Value: 120 m^3/m of drift
FRAC_DRIFT_NONLITH	Fraction of the drift that is filled with nonlithophysal rock Units: unitless	Function	MIN(1.0, NONLITH_VOL_ACCUM/MAX_ BLOCK_VOLUME)

Table 6-90. Definition of Parameters for the Waste Package Damage Abstractions

Parameter Name	Description/Definition	Type	Parameter Value
STATE_IorD	State of the waste package internals Units: unitless	Function of previous seismic events	Function of damage in the preceding seismic events: = 1 if the OCB is damaged, = 0 if the OCB is undamaged by any preceding seismic event
CYL_AREA_TAD	Cylindrical surface area of the OCB of the TAD-bearing waste package. This area does not include the end lids. Units: m^2	Constant	33.64 m^2
CYL_AREA_CDSP	Cylindrical surface area of the OCB of the CDSP waste package. This area is for the 5DHLW/DOE SNF Long waste package, and does not include the end lids. Units: m^2	Constant	33.05 m^2
PR_TADi23	Probability of rupture for the TAD-bearing waste package with intact internals and a 23-mm-thick OCB Units: unitless	Constant	0
PD_TADi23	Probability of damage for the TAD-bearing waste package with intact internals and a 23-mm-thick OCB Units: unitless	Lookup table	Bilinear function of PGV and RST: **PGV (m/s)** / **RST** 90 / 100 / 105 0.4 — 0 / 0 / 0 1.05 — 0 / 0 / 0 2.44 — 0 / 0 / 0 4.07 — 0.118 / 0 / 0
DA_TADi23_MU	Mean damaged area for the TAD-bearing waste package with intact internals and a 23-mm-thick OCB Units: m^2	Constant	0.00408 m^2
DA_TADi23_SIGMA	Standard deviation of damaged area for the TAD-bearing waste package with intact internals and a 23-mm-thick OCB Units: m^2	Constant	0.00130 m^2
DA_TADi23_GAMMA	Conditional damaged area for the TAD-bearing waste package with intact internals and a 23-mm-thick OCB Units: m^2	Random variable sampled once per seismic event	Gamma Distribution: Mean: DA_TADi23_MU, Standard Deviation: DA_TADi23_SIGMA
DA_TADi23	Final damaged area for the TAD-bearing waste package with intact internals and a 23-mm-thick OCB Units: m^2	Function	If (RN_DSF ≤ PD_TADi23), then DA_TADi23_GAMMA, else 0, where RN_DSF is the same random number between 0 and 1 that is identified in Table 6-88
PRinc_TADd	Probability of incipient rupture for the TAD-bearing waste package with degraded internals Units: unitless	Function of PGV	If PGV ≥ 0.40 m/s, then $(0.0120)(\text{PGV} - 0.40\ \text{m/s})^{1.7449}$, else 0.0

Table 6-90. Definition of Parameters for the Waste Package Damage Abstractions (Continued)

Parameter Name	Description/Definition	Type	Parameter Value
PRimmed_TADd	Probability of (Immediate) rupture for the TAD-bearing waste package with degraded internals Units: unitless	Function of PGV	If PGV ≥ 2.44 m/s, then $(0.0772)(PGV-2.44\ m/s)^{1.7449}$, else 0.0
PNoRup_TADd	Probability of no rupture for the TAD-bearing waste package with degraded internals Units: unitless	Function of PRinc_TADd and PRimmed_TADd	1 – PRinc_TADd – PRimmed_TADd
INC_TADd	Increment to determine rupture state of the TAD-bearing waste packages Units: unitless	Random variable sampled once per seismic event	Discrete distribution with the probability/value pairs: **INC_TADd** **Probability** 0 PNoRup_TADd 1 PRinc_TADd 2 PRimmed_TADd
CNT_TADd	Counter to determine the rupture state of the TAD-bearing waste packages Units: unitless	Function	CNT_TADd + INC_TADd, where CNT_TADd is initialized to 0 at the start of each realization and is incremented for each seismic event
RUP_AREA_TADd	Rupture area for the TAD-bearing waste package with degraded internals. This rupture area allows advective flow through the TAD-bearing waste packages for the remainder of the realization. Units: m^2	Function of CNT_TADd and FAILED_AREA_TAD	If (CNT_TADd ≥ 2) FAILED_AREA_TAD, else 0.0 Note: FAILED_AREA_TAD is defined in Table 6-93 and should be represented as a circumferential band around the waste package for transport analysis in TSPA
PD_TADd23	Probability of damage for the TAD-bearing waste package with degraded internals and a 23-mm-thick OCB Units: unitless	Lookup table	Bilinear function of PGV and RST: **PGV** **RST** **(m/s)** **90** **100** **105** 0.266 0 0 0 0.349 0.085 0 0 0.4 0.137 0.059 0 1.05 0.804 0.804 0.784 2.44 1 1 1 4.07 1 1 1
DA_TADd23_MU	Mean damaged area for the TAD-bearing waste package with degraded internals and a 23-mm-thick OCB Units: m^2	Function of PGV and RST	$(0.1096 - 0.00664*(RST - 100))*PGV^2 + (0.1722 - 0.01701*(RST - 100))*PGV + 0.0828 - 0.00661*(RST - 100)$
DA_TADd23_SIGMA	Standard deviation of damaged area for the TAD-bearing waste package with degraded internals and a 23-mm-thick OCB Units: m^2	Function of PGV and RST	$(0.0105 - 0.00098*(RST - 100))*PGV^2 + (0.2310 - 0.01373*(RST - 100))*PGV + 0.0829 - 0.01319*(RST - 100)$
DA_TADd23_GAMMA	Conditional damaged area for the TAD-bearing waste package with degraded internals and a 23-mm-thick OCB Units: m^2	Random variable sampled per seismic event	Gamma Distribution: Mean: DA_TADd23_MU, Standard Deviation: DA_TADd23_SIGMA

Table 6-90. Definition of Parameters for the Waste Package Damage Abstractions (Continued)

Parameter Name	Description/Definition	Type	Parameter Value
DA_TADd23	Final damaged area for the TAD-bearing waste package with degraded internals and a 23-mm-thick OCB Units: m^2	Function	If (RN_DSF ≤ PD_TADd23), then DA_TADd23_GAMMA, else 0, where RN_DSF is the same random number between 0 and 1 that is identified in Table 6-88
PD_TADd17	Probability of damage for the TAD-bearing waste package with degraded internals and a 17-mm-thick OCB Units: unitless	Lookup table	Bilinear function of PGV and RST: **PGV (m/s)** / **RST** 90 / 100 / 105 0.280: 0 / 0 / 0 0.351: 0.081 / 0 / 0 0.4: 0.137 / 0.059 / 0 1.05: 0.882 / 0.843 / 0.804 2.44: 1 / 1 / 1 4.07: 1 / 1 / 1
DA_TADd17_MU	Mean damaged area for the TAD-bearing waste package with degraded internals and a 17-mm-thick OCB Units: m^2	Function of PGV and RST	(0.1394 − 0.00838*(RST − 100))*PGV^2 + (0.1649 − 0.02224*(RST − 100))*PGV + 0.0766 − 0.00628*(RST − 100)
DA_TADd17_SIGMA	Standard deviation of damaged area for the TAD-bearing waste package with degraded internals and a 17-mm-thick OCB Units: m^2	Function of PGV and RST	(0.0902 − 0.00828*(RST − 100))*PGV^2 + (0.0170 + 0.00665*(RST − 100))*PGV + 0.1932 - 0.02851*(RST − 100)
DA_TADd17_GAMMA	Conditional damaged area for the TAD-bearing waste package with degraded internals and a 17-mm-thick OCB Units: m^2	Random variable sampled per seismic event	Gamma Distribution: Mean: DA_TADd17_MU, Standard Deviation: DA_TADd17_SIGMA
DA_TADd17	Final damaged area for the TAD-bearing waste package with degraded internals and a 17-mm-thick OCB Units: m^2	Function	If (RN_DSF ≤ PD_TADd17), then DA_TADd17_GAMMA, else 0, where RN_DSF is the same random number between 0 and 1 that is identified in Table 6-88
PP_23	Probability of puncture for any waste package surrounded by rubble with a 23-mm-thick OCB Units: unitless	Function of PGV	If PGV ≥ 1.05 m/s, then (0.0028)(PGV-1.05 m/s)$^{2.9007}$, else 0.0
PD_23	Probability of damage for any waste package surrounded by rubble with a 23-mm-thick OCB Units: unitless	Lookup table	Bilinear function of PGV and RST: **PGV (m/s)** / **RST** 90 / 100 / 105 0.4: 0 / 0 / 0 1.05: 0 / 0 / 0 2.44: 0 / 0 / 0 4.07: 0.294 / 0.118 / 0.059
DA_23_MU	Mean damaged area for any waste package surrounded by rubble with a 23-mm-thick OCB Units: % of surface area	Function of RST	0.0153492*RST^2 − 3.1814*RST + 165.834

Table 6-90. Definition of Parameters for the Waste Package Damage Abstractions (Continued)

Parameter Name	Description/Definition	Type	Parameter Value
DA_23_SIGMA	Standard deviation of damaged area for any waste package surrounded by rubble with a 23-mm-thick OCB Units: % of surface area	Function of RST	$0.025381*RST^2 - 5.26067*RST + 274.218$
DA_23_GAMMA	Conditional damaged area for any waste package surrounded by rubble with a 23-mm-thick OCB Units: % of surface area	Random variable sampled per seismic event	Gamma Distribution: Mean: DA_23_MU, Standard Deviation: DA_23_SIGMA
DA_23	Final damaged area for any waste package surrounded by rubble with a 23-mm-thick OCB Units: % of surface area	Function	If (RN_DSF ≤ PD_23), then DA_23_GAMMA, else 0, where RN_DSF is the same random number between 0 and 1 that is identified in Table 6-88
PP_17	Probability of puncture for any waste package surrounded by rubble with a 17-mm-thick OCB Units: unitless	Function of PGV	If PGV ≥ 0.40 m/s, then $(0.0210)(PGV-0.40\ m/s)^{1.6971}$, else 0.0
PP	Probability of puncture for any waste package surrounded by rubble Units: Unitless	Function of spatially averaged thickness of the OCB, PR_23 and PR_17	If ($t \geq$ 23-mm) PP_23, or if ($t \leq$ 17-mm) PP_17, else PP_17 + (PP_23 − PP_17)(t-17 mm)/ (6 mm), where t is the spatially averaged thickness (in mm) of the OCB at the time of the seismic event
PP_AREA	Puncture area for the waste package surrounded by rubble Units: m^2	Random variable sampled per seismic event	Uniform Distribution: Minimum Value: 0.0 m^2 Maximum Value: 0.1 m^2
PUNC_AREA	Area for advective flow through the waste package surrounded by rubble after a puncture occurs. This area allows advective flow through the waste packages for the remainder of the realization. Units: m^2	Function of PP and PP_AREA	If (RN_PUNC≤PP), then PP_AREA, else 0.0, where RN_PUNC is an independently sampled random number between 0 and 1
PD_17	Probability of damage for any waste package surrounded by rubble with a 17-mm-thick OCB Units: unitless	Lookup table	Bilinear function of PGV and RST: **PGV (m/s)** / **RST** 90 / 100 / 105 0.4 — 0 / 0 / 0 1.05 — 0 / 0 / 0 2.44 — 0.118 / 0 / 0 4.07 — 0.412 / 0.176 / 0.118
DA_17_MU	Mean damaged area for any waste package surrounded by rubble with a 17-mm-thick OCB Units: % of surface area	Function of RST	$0.0083948*RST^2 - 1.7755*RST + 94.0116$
DA_17_SIGMA	Standard deviation of damaged area for any waste package surrounded by rubble with a 17-mm-thick OCB Units: % of surface area	Function of RST	$0.007827*RST^2 - 1.6555*RST + 87.656$

Table 6-90. Definition of Parameters for the Waste Package Damage Abstractions (Continued)

Parameter Name	Description/Definition	Type	Parameter Value
DA_17_GAMMA	Conditional damaged area for any waste package surrounded by rubble with a 17-mm-thick OCB Units: % of surface area	Random variable sampled per seismic event	Gamma Distribution: Mean: DA_17_MU, Standard Deviation: DA_17_SIGMA
DA_17	Final damaged area for any waste package surrounded by rubble with a 17-mm-thick OCB Units: % of surface area	Function	If (RN_DSF ≤ PD_17), then DA_17_GAMMA, else 0, where RN_DSF is the same random number between 0 and 1 that is identified in Table 6-88
PR_CDSPi23	Probability of rupture for the CDSP waste package with intact internals and a 23-mm-thick OCB Units: unitless	Constant	0
PD_CDSPi23	Probability of damage for the CDSP waste package with intact internals and a 23-mm-thick OCB Units: unitless	Lookup table	Bilinear function of PGV and RST: **PGV (m/s)** / **RST: 90** / **100** / **105** 0.364 / 0 / 0 / 0 0.4 / 0.029 / 0 / 0 1.05 / 0.559 / 0 / 0 2.44 / 0.941 / 0.147 / 0 4.07 / 1 / 0.412 / 0
DA_CDSPi23_MU	Mean damaged area for the CDSP waste package with intact internals and a 23-mm-thick OCB Units: m^2	Function of PGV and RST	If (RST ≤ 100), − (0.0033)*(RST − 100)*PGV^2 − (0.00567)*(RST − 100)*PGV − (0.0004)*(RST − 100) + 0.0061, else − (0.0012)*(RST – 105)
DA_CDSPi23_SIGMA	Standard deviation of damaged area for the CDSP waste package with intact internals and a 23-mm-thick OCB Units: m^2 NOTE: Minor errors were discovered after this equation had been passed to TSPA. This table presents the correct values while the TSPA database has 0.0048 in place of 0.0041, 0.0014 in place of 0.0013, and −0.0010 in place of −0.0008. These errors produce insignificant changes in Figure 6-35 and have no impact on the TSPA.	Function of PGV and RST	If (RST ≤ 100), + (0.0001)*(RST − 100)*PGV^2 − (0.0138)*(RST − 100)*PGV + (0.0013)*(RST − 100) + 0.0041, else − (0.0008)*(RST – 105)
DA_CDSPi23_GAMMA	Conditional damaged area for the CDSP waste package with intact internals and a 23-mm-thick OCB Units: m^2	Random variable sampled per seismic event	Gamma Distribution: Mean: DA_CDSPi23_MU, Standard Deviation: DA_CDSPi23_SIGMA
DA_CDSPi23	Damaged area for the CDSP waste package with intact internals and a 23-mm-thick OCB Units: m^2	Function	If (RN_DSF ≤ PD_CDSPi23), then DA_CDSPi23_GAMMA, else 0, where RN_DSF is the same random number between 0 and 1 that is identified in Table 6-88

Table 6-90. Definition of Parameters for the Waste Package Damage Abstractions (Continued)

Parameter Name	Description/Definition	Type	Parameter Value
PRinc_CDSPd	Probability of incipient rupture for the CDSP waste package with degraded internals Units: unitless	Function of PGV	If PGV ≥ 1.05 m/s, then $(0.0158)(PGV - 1.05\ m/s)^{1.8586}$, else 0.0
PRimmed_CDSPd	Probability of (Immediate) rupture for the CDSP waste package with degraded internals Units: unitless	Function of PGV	If PGV ≥ 2.44 m/s, then $(0.0474)(PGV - 2.44\ m/s)^{1.8586}$, else 0.0
PNoRup_CDSPd	Probability of no rupture for the CDSP waste package with degraded internals Units: unitless	Function of PRinc_CDSPd and PRimmed_CDSPd	1 – PRinc_CDSPd – PRimmed_CDSPd
INC_CDSPd	Increment to determine rupture state of the CDSP waste packages Units: unitless	Random variable sampled once per seismic event	Discrete distribution with the probability/value pairs: **INC_CDSPd** **Probability** 0 PNoRup_CDSPd 1 PRinc_CDSPd 2 PRimmed_CDSPd
CNT_CDSPd	Counter to determine the rupture state of the CDSP waste packages Units: unitless	Function	CNT_CDSPd + INC_TADd, where CNT_CDSPd is initialized to 0 at the start of each realization and is incremented for each seismic event
RUP_AREA_CDSPd	Rupture area for the CDSP waste package with degraded internals. This rupture area allows advective flow through the failed area of the CDSP waste packages for the remainder of the realization. Units: m^2	Function of CNT_CDSPd and FAILED_AREA_CDSP	If (CNT_CDSPd ≥ 2) FAILED_AREA_CDSP. else 0.0 NOTE: FAILED_AREA_CDSP is defined in Table 6-93 and should be represented as a circumferential band around the waste package for transport analysis in TSPA
PD_CDSPd23	Probability of damage for the CDSP waste package with degraded internals and a 23-mm-thick OCB Units: unitless	Lookup table	Bilinear function of PGV and RST: **PGV (m/s)** / **RST 90** / **100** / **105** 0.285 / 0 / 0 / 0 0.364 / 0.060 / 0.060 / 0 0.4 / 0.088 / 0.088 / 0.029 1.05 / 0.588 / 0.588 / 0.559 2.44 / 0.941 / 0.941 / 0.941 4.07 / 1 / 1 / 1
DA_CDSPd23_MU	Mean damaged area for the CDSP waste package with degraded internals and a 23-mm-thick OCB Units: m^2	Function of PGV and RST	$(0.0637 - (0.0016)*(RST - 100))*PGV^2 + (0.2274 - (0.0277)*(RST - 100))*PGV + (-0.0144 + (0.0029)*(RST - 100))$
DA_CDSPd23_SIGMA	Standard deviation of damaged area for the CDSP waste package with degraded internals and a 23-mm-thick OCB Units: m^2	Function of PGV and RST	$(-0.0383 + (0.0059)*(RST - 100))*PGV^2 + (0.4623 - (0.0420)*(RST - 100))*PGV + (-0.0601 + (0.0034)*(RST - 100))$

Table 6-90. Definition of Parameters for the Waste Package Damage Abstractions (Continued)

Parameter Name	Description/Definition	Type	Parameter Value
DA_CDSPd23_GAMMA	Conditional damaged area for the CDSP waste package with degraded internals and a 23-mm-thick OCB Units: m^2	Random variable sampled per seismic event	Gamma Distribution: Mean: DA_CDSPd23_MU, Standard Deviation: DA_CDSPd23_SIGMA
DA_CDSPd23	Final damaged area for the CDSP waste package with degraded internals and a 23-mm-thick OCB Units: m^2	Function	If (RN_DSF ≤ PD_CDSPd23), then DA_CDSPd23_GAMMA, else 0, where RN_DSF is the same random number between 0 and 1 that is identified in Table 6-88
PD_CDSPd17	Probability of damage for the CDSP waste package with degraded internals and a 17-mm-thick OCB Units: unitless	Function of RST	Bilinear function of PGV and RST: **PGV (m/s)** / **RST 90** / **100** / **105** 0.219 / 0 / 0 / 0 0.338 / 0.097 / 0 / 0 0.346 / 0.103 / 0.007 / 0 0.4 / 0.147 / 0.059 / 0.029 1.05 / 0.676 / 0.676 / 0.382 2.44 / 0.941 / 0.941 / 0.882 4.07 / 1 / 1 / 1 See the NOTES to Table 6-77 regarding the differences between this table and the TSPA database
DA_CDSPd17_MU	Mean damaged area for the CDSP waste package with degraded internals and a 17-mm-thick OCB Units: m^2	Function of PGV and RST	(0.0670 − (0.0011)*(RST − 100))*PGV^2 + (0.1879 − (0.0376)*(RST − 100)) *PGV + (−0.0187 + (0.0034) *(RST − 100))

DA_CDSPd17_SIGMA	Standard deviation of damaged area for the CDSP waste package with degraded internals and a 17-mm-thick OCB
	Units: m^2
		Function of PGV and RST	If ((PGV > 0.4 m/s) or (RST < 102))
			(−0.0266 + (0.0078)*
			(RST − 100))*PGV^2
			+ (0.4066 − (0.0490)*
			(RST − 100))*PGV
			+ (−0.0605 + (0.0011)*
			(RST − 100)),
			else
			Use above equation, but set PGV equal to 0.4 m/s

DA_CDSPd17_GAMMA	Conditional damaged area for the CDSP waste package with degraded internals and a 17-mm-thick OCB Units: m^2	Random variable sampled per seismic event	Gamma Distribution: Mean: DA_CDSPd17_MU, Standard Deviation: DA_CDSPd17_SIGMA
DA_CDSPd17	Final damaged area for the CDSP waste package with degraded internals and a 17-mm-thick OCB Units: m^2	Function	If (RN_DSF ≤ PD_CDSPd17), then DA_CDSPd17_GAMMA, else 0, where RN_DSF is the same random number between 0 and 1 that is identified in Table 6-88

Table 6-91. Definition of Parameters for the Drip Shield Damage Abstractions

Parameter Name	Description/Definition	Type	Parameter Value
DSLOAD_LAMBDA	Mean value of the natural logarithm of the total dynamic load on the drip shield Units: unitless	Function of PGV and of the fraction of the drift that is filled with lithophysal rubble	(0.8333)ln(PGV) + 0.9145 +11.749 + ln(FRAC_DRIFT_LITH), where FRAC_DRIFT_LITH is defined in Table 6-89
DSLOAD_BETA	Standard deviation of the natural logarithm of the total dynamic load on the drip shield Units: unitless	Constant	0.536
DS_LOAD_LN	Natural logarithm of the total dynamic load on the drip shield Units: unitless	Random variable sampled each seismic event	Normal Distribution: Mean: DSLOAD_LAMBDA Standard Deviation: DSLOAD_BETA
DS_LOAD	Total dynamic load on the drip shield for this event Units: Pa	Function	Exp(DS_LOAD_LN)
DS_DA_PLATE_15	Damaged area on a single drip shield plate with 15-mm-thick plates Units: m^2	Lookup table as a function of the sampled value for DS_LOAD	**DS_LOAD (Pa)** / **DA (m^2)** $4.0 \times 10^{+5}$ / 0 $8.0 \times 10^{+5}$ / 0 $1.2 \times 10^{+6}$ / 1.24×10^{-3} $1.6 \times 10^{+6}$ / 9.43×10^{-3} $2.0 \times 10^{+6}$ / 1.38×10^{-2} $2.4 \times 10^{+6}$ / 2.09×10^{-2} $2.42 \times 10^{+6}$ / 2.14×10^{-2} $2.44 \times 10^{+6}$ / 2.22×10^{-2} $2.46 \times 10^{+6}$ / 2.24×10^{-2} $2.48 \times 10^{+6}$ / 2.29×10^{-2} $2.50 \times 10^{+6}$ / 2.31×10^{-2} $2.52 \times 10^{+6}$ / 2.39×10^{-2} $2.54 \times 10^{+6}$ / 2.52×10^{-2} $2.56 \times 10^{+6}$ / 2.55×10^{-2} $2.58 \times 10^{+6}$ / 2.61×10^{-2} $2.60 \times 10^{+6}$ / 2.64×10^{-2} $2.62 \times 10^{+6}$ / 2.67×10^{-2} $2.64 \times 10^{+6}$ / 2.70×10^{-2} $2.66 \times 10^{+6}$ / 2.72×10^{-2} $2.68 \times 10^{+6}$ / 2.83×10^{-2} $2.70 \times 10^{+6}$ / 2.90×10^{-2} $2.72 \times 10^{+6}$ / 3.11×10^{-2} $2.74 \times 10^{+6}$ / 3.47×10^{-2} $2.76 \times 10^{+6}$ / 3.71×10^{-2} $2.78 \times 10^{+6}$ / 4.24×10^{-2} $2.80 \times 10^{+6}$ / 4.71×10^{-2} $2.82 \times 10^{+6}$ / 3.36×10^{-1}

Table 6-91. Definition of Parameters for the Drip Shield Damage Abstractions (Continued)

Parameter Name	Description/Definition	Type	Parameter Value
DS_DA_PLATE_10	Damaged area on a single drip shield plate with 10-mm-thick plates Units: m^2	Lookup table as a function of DS_LOAD	**DS_LOAD (Pa)** / **DA (m^2)** $2.0 \times 10^{+5}$ / 0 $4.0 \times 10^{+5}$ / 0 $6.0 \times 10^{+5}$ / 0 $8.0 \times 10^{+5}$ / 1.33×10^{-3} $1.0 \times 10^{+6}$ / 7.39×10^{-3} $1.2 \times 10^{+6}$ / 1.29×10^{-2} $1.4 \times 10^{+6}$ / 1.71×10^{-2} $1.60 \times 10^{+6}$ / 1.94×10^{-2} $1.62 \times 10^{+6}$ / 1.97×10^{-2} $1.64 \times 10^{+6}$ / 2.02×10^{-2} $1.66 \times 10^{+6}$ / 2.04×10^{-2} $1.68 \times 10^{+6}$ / 2.06×10^{-2} $1.70 \times 10^{+6}$ / 2.07×10^{-2} $1.72 \times 10^{+6}$ / 2.14×10^{-2} $1.74 \times 10^{+6}$ / 2.27×10^{-2} $1.76 \times 10^{+6}$ / 2.53×10^{-2} $1.78 \times 10^{+6}$ / 3.44×10^{-2} $1.80 \times 10^{+6}$ / 2.53×10^{-1} $1.82 \times 10^{+6}$ / 2.71×10^{-1} $1.84 \times 10^{+6}$ / 2.73×10^{-1} $1.86 \times 10^{+6}$ / 2.79×10^{-1} $1.88 \times 10^{+6}$ / 2.89×10^{-1} $1.90 \times 10^{+6}$ / 2.91×10^{-1} $1.92 \times 10^{+6}$ / 2.95×10^{-1} $1.94 \times 10^{+6}$ / 3.04×10^{-1}
DS_DA_PLATE_5	Damaged area on a single drip shield plate with 5-mm-thick plates Units: m^2	Lookup table as a function of DS_LOAD	**DS_LOAD (Pa)** / **DA (m^2)** $1.0 \times 10^{+5}$ / 0 $2.0 \times 10^{+5}$ / 0 $3.0 \times 10^{+5}$ / 0 $4.0 \times 10^{+5}$ / 0 $5.0 \times 10^{+5}$ / 2.79×10^{-3} $6.0 \times 10^{+5}$ / 5.34×10^{-3} $7.0 \times 10^{+5}$ / 7.01×10^{-3} $8.0 \times 10^{+5}$ / 8.03×10^{-3} $8.2 \times 10^{+5}$ / 8.21×10^{-3} $8.4 \times 10^{+5}$ / 8.38×10^{-3} $8.6 \times 10^{+5}$ / 9.64×10^{-3} $8.8 \times 10^{+5}$ / 1.11×10^{-2} $9.0 \times 10^{+5}$ / 1.38×10^{-2} $9.2 \times 10^{+5}$ / 1.78×10^{-2} $9.4 \times 10^{+5}$ / 2.19×10^{-2} $9.6 \times 10^{+5}$ / 2.80×10^{-2} $9.8 \times 10^{+5}$ / 3.86×10^{-2} $1.0 \times 10^{+6}$ / 1.64×10^{-1} $1.02 \times 10^{+6}$ / 1.74×10^{-1} $1.04 \times 10^{+6}$ / 1.96×10^{-1} $1.06 \times 10^{+6}$ / 2.11×10^{-1} $1.08 \times 10^{+6}$ / 2.23×10^{-1} $1.10 \times 10^{+6}$ / 2.24×10^{-1}

Table 6-91. Definition of Parameters for the Drip Shield Damage Abstractions (Continued)

Parameter Name	Description/Definition	Type	Parameter Value
DS_DA_PLATE	Damaged area on a single drip shield plate with thickness *t* at the time of the seismic event Units: m^2	Lookup table as a function of the thickness, *t*, at the time of the seismic event	Linear interpolation within the following table as a function of the thickness of the drip shield plates at the time of the seismic event: **Thickness (mm)** — **Area (m^2)** 5 — DS_DA_PLATE_5 10 — DS_DA_PLATE_10 15 — DS_DA_PLATE_15 If the thickness is less than 5 mm, use the value of DS_DA_PLATE_5
DS_DA	Damaged area on the crown of the drip shield from this seismic event Units: m^2	Function	20*DS_DA_PLATE
PD_DSNL	Probability of damage to the drip shield or failure of the drip shield plates in the nonlithophysal units Units: unitless	Lookup table as a function of PGV and of the plate thickness at the time of the seismic event	Bilinear function of PGV and plate thickness: **PGV (m/s)** — **Plate Thickness mm) 15 / 10 / 5 / 0** 0.4 — 0.5 / 0.5 / 0.56 / 1 1.05 — 0.78 / 0.78 / 0.88 / 1 2.44 — 0.96 / 0.96 / 0.98 / 1 5.35 — 0.86 / 0.86 / 0.86 / 1 NOTE: if PGV is less than 0.40 m/s, then use the value at the 0.4 m/s PGV levels
PD_DSNL_STATE1	Conditional probability of State 1, with nonzero damaged area on the drip shield and no failures in the nonlithophysal units Units: unitless NOTE: Minor errors in the conditional probabilities for State 1 were discovered after this parameter had been defined in the TSPA database. This table presents the correct values, while the TSPA database has 0.79 in place of 0.81 and 0.16 in place of 0.18. These errors have no impact on the compliance case for the TSPA-LA because FEP 1.2.03.02.0B has been screened out of TSPA. These errors also have an insignificant impact on the low consequence argument that support the screening decision for FEP 1.2.03.02.0B.	Lookup table as a function of PGV and plate thickness at the time of the seismic event	Bilinear function of PGV and plate thickness: **PGV (m/s)** — **Plate Thickness (mm) 15 / 10 / 5** 0.4 — 1 / 1 / 0.56 1.05 — 0.95 / 0.87 / 0.34 2.44 — 0.94 / 0.73 / 0.18 5.35 — 0.81 / 0.33 / 0.05 NOTE: Use the conditional probability at 0.4 m/s if PGV is less than 0.40 m/s. Use the conditional probability at 5 mm if the plate thickness is less than 5 mm

Table 6-91. Definition of Parameters for the Drip Shield Damage Abstractions (Continued)

Parameter Name	Description/Definition	Type	Parameter Value
PD_DSNL_STATE2	Conditional probability of State 2, with nonzero damaged area on the drip shield and one drip shield failure as an advective barrier per every four drip shields in the nonlithophysal units Units: unitless NOTE: A minor error in the conditional probabilities for State 2 was discovered after this parameter had been defined in the TSPA database. This table presents the correct values, while the TSPA database has 0.1 in place of 0.16 for the 15-mm-thick plate. This error has no impact on the compliance case for the TSPA-LA because FEP 1.2.03.02.0B has been screened out of TSPA. This error also has an insignificant impact on the low consequence argument that support the screening decision for FEP 1.2.03.02.0B.	Lookup table as a function of PGV and plate thickness at the time of the seismic event	Bilinear function of PGV and plate thickness: **PGV (m/s) / Plate Thickness (mm): 15 / 10 / 5** 0.4 — 0 / 0 / 0.28 1.05 — 0.05 / 0.13 / 0.36 2.44 — 0.06 / 0.23 / 0.31 5.35 — 0.16 / 0.42 / 0.16 NOTE: Use the conditional probability at 0.4 m/s if PGV is less than 0.40 m/s. Use the conditional probability at 5 mm if the plate thickness is less than 5 mm
PD_DSNL_STATE3	Conditional probability of State 3, with nonzero damaged area on the drip shield and two drip shield failures as an advective barrier per every four drip shields in the nonlithophysal units Units: unitless	Lookup table as a function of PGV and plate thickness at the time of the seismic event	Bilinear function of PGV and plate thickness: **PGV (m/s) / Plate Thickness (mm): 15 / 10 / 5** 0.4 — 0 / 0 / 0.11 1.05 — 0 / 0 / 0.20 2.44 — 0 / 0.02 / 0.22 5.35 — 0.02 / 0.21 / 0.23 NOTE: Use the conditional probability at 0.4 m/s if PGV is less than 0.40 m/s. Use the conditional probability at 5 mm if the plate thickness is less than 5 mm
PD_DSNL_STATE4	Conditional probability of State 4, with nonzero damaged area on the drip shield and three drip shield failures as an advective barrier per every four drip shields in the nonlithophysal units Units: unitless	Lookup table as a function of PGV and plate thickness at the time of the seismic event	Bilinear function of PGV and plate thickness: **PGV (m/s) / Plate Thickness (mm): 15 / 10 / 5** 0.4 — 0 / 0 / 0 1.05 — 0 / 0 / 0.05 2.44 — 0 / 0.02 / 0.20 5.35 — 0 / 0.05 / 0.28 NOTE: Use the conditional probability at 0.4 m/s if PGV is less than 0.40 m/s. Use the conditional probability at 5 mm if the plate thickness is less than 5 mm

Table 6-91. Definition of Parameters for the Drip Shield Damage Abstractions (Continued)

Parameter Name	Description/Definition	Type	Parameter Value
PD_DSNL_STATE5	Conditional probability of State 5, with nonzero damaged area on the drip shield and all drip shields failed as advective barriers in the nonlithophysal units Units: unitless	Lookup table as a function of PGV and plate thickness at the time of the seismic event	Bilinear function of PGV and plate thickness: **PGV (m/s) / Plate Thickness (mm)** 15: 0.4 → 0; 1.05 → 0; 2.44 → 0; 5.35 → 0 10: 0.4 → 0; 1.05 → 0; 2.44 → 0; 5.35 → 0 5: 0.4 → 0.06; 1.05 → 0.05; 2.44 → 0.08; 5.35 → 0.28 NOTE: Use the conditional probability at 0.4 m/s if PGV is less than 0.40 m/s. Use the conditional probability at 5 mm if the plate thickness is less than 5 mm
STATE_DSNL	Conditional damaged state of the drip shield Units: unitless	Random variable sampled each seismic event	Discrete distribution with five-state conditional probabilities: **State / Conditional Probability** 1 PD_DSNL_STATE1 2 PD_DSNL_STATE2 3 PD_DSNL_STATE3 4 PD_DSNL_STATE4 5 PD_DSNL_STATE5
DA_4DSNL_MU	Conditional mean damaged area for four drip shields in the nonlithophysal units Units: m^2	Lookup table as a function of PGV and of the plate thickness at the time of the seismic event	Bilinear function of PGV and plate thickness: **PGV (m/s) / Plate Thickness (mm)** 15: 0.4 → 0.0052; 1.05 → 0.018; 2.44 → 0.037; 5.35 → 0.093 10: 0.4 → 0.013; 1.05 → 0.031; 2.44 → 0.056; 5.35 → 0.105 5: 0.4 → 0.0029; 1.05 → 0.0079; 2.44 → 0.013; 5.35 → 0.020 NOTE: Use the mean value at 0.4 m/s if PGV is less than 0.40 m/s. Use the mean value at 5 mm if the plate thickness is less than 5 mm
DA_4DSNL__SIGMA	Standard deviation of conditional damaged area for four drip shields in the nonlithophysal units Units: m^2	Lookup table as a function of PGV and of the plate thickness at the time of the seismic event	Bilinear function of PGV and plate thickness: **PGV (m/s) / Plate Thickness (mm)** 15: 0.4 → 0.0064; 1.05 → 0.031; 2.44 → 0.054; 5.35 → 0.088 10: 0.4 → 0.016; 1.05 → 0.046; 2.44 → 0.072; 5.35 → 0.085 5: 0.4 → 0.0025; 1.05 → 0.010; 2.44 → 0.012; 5.35 → 0.018 NOTE: Use the mean value at 0.4 m/s if PGV is less than 0.40 m/s. Use the mean value at 5 mm if the plate thickness is less than 5 mm
DA_4DSNL	Conditional damaged area for four drip shields in the nonlithophysal units Units: m^2	Random variable sampled each seismic event	Gamma Distribution: Mean: DA_4DSNL_MU Standard Deviation: DA_4DSNL_SIGMA

Table 6-91. Definition of Parameters for the Drip Shield Damage Abstractions (Continued)

Parameter Name	Description/Definition	Type	Parameter Value
DA_DSNL	Final damaged area per drip shields in the nonlithophysal units Units: m^2	Function	If (RN_DSF ≤ PD_DSNL), then (DA_4DSNL/4), else 0, where RN_DSF is the same random number between 0 and 1 that is identified in Table 6-88
FAIL_DSNL	Fraction of failed drip shields in the nonlithophysal units If drip shields fail, they fail as a barrier to advective flow	Function	If (RN_DSF ≤ PD_DSNL), then ((STATE_DSNL – 1)/4), else 0, where RN_DSF is the same random number between 0 and 1 that is identified in Table 6-88

Table 6-92. Definition of Parameters for the Cladding Damage Abstraction

Parameter Name	Description/Definition	Type	Parameter Value
CLAD_DAMAGE	Percent failed (perforated) cladding from vibratory ground motion Units: %	Constant	100% failed from the first seismic event

Table 6-93. Definition of Parameters for the Fault Displacement Damage Abstraction

Parameter Name	Description/Definition	Type	Parameter Value
AREA_TAD	Cross-sectional area of the TAD-bearing waste package in the TAD/Naval waste package group for fault displacement Units: m^2	Constant	2.78 m^2
AREA_CDSP	Cross-sectional area of the codisposal waste package group for fault displacement Units: m^2	Constant	3.28 m^2
FAILED_AREA_TAD	Distribution of failed area for the TAD-bearing waste package group for fault displacement Units: m^2	Random variable sampled each seismic event	Uniform Distribution: Minimum Value: 0.0 m^2 Maximum Value: AREA_TAD
FAILED_AREA_CDSP	Distribution of failed area for the codisposal waste package group for fault displacement Units: m^2	Random variable sampled each seismic event	Uniform Distribution: Minimum Value: 0.0 m^2 Maximum Value: AREA_CDSP
SURF_TAD	Total surface area for the average waste package in the TAD group for fault displacement. This surface area includes the end caps Units: m^2	Constant	40.10 m^2

Table 6-93. Definition of Parameters for the Fault Displacement Damage Abstraction (Continued)

Parameter Name	Description/Definition	Type	Parameter Value
SURF_CDSP	Total surface area for the average waste package in the CDSP group for fault displacement. This surface area includes the end caps Units: m^2	Constant	36.83 m^2
FRACTION_FAILED_AREA_TAD	Fraction of failed surface area for the TAD-bearing waste package group from fault displacement Units: dimensionless	Function	FAILED_AREA_TAD/SURF_TAD
FRACTION_FAILED_AREA_CDSP	Fraction of failed surface area for the CDSP waste package group from fault displacement Units: dimensionless	Function	FAILED_AREA_CDSP/SURF_CDSP
NO_TAD_FAILURES	Number of failed waste packages in the TAD/Naval group from fault displacement Units: integer NOTE: All fault-failed packages in the TAD-bearing group are located in a single, randomly chosen thermohydrologic and seepage environment in each realization. The environments for TAD and codisposal packages are chosen independently.	Function	Step function of the annual exceedance frequency, λ, for this event, based on a lookup table. **λ (1/yr) — # Failures** $> 2.2 \times 10^{-7}$ — 0 2.0×10^{-7} to 2.2×10^{-7} — 19.5 7.8×10^{-8} to 2.0×10^{-7} — 27.7 2.6×10^{-8} to 7.8×10^{-8} — 32.2 1×10^{-8} to 2.6×10^{-8} — 160.3 Fractional values can be rounded to the nearest integer. See the NOTES to Table 6-87 regarding the differences between this table and the TSPA database.
NO_CDSP_FAILURES	Number of failed waste packages from the codisposal group from fault displacement Units: integer NOTE: All fault-failed CDSP packages are located in a single, randomly chosen thermo-hydrologic and seepage environment in each realization. The environments for TAD and CDSP packages are chosen independently.	Function	Step function of the annual exceedance frequency, λ, for this event, based on a lookup table. **λ (1/yr) — # Failures** $> 2.5 \times 10^{-7}$ — 0 2.2×10^{-7} to 2.5×10^{-7} — 6.5 8.6×10^{-8} to 2.2×10^{-7} — 9.3 2.9×10^{-8} to 8.6×10^{-8} — 10.8 1.0×10^{-8} to 2.9×10^{-8} — 53.7 Fractional values can be rounded to the nearest integer. See the NOTES to Table 6-87 regarding the differences between this table and the TSPA database.
NO_DS_FD	Number of drip shields damaged by fault displacement. (Note that drip shields may have already failed from the plate or framework fragility analysis, so this calculation may be redundant.) Units: dimensionless	Function	NO_TAD_FAILURES + NO_CDSP_FAILURES
DS_DAMAGE_FD	Magnitude of drip shield damage for all shields failed by fault displacement. Units: %	Constant	100%

6.13 LIMITATIONS

The major limitations of the postclosure abstractions for the seismic scenario class are as follows:

- Waste package internals are assumed to degrade as structural elements after the OCB is first damaged by a seismic event (Assumption 5.4, Section 5). More exactly, the internals degrade as a structural component by the time of the next seismic event after the first seismic event that breaches the waste package. This approach is conservative because a waste package with degraded internals has significantly greater deformation and probability of rupture relative to a waste package with intact internals (see Sections 6.5.1 versus 6.5.2 and 6.6.1 versus 6.6.2). However, this approach underestimates the structural capacity of stainless steel internal components, such as the 2-in-thick inner vessel or the TAD canister itself, for screening of criticality-related issues during a 10,000-year period.

- Spatial variability in the mechanical response of EBS components to vibratory ground motion has not been represented in the TSPA. In other words, damage to the waste package and drip shield from vibratory ground motion is constant throughout the repository for each seismic event. Although spatial variability is not included within the TSPA, it has been included in the kinematic calculations through the variability of friction factors on a package-by-package basis and in the abstraction of damaged areas for the two or three central waste packages in the kinematic calculations.

  Lack of spatial variability is reasonable for estimating the mean dose from the seismic scenario class. The mean dose is accurately estimated because the sum of the mean doses from groups of waste packages with different damage levels is equal to the mean of the sum of the doses from the individual groups. In other words, using a constant mean value for the damage is an accurate approach for calculating the mean total dose from the repository. On the other hand, the coefficient of variation (i.e., the variability about the mean) of the total dose over all realizations is overestimated without spatial variability. If damage to waste package or drip shield is constant and perfectly correlated everywhere in the repository, realizations with very high or very low damage produce a more extreme response for the dose than a realization with damage that varies spatially between the high and low values.

- Structural response calculations for the waste package surrounded by rubble are based on the TAD-bearing waste package with degraded internals. Section 6.9.10 provides the rationale for using the results for the TAD-bearing waste package with degraded internals for the codisposal waste package with degraded internals.

- The internals of the waste package surrounded by rubble are always degraded. The use of degraded internals is consistent with the fact that the waste package becomes surrounded by rubble at late times, after the drip shield plates have failed and allowed rubble to contact the waste package. The use of degraded internals is conservative because damage to a waste package with degraded internals is observed to be significantly greater than damage to a waste package with intact internals (see Sections 6.5.1 versus 6.5.2 and 6.6.1 versus 6.6.2).

6.14 TECHNICAL BASIS OF CALCULATIONS

The abstraction for damage from fault displacement is not considered a model and, since it is not a model, it is not validated per SCI-PRO-006. However, it is useful to justify that this abstraction is a calculation and that it provides a reasonable representation of the variability and uncertainty in damage to the EBS components from fault displacement. The analysis of the standoff distance from known secondary faults in Appendix D is also considered a calculation because it is based on established engineering practice, as explained in this section.

The abstraction for damage to the waste package and drip shield from fault displacement is based on the mean hazard curves for displacement on known and generic faults in the repository block and on the available clearances between EBS components. The analysis of damage from fault displacement demonstrates that there is no damage from faulting until an annual exceedance frequency less than 2.5×10^{-7} per year is reached (Table 6-67). In other words, only the largest, very low probability fault displacements have the potential to damage the EBS components.

Fault displacement is conceptualized to damage the EBS components when the fault displacement is greater than the available clearance between or around EBS components. The performance of EBS components is estimated from a comparison of hazard curves and engineering clearances. This comparison is useful because it evaluates the performance of EBS components using a standard engineering approach. The use of a standard engineering approach, without model development, meets the requirements for a calculation under SCI-PRO-005, *Scientific Analyses and Calculations*.

If a package is damaged by fault displacement, the damaged area on the waste package is defined as a uniform distribution with a lower bound of 0 and an upper bound given by the lid area. The lower bound represents a situation with minor crimping of the waste package; the upper bound represents a situation in which the welds fail and the lid completely separates from the waste package. These damage states are intended to be bounding conditions because there is high uncertainty in the state of the drift, the invert, and the EBS components after a major fault displacement.

The calculation for fault displacement has been compared to an alternative conceptual model proposed by Waiting et al. (2003 [DIRS 164449]). This comparison is not required for a calculation but is useful for justifying the technical approach in Section 6.11 and is performed without the use of mathematical models. There is very reasonable agreement between the calculation in this report and the results from the alternative conceptual model, considering that the alternate model is based on historical data for fault displacement in the western United States and that the calculation is based on hazard curves specific to Yucca Mountain. Based on

site-specific information, there are 43 locations where known faults intersect the planned emplacement drifts (Table 6-60), plus an estimated 171 locations where unmapped faults could intersect the drifts (Section 6.11.2.2), for a total of 214 fault intersections. The alternative conceptual model predicts 191 fault intersections (Section 6.11.6). Similarly, the probability-weighted number of waste package failures is predicted to be 1.1×10^{-5} for the damage abstraction (Table 6-68), within the range of 1.9×10^{-6} to 1.9×10^{-5} predicted by the alternative conceptual model (Section 6.11.6). This agreement provides added confidence in the calculation for fault displacement.

The analysis of the standoff distance from known secondary faults in Appendix D is also considered a calculation because it is based on established engineering practice using the Particle Flow Code. The Particle Flow Code in two dimensions (PFC2D V. 2.0. STN: 10828-2.0-00 [DIRS 161950]) is used here to simulate the shear movement on a vertical fault that intersects a drift filled with circular rubble particles. The PFC2D program simulates the differential movement of the solid rock walls on either side of the fault and the subsequent force interaction and frictional sliding of the circular particles. This application of the PFC2D program to the response of rubble is considered to be an established engineering practice for the following reasons:

- Modeling of the force interaction and frictional sliding between circular particles is simplistic in nature and does not require complex models for the constitutive behavior of the rubble.

- PFC2D was developed for a consortium of mining companies to simulate the flow, movement and draw of rock rubble created during caving operations in a mine. As such, PFC2D is used as a tool by the mining industry for prediction of rock rubble interaction and flow (Brown 2003 [DIRS 169527]).

- PFC2D is a standard, commercially-available numerical code that has been in use for over 15 years. It has been used for extensive engineering calculations of the static and dynamic mechanical response of particulate materials, including rock rubble, soils, powders, and nanoparticles (see, for example, Konietsky 2003 [DIRS 162198]).

Application of PFC2D to simulation of rock rubble in a faulted drift is considered a calculation because it is a standard engineering application for the PFC2D software and because new model development is not required to perform this calculation.

7. VALIDATION

This report develops damage abstractions for the response of EBS components to seismic hazards at a geologic repository in Yucca Mountain, Nevada. It also defines the methodology for using these abstractions in a seismic scenario class for the TSPA-LA. The seismic hazards addressed are vibratory ground motion, fault displacement, and rockfall induced by ground motion. The EBS components are the drip shield and waste package. Consistent with its intended use, *Technical Work Plan for: Calculation of Waste Package and Drip Shield Response to Vibratory Ground Motion and Revision of the Seismic Consequence Abstraction* (SNL 2007 [DIRS 179869]) specifies model validation Level II for the seismic damage abstractions for the waste package and drip shield.

The abstraction for damage to EBS components from fault displacement is a calculation because it is based on a standard engineering approach, without requiring development of a new mathematical model. Since this abstraction is not a model, it is not validated per SCI-PRO-006, *Models*. The analysis of the standoff distance from known secondary faults in Appendix D is also considered a calculation because it is based on established engineering practice using the particle flow code, PFC2D, and because new mathematical models are not being developed.

7.1 LEVEL I VALIDATION

The TWP (SNL 2007 [DIRS 179869], Section 2.3.1) specifies that the seismic damage abstractions will be validated to the Level II criteria for models of higher relative importance. A Level II validation includes items 1 through 6 for Level I validation, per Attachment 3 of SCI-PRO-002, *Planning for Science Activities*. The development of the seismic damage abstractions has included Level I validation activities that build confidence and verify and justify that the technical approach is adequate and reasonable.

1. *Evaluate and select input parameters and/or data that are adequate for the model's intended use* (SCI-PRO-002, Attachment 3, Level I Validation (1))

   The types and quality of the data selected as inputs build confidence in the seismic damage abstractions. The major inputs to the seismic damage abstractions have been generated by structural response calculations and by coupled rockfall/structural response calculations (SNL 2007 [DIRS 178851]) that are specifically designed to evaluate the mechanical response of the drip shield and waste package to seismic events. These calculations explicitly consider future states of the system, including the degradation of EBS components by general corrosion and changes to the in-drift configuration of EBS components due to drift collapse and drip shield failure. The outputs from these calculations provide most of the inputs to the seismic damage abstractions, which are obtained from controlled sources. Section 4.1 provides a discussion of the inputs and Table 4-1 identifies the data and design parameters used to develop the abstractions. Additional information that corroborates Table 4-1 and therefore builds additional confidence is discussed in Section 6.2. Thus, this requirement can be considered satisfied.

The results from the structural response calculations in *Mechanical Assessment of Degraded Waste Packages and Drip Shields Subject to Vibratory Ground Motion* (SNL 2007 [DIRS 178851]) are considered appropriate for their intended use for several reasons. First, the calculations are based on standard, commercially available software that has demonstrated the capability to accurately analyze impact processes, kinematic response, and coupled rockfall/structural response. Second, the finite-element representation of EBS components and the discrete-element representation of rockfall are designed to accurately represent the response of the rock mass and the potential damage from dynamic seismic loads. And lastly, the ground motions for the calculations are based on state-of-the-art techniques for representing seismic phenomena.

The rockfall analyses are also performed with commercially available software using models that have been validated for their intended application to lithophysal and nonlithophysal tuffs. This model validation is documented in Section 7 of *Drift Degradation Analysis* (BSC 2004 [DIRS 166107]).

2. *Formulate defensible assumptions and simplifications that are adequate for the model's intended use* (SCI-PRO-002, Attachment 3, Level I Validation (2))

   The key assumptions for developing these abstractions are presented in Section 5. In general, the seismic damage abstractions are designed to represent the deformation and failure of EBS components with an accuracy that is commensurate with the application, based on (1) the computational results from rockfall analyses, structural response calculations, and coupled rockfall/structural response calculations and (2) the level of detail captured by the TSPA model for the compliance case.

   A key simplification for the abstractions relates to spatial variability of damage within the repository. Spatial variability has not been represented in the seismic damage abstractions for EBS components in response to vibratory ground motion. In other words, damage to the waste package and drip shield from vibratory ground motion is constant throughout the repository. Although spatial variability is not directly included within the TSPA, it is indirectly included in the kinematic calculations through the variability of friction factors on a package-by-package basis. The resulting spatial variability for the three central TAD-bearing waste packages and for the two central codisposal waste packages is included in the abstraction of damaged areas from the kinematic calculations.

   Lack of spatial variability is reasonable for estimating the mean dose from the seismic scenario class but overestimates the coefficient of variation for the dose. The mean dose is accurately estimated because the sum of the mean doses from groups of waste packages with different damage levels is equal to the mean of the sum of the doses from the individual groups. In other words, using a constant mean value for the damage is an accurate approach for calculating the mean total dose. On the other hand, the coefficient of variation (i.e., the variability about the mean) of the total dose over all realizations is overestimated without spatial variability. If the waste package damage is constant and perfectly correlated everywhere in the repository, realizations with very high or very low

damage produce a more extreme response for the dose than realizations with damage that varies spatially between the high and low values.

A second key simplification relates to the use of the spatially averaged thickness of the OCB for the finite-element and discrete-element models of the waste package. While surface imperfections, residual stresses from welding, and local chemical environments may result in variable corrosion rates on the OCB, the spatially averaged thickness of the OCB is most relevant to the overall structural response of the waste package. The damaged area from the kinematic response of the waste package is dominated by waste package-to-pallet impacts. These impacts involve contact of the pallet with a significant area on the surface of the waste package, thereby averaging the impact loads across regions with multiple OCB thicknesses due to nonuniform corrosion. If rubble surrounds the waste package, then the seismic loads are spread over the whole surface of the waste package, again providing a mechanism to average the loads over the surface of the waste package. In both of these cases, the spatially averaged thickness of the OCB provides an appropriate measure of structural deformation and damaged area.

A third key simplification is that the static load from rockfall is based on lithophysal rubble because the static lithophysal load is greater than to the static load from nonlithophysal rockfall. Rockfall in lithophysal rock has significantly greater volume (see Figure 6-58 and Section 6.7.2.1) than rockfall in nonlithophysal rock, resulting in greater static loads from lithophysal rockfall at a given point in time. The load from lithophysal rubble is usually treated as a uniform load because the typical rubble size of 0.1 m to 0.3 m (BSC 2004 [DIRS 166107], Section 6.4.1.1) is significantly less than typical length scales of the waste package or drip shield. For example, the width of the drip shield is 2,535 mm or approximately 2.5 m (SNL 2007 [DIRS 179354], Table 4-2, Item Number 07-01 for external width at base of drip shield), much greater than the typical dimensions of rubble particulates. Similarly, the diameter of the TAD-bearing waste package is 1,881.6 mm or approximately 1.9 m (SNL 2007 [DIRS 179394], Table 4-3), again significantly greater than the typical particulate size in lithophysal rubble.

This requirement can be considered satisfied.

3. *Ensure consistency with physical principals, such as conservation of mass, energy, and momentum, to an appropriate degree commensurate with the model's intended use* (SCI-PRO-002, Attachment 3, Level I Validation (3))

   Consistency with physical principles, such as conservation of mass, energy, and momentum, is maintained because the abstractions are based on detailed structural response calculations and coupled rockfall/structural response calculations that predict dynamic or quasi-static response using the three conservation laws. Structural calculations for the response of large engineered components (e.g., waste package and drip shield) due to impact and vibration is a well-established technology. The deformation of these types of structures has been evaluated with standard, commercially available finite-element programs. As a result, there is high confidence in the results from the computational process because of the extensive testing of commercial software

on a wide variety of problems, including impact calculations. In addition, each computational study is based on other supporting calculations that provide additional confidence in the results. This software has been qualified for its intended use under IT-PRO-0011, *Software Management*. The finite-element models for the structural response calculations have been validated to the Level II requirements in SCI-PRO-006.

The failure criteria for Alloy 22, Titanium Grade 7, and Titanium Grade 29 have been selected in a manner that is consistent with physical principles. One failure criterion is based on consideration of potential SCC due to residual tensile stress. The rationale and experimental basis for selection of the RSTs for potential SCC is documented in *Stress Corrosion Cracking of the Drip Shield, the Waste Package Outer Barrier, and the Stainless Steel Structural Material* (SNL 2007 [DIRS 181953], Sections 6.2 and 6.5). A second failure criterion is based on the ultimate tensile strain for tearing and rupture. This failure criterion includes a "knockdown" factor to adjust the uniaxial data for ultimate tensile strain in a multidimensional stress field. The failure criteria are considered appropriate for their intended use because they are a conservative interpretation of the experimental data for the corrosion of Alloy 22 and Titanium Grade 7 under conditions relevant to Yucca Mountain, are consistent with handbook or catalog data for the ultimate uniaxial tensile strain, and are consistent with current scientific understanding.

This requirement can be considered satisfied.

4. *Represent important future state (aleatoric), parameter (epistemic), and alternative model uncertainties to an appropriate degree commensurate with the model's intended use* (SCI-PRO-002, Attachment 3, Level I Validation (4))

The uncertainty in future states of the EBS components has been represented by three idealized configurations, as shown in Figure 6-2. Figure 6-2(a) represents the as-emplaced EBS configuration, with an intact drip shield and minimal rockfall in the drifts. Figure 6-2(b) represents an intermediate state of the system where the legs of the drip shield have buckled under combined rockfall/seismic load, but the drip shield plates remain intact. Figure 6-2(c) represents the final state of the system, in which rubble surrounds the waste package after failure of the drip shield plates. The transition between these configurations is determined by fragility curves for the drip shield framework and plates, based on the intensity of the seismic event and on the thickness of drip shield components and accumulated rockfall load at the time of the seismic event.

The abstractions for failure and damaged areas on the waste package and drip shield due to vibratory ground motion and rockfall induced by vibratory ground motion are a function of the intensity of the seismic event (measured by peak ground velocity), of the RSTs for Alloy 22 and Titanium Grade 7, of the spatially averaged thickness of the OCB, and of the thicknesses of the drip shield framework and plates at the time of the seismic event. The damaged areas exhibit substantial variability induced by the uncertainties in seismic ground motions, and minor variability due to the uncertainties in metal-to-metal and metal-to-rock friction coefficients. The potential variations in material properties for

EBS components in the structural response calculations have been represented in a bounding manner by evaluating material properties at 60°C.

Alternate conditional probability distributions have been considered to represent the damaged areas on the waste package and drip shield. These alternate distributions include the gamma, normal, log-normal, Weibull and triangular distributions, as presented in Sections 6.5.1.4, 6.5.2.4, 6.6.1.4, 6.6.2.4, 6.7.1.3, 6.7.2.4, 6.9.4, and 6.10.2.8.

This variability in the seismic damage abstractions is directly propagated into the TSPA compliance case by defining random (stochastic) parameters that are sampled during each realization or for each seismic event. A more detailed discussion can be found in Section 8.2 under Acceptance Criterion 3: Data Uncertainty Is Characterized and Propagated Through the Model Abstraction**.** Treatment of model uncertainty is discussed in Section 8.2 under Acceptance Criterion 4: Model Uncertainty Is Characterized and Propagated Through the Model Abstraction.

This requirement can be considered satisfied.

5. *Ensure simulation conditions have been designed to span the range of intended use and avoid inconsistent outputs or that those inconsistencies can be adequately explained and demonstrated to have little impact on results* (SCI-PRO-002, Attachment 3, Level I Validation (5))

   Kinematic damage abstractions have been developed for three future states of the TAD-bearing waste package and of the codisposal waste package:

   - 23-mm-thick OCB with intact internals
   - 23-mm-thick OCB with degraded internals
   - 17-mm-thick OCB with degraded internals.

   Each abstraction defines the probability of rupture, the probability of damage, and the conditional probability distributions for nonzero damaged area, all as functions of PGV and/or RST. The abstractions are based on computational results for (1) 17 sets of ground motions at each of four PGV levels: 0.4 m/s, 1.05 m/s, 2.44 m/s, and 4.07 m/s, and (2) damaged areas for 90%, 100%, and 105% RST. The resulting damage abstractions span the full range of PGV and RST for the seismic scenario. The spatially averaged OCB thicknesses of 23 mm and 17 mm are intended to represent the potential thicknesses of the OCB over a 1,000,000 year period. The appropriateness of the 17-mm-thick OCB must be verified by results with the general corrosion models for the TSPA compliance case.

   Two damage abstractions have been developed for a waste package with degraded internals that is surrounded by lithophysal rubble:

   - 23-mm-thick OCB with degraded internals
   - 17-mm-thick OCB with degraded internals.

A case with intact internals was not performed for the waste package surrounded by rubble. The waste package becomes surrounded by rubble after the drip shield framework and drip shield plates have failed during a seismic event. This is expected to occur at late times after repository closure, when the OCB is likely to be breached by potential SCC, resulting in degraded internals inside the waste package. Regardless of the time scale, the damage abstractions for degraded internals provide an upper bound for the damaged areas relative to the response with intact internals, so this approach is conservative.

Lithophysal rubble was selected for the dynamic load on the waste package. Rockfall in lithophysal rock has significantly greater volume than rockfall in nonlithophysal rock (see Section 6.7.2.1), resulting in greater static loads from lithophysal rockfall at a given point in time. The abstractions for the mechanical response of a waste package surrounded by rubble to a seismic event are based on the TAD-bearing waste package with degraded internals. The response of the TAD-bearing waste package is expected to be similar to the response of the codisposal waste package when the internals are degraded, so a single damage abstraction has been developed for both types of waste packages. The rationale for the similarity of response is explained in Section 6.9.10.

Each abstraction defines the probability of puncture, the probability of damage, and the conditional probability distributions for conditional damaged area, all as functions of PGV and/or RST. The abstractions are based on computational results for (1) 17 sets of ground motions at each of four PGV levels: 0.4 m/s, 1.05 m/s, 2.44 m/s, and 4.07 m/s, and (2) damaged areas for 90%, 100%, and 105% RST. The resulting damage abstractions span the full range of PGV and RST for the seismic scenario. The spatially averaged OCB thicknesses of 23 mm and 17 mm are intended to represent the potential thicknesses of the OCB over a 1,000,000-year period. The appropriateness of the 17-mm-thick OCB must be verified by results with the general corrosion models for the TSPA compliance case.

Drip shield damage abstractions and fragility curves have been developed for three future states of the drip shield:

- The initial or intact state, with 15-mm-thick plates
- A degraded state with 10-mm-thick plates and a 5-mm reduction for all other drip shield components
- A degraded state with 5-mm-thick plates and a 10-mm reduction for all other drip shield components.

Each drip shield damage abstraction defines the probability of plate failure, the probability of damage, and the conditional probability distributions for nonzero damaged area, all as functions of PGV. RST is not a variable because Titanium Grade 7 has a constant, bounding value for RST. The abstractions are based on quasi-static (rather than dynamic) calculations with loads that go from zero up to the loads at ultimate failure.

The resulting damage abstractions span the full range of PGV values and of rockfall or rock block loading for the seismic scenario.

The drip shield fragility curves define the probability of plate rupture or the probability of buckling of the sidewalls of the drip shield. The fragility curves are a function of the static rockfall load, the thickness of drip shield components, and the peak vertical acceleration from a seismic event. The fragility curves span the full range of structural response and seismic loading.

This requirement can be considered satisfied.

6. *Ensure that model predictions (performance parameters) adequately represent the range of possible outcomes, consistent with important uncertainties and modeling assumptions, conceptualizations, and implementation* (SCI-PRO-002, Attachment 3, Level I Validation (6))

   The seismic damage abstractions span the full range of intended use by covering the full range of peak ground velocities from the bounded PGV hazard curve that can cause damage to the waste package (see Section 6.4), by defining the long-term degradation of EBS components (see Sections 6.1.2, 6.5, 6.6, 6.9, and 6.10), by defining appropriate failure mechanisms and damage mechanisms for the waste package and drip shield (see Section 6.1.4), and by consideration of the potential for drift collapse and drip shield failure (see Sections 6.7 and 6.8).

   This requirement can be considered satisfied.

7.2 VALIDATION TO LEVEL II CRITERIA

The seismic damage abstractions for the waste package and drip shield define the probability of component failure, the probability of damage on the component, and the conditional (nonzero) damaged areas on the component. The probability of component failure and the probability of damage are functions of PGV and/or RST and the thickness of the component. The conditional (nonzero) damaged area is a random variable that is a function of PGV, RST, and the thickness of the component. The appropriate functions and conditional probability distributions have been developed and documented in Microsoft Excel spreadsheets. The numerical values in these spreadsheets have been verified during the checking process for this model report. The input data, formulas, and output data for these spreadsheets are described in Appendix B of this report. Electronic copies of the spreadsheets are archived in an output DTN from this model report, DTN: MO0703PASDSTAT.001.

The abstractions for kinematic damage to the waste package, for the waste package surrounded by rubble, for the drip shield fragility curves, and for the damage to the drip shield will be validated by (1) corroboration of the abstraction model results to the results of the validated structural response model from which the abstraction is derived and (2) a technical review by a reviewer for postdevelopment model validation (SNL 2007 [DIRS 179869], Sections 2.3.2.1 and 2.3.2.2). The independent technical review has been performed by Dr. Gabriel Toro and is discussed further in Section 7.2.2. These steps provide validation to the fifth and seventh methods in Section 6.3.2 of SCI-PRO-006.

7.2.1 Corroboration of Abstraction Model Results (Seventh Method in SCI-PRO-006)

Table 7-1 provides a brief summary of the figures in this report and in output DTN: MO0703PASDSTAT.001 that demonstrate the corroboration of the output from the abstraction models with the results from the validated structural response models and the validated rockfall/structural response models. The damage abstraction for fault displacement is not listed in Table 7-1 because it is not a model and does not require validation.

Table 7-1. Summary of Corroborations of Abstraction Model Results to the Underlying Data

Kinematic Response of TAD-Bearing Waste Package	
- 23-mm-Thick OCB with Intact Internals and 90% RST to 105% RST	- Probability of damage is presented in Table 6-4 and in Figure 6-8. These data are directly represented in the damage abstraction as a lookup table that is a function of PGV and RST in the TSPA. - Figure 6-9 is a Q-Q plot that demonstrates the very good comparison of nonzero damaged area at 4.07 m/s PGV level and 90% RST with a gamma distribution. - The results in Figure 6-9 provide an upper bound for all PGV levels less than 4.07 m/s and all RST levels greater than 90%.
- 23-mm-Thick OCB with Degraded Internals and 90% RST	- Figure 6-11 demonstrates that a linear least-squares fit in log space provides an excellent representation of the data for probability of incipient rupture. - Figure 6-12 demonstrates the excellent agreement between the power-law fits and the data for incipient rupture and (immediate) rupture. - Probability of damage is presented in a table and figure in output DTN: MO0703PASDSTAT.001, File *Kinematic Damage Abstraction 23-mm Degraded.xls*, worksheet "Prob of Damage – New." These data are directly represented in the damage abstraction as a lookup table that is a function of PGV and RST in the TSPA. - The Q-Q plots for nonzero damaged areas at 0.4 m/s, 1.05 m/s, 2.44 m/s, and 4.07 m/s PGV levels demonstrate that gamma distributions provide an excellent representation of the nonzero damaged areas, as documented in output DTN: MO0703PASDSTAT.001, File *Kinematic Damage Abstraction 23-mm Degraded.xls*, worksheet "Gamma for 90%_d23." - Quadratic fits as a function of PGV provide an excellent fit to the underlying data for the mean and standard deviation of the nonzero damaged areas, as documented in output DTN: MO0703PASDSTAT.001, File *Kinematic Damage Abstraction 23-mm Degraded.xls*, worksheet "Gamma for 90%_d23." - The percentiles on a gamma distribution provide a reasonable representation of the full range of nonzero damaged areas, as documented in output DTN: MO0703PASDSTAT.001, File *Kinematic Damage Abstraction 23-mm Degraded.xls*, worksheet "Gamma for 90%_d23."
- 23-mm-Thick OCB with Degraded Internals and 90% RST to 105% RST	- The quadratic fits as a function of PGV and RST are in excellent agreement with the underlying data for the mean and standard deviation of the nonzero damaged areas, as documented in output DTN: MO0703PASDSTAT.001, File *Kinematic Damage Abstraction 23-mm Degraded.xls*, worksheet "Dependence on RST."

Table 7-1. Summary of Corroborations of Abstraction Model Results to the Underlying Data (Continued)

Kinematic Response of TAD-Bearing Waste Package (Continued)	
- 17-mm-Thick OCB with Degraded Internals and 90% RST	- Figure 6-11 demonstrates that a linear least-squares fit in log space provides an excellent representation of the data for probability of incipient rupture. - Figure 6-12 demonstrates the excellent agreement between the power-law fits and the data for incipient rupture and (immediate) rupture. - Probability of nonzero damage is presented in Table 6-11 and Figure 6-14. These data are directly represented in the damage abstraction as a lookup table that is a function of PGV and RST in the TSPA. - Figures 6-15 to 6-18 are Q-Q plots that demonstrate the very-good to excellent comparisons of the nonzero damaged areas at 0.4 m/s, 1.05 m/s, 2.44 m/s, and 4.07 m/s PGV levels with gamma distributions. - Figure 6-19 demonstrates the excellent agreement between quadratic fits as a function of PGV to the underlying data for the mean and standard deviation of the nonzero damaged areas. - Figure 6-20 demonstrates that the percentiles on the gamma distributions provide a reasonable representation of the full range of nonzero damaged areas.
- 17-mm-Thick OCB with Degraded Internals and 90% RST to 105% RST	- Figures 6-23 and 6-24 demonstrate the excellent agreement between quadratic fits as a function of PGV and RST and the underlying data for the mean and standard deviation of the nonzero damaged areas.
Kinematic Response of CDSP Waste Package	
- 23-mm-Thick OCB with Intact Internals and 90% RST	- Probability of damage is presented in Table 6-16 and in Figure 6-27. These data are directly represented in the damage abstraction as a lookup table that is a function of PGV and RST in the TSPA. - Figures 6-28 to 6-31 are Q-Q plots that demonstrate the very good to excellent comparisons of the nonzero damaged areas at the 0.4 m/s, 1.05 m/s, 2.44 m/s, and 4.07 m/s PGV levels with gamma distributions. - Figure 6-32 demonstrates the excellent agreement between quadratic fits as a function of PGV and the underlying data for the mean and standard deviation of the nonzero damaged areas. - Figure 6-33 demonstrates that the percentiles on the gamma distributions provide a reasonable representation of the full range of nonzero damaged areas.
- 23-mm-Thick OCB with Intact Internals and 90% RST to 105% RST	- Figures 6-34 and 6-35 demonstrate the excellent agreement between quadratic fits as a function of PGV and RST to the underlying data for the mean and standard deviation of the nonzero damaged areas.
- 23-mm-Thick OCB with Degraded Internals and 90% RST	- Figure 6-38 demonstrates the excellent agreement between the power-law fits and the data for incipient rupture and (immediate) rupture. - Probability of damage is presented in a table and figure in output DTN: MO0703PASDSTAT.001, File *CDSP Kinematic Damage Abstraction 23-mm Degraded.xls*, worksheet "Prob of Damage – New." These data are directly represented in the damage abstraction as a lookup table that is a function of PGV and RST in the TSPA. - The Q-Q plots for nonzero damaged areas at 0.4 m/s, 1.05 m/s, 2.44 m/s, and 4.07 m/s PGV levels demonstrate that gamma distributions provide an excellent representation of the nonzero damaged areas, as documented in output DTN: MO0703PASDSTAT.001, File *CDSP Kinematic Damage Abstraction 23-mm Degraded.xls*, worksheet "Gamma for 90%_d23." - Quadratic fits as a function of PGV provide an excellent fit to the underlying data for the mean and standard deviation of the nonzero damaged areas, as documented in output DTN: MO0703PASDSTAT.001, File *CDSP Kinematic Damage Abstraction 23-mm Degraded.xls*, worksheet "Gamma for 90%_d23." - The percentiles on a gamma distribution provide a reasonable representation of the full range of nonzero damaged areas, as documented in output DTN: MO0703PASDSTAT.001, File *CDSP Kinematic Damage Abstraction 23-mm Degraded.xls*, worksheet "Gamma for 90%_d23."

Table 7-1. Summary of Corroborations of Abstraction Model Results to the Underlying Data (Continued)

Kinematic Response of CDSP Waste Package (Continued)	
- 23-mm-Thick OCB with Degraded Internals and 90% RST to 105% RST	- The quadratic fits as a function of PGV and RST are in excellent agreement with the underlying data for the mean and standard deviation of the nonzero damaged areas, as documented in output DTN: MO0703PASDSTAT.001, File *CDSP Kinematic Damage Abstraction 23-mm Degraded.xls*, worksheet "Dependence on RST."
- 17-mm-Thick OCB with Degraded Internals and 90% RST	- Figure 6-38 demonstrates the excellent agreement between the power law fits and the data for incipient rupture and (immediate) rupture. - Probability of damage is presented in Table 6-26 and Figure 6-40. These data are directly represented in the damage abstraction as a lookup table that is a function of PGV and RST in the TSPA. - Figures 6-41 to 6-44 are Q-Q plots that demonstrate the very good to excellent comparisons of the nonzero damaged areas at 0.4 m/s, 1.05 m/s, 2.44 m/s, and 4.07 m/s PGV levels with gamma distributions. - Figure 6-45 demonstrates the excellent agreement between quadratic fits as a function of PGV to the underlying data for the mean and standard deviation of the nonzero damaged areas. - Figure 6-46 demonstrates that the percentiles on the gamma distributions provide a reasonable representation of the full range of nonzero damaged areas.
- 17-mm-Thick OCB with Degraded Internals and 90% RST to 105% RST	- Comparisons of the quadratic fits as a function of PGV and RST to the underlying data for the mean and standard deviation of the nonzero damaged areas are presented in Figures 6-49 and 6-50. These figures demonstrate excellent agreement with the underlying data for the mean and standard deviation of the nonzero damaged areas.
Lithophysal Rubble Volume	
- Probability of rockfall is presented in Table 6-29 and Figure 6-52. These data are directly represented in the damage abstraction as a lookup table that is a function of PGV in the TSPA. - Figure 6-53 through Figure 6-55 are Q-Q plots that demonstrate the very good to excellent comparisons of the nonzero rockfall volumes at 0.4 m/s, 1.05 m/s, and 2.44 m/s PGV levels with gamma distributions. - Figure 6-56 demonstrates the excellent agreement between quadratic fits as a function of PGV to the underlying data for the mean and standard deviation of the nonzero rockfall volumes. - Figure 6-57demonstrates that the percentiles on the gamma distributions provide a reasonable representation of the full range of nonzero rockfall volumes.	
Nonlithophysal Rockfall Volume	
- Probability of rockfall in the nonlithophysal units is represented by the data for the lithophysal units in Table 6-29 and Figure 6-52. The lithophysal data provide an upper bound for the probability of rockfall in the nonlithophysal units. These data are directly represented in the damage abstraction as a lookup table that is a function of PGV in the TSPA. - Figures 6-59 to 6-61 are Q-Q plots that demonstrate the very-good to excellent comparisons of the nonzero rockfall volumes at 1.05 m/s, 2.44 m/s, and 5.35 m/s PGV levels with gamma distributions. - Figure 6-62 demonstrates the excellent agreement between quadratic fits as a function of PGV to the underlying data for the mean and standard deviation of the nonzero rockfall volumes. - Figure 6-63 demonstrates that the percentiles on the gamma distributions provide a reasonable representation of the full range of nonzero rockfall volumes.	

Table 7-1. Summary of Corroborations of Abstraction Model Results to the Underlying Data (Continued)

Drip Shield Plate Fragility
- Figure 6-64 demonstrates the least-squares fit for the mean of *ln*(PGA-V) versus PGV-H1. - Figure 6-65 is a Q-Q plot that demonstrates the excellent comparison for the residuals of *ln*(PGA-V) relative to the least squares fit with a normal distribution. - Figure 6-66 demonstrates that the percentiles on the log-normal distributions provide an excellent representation of the full range of values for PGA-V. - Figure 6-67 is a Q-Q plot that demonstrates the excellent comparison for the residuals of the lithophysal rockfall load on the crown of the drip shield relative to the average crown pressure with a log-normal distribution. - Figure 6-68 demonstrates that a linear function of plate thickness provides an excellent fit for the ultimate plastic load capacity data for the drip shield plates. - Figures 6-69 to 6-71 plot the probability of plate rupture as a function of PGV and plate thickness. These data are directly represented in the damage abstraction as a lookup table that is a function of plate thickness, rockfall load, and PGV in the TSPA.
Drip Shield Framework Fragility
- Figure 6-64 demonstrates the least-squares fit for the mean of *ln*(PGA-V) versus PGV-H1. - Figure 6-65 is a Q-Q plot that demonstrates the excellent comparison for the residuals of *ln*(PGA-V) relative to the least squares fit with a normal distribution. - Figure 6-66 demonstrates that the percentiles on the log-normal distributions provide an excellent representation of the full range of values for PGA-V. - Figure 6-67 is a Q-Q plot that demonstrates the excellent comparison for the residuals of the lithophysal rockfall load on the crown of the drip shield relative to the average crown pressure with a log-normal distribution. - Figure 6-72 demonstrates that a linear function of plate thickness provides an excellent representation of the mean value of the ultimate plastic load capacity data for the drip shield framework. - Figures 6-74 to 6-76 plot the probability of framework collapse as a function of PGV and plate thickness. These data are directly represented in the damage abstraction as a lookup table that is a function of component thickness, rockfall load, and PGV in the TSPA.
TAD-Bearing Waste Package with Degraded Internals and Surrounded by Rubble
- Figure 6-78 demonstrates that a linear least-squares fit in *ln* space provides an excellent representation of the data for probability of puncture. - Figure 6-79 demonstrates the excellent agreement between the power law fits and the data for puncture. - Figures 6-80 and 6-81 present the probability of damage for the 23-mm-thick and 17-mm-thick OCBs, respectively. These data, which are summarized in Table 6-44, are directly represented in the damage abstraction as a lookup table that is a function of PGV and RST in the TSPA. - Figures 6-82 and 6-83 are Q-Q plots that demonstrate the very good comparisons of the nonzero damaged areas with gamma distributions for the 17-mm-thick OCB at the 4.07 m/s PGV level for 90% RST and 100% RST, respectively. - Figure 6-84 demonstrates the excellent agreement between quadratic fits as a function of RST to the underlying data for the mean and standard deviation of the nonzero damaged areas for the 17-mm-thick OCB at the 4.07 m/s PGV level. - Figure 6-85 demonstrates that the percentiles on the gamma distributions provide a reasonable representation of the full range of nonzero damaged areas for the 17-mm-thick OCB at the 4.07 m/s PGV level. - The results for the 4.07 m/s PGV level provide an upper bound for all PGV levels for the 17-mm-thick OCB, as discussed in Section 6.9.3. - Figure 6-87 is a Q-Q plot that demonstrates reasonable comparison of the nonzero damaged areas with a gamma distribution for the 23-mm-thick OCB at 4.07 m/s PGV levels and 90% RST. - Figure 6-88 demonstrates the excellent agreement between quadratic fits as a function of RST to the underlying data for the mean and standard deviation of the nonzero damaged areas for the 23-mm-thick OCB at the 4.07 m/s PGV level. - Figure 6-89 demonstrates that the percentiles on the gamma distributions provide a reasonable representation of the full range of nonzero damaged areas for the 23-mm-thick OCB at the 4.07 m/s PGV level. - The results for the 4.07 m/s PGV level provide an upper bound for all PGV levels, as discussed in Section 6.9.5.

Table 7-1. Summary of Corroborations of Abstraction Model Results to the Underlying Data (Continued)

Drip Shield Damaged Area—Lithophysal Units
- Figure 6-92 demonstrates the least-squares fit for the mean of *ln*(PGA-V+1) versus PGV-H1. - Figure 6-93 is a Q-Q plot that demonstrates the excellent comparison for the residuals of *ln*(PGA-V+1) relative to the least squares fit with a normal distribution. - Figure 6-94 demonstrates that the percentiles on the log-normal distributions provide an excellent representation of the full range of values for (PGA-V+1). - Figures 6-95 to 6-97 plot the cumulative distribution functions for damaged area at the 1.05 m/s, 2.44 m/s, and 4.07 m/s PGV levels, respectively. These data are directly represented in the damage abstraction as lookup tables that are a function of dynamic load and plate thickness in the TSPA.
Drip Shield Damage—Nonlithophysal Units
- Table 6-53 defines the probability of damage/plate failure from large rock block impacts. These data are directly represented in the damage abstraction as lookup tables that are a function of component thickness and PGV in the TSPA. - Table 6-54 defines the probability of Damage States 1 through 5. These data are directly represented in the damage abstraction as lookup tables that are a function of PGV and component thickness in the TSPA. - Figures 6-99 to 6-101 are Q-Q plots that demonstrate excellent comparison of the nonzero damaged areas on the crown of a drip shield with 15-mm-thick, 10-mm-thick, and 5-mm-thick plates, respectively, for the 2.44 m/s PGV level relative to gamma distributions. Q-Q plots relative to gamma distributions for the 0.4 m/s, 1.05 m/s, and 5.35 m/s PGV levels at the 15 mm, 10 mm, and 5 mm plate thicknesses are in output DTN: MO0703PASDSTAT.001, File *Nonlith Damage Abstraction for DS.xls*, worksheets “0.4 ms PGV 15-mm Plate,” “0.4 ms PGV 10-mm Plate,” “0.4 ms PGV 5-mm Plate,” “1.05 ms PGV 15-mm Plate,” “1.05 ms PGV 10-mm Plate,” “1.05 ms PGV 5-mm Plate,” “5.35 ms PGV 15-mm Plate,” “5.35 ms PGV 10-mm Plate,” and “5.35 ms PGV 5-mm Plate.” - Figures 6-102 to 6-104 demonstrate that the percentiles of the gamma distributions for the 15-mm-thick, 10-mm-thick, and 5-mm-thick plates, respectively, provide a reasonable representation of the full range of nonzero damaged areas on the crown of the drip shield.

7.2.2 Independent Technical Review by Dr. Gabriel Toro (Fifth Method in SCI-PRO-006)

An independent technical review for postdevelopment model validation has been performed by Dr. Gabriel R. Toro of Risk Engineering, Inc. Dr. Toro has not been involved in any aspect of the development of the seismic damage abstractions. The complete text of Dr. Toro’s review is in Appendix C. His general conclusions are as follows:

> *The preceding review identifies a large number of issues, but most of them represent areas needing clarification (it may well be, however, that the reviewer failed to understand them despite their clarity or that explanations were provided elsewhere in the report), or suggestions for improvements in future versions of the report.*
>
> *The only potentially serious issue that was identified in the review is the difficulty to establish the probabilities of nonzero damage for moderate and low values of PGV, given the limitation of 17 time histories. Increasing the number of time histories in order to attain a purely statistical resolution of this problem may be impractical. The preferred solution is probably to look for additional arguments to justify these probabilities of zero. If this does not succeed, one would have to devise alternative approaches that rely more on mechanics and probability and less on brute-force statistics (i.e., counting).*

> *In addition, the effects of the cutoff of 0.0024 m^2 should be investigated, and the potential problems identified in Sections 6.10.1.3 and 6.10.2.2 should be explained or resolved.*
>
> *Aside from these issues, my overall conclusion is that the abstractions contained in this report are adequate in terms of accuracy and treatment of uncertainty, despite the difficulty of this task. The approach followed is sound and it is well documented by means of Q-Q plots and plots of the data and quantiles as a function of PGV. In addition, the report contains an adequate characterization of the limitations of these abstractions.*

The results from this independent review are a confirmation of the adequacy of the seismic damage abstractions, based on Dr. Toro's overall conclusion. A YMP response to the detailed items identified by Dr. Toro is contained in Appendix C.

7.3 VALIDATION SUMMARY

The seismic damage abstractions have been validated by applying acceptance criteria based on an evaluation of the model's relative importance to the potential performance of the repository system. All validation requirements defined in the applicable TWP (SNL 2007 [DIRS 179869], Sections 2.3.2.1 and 2.3.2.2) have been fulfilled. Requirements for Level II model validation have also been satisfied. The model development activities and postdevelopment validation activities, as described here, establish the scientific bases for the seismic damage abstractions. Based on this, the *Seismic Consequences Abstraction* report and its components are considered to be sufficiently accurate and adequate for the representation of seismically induced damage to EBS components in the TSPA and for the level of confidence required for each component's damage abstraction relative to its importance to the performance of the repository system.

INTENTIONALLY LEFT BLANK

8. CONCLUSIONS

8.1 SUMMARY

The main purpose of this work is to develop abstractions for the response of EBS components to seismic hazards at a geologic repository at Yucca Mountain, Nevada, and to define the methodology for using these abstractions in a seismic scenario class for the TSPA compliance case for the license application. The seismic hazards are vibratory ground motion, fault displacement, and rockfall due to ground motion. The EBS components are the drip shield and the waste package. The following abstractions for seismically-induced damage have been developed:

- Abstractions for the kinematic response of the TAD-bearing waste package to vibratory ground motion
- Abstractions for the kinematic response of the codisposal waste package to vibratory ground motion
- Abstraction for lithophysal rubble volume and nonlithophysal rockfall volume in response to vibratory ground motion
- Fragility curves for the drip shield plates in response to the combined loads from vibratory ground motion and from rockfall that accumulates on the drip shield
- Fragility curves for the drip shield framework in response to the combined loads from vibratory ground motion and from rockfall that accumulates on the drip shield
- Abstractions for the TAD-bearing waste package surrounded by rubble in response to vibratory ground motion
- Abstraction for drip shield damage due to impact from large rock blocks induced by vibratory ground motion
- Abstraction for the drip shield partly or completely surrounded by lithophysal rubble in response to vibratory ground motion
- Damage to the waste package, drip shield, and fuel rod cladding from fault displacement.

The recommended implementation of these abstractions and their associated input parameters are defined in Section 6.12.2 and in Tables 6-88 to 6-93. The statistical analyses that define the abstractions are documented in output DTN: MO0703PASDSTAT.001. The computational algorithm and the TSPA parameters can be referenced through output DTN: MO0703PASEISDA.002. The recommended implementation of damage from fault displacement for criticality analyses is defined in Section 6.11.7. The calculations for Section 6.11.7 can be referenced through output DTN: MO0705FAULTABS.000. The calculation for the vertical component of PGA for the drip shield fragility calculations is documented in output DTN: MO0702PAFRAGIL.000. The calculation of the relative abundance of rock mass categories in lithophysal units is documented in output

DTN: MO0705ROCKMASS.000. The analysis for fault displacement standoff distance in Appendix D is documented in output DTN: MO0707STANDOFF.000.

The major limitations of the postclosure abstractions for the seismic scenario class are as follows:

- Waste package internals are assumed to degrade as structural elements after the OCB is first damaged by a seismic event (Assumption 5.4, Section 5). More exactly, the internals degrade as a structural component by the time of the next seismic event after the first seismic event that breaches the waste package. This approach maximizes damage estimates because a waste package with degraded internals has significantly greater deformation and rupture probability relative to a waste package with intact internals (see Sections 6.5.1 versus 6.5.2 and 6.6.1 versus 6.6.2). However, this approach underestimates the structural capacity of stainless steel internal components, such as the 2-in-thick inner vessel or the TAD canister itself, for screening of criticality-related issues during a 10,000-yr period.

- Spatial variability in the mechanical response of EBS components to vibratory ground motion has not been represented in the TSPA. In other words, damage to the waste package and drip shield from vibratory ground motion is constant throughout the repository for each seismic event. Although spatial variability is not included within the TSPA, it has been included in the kinematic calculations through the variability of friction factors on a package-by-package basis and in the abstraction of damaged areas for the two or three central waste packages in the kinematic calculations.

  Lack of spatial variability is reasonable for estimating the mean dose from the seismic scenario class. The mean dose is accurately estimated because the sum of the mean doses from groups of waste packages with different damage levels is equal to mean of the sum of the doses from the individual groups. In other words, using a constant mean value for the damage is an accurate approach for calculating the mean total dose from the repository. On the other hand, the coefficient of variation (i.e., the variability about the mean) of the total dose over all realizations is overestimated without spatial variability. If damage to waste package or drip shield is constant and perfectly correlated everywhere in the repository, realizations with very high or very low damage produce a more extreme response for the dose than a realization with damage that varies spatially between the high and low values.

- Structural response calculations for the waste package surrounded by rubble are based on the TAD-bearing waste package with degraded internals. Section 6.9.10 provides the rationale for using the results for the TAD-bearing waste package with degraded internals for the codisposal waste package with degraded internals.

- The internals of the waste package surrounded by rubble are always modeled as degraded. The use of degraded internals is consistent with the fact that the waste package becomes surrounded by rubble at late times, after the drip shield plates have failed and allowed rubble to contact the waste package. The use of degraded internals provides an upper bound because damage to a waste package with degraded internals is observed to be significantly greater than damage to a waste package with intact internals (see Sections 6.5.1 versus 6.5.2 and 6.6.1 versus 6.6.2).

These limitations should be considered during subsequent TSPA calculations.

8.2 HOW THE ACCEPTANCE CRITERIA ARE ADDRESSED

Acceptance Criterion 1: System Description and Model Integration Are Adequate.

(1) *Total system performance assessment adequately incorporates important design features, physical phenomena, and couplings, and uses consistent and appropriate assumptions throughout the mechanical disruption of engineered barrier abstraction process*.

Response: Section 6 explains the basis for the damage abstractions for the waste package (Sections 6.5, 6.6, 6.9, and 6.11) and drip shield (Sections 6.8, 6.10, and 6.11) in response to vibratory ground motion and fault displacement. The structural response calculations in *Mechanical Assessment of Degraded Waste Packages and Drip Shields Subject to Vibratory Ground Motion* (SNL 2007 [DIRS 178851]) include the mechanical coupling between EBS components and the mechanical coupling between rockfall and EBS components in defining damaged areas on the drip shield and waste package. Sections 6.6, 6.8, and 6.10.2 consider the potential damage to the EBS components from rockfall induced by vibratory ground motion. Section 6.7 defines the accumulation of rockfall from multiple seismic events, which is the basis for defining changes in the in-drift environment after drift collapse from a seismic event. Collectively, these sections address the methodology for incorporating design features, seismic response, and mechanical couplings within the damage abstractions for the seismic scenario class. Specific aspects of the methodology are as follows:

- The abstractions for damaged areas on the waste package are based on a statistically robust sampling of uncertain parameters, including the ground motion time histories, rock fracture patterns, rock compressive strength, and friction coefficients (Sections 6.5, 6.6, and 6.9). The abstractions are based on rockfall analyses and structural response calculations that use current design information, consistent assumptions, and consistent material properties.

- All abstractions are based on the mean hazard curves for ground motion and fault displacement, as discussed in Section 6.4. This approach is consistent with Brocoum (2001 [DIRS 159576], enclosure).

- Degradation of the drip shield and waste package is addressed by producing separate damage abstractions for discrete thicknesses of the OCB of the waste package and for discrete thickness of the drip shield components (plates and framework). These discrete thicknesses span the expected range of response for the peak dose assessment.

- Material properties for structural response calculations are based on a temperature of 60°C, resulting in material properties than maximize strain and deformation for 99% of the first 1,000,000 years after repository closure. A sensitivity study (SNL 2007 [DIRS 178851], Section 6.3.2.2.2) indicates that damaged area is relatively insensitive to the temperature for material properties, based on evaluations at 90°C and 150°C.

- Failure of the drip shield plates and drip shield framework are incorporated into the seismic scenario class through fragility curves. The potential for rupture or puncture of a highly degraded waste package is represented in the seismic damage abstractions. Rockfall is analyzed with state-of-the-art computer codes that are used for other drift degradation analyses.

- All relevant seismic-related FEPs are considered in Section 6.3. The seismic-related FEPs in Table 6-2 are directly included in these abstractions.

(2) The description of geological and engineering aspects of design features, physical phenomena, and couplings, that may affect mechanical disruption of engineered barriers, is adequate. For example, the description includes materials used in the current designs for EBS components, environmental effects (e.g., temperature, water chemistry, humidity, radiation, etc.) on these materials, and mechanical-failure processes and concomitant failure criteria used to assess the performance capabilities of these materials. Conditions and assumptions in the abstraction of mechanical disruption of engineered barriers are readily identified and consistent with the body of data presented in Section 6.

Response: The structural response calculations and kinematic calculations in *Mechanical Assessment of Degraded Waste Packages and Drip Shields Subject to Vibratory Ground Motion* (SNL 2007 [DIRS 178851]) include the mechanical coupling between EBS components and the mechanical coupling between rockfall and EBS components in defining damaged areas on the drip shield and waste package. Section 6 explains the basis for the damage abstractions for the waste package (Sections 6.5, 6.6, 6.9, and 6.11) and drip shield (Sections 6.8, 6.10, and 6.11) in response to vibratory ground motion and fault displacement. Sections 6.6, 6.8, and 6.10.2 consider the potential damage to the EBS components from rockfall induced by vibratory ground motion. Section 6.7 defines the accumulation of rockfall from multiple seismic events, which is the basis for defining changes in the in-drift environment after drift collapse from a seismic event. These sections collectively address the methodology for incorporating design features, physical phenomena, and the mechanical coupling between these phenomena in the seismic damage abstractions. Specific aspects of the methodology are as follows:

- All abstractions are based on the mean hazard curves for ground motion and fault displacement, as discussed in Section 6.4. This is consistent with Brocoum (2001 [DIRS 159576], enclosure).

- Degradation of the drip shield and waste package is addressed by producing separate damage abstractions for discrete thicknesses of the OCB of the waste package and for discrete thickness of the drip shield components (plates and framework). These discrete thicknesses span the expected range of response for the peak dose assessment.

- Material properties for structural response calculations are based on a temperature of 60°C, resulting in material properties that maximize strain and deformation for 99% of the first 1,000,000 years after repository closure. A sensitivity study (SNL 2007 [DIRS 178851], Section 6.3.2.2.2) indicates that damaged area is relatively insensitive to the temperature for material properties, based on evaluations at 90°C and 150°C.

- The failure mechanisms for the EBS components are defined in Section 6.1.4. The potential for tearing or rupture of EBS components is based on the ultimate tensile strain for Alloy 22 and Titanium Grade 7, with an appropriate "knockdown" factor for triaxiality. A second failure criterion is based on a RST for initiation of potential SCC, as explained in Section 6.1.4 and 6.1.5. The experimental basis for the second failure criterion is defined in the references cited in this report.

(3) *The abstraction of mechanical disruption of engineered barriers uses assumptions, technical bases, data, and models that are appropriate and consistent with other related U.S. Department of Energy abstractions. For example, assumptions used for mechanical disruption of engineered barriers are consistent with the abstraction of degradation of engineered barriers as given in Yucca Mountain Review Plan, Final Report (NRC 2003 [DIRS 163274], Section 2.2.1.3.1). The descriptions and technical bases provide transparent and traceable support for the abstraction of mechanical disruption of engineered barriers*.

Response: The seismic scenario class generally uses the same assumptions, technical bases, and data and process models as the nominal scenario class. The major exception to this is that failure of EBS components is based on mechanical failure mechanisms for the waste package and drip shield in response to multiple seismic events. Specific aspects of the seismic scenario class are as follows:

- All abstractions are based on the mean hazard curves for ground motion and fault displacement, as discussed in Section 6.4. This is consistent with Brocoum (2001 [DIRS 159576], enclosure).

- The analysis of rockfall for the seismic scenario class and for the nominal scenario class is based on the same set of computer codes (BSC 2004 [DIRS 166107]). Similarly, the LS-DYNA code is used for some design calculations and for all of the structural response calculations for the seismic scenario class (Sections 6.5 and 6.6).

- The thickness of EBS components at the time of the seismic event is an input to the seismic damage abstractions that is based on the results from general corrosion modeling in other the TSPA elements. This approach ensures consistency between general corrosion and the seismic damage abstractions.

- The RST for failure of Alloy 22 is also used as the threshold for initiation of potential SCC in the representation of corrosion processes on the waste package (SNL 2007 [DIRS 181953], Sections 6.2 and 6.5).

(4) *Boundary and initial conditions used in the total system performance assessment abstraction of mechanical disruption of engineered barriers are propagated throughout its abstraction approaches*.

Response: The structural response calculations and the coupled rockfall/structural response calculations are based on 17 ground motions at each of the 0.4 m/s, 1.05 m/s, 2.44 m/s, and 4.07 m/s PGV levels. Older rockfall analyses use 15 ground motions at the 1.05 m/s, 2.44 m/s, and 5.35 m/s PGV levels. The same sets of ground motions are used for both analyses; only the total number differs, and this difference is not considered significant. Other boundary and initial conditions that ensure consistency are as follows:

- The abstractions for damaged areas on the waste package are based on a statistically robust sampling of uncertain parameters, including the ground motion time histories, rock fracture patterns, rock compressive strength, and friction coefficients (Sections 6.5, 6.6, 6.7, and 6.9). The abstractions are based on rockfall analyses and structural response calculations that use consistent boundary conditions and initial conditions.

- The abstractions for the ultimate plastic load capacity of the drip shield plates and drip shield framework are based on a range of boundary conditions for the plates to encompass uncertainty in the structural response. The fragility curves for the drip shield plates and drip shield framework encompass this uncertainty as well as the uncertainties in rockfall loads and in the peak vertical acceleration as a function of PGV.

- All abstractions are based on the mean hazard curves for ground motion and fault displacement, as discussed in Section 6.4. This is consistent with Brocoum (2001 [DIRS 159576], enclosure).

- Material properties for structural response calculations are based on a temperature of 60°C, resulting in material properties that maximize strain and deformation for 99% of the first 1,000,000 years after repository closure. A sensitivity study (SNL 2007 [DIRS 178851], Section 6.3.2.2.2) indicates that damaged area is relatively insensitive to the temperature for material properties, based on evaluations at 90°C and 150°C.

(5) *Sufficient data and technical bases to assess the degree to which features, events, and processes have been included in this abstraction are provided.*

Response: The seismic-related FEPs in Table 6-2 are directly included in these abstractions. Damage to EBS components from ground motion, rockfall, drift collapse, and shear due to fault displacement have been considered in the abstractions for the seismic scenario class or in the structural response calculations that support the abstractions.

Acceptance Criterion 2: Data Are Sufficient for Model Justification.

(1) *Geological and engineering values, used in the license application to evaluate mechanical disruption of engineered barriers, are adequately justified. Adequate descriptions of how the data were used, interpreted, and appropriately synthesized into the parameters are provided.*

Response: The underlying data for geologic properties and for engineering material properties are generally not directly used in the development of the seismic abstractions, with the exception of the residual stress failure criteria for Alloy 22. Justification of the appropriate values is provided through external references. These justifications are based on experimental data for potential SCC, on handbook values and manufacturer's literature for the elastic and inelastic properties of EBS component materials, and on expert elicitation for the seismic hazard curves. Specific source documents that support development of the seismic scenario class are as follows:

- The residual stress failure criteria are based on experimental data for the initiation of potential SCC in Alloy 22 and Titanium Grade 7 (SNL 2007 [DIRS 181953], Section 6.2.2 for Alloy 22 and Section 6.8.3 for titanium alloys).

- The constitutive relationships for Alloy 22 and for Titanium Grade 7 are based on material properties in the published literature. More specifically, the Young's modulus, Poisson's ratio, yield strength, and friction factors are based on data in published literature (SNL 2007 [DIRS 178851], Section 4.1.2).

- Hazard curves are based on the results of an expert elicitation (CRWMS M&O 1998 [DIRS 103731]; DTN: MO0401MWDRPSHA.000 [DIRS 183046], with files listed in Table 4-1). The ground motion time histories for the rockfall analyses and structural response calculations have been developed in a manner that is consistent with and builds upon the results of this expert elicitation.

(3) *Data on geology of the natural system, engineering materials, and initial manufacturing defects, used in the total system performance assessment abstraction, are based on appropriate techniques. These techniques may include laboratory experiments, site-specific field measurements, natural analog research, and process-level modeling studies. As appropriate, sensitivity or uncertainty analyses used to support the U.S. Department of Energy total system performance assessment abstraction are adequate to determine the possible need for additional data.*

Response: As with the response to Subcriterion 1 above, the underlying data for the seismic scenario class are based on experimental data for potential SCC, on handbook values and manufacturer's literature for the elastic and inelastic properties of EBS component materials, and on expert elicitation. Specific sources that support development of the seismic scenario class are as follows:

- The residual stress failure criteria are based on experimental data for the initiation of potential SCC in Alloy 22 and Titanium Grade 7 (SNL 2007 [DIRS 181953], Section 6.2.2 for Alloy 22 and Section 6.8.3 for titanium alloys).

- The constitutive relationships for Alloy 22 and for Titanium Grade 7 are based on material properties in the published literature. More specifically, the Young's modulus, Poisson's ratio, yield strength, and friction factors are based on data in published literature (SNL 2007 [DIRS 178851], Section 4.1.2).

- Hazard curves are based on the results of an expert elicitation (CRWMS M&O 1998 [DIRS 103731]; DTN: MO0401MWDRPSHA.000 [DIRS 183046], with files listed in Table 4-1). The ground motion time histories for the rockfall analyses and structural response calculations have been developed in a manner that is consistent with and builds upon the results of this expert elicitation.

(4) *Engineered barrier mechanical failure models for disruption events are adequate. For example, these models may consider effects of prolonged exposure to the expected emplacement drift environment, material test results not specifically designed or performed for the Yucca Mountain site, and engineered barrier component fabrication flaws.*

Response: The long-term evolution of the EBS is discussed in Section 6.1.1 and the potential failure modes of EBS components are analyzed in Section 6.1.4. Based on this discussion, potential SCC and puncture or tearing at the ultimate tensile strain are the expected failure mechanism for EBS components during a seismic event. The constitutive relationships for Alloy 22 and for Titanium Grade 7 are based on material properties in the published literature. More specifically, the Young's modulus, Poisson's ratio, yield strength, and friction factors are based on data in published literature, as summarized in *Mechanical Assessment of Degraded Waste Packages and Drip Shields Subject to Vibratory Ground Motion* (SNL 2007 [DIRS 178851], Section 4.1.2).

Acceptance Criterion 3: Data Uncertainty Is Characterized and Propagated Through the Model Abstraction.

Data uncertainty is explicitly included in the seismic abstractions for the TSPA compliance case for the license application. In the PSHA, parameter uncertainty and model uncertainty were directly incorporated into the seismic hazard curves that are direct inputs to the fault displacement damage abstraction and the computational methodology for the seismic scenario class. Geotechnical parameter uncertainty is also included in the ground motion time histories that are direct inputs to the rockfall analyses and structural response calculations that provide the basis for the damage abstractions. Uncertainty in the input parameters for the structural response calculation and rockfall analyses is described next, followed by information on Subcriteria (1), (2), and (3) for this acceptance criterion.

Uncertainty in Input Parameters for Structural Response Calculations—The structural response calculations for the waste package and drip shield in response to vibratory ground motions include three major sources of data uncertainty: (1) the ground motion time histories (aleatory

uncertainty), (2) the metal-to-metal friction coefficient (epistemic uncertainty), and (3) the metal-to-rock friction coefficient (epistemic uncertainty):

- Multiple three-component ground motion time histories are used to represent the uncertainty in the seismic forcing functions at PGV levels of 0.4 m/s, 1.05 m/s, 2.44 m/s, and 4.07 m/s. One horizontal component of each ground motion set is scaled to have the same horizontal PGV because its uncertainty has been incorporated into the hazard curves during the PSHA. However, the peak ground acceleration and the duration of the time histories span a wide range of response.

- The metal-to-metal friction coefficient between the waste package and emplacement pallet varies from 0.2 to 0.8 to represent the uncertainty in its value. The friction coefficient affects the onset of sliding and dissipation of energy for the EBS components as a function of the amplitude of the ground motion. The static and dynamic friction coefficients are taken to be equal within the broad range (0.2 to 0.8) defined for this parameter. However, the importance of friction is anticipated to diminish with increasing ground motion level because the EBS components begin to slide almost immediately for high amplitude ground motions.

- The metal-to-rock friction coefficient between the emplacement pallet and the invert or between the drip shield and the invert varies from 0.2 to 0.8 to represent the uncertainty in its value. Again, the friction coefficient affects the onset of sliding and dissipation of energy for the unanchored EBS components as a function of the amplitude of the ground motion. However, the importance of friction is anticipated to diminish with increasing amplitude of the ground motions.

The selection of friction coefficients as major sources of uncertainty, in addition to the ground motions, is based on the potential for frictional forces to influence the kinematics of EBS components. Variability of friction coefficients may be important if damage varies significantly with the relative motions or impacts between adjacent structures.

The variations of these uncertain input parameters are simultaneously included in the structural response calculations for each ground motion at each seismic hazard level. This is accomplished by a Monte Carlo procedure that ensures robust sampling of the uncertain parameters over their full ranges. The Monte Carlo procedure and the sampled values of the three uncertain input parameters are described and documented in *Sampling of Stochastic Input Parameters for Rockfall and Structural Response Calculations Under Vibratory Ground Motion* (BSC 2004 [DIRS 169999], Section 6.4).

The results from the kinematic calculations and the associated catalogs for damaged areas are post-processed to determine the damaged areas on the waste package. The seismic abstractions for the waste package and drip shield make use of two failure criteria: a RST and the ultimate tensile strain. If the residual stress from mechanical damage exceeds the stress threshold for the barrier, then the affected area(s) are represented as a network of stress corrosion cracks. The RST for the waste package is based on a uniform distribution between 90% and 105% of the yield strength for Alloy 22. Postprocessing of the output from the combined kinematic calculations and catalogs determines the damaged areas corresponding to the 90%, 100%, and

105% RST levels. The coupled rockfall/structural response calculations for a waste package surrounded by rubble use a similar approach, although the damaged areas exceeding the RSTs are determined directly from the finely zoned finite-element mesh. The RST for Titanium Grade 7 in the drip shield plates is set to a constant value of 80% of its yield strength, so no uncertainty is propagated into the TSPA compliance case for damaged area on the drip shield from vibratory ground motion.

Calculations for large rock block impacts on drip shield in nonlithophysal units incorporate a similar methodology for plate failure, based on the ultimate tensile strain for Titanium Grade 7 and a "knockdown" factor of 2 (the maximum value) for triaxiality of the stress field. The use of the maximum triaxiality factor provides an upper bound for plate failure, so uncertainty has not been propagated into the TSPA compliance case.

Abstractions for rupture and puncture of the waste package are based on the accumulated deformations of the corroded OCB, based on the results from catalog calculations for damaged area and from the structural response calculations for a waste package surrounded by rubble.

Uncertainty in Input Parameters for Rockfall Analyses—All rockfall analyses include the ground motion time histories as a major source of uncertainty (Section 6.7). Fifteen ground motions represent the uncertainty in the seismic forcing functions at the 1.05-m/s, 2.44-m/s, and 5.35-m/s PGV levels. In the lithophysal units, the rock compressive strength is an uncertain input parameter that is represented as five discrete levels of rock strength, ranging from low (5 MPa) to high (30 MPa). In the nonlithophysal units, the synthetic fracture pattern is an uncertain input parameter. The synthetic fracture pattern is a representation of the fracture system geometry in three dimensions. The fracture geometry (but not the fracture properties; see below) is defined by 105 synthetic fracture patterns that are used in the rockfall analyses for the nonlithophysal units. The variations in these uncertain parameters are simultaneously included in the rockfall analyses at each seismic hazard level (BSC 2004 [DIRS 166107]).

The stochastic input parameters for the rockfall analyses are based on engineering judgment. For example, the rock compressive strength is a key parameter for drift failure in a continuum material, while the fracture geometry is a key parameter for identifying the size and location of rock blocks that can be shaken loose from the walls of a drift. Fracture properties such as cohesion and sliding friction can also be important in the nonlithophysal units but are represented using minimal values rather than being incorporated into the stochastic sampling scheme.

Rockfall analyses for lithophysal units predict rubble volume at three PGV levels. The rockfall volume from individual seismic events can accumulate over long periods of time, eventually filling the emplacement drifts. The uncertainty in rockfall volume in lithophysal and nonlithophysal units is explicitly represented in the seismic damage abstractions. Rockfall analyses for the nonlithophysal units predict a wide range of block sizes and velocities that can be ejected from the drift walls and impact the drip shield. More specifically, each rockfall analysis for the nonlithophysal unit predicts a complex, time-dependent sequence of rock blocks that impact the drip shield at varying locations and velocities. Individual impacts can cause damage to the drip shield and sometimes failure of the drip shield plates if the block has enough mass and kinetic energy. The sequence of nonlithophysal rock blocks during a given ground motion determines the total damage to the drip shield plates for the seismic damage abstractions.

Propagation of Uncertainty Into TSPA—The calculations of damaged area on the waste package and drip shield due to vibratory ground motions exhibit substantial variability induced by the uncertainties in seismic ground motions and other input parameters. This variability has been directly represented in the TSPA-LA by defining conditional probability distributions that are sampled during each realization of the seismic scenario class. For example:

- For a given value of PGV, the kinematic damage to the waste package from vibratory ground motion is represented as (1) the probability of rupture, (2) the probability of damage, and (3) if damage occurs, gamma distributions for the range of damaged area across all PGV levels of interest. A similar approach defines the probability of puncture, the probability of damage, and the conditional probability distributions for nonzero damaged area on a waste package surrounded by rubble. This approach explicitly propagates the uncertainty in the conditional damaged areas into the TSPA calculations for the seismic scenario class.

- The damage to the drip shield from large rock block impacts in nonlithophysal units is also represented as (1) the probability of damage/failure, (2) if damage/failure occur, the conditional probability for five different damage/failure states, and (3) the conditional (nonzero) damaged areas on the drip shield plates. This approach explicitly propagates the uncertainty in the failure state and nonzero damaged area into the TSPA calculations for the seismic scenario class.

- The uncertainty in the RST for Alloy 22 has been propagated into the abstraction for the TSPA-LA. The damaged areas on the waste packages are based on separate damage abstractions for the 90%, 100%, and 105% RST levels for Alloy 22. This approach directly maintains the range in damaged areas due to the uncertainty in the RST into the TSPA calculations for the seismic scenario class.

A final aspect of data uncertainty is related to the finite sample size that forms the basis for the seismic damage abstractions. The kinematic calculations for the TAD-bearing and codisposal waste packages produce up to 51 and 34 nonzero observations for damaged areas, respectively, at each PGV level. However, the number of nonzero observations can be significantly smaller at low PGV levels because many observations result in zero damage. A similar situation occurs with the calculations for the waste package surrounded by rubble. These calculations have a maximum of 17 observations at each PGV level, but many observations produce zero damage even at the 4.07 m/s PGV level. The process of developing the damage abstractions for a waste package surrounded by rubble acknowledges the limited number of data points, as discussed in Sections 6.9.3 and 6.9.5.

It is possible to augment the calculated values for the mean nonzero damaged areas with an analysis based on the central limit theorem in statistics. This approach has not been used for the seismic damage abstractions because the structural response calculations overestimate the damaged areas from seismic events. This bias arises from several sources:

- The kinematic methodology produces much larger values for damaged areas at the 0.4 m/s PGV level in comparison to the single waste package calculations. The computational results reported in Table 6-8 indicate that damaged areas for single waste

package calculations with a finely zoned finite-element grid are at least two orders of magnitude lower than the damaged areas with the kinematic methodology for the same ground motion and friction factors. The computational results reported in Table 6-23 for the codisposal waste package indicate that damaged areas for single waste package calculations are a factor of 2.7 to 38 less than the damaged areas with the kinematic methodology. This effect is anticipated to persist, although to a lesser extent, at higher PGV levels; however, it is not possible to quantify the difference in damaged areas at higher PGV levels with single waste package calculations[18].

- The structural response calculations are based on ground motions whose second horizontal and vertical components are unbounded, in the sense that these components can have PGV values that exceed the maximum value of 4.07 m/s on the bounded hazard curve. This effect is potentially significant at the 2.44 m/s and 4.07 m/s PGV levels.

- Material properties are based on 60°C, which results in material properties that maximize strain and deformation beyond 10,000 years after repository closure. The sensitivity to material properties is probably a secondary effect in comparison to the impacts from the kinematic methodology and unbounded ground motions, as discussed in the first two bullets above.

These bulletized features result in overestimates of the mean nonzero damaged areas for the seismic damage abstractions.

Discussion for Subcriteria (1), (2), and (3)

(1) *Models use parameter values, assumed ranges, probability distributions, and bounding assumptions that are technically defensible, reasonably account for uncertainties and variabilities, and do not result in an under-representation of the risk estimate*.

Response: The above discussion directly addresses the technical defensibility, uncertainty, and variabilities in parameter values. Specific examples include:

- Rockfall models and structural response calculations use parameter values and parameter ranges that are defensible and account for variabilities in rock properties and fracture patterns and uncertainties in ground motion time histories and friction coefficients.

- A major uncertainty in the response of the lithophysal zone is the rock compressive strength. This parameter is sampled from five levels for the rockfall analyses.

[18] Single waste package calculations cannot be performed at higher PGV levels because they do not represent the interactions between adjacent waste packages, resulting in different kinematics that are not comparable to the kinematic methodology with its multiple waste packages.

- Material properties for structural response calculations are based on a temperature of 60°C, resulting in material properties that maximize strain and deformation for 99% of the first 1,000,000 years after repository closure. A sensitivity study (SNL 2007 [DIRS 178851], Section 6.3.2.2.2) indicates that damaged area is relatively insensitive to the temperature for material properties, based on evaluations at 90°C and 150°C.

(2) *Process-level models used to represent mechanically disruptive events, within the emplacement drifts at the proposed Yucca Mountain repository, are adequate. Parameter values are adequately constrained by Yucca Mountain site data, such that the effects of mechanically disruptive events on engineered barrier integrity are not underestimated. Parameters within conceptual models for mechanically disruptive events are consistent with the range of characteristics observed at Yucca Mountain.*

Response: The LS-DYNA code and the UDEC code are used to determine the mechanical response of EBS components to vibratory ground motion. LS-DYNA is used for both design calculations and for the structural response calculations for the seismic scenario class (Sections 6.5 and 6.6). The analysis of rockfall for the seismic scenario class and for the nominal scenario class is based on state-of-the-art computer codes, UDEC and 3DEC, that can represent continuum and discontinuous response of rock in the lithophysal and nonlithophysal units of the repository (Section 6.9 and BSC 2004 [DIRS 166107]). The appropriateness of the parameters within LS-DYNA and for the rockfall analyses with UDEC are discussed in underlying documents, such as *Drift Degradation Analysis* (BSC 2004 [DIRS 166107]) and *Mechanical Assessment of Degraded Waste Packages and Drip Shields Subject to Vibratory Ground Motion* (SNL 2007 [DIRS 178851]), and are beyond the scope of this document.

(3) *Uncertainty is adequately represented in parameter development for conceptual models, process-level models, and alternative conceptual models considered in developing the assessment abstraction of mechanical disruption of engineered barriers. This may be done either through sensitivity analyses or use of conservative limits.*

Response: The discussion preceding Subcriterion (1) directly addresses the incorporation of parameter uncertainty into the abstraction process. Specific examples include:

- The rock compressive strength, a major uncertainty in the response of the lithophysal zone. This parameter is sampled from five levels for the rockfall analyses.

- The fracture geometry and fracture properties, a major uncertainty in the response of the nonlithophysal zone. These uncertainties are represented by the use of numerous synthetic joint fracture patterns that are generated in a statistically sound manner and incorporated into the rockfall analyses for the nonlithophysal zones.

- Material properties for structural response calculations, which are based on a temperature of 60°C, resulting in material properties that maximize strain and deformation for 99% of the first 1,000,000 years after repository closure. A sensitivity study (SNL 2007 [DIRS 178851], Section 6.3.2.2.2) indicates that damaged area is relatively insensitive to the temperature for material properties, based on evaluations at 90°C and 150°C.

- Two discrete thicknesses of the waste package outer corrosion barrier, 23 mm and 17 mm, which represent waste package degradation in the structural response calculations. Three discrete thicknesses of the drip shield plates, 15 mm, 10 mm, and 5 mm, represent drip shield degradation in the structural response calculations. These plate thicknesses correspond to reductions of 0 mm, 5 mm, and 10 mm in other components of the drip shield framework. These results provide the basis for the seismic damage abstractions, which must span the full range of EBS component thicknesses for the seismic scenario class.

- Uncertainty and variability in damaged areas of the waste package and drip shield, which are represented in the abstractions as conditional probability distributions that are sampled by the Monte Carlo approach for the TSPA compliance case for the license application.

Acceptance Criterion 4: Model Uncertainty Is Characterized and Propagated Through the Model Abstraction.

The seismic consequence abstractions have considered alternative conceptual models for the conditional probability distributions representing damaged areas on the waste package, damaged areas on the drip shield, and the volume of rockfall from a seismic event. Gamma distributions generally provided simpler and more accurate representations of the statistical observations than normal, log-normal, log-triangular, and Weibull distributions. The exception to the use of gamma distributions is that the fragility analyses have used log-normal representations to simplify manipulation of products and quotients of random variables.

The damage abstraction for fault displacement has been compared to an alternative conceptual model proposed by Waiting et al. (2003 [DIRS 164449]). There is excellent agreement between the damage abstraction in this report and the alternative conceptual model, considering that the alternate model is based on historical data for fault displacement in the western United States and that the damage abstraction is based on hazard curves specific to Yucca Mountain. For example, the number of fault intersections predicted by the damage abstraction is 214, versus 191 for the alternative conceptual model. Similarly, the probability weighted number of waste package failures is predicted to be 1.1×10^{-5} for the damage abstraction, within the range of 1.9×10^{-6} to 1.9×10^{-5} for the alternative conceptual model. This agreement provides added confidence in the damage abstraction for fault displacement.

Discussion for Subcriteria (2) and (3)

(2) *Consideration of conceptual model uncertainty is consistent with available site characterization data, laboratory experiments, field measurements, natural analog information and process-level modeling studies; and the treatment of conceptual model uncertainty does not result in an under-representation of the risk estimate*.

Response: The above discussion directly addresses how conceptual model uncertainty has been incorporated into the abstractions for the seismic scenario class. Specific examples include:

- The hazard curves for vibratory ground motion and fault displacement, which were developed from an expert elicitation (CRWMS M&O 1998 [DIRS 103731]). This elicitation process explicitly considered conceptual model uncertainty during its development of the hazard curves.

- Grid convergence studies and alternate finite-element representations, which have been evaluated for the rockfall models (BSC 2004 [DIRS 166107]) and for the structural response calculations (SNL 2007 [DIRS 178851]). Calculations and analyses have been performed with the most appropriate numerical representations, so this particular source of model uncertainty is not propagated through the damage abstractions for the TSPA compliance case for the license application.

(3) *Appropriate alternative modeling approaches are investigated that are consistent with available data and current scientific knowledge, and appropriately consider their results and limitations using tests and analyses that are sensitive to the processes modeled.*

Response: The discussion before Subcriterion (2) directly addresses how alternate modeling approaches are addressed. Specific examples include:

- The hazard curves for vibratory ground motion and fault displacement, which are developed from an expert elicitation (CRWMS M&O 1998 [DIRS 103731]). The individual groupings of experts developed and weighted alternative conceptual models for defining the seismic hazards at Yucca Mountain.

- Grid convergence studies and alternate finite element representations, which have been performed for the rockfall models (BSC 2004 [DIRS 166107]) and for the structural response calculations (SNL 2007 [DIRS 178851]). Calculations and analyses have been performed with the most appropriate numerical representations, so this particular source of model uncertainty is not propagated through the damage abstractions for the TSPA compliance case for the license application.

- Alternative modeling approaches, which have been evaluated for the conceptual and computational models of lithophysal and nonlithophysal rock (BSC 2004 [DIRS 166107]) but are beyond the scope of this document.

- The damage abstraction for fault displacement, which has been compared to an alternative conceptual model proposed by Waiting et al. (2003 [DIRS 164449]).

Acceptance Criterion 5: Model Abstraction Output Is Supported by Objective Comparisons.

(1) *Models implemented in this total system performance assessment abstraction provide results consistent with output from detailed process-level models and/or empirical observations (laboratory and field testings and/or natural analogs).*

Response: The consistency of the seismic damage abstractions with the detailed output from the structural response calculations and coupled rockfall/structural response calculations is summarized in Table 8-1, which is identical to Table 7-1.

(2) *Outputs of mechanical disruption of engineered barrier abstractions reasonably produce or bound the results of corresponding process-level models, empirical observations, or both.*

Response: Objective comparisons between the calculated damage to EBS components and the corresponding abstractions for the TSPA compliance case are presented in Table 8-1.

(3) *Well-documented procedures, that have been accepted by the scientific community to construct and test the mathematical and numerical models, are used to simulate mechanical disruption of engineered barriers.*

Response: The objective comparisons in Table 8-1 are an accepted method for comparing abstractions with the underlying data from structural response calculations or for defining the bounding response of EBS components.

Table 8-1. Comparison of Seismic Abstractions with Objective Evidence

Kinematic Response of TAD-Bearing Waste Package	
- 23-mm-Thick OCB with Intact Internals and 90% RST to 105% RST	- Probability of damage is presented in Table 6-4 and in Figure 6-8. These data are directly represented in the damage abstraction as a lookup table that is a function of PGV and RST in the TSPA. - Figure 6-9 is a Q-Q plot that demonstrates the very good comparison of nonzero damaged area at 4.07 m/s PGV level and 90% RST with a gamma distribution. - The results in Figure 6-9 provide an upper bound for all PGV levels less than 4.07 m/s and all RST levels greater than 90%.
- 23-mm-Thick OCB with Degraded Internals and 90% RST	- Figure 6-11 demonstrates that a linear least-squares fit in log space provides an excellent representation of the data for probability of incipient rupture. - Figure 6-12 demonstrates the excellent agreement between the power-law fits and the data for incipient rupture and (immediate) rupture. - Probability of damage is presented in a table and figure in output DTN: MO0703PASDSTAT.001, File *Kinematic Damage Abstraction 23-mm Degraded.xls*, worksheet "Prob of Damage – New." These data are directly represented in the damage abstraction as a lookup table that is a function of PGV and RST in the TSPA. - The Q-Q plots for nonzero damaged areas at 0.4 m/s, 1.05 m/s, 2.44 m/s, and 4.07 m/s PGV levels demonstrate that gamma distributions provide an excellent representation of the nonzero damaged areas, as documented in output DTN: MO0703PASDSTAT.001, File *Kinematic Damage Abstraction 23-mm Degraded.xls*, worksheet "Gamma for 90%_d23."

Table 8-1. Comparison of Seismic Abstractions with Objective Evidence (Continued)

Kinematic Response of TAD-Bearing Waste Package (Continued)	
	- Quadratic fits as a function of PGV provide an excellent fit to the underlying data for the mean and standard deviation of the nonzero damaged areas, as documented in output DTN: MO0703PASDSTAT.001, File *Kinematic Damage Abstraction 23-mm Degraded.xls*, worksheet "Gamma for 90%_d23." - The percentiles on a gamma distribution provide a reasonable representation of the full range of nonzero damaged areas, as documented in output DTN: MO0703PASDSTAT.001, File *Kinematic Damage Abstraction 23-mm Degraded.xls*, worksheet "Gamma for 90%_d23."
- 23-mm-Thick OCB with Degraded Internals and 90% RST to 105% RST	- The quadratic fits as a function of PGV and RST are in excellent agreement with the underlying data for the mean and standard deviation of the nonzero damaged areas, as documented in output DTN: MO0703PASDSTAT.001, File *Kinematic Damage Abstraction 23-mm Degraded.xls*, worksheet "Dependence on RST."
- 17-mm-Thick OCB with Degraded Internals and 90% RST	- Figure 6-11 demonstrates that a linear least-squares fit in log space provides an excellent representation of the data for probability of incipient rupture. - Figure 6-12 demonstrates the excellent agreement between the power-law fits and the data for incipient rupture and (immediate) rupture. - Probability of nonzero damage is presented in Table 6-11 and Figure 6-14. These data are directly represented in the damage abstraction as a lookup table that is a function of PGV and RST in the TSPA. - Figures 6-15 to 6-18 are Q-Q plots that demonstrate the very-good to excellent comparisons of the nonzero damaged areas at 0.4 m/s, 1.05 m/s, 2.44 m/s, and 4.07 m/s PGV levels with gamma distributions. - Figure 6-19 demonstrates the excellent agreement between quadratic fits as a function of PGV to the underlying data for the mean and standard deviation of the nonzero damaged areas. - Figure 6-20 demonstrates that the percentiles on the gamma distributions provide a reasonable representation of the full range of nonzero damaged areas.
- 17-mm-Thick OCB with Degraded Internals and 90% RST to 105% RST	- Figures 6-23 and 6-24 demonstrate the excellent agreement between quadratic fits as a function of PGV and RST and the underlying data for the mean and standard deviation of the nonzero damaged areas.
Kinematic Response of CDSP Waste Package	
- 23-mm-Thick OCB with Intact Internals and 90% RST	- Probability of damage is presented in Table 6-16 and in Figure 6-27. These data are directly represented in the damage abstraction as a lookup table that is a function of PGV and RST in the TSPA. - Figures 6-28 to 6-31 are Q-Q plots that demonstrate the very good to excellent comparisons of the nonzero damaged areas at the 0.4 m/s, 1.05 m/s, 2.44 m/s, and 4.07 m/s PGV levels with gamma distributions. - Figure 6-32 demonstrates the excellent agreement between quadratic fits as a function of PGV and the underlying data for the mean and standard deviation of the nonzero damaged areas. - Figure 6-33 demonstrates that the percentiles on the gamma distributions provide a reasonable representation of the full range of nonzero damaged areas.

Table 8-1. Comparison of Seismic Abstractions with Objective Evidence (Continued)

Kinematic Response of CDSP Waste Package (Continued)	
- 23-mm-Thick OCB with Intact Internals and 90% RST to 105% RST	- Figures 6-34 and 6-35 demonstrate the excellent agreement between quadratic fits as a function of PGV and RST to the underlying data for the mean and standard deviation of the nonzero damaged areas.
- 23-mm-Thick OCB with Degraded Internals and 90% RST	- Figure 6-38 demonstrates the excellent agreement between the power-law fits and the data for incipient rupture and (immediate) rupture. - Probability of damage is presented in a table and figure in output DTN: MO0703PASDSTAT.001, File *CDSP Kinematic Damage Abstraction 23-mm Degraded.xls*, worksheet "Prob of Damage – New." These data are directly represented in the damage abstraction as a lookup table that is a function of PGV and RST in the TSPA. - The Q-Q plots for nonzero damaged areas at 0.4 m/s, 1.05 m/s, 2.44 m/s, and 4.07 m/s PGV levels demonstrate that gamma distributions provide an excellent representation of the nonzero damaged areas, as documented in output DTN: MO0703PASDSTAT.001, File *CDSP Kinematic Damage Abstraction 23-mm Degraded.xls*, worksheet "Gamma for 90%_d23." - Quadratic fits as a function of PGV provide an excellent fit to the underlying data for the mean and standard deviation of the nonzero damaged areas, as documented in output DTN: MO0703PASDSTAT.001, File *CDSP Kinematic Damage Abstraction 23-mm Degraded.xls*, worksheet "Gamma for 90%_d23." - The percentiles on a gamma distribution provide a reasonable representation of the full range of nonzero damaged areas, as documented in output DTN: MO0703PASDSTAT.001, File *CDSP Kinematic Damage Abstraction 23-mm Degraded.xls*, worksheet "Gamma for 90%_d23."
- 23-mm-Thick OCB with Degraded Internals and 90% RST to 105% RST	- The quadratic fits as a function of PGV and RST are in excellent agreement with the underlying data for the mean and standard deviation of the nonzero damaged areas, as documented in output DTN: MO0703PASDSTAT.001, File *CDSP Kinematic Damage Abstraction 23-mm Degraded.xls*, worksheet "Dependence on RST."
- 17-mm-Thick OCB with Degraded Internals and 90% RST	- Figure 6-38 demonstrates the excellent agreement between the power law fits and the data for incipient rupture and (immediate) rupture. - Probability of damage is presented in Table 6-26 and Figure 6-40. These data are directly represented in the damage abstraction as a lookup table that is a function of PGV and RST in the TSPA. - Figures 6-41 to 6-44 are Q-Q plots that demonstrate the very good to excellent comparisons of the nonzero damaged areas at 0.4 m/s, 1.05 m/s, 2.44 m/s, and 4.07 m/s PGV levels with gamma distributions. - Figure 6-45 demonstrates the excellent agreement between quadratic fits as a function of PGV to the underlying data for the mean and standard deviation of the nonzero damaged areas. - Figure 6-46 demonstrates that the percentiles on the gamma distributions provide a reasonable representation of the full range of nonzero damaged areas.
- 17-mm-Thick OCB with Degraded Internals and 90% RST to 105% RST	- Comparisons of the quadratic fits as a function of PGV and RST to the underlying data for the mean and standard deviation of the nonzero damaged areas are presented in Figures 6-49 and 6-50. These figures demonstrate excellent agreement with the underlying data for the mean and standard deviation of the nonzero damaged areas.

Table 8-1. Comparison of Seismic Abstractions with Objective Evidence (Continued)

Lithophysal Rubble Volume
- Probability of rockfall is presented in Table 6-29 and Figure 6-52. These data are directly represented in the damage abstraction as a lookup table that is a function of PGV in the TSPA. - Figure 6-53 through Figure 6-55 are Q-Q plots that demonstrate the very good to excellent comparisons of the nonzero rockfall volumes at 0.4 m/s, 1.05 m/s, and 2.44 m/s PGV levels with gamma distributions. - Figure 6-56 demonstrates the excellent agreement between quadratic fits as a function of PGV to the underlying data for the mean and standard deviation of the nonzero rockfall volumes. - Figure 6-57 demonstrates that the percentiles on the gamma distributions provide a reasonable representation of the full range of nonzero rockfall volumes.
Nonlithophysal Rockfall Volume
- Probability of rockfall in the nonlithophysal units is represented by the data for the lithophysal units in Table 6-29 and Figure 6-52. The lithophysal data provide an upper bound for the probability of rockfall in the nonlithophysal units. These data are directly represented in the damage abstraction as a lookup table that is a function of PGV in the TSPA. - Figures 6-59 to 6-61 are Q-Q plots that demonstrate the very-good to excellent comparisons of the nonzero rockfall volumes at 1.05 m/s, 2.44 m/s, and 5.35 m/s PGV levels with gamma distributions. - Figure 6-62 demonstrates the excellent agreement between quadratic fits as a function of PGV to the underlying data for the mean and standard deviation of the nonzero rockfall volumes. - Figure 6-63 demonstrates that the percentiles on the gamma distributions provide a reasonable representation of the full range of nonzero rockfall volumes.
Drip Shield Plate Fragility
- Figure 6-64 demonstrates the least-squares fit for the mean of *ln*(PGA-V) versus PGV-H1. - Figure 6-65 is a Q-Q plot that demonstrates the excellent comparison for the residuals of *ln*(PGA-V) relative to the least squares fit with a normal distribution. - Figure 6-66 demonstrates that the percentiles on the log-normal distributions provide an excellent representation of the full range of values for PGA-V. - Figure 6-67 is a Q-Q plot that demonstrates the excellent comparison for the residuals of the lithophysal rockfall load on the crown of the drip shield relative to the average crown pressure with a log-normal distribution. - Figure 6-68 demonstrates that a linear function of plate thickness provides an excellent fit for the ultimate plastic load capacity data for the drip shield plates. - Figures 6-69 to 6-71 plot the probability of plate rupture as a function of PGV and plate thickness. These data are directly represented in the damage abstraction as a lookup table that is a function of plate thickness, rockfall load, and PGV in the TSPA.
Drip Shield Framework Fragility
- Figure 6-64 demonstrates the least-squares fit for the mean of *ln*(PGA-V) versus PGV-H1. - Figure 6-65 is a Q-Q plot that demonstrates the excellent comparison for the residuals of *ln*(PGA-V) relative to the least squares fit with a normal distribution. - Figure 6-66 demonstrates that the percentiles on the log-normal distributions provide an excellent representation of the full range of values for PGA-V. - Figure 6-67 is a Q-Q plot that demonstrates the excellent comparison for the residuals of the lithophysal rockfall load on the crown of the drip shield relative to the average crown pressure with a log-normal distribution. - Figure 6-72 demonstrates that a linear function of plate thickness provides an excellent representation of the mean value of the ultimate plastic load capacity data for the drip shield framework. - Figures 6-74 to 6-76 plot the probability of framework collapse as a function of PGV and plate thickness. These data are directly represented in the damage abstraction as a lookup table that is a function of component thickness, rockfall load, and PGV in the TSPA.

Table 8-1. Comparison of Seismic Abstractions with Objective Evidence (Continued)

TAD-Bearing Waste Package with Degraded Internals and Surrounded by Rubble
- Figure 6-78 demonstrates that a linear least-squares fit in *ln* space provides an excellent representation of the data for probability of puncture. - Figure 6-79 demonstrates the excellent agreement between the power law fits and the data for puncture. - Figures 6-80 and 6-81 present the probability of damage for the 23-mm-thick and 17-mm-thick OCBs, respectively. These data, which are summarized in Table 6-44, are directly represented in the damage abstraction as a lookup table that is a function of PGV and RST in the TSPA. - Figures 6-82 and 6-83 are Q-Q plots that demonstrate the very good comparisons of the nonzero damaged areas with gamma distributions for the 17-mm-thick OCB at the 4.07 m/s PGV level for 90% RST and 100% RST, respectively. - Figure 6-84 demonstrates the excellent agreement between quadratic fits as a function of RST to the underlying data for the mean and standard deviation of the nonzero damaged areas for the 17-mm-thick OCB at the 4.07 m/s PGV level. - Figure 6-85 demonstrates that the percentiles on the gamma distributions provide a reasonable representation of the full range of nonzero damaged areas for the 17-mm-thick OCB at the 4.07 m/s PGV level. - The results for the 4.07 m/s PGV level provide an upper bound for all PGV levels for the 17-mm-thick OCB, as discussed in Section 6.9.3. - Figure 6-87 is a Q-Q plot that demonstrates reasonable comparison of the nonzero damaged areas with a gamma distribution for the 23-mm-thick OCB at 4.07 m/s PGV levels and 90% RST. - Figure 6-88 demonstrates the excellent agreement between quadratic fits as a function of RST to the underlying data for the mean and standard deviation of the nonzero damaged areas for the 23-mm-thick OCB at the 4.07 m/s PGV level. - Figure 6-89 demonstrates that the percentiles on the gamma distributions provide a reasonable representation of the full range of nonzero damaged areas for the 23-mm-thick OCB at the 4.07 m/s PGV level. - The results for the 4.07 m/s PGV level provide an upper bound for all PGV levels, as discussed in Section 6.9.5.
Drip Shield Damaged Area—Lithophysal Units
- Figure 6-92 demonstrates the least-squares fit for the mean of *ln*(PGA-V+1) versus PGV-H1. - Figure 6-93 is a Q-Q plot that demonstrates the excellent comparison for the residuals of *ln*(PGA-V+1) relative to the least squares fit with a normal distribution. - Figure 6-94 demonstrates that the percentiles on the log-normal distributions provide an excellent representation of the full range of values for (PGA-V+1). - Figures 6-95 to 6-97 plot the cumulative distribution functions for damaged area at the 1.05 m/s, 2.44 m/s, and 4.07 m/s PGV levels, respectively. These data are directly represented in the damage abstraction as lookup tables that are a function of dynamic load and plate thickness in the TSPA.
Drip Shield Damage—Nonlithophysal Units
- Table 6-53 defines the probability of damage/plate failure from large rock block impacts. These data are directly represented in the damage abstraction as lookup tables that are a function of component thickness and PGV in the TSPA. - Table 6-54 defines the probability of Damage States 1 through 5. These data are directly represented in the damage abstraction as lookup tables that are a function of PGV and component thickness in the TSPA. - Figures 6-99 to 6-101 are Q-Q plots that demonstrate excellent comparison of the nonzero damaged areas on the crown of a drip shield with 15-mm-thick, 10-mm-thick, and 5-mm-thick plates, respectively, for the 2.44 m/s PGV level relative to gamma distributions. Q-Q plots relative to gamma distributions for the 0.4 m/s, 1.05 m/s, and 5.35 m/s PGV levels at the 15mm, 10 mm, and 5 mm plate thicknesses are in output DTN: MO0703PASDSTAT.001, File *Nonlith Damage Abstraction for DS.xls*, worksheets “0.4 ms PGV 15-mm Plate,” “0.4 ms PGV 10-mm Plate,” “0.4 ms PGV 5-mm Plate,” “1.05 ms PGV 15-mm Plate,” “1.05 ms PGV 10-mm Plate,” “1.05 ms PGV 5-mm Plate,” “5.35 ms PGV 15-mm Plate,” “5.35 ms PGV 10-mm Plate,” and “5.35 ms PGV 5-mm Plate.” - Figures 6-102 to 6-104 demonstrate that the percentiles of the gamma distributions for the 15-mm-thick, 10-mm-thick, and 5-mm-thick plates, respectively, provide a reasonable representation of the full range of nonzero damaged areas on the crown of the drip shield.

9. INPUTS AND REFERENCES

The following is a list of the references cited in this document. Column 2 represents the unique six digit Document Input Reference System (DIRS) number, which is placed in the text following the reference callout (e.g., BSC 2004 [DIRS 170027]). The purpose of these numbers is to assist in locating a specific reference. Within the reference list, multiple sources by the same author (e.g., BSC 2004) are sorted numerically by DIRS number.

9.1 DOCUMENTS CITED

100029 Barr, D.L.; Moyer, T.C.; Singleton, W.L.; Albin, A.L.; Lung, R.C.; Lee, A.C.; Beason, S.C.; and Eatman, G.L.W. 1996. *Geology of the North Ramp — Stations 4+00 to 28+00, Exploratory Studies Facility, Yucca Mountain Project, Yucca Mountain, Nevada.* Denver, Colorado: U.S. Geological Survey. ACC: MOL.19970106.0496.

126811 Brady, B.H.G. and Brown, E.T. 1985. *Rock Mechanics for Underground Mining.* London, United Kingdom: George Allen and Unwin. TIC: 226226.

159576 Brocoum, S. 2001. "Transmittal of Report Addressing Key Technical Issues (KTI) Structural Deformation and Seismicity (SDS)." Letter from S. Brocoum (DOE/YMSCO) to C.W. Reamer (NRC), October 25, 2001, OL&RC:TCG-0140, with enclosure. ACC: MOL.20020304.0297; MOL.20030714.0094.

169527 Brown, E.T. 2003. *Block Caving Geomechanics.* JKMRC Monograph Series in Mining and Mineral Processing 3. Indooroopilly, Queensland, Australia: Julius Kruttschnitt Mineral Research Centre. TIC: 256115.

162293 BSC (Bechtel SAIC Company) 2003. *21-PWR Waste Package Side and End Impacts.* 000-00C-DSU0-01000-000-00B. Las Vegas, Nevada: Bechtel SAIC Company. ACC: ENG.20030227.0067; ENG.20050829.0004.

168030 BSC 2004. *Characterize Framework for Seismicity and Structural Deformation at Yucca Mountain, Nevada.* ANL-CRW-GS-000003 REV 00 Errata 001. Las Vegas, Nevada: Bechtel SAIC Company. ACC: MOL.20000510.0175; DOC.20040223.0007.

170027 BSC 2004. *Development of Earthquake Ground Motion Input for Preclosure Seismic Design and Postclosure Performance Assessment of a Geologic Repository at Yucca Mountain, NV.* MDL-MGR-GS-000003 REV 01. Las Vegas, Nevada: Bechtel SAIC Company. ACC: DOC.20041111.0006; DOC.20051130.0003.

166107 BSC 2004. *Drift Degradation Analysis.* ANL-EBS-MD-000027 REV 03. Las Vegas, Nevada: Bechtel SAIC Company. ACC: DOC.20040915.0010; DOC.20050419.0001; DOC.20051130.0002; DOC.20060731.0005.

170029 BSC 2004. *Geologic Framework Model (GFM2000)*. MDL-NBS-GS-000002 REV 02. Las Vegas, Nevada: Bechtel SAIC Company. ACC: DOC.20040827.0008.

169753 BSC 2004. *Mechanical Assessment of the Drip Shield Subject to Vibratory Motion and Dynamic and Static Rock Loading.* CAL-WIS-AC-000002 REV 00A. Las Vegas, Nevada: Bechtel SAIC Company. ACC: DOC.20041028.0004; DOC.20050830.0003.

169999 BSC 2004. *Sampling of Stochastic Input Parameters for Rockfall Calculations and for Structural Response Calculations Under Vibratory Ground Motion.* ANL-EBS-PA-000009 REV 01. Las Vegas, Nevada: Bechtel SAIC Company. ACC: DOC.20040901.0004.

173172 BSC 2005. *Mechanical Assessment of the Waste Package Subject to Vibratory Ground Motion.* CAL-WIS-AC-000001 REV 0B. Las Vegas, Nevada: Bechtel SAIC Company. ACC: DOC.20050823.0001; DOC.20050830.0005.

170137 BSC 2005. *Peak Ground Velocities for Seismic Events at Yucca Mountain, Nevada.* ANL-MGR-GS-000004 REV 00. Las Vegas, Nevada: Bechtel SAIC Company. ACC: DOC.20050223.0002; DOC.20050725.0002.

103635 Budnitz, R.J.; Apostolakis, G.; Boore, D.M.; Cluff, L.S.; Coppersmith, K.J.; Cornell, C.A.; and Morris, P.A. 1997. *Recommendations for Probabilistic Seismic Hazard Analysis: Guidance on the Uncertainty and Use of Experts.* NUREG/CR-6372. Two volumes. Washington, D.C.: U.S. Nuclear Regulatory Commission. TIC: 235076; 235074.

144357 Chun, R.; Witte, M.; and Schwartz, M. 1987. *Dynamic Impact Effects on Spent Fuel Assemblies.* UCID-21246. Livermore, California: Lawrence Livermore National Laboratory. ACC: HQX.19881020.0031.

103731 CRWMS M&O (Civilian Radioactive Waste Management System Management and Operating Contractor) 1998. *Probabilistic Seismic Hazard Analyses for Fault Displacement and Vibratory Ground Motion at Yucca Mountain, Nevada.* Milestone SP32IM3, September 23, 1998. Three volumes. Las Vegas, Nevada: CRWMS M&O. ACC: MOL.19981207.0393.

101557 Day, W.C.; Potter, C.J.; Sweetkind, D.S.; Dickerson, R.P.; and San Juan, C.A. 1998. *Bedrock Geologic Map of the Central Block Area, Yucca Mountain, Nye County, Nevada.* Miscellaneous Investigations Series Map I-2601. Washington, D.C.: U.S. Geological Survey. ACC: MOL.19980611.0339.

155943 DOE (U.S. Department of Energy) 2002. *Yucca Mountain Science and Engineering Report.* DOE/RW-0539, Rev. 1. Washington, D.C.: U.S. Department of Energy, Office of Civilian Radioactive Waste Management. ACC: MOL.20020404.0042.

182051 DOE 2007. *Quality Assurance Requirements and Description.* DOE/RW-0333P, Rev. 19. Washington, D. C.: U.S. Department of Energy, Office of Civilian Radioactive Waste Management. ACC: DOC.20070717.0006.

161776 Duncan, J.M.; Byrne, P.; Wong, K.S.; and Mabry, P. 1980. *Strength, Stress-Strain and Bulk Modulus Parameters for Finite Element Analyses of Stresses and Movements in Soil Masses.* UCB/GT/80-01. Berkeley, California: University of California, College of Engineering, Office of Research Services. TIC: 253873.

157677 Eatman, G.L.W.; Singleton, W.L.; Moyer, T.C.; Barr, D.L.; Albin, A.L.; Lung, R.C.; and Beason, S.C. 1997. *Geology of the South Ramp - Station 55+00 to 78+77, Exploratory Studies Facility, Yucca Mountain Project, Yucca Mountain, Nevada.* Denver, Colorado: U.S. Department of Energy. ACC: MOL.19980127.0396.

166226 GoldSim Technology Group. 2003. *User's Guide, GoldSim Probabilistic Simulation Environment.* Version 8.01. Redmond, Washington: Golder Associates. TIC: 255170.

101966 Goodman, R.E. 1980. *Introduction to Rock Mechanics*. New York, New York: John Wiley & Sons. TIC: 218828.

146529 Hahn, G.J. and Shapiro, S.S. 1967. *Statistical Models in Engineering.* New York, New York: John Wiley & Sons. TIC: 247729.

162198 Konietzky, H. 2003. "Preface." *Numerical Modeling in Micromechanics via Particle Methods, Proceedings of the 1st International PFC Symposium, Gelsenkirchen, Germany, 6-8 November 2002.* Konietzky, H., ed. Page ix. Exton, Pennsylvania: A.A. Balkema. TIC: 253950.

179773 Laubscher, D.H. 1994. "Cave Mining--State of the Art." *Journal of the South African Institute of Mining and Metallurgy, 94,* (10), 279-293. Johannesburg, South Africa: South African Institute of Mining and Metallurgy. TIC: 259288.

163996 McGarr, A. 1984. "Some Applications of Seismic Source Mechanism Studies to Assessing Underground Hazard." *Proceedings of the 1st International Congress on Rockbursts and Seismicity in Mines, Johannesburg, 1982.* Gay, N.C. and Wainwright, E.H., eds. Pages 199-208. Johannesburg, South Africa: South African Institute of Mining and Metallurgy. TIC: 254652.

157510 McGuire, R.K.; Silva, W.J.; and Costantino, C.J. 2001. *Technical Basis for Revision of Regulatory Guidance on Design Ground Motions: Hazard- and Risk-Consistent Ground Motion Spectra Guidelines.* NUREG/CR-6728. Washington, D.C.: U.S. Nuclear Regulatory Commission. TIC: 251294.

106342 Menges, C.M. and Whitney, J.W. 1996. "Distribution of Quaternary Faults in the Site Area." Chapter 4.2 of *Seismotectonic Framework and Characterization of Faulting at Yucca Mountain, Nevada.* Whitney, J.W., ed. Milestone 3GSH100M. Denver, Colorado: U.S. Geological Survey. TIC: 237980. ACC: MOL.19970129.0041.

149850 Mongano, G.S.; Singleton, W.L.; Moyer, T.C.; Beason, S.C.; Eatman, G.L.W.; Albin, A.L.; and Lung, R.C. 1999. *Geology of the ECRB Cross Drift - Exploratory Studies Facility, Yucca Mountain Project, Yucca Mountain, Nevada.* Deliverable SPG42GM3. Denver, Colorado: U.S. Geological Survey. ACC: MOL.20000324.0614.

151246 Newmark, N.M. and Rosenblueth, E. 1971. *Fundamentals of Earthquake Engineering.* Civil Engineering and Engineering Mechanics Series. Englewood Cliffs, New Jersey: Prentice-Hall. TIC: 248548.

163274 NRC (U.S. Nuclear Regulatory Commission) 2003. *Yucca Mountain Review Plan, Final Report.* NUREG-1804, Rev. 2. Washington, D.C.: U.S. Nuclear Regulatory Commission, Office of Nuclear Material Safety and Safeguards. TIC: 254568.

102072 Sanders, T.L.; Seager, K.D.; Rashid, Y.R.; Barrett, P.R.; Malinauskas, A.P.; Einziger, R.E.; Jordan, H.; Duffey, T.A.; Sutherland, S.H.; and Reardon, P.C. 1992. *A Method for Determining the Spent-Fuel Contribution to Transport Cask Containment Requirements.* SAND90-2406. Albuquerque, New Mexico: Sandia National Laboratories. ACC: MOV.19960802.0116.

180778 SNL (Sandia National Laboratories) 2007. *General Corrosion and Localized Corrosion of the Drip Shield.* ANL-EBS-MD-000004 REV 02 ADD 01. Las Vegas, Nevada: Sandia National Laboratories. ACC: DOC.20060427.0002; DOC.20070807.0004.

178851 SNL 2007. *Mechanical Assessment of Degraded Waste Packages and Drip Shields Subject to Vibratory Ground Motion.* MDL-WIS-AC-000001 REV 00. Las Vegas, Nevada: Sandia National Laboratories. ACC: DOC.20070917.0006.

181383 SNL 2007. *Multiscale Thermohydrologic Model.* ANL-EBS-MD-000049 REV 03 ADD 01. Las Vegas, Nevada: Sandia National Laboratories. ACC: DOC.20070831.0003.

181953 SNL 2007. *Stress Corrosion Cracking of Waste Package Outer Barrier and Drip Shield Materials.* ANL-EBS-MD-000005 REV 04. Las Vegas, Nevada: Sandia National Laboratories. ACC: DOC.20070913.0001.

179869 SNL 2007. *Technical Work Plan for: Calculation of Waste Package and Drip Shield Response to Vibratory Ground Motion and Revision of the Seismic Consequence Abstraction.* TWP-MGR-GS-000004 REV 01 ICN 02. Las Vegas, Nevada: Sandia National Laboratories. ACC: DOC.20070416.0003.

179567 SNL 2007. *Total System Performance Assessment Data Input Package for Requirements Analysis for DOE SNF/HLW and Navy SNF Waste Package Physical Attributes Basis for Performance Assessment.* TDR-TDIP-ES-000009 REV 00. Las Vegas, Nevada: Sandia National Laboratories. ACC: DOC.20070921.0009.

179354 SNL 2007. *Total System Performance Assessment Data Input Package for Requirements Analysis for Engineered Barrier System In-Drift Configuration.* TDR-TDIP-ES-000010 REV 00. Las Vegas, Nevada: Sandia National Laboratories. ACC: DOC.20070921.0008.

179466 SNL 2007. *Total System Performance Assessment Data Input Package for Requirements Analysis for Subsurface Facilities.* TDR-TDIP-PA-000001 REV 00. Las Vegas, Nevada: Sandia National Laboratories. ACC: DOC.20070921.0007.

179394 SNL 2007. *Total System Performance Assessment Data Input Package for Requirements Analysis for Transportation Aging and Disposal Canister and Related Waste Package Physical Attributes Basis for Performance Assessment.* TDR-TDIP-ES-000006 REV 00. Las Vegas, Nevada: Sandia National Laboratories. ACC: DOC.20070918.0005.

164449 Waiting, D.J.; Stamatakos, J.A.; Ferrill, D.A.; Sims, D.W.; Morris, A.P.; Justus, P.S.; and Ibrahim, A.K. 2003. "Methodologies for the Evaluation of Faulting at Yucca Mountain, Nevada." *Proceedings of the 10th International High-Level Radioactive Waste Management Conference (IHLRWM), March 30-April 2, 2003, Las Vegas, Nevada.* Pages 377-387. La Grange Park, Illinois: American Nuclear Society. TIC: 254559.

9.2 CODES, STANDARDS, REGULATIONS, AND PROCEDURES

180319 10 CFR 63. 2007. Energy: Disposal of High-Level Radioactive Wastes in a Geologic Repository at Yucca Mountain, Nevada. Internet Accessible.

IM-PRO-002, *Control of the Electronic Management of Information*

IM-PRO-003, *Software Management*

SCI-PRO-002, *Planning for Science Activities*

SCI-PRO-003, *Document Review*

SCI-PRO-005, *Scientific Analyses and Calculations*

SCI-PRO-006, *Models*

TST-PRO-001, *Submittal and Incorporation of Data to the Technical Data Management System*

9.3 SOFTWARE CODES

172925 LS-DYNA SMP D V. 970.3858. 2005. OSF1 V5.1. STN: 10300-970.3858-02.

178801 LS-DYNA V. 971.7600.398. 2007. RedHat Linux Chaos 3.0. STN: 10300-971.7600.398-00.

161950 PFC2D V. 2.0. 2002. WINDOWS 2000/NT 4.0. STN: 10828-2.0-00.

161949 UDEC V. 3.1 Sub-Release 3.10.109. 2002. WINDOWS 2000/NT 4.0. STN: 10173-3.1-00.

9.4 SOURCE DATA, LISTED BY DATA TRACKING NUMBER

177299 GS031083114222.002. Direct Shear Data from Selected Samples of the Topopah Spring Tuff. Submittal date: 06/02/2004.

179406 LL0702PA055SPC.002. LS-DYNA Single Waste Package Damaged Area Analyses for the TAD-Bearing Waste Package. Submittal date: 02/21/2007.

179644 LL0703PA007SPC.005. LS-DYNA Single Waste Package Damaged Area Analyses for the 5-DHLW/DOE SNF-Long Co-Disposal Waste Package. Submittal date: 03/06/2007.

179775 LL0703PA029SPC.014. Rupture Probability for the LS-DYNA Kinematic Analyses for the 5-DHLW/DOE SNF-Long Co-Disposal Waste Package and the TAD-Bearing Waste Package. Submittal date: 03/13/2007.

180735 LL0704PA048SPC.023. LS-DYNA Kinematic Damaged Area Analyses for the TAD-Bearing Waste Package April 2007. Submittal date: 05/01/2007.

180736 LL0704PA049SPC.024. LS-DYNA Kinematic Damaged Area Analyses for the 5-DHLW/DOE SNF-Long Co-Disposal Waste Package April 2007. Submittal date: 05/01/2007.

180819 LL0704PA050SPC.025. LS-DYNA Kinematic Waste Package-to-Drip Shield Analyses. Submittal date: 05/01/2007.

182137 LL0706MG004SPC.001. Peak Acceleration of Waste Package Internals from Impacts with Waste Packages and Pallets. Submittal date: 06/06/2007.

162713 MO0210PGVPB107.000. Design Peak Ground Velocity for the Repository Level (Point B) at 10-7 Annual Exceedance Probability. Submittal date: 10/17/2002.

161869 MO0301SPASIP27.004. Sampling of Stochastic Input Parameters for Rockfall Calculations and for Structural Response Calculations Under Vibratory Ground Motions. Submittal date: 01/15/2003.

162712 MO0303DPGVB106.002. Design Peak Ground Velocity for the Repository Level (Point B) at 10-6 Annual Exceedance Probability. Submittal date: 03/10/2003.

183046 MO0401MWDRPSHA.000. Results of the Yucca Mountain Probabilistic Seismic Hazard Analysis (PSHA). Submittal date: 09/19/2007.

169099 MO0401SEPPGVRL.022. Peak Ground Velocity for the Repository Level (Point B) at 10-5 Annual Exceedance Frequency. Submittal date: 01/26/2004.

168890 MO0402AVDTM105.001. Acceleration, Velocity, and Displacement Time Histories for the Repository Level at 10-5 Annual Exceedance Frequency. Submittal date: 02/09/2004.

168891 MO0403AVDSC106.001. Acceleration, Velocity, and Displacement Time Histories for the Repository Level at 10-6 Annual Exceedance Frequency. Submittal date: 03/09/2004.

168892 MO0403AVTMH107.003. Acceleration, Velocity, and Displacement Time Histories for the Repository Level at 10-7 Annual Exceedance Frequency. Submittal date: 03/22/2004.

170437 MO0404PGVRL104.000. Peak Ground Velocity for the Repository Level (Point B) at 10-4 Annual Exceedance Frequency. Submittal date: 04/23/2004.

170873 MO0407MWDDSLCR.000. Drip Shield Load in Collapsed Lithophysal Rock. Submittal date: 07/21/2004.

172682 MO0501BPVELEMP.001. Bounded Horizontal Peak Ground Velocity Hazard at the Repository Waste Emplacement Level. Submittal date: 01/11/2005.

178831 MO0611ROCKFALL.000. Seismic Rockfall Analysis for Emplacement Drifts in Lithophysal Rock Mass Subject to Various Vibratory Ground Motion Levels. Submittal date: 11/28/2006.

182035 MO0612WPOUTERB.000. Output from General and Localized Corrosion of Waste Package Outer Barrier Report. Submittal date: 07/18/2007.

182334 MO0701DRIPSHLD.000. The Input Data and Results of Analysis of the Drip Shield Plate and Framework Fragility, Drip Shield Failure Modes, Effects of Uneven Invert Settlement on Drip Shield Stability, and Deformation and Damage of the Waste Package Loaded by Collapsed Drip Shield. Submittal date: 08/07/2007.

179925 MO0702PASTREAM.001. Waste Stream Composition and Thermal Decay Histories for LA. Submittal date: 02/15/2007.

180514 MO0702PASTRESS.002. Output DTN of Model Report, "Stress Corrosion Cracking of Waste Package Outer Barrier and Drip Shield Materials," ANL-EBS-MD-000005. Submittal date: 04/24/2007.

179314 MO0702POSTRUBB.000. Post-Processing Results for Analysis of the Waste Package Surrounded by Rubble Subjected to Seismic Ground Motion. Submittal date: 02/20/2007.

179662 MO0703PADSBLOC.000. Drip Shield Damage Due to Block Impact and Distributed Loading. Submittal date: 03/09/2007.

179895 MO0703SUMM3DEC.000. Summary of 3DEC Nonlithophysal Rockfall Model Results. Submittal date: 03/15/2007.

180634 MO0704PUNCTURE.000. Puncture Probability for the Outer Corrosion Barrier of the TAD-Bearing Waste Package When the Package Surrounded with Rubble and with Degraded Internals is Subjected to Strong Seismic Ground Motions. Submittal date: 04/25/2007.

181613 MO0706SPAFEPLA.001. FY 2007 LA FEP List and Screening. Submittal date: 06/20/2007.

182092 MO0707FAULTEMP.000. Fault/Emplacement Drift Intersections. Submittal date: 07/19/2007.

9.5 PRODUCT OUTPUT, LISTED BY DATA TRACKING NUMBER

MO0702PAFRAGIL.000. Calculation of PGA-V at 3 PGV Levels. Submittal date: 02/12/2007.

MO0703PASDSTAT.001. Statistical Analyses for Seismic Damage Abstractions. Submittal date: 09/21/2007.

MO0703PASEISDA.002. Seismic Damage Abstractions for TSPA Compliance Case. Submittal date: 09/21/2007.

MO0705FAULTABS.000. Assessment of Waste Package Failure Due to Fault Displacement for Criticality. Submittal date: 09/21/2007.

MO0705ROCKMASS.000. Rock Mass Category Percentages. Submittal date: 05/31/2007.

MO0707STANDOFF.000. Fault Standoff Analysis. Submittal date: 07/18/2007.

INTENTIONALLY LEFT BLANK

APPENDIX A
CLADDING DAMAGE ABSTRACTION

APPENDIX A
CLADDING DAMAGE ABSTRACTION

The compliance case for the TSPA-LA is not taking credit for the fuel rod cladding as a barrier to radionuclide release, so a cladding damage abstraction is not needed for the compliance case. However, a cladding damage abstraction has been developed to support the Performance Margin Analysis (PMA) for the TSPA-LA.

A.1 CLADDING FAILURE CRITERIA

The integrity of fuel rod cladding during cask drop or tip-over incidents has been extensively studied for Zircaloy-clad light water reactor spent fuel assemblies (Chun et al. 1987 [DIRS 144357]; Sanders et al. 1992 [DIRS 102072]). The work by Chun et al. (1987 [DIRS 144357]) is more useful here because it explicitly calculates *g*-loads for axial buckling and for yielding due to side drops. The range of *g*-loads for failure due to axial buckling varies between 82 *g*'s for the Westinghouse 17×17 fuel assembly to 252 *g*'s for the Combustion Engineering 16×16 fuel assembly (Chun et al. 1987 [DIRS 144357], Table 4]). The range of *g*-loads for yielding due to side drops varies between 63 *g*'s for a Westinghouse 17×17 fuel assembly to 211 *g*'s for a Combustion Engineering 16×16 fuel assembly (Chun et al. 1987 [DIRS 144357], Table 4). The actual *g*-loads for failure may be lower because: (1) the weight of the fuel pellets is not transferred to the cladding (Chun et al. 1987 [DIRS 144357], p. 2) and (2) the potential effects of cladding defects or existing failures are not included in the analysis. These effects increase the inertial mass or weaken the clad, possibly causing failure at lower *g*-loads. Because the corrosion rate for Zircaloy alloys is extremely low, if not essentially zero, thinning of the cladding is not considered here.

Based on these considerations, the criteria for cladding failure are conservatively defined as an axial load of 82 g's or a lateral load of 63 g's.

A.2 G LOADS ON WASTE PACKAGE INTERNALS

As discussed in Section 6.5, the results from kinematic analyses are converted to damaged area based on catalogs or lookup tables for damaged area from individual waste package-to-pallet impacts and from individual end-to-end impacts between adjacent waste packages. The calculations for the catalogs use a highly refined finite-element grid that is appropriate for defining the average g load on the waste package internals as a function of relative impact velocity. The average g load is used here because it reduces the numerical sensitivity in acceleration time histories with the LS-DYNA software (V. 970.3858 STN: 10300-970.3858-02 [DIRS 172925]; V. 971.7600.398 STN: 10300-971.7600.398-00 [DIRS 178801]). The catalogs with intact internals are the basis for this analysis because the focus here is on failure of intact fuel rods and because the representation of degraded internals as a sandy material tends to reduce g loads during impact relative to the higher structural stiffness of the intact internals.

An analysis of the catalog calculations for the maximum g loads on waste package internals from package-to-pallet and package-to-package impacts provides the following information:

- The maximum lateral acceleration from the impact of the TAD-bearing or codisposal waste package on an emplacement pallet at 10 m/s is 43 g's (DTN: LL0706MG004SPC.001 [DIRS 182137], File *Catalog_analyses_accel.xls*, worksheets "NavalLong TAD WPP" and "CDSP WPP"). This acceleration is significantly less than the cladding failure criterion of 63 g's. Based on this information, the cladding is not expected to fail from waste package-to-pallet impacts.

- The maximum axial acceleration from end-to-end impacts of two TAD-bearing waste packages is 72 g's for an impact velocity of 9 m/s (DTN: LL0706MG004SPC.001 [DIRS 182137], File *Catalog_analyses_accel.xls*, worksheet "NavalLong TAD WPWP").

- The maximum axial acceleration for a codisposal waste package from end-to-end impacts of a TAD-bearing and a codisposal waste package is 75 g's for an impact velocity of 4 m/s, 111 g's for an impact velocity of 6 m/s, and 164 g's for an impact velocity of 9 m/s (DTN: LL0706MG004SPC.001 [DIRS 182137], File *Catalog_analyses_accel.xls*, worksheet "CDSP WPWP").

- The maximum axial acceleration for a TAD-bearing waste package from end-to-end impacts of a TAD-bearing and a codisposal waste package is 75 g's for an impact velocity of 6 m/s and 88 g's for an impact velocity of 9 m/s (DTN: LL0706MG004SPC.001 [DIRS 182137], File *Catalog_analyses_accel.xls*, worksheet "CDSP WPWP").

Based on the results in the final two bullets, an axial impact velocity of 4 m/s is assigned as the velocity threshold for cladding failure in the codisposal waste package, and an axial impact velocity of 6 m/s is assigned as the velocity threshold for cladding failure in the TAD-bearing waste package.

A.3 NUMBER OF END-TO-END IMPACTS EXCEEDING THE VELOCITY THRESHOLD

The kinematic calculations indicate that six realizations have axial impact velocities for codisposal waste packages exceeding 4 m/s, with one realization at the 2.44 m/s PGV level and five realizations at the 4.07 m/s PGV level (DTN: LL0706MG004SPC.001 [DIRS 182137], File *Catalog_analyses_accel.xls*, worksheet "Max Vel CDSP-NavalLongTAD"). Given that there are 17 ground motions at each PGV level, the (conditional) probability of cladding failure in a codisposal waste package is (1/17) = 0.0588 at the 2.44 m/s PGV level and (5/17) = 0.294 at the 4.07 m/s PGV level. The corresponding probabilities at the 0.4 m/s PGV level and at the 1.05 m/s PGV level are 0.

The kinematic calculations also indicate that only one realization at the 4.07 m/s PGV level has an axial impact velocity exceeding 6 m/s for the TAD-bearing waste package (DTN: LL0706MG004SPC.001 [DIRS 182137], File *Catalog_analyses_accel.xls*, worksheet "Max Vel CDSP-NavalLongTAD"). The conditional probability of cladding failure in the TAD-bearing waste package is (1/17) = 0.0588 at the 4.07 m/s PGV level. The corresponding probabilities at the 0.4 m/s, 1.05 m/s, and 2.44 m/s PGV levels are 0.

A.4 DAMAGE ABSTRACTIONS FOR CLADDING WITH INTACT INTERNALS

The (conditional) probability of cladding failure in codisposal waste packages with intact internals is represented as a power law of the form $a(\text{PGV} - 1.05)^b$, similar to the approach for rupture or puncture probability in Sections 6.5.2.1, 6.6.2.1, and 6.9.1. This function goes to 0 at the 1.05 m/s PGV level, consistent with the kinematic data. Given that there are 17 ground motions at each PGV level, the (conditional) probability of cladding failure is (1/17) = 0.0588 at the 2.44 m/s PGV level and (5/17) = 0.294 at the 4.07 m/s PGV level. The coefficients a and b are calculated as: $b = \log(0.0588/0.294)/\log((2.44 - 1.05)/(4.07 - 1.05)) = 2.07$ and $a = (0.294)/(4.07 - 1.05)^{2.074} = 0.0298$.

The (conditional) probability of cladding failure in TAD-bearing waste packages with intact internals is represented as a power-law function of the form $c(\text{PGV}–2.44)^d$. This functional form goes to 0 at the 2.44 m/s PGV level, consistent with the kinematic data. However, there is only one nonzero data point, so there is not enough data to define the coefficients c and d. A reasonable simplification is to set the value of d equal to 2.07, the same value as b. The value of c is then calculated as $c = (0.0588)/(4.07 - 2.44)^{2.07} = 0.0214$.

Equations A-1 and A-2 summarize these results:

$$P_{\text{Clad\_Fail\_CDSP}} = \text{If (PGV}\geq 1.05\text{ m/s) } (0.0298)(\text{PGV} - 1.05)^{2.07}\text{, else 0.0} \qquad \text{(Eq. A-1)}$$

$$P_{\text{Clad\_Fail\_TAD}} = \text{If (PGV}\geq 2.44\text{ m/s) } (0.0214)(\text{PGV} - 2.44)^{2.07}\text{, else 0.0.} \qquad \text{(Eq. A-2)}$$

A.5 CONSEQUENCE OF CLADDING FAILURE

If the cladding fails in the TAD-bearing waste packages during a seismic event, then the cladding in this waste package type is 100% perforated throughout the repository. Similarly, if the cladding fails in the codisposal waste packages during a seismic event, then the cladding in this waste package type is 100% perforated throughout the repository. Once the cladding fails, it remains failed for the remainder of the realization.

INTENTIONALLY LEFT BLANK

APPENDIX B
DESCRIPTION OF INPUTS, FORMULAS, AND OUTPUTS FOR SPREADSHEETS IN OUTPUT DTN: MO0703PASDSTAT.001

APPENDIX B
DESCRIPTION OF INPUTS, FORMULAS, AND OUTPUTS FOR SPREADSHEETS IN OUTPUT DTN: MO0703PASDSTAT.001

B.1 DESCRIPTION OF INPUTS FOR SPREADSHEETS IN OUTPUT DTN: MO0703PASDSTAT.001

Table B-1 identifies the data inputs and their sources for the spreadsheets in *Statistical Analyses for Seismic Damage Abstractions*, output DTN: MO0703PASDSTAT.001. The first column, Input, provides a brief description of the input data. The second column, Location in File, identifies the worksheet/cells that reproduce the data from the source. These worksheets/cells are in the spreadsheets in output DTN: MO0703PASDSTAT.001. The third column, Source, identifies the DTN that is the source of the input data for the spreadsheet. The sources for the data inputs are also identified in the "ReadMe" worksheet that is included in each Excel file.

Table B-1. Input to Spreadsheets in Output DTN: MO0703PASDSTAT.001

Input	Location in File ("Worksheet")	Source
CDSP Kinematic Damage Abstraction 17-mm Degraded.xls		
End-to-End WP Impacts	"WP-WP Data" Cells: A3:G149	DTN: LL0704PA049SPC.024 [DIRS 180736], File *CDSP_kinematic_analyses_DA_summary.xls*
WP-Pallet Impacts	"WP-Pallet Data" Cells: A3:G149	DTN: LL0704PA049SPC.024 [DIRS 180736], File *CDSP_kinematic_analyses_DA_summary.xls*
Damage Area from Single WP Calculations	"Prob of Damage Anal. 17-mm OCB" Cells: A9:F13	DTN: LL0703PA007SPC.005 [DIRS 179644], File *CDSP_1WP_analyses_DA_summary.xls*
TAD Data for Mean and Standard Deviation	"CDSP-TAD Comparison" Cells: A21:E33	Output DTN: MO0703PASDSTAT.001, File *Kinematic Damage Abstraction 17-mm Degraded.xls*
CDSP Kinematic Damage Abstraction 23-mm Degraded.xls		
End-to-End WP Impacts	"WP-WP Data" Cells: A3:G149	DTN: LL0704PA049SPC.024 [DIRS 180736], File *CDSP_kinematic_analyses_DA_summary.xls*
WP-Pallet Impacts	"WP-Pallet Data" Cells: A3:G149	DTN: LL0704PA049SPC.024 [DIRS 180736], File *CDSP_kinematic_analyses_DA_summary.xls*
Damage Area from Single WP Calculations	"Prob of Damage Anal. 23-mm OCB" Cells: A9:F13	DTN LL0703PA007SPC.005 [DIRS 179644], File *CDSP_1WP_analyses_DA_summary.xls*
CDSP Kinematic Damage Abstraction 23-mm Intact.xls		
End-to-End WP Impacts	"WP-WP Data" Cells: A3:G149	DTN: LL0704PA049SPC.024 [DIRS 180736], File *CDSP_kinematic_analyses_DA_summary.xls*
WP-Pallet Impacts	"WP-Pallet Data" Cells: A3:G149	DTN: LL0704PA049SPC.024 [DIRS 180736], File *CDSP_kinematic_analyses_DA_summary.xls*
Damage Area from Single WP Calculations	"Prob of Damage Anal. 23-mm OCB" Cells: A9:F13	DTN: LL0703PA007SPC.005 [DIRS 179644], File *CDSP_1WP_analyses_DA_summary.xls*

Table B-1. Input to Spreadsheets in Output DTN: MO0903PASDSTAT.001 (Continued)

Input	Location in File ("Worksheet")	Source
DS Damaged Areas with Rubble.xls		
Damage Catalog	"1.05 ms PGV – Case 1 BCs" Cells: A9:F34 "2.44 ms PGV – Case 1 BCs" Cells: A9:F34 "4.07 ms PGV – Case 1 BCs" Cells: A9:F34	DTN: MO0703PADSBLOC.000 [DIRS 179662], File *DS plate damage due to distributed loads.xls*, worksheet: "Case 1 boundary condition"
	"1.05 ms PGV – Case 2 BCs" Cells: A9:F38 "2.44 ms PGV – Case 2 BCs" Cells: A9:F38 "4.07 ms PGV – Case 2 BCs" Cells: A9:F38	DTN: MO0703PADSBLOC.000 [DIRS 179662], File *DS plate damage due to distributed loads.xls*, worksheet: "Case 2 boundary condition"
PGV-H1	"PGV-H1 to (A+1) Regression" Cells: B15:B31	DTN: MO0402AVDTM105.001 [DIRS 168890], Files *matxh1.vts* in *vts.zip* where x = 01, 02, …, 16, and 17
	"PGV-H1 to (A+1) Regression" Cells: B32:B48	DTN: MO0403AVDSC106.001 [DIRS 168891], Files *matxh1.vts* in *vts.zip* where x = 01, 02, …, 16, and 17
	"PGV-H1 to (A+1) Regression" Cells: B49:B65	DTN: MO0403AVTMH107.003 [DIRS 168892], Files *matxh1.vts* in *vts.zip* where x = 01, 02, …, 16, and 17
PGA-V	"PGV-H1 to (A+1) Regression" Cells: C15:C65	Output DTN: MO0702PAFRAGIL.000, Files *MATxV_105.xls, MATxV_244.xls,* and *MATxV_535.xls* in *Calculation_of_PGA_V_at_3_PGV_Levels.zip*, where x = 01, 02, …, 16, and 17
Average Pressure on DS Segments	"Load" Cells: B8:B13	DTN: MO0407MWDDSLCR.000 [DIRS 170873], File *final drip shield quasi-static pressures.xls*, worksheet "data", average of data in cells: C14:C23, F14:F23, I14:I23, L14:L23, O14:O23, R14:R23
Fault Displacement Abstraction.xls		
Emplacement Drift Diameter	"Tables" Cell: C6	SNL 2007 [DIRS 179354], Table 4-1, Item Number 01-10
Invert Thickness	"Tables" Cell: C7	SNL 2007 [DIRS 179354], Table 4-1, Item Number 01-10A
DS Height (exterior)	"Tables" Cell: C8	SNL 2007 [DIRS 179354], Table 4-2, Item Number 07-01
DS Height (interior)	"Tables" Cell: C9	SNL 2007 [DIRS 179354], Table 4-2, Item Number 07-01
Clearance above DS	"Tables" Cell: C10	SNL 2007 [DIRS 179354], Table 4-2, Item Number 07-01
Outer Diameter of TAD WP	"Tables" Cell: B20	SNL 2007 [DIRS 179394], Table 4-3
Outer Diameter of Naval-Long WP	"Tables" Cell: B21	SNL 2007 [DIRS 179567], Table 4-6
Outer Diameter of Naval-Short WP	"Tables" Cell: B22	SNL 2007 [DIRS 179567], Table 4-7
Outer Diameter of 5DHLW/DOE SNF Short WP	"Tables" Cell: B23	SNL 2007 [DIRS 179567], Table 4-8
Outer Diameter of 5DHLW/DOE SNF-Long WP	"Tables" Cell: B24	SNL 2007 [DIRS 179567], Table 4-9
Outer Diameter of 2-MCO/2-DHLW WP	"Tables" Cell: B25	SNL 2007 [DIRS 179567], Table 4-10

Table B-1. Input to Spreadsheets in Output DTN: MO0703PASDSTAT.001 (Continued)

Input	Location in File ("Worksheet")	Source
***Fault Displacement Abstraction.xls* (Continued)**		
Drift Intersections with Sever Wash, Drill Hole Wash, Pagany Wash, West Ghost Dance, and Sundance Faults	"Tables" Cells: A44:B94	DTN: MO0707FAULTEMP.000 [DIRS 182092], File *Output xls* with results summarized in the *ReadMe* file
Numbering of Drifts	"Tables" Cell: A41	SNL 2007 [DIRS 179466] Table 4-1, Item 01-02
Fault Displacement Summary Information	"Tables" Cells: A108:F121	DTN: MO0401MWDRPSHA.000 [DIRS 183046]
WP (TAD) Length	"Tables" Cell: B132	SNL 2007 [DIRS 179394], Table 4-3
WP (Excluding TAD) Length	"Tables" Cells: B133:B137	2007 [DIRS 179567], Tables 4-6 to 4-10
Waste Package Inventory	"Tables" Cells: C132:C137	Design Basis Inventory: DTN: MO0702PASTREAM.001 [DIRS 179925], File *DTN-Inventory-Rev00.xls*, worksheet "UNIT CELL", cells B14:L15
Hazard Curve Data (Solitario Canyon Fault)	"Hazard Calcs" Cells: A10:B21	DTN: MO0401MWDRPSHA.000 [DIRS 183046], File */disp/tot_haz/s2.frac_mean.gz*
Hazard Curve Data (Drill Hole Wash Fault)	"Hazard Calcs" Cells: A30:B41	DTN: MO0401MWDRPSHA.000 [DIRS 183046], File */disp/tot_haz/s3.frac_mean.gz*
Hazard Curve Data (Ghost Dance Fault)	"Hazard Calcs" Cells: A50:B61	DTN: MO0401MWDRPSHA.000 [DIRS 183046], File */disp/tot_haz/*s4rev.frac_mean.gz
Hazard Curve Data (Sundance Fault)	"Hazard Calcs" Cells: A70:B81	DTN: MO0401MWDRPSHA.000 [DIRS 183046], File */disp/tot_haz/*s5rev.frac_mean.gz
Hazard Curve Data (Site s7a)	"Hazard Calcs" Cells: A90:B101	DTN: MO0401MWDRPSHA.000 [DIRS 183046], File */disp/tot_haz/s7a.frac_mean.gz*
Hazard Curve Data (Site s7b)	"Hazard Calcs" Cells: A110:B121	DTN: MO0401MWDRPSHA.000 [DIRS 183046], File */disp/tot_haz/s7b.frac_mean.gz*
Hazard Curve Data (Site s7c)	"Hazard Calcs" Cells: A130:B141	DTN: MO0401MWDRPSHA.000 [DIRS 183046], File */disp/tot_haz/s7c.frac_mean.gz*
Hazard Curve Data (Site s7d)	"Hazard Calcs" Cells: A150:B161	DTN: MO0401MWDRPSHA.000 [DIRS 183046], File */disp/tot_haz/s7d.frac_mean.gz*
Hazard Curve Data (Site s8a)	"Hazard Calcs" Cells: A170:B181	DTN: MO0401MWDRPSHA.000 [DIRS 183046], File */disp/tot_haz/s8a.frac_mean.gz*
Hazard Curve Data (Site s8b)	"Hazard Calcs" Cells: A190:B201	DTN: MO0401MWDRPSHA.000 [DIRS 183046], File */disp/tot_haz/s8b.frac_mean.gz*
Hazard Curve Data (Site s8c)	"Hazard Calcs" Cells: A210:B221	DTN: MO0401MWDRPSHA.000 [DIRS 183046], Files */displ/tot_haz/s8c.frac_mean.gz*
Frame Fragility Analysis.xls		
PGV-H1 (1.05 m/s)	"PGV-H1 to A Correlation" Cells: B13:B29	DTN: MO0402AVDTM105.001 [DIRS 168890], Files *matxh1.vts* in *vts.zip*, where x = 01, 02, 03,…, 16, and 17
PGV-H1 (2.44 m/s)	"PGV-H1 to A Correlation" Cells: B30:B46	DTN: MO0403AVDSC106.001 [DIRS 168891], Files *matxh1.vts* in *vts.zip*, where x = 01, 02, 03,…, 16, and 17
PGV-H1 (5.35 m/s)	"PGV-H1 to A Correlation" Cells: B47:B63	DTN: MO0403AVTMH107.003 [DIRS 168892], Files *matxh1.vts* in *vts.zip*, where x = 01, 02, 03,…, 16, and 17
PGA-V	"PGV-H1 to A Correlation" Cells: C13:C63	Output DTN: MO0702PAFRAGIL.000, Files *MATxV_105.xls, MATxV_244.xls,* and *MATxV_535.xls,* where x = 01, 02, 03, …, 16, and 17.

Table B-1. Input to Spreadsheets in Output DTN: MO0703PASDSTAT.001 (Continued)

Input	Location in File ("Worksheet")	Source
***Frame Fragility Analysis.xls* (Continued)**		
Average Pressure on DS Segments	"Load and Capacity" Cells: B8:B13	DTN: MO0407MWDDSLCR.000 [DIRS 170873], File *final drip shield quasi-static pressures.xls*, worksheet "data", average of data in cells: C14:C23, F14:F23, I14:I23, L14:L23, O14:O23, R14:R23
Plastic Load Capacity of DS	"Load and Capacity" Cells: B50:C52	DTN: MO0701DRIPSHLD.000 [DIRS 182334], File *summary DS framework fragility.xls,* worksheet "limit load" Cells: E3:E5, B3:B5
Kinematic Damage Abstraction 17-mm Degraded.xls		
End-to-End WP Impacts	"WP-WP Data" Cells: A4:M217	DTN: LL0704PA048SPC.023 [DIRS 180735], File *NavalLong_TAD_kinematic_analyses_DA_summary.xls*
WP-Pallet Impacts	"WP-Pallet Data" Cells: A4:M217	DTN: LL0704PA048SPC.023 [DIRS 180735], File *NavalLong_TAD_kinematic_analyses_DA_summary.xls*
Damage Area from Single WP Calculations	"Prob of Damage Anal. 17-mm OCB" Cells: A9:F11	DTN: LL0702PA055SPC.002 [DIRS 179406], File *NavalLong_TAD_1WP_analyses_DA_summary.xls*
Kinematic Damage Abstraction 23-mm Degraded.xls		
End-to-End WP Impacts	"WP-WP Data" Cells: A4:M217	DTN: LL0704PA048SPC.023 [DIRS 180735], File *NavalLong_TAD_kinematic_analyses_DA_summary.xls*
WP-Pallet Impacts	"WP-Pallet Data" Cells: A4:M217	DTN: LL0704PA048SPC.023 [DIRS 180735], File *NavalLong_TAD_kinematic_analyses_DA_summary.xls*
Damage Area from Single WP Calculations	"Prob of Damage Anal. 23-mm OCB" Cells: A9:F11	DTN: LL0702PA055SPC.002 [DIRS 179406], File *NavalLong_TAD_1WP_analyses_DA_summary.xls*
Kinematic Damage Abstraction 23-mm Intact.xls		
End-to-End WP Impacts	"WP-WP Data" Cells: A4:M217	DTN: LL0704PA048SPC.023 [DIRS 180735], File *NavalLong_TAD_kinematic_analyses_DA_summary.xls*
WP-Pallet Impacts	"WP-Pallet Data" Cells: A4:M217	DTN: LL0704PA048SPC.023 [DIRS 180735], File *NavalLong_TAD_kinematic_analyses_DA_summary.xls*
Lith Rubble Abstraction.xls		
Rockfall Area	"Data" Cells: A1:D17	DTN: MO0611ROCKFALL.000 [DIRS 178831], File *summary.xls*
Ground Motion Number and Rock Mass Category	"Probability of Rockfall" Cells: B15:C29	BSC 2004 [DIRS 166107], Table 6-44
Weighting for Rock Mass Categories	"Probability of Rockfall" Cells: B34:B38	Output DTN: MO0705ROCKMASS.000, File *Rock Mass Category Percentages.xls*, worksheet "Sheet1"
Range of V0	"Exceed Prob for V > V0" Cells: B3, L3, P3	Section 6.7.1.5 in this report
λ_{max}	"Exceed Prob for V > V0" Cells: B5, L5, P5	Section 6.4.3 in this report
λ_{min}	"Exceed Prob for V > V0" Cells: B6, L6, P6	10 CFR 63.114 (d) [DIRS 180319], Requirement: "*consider only events that have at least one chance in 10,000 of occurring over 10,000 years*"
Bounded Hazard Curve	"Data for Bounded Hazard" Cells: A13:B89	DTN: MO0501BPVELEMP.001 [DIRS 172682], worksheet "Bounded Horizontal PGV Hazard" in the file *Bounded Horizontal Peak Ground Velocity Hazard at the Repository Waste Emplacement Level.xls*

Table B-1. Input to Spreadsheets in Output DTN: MO0703PASDSTAT.001 (Continued)

Input	Location in File ("Worksheet")	Source
Nonlith Damage Abstraction for DS .xls		
Damaged Areas on the DS	"Data Catalogs" Cells: C7:E13	DTN: MO0703PADSBLOC.000 [DIRS 179662], File *DS damage due to large block impacts.xls*, worksheet "damaged area"
Maximum Plastic Strain in the DS Plates	"Data Catalogs" Cells: K7:M13	DTN: MO0703PADSBLOC.000 [DIRS 179662], File *DS damage due to large block impacts.xls*, worksheet "max plate plastic strains"
Nonlith Damage Abstraction for DS .xls		
Maximum Plastic Strain in the Axial Stiffeners of the DS	"Data Catalogs" Cells: S7:U13	DTN: MO0703PADSBLOC.000 [DIRS 179662], File *DS damage due to large block impacts.xls*, worksheet "max stiffener plastic strains"
Nonlith Rockfall Characteristics in Emplacement Drifts (0.4 m/s)	"0.4 ms PGV 15-mm Plate" Cells A22:H449 "0.4 ms PGV 10-mm Plate" Cells: A22:H449 "0.4 ms PGV 5-mm Plate" Cells: A22:H449	DTN: MO0703SUMM3DEC.000 [DIRS 179895], File *nonlith rockfall characteristics in emplacement drifts for 1e-4 gm.xls*
Nonlith Rockfall Characteristics in Emplacement Drifts (1.05 m/s)	"1.05 ms PGV 15-mm Plate" Cells: A22:H1788 "1.05 ms PGV 10-mm Plate" Cells: A22:H1788 "1.05 ms PGV 5-mm Plate" Cells: A22:H1788	DTN: MO0703SUMM3DEC.000 [DIRS 179895], File *nonlith rockfall characteristics in emplacement drifts for 1e-5 gm.xls*
Nonlith Damage Abstraction for DS .xls **(Continued)**		
Nonlith Rockfall Characteristics in Emplacement Drifts (2.44 m/s)	"2.44 ms PGV 15-mm Plate" Cells: A22:H2818 "2.44 ms PGV 10-mm Plate" Cells: A22:H2818 "2.44 ms PGV 5-mm Plate" Cells: A22:H2818	DTN: MO0703SUMM3DEC.000 [DIRS 179895], File *nonlith rockfall characteristics in emplacement drifts for 1e-6 gm.xls*
Nonlith Rockfall Characteristics in Emplacement Drifts (5.35 m/s)	"5.35 ms PGV 15-mm Plate" Cells: A22:H3408 "5.35 ms PGV 10-mm Plate" Cells: A22:H3408 "5.35 ms PGV 5-mm Plate" Cells: A22:H3408	DTN: MO0703SUMM3DEC.000 [DIRS 179895], Files *nonlith rockfall characteristics in emplacement drifts for 1e-7 gm.xls*
Nonlith Rockfall Abstraction.xls		
Lithophysal Rockfall Volumes	"Lith Versus Nonlith" Cells: D13:F27	DTN: MO0611ROCKFALL.000 [DIRS 178831], File *summary.xls*
Ground Motion Number and Rock Mass Category	"Lith Versus Nonlith" Cells: B13:C27	BSC 2004 [DIRS 166107], Table 6-44
Nonlithophysal Rockfall Volume (1.05 m/s)	"Lith Versus Nonlith" Cells: H13:K62	DTN: 0703SUMM3DEC.000 [DIRS 179895], File *nonlith rockfall characteristics in emplacement drifts for 1e-5 gm.xls*
Nonlithophysal Rockfall Volume (2.44 m/s)	"Lith Versus Nonlith" Cells: O13:R62	DTN: O0703SUMM3DEC.000 [DIRS 179895], File *nonlith rockfall characteristics in emplacement drifts for 1e-6 gm.xls*
Nonlithophysal Rockfall Volume (5.35 m/s)	"Lith Versus Nonlith" Cells: V13:Y56	DTN: MO0703SUMM3DEC.000 [DIRS 179895], Files *nonlith rockfall characteristics in emplacement drifts for 1e-7 gm.xls*

Table B-1. Input to Spreadsheets in Output DTN: MO0703PASDSTAT.001 (Continued)

Input	Location in File ("Worksheet")	Source
Plate Fragility Analysis.xls		
PGV-H1 (1.05 m/s)	"PGV-H1 to A Correlation" Cells: B13:B29	DTN: MO0402AVDTM105.001 [DIRS 168890], Files *matxh1.vts* in *vts.zip* where x = 01, 02, …, 16, and 17
PGV-H1 (2.44 m/s)	"PGV-H1 to A Correlation" Cells: B30:B46	DTN: MO0403AVDSC106.001 [DIRS 168891], Files *matxh1.vts* in *vts.zip* where x = 01, 02, …, 16, and 17
PGV-H1 (5.35 m/s)	"PGV-H1 to A Correlation" Cells: B47:B63	DTN: MO0403AVTMH107.003 [DIRS 168892], Files *matxh1.vts* in *vts.zip* where x = 01, 02, …, 16, and 17
PGA-V	"PGV-H1 to A Correlation" Cells: C13:C63	Output DTN: MO0702PAFRAGIL.000, Files *MATxV_105.xls, MATxV_244.xls,* and *MATxV_535.xls,* where x = 01, 02, 03, …, 16, and 17
***Plate Fragility Analysis.xls* (Continued)**		
Average Pressure on DS Segments	"Load and Capacity" Cells: B8:B13	DTN: MO0407MWDDSLCR.000 [DIRS 170873], File *final drip shield quasi-static pressure.xls*, worksheet "data", average of data in cells: C14:C23, F14:F23, I14:I23, L14:L23, O14:O23, R14:R23
Plastic Load Capacity of DS	"Load and Capacity" Cells: B49:B51 and D49:D51	DTN: MO0701DRIPSHLD.000 [DIRS 182334], File *summary DS plate fragility.xls,* worksheet "limit load", Cells: E3:E5, B3:B5
Rupture and Puncture Abstractions.xls		
CDSP Rupture Probabilities	"CDSP Kinematic Data" Cells: A4:I150	DTN: LL0703PA029SPC.014 [DIRS 179775], File *kinematic_analyses_rupture_summary.xls,* worksheet "CDSP summary"
TAD Rupture Probabilities	"TAD Kinematic Data" Cells: A4:I218	DTN: LL0703PA029SPC.014 [DIRS 179775], File *kinematic_analyses_rupture_summary.xls,* worksheet "Naval Long TAD Summary"
TAD Probabilities of Puncture	"TAD Rubble Data" Cells: A5:E48	DTN: MO0704PUNCTURE.000 [DIRS 180634], File *Puncture Probability Data – WP Surrounded by Rubble.xls*, worksheet "TAD Rubble Data"
WP-Rubble Damage Abstraction 17-mm Degraded.xls		
Damaged Areas on WP Surrounded by Lithophysal Rubble	"Data at 0.40 mps PGV" Cells: A15:R24 "Data at 1.05 mps PGV" Cells: A15:R24 "Data at 2.44 mps PGV" Cells: A15:R24 "Data at 4.07 mps PGV" Cells: A15:R24	DTN: MO0702POSTRUBB.000 [DIRS 179314], File *17mm.xls*

Table B-1. Input to Spreadsheets in Output DTN: MO0703PASDSTAT.001 (Continued)

Input	Location in File ("Worksheet")	Source
WP-Rubble Damage Abstraction 23-mm Degraded.xls		
Damaged Areas on WP Surrounded by Lithophysal Rubble	"Data at 0.40 mps PGV" Cells: A15:R24 "Data at 1.05 mps PGV" Cells: A15:R24 "Data at 2.44 mps PGV" Cells: A15:R24 "Data at 4.07 mps PGV" Cells: A15:R24	DTN: MO0702POSTRUBB.000 [DIRS 179314], File *23mm.xls*

Sources: Output DTN: MO0703PASDSTAT.001, Files: *CDSP Kinematic Damage Abstraction 17-mm Degraded.xls, CDSP Kinematic Damage Abstraction 23-mm Degraded.xls, CDSP Kinematic Damage Abstraction 23-mm Intact.xls, DS Damaged Areas with Rubble.xls, Fault Displacement Abstraction.xls, Frame Fragility Analysis.xls, Kinematic Damage Abstraction 17-mm Degraded.xls, 23-mm Degraded.xls, Kinematic Damage Abstraction 23-mm Intact.xls, Lith Rubble Abstraction.xls, Nonlith Damage Abstraction for DS.xls, Nonlith Rockfall Abstraction.xls, Plate Fragility Analysis.xls, Rupture and Puncture Abstractions.xls, WP-Rubble Damage Abstraction 17-mm Degraded.xls,* and *WP-Rubble Damage Abstraction 23-mm Degraded.xls.*

NOTES: In Section *Lith Rubble Abstraction.xls*, "Exceed Prob for V greater than V0" refers to the exceedance probability for rockfall volume, V, greater than a given value, V0.

CDSP = codisposal; DS = drip shield; TAD = transportation, aging, and disposal (canister); WP = waste package.

B.2 DESCRIPTION OF FORMULAS IN THE SPREADSHEETS IN OUTPUT DTN: MO0703PASDSTAT.001

Table B-2 identifies the formulas in the spreadsheets in *Statistical Analyses for Seismic Damage Abstractions*, output DTN: MO0703PASDSTAT.001. The first column identifies the formula or function. The second column identifies the worksheet/cells that employ the formula. These worksheets/cells are in the spreadsheets in output DTN: MO0703PASDSTAT.001. The third column identifies the direct inputs to the formula or function, and the fourth column identifies the output values for the function.

Table B-2. Formulas[19] used in Spreadsheets in Output DTN: MO0703PASDSTAT.001

Formula (Bold), Function	Location in File ("Worksheet")	Input (Location in file or value if directly entered) in Order of Use in Formula	Output (Value)
CDSP Kinematic Damage Abstraction 17-mm Degraded.xls			
A + B, Calculates the Total Damage Area by Adding the Damage from the WP-WP Impacts to the Damage from the WP-Pallet Impacts	"WP Total" Cells: E5:G38, E46:G79, E87:G120, E128:G161	Corresponding cells in "WP-WP Data" and "WP-Pallet Data"	Total Damage Area

[19] All built-in Excel commands used in the spreadsheets are documented in this table. In addition, calculations of primary importance to the output of a worksheet were included. By default, basic arithmetic (addition, subtraction, multiplication, division, and exponentials) were not included in this table, the exception being calculations of primary importance to the output of the spreadsheets. Specific output was included when deemed significant.

Table B-2. Formulas used in Spreadsheets in Output DTN: MO0703PASDSTAT.001 (Continued)

Formula (Bold), Function	Location in File ("Worksheet")	Input (Location in file or value if directly entered) in Order of Use in Formula	Output (Value)
CDSP Kinematic Damage Abstraction 17-mm Degraded.xls **(Continued)**			
Built-in Excel Command: **FREQUENCY (data_array, bins_array)**, Counts the Number of Zeros in the Input Cells	"WP Total" Cell: E39:G39, E80:G80, G121:G121, G162:G162	"WP Total" Cells: E5:E38, 0	Number of Zeros
	"WP Total" Cell: F39	"WP Total" Cells: F5:F38, 0	
	"WP Total" Cell: G39	"WP Total" Cells: G5:G38, 0	
	"WP Total" Cell: E80	"WP Total" Cells: E46:E79, 0	
	"WP Total" Cell: F80	"WP Total" Cells: F46:F79, 0	
	"WP Total" Cell: F80	"WP Total" Cells: G46:G79, 0	
	"WP Total" Cell: E121	"WP Total" Cells: E87:E120, 0	
	"WP Total" Cell: F121	"WP Total" Cells: F87:F120, 0	
	"WP Total" Cell: G121	"WP Total" Cells: G87:G120, 0	
	"WP Total" Cell: E162	"WP Total" Cells: E128:E161, 0	
	"WP Total" Cell: F162	"WP Total" Cells: F128:F161, 0	
	"WP Total" Cell: G162	"WP Total" Cells: G128:G161, 0	
	"Prob of Damage Anal. 17-mm OCB" Cell: E54	"Prob of Damage Anal. 17-mm OCB" Cells: E20:E53	
	"Prob of Damage Anal. 17-mm OCB" Cell: F54	"Prob of Damage Anal. 17-mm OCB" Cell: F20:F53	
	"Prob of Damage Anal. 17-mm OCB" Cell: G54	"Prob of Damage Anal. 17-mm OCB" Cell: G20:G53	
	"Prob of Damage Anal. 17-mm OCB" Cell: H54	"Prob of Damage Anal. 17-mm OCB" Cell: H20:H53	
	"Prob of Damage Anal. 17-mm OCB" Cell: I54	"Prob of Damage Anal. 17-mm OCB" Cell: I20:I53	
	"Prob of Damage Anal. 17-mm OCB" Cell: J54	"Prob of Damage Anal. 17-mm OCB" Cell: J20:J53	
(A-B) / A, Calculates the Probability of Damage Using the Number of Zero Damage Areas and the Total Number of Damage Areas	"WP Total" Cell: E40	34, "WP Total" Cell: E39	0.235
	"WP Total" Cell: F40	34, "WP Total" Cell: F39	0.235
	"WP Total" Cell: G40	34, "WP Total" Cell: G39	0.088
	"WP Total" Cell: E81	34, "WP Total" Cell: E80	0.676
	"WP Total" Cell: F81	34, "WP Total" Cell F80	0.676
	"WP Total" Cell: G81	34, "WP Total" Cell: G80	0.382
	"WP Total" Cell: E122	34, "WP Total" Cell: E121	0.941
	"WP Total" Cell: F122	34, "WP Total" Cell F121	0.941
	"WP Total" Cell: G122	34, "WP Total" Cell: G121	0.882
	"WP Total" Cell: E163	34, "WP Total" Cell: E160	1
	"WP Total" Cell: F163	34, "WP Total" Cell F160	1
	"WP Total" Cell: G163	34, "WP Total" Cell: G160	1
	"Prob of Damage Anal. 17-mm OCB" Cell: E55	34, "Prob of Damage Anal. 17-mm OCB" Cell: E55	0.235
	"Prob of Damage Anal. 17-mm OCB" Cell: F55	34, "Prob of Damage Anal. 17-mm OCB" Cell: F55	0.235
	"Prob of Damage Anal. 17-mm OCB" Cell: G55	34, "Prob of Damage Anal. 17-mm OCB" Cell: G55	0.088

Table B-2. Formulas used in Spreadsheets in Output DTN: MO0703PASDSTAT.001 (Continued)

Formula (Bold), Function	Location in File ("Worksheet")	Input (Location in file or value if directly entered) in Order of Use in Formula	Output (Value)
***CDSP Kinematic Damage Abstraction 17-mm Degraded.xls* (Continued)**			
	"Prob of Damage Anal. 17-mm OCB" Cell: H55	34, "Prob of Damage Anal. 17-mm OCB" Cell: H55	0.147
	"Prob of Damage Anal. 17-mm OCB" Cell: I55	34, "Prob of Damage Anal. 17-mm OCB" Cell: I55	0.059
	"Prob of Damage Anal. 17-mm OCB" Cell: J55	34, "Prob of Damage Anal. 17-mm OCB" Cell: J55	0
Built-in Excel Command: **AVERAGE (number1, number2,…)**, Calculates the Mean of the Numbers in the Input Cells	"WP Total" Cell: E41	"WP Total" Cells: E5:E38	0.041
	"WP Total" Cell: F41	"WP Total" Cells: F5:F38	0.014
	"WP Total" Cell: G41	"WP Total" Cells: G5:G38	0.002
	"WP Total" Cell: E82	"WP Total" Cells: E46:E79	0.435
	"WP Total" Cell: F82	"WP Total" Cells: F46:F79	0.181
	"WP Total" Cell: G82	"WP Total" Cells: G46:G79	0.075
	"WP Total" Cell: E123	"WP Total" Cells: E87:E120	1.671
	"WP Total" Cell: F123	"WP Total" Cells: F87:F120	0.781
	"WP Total" Cell: G123	"WP Total" Cells: G87:G120	0.359
	"WP Total" Cell: E164	"WP Total" Cells: E128:E161	3.535
	"WP Total" Cell: F164	"WP Total" Cells: F128:F161	1.858
	"WP Total" Cell: G164	"WP Total" Cells: G128:G161	0.973
	"Gamma for 90%_d17" Cell: C17	"Gamma for 90%_d17" Cells: C8:C15	0.174
	"Gamma for 90%_d17" Cell: C50	"Gamma for 90%_d17" Cells: C26:C48	0.643
	"Gamma for 90%_d17" Cell: C90	"Gamma for 90%_d17" Cells: C57:C88	1.775
	"Gamma for 90%_d17" Cell: C132	"Gamma for 90%_d17" Cells: C97:C130	3.535
	"Log-Normal for 90%_d17" Cell: C17	"Log-Normal for 90%_d17" Cells: D8:D15	-2.443
	"Log-Normal for 90%_d17" Cell: C49	"Log-Normal for 90%_d17" Cells: D25:D47	-1.443
	"Log-Normal for 90%_d17" Cell: C87	"Log-Normal for 90%_d17" Cells: D54:D85	0.176
	"Log-Normal for 90%_d17" Cell: C127	"Log-Normal for 90%_d17" Cells: D92:D125	1.104
	"Gamma for 100%_d17" Cell: C17	"Gamma for 100%_d17" Cells: C8:C15	0.059
	"Gamma for 100%_d17" Cell: C48	"Gamma for 100%_d17" Cells: C24:C4	0.268
	"Gamma for 100%_d17" Cell: C88	"Gamma for 100%_d17" Cells: C55:C86	0.830
	"Gamma for 100%_d17" Cell: C130	"Gamma for 100%_d17" Cells: C95:C128	1.858
	"Gamma for 105%_d17" Cell: C12	"Gamma for 105%_d17" Cells: C8:C10	0.023

Table B-2. Formulas used in Spreadsheets in Output DTN: MO0703PASDSTAT.001 (Continued)

Formula (Bold), Function	Location in File ("Worksheet")	Input (Location in file or value if directly entered) in Order of Use in Formula	Output (Value)
***CDSP Kinematic Damage Abstraction 17-mm Degraded.xls* (Continued)**			
Built-in Excel Command: **AVERAGE (number1, number2,…)**, Calculates the Mean of the Numbers in the Input Cells (Continued)	"Gamma for 105%_d17" Cell: C37	"Gamma for 105%_d17" Cells: C23:C35	0.196
	"Gamma for 105%_d17" Cell: C75	"Gamma for 105%_d17" Cells: C44:C73	0.407
	"Gamma for 105%_d17" Cell: C117	"Gamma for 105%_d17" Cell: C82:C115	0.973
Built-in Excel Command: **STDEV (number1, number2,…)**, Calculates the Standard Deviation of the Numbers in the Input Cells	"WP Total", Cell: E42	"WP Total", Cells: E5:E38	0.129
	"WP Total", Cell: F42	"WP Total", Cells: F5:F38	0.045
	"WP Total", Cell: G42	"WP Total", Cells: G5:G38	0.010
	"WP Total", Cell: E83	"WP Total", Cells: E46:E79	0.743
	"WP Total", Cell: F83	"WP Total", Cells: F46:F79	0.327
	"WP Total", Cell: G83	"WP Total", Cells: G46:G79	0.153
	"WP Total", Cell: E124	"WP Total", Cells: E87:E120	1.467
	"WP Total", Cell: F124	"WP Total", Cells: F87:F120	0.758
	"WP Total", Cell: G124	"WP Total", Cells: G87:G120	0.401
	"WP Total", Cell: E165	"WP Total", Cells: E128:E161	1.858
	"WP Total", Cell: F165	"WP Total", Cells: F128:F161	1.159
	"WP Total", Cell: G165	"WP Total", Cells: G128:G161	0.717
	"Gamma for 90%_d17" Cell: C18	"Gamma for 90%_d17" Cells: C8:C15	0.228
	"Gamma for 90%_d17" Cell: C51	"Gamma for 90%_d17" Cells: C26:C48	0.830
	"Gamma for 90%_d17" Cell: C91	"Gamma for 90%_d17" Cells: C57:C88	1.449
	"Gamma for 90%_d17" Cell: C133	"Gamma for 90%_d17" Cells: C97:C130	1.858
	"Log-Normal for 90%_d17" Cell: C18	"Log-Normal for 90%_d17" Cells: D8:D15	1.313
	"Log-Normal for 90%_d17" Cell: C50	"Log-Normal for 90%_d17" Cells: D25:D47	1.621
	"Log-Normal for 90%_d17" Cell: C88	"Log-Normal for 90%_d17" Cells: D54:D85	1.001
	"Log-Normal for 90%_d17" Cell: C128	"Log-Normal for 90%_d17" Cells: D92:D125	0.616
	"Gamma for 100%_d17" Cell: C18	"Gamma for 100%_d17" Cells: C8:C15	0.080
	"Gamma for 100%_d17" Cell: C49	"Gamma for 100%_d17" Cells: C24:C4	0.369
	"Gamma for 100%_d17" Cell: C89	"Gamma for 100%_d17" Cells: C55:C86	0.755
	"Gamma for 100%_d17" Cell: C130	"Gamma for 100%_d17" Cells: C95:C128	1.159
	"Gamma for 105%_d17" Cell: C13	"Gamma for 105%_d17" Cells: C8:C10	0.031

Table B-2. Formulas used in Spreadsheets in Output DTN: MO0703PASDSTAT.001 (Continued)

Formula (Bold), Function	Location in File ("Worksheet")	Input (Location in file or value if directly entered) in Order of Use in Formula	Output (Value)
***CDSP Kinematic Damage Abstraction 17-mm Degraded.xls* (Continued)**			
Built-in Excel Command: **STDEV (number1, number2,…)**, Calculates the Standard Deviation of the Numbers in the Input Cells (Continued)	"Gamma for 105%_d17" Cell: C38	"Gamma for 105%_d17" Cells: C23:C35	0.197
	"Gamma for 105%_d17" Cell: C76	"Gamma for 105%_d17" Cells: C44:C73	0.403
	"Gamma for 105%_d17", Cell: C118	"Gamma for 105%_d17" Cell: C82:C115	0.717
(Y1-Y2)/(X1-X2), Calculates the Linear Slope Between Two Points	"Prob of Damage – New" Cells: B19:D19 "Dependence on RST" Cells: B39:D39 and O39:Q39	Corresponding Points that are Used to Calculate Slope	Slope
-Y1/Slope+X1, Calculates the X-Intercept Given a Point and Slope	"Prob of Damage – New" Cells: B20:D20	Corresponding Slope and Point that are Used to Calculate X-Intercept	X - Intercept
Y1+Slope*(x – X1), Calculates the y given an x for a linear equation of the form y = Slope*x + Y-Intercept	"Prob of Damage – New" Cells: B21:B24, C21:C23, D21 "Dependence on RST" Cells: B27:E28	Corresponding Point, x, and Slope Used to Calculate y	y
(Mean/Standard Deviation)^2, Calculates Alpha, One of the Inputs to the Gamma Distribution	"Gamma for 90%_d17" Cells: C19, C52, C92, C134	"Gamma for 90%_d17" Cells: C17:C18, C50:C51, C90:C91, C132:C133	0.586, 0.601, 1.501, 3.621
	"Gamma for 90%_d17" Cells: D171:D183	"Gamma for 90%_d17" Cells: B171:B183, C171:C183	Alpha
	"Gamma for 100%_d17" Cells: C19, C50, C90, C132	"Gamma for 100%_d17" Cells: C12:C13, C37:C38, C75:C76, C117:C118	0.535, 0.527, 1.207, 2.568
	"Gamma for 100%_d17" Cells: D174:D186	"Gamma for 100%_d17" Cells: B174:B186, C174:C186	Alpha
	"Gamma for 105%_d17" Cells: C14, C39, C77, C119	"Gamma for 105%_d17" Cells: C12:C13, C37:C38, C75:C76, C117:C118	0.539, 0.986, 1.017, 1.841
	"Gamma for 105%_d17" Cells: D159:D171	"Gamma for 105%_d17" Cells: B159:B171, C159:C171	Alpha
(Standard Deviation)^2 / Mean, Calculates Beta, One of the Inputs to the Gamma Distribution	"Gamma for 90%_d17" Cells: C20, C53, C93, C135	"Gamma for 90%_d17" Cells: C17:C18, C50:C51, C90:C91, C132:C133	0.298, 1.071, 1.183, 0.976
	"Gamma for 90%_d17" Cells: E171:E183	"Gamma for 90%_d17" Cells: C171:C183, B171:B183	Beta
	"Gamma for 100%_d17" Cells: C20, C51, C91, C133	"Gamma for 100%_d17" Cells: C12:C13, C37:C38, C75:C76, C117:C118	0.110, 0.508, 0.687, 0.724
	"Gamma for 100%_d17" Cells: E174:E186	"Gamma for 100%_d17" Cells: C174:C186, B174:B186	Beta
	"Gamma for 105%_d17" Cells: C15, C40, C78, C120	"Gamma for 105%_d17" Cells: C12:C13, C37:C38, C75:C76, C117:C118	0.043, 0.199, 0.400, 0.528
	"Gamma for 105%_d17" Cells: E159:E171	"Gamma for 105%_d17" Cells: C159:C171, B159:B171	Beta

Table B-2. Formulas used in Spreadsheets in Output DTN: MO0703PASDSTAT.001 (Continued)

Formula (Bold), Function	Location in File ("Worksheet")	Input (Location in file or value if directly entered) in Order of Use in Formula	Output (Value)
***CDSP Kinematic Damage Abstraction 17-mm Degraded.xls* (Continued)**			
Built-in Excel Command: **GAMMAINV (probability, alpha, beta)**, Calculates the Inverse of the Gamma Cumulative Distribution Using the Probability Associated with the Distribution, Alpha, and Beta	"Gamma for 90%_d17" Cells: D8:D15, D26:D48, D57:D88, D97:D130	"Gamma for 90%_d17" Cells: E8:E15, C19, C20, E26:E48, C52, C53, E57:E88, C92, C93, E97:E130, C134, C135	Inverse of Gamma Distribution Used for Comparison in Q-Q Plot
	"Gamma for 100%_d17" Cells: D8:D15, D24:D46, D55:D86, D95:D128	"Gamma for 100%_d17" Cells: E8:E15, C19, C20, E24:E46, C50, C51, E55:E86, C90, C91, E95:E128, C132, C133	
	"Gamma for 105%_d17" Cells: D8:D10, D23:D35, D44:D73, D82:D115	"Gamma for 105%_d17" Cells: E8:E10, C14, C15, E23:E35, C39, C40, E44:E73, C77, C78, E82:E115, C119, C120	
	"Gamma for 90%_d17" Cells: F171:J183	"Gamma for 90%_d17" Cells: F169:J169, D171:D183, E171:E183	Inverse of Gamma Distribution Used to Generate Non-exceedance Curves for Comparison to All Data
	"Gamma for 100%_d17" Cells: F174:J186	"Gamma for 100%_d17" Cells: F172:J172, D174:D186, E174:E186	
	"Gamma for 105%_d17" Cells: F159:J171	"Gamma for 90%_d17" Cells: F157:J157, D159:D171, E159:E171	
Built-in Excel Command: **Add Trendline (chart input),** Calculates the Quadratic Fit to the Data of the Form $y = ax^2 + bx + c$	"Gamma for 90%_d17" Cells: B154:D155	"Gamma for 90%_d17" Cells: B147:E149"	a, b, and c for the Mean and Standard Deviation
	"Gamma for 100%_d17" Cells: B155:D156	"Gamma for 100%_d17" Cells: B148:E150"	
	"Gamma for 105%_d17" Cells: B139:D140	"Gamma for 90%_d17" Cells: B132:E134"	
Built-in Excel Command: **ln(number)**, Calculates the Natural-Log of a Number	"Log-Normal for 90%_d17" Cells: D8:D15, D25:D47, D54:D85, D92:D125	"Log-Normal for 90%_d17" Cells: C8:C15, C25:C47, C54:C85, C92:C125	ln(input)
Built-in Excel Command: **exp(number)**, Calculates the Exponent Applied to the Base e	"Log-Normal for 90%_d17" Cells: F8:F15, F25:F47, F54:F85, F92:F125	"Log-Normal for 90%_d17" Cells: E8:E15, E25:E47, E54:E85, E92:E125	e^{input}
Built-in Excel Command: **NORMINV (probability, mean, standard deviation)**, Calculates the Inverse of the Normal Cumulative Distribution for the Given Inputs	"Log-Normal for 90%_d17" Cells: E8:E15, E25:E47, E54:E85, E92:E125	"Log-Normal for 90%_d17" Cells: G8:G15, C17, C18, G25:G47, C49, C50, G54:G85, C87, C88, G92:G125, C127, C128	Inverse of Normal Distribution Used for Comparison in Q-Q Plot

Table B-2. Formulas used in Spreadsheets in Output DTN: MO0703PASDSTAT.001 (Continued)

Formula (Bold), Function	Location in File ("Worksheet")	Input (Location in file or value if directly entered) in Order of Use in Formula	Output (Value)
***CDSP Kinematic Damage Abstraction 17-mm Degraded.xls* (Continued)**			
|expected – actual| * 100 / expected, Calculates the Percent Error	"Gamma for 90%_d17" Cells: F8:F15, F26:F48, F57:F88, F97:F130	"Gamma for 90%_d17" Cells: C8:D15, C26:D48, C57:D88, C97:D130	% Error
	"Log-Normal for 90%_d17" Cells: H8:H15, H25:H47, H54:H85, H92:H125	"Log-Normal for 90%_d17" Cells: C8:C15, F8:F15, C25:C47, F25:F47, C54:C85, F54:F85, C92:C125, F92:F125	
	"Gamma for 100%_d17" Cells: F8:F15, F24:F46, F55:F86, F95:F128	"Gamma for 100%_d17" Cells: C8:D15, C24:D46, C55:D86, C95:D128	
	"Gamma for 105%_d17" Cells: F8:F10, F23:F35, F44:F73, F82:F115	""Gamma for 105%_d17" Cells: C8:D10, C23:D35, C44:D73, C82:D115	
(expected – actual)^2, Calculates the Squared Difference	"Gamma for 90%_d17" Cells: G8:G15, G26:G48, G57:G88, G97:G130	"Gamma for 90%_d17" Cells: C8:D15, C26:D48, C57:D88, C97:D130	Squared Difference
	"Log-Normal for 90%_d17" Cells: I8:I15, I25:I47, I54:I85, I92:I125	"Log-Normal for 90%_d17" Cells: C8:C15, F8:F15, C25:C47, F25:F47, C54:C85, F54:F85, C92:C125, F92:F125	
	"Gamma for 100%_d17" Cells: G8:G15, G24:G46, G55:G86, G95:G128	"Gamma for 100%_d17" Cells: C8:D15, C24:D46, C55:D86, C95:D128	
	"Gamma for 105%_d17" Cells: G8:G10, G23:G35, G44:G73, G82:G115	""Gamma for 105%_d17" Cells: C8:D10, C23:D35, C44:D73, C82:D115	
$a_i = a_1 + \sum_{j=2}^{i} \frac{1}{n}$ $a_1 = \frac{1}{2n}$ n = # of cases with nonzero damage areas, Calculates the Cumulative Probability	"Gamma for 90%_d17" Cells: E8:E15, E26:E48, E57:E88, E97:E130 "Log-Normal for 90%_d17" Cells: G8:G15, G25:G47, G54:G85, G92:G125 "Gamma for 100%_d17" Cells: E8:E15, E24:E46, E55:E86, E95:E128 "Gamma for 105%_d17" Cells: E8:E10, E23:E35, E44:E73, E82:E115	Number of Nonzero Damaged Areas for Given PGV Level	Cumulative Probability
CDSP Kinematic Damage Abstraction 23-mm Degraded.xls			
All of the formulas used in this file are used in the file *CDSP Kinematic Damage Abstraction 17-mm Degraded.xls*. For documentation of the formulas used in this file, refer to documentation of formulas used in the file *CDSP Kinematic Damage Abstraction 17-mm Degraded.xls*.			
CDSP Kinematic Damage Abstraction 23-mm Intact.xls			
All of the formulas used in this file are used in the file *CDSP Kinematic Damage Abstraction 17-mm Degraded.xls*. For documentation of the formulas used in this file, refer to documentation of formulas used in the file *CDSP Kinematic Damage Abstraction 17-mm Degraded.xls*.			

Table B-2. Formulas used in Spreadsheets in Output DTN: MO0703PASDSTAT.001 (Continued)

Formula (Bold), Function	Location in File ("Worksheet")	Input (Location in file or value if directly entered) in Order of Use in Formula	Output (Value)
DS Damaged Areas with Rubble.xls			
Built-in Excel Command: **ln(number)**, Calculates the Natural-Log of a Number	"Load" Cells: C8:C13	"Load" Cells: B8:B13	ln(input)
	"PGV-H1 to (A+1) Regression" Cells: E15:E65	"PGV-H1 to (A+1) Regression" Cells: B15:B65	
	"PGV-H1 to (A+1) Regression" Cells: F15:F65	"PGV-H1 to (A+1) Regression" Cells: D15:D65	
A - Mean, Calculates the Residual	"Load" Cells: D8:D13	"Load" Cells" C8:C13, C15	Residual
	"PGV-H1 to (A+1) Regression" Cells" O15:O65	"PGV-H1 to (A+1) Regression" Cells" F15:F65, 0.833*(E15:E65)+0.9145	
$a_i = a_1 + \sum_{j=2}^{i} \frac{1}{n}$ $a_1 = \frac{1}{2n}$ n = # of cases with nonzero values, Calculates the Quantile	"Load" Cells: F8:F13	Number of Cases with Nonzero Average Pressure on the Segments	Quantile
	"PGV-H1 to (A+1) Regression" Cells: Q15:Q65	Number of Realizations per PGV Level	
Built-in Excel Command: **NORMINV (probability, mean, standard deviation)**, Calculates the Inverse of the Normal Cumulative Distribution for the Given Inputs	"Load" Cells: G8:G13	"Load" Cells: F8:F13, E15, E16	Inverse of Normal Distribution Used for Comparison in Q-Q Plot
	"PGV-H1 to (A+1) Regression" Cells: R15:R65	"PGV-H1 to (A+1) Regression" Cells: Q15:Q65, P66, P67	
Built-in Excel Command: **exp(number)**, Calculates the Exponent Applied to the Base e	"Load" Cells: H8:H13	"Load" Cells: G8:G13, C15	e^{input}
	"PGV-H1 to (A+1) Regression" Cells: AD23:AD34	"PGV-H1 to (A+1) Regression" Cells: AC23:AC34	
	"PGV-H1 to (A+1) Regression" Cells: AE23:AE34	"PGV-H1 to (A+1) Regression" (Cells: AC23:AC34) – 1.645*P67	
	"PGV-H1 to (A+1) Regression" Cells: AF23:AF34	"PGV-H1 to (A+1) Regression" (Cells: AC23:AC34) + 1.645*P67	
	"4.07 ms PGV – Case 2 BCs" Cells: D55:D66, L55:L66, T55:T66	"4.07 ms PGV – Case 2 BCs" Cells: C55:C66; K55:K66; S55:S66	
	"4.07 ms PGV – Case 1 BCs" Cells: D55:D66, L55:L66, T55:T66	"4.07 ms PGV – Case 1 BCs" Cells: C55:C66; K55:K66; S55:S66	
	"2.44 ms PGV – Case 2 BCs" Cells: D55:D66, L55:L66, T55:T66	"2.44 ms PGV – Case 2 BCs" Cells: C55:C66; K55:K66; S55:S66	
	"2.44 ms PGV – Case 1 BCs" Cells: D55:D66, L55:L66, T55:T66	"2.44 ms PGV – Case 1 BCs" Cells: C55:C66; K55:K66; S55:S66	
	"1.05 ms PGV – Case 2 BCs" Cells: D57:D68, L57:L68, T57:T68	"1.05 ms PGV – Case 2 BCs" Cells: C57:C68; K57:K68; S57:S68	
	"1.05 ms PGV – Case 1 BCs" Cells: D54:D65, L54:L65, T54:T65	"1.05 ms PGV – Case 1 BCs" Cells: C54:C65; K54:K65; S54:S65	

Table B-2. Formulas used in Spreadsheets in Output DTN: MO0703PASDSTAT.001 (Continued)

Formula (Bold), Function	Location in File ("Worksheet")	Input (Location in file or value if directly entered) in Order of Use in Formula	Output (Value)
***DS Damaged Areas with Rubble.xls* (Continued)**			
Built-in Excel Command: **AVERAGE (number1, number2,…)**, Calculates the Mean of the Numbers in the Input Cells	"Load" Cells: B15:E15	"Load" Cells: B8:E13	Mean of the Input Data
	"PGV-H1 to (A+1) Regression" Cells: O66:P66	"PGV-H1 to (A+1) Regression" Cells: O15:O65, P15:P65	
Built-in Excel Command: **STDEV (number1, number2,…)**, Calculates the Standard Deviation of the Numbers in the Input Cells	"Load" Cells: B16:E16	"Load" Cells: B8:E13	Standard Deviation of the Input Data
	"PGV-H1 to (A+1) Regression" Cells: L51:L53	"PGV-H1 to (A+1) Regression" Cells: F15:F31, F32:F48, F49:F65	
	"PGV-H1 to (A+1) Regression" Cells: O67:P67	"PGV-H1 to (A+1) Regression" Cells: O15:O65, P15:P65	
A + 1, Calculates A + 1 to Show that A + 1 Follows a Log-Normal Distribution	"PGV-H1 to (A+1) Regression" Cells: D15:D65	"PGV-H1 to (A+1) Regression" Cells: C15:C65	A + 1
Built-in Excel Command: **Add Trendline (chart input),** Calculates the Linear Fit to the Data of the Form y = m*x + b, and the R^2 value	"PGV-H1 to (A+1) Regression" Plot in Cells: G15:N47	"PGV-H1 to (A+1) Regression" Cells: E15:E65, F15:F65	ln(A+1) = 0.8333 * ln(PGV-H1) + 0.9145, R^2 = 0.5429
0.8333*ln(x) + 0.9145, Used to Calculate ln(A+1)	"PGV-H1 to (A+1) Regression" Cells: AC23:AC34	"PGV-H1 to (A+1) Regression" Cells: AB23:AB34	ln(A+1)
	"4.07 ms PGV – Case 2 BCs" Cells: D43, L43, T43	"4.07 ms PGV – Case 2 BCs" Cells: D42, L42, T42	
	"4.07 ms PGV – Case 1 BCs" Cells: D43, L43, T43	"4.07 ms PGV – Case 1 BCs" Cells: D42, L42, T42	
	"2.44 ms PGV – Case 2 BCs" Cells: D43, L43, T43	"2.44 ms PGV – Case 2 BCs" Cells: D42, L42, T42	
	"2.44 ms PGV – Case 1 BCs" Cells: D43, L43, T43	"2.44 ms PGV – Case 1 BCs" Cells: D42, L42, T42	
	"1.05 ms PGV – Case 2 BCs" Cells: D45, L45, T45	"1.05 ms PGV – Case 2 BCs" Cells: D44, L44, T44	
	"1.05 ms PGV – Case 1 BCs" Cells: D42, L42, T42	"1.05 ms PGV – Case 1 BCs" Cells: D41, L41, T41	
Mean[ln(A+1)] + ln(f) + Mean[ln(P_{stat})], Calculates the Mean of ln(f*P_{stat}*(A+1))	"4.07 ms PGV – Case 2 BCs" Cells: D48, L48, T48	"4.07 ms PGV – Case 2 BCs" Cells: D43, D47, D45; L43, L47, L45; T43, T47, T45	Mean of ln(f*P_{stat}*(A+1))
	"4.07 ms PGV – Case 1 BCs" Cells: D48, L48, T48	"4.07 ms PGV – Case 1 BCs" Cells: D43, D47, D45; L43, L47, L45; T43, T47, T45	
	"2.44 ms PGV – Case 2 BCs" Cells: D48, L48, T48	"2.44 ms PGV – Case 2 BCs" Cells: D43, D47, D45; L43, L47, L45; T43, T47, T45	

Table B-2. Formulas used in Spreadsheets in Output DTN: MO0703PASDSTAT.001 (Continued)

Formula (Bold), Function	Location in File ("Worksheet")	Input (Location in file or value if directly entered) in Order of Use in Formula	Output (Value)
***DS Damaged Areas with Rubble.xls* (Continued)**			
Mean[ln(A+1)] + ln(f) + Mean[ln(P_{stat})], Calculates the Mean of ln(f*P_{stat}*(A+1)) (Continued)	"2.44 ms PGV – Case 1 BCs" Cells: D48, L48, T48	"2.44 ms PGV – Case 1 BCs" Cells: D43, D47, D45; L43, L47, L45; T43, T47, T45	
	"1.05 ms PGV – Case 2 BCs" Cells: D50, L50, T50	"1.05 ms PGV – Case 2 BCs" Cells: D45, D49, D47, L45, L49, L47, T45, T49, T47	
	"1.05 ms PGV – Case 1 BCs" Cells: D47, L47, T47	"1.05 ms PGV – Case 1 BCs" Cells: D42, D46, D44; L42, L46, L44; T42 T46, T44	
Built-in Excel Command: **SQRT(A2+B2)**, Calculates Beta of ln(f*P_{stat}*(A+1))	"4.07 ms PGV – Case 2 BCs" Cells: D49, L49, T49	"4.07 ms PGV – Case 2 BCs" Cells: D44, D46; L44, L46; T44, T46	Beta
	"4.07 ms PGV – Case 1 BCs" Cells: D49, L49, T49	"4.07 ms PGV – Case 1 BCs" Cells: D44, D46; L44, L46; T44, T46	
	"2.44 ms PGV – Case 2 BCs" Cells: D49, L49, T49	"2.44 ms PGV – Case 2 BCs" Cells: D44, D46; L44, L46; T44, T46	
	"2.44 ms PGV – Case 1 BCs" Cells: D49, L49, T49	"2.44 ms PGV – Case 1 BCs" Cells: D44, D46; L44, L46; T44, T46	
	"1.05 ms PGV – Case 2 BCs" Cells: D51, L51, T51	"1.05 ms PGV – Case 2 BCs" Cells: D46, D48; L46, L48; T46, T48	
	"1.05 ms PGV – Case 1 BCs" Cells: D48, L48, T48	"1.05 ms PGV – Case 1 BCs" Cells: D43, D45; L43, L45; T43, T45	
Built-in Excel Command: **NORMSINV (probability)**, Calculates the Inverse of the Standard Normal Cumulative Distribution for a Given Probability	"4.07 ms PGV – Case 2 BCs" Cells: B55:B66, J55:J66, R55:R66	"4.07 ms PGV – Case 2 BCs" Cells: A55:A66, I55:I66, Q55:Q66	"z" for Normal Distribution
	"4.07 ms PGV – Case 1 BCs" Cells: B55:B66, J55:J66, R55:R66	"4.07 ms PGV – Case 1 BCs" Cells: A55:A66, I55:I66, Q55:Q66	
	"2.44 ms PGV – Case 2 BCs" Cells: B55:B66, J55:J66, R55:R66	"2.44 ms PGV – Case 2 BCs" Cells: A55:A66, I55:I66, Q55:Q66	
	"2.44 ms PGV – Case 1 BCs" Cells: B55:B66, J55:J66, R55:R66	"2.44 ms PGV – Case 1 BCs" Cells: A55:A66, I55:I66, Q55:Q66	
	"1.05 ms PGV – Case 2 BCs" Cells: B57:B68, J57:J68, R57:R68	"1.05 ms PGV – Case 2 BCs" Cells: A57:A68, I57:I68, Q57:Q68	
	"1.05 ms PGV – Case 1 BCs" Cells: B54:B65, J54:J65, R54:R65	"1.05 ms PGV – Case 1 BCs" Cells: A54:A65, I54:I65, Q54:Q65	
Mean of [ln(f*P_{stat}*(A+1))] + z*Beta, Calculates the ln of the Dynamic Load	"4.07 ms PGV – Case 2 BCs" Cells: C55:C66, K55:K66, S55:S66	"4.07 ms PGV – Case 2 BCs" Cells: D48, B55:B66, D49; L48, J55:J66, L49; T48, R55:R66, T49	Ln of Dynamic Load
	"4.07 ms PGV – Case 1 BCs" Cells: C55:C66, K55:K66, S55:S66	"4.07 ms PGV – Case 1 BCs" Cells: D48, B55:B66, D49; L48, J55:J66, L49; T48, R55:R66, T49	
	"2.44 ms PGV – Case 2 BCs" Cells: C55:C66, K55:K66, S55:S66	"2.44 ms PGV – Case 2 BCs" Cells: D48, B55:B66, D49; L48, J55:J66, L49; T48, R55:R66, T49	
	"2.44 ms PGV – Case 1 BCs" Cells: C55:C66, K55:K66, S55:S66	"2.44 ms PGV – Case 1 BCs" Cells: D48, B55:B66, D49; L48, J55:J66, L49; T48, R55:R66, T49	

Table B-2. Formulas used in Spreadsheets in Output DTN: MO0703PASDSTAT.001 (Continued)

Formula (Bold), Function	Location in File ("Worksheet")	Input (Location in file or value if directly entered) in Order of Use in Formula	Output (Value)
***DS Damaged Areas with Rubble.xls* (Continued)**			
Mean of [ln(f*P_{stat}*(A+1))] + z*Beta, Calculates the ln of the Dynamic Load (Continued)	"1.05 ms PGV – Case 2 BCs" Cells: C57:C68, K57:K68, S57:S68	"1.05 ms PGV – Case 2 BCs" Cells: D50, B57:B68, D51; L50, J57:J68, L51; T50, R57:R68, T50	
	"1.05 ms PGV – Case 1 BCs" Cells: C54:C65, K54:K65, S54:S65	"1.05 ms PGV – Case 1 BCs" Cells: D47, B54:B65, D48; L47, J54:J65, L48; T47, R54:R65, T48	
Built-in Excel Command: **FORECAST(x, known_y's, known_x's)**, Calculates, or predicts, a future value by using existing values using linear regression	"4.07 ms PGV – Case 2 BCs" Cells: Cells: G66, M64:M66, N62:N66, O58:O64, U59:U65, V58:V64, W56:W61	"4.07 ms PGV – Case 2 BCs" Cells: D66, F14:F15, E14:E15; L64:L66, B13:B16, A13:A16; L62:L66, D14:D28, C14:C28; L58:L64, F14:F24, E14:E24; T59:T65, B13:B20, A13:A20; T58:T64, D14:D28, C14:C28; T56:T61, F15:F34, E15:E34	Damaged Area
	"4.07 ms PGV – Case 1 BCs" Cells: Cells: M65:M66, N64:N66, O59:O64, U62:U65, V59:V64, W56:W61	"4.07 ms PGV – Case 1 BCs" Cells: L65:L66, B14:B16, A14:A16; L64:L66, D15:D20, C15:C20; L59:L64, F15:F24, E15:E24; T62:T65, B14:B18, A14:A18; T59:T64, D15:D20, C15:C20; T56:T61, F15:F34, E15:E34	
	"2.44 ms PGV – Case 2 BCs" Cells: Cells: M66, N65:N66, O60:O65, U62:U66, V60:V65, W58:W63	"2.44 ms PGV – Case 2 BCs" Cells: L66, B13:B14, A13:A14; L65:L66, D15:D17, C15:C17; L60:L65, F14:F20, E14:E20; T62:T66, B13:B17, A13:A17; T60:T65, D14:D20, C14:C20; T58:T63, F15:F27, E15:E27	
	"2.44 ms PGV – Case 1 BCs" Cells: N65:N66, O62:O65, U65:U66, V62:V65, W58:W63	"2.44 ms PGV – Case 1 BCs" Cells: L65:L66, D15:D17, C15:C17; L62:L65, F15:F20, E15:E20; T65:T66, B15:B17, A15:A17; T62:T65, D15:D20, C15:C20; T58:T63, F15:F27, E15:E27	
	"1.05 ms PGV – Case 2 BCs" Cells: O67:O68, U68, V67:V68, W64:W67	"1.05 ms PGV – Case 2 BCs" Cells: L67:L68, F14:F17, E14:E17; T68, B13:B14, A13:A14; T67:T68, D14:D17, C14:C17; T64:T67, F15:F19, E15:E19	
	"1.05 ms PGV – Case 1 BCs" Cells: O65, V65, W61:W64	"1.05 ms PGV – Case 1 BCs" Cells: L65, F16:F17, E16:E17; T65, D16:D17, C16:C17; T61:T64, F15:F19, E15:E19	

Table B-2. Formulas used in Spreadsheets in Output DTN: MO0703PASDSTAT.001 (Continued)

Formula (Bold), Function	Location in File ("Worksheet")	Input (Location in file or value if directly entered) in Order of Use in Formula	Output (Value)
Fault Displacement Abstraction.xls			
Built-in Excel Command: **SUM(Number1, Number 2, …)**	"Tables" Cells: C138, B149, C147, C148, C149, E149, C189, D189	"Tables" Cells: C132:C137; B147:B148; C132:C134; C135:C137; C147:B148; E147:E148; C185:C188; D185:D188	Total of Input Values
Built-in Excel Command: **COUNTA(value1, value2, …)**, counts the number of cells that are not empty	"Tables" Cells: B185:B187	"Tables" Cells: B46:B61, B64:B71, B74:B75; B78:B88; B91:B94	WPs Impacted by Each Fault
Built-in Excel Command: **PI()**, Provides the Number π for Calculations	"Tables" Cells: G147:G148	N/A	π
Built-in Excel Command: **LOG(Number)**, Calculates the Logarithm of a Number, Base 10, for Use in a Power Law Fit	"Hazard Calcs" Cells: F11:F14, G20:G22, F32:F34, G40:G42, F52:F54, G60:G62, F72:F74, G80:G82, F92:F94, G100:G102, F112:F114, G120:G122, F132:F134, G140:G142, G160:G162, F172:F174, G180:G182, F192:F194, G200:G202, F212:F214, G220:G222,	"Hazard Calcs" Cells: A17:B21, A36:B41, A56:B60, A75:B80, A94:B99, A113:B119, A130:B133, A137:B139, A157:B159, A174:B179, A192:B199, A210:B213, A217:B219	Log(number)
Frame Fragility Analysis.xls			
Built-in Excel Command: **SQRT(number),** Calculates the Square Root of the Input Number	"2-mm Full Load" Cells: D20, L20, T20, AB20, AJ20	"2-mm Full Load" Cells: D18:D19, L18:L19, T18:T19, AB18:AB19, AJ18:AJ19	Square Root of Input
	"5-mm Full Load" Cells: D20, L20, T20, AB20, AJ20	"5-mm Full Load" Cells: D18:D19, L18:L19, T18:T19, AB18:AB19, AJ18:AJ19	
	"10-mm Full Load" Cells: C20, L20, T20, AB20, AJ20	"10-mm Full Load" Cells: C18:C19, L18:L19, T18:T19, AB18:AB19, AJ18:AJ19	
	"15-mm Full Load" Cells: D20, L20, T20, AB20	"15-mm Full Load" Cells: D18:D19, L18:L19, T18:T19, AB18:AB19	
	"2-mm 50% Load" Cells: D20, L20, T20, AB20, AJ20	"2-mm 50% Load" Cells: D18:D19, L18:L19, T18:T19, AB18:AB19, AJ18:AJ19	
	"5-mm 50% Load" Cells: C20, L20, T20, AB20, AJ20	"5-mm 50% Load" Cells: C18:C19, L18:L19, T18:T19, AB18:AB19, AJ18:AJ19	
	"10-mm 50% Load" Cells: D20, L20, T20, AB20	"10-mm 50% Load" Cells: D18:D19, L18:L19, T18:T19, AB18:AB19	
	"15-mm 50% Load" Cells: D20, L20, T20, AB20	"15-mm 50% Load" Cells: D18:D19, L18:L19, T18:T19, AB18:AB19	
	"2-mm 10% Load" Cells: D20, L20, T20, AB20	"2-mm 10% Load" Cells: D18:D19, L18:L19, T18:T19, AB18:AB19	

Table B-2. Formulas used in Spreadsheets in Output DTN: MO0703PASDSTAT.001 (Continued)

Formula (Bold), Function	Location in File ("Worksheet")	Input (Location in file or value if directly entered) in Order of Use in Formula	Output (Value)
Frame Fragility Analysis.xls **(Continued)**			
Built-in Excel Command: **SQRT(number),** Calculates the Square Root of the Input Number (Continued)	"5-mm 10% Load" Cells: D20, L20, T20, AB20	"5-mm 10% Load" Cells: D18:D19, L18:L19, T18:T19, AB18:AB19	
	"10-mm 10% Load" Cells: D20, L20, T20, AB20	"10-mm 10% Load" Cells: D18:D19, L18:L19, T18:T19, AB18:AB19	
	"15-mm 10% Load" Cells: D20	"15-mm 10% Load" Cells: D18:D19	
	"Load and Capacity" Cells: F49:F52	"Load and Capacity" Cell: E50	
Built-in Excel Command: **ln(number),** Calculates the natural-log of the input	"2-mm Full Load" Cells: B26:B81, F26:F80, J26:J69, N26:N68, R26:R68, V26:V67, Z26:Z82, AD26:AD81, AH26:AH91, AL26:AL90	"2-mm Full Load" Cells: A26:A81, E26:E80, I26:I69, M26:M68, Q26:Q68, U26:U67, Y26:Y82, AC26:AC81, AG26:AG91, AK26:AK90	ln(input)
	"5-mm Full Load" Cells: B26:B63, F26:F62, J26:J63, N26:N62, R26:R63, V26:V62, Z26:Z77, AD26:AD76, AH26:AH78, AL26:AL77	"5-mm Full Load" Cells: A26:A63, E26:E62, I26:I63, M26:M62, Q26:Q63, U26:U62, Y26:Y77, AC26:AC76, AG26:AG78, AK26:AK77	
	"10-mm Full Load" Cells: B26:B64, F26:F63, J26:J69, N26:N68, R26:R69, V26:V68, Z26:Z77, AD26:AD76, AH26:AH81, AL26:AL80	"10-mm Full Load" Cells: A26:A64, E26:E63, I26:I69, M26:M68, Q26:Q69, U26:U68, Y26:Y77, AC26:AC76, AG26:AG81, AK26:AK80	
	"15-mm Full Load" Cells: B26:B74, F26:F73, J26:J75, N26:N74, R26:R83, V26:V82, Z26:Z84, AD26:AD83	"15-mm Full Load" Cells: A26:A74, E26:E73, I26:I75, M26:M74, Q26:Q83, U26:U82, Y26:Y84, AC26:AC83	
	"2-mm 50% Load" Cells: B26:B82, F26:F81, J26:J69, N26:N68, R26:R78, V26:V77, Z26:Z88, AD26:AD87, AH26:AH89, AL26:AL88	"2-mm 50% Load" Cells: A26:A82, E26:E81, I26:I69, M26:M68, Q26:Q78, U26:U77, Y26:Y88, AC26:AC87, AG26:AG89, AK26:AK88	
	"5-mm 50% Load" Cells: B26:B64, F26:F63, J26:J68, N26:N67, R26:R68, V26:V67, Z26:Z82, AD26:AD81, AH26:AH93, AL92:AL88	"5-mm 50% Load" Cells: A26:A64, E26:E63, I26:I68, M26:M67, Q26:Q68, U26:U67, Y26:Y82, AC26:AC81, AG26:AG93, AK26:AK92	
	"10-mm 50% Load" Cells: B26:B66, F26:F65, J26:J66, N26:N65, R26:R66, V26:V65, Z26:Z66, AD26:AD65	"10-mm 50% Load" Cells: A26:A66, E26:E65, I26:I66, M26:M65, Q26:Q66, U26:U65, Y26:Y66, AC26:AC65	
	"15-mm 50% Load" Cells: B26:B66, F26:F65, J26:J66, N26:N65, R26:R66, V26:V65, Z26:Z66, AD26:AD65	"15-mm 50% Load" Cells: A26:A66, E26:E65, I26:I66, M26:M65, Q26:Q66, U26:U65, Y26:Y66, AC26:AC65	
	"2-mm 10% Load" Cells: B26:B79, F26:F78, J26:J79, N26:N78, R26:R89, V26:V88, Z26:Z95, AD26:AD94	"2-mm 10% Load" Cells: A26:A79, E26:E78, I26:I79, M26:M78, Q26:Q89, U26:U88, Y26:Y95, AC26:AC94	
	"5-mm 10% Load" Cells: B26:B71, F26:F70, J26:J75, N26:N74, R26:R78, V26:V77, Z26:Z87, AD26:AD86	"5-mm 10% Load" Cells: A26:A71, E26:E70, I26:I75, M26:M74, Q26:Q78, U26:U77, Y26:Y87, AC26:AC86	

Table B-2. Formulas used in Spreadsheets in Output DTN: MO0703PASDSTAT.001 (Continued)

Formula (Bold), Function	Location in File ("Worksheet")	Input (Location in file or value if directly entered) in Order of Use in Formula	Output (Value)
***Frame Fragility Analysis.xls* (Continued)**			
Built-in Excel Command: **ln(number),** Calculates the natural-log of the input (Continued)	"10-mm 10% Load" Cells: B26:B70, F26:F69, J26:J84, N26:N83, R26:R95, V26:V94, Z26:Z95, AD26:AD94	"10-mm 10% Load" Cells: A26:A70, E26:E69, I26:I84, M26:M83, Q26:Q95, U26:U94, Y26:Y95, AC26:AC94	
	"15-mm 10% Load" Cells: B26:B76, F26:F75	"15-mm 10% Load" Cells: A26:A76, E26:E75	
	"PGV-H1 to A Correlation" Cells:D13:D63, E13:E63, AB21:AB32	"PGV-H1 to A Correlation" Cells: B13:B63, C13:C63, AA21:AA32	
	"Load and Capacity" Cells: C8:C13, D23, D25, E50:E52, G49:G52	"Load and Capacity" Cells: B8:B13; 2; 10; D50:D52, B50:B52; B49:B52	
Built-in Excel Command: **NORMDIST(x, mean, standard_dev, TRUE)**, Calculates the Cumulative Distribution for the Specified Mean and Standard Deviation	"2-mm Full Load" Cells: B26:B81, F26:F80, J26:J69, N26:N68, R26:R68, V26:V67, Z26:Z82, AD26:AD81, AH26:AH91, AL26:AL90	"2-mm Full Load" Cells: A26:A81, D13, D14; E26:E80, D17, D20; I26:I69, L13, L14; M26:M68, L17, L20; Q26:Q68, T13, T14; U26:U67, T17, T20; Y26:Y82, AB13, AB14; AC26:AC81, AB17, AB20; AG26:AG91, AJ13, AJ14; AK26:AK90, AJ17, AJ20	Cumulative Probability for Use in Log-Normal Distribution and (P_{cap}/P_{stat}) < A+1
	"5-mm Full Load" Cells: B26:B63, F26:F62, J26:J63, N26:N62, R26:R63, V26:V62, Z26:Z77, AD26:AD76, AH26:AH78, AL26:AL77	"5-mm Full Load" Cells: A26:A63, D13, D14; E26:E62, D17, D20; I26:I63, L13, L14; M26:M62, L17, L20; Q26:Q63, T13, T14; U26:U62, T17, T20; Y26:Y77, AB13, AB14; AC26:AC76, AB17, AB20; AG26:AG78, AJ13, AJ14; AK26:AK77, AJ17, AJ20	
	"10-mm Full Load" Cells: B26:B64, F26:F63, J26:J69, N26:N68, R26:R69, V26:V68, Z26:Z77, AD26:AD76, AH26:AH81, AL26:AL80	"10-mm Full Load" Cells: A26:A64, C13, C14; E26:E63, C17, C20; I26:I69, L13, L14; M26:M68, L17, L20; Q26:Q69, T13, T14; U26:U68, T17, T20; Y26:Y77, AB13, AB14; AC26:AC76, AB17, AB20; AG26:AG81, AJ13, AJ14; AK26:AK80, AJ17, AJ20	
	"15-mm Full Load" Cells: B26:B74, F26:F73, J26:J75, N26:N74, R26:R83, V26:V82, Z26:Z84, AD26:AD83	"15-mm Full Load" Cells: A26:A74, D13, D14; E26:E73, D17, D20; I26:I75, L13, L14; M26:M74, L17, L20; Q26:Q83, T13, T14; U26:U82, T17, T20; Y26:Y84, AB13, AB14; AC26:AC83, AB17, AB20;	
	"2-mm 50% Load" Cells: B26:B82, F26:F81, J26:J69, N26:N68, R26:R78, V26:V77, Z26:Z88, AD26:AD87, AH26:AH89, AL26:AL88	"2-mm 50% Load" Cells: A26:A82, D13, D14; E26:E81, D17, D20; I26:I69, L13, L14; M26:M68, L17, L20; Q26:Q78, T13, T14; U26:U77, T17, T20; Y26:Y88, AB13, AB14; AC26:AC87, AB17, AB20; AG26:AG89, AJ13, AJ14; AK26:AK88, AJ17, AJ20	

Table B-2. Formulas used in Spreadsheets in Output DTN: MO0703PASDSTAT.001 (Continued)

Formula (Bold), Function	Location in File ("Worksheet")	Input (Location in file or value if directly entered) in Order of Use in Formula	Output (Value)
***Frame Fragility Analysis.xls* (Continued)**			
Built-in Excel Command: **NORMDIST(x, mean, standard_dev, TRUE)**, Calculates the Cumulative Distribution for the Specified Mean and Standard Deviation (Continued)	"5-mm 50% Load" Cells: B26:B64, F26:F63, J26:J68, N26:N67, R26:R68, V26:V67, Z26:Z82, AD26:AD81, AH26:AH93, AL92:AL88	"5-mm 50% Load" Cells: A26:A64, C13, C14; E26:E63, C17, C20; I26:I68, L13, L14; M26:M67, L17, L20; Q26:Q68, T13, T14; U26:U67, T17, T20; Y26:Y82, AB13, AB14; AC26:AC81, AB17, AB20; AG26:AG93, AJ13, AJ14; AK26:AK92, AJ17, AJ20	
	"10-mm 50% Load" Cells: B26:B66, F26:F65, J26:J66, N26:N65, R26:R66, V26:V65, Z26:Z66, AD26:AD65	"10-mm 50% Load" Cells: A26:A66, D13, D14; E26:E65, D17, D20; I26:I66, L13, L14; M26:M65, L17, L20; Q26:Q66, T13, T14; U26:U65, T17, T20; Y26:Y66, AB13, AB14; AC26:AC65, AB17, AB20	
	"15-mm 50% Load" Cells: B26:B66, F26:F65, J26:J66, N26:N65, R26:R66, V26:V65, Z26:Z66, AD26:AD65	"15-mm 50% Load" Cells: A26:A66, D13, D14; E26:E65, D17, D20; I26:I66, L13, L14; M26:M65, L17, L20; Q26:Q66, T13, T14; U26:U65, T17, T20; Y26:Y66, AB13, AB14; AC26:AC65, AB17, AB20	
	"2-mm 10% Load" Cells: B26:B79, F26:F78, J26:J79, N26:N78, R26:R89, V26:V88, Z26:Z95, AD26:AD94	"2-mm 10% Load" Cells: A26:A79, D13, D14; E26:E78, D17, D20; I26:I79, L13, L14; M26:M78, L17, L20; Q26:Q89, T13, T14; U26:U88, T17, T20; Y26:Y95, AB13, AB14; AC26:AC94, AB17, AB20	
	"5-mm 10% Load" Cells: B26:B71, F26:F70, J26:J75, N26:N74, R26:R78, V26:V77, Z26:Z87, AD26:AD86	"5-mm 10% Load" Cells: A26:A71, D13, D14; E26:E70, D17, D20; I26:I75, L13, L14; M26:M74, L17, L20; Q26:Q78, T13, T14; U26:U77, T17, T20; Y26:Y87, AB13, AB14; AC26:AC86, AB17, AB20	
	"10-mm 10% Load" Cells: B26:B70, F26:F69, J26:J84, N26:N83, R26:R95, V26:V94, Z26:Z95, AD26:AD94	"10-mm 10% Load" Cells: A26:A70, D13, D14; E26:E69, D17, D20; I26:I84, L13, L14; M26:M83, L17, L20; Q26:Q95, T13, T14; U26:U94, T17, T20; Y26:Y95, AB13, AB14; AC26:AC94, AB17, AB20	
	"15-mm 10% Load" Cells: B26:B76, F26:F75	"15-mm 10% Load" Cells: A26:A76, D13, D14; E26:E75, D17, D20	
Built-in Excel Command: **SUM(Number1, Number 2, …)**, Sums the Values in the Input Cells	"2-mm Full Load" Cells: G83, O71, W70, AE84, AM93	"2-mm Full Load" Cells: G26:G80, O26:O68, W26:W67, AE26:AE81, AM26:AM90	Total Probability of Failure (Static + Seismic Load > Plastic Capacity)
	"5-mm Full Load" Cells: G65, O65, W65, AE79, AM80	"5-mm Full Load" Cells: G26:G64, O26:O64, W26:W64, AE26:AE78, AM26:AM79	
	"10-mm Full Load" Cells: G66, O71, W71, AE79, AM81	"10-mm Full Load" Cells: G26:G62, O26:O68, W26:W68, AE26:AE76, AM26:AM78	

Table B-2. Formulas used in Spreadsheets in Output DTN: MO0703PASDSTAT.001 (Continued)

Formula (Bold), Function	Location in File ("Worksheet")	Input (Location in file or value if directly entered) in Order of Use in Formula	Output (Value)
***Frame Fragility Analysis.xls* (Continued)**			
Built-in Excel Command: **SUM(Number1, Number 2, …)**, Sums the Values in the Input Cells (Continued)	"15-mm Full Load" Cells: G76, O77, W85, AE86	"15-mm Full Load" Cells: G26:G73, O26:O74, W26:W82, AE26:AE83	
	"2-mm 50% Load" Cells: G84, O71, W80, AE90, AM91	"2-mm 50% Load" Cells: G26:G81, O26:O68, W26:W77, AE26:AE87, AM26:AM88	
	"5-mm 50% Load" Cells: G66, O70, W70, AE84, AM91	"5-mm 50% Load" Cells: G26:G63, O26:O67, W26:W67, AE26:AE81, AM26:AM88	
	"10-mm 50% Load" Cells: G68, O68, W68, AE68	"10-mm 50% Load" Cells: G26:G65, O26:O65, W26:W65, AE26:AE65	
	"15-mm 50% Load" Cells: G68, O68, W68, AE68	"15-mm 50% Load" Cells: G26:G65, O26:O65, W26:W65, AE26:AE65	
	"2-mm 10% Load" Cells: G81, O81, W91, AE97	"2-mm 10% Load" Cells: G26:G78, O26:O78, W26:W88, AE26:AE94	
	"5-mm 10% Load" Cells: G73, O77, W80, AE89	"5-mm 10% Load" Cells: G26:G70, O26:O74, W26:W77, AE26:AE86	
	"10-mm 10% Load" Cells: G72, O86, W97, AE97	"10-mm 10% Load" Cells: G26:G69, O26:O83, W26:W94, AE26:AE94	
	"15-mm 10% Load" Cells: G78	"15-mm 10% Load" Cells: G26:G75	
Built-in Excel Command: **STDEV(Number1, Number2,…)**, Calculates the Standard Deviation of the Input Numbers	"PGV-H1 to A Correlation" Cells K49:K51	"PGV-H1 to A Correlation" Cells: E13:E29, E30:E46, E47:E63	Beta for 1.05 m/s, 2.44 m/s, and 5.35 m/s
	"PGV-H1 to A Correlation" Cells: N65:O75	"PGV-H1 to A Correlation" Cells: N13:N63, O13:O63	Standard Deviation of Input
	"Load and Capacity" Cells: B16:E16	"Load and Capacity" Cells: B8:B13, C8:C13, D8:D13, E8:E13	
Built-in Excel Command: **AVERAGE (Number1, Number 2, …)**, Calculates the Mean of the Input Numbers	"PGV-H1 to A Correlation" Cells: N64:O64	"PGV-H1 to A Correlation" Cells" N14:N63, O13:O63	Mean of Input
	"Load and Capacity" Cells: B15:E15	"Load and Capacity" Cells: B8:B13, C8:C13, D8:D13, E8:E13	
Built-in Excel Command: **Add Trendline (chart input),** Calculates the Linear Fit to the Data of the Form y = m*x + b, and the R^2 value	"PGV-H1 to (A+1) Correlation" Plot in Cells: F13:M45	"PGV-H1 to (A+1) Correlation" Cells: D13:E63, E13:E63	ln(A) = 1.1079 * ln(PGV-H1) + 0.3514, R^2 = 0.5316
Built-in Excel Command: **NORMINV (probability, mean, standard_dev)**, Calculates the Inverse of the Normal Cumulative Distribution for the Specified Mean and Standard Deviation	"PGV-H1 to (A+1) Correlation" Cells:Q13:Q63	"PGV-H1 to (A+1) Correlation" Cells: P13:P63, O64, O65	Value for Normal Distribution
	"Load and Capacity" Cells: G8:G13	"Load and Capacity" Cells: F8:F13, E15, E16	

Table B-2. Formulas used in Spreadsheets in Output DTN: MO0703PASDSTAT.001 (Continued)

Formula (Bold), Function	Location in File ("Worksheet")	Input (Location in file or value if directly entered) in Order of Use in Formula	Output (Value)
***Frame Fragility Analysis.xls* (Continued)**			
Built-in Excel Command: **exp(number)**, Calculates the Number Applied to the Base e	"PGV-H1 to (A+1) Correlation" Cells: AC21:AC32, AD21:AD32, AE21:AE32	"PGV-H1 to (A+1) Correlation" Cells: AB21:AB32; AB21:AB32, O65; AB21:AB32, O65	e^{input}
	"Load and Capacity" Cells: H8:H13, D21, N49:N52, O49:O52, P49:P52, Q49:Q52, R49:R52	"Load and Capacity" Cells: C15, G8:G13; D19; M49:M52, E50; M49:M52, F49:F52; M49:M52, F49:F52; M49:M52, F49:F52; M49:M52, F49:F52;	
Built-in Excel Command: **ABS(Number)**, Calculates the Absolute Value of a Number	"Load and Capacity" Cells: D50:D52	"Load and Capacity" Cells: B50:B52, C50:C52	|input|
Kinematic Damage Abstraction 17-mm Degraded.xls			
The majority of the formulas used in this file are used in the file *CDSP Kinematic Damage Abstraction 17-mm Degraded.xls*. For documentation of the formulas used in this file, refer to documentation of formulas used in the file *CDSP Kinematic Damage Abstraction 17-mm Degraded.xls*. Formulas not found in the file *CDSP Kinematic Damage Abstraction 17-mm Degraded.xls* are described below.			
$\varepsilon + (\beta - \varepsilon)*((-1)*\ln(1-\text{Probability}))^{1/\alpha}$, Calculates the Weibull Value	"Weibull for 90%_d17" Cells: D7:D27, I7:I51, N7:N57, S7:S57, AK8:AO20	"Weibull for 90%_d17" Cells: D30, D29, C7:C27, D28; I54, I53, H7:H51, I52; N60, N59, M7:M57, N58; S60, S59, R7:R57, S58; AJ8:AJ20, AI8:AI20, AK6:AO6, AH8:AH20	Weibull Value
Kinematic Damage Abstraction 23-mm Degraded.xls			
All of the formulas used in this file are used in the file *Kinematic Damage Abstraction 17-mm Degraded.xls*. For documentation of the formulas used in this file, refer to documentation of formulas used in the file *Kinematic Damage Abstraction 17-mm Degraded.xls*.			
Kinematic Damage Abstraction 23-mm Intact.xls			
All of the formulas used in this file are used in the file *Kinematic Damage Abstraction 17-mm Degraded.xls*. For documentation of the formulas used in this file, refer to documentation of formulas used in the file *Kinematic Damage Abstraction 17-mm Degraded.xls*.			
Lith Rubble Abstraction.xls			
Built-in Excel Command: **AVERAGE (Number1, Number 2, …)**, Calculates the Mean of the Input Numbers	"Data" Cells: B18:D18	"Data" Cells: B3:D17	Average Rockfall Area
	"Gamma Abstraction" Cells: G16, E44, E69	"Gamma Abstraction" Cells: G13:G15; E33:E43; E58:E68	
	"Log-Normal Abstraction" Cells: G16, F42, F62	"Log-Normal Abstraction" Cells: G13:G15; F31:F41; F51:F61	Average of ln of Rockfall Area
Built-in Excel Command: **Add Trendline (chart input),** Calculates the Linear Fit to the Data of the Form y = m*x + b, and the R^2 Value	"Probability of Rockfall" Plot Cells: G12:N37	"Probability of Rockfall" Cells: D43:D45, J38:K41	Weighted Probability of Rockfall = 1.288 * PGV-H1 – 0.353

Table B-2. Formulas used in Spreadsheets in Output DTN: MO0703PASDSTAT.001 (Continued)

Formula (Bold), Function	Location in File ("Worksheet")	Input (Location in file or value if directly entered) in Order of Use in Formula	Output (Value)
***Lith Rubble Abstraction.xls* (Continued)**			
Built-in Excel Command: **Add Trendline (chart input),** Calculates the Quadratic Fit to the Data of the Form y = a*x2 + b*x + c	"Gamma Abstraction" Plot Cells:Q7:V26, Q27:Q47	"Gamma Abstraction" Cells: S4:U5; S4:U4, S6:U6	a, b, and c for the Mean and Standard Deviation
	"Log-Normal Abstraction" Plot Cells: P8:V27, P31:V51	"Log-Normal Abstraction" Cells: R4:T5; R4:T4, R6:T6	
Built-in Excel Command: **STDEV(Number1, Number2,…)**, Calculates the Standard Deviation of the Input Numbers	"Gamma Abstraction" Cells: G17, E45, E70	"Gamma Abstraction" Cells: G13:G15; E33:E43; E58:E68	Standard Deviation of Input
	"Log-Normal Abstraction" Cells: G17, F43, F63	"Log-Normal Abstraction" Cells: G13:G15; F31:F41; F51:F61	
$(\mu / \sigma)^2$, Calculates Alpha	"Gamma Abstraction" Cells: G18, E46, E71, Z9:Z20	"Gamma Abstraction" Cells: G16, G17; E44, E45; E69, E70; X9:X20, Y9:Y20	Alpha
	"Exceed Prob for V > V0" Cells: E15:E54	"Exceed Prob for V > V0" Cells: C15:C54, D15:D54	
$(\sigma)^2 / \mu$, Calculates Beta	"Gamma Abstraction" Cells: G19, E47, E72, AA9:AA20	"Gamma Abstraction" Cells: G17, G16; E45, E44; E70, E69; Y9:Y20, X9:X20	Beta
	"Exceed Prob for V > V0" Cells: F15:F54	"Exceed Prob for V > V0" Cells: D15:D54, C15:C54	
$a_i = a_1 + \sum_{j=2}^{i} \frac{1}{n}$ $a_1 = \frac{1}{2n}$ n = # of cases with nonzero damage areas, Calculates the Cumulative Probability	"Gamma Abstraction" Cells: H13:H15, F33:F43, F58:F68 "Log-Normal Abstraction" Cells: H13:H15, G31:G41, G51:G61	Number of Nonzero Damaged Areas for Given PGV Level	Cumulative Probability
Built-in Excel Command: **GAMMAINV (probability, alpha, beta)**, Calculates the Inverse of the Gamma Cumulative Distribution Using the Probability Associated with the Distribution, Alpha, and Beta	"Gamma Abstraction" Cells: I13:I15, G33:G43, G58:G68, AB9:AF20	"Gamma Abstraction" Cells: H13:H15, G18, G19; F33:F43, E46, E47; F58:F68, E71, E72; AB5:AF5, Z9:Z20, AA9:AA20	Rockfall Area From Gamma Distribution
Built-in Excel Command: **SUM(Number1, Number2, …)**; Sums the Values in the Input Cells	"Gamma Abstraction" Cells: J17, H45, H70	"Gamma Abstraction" Cells: J13:J15; H33:H43; H58:H68	Sum(Input)
	"Log-Normal Abstraction" Cells: J17, I42, I63	"Log-Normal Abstraction" Cells: J13:J15; I31:I41; I51:I61	
	"Exceed Prob for V > V0" Cells: I56, M56, Q56	"Exceed Prob for V > V0" Cells: I15:I54; M15:M54; Q 15:Q54	

Table B-2. Formulas used in Spreadsheets in Output DTN: MO0703PASDSTAT.001 (Continued)

Formula (Bold), Function	Location in File ("Worksheet")	Input (Location in file or value if directly entered) in Order of Use in Formula	Output (Value)
***Lith Rubble Abstraction.xls* (Continued)**			
Built-in Excel Command: **ln(number),** Calculates the natural-log of the input	"Log-Normal Abstraction" Cells: G13:G15, F31:F41, F51:F61	"Log-Normal Abstraction" Cells: E19, E13, E17; E31:E41; E51:E61	ln(input)
	"Data for Bounded Hazard" Cells: C13, C17, C21, C26, C29, C33, C37, C41, C45, C49, C54, C58, C62, C66, C70, C74, C78, C82, C86	"Data for Bounded Hazard" Cells: B17, B13, A17, A13, B21, A21, B26:A26, B29, A29, B33, A33, B37, A37, B41, A41, B45, A45, B49, A49, B54, A54, B58, A58, B62, A62, B66, A66, B70, A70, B74, A74, B78, A78, B82, A82, B86, A86, B89, A89	B for Power Law Fit
Built-in Excel Command: **NORMINV (probability, mean, standard_dev)**, Calculates the Inverse of the Normal Cumulative Distribution for the Specified Mean and Standard Deviation	"Log-Normal Abstraction" Cells: I13:I15, H31:H41, H51:H61, AA9:AE18	"Log-Normal Abstraction" Cells: H13:H15, G16, G17; G31:G41, F42, F43; G51:G61, F62, F63; AA5:AE5, Y9:Y18, Z9:Z18	ln (Rockfall Area) from Normal Distribution
Built-in Excel Command: **exp(number)**, Calculates the Exponent Applied to the Base e	"Log-Normal Abstraction" Cells: I13:I15, H31:H41, H51:H61, AA9:AE18	"Log-Normal Abstraction" Cells: H13:H15, G16, G17; G31:G41, F42, F43; G51:G61, F62, F63; AA5:AE5, Y9:Y18, Z9:Z18	Rockfall Area from Normal Distribution
	"Exceed Prob for V > V0" Cells: B8, L8, P8	"Exceed Prob for V > V0" Cells: B4, B7; L4, L7; P4, P7	e^{input}
Built-in Excel Command: **MIN(Number1, Number2, …)**, Returns the Smallest Value in the Inputs	"Exceed Prob for V > V0" Cells: B15:B54	1, Max(0,("Exceed Prob for V > V0" Cells: A15:A54)*1.2888-0.353)	Min(Input)
Built-in Excel Command **Max(Number1, Number2, …)**, Returns the Largest Value in the Inputs	"Exceed Prob for V > V0" Cells: B15:B54	0,("Exceed Prob for V > V0" Cells: A15:A54)*1.2888-0.353)	Max(Input)
Built-in Excel Command **GAMMADIST(x, alpha, beta, TRUE)**, Calculates the Cumulative Gamma Distribution	"Exceed Prob for V > V0" Cells: G15:G54, L15:L54, P15:P54	"Exceed Prob for V > V0" Cells: B3, E15:E54, F15:F54; L3, E15:E54, F15:F54; P3, E15:E54, F15:F54	Exceedance Probability Rockfall Volume > V0

Table B-2. Formulas used in Spreadsheets in Output DTN: MO0703PASDSTAT.001 (Continued)

Formula (Bold), Function	Location in File ("Worksheet")	Input (Location in file or value if directly entered) in Order of Use in Formula	Output (Value)
Nonlith Damage Abstraction for DS.xls[20]			
Built-in Excel Command: **FORECAST(x, known_y's, known_x's)**, Calculates, or predicts, a future value by using existing values using linear regression	"Plot 15-mm" Cells: B23:B25, B27:B38	"Plot 15-mm" Cells: A23:A25, C6:C7, B6:B7; A27:B38, C7:C9, B7:B9;	Mean at a Given PGV
	"Plot 15-mm" Cells: C23:C38	"Plot 15-mm" Cells: A23:A38, C14:C17, B14:B17	Standard Deviation at a Given PGV
	"Plot 10-mm" Cells: B23:B25, B27:B38, C23:C38	"Plot 10-mm" Cells: A23:A25, C6:C7, B6:B7; A27:B38, C7:C9, B7:B9;	Mean at a Given PGV
	"Plot 10-mm" Cells: C23:C38	"Plot 10-mm" Cells: A23:A38, C14:C17, B14:B17	Standard Deviation at a Given PGV
	"Plot 5-mm" Cells: B23:B25, B27:B38	"Plot 5-mm" Cells: A23:A25, C6:C7, B6:B7; A27:B38, C7:C9, B7:B9;	Mean at a Given PGV
	"Plot 5-mm" Cells: C23:C38	"Plot 5-mm" Cells: A23:A38, C14:C17, B14:B17	Standard Deviation at a Given PGV
	"0.4 ms PGV 15-mm Plate" Cell: U22	"0.4 ms PGV 15-mm Plate" ln(Cell T22), Cells: R8:R9, Q8:Q9;	Strain Level
	"0.4 ms PGV 15-mm Plate" Cells: V22:V90	"0.4 ms PGV 15-mm Plate" ln(Cells: T22:T90), X8:X11, W8:W11	Damaged Area
$(\mu / \sigma)^2$, Calculates Alpha	"Plot 15-mm" Cells: D23:D38	"Plot 15-mm" Cells: B23:B38, C23:C38	Alpha
	"Plot 10-mm" Cells: D23:D38	"Plot 10-mm" Cells: B23:B38, C23:C38	
	"Plot 5-mm" Cells: D23:D38	"Plot 5-mm" Cells: B23:B38, C23:C38	
	"0.4 ms PGV 15-mm Plate" Cell: AJ41	"0.4 ms PGV 15-mm Plate" Cell: AJ22:AJ37	
$(\sigma)^2 / \mu$, Calculates Beta	"Plot 15-mm" Cells: E23:E38	"Plot 15-mm" Cells: C23:C38, B23:B38	Beta
	"Plot 10-mm" Cells: E23:E38	"Plot 10-mm" Cells: C23:C38, B23:B38	
	"Plot 5-mm" Cells: E23:E38	"Plot 5-mm" Cells: C23:C38, B23:B38	
	"0.4 ms PGV 15-mm Plate" Cell: AJ42	"0.4 ms PGV 15-mm Plate" Cell: AJ22:AJ37	

[20] The formulas found in the following worksheets: "0.4 ms PGV 10-mm Plate," "0.4 ms PGV 5-mm Plate," "1.05 ms PGV 15-mm Plate," "1.05 ms PGV 10-mm Plate," "1.05 ms PGV 5-mm Plate," "2.44 ms PGV 15-mm Plate," "2.44 ms PGV 10-mm Plate," "2.44 ms PGV 5-mm Plate," "5.35 ms PGV 15-mm Plate," "5.35 ms PGV 10-mm Plate," and "5.35 ms PGV 5-mm Plate" were not documented in this table. The format of these worksheets is identical to that of "0.4 ms PGV 15-mm Plate." All of the formulas in these worksheets can be found in "0.4 ms PGV 15-mm Plate." Refer to documentation of the formulas in "0.4 ms PGV 15-mm Plate" for documentation of the formulas found in : "0.4 ms PGV 10-mm Plate," "0.4 ms PGV 5-mm Plate," "1.05 ms PGV 15-mm Plate," "1.05 ms PGV 10-mm Plate," "1.05 ms PGV 5-mm Plate," "2.44 ms PGV 15-mm Plate," "2.44 ms PGV 10-mm Plate," "2.44 ms PGV 5-mm Plate," "5.35 ms PGV 15-mm Plate," "5.35 ms PGV 10-mm Plate," and "5.35 ms PGV 5-mm Plate."

Table B-2. Formulas used in Spreadsheets in Output DTN: MO0703PASDSTAT.001 (Continued)

Formula (Bold), Function	Location in File ("Worksheet")	Input (Location in file or value if directly entered) in Order of Use in Formula	Output (Value)
***Nonlith Damage Abstraction for DS.xls* (Continued)**			
Built-in Excel Command: **GAMMAINV (probability, alpha, beta)**, Calculates the Inverse of the Gamma Cumulative Distribution Using the Probability Associated with the Distribution, Alpha, and Beta	"Plot 15-mm" Cells: F23:J38	"Plot 15-mm" Cells: F21:J21, D23:D38, E23:E38	Damage Area from Gamma Distribution
	"Plot 10-mm" Cells: F23:J38	"Plot 10-mm" Cells: F21:J21, D23:D38, E23:E38	
	"Plot 5-mm" Cells: F23:J38	"Plot 5-mm" Cells: F21:J21, D23:D38, E23:E38	
	"0.4 ms PGV 15-mm Plate" Cells: AJ22:AJ37	"0.4 ms PGV 15-mm Plate" Cells: AI22:AI37, AJ41, AJ42	
Built-in Excel Command: **ATAN2(x_num, y_num)**, Calculates the Angle from the x-axis to a Line Containing the Origin and a point with the specified x- and y-coordinates	"Data Catalogs" Cells: K47:K1813	"Data Catalogs" Cells: H47:H1813, G47:G1813	Used with IF Statement to Calculate Impact Angle
	"0.4 ms PGV 15-mm Plate" Cells: K22:K449	"0.4 ms PGV 15-mm Plate" Cells: H22:H449, G22:G449	
Built-in Excel Command: **IF(logical_test, value_if_true, value_if_false),** Returns a Value Dependent Upon the Conditions Specified	"Data Catalogs" Cells: K47:K1813	ATAN2("Data Catalogs" Cells: H47:H1813, G47:G1813)* 180/3.14 < 0, 360 + ATAN2("Data Catalogs" Cells: H47:H1813, G47:G1813)* 180/3.14, ATAN2("Data Catalogs" Cells: H47:H1813, G47:G1813)* 180/3.14	Impact Angle
	"0.4 ms PGV 15-mm Plate" Cells: K22:K449	ATAN2("Data Catalogs" Cells: H22:H449, G22:G449)* 180/3.14 < 0, 360 + ATAN2("Data Catalogs" Cells: H22:H449, G22:G449)* 180/3.14, ATAN2("Data Catalogs" Cells: H22:H449, G22:G449)* 180/3.14	
	"0.4 ms PGV 15-mm Plate" Cells: AD28, AD29 AD33, AD34, AD38, AD43, AD47, AD54, AD55, AD56, AD57, AD78, AD82, AD84, AD86, AD90	Nested If Statements: First Test Determines How Many Block Impacts Cause Failure, Second Test Determines the Distance Between Rock Block Impacts, and Subsequently How Many Drip Shields Fail "0.4 ms PGV 15-mm Plate" Cells:AA22:AA90. Y22:Y90	Determines the Number of DS Failures per Case
	"0.4 ms PGV 15-mm Plate" Cells: BF22:BF37	"0.4 ms PGV 15-mm Plate" BD22:BD37<BF42, BF41+SQRT(BE22:BE37*(BF42-BF41)*(BF43-BF41)), BF43-SQRT((1-BE22:BE37)*(BF43-BF41)*(BF43-BF42))	ln(DA) on Fitted Log-Triangular Distribution

Table B-2. Formulas used in Spreadsheets in Output DTN: MO0703PASDSTAT.001 (Continued)

Formula (Bold), Function	Location in File ("Worksheet")	Input (Location in file or value if directly entered) in Order of Use in Formula	Output (Value)
***Nonlith Damage Abstraction for DS.xls* (Continued)**			
Built-in Excel Command: **ROW(reference)**, Returns the Row Number of a Reference	"Data Catalogs" Cells: N47:N1813	"Data Catalogs" Cells: M47:M1813	Used to Calculate the Percentile
Built-in Excel Command: **ATAN(number)**, Calculates the Arctangent of a Number	"Data Catalogs" Cell: Y45	"Data Catalogs" Cell Y42 / Cell Y43	Angle in Radians
Built-in Excel Command: **DEGREES(angle)**, Converts Radians into Degrees	"Data Catalogs" Cell: Y45	ATAN("Data Catalogs" Cell Y42 / Cell Y43)	Angle in Degrees
Built-in Excel Command: **ln(number),** Calculates the natural-log of the input	"0.4 ms PGV 15-mm Plate" Cells: Q7:Q13, W7:W13, U22, V22:V90, AS22:AS37, BD22:BD37	"0.4 ms PGV 15-mm Plate" Cells: P7:P13; V7:V13; T22; T22:T90; AR22:AR37; BC22:BC37	ln(Impact Energy)
	"0.4 ms PGV 15-mm Plate" Cells: AS22:AS37, BD22:BD37	"0.4 ms PGV 15-mm Plate" Cells: AR22:AR37; BC22:BC37	ln(damaged area)
Built-in Excel Command: **SUM(Number1, Number2,….)**, Calculates the Sum of the Inputs	"0.4 ms PGV 15-mm Plate" Cells: AC28, AC33, AC38, AC43, AC47, AC54, AC78, AC82, AC84, AC86, AC90, AB93, AC93	"0.4 ms PGV 15-mm Plate" Cells: AB22:AB28; AB30:AB33; AB35:AB38; AB39:AB43; AB44:AB47; AB48:AB54; AB58:AB78; AB79:AB82; AB83:AB84; AB85:AB86; AB87:AB90; AB22:AB90; AC22:AC90	Sum of Damaged Area
	"0.4 ms PGV 15-mm Plate" Cell: AC95	"0.4 ms PGV 15-mm Plate" Cells: AD22:AD90	Number of DS Failures
	"0.4 ms PGV 15-mm Plate" Cell: BH41	"0.4 ms PGV 15-mm Plate" Cells: BH22:BH37	Sum of Squared Differences
Built-in Excel Command: **COUNTIF(range, criteria),** Counts the Number of Cells that Meet the Given Criteria	"0.4 ms PGV 15-mm Plate" Cells: AC96:AC99	"0.4 ms PGV 15-mm Plate" Cells: AD22:AD90, 1; AD22:AD90, 2; AD22:AD90, 3; AD22:AD90,4	Number of Cases with DS Failure
	"0.4 ms PGV 15-mm Plate" Cells: AD28, AD29 AD33, AD34, AD38, AD43, AD47, AD54, AD55, AD56, AD57, AD78, AD82, AD84, AD86, AD90	"0.4 ms PGV 15-mm Plate" Cells: AA22:AA28; AA29; AA30:AA33; AD34; AA35:AA38; AA39:AA43; AA44:AA47; AA48:AA54; AA55; AA56; AA57; AA58:AA78; AA79:AA82; AA83:AA84; AA85:AA86; AA87:AA90;	Number of Failures
	"0.4 ms PGV 15-mm Plate" Cell: AG55	"0.4 ms PGV 15-mm Plate" Cells: AG22:AG53, >0	Number of Cases with Damage Area

Table B-2. Formulas used in Spreadsheets in Output DTN: MO0703PASDSTAT.001 (Continued)

Formula (Bold), Function	Location in File ("Worksheet")	Input (Location in file or value if directly entered) in Order of Use in Formula	Output (Value)
***Nonlith Damage Abstraction for DS.xls* (Continued)**			
Built-in Excel Command: **LOOKUP (lookup_value, lookup_vector, result_vector)**, Looks in a One-Row Range for a Value and Returns a value from the Same Position in a Second One-Row Range	"0.4 ms PGV 15-mm Plate" Cells: AD28, AD29 AD33, AD34, AD38, AD43, AD47, AD54, AD55, AD56, AD57, AD78, AD82, AD84, AD86, AD90	Max(x-imp)-Min(x-impact), {0, 2.75, 8.25, 13.75}, {1, 2, 3, 4} "0.4 ms PGV 15-mm Plate" Cells: Y22:Y25, Y29, Y30:Y33, Y34, Y35:Y38, Y39:Y42, Y44:Y47, Y48:Y51, Y55, Y56, Y57, Y58:Y61, Y79:Y82, Y83:Y84, Y85:Y86, Y87:Y90	Determines the Number of DS Failures Using the Maximum Distance Between Impacts to the DS
$a_i = a_1 + \sum_{j=2}^{i} \frac{1}{n}$ $a_1 = \frac{1}{2n}$ n = # of cases with nonzero damage areas, Calculates the Cumulative Probability	"0.4 ms PGV 15-mm Plate" Cells: AI22:AI37, AT22:AT37, BE22:BE37	Number of Nonzero Damaged Areas for Given PGV Level	Cumulative Probability
Built-in Excel Command: **AVERAGE (Number1, Number 2, …)**, Calculates the Mean of the Input Numbers	"0.4 ms PGV 15-mm Plate" Cell: AJ39, AS39	"0.4 ms PGV 15-mm Plate" Cells: AH22:AH37; AS22:AS37	Mean of Damaged Area
Built-in Excel Command: **STDEV(Number1, Number2,…)**, Calculates the Standard Deviation of the Input Numbers	"0.4 ms PGV 15-mm Plate" Cell: AJ40; AS40	"0.4 ms PGV 15-mm Plate" Cells: AH22:AH37; AS22:AS37	Standard Deviation of Damaged Area
Built-in Excel Command: **NORMINV (probability, mean, standard_dev)**, Calculates the Inverse of the Normal Cumulative Distribution for the Specified Mean and Standard Deviation	"0.4 ms PGV 15-mm Plate" Cells: AU22:AU37	"0.4 ms PGV 15-mm Plate" Cells: AT22:AT37, AS39, AS40	ln (damage area) from Normal Distribution
Built-in Excel Command: **exp(number)**, Calculates the Exponent Applied to the Base e	"0.4 ms PGV 15-mm Plate" Cells: AU22:AU37	NORMINV("0.4 ms PGV 15-mm Plate" Cells: AT22:AT37, AS39, AS40)	Damage Area from Normal Distribution
	"0.4 ms PGV 15-mm Plate" Cells: BG22:BG37	"0.4 ms PGV 15-mm Plate" Cells: BF22:BF37	Damage Area on Fitted Log-Triangular Distribution

Table B-2. Formulas used in Spreadsheets in Output DTN: MO0703PASDSTAT.001 (Continued)

Formula (Bold), Function	Location in File ("Worksheet")	Input (Location in file or value if directly entered) in Order of Use in Formula	Output (Value)
***Nonlith Damage Abstraction for DS.xls* (Continued)**			
Built-in Excel Command: **SQRT(number),** Calculates the Square Root of the Input Number	"0.4 ms PGV 15-mm Plate" Cells: BF22:BF37	(A*(B-C)*(D-C)) or ((1-A)*(D-C)*(D-B)) "0.4 ms PGV 15-mm Plate" Cells: BE22:BE37, BF42, BF41, BF43	Part of Input to IF Statement
Built-in Excel Command: **Solver**, Solves for a Given Cell by Minimizing Another Cell	"0.4 ms PGV 15-mm Plate" Cell: BH41	"0.4 ms PGV 15-mm Plate" Cell: BF42	ln(b), Mod
Nonlith Rockfall Abstraction.xls			
Built-in Excel Command: **AVERAGE (Number1, Number 2, …)**, Calculates the Mean of the Input Numbers	"Lith Versus Nonlith" Cells: D28:F28, K63, L63, R63, S53, Y57, Z57	"Lith Versus Nonlith" Cells: D13:D27; E13:E27; F13:F27; K13:K62; L13:L62; R13:R62; S13:S62; Y13:Y56; Z13:Z56	Mean of all Rockfall Volume
	"Lith Versus Nonlith" Cells: D31:F31, K66, L66, R66, S66	"Lith Versus Nonlith" Cells: D13, D16, D18, D19, D21, D23, D24; E13:E27; F13:F27; K13:K57, K59:K62; L13:L57, L59:L63; R13:R62; S13:S62	Mean of Rockfall Volume Greater than Zero
	"Gamma Abstractions" Cells: E64, T64, AI58	"Gamma Abstractions" Cells: E14:E62; T14:T63; AI14:AI57	Mean of Rockfall Volume
	"Log-Normal Abstractions" Cells: F64, V64, AL58	"Log-Normal Abstractions" Cells: F14:F62; V14:V63; AL14:AL57	Mean of ln of Rockfall Volume
Built-in Excel Command: **STDEV(Number1, Number2,…)**, Calculates the Standard Deviation of the Input Numbers	"Lith Versus Nonlith" Cells: D29:F29, K64, L64, R64, S64, Y58, Z58	"Lith Versus Nonlith" Cells: D13:D27; E13:E27; F13:F27; K13:K62; L13:L64; R13:R62; S13:S62; Y13:Y56; Z13:Z56	Standard Deviation of all Rockfall Volume
	"Lith Versus Nonlith" Cells: D32:F32, K67, L67, R67, S67	"Lith Versus Nonlith" Cells: D13, D16, D18, D19, D21, D23, D24; E13:E27; F13:F27; K13:K57, K59:K62; L13:L57, L59:L62; R13:R62; S13:S62	Standard Deviation of Rockfall Volume Greater than Zero
	"Gamma Abstractions" Cells: E65, T65, AI59	"Gamma Abstractions" Cells: E14:E62; T14:T63; AI14:AI57	Standard Deviation of Rockfall Volume
	"Log-Normal Abstractions" Cells: F65, V65, AL59	"Log-Normal Abstractions" Cells: F14:F62; V14:V63; AL14:AL57	Standard Deviation of ln of Rockfall Volume

Table B-2. Formulas used in Spreadsheets in Output DTN: MO0703PASDSTAT.001 (Continued)

Formula (Bold), Function	Location in File ("Worksheet")	Input (Location in file or value if directly entered) in Order of Use in Formula	Output (Value)
***Nonlith Rockfall Abstraction.xls* (Continued)**			
$a_i = a_1 + \sum_{j=2}^{i} \frac{1}{n}$ $a_1 = \frac{1}{2n}$ n = # of cases with nonzero damage areas, Calculates the Cumulative Probability	"Gamma Abstractions" Cells: F14:F62, U14:U63, AJ14:AJ57	Number of Nonzero Damaged Areas for Given PGV Level	Cumulative Probability
	"Log-Normal Abstractions" Cells: G14:G62, W14:W63, AM14:AM57		
(μ / σ)^2, Calculates Alpha	"Gamma Abstractions" Cells: E66, T66, AI60, BC16:BC31	"Gamma Abstractions" Cells: E64, E65; T64, T65; AI58, AI59; BA16:BA31, BB16:BB31	Alpha
	"Log-Normal Abstractions" Cells: BF16:BF30	"Log-Normal Abstractions" Cells: BD16:BD30, BE16:BE30	
(σ)^2 / μ, Calculates Beta	"Gamma Abstractions" Cells: E67, T67, AI61, BD16:BD31	"Gamma Abstractions" Cells: E65, E64; T65, T64; AI59, AI58; BB16:BB31, BA16:BA31	Beta
	"Log-Normal Abstractions" Cells: BG16:BG0	"Log-Normal Abstractions" Cells: BE16:BE30, BD16:BD30	
Built-in Excel Command: **GAMMAINV (probability, alpha, beta)**, Calculates the Inverse of the Gamma Cumulative Distribution Using the Probability Associated with the Distribution, Alpha, and Beta	"Gamma Abstractions" Cells: G14:G62, V14:V63, AK14:AK57, BE16:BI31	"Gamma Abstractions" Cells: F14:F62, E66, E67; U14:U63, T66, T67;AJ14:AJ57, AI60, AI61; BE14:BI14, BC16:BC31, BD16:BD31	Rockfall Volume from Gamma Distribution
Built-in Excel Command: **Add Trendline (chart input),** Calculates the Quadratic Fit to the Data of the Form y = a*x2 + b*x + c	"Gamma Abstractions" Plot Cells: AT18:AY37	"Gamma Abstractions" Cells: AV15:AX16	Mean = -0.0142 * PGV^2 + 0.2064 * PGV + 0.0387
	"Gamma Abstractions" Plot Cells: AT38:AY58	"Gamma Abstractions" Cells: AV15:AX15, AV17:AX17	Standard Deviation = -0.037 * PGV^2 + 0.3057 * PGV + 0.0696
	"Log-Normal Abstractions" Plot Cells: AW18:AW37	"Log-Normal Abstractions" Cells: AY15:BA16	Mean = -0.1092 * PGV^2 + 1.1008 * PGV – 3.4932
	"Log-Normal Abstractions" Plot Cells: AW39:AW58	"Log-Normal Abstractions" Cells: AY15:BA15, AY17:BA17	Standard Deviation = 0.0222 * PGV^2 – 0.2587 * PGV + 1.7632

Table B-2. Formulas used in Spreadsheets in Output DTN: MO0703PASDSTAT.001 (Continued)

Formula (Bold), Function	Location in File ("Worksheet")	Input (Location in file or value if directly entered) in Order of Use in Formula	Output (Value)
***Nonlith Rockfall Abstraction.xls* (Continued)**			
Built-in Excel Command: **NORMINV (probability, mean, standard_dev)**, Calculates the Inverse of the Normal Cumulative Distribution for the Specified Mean and Standard Deviation	"Log-Normal Abstractions" Cells: H14:H62, X14:X63, AN14:AN57, BH16:BL30	"Log-Normal Abstractions" Cells: G14:G62, F64, F65; W14:W63, W64, W65; AM14:AM57, AL58, AL59; BH14:BL14, BD16:BD30, BE16:BE30	ln (Rockfall Volume) from Log-Normal Distribution
Built-in Excel Command: **exp(number)**, Calculates the Exponent Applied to the Base e	"Log-Normal Abstractions" Cells: H14:H62, X14:X63, AN14:AN57, BH16:BL30	"Log-Normal Abstractions" NORMINV(Cells: G14:G62, F64, F65); NORMINV(Cells: W14:W63, V64, V65); NORMINV(Cells: AM14:AM57, AL58, AL59) NORMINV(Cells: BH14:BL14, BD16:BD30, BE16:BE30)	Rockfall Volume from Log-Normal Distribution
Built-in Excel Command: **ln(number),** Calculates the natural-log of the input	"Log-Normal Abstractions" Cells: F14:F62, V14:V63, AL14:AL57	"Log-Normal Abstractions" Cells: E14:E62; U14:U63; AK14:AK57	ln(Rockfall Volume)
Plate Fragility Analysis.xls			
All of the formulas used in this file are used in the file *Frame Fragility Analysis.xls*. For documentation of the formulas used in this file, refer to documentation of formulas used in the file *Frame Fragility Analysis.xls*.			
Rupture and Puncture Abstractions.xls			
Built-in Excel Command: **AVERAGE (Number1, Number 2, …)**, Calculates the Mean of the Input Numbers	"CDSP Kinematic Abstraction" Cells: D10:D13, K10:K13	"CDSP Kinematic Abstraction" Cells: B10:C10; B11:C11; B12:C12; B13:C13; I10:J10; I11:J11; I12:J12; I13:J13	Average of Probability of Incipient or Immediate Rupture
	"TAD Kinematic Abstraction" Cells: D10:D13, M10:M13	"TAD Kinematic Abstraction" Cells: B10:C10; B11:C11; B12:C12; B13:C13; K10:L10; K11:L11; K12:L12; K13:L13	
	"TAD Rubble Data" Cells: L25:O25, L49:O49	"TAD Rubble Data" Cells: L8:L4; M8:M24; N8:N24; O8:O24; L32:L48; M34:M48; N32:N48; O32:O48	Average of Probability of Rupture (Puncture)
Built-in Excel Command: **LOG(Number)**, Calculates the Logarithm of a Number, Base 10, for Use in a Power Law Fit	"CDSP Kinematic Abstraction" Cell: B17	"CDSP Kinematic Abstraction" (Cell D12/ Cell D13); ((Cell A12 – 1.05)/(Cell A13 – 1.05))	log(input) Used to Calculate b in: $a(PGV-1.05)^b$

Table B-2. Formulas used in Spreadsheets in Output DTN: MO0703PASDSTAT.001 (Continued)

Formula (Bold), Function	Location in File ("Worksheet")	Input (Location in file or value if directly entered) in Order of Use in Formula	Output (Value)
***Rupture and Puncture Abstractions.xls* (Continued)**			
Built-in Excel Command: **ln(number),** Calculates the natural-log of the input	"TAD Kinematic Abstraction" Cells: C19:C21, D19:D21	"TAD Kinematic Abstraction" Cells: A19:A21; B19:B21	ln(input) for use in Power Law Function
	"TAD Rubble Abstraction" Cells: C19:D21	"TAD Rubble Abstraction" Cells: A19:A21; B19:B21	
Built-in Excel Command: **PI(),** Provides the Number π for Calculations	"TAD Rubble Data" Cells: G8:J24, G32:J48	NA	π
Built-in Excel Command **Max(Number1, Number2, …)**, Returns the Largest Value in the Inputs	"TAD Rubble Data" Cells: L8:O24, L32:O48	"TAD Rubble Data" Cells: 0, (Q11 - G8:J24) / (Q11 – 0.5) 0, (Q11 - G32:J48) / (Q11 – 0.5)	Probability of Rupture (Puncture)
Built-in Excel Command: **Add Trendline (chart input),** Calculates the Linear Fit to the Data of the Form y = m*x + b, and the R^2 Value	"TAD Kinematic Abstraction" Plot Cells: E8:I31	"TAD Kinematic Abstraction" Cells: C19:D21	ln(Prob. of Incipient Rupture) = 1.7449 * ln(PGV) – 4.4204 R^2 = 0.9959
	"TAD Rubble Abstraction" Plot Cells: E8:I31	"TAD Rubble Abstraction" Cells: C19:D21	ln(Prob. of Puncture) = 1.6971 * ln(PGV) – 3.8656 R^2 = 0.9958
***WP-Rubble Damage Abstraction 17-mm Degraded.xls*[21]**			
Built-in Excel Command: **SQRT(number),** Calculates the Square Root of the	"Data at 0.40 mps PGV" Cells: B4:R4	4/3	1.1547
Built-in Excel Command: **AVERAGE (Number1, Number 2, …)**, Calculates the Mean of the Input Numbers	"Data at 0.40 mps PGV" Cells: S4:S12	"Data at 0.40 mps PGV" Cells: A4:R12	Average (input)
	"ACMs at 4.07 PGV" Cells: S8:S10, T8:T10, B25, B69, M25, M69, X25, X69, AI69	"ACMs at 4.07 PGV" Cells: B8:R8; B9:R9; B10:R10; L8:R8; P9:R9; Q10:R10; B18:B24; B66:B68; M18:M24; M66:M68; X18:X24; X66:X68; AI66:AI68	

[21] The formulas used in worksheets "Data at 1.04 mps PGV", "Data at 2.44 mps PGV", and "Data at 4.07 mps PGV" were not documented in this table because these worksheets use the same format and equations as the worksheet "Data at 0.40 mps PGV". For questions regarding these three worksheets, refer to the documentation of the worksheet "Data at 0.40 mps PGV".
The formulas used in the worksheet "Gamma Abstraction – Modified" were not documented in this table because this worksheet uses the same format and equations as the worksheet "Gamma Abstraction". For questions regarding the formulas found in "Gamma Abstraction – Modified", refer to the documentation for the worksheet "Gamma Abstraction".

Table B-2. Formulas used in Spreadsheets in Output DTN: MO0703PASDSTAT.001 (Continued)

Formula (Bold), Function	Location in File ("Worksheet")	Input (Location in file or value if directly entered) in Order of Use in Formula	Output (Value)
***WP-Rubble Damage Abstraction 17-mm Degraded.xls* (Continued)**			
Built-in Excel Command: **AVERAGE (Number1, Number 2, …)**, Calculates the Mean of the Input Numbers (Continued)	"Gamma Abstraction" Cells: C21, E21, G21	"Gamma Abstraction" Cells: C14:C20; E14:E20; G14:G20	
	"Log-Normal Abstraction" Cells: D21, G21, J21	"Log-Normal Abstraction" Cells: D14:D20; G14:G16; J14:J15	
	"Expected Damage" Cell:D17	"Data at 2.44 mps PGV" Cells: M10, N10	
Built-in Excel Command: **Median(Number1, Number2, ...)**, Returns the Median of the Given Input	"Data at 0.40 mps PGV" Cells: T4:T12	"Data at 0.40 mps PGV" Cells: A4:R12	Median (input)
Built-in Excel Command: **MAX(Number1, Number2, …)**, Returns the Maximum of the Given Input	"Data at 0.4 mps PGV" Cells: U4:U12	"Data at 0.4 mps PGV" Cells: B4:R12	Max(input)
Built-in Excel Command: **STDEV(Number1, Number2,…)**, Calculates the Standard Deviation of the Input Numbers	"ACMs at 4.07 PGV" Cells: U8:U10, B26, B70, M26, M70, X26, X70, AI70	"ACMs at 4.07 PGV" Cells: L8:R8; P9:R9; Q10:R10; B18:B24; B66:B68; M18:M24; M66:M68; X18:X24; X66:X68; AI66:AI68	Standard Deviation (input)
	"Gamma Abstraction" Cells: C22, E22, G22	"Gamma Abstraction" Cells: C14:C20; E14:E20; G14:G20	
$a_i = a_1 + \sum_{j=2}^{i} \frac{1}{n}$ $a_1 = \frac{1}{2n}$ n = # of cases with nonzero damage areas, Calculates the Cumulative Probability	"ACMs at 4.07 PGV" Cells: C18:C24, C66:C68, N18:N24, N66:N68, Y66:Y68, AJ66:AJ68	Number of Nonzero Damaged Areas for Given PGV Level	Cumulative Probability
Built-in Excel Command: **GAMMAINV (probability, alpha, beta)**, Calculates the Inverse of the Gamma Cumulative Distribution Using the Probability Associated with the Distribution, Alpha, and Beta	"ACMs at 4.07 PGV" Cells: D18:D24, D66:D68	"ACMs at 4.07 PGV" Cells: (C18:C24, $(B25/B26)^2$, $B26^2/B25$) (C66:C68, $(B69/B70)^2$, $B70^2/B69$)	Surface Area from Gamma Distribution
	"Gamma Abstraction" Cells: Q20:U26	"Gamma Abstraction" Cells: Q18:U18, O20:O26, P20:P26	

Table B-2. Formulas used in Spreadsheets in Output DTN: MO0703PASDSTAT.001 (Continued)

Formula (Bold), Function	Location in File ("Worksheet")	Input (Location in file or value if directly entered) in Order of Use in Formula	Output (Value)
***WP-Rubble Damage Abstraction 17-mm Degraded.xls* (Continued)**			
Built-in Excel Command: **SUM(Number1, Number2,….)**, Calculates the Sum of the Inputs	"ACMs at 4.07 PGV" Cells: E27, E71, P49, AA27	"ACMs at 4.07 PGV" Cells: E18:E24; E66:E68; P42:P48; AA18:AA24	Sum(input)
Built-in Excel Command: **ln(number),** Calculates the natural-log of the input	"ACMs at 4.07 PGV" Cells: M18:M24, X66:X68	"ACMs at 4.07 PGV" Cells: B18:B24; P9:R9	ln(input)
	"Log-Normal Abstraction" Cells: D14:D20; G14:16; J14:J15	"Log-Normal Abstraction" Cells: C14:C20; P9:R9; I14:I15	
Built-in Excel Command: **NORMINV (probability, mean, standard_dev)**, Calculates the Inverse of the Normal Cumulative Distribution for the Specified Mean and Standard Deviation	"ACMs at 4.07 PGV" Cells: O18:O24, O42:O48, O66:O68, Z66:Z68, Z80:Z82	"ACMs at 4.07 PGV" Cells: N18:N24, M25, M26; N42:N48, M25, M26; N66:N68, M69, M70; Y66:Y68, X69, X70; Y80:Y82, X69, X70;	ln(Surface Area)
	"Log-Normal Abstraction" Cells: O15:S21	"Log-Normal Abstraction" Cells: (NORMINV(O13:S13, M15:M21, N15:N21))	
Built-in Excel Command: **exp(number)**, Calculates the Exponent Applied to the Base e	"ACMs at 4.07 PGV" Cells: O42:O48, Z80:Z82	"ACMs at 4.07 PGV" Cells: (NORMINV(N42:N48, M25, M26)) (NORMINV(Y80:Y82, X69, X70))	e^{input} Surface Area from Log-Normal Distribution
	"Log-Normal Abstraction" Cells: O15:S21	"Log-Normal Abstraction" Cells: (NORMINV(O13:S13, M15:M21, N15:N21))	
$\varepsilon + (\beta - \varepsilon)*((-1)*\ln(1-\text{Probability}))^{1/\alpha}$, Calculates the Weibull Value	"ACMs at 4.07 PGV" Cells: Z18:Z24, AK66:AK68	"ACMs at 4.07 PGV" Cells: X29, X28, Y18:Y24, X27; AI73, AI72, AJ66:AJ68, AI71	Weibull Value
Built-in Excel Command: **Solver**, Solves for a Given Cell by Minimizing Another Cell	"ACMs at 4.07 PGV" Cells: AA27, AL74	"ACMs at 4.07 PGV" Cells: X27:X29; AI71:AI73	Sum of Squared Differences Minimized Using Solver
Built-in Excel Command: **Add Trendline (chart input),** Calculates the Quadratic Fit to the Data of the Form y = a*x2 + b*x + c	"Gamma Abstraction" Plot Cells: B29:F48, F29:K48	"Gamma Abstraction" Cells: B26:C28; G26:H28	Mean = 0.0083948 * $(\%YS)^2$ – 1.7755048 * (%YS) + 94.0116400 Standard Deviation = 0.011194 * $(\%YS)^2$ – 2.319894 * (%YS) + 120.182831

Table B-2. Formulas used in Spreadsheets in Output DTN: MO0703PASDSTAT.001 (Continued)

Formula (Bold), Function	Location in File ("Worksheet")	Input (Location in file or value if directly entered) in Order of Use in Formula	Output (Value)
***WP-Rubble Damage Abstraction 17-mm Degraded.xls* (Continued)**			
Built-in Excel Command: **Add Trendline (chart input),** Calculates the Quadratic Fit to the Data of the Form y = a*x2 + b*x + c (Continued)	"Log-Normal Abstraction" Plot Cells: A28:D47, F28:J47	"Log-Normal Abstraction" Cells: B25:C27; F25:G27	Mean = -0.005880 * $(\%YS)^2$ + 0.992618 * (%YS) – 41.399671 Standard Deviation = 0.002068 * $(\%YS)^2$ – 0.481918 *(%YS) + 27.84936
$(\mu / \sigma)^2$, Calculates Alpha	"Gamma Abstraction" Cells: O20:O26	"Gamma Abstraction" Cells M20:M26, N20:N26	Alpha
$(\sigma)^2 / \mu$, Calculates Beta	"Gamma Abstraction" Cells: P20:P26	"Gamma Abstraction" Cells: N20:N26, M20:M26	Beta
WP-Rubble Damage Abstraction 23-mm Degraded.xls			
All of the formulas used in this file are used in the file *WP-Rubble Damage Abstraction 17-mm Degraded.xls*. For documentation of the formulas used in this file, refer to documentation of formulas used in the file *WP-Rubble Damage Abstraction 17-mm Degraded.xls*.			

Sources: Output DTN: MO0703PASDSTAT.001, Files *CDSP Kinematic Damage Abstraction 17-mm Degraded.xls*, *CDSP Kinematic Damage Abstraction 23-mm Degraded.xls*, *CDSP Kinematic Damage Abstraction 23-mm Intact.xls*, *DS Damaged Areas with Rubble.xls*, *Fault Displacement Abstraction.xls*, *Frame Fragility Analysis.xls*, *Kinematic Damage Abstraction 17-mm Degraded.xls*, *23-mm Degraded.xls*, *Kinematic Damage Abstraction 23-mm Intact.xls*, *Lith Rubble Abstraction.xls*, *Nonlith Damage Abstraction for DS.xls*, *Nonlith Rockfall Abstraction.xls*, *Plate Fragility Analysis.xls*, *Rupture and Puncture Abstractions.xls*, *WP-Rubble Damage Abstraction 17-mm Degraded.xls*, and *WP-Rubble Damage Abstraction 23-mm Degraded.xls*.

B.3 DESCRIPTION OF OUTPUTS FROM THE SPREADSHEETS IN OUTPUT DTN: MO0703PASDSTAT.001

Table B-3 identifies the outputs from the 16 spreadsheets in Statistical Analyses for Seismic Damage Abstractions, output DTN: MO0703PASDSTAT.001. The first column describes the type and nature of the output. The second column identifies the worksheet/cells that produce the output. These worksheets/cells are in the spreadsheets in output DTN: MO0703PASDSTAT.001. The third column identifies the location in this report where the output from the spreadsheet is presented.

Table B-3. Outputs in Spreadsheets in Output DTN: MO0703PASDSTAT.001

Description of Output	Location in File ("Worksheet")	Location in Report
CDSP Kinematic Damage Abstraction 17-mm Degraded.xls		
Table Documenting the Probability of Damage for the Codisposal WP with 17-mm-Thick OCB and Degraded Internals	"Prob of Damage – Old" Cells: A6:D13	Section 6.6.2.2, Table 6-21
Existence of 1 End-to-End Impact of Adjacent WPs at the 0.4 m/s PGV Level	"WP-WP Data" Cells: D5:D38	Section 6.6.2.2
Plot of Probability of Damage Based on Kinematic Calculations for the Codisposal WP with 17-mm-Thick OCB and Degraded Internals	"Prob of Damage – Old" Cells: E4:R32	Section 6.6.2.2, Figure 6-38
Table Documenting a Comparison of Damaged Area for the Codisposal WP with 17-mm-Thick OCB and Degraded Internals	"Prob of Damage Anal. 17-mm OCB" Cells: A6:I12	Section 6.6.2.2, Table 6-22
Table Documenting the Reinterpretation of Nonzero Damage for a Codisposal WP with 17-mm-Thick OCB and Degraded Internals at the 0.4 m/s PGV Level	"Prob of Damage Anal. 17-mm OCB" Cells: A16:Q53	Section 6.6.2.2, Table 6-23
Plot of Probability of Damage with Reinterpreted Damage States for the Codisposal WP with 17-mm-Thick OCB and Degraded Internals	"Prob of Damage – New" Cells: E5:O26	Section 6.6.2.2, Figure 6-39
Table Documenting the PGV-Intercepts for the Codisposal WP with Degraded Internals	"Prob of Damage – New" Cells: A14:D20	Section 6.6.2.2, Table 6-24
Table Documenting the Revised Probability of Damage for the Codisposal WP with Intact Internals	"Prob of Damage – New" Cells: A29:D38	Section 6.6.2.2, Table 6-25 Section 6.12.2, Step10, Table 6-76
Q-Q Plots for Conditional Damaged Areas versus a Gamma Distribution for the Codisposal WP with 17-mm-Thick OCB and Degraded Internals at 0.4 m/s, 1.05 m/s, 2.44 m/s, and 4.07 m/s PGV Level and 90% RST	"Gamma for 90%_d17" Cells: H7:O21, H25:O48, H56:O79, H96:O120	Section 6.6.2.3, Figures 6-40 through 6-43
Table Documenting the Mean and Standard Deviations for the Conditional Damaged Areas for the 17-mm-Thick OCB with Degraded Internals	"Gamma for 90%_d17" Cells: A146:E149 "Gamma for 100%_d17" Cells: A147:E150 "Gamma for 105%_d17" Cells: A131:E134	Section 6.6.2.3, Table 6-26
Plot of Quadratic Fits to the Mean and Standard Deviation of Conditional Damaged Areas for the Codisposal WP with 17-mm-Thick OCB and Degraded Internals at 90% RST	"Gamma for 90%_d17" Cells: G145:N167, N145:U167	Section 6.6.2.3, Figure 6-44
Plot of the Comparison of Percentiles on the Gamma Distributions to Conditional Damaged Areas for the Codisposal Waste Package with 17-mm-Thick OCB and Degraded Internals	"Gamma for 90%_d17" Cells: A187:J216	Section 6.6.2.3, Figure 6-45
μ = (-0.0011*(RST - 100) + 0.0670)*PGV^2 + (-0.0376*(RST - 100) + 0.1879)*PGV + (0.0034*(RST - 100) - 0.0187)	"Dependence on RST" Cells: A42:J42	Section 6.6.2.3, Equation 6.6-2 Section 6.12.2, Step 11, Table 6-77
σ = (0.0078*(RST - 100) - 0.0266)*PGV^2 + (-0.0490*(RST - 100) + 0.4066)*PGV + (0.0011*(RST - 100) - 0.0605)	"Dependence on RST" Cells: N42:W42	Section 6.6.2.3, Equation 6.6-3 Section 6.12.2, Step 11, Table 6-77

Table B-3. Outputs in Spreadsheets in Output DTN: MO0703PASDSTAT.001 (Continued)

Description of Output	Location in File ("Worksheet")	Location in Report
***CDSP Kinematic Damage Abstraction 17-mm Degraded.xls* (Continued)**		
Plot Demonstrating that Linear Scaling Provides a Reasonable Estimate of the Mean Conditional Damaged Area at 105% RST	"Dependence on RST" Cells: F9:M32	Section 6.6.2.3, Figure 6-46
Plot Demonstrating that Linear Scaling Provides a Reasonable Estimate of the Standard Deviation of Conditional Damaged Area at 105% RST	"Dependence on RST" Cells: M9:S32	Section 6.6.2.3, Figure 6-47
Plot of Comparison of Equation 6.6-2 to the Mean of the Conditional Damaged Areas	"Dependence on RST" Cells: A51:G79	Section 6.6.2.4, Figure 6-48
Plot of Comparison of Equation 6.6-3 to the Standard Deviation of the Conditional Damaged Areas	"Dependence on RST" Cells: N52:T80	Section 6.6.2.4, Figure 6-49
Q-Q Plot for Conditional Damaged Areas versus a Log-Normal Distribution for the Codisposal WP with 17-mm-Thick OCB and Degraded Internals at 1.05 m/s PGV Level and 90% RST	"Log-Normal for 90%_d17" Cells: J24:P44	Section 6.6.2.4, Figure 6-50
Plot of Comparison of Mean Conditional Damaged Areas for the Kinematic Response of the TAD-Bearing and Codisposal WPs	"CDSP-TAD Comparison" Cells: F4:M27	Section 6.9.9, Figure 6-89
Plot of Comparison of Standard Deviations for the Conditional Damaged Areas from the Kinematic Response of the TAD-Bearing and Codisposal WPS	"CDSP-TAD Comparison" Cells: M4:S27	Section 6.9.9, Figure 6-90
CDSP Kinematic Damage Abstraction 23-mm Degraded.xls		
Table Documenting the Probability of Damage for the Codisposal WP with 23-mm-Thick OCB and Degraded Internals	"Prob of Damage – Old" Cells: A6:D13	Section 6.6.2.2, Table 6-21
Revised Damage States and Probabilities for the Codisposal WP with 23-mm-Thick OCB and Degraded Internals	"Prob of Damage Anal. 23-mm OCB" Cells: A16:Q55	Section 6.6.2.2
Table Documenting the PGV-Intercepts for the Codisposal WP with Degraded Internals	"Prob of Damage – New" Cells: A14:D20	Section 6.6.2.2, Table 6-24
Table Documenting the Revised Probability of Damage for the Codisposal WP with Intact Internals	"Prob of Damage – New" Cells: A26:D34	Section 6.6.2.2, Table 6-25 Section 6.12.2, Step 10, Table 6-76
Table Documenting the Gamma Distribution Parameters for the Conditional Damaged Areas on the Codisposal WP	"Dependence on RST" Cells: A42:J42, M42:V42	Section 6.12.2, Step 11, Table 6-77
CDSP Kinematic Damage Abstraction 23-mm Intact.xls		
Table Documenting the Probability of Damage for the Codisposal Waste Package with 23-mm-Thick OCB and Intact Internals	"Prob of Damage – Old" Cells: A7:D14	Section 6.6.1.2, Table 6-13
Plot of the Probability of Damage for the Codisposal WP with 23-mm-Thick OCB and Intact Internals	"Prob of Damage – Old" Cells: F4:S39	Section 6.6.1.2, Figure 6-25

Table B-3. Outputs in Spreadsheets in Output DTN: MO0703PASDSTAT.001 (Continued)

Description of Output	Location in File ("Worksheet")	Location in Report
***CDSP Kinematic Damage Abstraction 23-mm Intact.xls* (Continued)**		
Table Documenting the Reinterpretation of Nonzero Damage for a Codisposal WP at the 0.4 m/s PGV Level	"Prob of Damage Anal. 23-mm OCB" Cells: A16:Q53	Section 6.6.1.2, Table 6-14
Table Documenting the Revised Probability of Damage for the Codisposal WP with 23-mm-Thick OCB and Intact Internals	"Prob of Damage – New" Cells: A24:D31	Section 6.6.1.2, Table 6-15 Section 6.12.2, Step 10, Table 6-76
Plot of the Probability of Damage with Reinterpreted Damage States for the Codisposal WP with 23-mm-Thick OCB and Intact Internals	"Prob of Damage – New" Cells: E4:P26	Section 6.6.1.2, Figure 6-26
Table Documenting the Mean and Standard Deviations of the Conditional Damaged Areas for the 23-mm-Thick OCB with Intact Internals	"Gamma for 90%_i23" Cells: A138:E141 "Gamma for 100%_i23" Cells: D54:E57 "WP Total" Cells: F41:G42, F82:G83, G123:G124, G164:G165	Section 6.6.1.3, Table 6-16
Q-Q Plot for Conditional Damaged Areas versus a Gamma Distribution for the Codisposal WP with 23-mm-Thick OCB and Intact Internals at 0.4 m/s, 1.05 m/s, 2.44 m/s, and 4.07 m/s PGV and 90% RST	"Gamma for 90%_i23" Cells: I7:O21, I24:O45, I51:O73, I91:O112	Section 6.6.1.3, Figures 6-27 through 6-30
Plot of Quadratic Fits to the Mean and Standard Deviation of Conditional Damaged Areas for the Codisposal WP with 23-mm-Thick OCB and Intact Internals at 90% RST	"Gamma for 90%_i23" Cells: F138:M161, N138:T161	Section 6.6.1.3, Figure 6-31
Plot of Comparison of Percentiles on the Gamma Distributions to Conditional Damaged Areas for the Codisposal Waste Package with 23-mm-Thick OCB and Intact Internals at 90% RST	"Gamma for 90%_i23" Cells: A185:H216	Section 6.6.1.3, Figure 6-32
Table Documenting the Gamma Distribution Parameters for the Conditional Damaged Areas on the Codisposal WP with 23-mm-Thick OCB and Intact Internals	"Dependence on RST" Cells: A41:J44, N41:W44	Section 6.6.1.3, Table 6-18 Section 6.12.2, Step 11, Table 6-77
Plot of Comparison of Equations in Table 6-18 to the Mean of the Conditional Damaged Areas	"Dependence on RST" Cells: A54:G76	Section 6.6.1.3, Figure 6-33
Plot of Comparison of Equations in Table 6-18 to the Standard Deviation of the Conditional Damaged Areas	"Dependence on RST" Cells: N584:T81	Section 6.6.1.3, Figure 6-34
Plot of Expected Damage Area for the Codisposal Waste Package with 23-mm-Thick OCB and Intact Internals	"Expected Damage" Cells: E4:O29	Section 6.6.1.3, Figure 6-35
Q-Q Plot of Conditional Damaged Areas versus a Log-Normal Distribution for the Codisposal Waste Package with 23-mm-Thick OCB and Intact Internals at 1.05 m/s PGV Level and 90% RST	"Log-Normal for 90%_i23" Cells: K20:Q41	Section 6.6.1.4, Figure 6-36

Table B-3. Outputs in Spreadsheets in Output DTN: MO0703PASDSTAT.001 (Continued)

Description of Output	Location in File ("Worksheet")	Location in Report
DS Damaged Areas with Rubble.xls		
Plot of Least Squares Fit for *ln(A+1)* versus *ln(PGV-H1)*	"PGV-H1 to (A+1) Regression" Cells: G15:N47	Section 6.10.1.2, Figure 6-91
Q-Q Plot for the Residuals of *ln(A+1)* versus a Normal Distribution	"PGV-H1 to (A+1) Regression" Cells: S15:AA47	Section 6.10.1.2, Figure 6-92
Plot of Comparison of Percentiles on the Log-Normal Distributions with Observations for (A+1)	"PGV-H1 to (A+1) Regression" Cells: AG16:AP50	Section 6.10.1.2, Figure 6-93
$B_{(A+1)}$ = 0.515	"PGV-H1 to (A+1) Regression" Cell: O67	Section 6.10.1.2, Equation 6.10-5
Plot of Cumulative Distribution Function for Damaged Area at 1.05 m/s, 2.44 m/s, and 4.07 m/s PGV Level with 100% Rockfall Load	"Summary" Cells: A5:J31, J5:T31, A35:J62	Section 6.10.1.3, Figures 6-94 through 6-96
Fault Displacement Abstraction.xls		
Table Documenting the Maximum Allowable Displacement with Drift Collapse for an Intact Drip Shield	"Tables" Cells: C20:C25	Section 6.11.1.1, Table 6-57
Table Documenting the Maximum Allowable Displacement after Drip Shield Failure	"Tables" Cells: B31:B36	Section 6.11.1.2, Table 6-58
Table Documenting Fault Displacement from Mean Hazard Curves	"Hazard Calcs" Cells: H10:H14, H30:H34, H50:H54, H70:H74, H90:H94, H110:H114, H130:H134, H150:H154, H170:H174, H190:H194, H210:H214	Section 6.11.3, Table 6-60
Table Documenting the Maximum Allowable Fault Displacements Before a WP Group is Pinned	"Tables" Cells: B31 and B36	Section 6.11.4, Table 6-62
Table Documenting the Parameters for Simplified Groups of WPs	"Tables" Cells: D147:D148, F147:G148, C147:C148, B147:B148, E147:E148	Section 6.11.4, Table 6-63
Table Documenting Fault Displacement at the 10−4, 105, 106, 107, and 108 Annual Exceedance Frequencies	"Tables" Cells: A110:F121	Section 6.11.3, Table 6-61
Table Documenting the Mean Annual Exceedance Frequencies that Cause WP Failure	"Tables" Cells: B169:B174, C169:C174	Section 6.11.4, Table 6-64
Table Documenting the Expected Number of WPs Emplaced on Each Fault	"Tables" Cells: B185:D188	Section 6.11.4, Table 6-65
Table Documenting the Expected Number of WP Failures versus Annual Exceedance Frequency	"Tables" Cells: A196:D200	Section 6.11.5, Table 6-66 Section 6.12.2, Step 21, Table 6-86
Frame Fragility Analysis.xls		
Plot of Plastic Load Capacity of the Framework as a Function of Plate Thickness and Boundary Conditions	"Load and Capacity" Cells: D53:K80	Section 6.8.3.2, Figure 6-71
Table Documenting Log-Normal Parameters for the Ultimate Load Capacity of the Drip Shield Framework	"Load and Capacity" Cells: E50:G52	Section 6.8.3.2, Table 6-38
Plot of Comparison of Percentiles on the Log-Normal Distributions with Plastic Load Capacity of the Drip Shield Framework	"Load and Capacity" Cells: L53:R80	Section 6.8.3.2, Figure 6-72

Table B-3. Outputs in Spreadsheets in Output DTN: MO0703PASDSTAT.001 (Continued)

Description of Output	Location in File ("Worksheet")	Location in Report
***Frame Fragility Analysis.xls* (Continued)**		
Table Documenting the Probability of Failure for the Drip Shield Framework	"Summary" Cells: A5:E13, A16:E24, A27:E35	Section 6.8.3.3, Table 6-39 Section 6.12.2, Step 8, Table 6-75
Plots of the Probability of Collapse of the Drip Shield Framework for 10%, 50%, and 100% Rockfall Load	"Summary" Cells: N12:U36, G27:N51, G2:N26	Section 6.8.3.3, Figures 6-73 through 6-75
Kinematic Damage Abstraction 17-mm Degraded.xls		
Table Documenting Preliminary Probability of Damage for the TAD-Bearing WP with Degraded Internals	"Prob of Damage – Old" Cells: A7:D13	Section 6.5.2.2, Table 6-7
Plot of Preliminary Probability of Damage Based on Kinematic Calculations for the TAD-Bearing WP with 17-mm-Thick OCB and Degraded Internals	"Prob of Damage – Old" Cells: E4:M29	Section 6.5.2.2, Figure 6-12
Zero End-to-End Impacts of Adjacent Packages at the 0.40 m/s PGV Level	"WP-WP Data" Cells: D5:D55	Section 6.5.2.2
Table Documenting Comparison of Damaged Area for the TAD-Bearing WP with 17-mm Thick OCB and Degraded Internals Using Different Analytical Methods at the 0.4 m/s PGV Level	"Prob of Damage Anal. 17-mm OCB" Cells: A6:F11	Section 6.5.2.2, Table 6-8
Table Documenting Reinterpretation of Nonzero Damage for a TAD-Bearing Waste Package at the 0.4 m/s PGV Level	"Prob of Damage Anal. 17-mm OCB" Cells: B14:K68	Section 6.5.2.2, Table 6-9
Plot of Revised Probability of Damage with Reinterpreted Damage States for the TAD-Bearing WP with 17-mm Thick OCB and Degraded Internals	"Prob of Damage – New" Cells: E5:M29	Section 6.5.2.2, Figure 6-13
Table Documenting PGV-Intercepts for the TAD-Bearing WP with Degraded Internals	"Prob of Damage – New" Cells: A17:D24	Section 6.5.2.2, Table 6-10
Table Documenting Revised Probability of Damage for the TAD-Bearing WP with Degraded Internals	"Prob of Damage – New" Cells: A32:D41	Section 6.5.2.2, Table 6-11 Section 6.12.2, Step 13, Table 6-78
Q-Q Plot for Conditional Damaged Area versus a Gamma Distribution for the TAD-Bearing WP with 17-mm-Thick OCB and Degraded Internals at 90% RST and 0.4 m/s, 1.05 m/s, 2.44 m/s, and 4.07 m/s PGV Level	"Gamma for 90%_d17" Cells: V7:Z32, V37:Z62, V65:Z91, AA65:AF91	Section 6.5.2.3, Figures 6-14 through 6-17
Table Documenting Mean and Standard Deviations of the Conditional Damaged Areas for the 17-mm-Thick OCB with Degraded Internals	"Gamma for 90%_d17" Cells: AB4:AF7 "Gamma for 100%_d17" Cells: Y4:AC7 "Gamma for 105%_d17" Cells: Y4:AC7	Section 6.5.2.3, Table 6-12
Plot of Quadratic Fits to the Mean and Standard Deviation of Conditional Damaged Areas for the TAD-Bearing Waste Package with 17-mm-Thick OCB and Degraded Internals at 90% RST	"Gamma for 90%_d17" Cells: AB9:AF29, AB31:AF51	Section 6.5.2.3, Figure 6-18

Table B-3. Outputs in Spreadsheets in Output DTN: MO0703PASDSTAT.001 (Continued)

Description of Output	Location in File ("Worksheet")	Location in Report
***Kinematic Damage Abstraction 17-mm Degraded.xls* (Continued)**		
Plot of the Comparison of Percentiles on the Gamma Distributions to Conditional Damaged Areas for the TAD-Bearing Waste Package with 17-mm-Thick OCB and Degraded Internals at 90% RST	"Gamma for 90%_d17" Cells: AI21:AQ53	Section 6.5.2.3, Figure 6-19
Plot Demonstrating that Linear Scaling Provides a Conservative Estimate of the Mean Conditional Damaged Area at 105% RST	"Dependence on RST" Cells: F8:L32	Section 6.5.2.3, Figure 6-20
Plot Demonstrating that Linear Scaling Provides a Conservative Estimate of the Standard Deviation of the Conditional Damaged Area at 105% RST	"Dependence on RST" Cells: L8:S32	Section 6.5.2.3, Figure 6-21
μ = (-0.00838*(RST - 100) + 0.1394)*PGV^2 + (-0.02224*(RST - 100) + 0.1649)*PGV + (-0.00628*(RST - 100) + 0.0766)	"Dependence on RST" Cells: A41:K41	Section 6.5.2.3, Equation 6.5-2 Section 6.12.2, Step 14, Table 6-79
σ = (-0.00828*(RST - 100) + 0.0902)*PGV^2 + (0.00665*(RST - 100) + 0.0170)*PGV + (-0.02851*(RST - 100) + 0.1932)	"Dependence on RST" Cells: L41:W41	Section 6.5.2.3, Equation 6.5-3 Section 6.12.2, Step 14, Table 6-79
Plot of Comparison of Equation 6.5-2 to the Mean of the Conditional Damaged Areas	"Dependence on RST" Cells: B47:H71	Section 6.5.2.4, Figure 6-22
Plot of Comparison of Equation 6.5-3 to the Standard Deviation of the Conditional Damaged Areas	"Dependence on RST" Cells: L47:R71	Section 6.5.2.4, Figure 6-23
Q-Q Plot of Conditional Damaged Areas versus a Log-Normal Distribution for the TAD-Bearing Waste Package with 17-mm-Thick OCB and Degraded Internals at 1.05 m/s PGV Level and 90% RST	"Log-Normal for 90%_d17", Cells: S37:W62	Section 6.5.2.4, Figure 6-24
Kinematic Damage Abstraction 23-mm Degraded.xls		
Table Documenting Preliminary Probability of Damage for the TAD-Bearing WP with Degraded Internals	"Prob of Damage – Old" Cells: A7:D13	Section 6.5.2.2, Table 6-7
Table Documenting PGV-Intercepts fro the TAD-Bearing WP with Degraded Internals	"Prob of Damage – New" Cells: A17:D24	Section 6.5.2.2, Table 6-10
Table Documenting Revised Probability of Damage for the TAD-Bearing WP with Degraded Internals	"Prob of Damage – New" Cells: A37:D46	Section 6.5.2.2, Table 6-11 Section 6.12.2, Step 13, Table 6-78
Table Documenting Gamma Distribution Parameters for the Conditional Damaged Areas on the TAD-Bearing WP	"Dependence on RST" Cells: A41:K41, L41:W41	Section 6.12.2, Step 14, Table 6-79
Kinematic Damage Abstraction 23-mm Intact.xls		
Table Documenting Probability of Damage for the TAD-Bearing WP with 23-mm-Thick OCB and Intact Internals	"Probability of Damage" Cells: A6:D12	Section 6.5.1.2, Table 6-4 Section 6.12.2, Step 13, Table 6-78
Plot of the Probability of Damage for the TAD-Bearing WP with 23-mm-Thick OCB and Intact Internals	"Probability of Damage" Cells: E4:M28	Section 6.5.1.2, Figure 6-7

Table B-3. Outputs in Spreadsheets in Output DTN: MO0703PASDSTAT.001 (Continued)

Description of Output	Location in File ("Worksheet")	Location in Report
***Kinematic Damage Abstraction 23-mm Intact.xls* (Continued)**		
Mean and Standard Deviation for Gamma Distribution	"ACM for 90%_i23" Cells: H13, H14	Section 6.5.1.3
Q-Q Plot for Conditional Nonzero Damaged Areas versus a Gamma Distribution for the TAD-Bearing WP with 23-mm Thick OCB and Intact Internals	"ACM for 90%_i23" Cells: N7:S33	Section 6.5.1.3, Figure 6-8
Plot of Expected Damage Area for the TAD-Bearing WP with 23-mm-Thick OCB and Intact Internals	"Expected Damage" Cells: E4:M28	Section 6.5.1.4, Figure 6-9
Table Documenting the Gamma Distribution Parameters for the Conditional Damaged Areas on the TAD-Bearing WP	"ACM for 90%_i23" Cells: H13:H14	Section 6.12.2, Step 14, Table 6-79
Lith Rubble Abstraction.xls		
Plot of Weighted Probability of Lithophysal Rock Volume Caving into the Drifts	"Probability of Rockfall" Cells: G12:N37	Section 6.7.1.1, Figure 6-51
Q-Q Plots for Conditional Lithophysal Rock Volume versus a Gamma Distribution at the 0.4 m/s, 1.05 m/s, and 2.44 m/s PGV Level	"Gamma Abstraction" Cells: K8:P29, I32:O53, I57:O78	Section 6.7.1.2, Figures 6-52 through 6-54
Table Documenting the Mean and Standard Deviations of the Conditional Lithophysal Rock Volumes	"Gamma Abstraction" Cells: Q4:U6	Section 6.7.1.2, Table 6-29
Plot of Quadratic Fits to the Mean and Standard Deviation of Conditional Lithophysal Rock Volume	"Gamma Abstraction" Cells: Q7:V26, Q27:V47	Section 6.7.1.2, Figure 6-55
Plot of Comparison of Percentiles on the Gamma Distributions for Conditional Lithophysal Rock Volumes	"Gamma Abstraction" Cells: W21:AG53	Section 6.7.1.2, Figure 6-56
Probabilities that the Volume of Rockfall from all Relevant Seismic Events Exceeds the Volume for Drift Collapse	"Exceed Prob for V>V0" Cells: I56, M56, Q56	Section 6.7.1.7.4
Nonlith Damage Abstraction for DS .xls		
Impact Energies Associated with Selected Rocks: 99.9th 99th, 90th, 70th, 40th, and 20th Percentiles	"Data Catalogs" Cells: A35:O42	Section 6.10.2.2
Table Documenting the Characteristics of Representative Rock Blocks	"Data Catalogs" Cells: J27:J33, C27:C33, K27:K33, N27:N33, A35: O42	Section 6.10.2.2, Table 6-49
Table Documenting Damaged Areas and Plate Failures for the 2.44 m/s PGV Level with 10-mm-Thick Plates	"2.44 ms PGV 10-mm Plate" Cells: AF22:AG71, AD22:AD746	Section 6.10.2.3, Table 6-51
Table Documenting the Probability of Damage/Plate Failures from Rock Block Impacts	"Summary" Cells: I12:L18	Section 6.10.2.4, Table 6-52 Section 6.12.2, Step 18, Table 6-82
Table Documenting Conditional Probabilities of Damage States 1 through 5	"Summary" Cells: H44:K83	Section 6.10.2.5, Table 6-53 Section 6.12.2, Step 18, Table 6-83
Table Documenting Mean and Standard Deviations of the Conditional Damaged Areas for Realizations of Rock Block Impacts on the Drip Shield	"Summary" Cells: B20:E34	Section 6.10.2.6, Table 6-54 Section 6.12.2, Step 18, Table 6-84

Table B-3. Outputs in Spreadsheets in Output DTN: MO0703PASDSTAT.001 (Continued)

Description of Output	Location in File ("Worksheet")	Location in Report
Nonlith Damage Abstraction for DS .xl* (Continued)*s		
Q-Q Plots for Conditional Nonzero Damaged Area from Rock Block Impacts versus a Gamma Distribution at 2.44 m/s PGV Level with 15-mm, 10-mm, and 5-mm Plate Thickness	"2.44 ms PGV 15-mm Plate" Cells: AK22:AQ74 "2.44 ms PGV 10-mm Plate" Cells: AK22:AQ47 "2.44 ms PGV 5-mm Plate" Cells: AK22:AQ47	Section 6.10.2.7, Figures 6-98 through 6-100
Plots of Comparison of Percentiles on the Gamma Distributions to Conditional Damaged Areas for the 15-mm, 10-mm, and 5-mm-Thick Plates	"Plot 15-mm" Cells: A42:J71 "Plot 10-mm" Cells: A42:J71 "Plot 5-mm" Cells: A42:J71	Section 6.10.2.7, Figures 6-101 through 6-103
Q-Q Plot for Conditional Nonzero Damaged Area from Rock Block Impacts versus a Log-Normal Distribution at 2.44 m/s PGV Level with 10-mm-Thick Plates	"2.44 ms PGV 10-mm Plate" Cells: AV22:BB47	Section 6.10.2.8, Figure 6-104
Q-Q Plot for Conditional Nonzero Damaged Area from Rock Block Impacts versus a Log-Triangular Distribution	"2.44 ms PGV 10-mm Plate" Cells: BI22:BO47	Section 6.10.2.8, Figure 6-105
Nonlith Rockfall Abstraction.xls		
Table Documenting Data for Rockfall Volume in Nonlithophysal Rock	"Lith Versus Nonlith" Cells: K13:L67, R13:S67, Y13:Z58	Section 6.7.2, Table 6-30
Table with a Comparison of Statistical Parameters for Conditional Rock Volumes in Lithophysal and Nonlithophysal Rock	"Lith Versus Nonlith" Cells: A35:G38	Section 6.7.2.1, Table 6-31
Plot of Comparison of Rockfall Volumes in Lithophysal and Nonlithophysal Rock	"Lith Versus Nonlith" Cells: AJ10:AR37	Section 6.7.2.1, Figure 6-57
Q-Q Plots for Conditional Nonlithophysal Rock Volume versus a Gamma Distribution at the 1.05 m/s, 2.44 m/s, and 5.35 m/s PGV Level	"Gamma Abstractions" Cells: H13:O36, W13:AD36, AL13:AS36	Section 6.7.2.3, Figures 6-58 through 6-60
Plot of Quadratic Fits to the Mean and Standard Deviation of Conditional Nonlithophysal Rock Volume	"Gamma Abstractions" Cells: AT18:AY38, AT38:AY58	Section 6.7.2.3, Figure 6-61
Plot of Comparison of Percentiles on the Gamma Distributions for Conditional Nonlithophysal Rock Volumes	"Gamma Abstractions" Cells: AZ32:BJ65	Section 6.7.2.4, Figure 6-62
Plate Fragility Analysis.xls		
β_A = 0.700	"PGV-H1 to A Correlation" Cell: N65	Section 6.8.1.1, Equation 6.8-14
Logarithmic Standard Deviation at 1.05 m/s, 2.44 m/s, and 5.35 m/s PGV Level	"PGV-H1 to A Correlation" Cells: K49:K51	Section 6.8.1.1 Table 6-32
Plot of Correlation of Peak Vertical Acceleration with PGV-H1	"PGV-H1 to A Correlation" Cells: F13:M45	Section 6.8.1.1, Figure 6-63
Q-Q Plot for a Normal Distribution Versus the Residuals of *ln(A)* with Respect to the Least Squares Fit, λ_A	"PGV-H1 to A Correlation" Cells: R13:Z45	Section 6.8.1.1, Figure 6-64
Plot of Comparison of Percentiles on the Log-Normal Distributions with Peak Vertical Acceleration	"PGV-H1 to A Correlation" Cells: AF14:AO48	Section 6.8.1.1, Figure 6-65
Q-Q Plot for a Log-Normal Distribution Versus the Residuals of the Logarithm of Average Pressure with λ_{STAT}	"Load and Capacity" Cells: J1:P21	Section 6.8.1.2, Figure 6-66

Table B-3. Outputs in Spreadsheets in Output DTN: MO0703PASDSTAT.001 (Continued)

Description of Output	Location in File ("Worksheet")	Location in Report
***Plate Fragility Analysis.xls* (Continued)**		
Plot of Plastic Load Capacity as a Function of Plate Thickness and Boundary Conditions	"Load and Capacity" Cells: F52:M79	Section 6.8.2.1, Figure 6-67
Table Documenting the Probability of Failure for the Drip Shield Plates	"Summary" Cells: A6:E14, A17:E25, A28:E36	Section 6.8.2.2, Table 6-35 Section 6.12.2, Step 7, Table 6-74
Plot of Probability of Failure of the Drip Shield Plates for 10%, 50% and 100% Rockfall Load	"Summary" Cells: N13:U37, G30:N54, G4:N27	Section 6.8.2.2, Figures 6-68 through 6-90
Rupture and Puncture Abstractions.xls		
Table Documenting Average Probability Data for Incipient Rupture and Rupture of the TAD-Bearing WP with Degraded Internals	"TAD Kinematic Abstraction" Cells: D10:D13, M10:M13	Section 6.5.2.1, Table 6-6
Coefficients c and d for Power Law Fit for TAD-Bearing WP	"TAD Kinematic Abstraction" Cells: K16:K17	Section 6.5.2.1
Plot of Least-Squares Fit for Power-Law Dependence for Probability of Incipient Rupture for TAD-Bearing WP	"TAD Kinematic Abstraction" Cells: E8:I31	Section 6.5.2.1, Figure 6-10
Plot of Comparison of Power-Law Dependence with Probability Data for Incipient Rupture and for Rupture for TAD-Bearing WP	"TAD Kinematic Abstraction" Cells: E31:I55	Section 6.5.2.1, Figure 6-11
Table Documenting the Average Probability Data for Incipient Rupture and Rupture for the Codisposal WP with Degraded Internals	"CDSP Kinematic Abstraction" Cells: D10:D13, K10:K13	Section 6.6.2.1, Table 6-20
Coefficients a, b, c, and d for Power-Law Fit for Codisposal WP	"CDSP Kinematic Abstraction" Cells: B17:B18, H17:H18	Section 6.6.2.1
Plot of Comparison of Power-Law Dependence with Probability Data for Incipient Rupture and for Rupture for Codisposal WP with Degraded Internals	"CDSP Kinematic Abstraction" Cells: C17:G40	Section 6.6.2.1, Figure 6-37
Plot of Least Squares Fit for Power Law Dependence for Probability of Rupture for TAD-Bearing WP Surrounded by Rubble with 17-mm OCB and Degraded Internals	"TAD Rubble Abstraction" Cells: E8:I31	Section 6.9.1, Figure 6-77
Numerical Values of c and d for Power Law Fit for Average Probability of Rupture	"TAD Rubble Abstraction" Cells: K16:K17	Section 6.9.1
Plot of Power-Law Dependence for Probability of Puncture for the TAD-Bearing WP Surrounded by Rubble with 23-mm and 17-mm OCB and Degraded Internals	"TAD Rubble Abstraction" Cells: E32:I55	Section 6.9.1, Figure 6-78
WP-Rubble Damage Abstraction 17-mm Degraded.xls		
Plot of Probability of Damage for the TAD-Bearing WP Surrounded by Rubble for the 17-mm-Thick OCB and Degraded Internals	"Probability of Damage" Cells: E4:M29	Section 6.9.2, Figure 6-80
Table Documenting the Probability of Damage for the WP Surrounded by Rubble	"Probability of Damage" Cells: A4:D9	Section 6.9.2, Table 6-43 Section 6.12.2, Step 16, Table 6-80

Table B-3. Outputs in Spreadsheets in Output DTN: MO0703PASDSTAT.001 (Continued)

Description of Output	Location in File ("Worksheet")	Location in Report
***WP-Rubble Damage Abstraction 17-mm Degraded.xls* (Continued)**		
Q-Q Plot for Conditional Damaged Areas versus a Gamma Distribution for the TAD-Bearing WP Surrounded by Rubble at 4.07 m/s PGV Level and 90% RST	"ACMs at 4.07 PGV" Cells: F13:K35	Section 6.9.3, Figure 6-81
Table Documenting the Mean and Standard Deviations of the Conditional Damaged Areas for the 17-mm-Thick OCB with Degraded Internals	"Data at 2.44 mps PGV" Cells: V10, W10 "Gamma Abstraction" Cells: C21, C22, E21, E22, G21, G22	Section 6.9.3, Table 6-44
Q-Q Plot for Conditional Damaged Areas versus a Gamma Distribution for the TAD-Bearing WP Surrounded by Rubble at 4.01 m/s PGV Level and 100% RST	"ACMs at 4.07 PGV" Cells: F61:K83	Section 6.9.3, Figure 6-82
Table Documenting the Mean and Modified Standard Deviations of the Conditional Damaged Areas for the 17-mm-Thick OCB with Degraded Internals	"Data at 2.44 mps PGV" Cells: V10, W10 "Gamma Abstraction - Modified" Cells: C22, C23, E22, E23, G22, G23	Section 6.9.3, Table 6-45
Plot of Quadratic Fits to the Mean and Standard Deviation of Conditional Damaged Areas for the TAD-Bearing WP Surrounded by Rubble for the 17-mm-Thick OCB with Degraded Internals at the 4.07 m/s PGV Level	"Gamma Abstraction – Modified" Cells: B30:F49, F30:K49	Section 6.9.3, Figure 6-83
Plot of the Comparison of Percentiles on the Gamma Distributions to Conditional Damaged Areas for the TAD-Bearing WP Surrounded by Rubble at the 4.07 m/s PGV Level	"Gamma Abstraction – Modified" Cells: M28:S50	Section 6.9.3, Figure 6-84
Plot of the Expected Damage Area for the TAD-Bearing WP Surrounded by Rubble	"Expected Damage" Cells: E4:N28	Section 6.9.4, Figure 6-85
Gamma Distribution Parameters for Conditional Damaged Areas on the TAD-Bearing WP Surrounded by Rubble	"Gamma Abstraction – Modified" Cells: B30:F49, F30:K49	Section 6.12.2, Step 17, Table 6-81
WP-Rubble Damage Abstraction 23-mm Degraded.xls		
Plot of Probability of Damage for the TAD-Bearing WP Surrounded by Rubble for the 23-mm-Thick OCB and Degraded Internals	"Probability of Damage" Cells: F4:N28	Section 6.9.2, Figure 6-79
Table Documenting the Probability of Damage for the WP Surrounded by Rubble	"Probability of Damage" Cells: A4:D9	Section 6.9.2, Table 6-43 Section 6.12.2, Step 16, Table 6-80
Q-Q Plot for Conditional Damaged Areas versus a Gamma Distribution for the TAD-Bearing WP Surrounded by Rubble	"ACMs at 4.07 PGV" Cells: F14:K36	Section 6.9.5, Figure 6-86
Table Documenting the Mean and Standard Deviations of the Conditional Damaged Areas for the 23-mm-Thick OCB with Degraded Internals	"Gamma Abstraction – Modified" Cells: C20:C21, E20:E21, G20:G21	Section 6.9.5, Table 6-46
Plot of Quadratic Fits to the Mean and Standard Deviation of Conditional Damaged Areas for the TAD-Bearing WP Surrounded by Rubble at the 4.07 m/s PGV Level	"Gamma Abstraction – Modified" Cells: B27:K46	Section 6.9.5, Figure 6-87

Table B-3. Outputs in Spreadsheets in Output DTN: MO0703PASDSTAT.001 (Continued)

Description of Output	Location in File ("Worksheet")	Location in Report
***WP-Rubble Damage Abstraction 23-mm Degraded.xls* (Continued)**		
Plot of Comparison of Percentiles on the Gamma Distributions to Conditional Damaged Areas for the TAD-Bearing WP Surrounded by Rubble at the 4.07 m/s PGV Level	"Gamma Abstraction – Modified" Cells: M28:S51	Section 6.9.5, Figure 6-88
Gamma Distribution Parameters for Conditional Damaged Areas on the TAD-Bearing WP Surrounded by Rubble	"Gamma Abstraction – Modified" Cells: B27:F46, G27:K46	Section 6.12.2, Step 17, Table 6-81

Sources: DTN: MO0703PASDSTAT.001, Files *CDSP Kinematic Damage Abstraction 17-mm Degraded.xls*, *CDSP Kinematic Damage Abstraction 23-mm Degraded.xls*, *CDSP Kinematic Damage Abstraction 23-mm Intact.xls*, *DS Damaged Areas with Rubble.xls*, *Fault Displacement Abstraction.xls*, *Frame Fragility Analysis.xls*, *Kinematic Damage Abstraction 17-mm Degraded.xls*, *23-mm Degraded.xls*, *Kinematic Damage Abstraction 23-mm Intact.xls*, *Lith Rubble Abstraction.xls*, *Nonlith Damage Abstraction for DS.xls*, *Nonlith Rockfall Abstraction.xls*, *Plate Fragility Analysis.xls*, *Rupture and Puncture Abstractions.xls*, *WP-Rubble Damage Abstraction 17-mm Degraded.xls*, and *WP-Rubble Damage Abstraction 23-mm Degraded.xls*.

INTENTIONALLY LEFT BLANK

APPENDIX C
INDEPENDENT TECHNICAL REVIEW FOR POSTDEVELOPMENT MODEL VALIDATION OF THE SEISMIC DAMAGE ABSTRACTIONS

BY DR. GABRIEL R. TORO

APPENDIX C

INDEPENDENT TECHNICAL REVIEW OF DAMAGE ABSTRACTIONS IN SEISMIC CONSEQUENCE ABSTRACTION REPORT (MDL-WIS-PA-000003 REV 03A AND REV03F)[22]

PREPARED BY
GABRIEL R. TORO
RISK ENGINEERING, INC.
REV 0—September 2, 2007

INTRODUCTION

I have performed a technical review of seismic damage abstractions contained in Chapter 6 of the report titled "Seismic Consequence Abstraction" (MDL-WIS-PA-000003 REV03A) and I have reviewed some of the associated spreadsheets in DTN MO0703PASDSTAT.001, according to the criteria contained in Section 2.3.2.3 of TWP-MGR-GS-000004 REV 01 ICN 02.

There are a few areas, however, where I identified some potential problems or limitations with the abstractions. My comments below are concerned mainly with these areas. In my view, most or all of these problems or limitations may be resolved by means of additional sensitivity calculations or clarifications in the report.

SPECIFIC COMMENTS

The comments are organized by Section, but many of the issues I identified apply to multiple abstractions. A few editorial comments are also included.

6.4.2 Site-Specific Ground Motions

The PGV scaling approach employed, where all components of the ground motion are scaled by the same factor, is conservative because it does not take into account the phenomenon of "regression to the mean," as briefly explained below.

De-aggregation results indicate that the high amplitudes associated with annual exceedence probabilities of the hazard curve are largely due to high values of epsilon (see PSHA report for definition of epsilon and for deaggregation results). Therefore, the H1 component of motion (i.e., the component that we are explicitly controlling) has a high value of epsilon(PGV). Because the values of epsilon for different components of motion or for different ground motion characteristics are not fully correlated, one would expect that (conditional on the high epsilon(PGV) for the H1 component), the other components and ground motion measures would have somewhat lower values of their corresponding epsilons.

If the transverse two and vertical components of motion are important contributors to damage, then the scaling approach employed may introduce significant conservatism (unless the

[22] EDITORIAL NOTE: Dr. Toro's review is presented in this appendix in standard typeface. Yucca Mountain Project responses to Dr. Toro's comments have been inserted into Dr. Toro's review and are shown in an italic typeface.

associated correlation coefficients are high). On the other hand, the use of rational approaches for the joint treatment of multiple components or measures of ground motion in PSHA and in performance assessment is beyond the current state of practice, despite a few pioneering papers published recent years (e.g., Bazzurro and Cornell, 2002; Baker and Cornell, 2006).

Response: *There is general agreement that the current sets of postclosure ground motions are conservative because of the issue identified by Dr. Toro and because two of the ground motion components are "unbounded". Although the first horizontal component of each ground motion incorporates a physical limit for the response of the lithophysal rock based on the maximum strain criterion discussed in Section 6.4.3 of this report, this limit is not applied to the second horizontal and vertical components of the ground motion. With this procedure, the current sets of ground motions often have higher values of PGV in the second horizontal or vertical components than the PGV for the first horizontal component. The current sets of ground motions are therefore expected to provide a conservative bias to the seismic damage abstractions for the license application. The degree of conservatism may be quantified if revised postclosure ground motions become available in the future.*

6.5.1.2 Probability of Damage (for TAD-Bearing Waste Package)

a. **Sample size.** The kinematic calculations indicate no damage for PGV values other than 4.07 m per second, but these results are based on calculations performed with only 17 sets of time histories. This sample size makes it impossible to resolve probabilities lower than 1/17=0.0588 (and, moreover, probabilities of this order will be poorly resolved). If one considers that packages I, J, and K, appear (at first glance) to be behaving independently, the above resolution threshold diminishes to 1/51=0.0196 for the TAD packages. One could argue that this probability is negligible, but one must also consider that events with lower PGVs are much more frequent than stronger events, as indicated by Figure 6-7 or Table 6-3[23]. For instance, earthquakes with PGV of 1 m per second are approximately a thousand times more frequent than those with PGV of 4 m per second. The same problem arises in a number of other abstractions, where the probability of nonzero damage is found to be zero based on these 17 time histories. This potentially serious problem is mitigated by at least two factors, as follows: (a) the kinematic results appear to be very conservative for these low PGVs, as demonstrated, for example, in Table 6-8; (b) the damaged areas are expected to be smaller for these lower values for PGV. Nonetheless, I feel that this issue needs to be addressed in more detail.

   Response: *Each seismic damage abstraction represents the damaged area as two "models": (1) the probability that a positive damaged area will occur during a seismic event and (2) a conditional probability distribution for the resulting damaged area, conditional on damage occurring. This separation is convenient for developing the abstractions because it eliminates observations with zero damage from the conditional probability distributions, making it easier to evaluate the use of log-normal, gamma, and other probability distributions to represent the nonzero*

[23] Strictly speaking, this comparison should be made in terms of occurrence frequencies and not in terms of exceedence frequencies. In practice, the hazard curve in Figure 6-7 and the associated rate-density curve (i.e., minus the derivative of the hazard curve) have very similar shapes.

damaged areas. This separation is not important for TSPA because the response in the seismic scenario is based on the product of these two models. In other words, all of the available data are used to define the expected damaged area, which is the important quantity for TSPA and can be thought of as the product of the probability of damage and the (conditional) mean damaged area. From the viewpoint of expected damaged area, both the probability of damage and the mean conditional damaged area become smaller as PGV becomes smaller. In addition, each of these models (i.e., functions) is based on data from the whole range of PGV values, so the behavior near the zero damage level, corresponding to low values of PGV, is based on more than the 17 or 51 data points at each PGV level.

b. **Damage Area Cutoff.** A cutoff of 0.0024 m^2 was introduced in order to resolve problems created by the spatial resolution of the finite element model used in the kinematic calculations. This cutoff may cause two problems, as follows: (1) underestimation of the probability of nonzero damage (the most important of the two problems; see discussion above regarding the importance of this probability for low values of PGV), and (b) this cutoff may distort the conditional distribution of damaged area. Examination of the Q-Q plots suggest that the second problem is less significant. I suggest that the effect of this cutoff be investigated by means of sensitivity analyses.

Response: *The rationale for the 0.0024 m^2 cut-off is based on the numerical limitations of the finite-element mesh for the damage catalogs (see Section 6.5) and the need to interpolate for damaged area in the kinematic methodology. This methodology produces conservative results at low PGV levels, as noted by Dr. Toro (see item (a) above). The differences in magnitude of damaged area from the kinematic approach and from the single waste package calculations are significantly greater than the 0.0024 m^2 cutoff. For the TAD-bearing waste package with degraded internals, the single waste package model has zero damage when the kinematic damage areas are less than 0.24 m^2, as discussed in Section 6.5.2.2. For the codisposal waste package with degraded internals, the single waste package model has zero damage when the kinematic areas are less than 0.057 m^2, as discussed in Section 6.6.2.2. These values are a factor of 100 and 24 (respectively) greater than the numerical cut-off of 0.0024 m^2. This comparison provides convincing evidence that the 0.0024 m^2 cutoff represents numerical noise in the finite-element grid and kinematic interpolation process, particularly at the 0.4 m/s PGV level, rather than a significant bias in the probability of nonzero damage.*

6.5.2.1 Probability of Rupture (for TAD Package with 17-mm-Thick OCB with Degraded Internals)

Distribution of Failed Area. No justification is provided for the choice of a uniform distribution shape (a justification is provided for the limits of this distribution, however). If this is an important assumption, with a significant effect on the TSPA results, a justification should be provided.

Response: *The sensitivity of TSPA results to the type of conditional probability distribution for failed area is not known at this time.*

6.5.2.3 Conditional Probability Distributions for Nonzero Damaged Area (for TAD Package with 17-mm-Thick OCB with Degraded Internals)

Some of the higher points on the Q-Q plots in Figures 6-15 through 6-18 appear to deviate from the 1-1 line. Upon closer examination, one notices that these points correspond to very high percentiles of the conditional distribution and that points in the mean $\pm$ 2 sigma range are close to the 1-1 line. Therefore, these deviations are not a source of concern.

Also, examination of the means and standard deviations in Table 6-12 indicate that the coefficient of variation seems to decrease as PGV increases. This is actually the result that one would expect. A gamma distribution with a coefficient of variation of 1.0 or greater has an exponential-like shape, with its most-likely (or modal) value at zero (this is what one would expect when the probability of non-damage is low). In contrast, a gamma distribution with a lower coefficient of variation has a normal-like shape, with a most-likely value in the middle of the distribution. The distribution becomes more symmetrical and normal-like as the coefficient of variation decreases (possibly as a result of having multiple disjoint areas of damage with random sizes).

Response: *This is a very useful insight into the behavior of the conditional nonzero damaged areas and the associated gamma distributions from the kinematic model.*

6.6.1.3 Conditional Probability Distribution for Nonzero Damaged Area (for CDSP Package with Intact Internals)

For 100% residual-stress threshold (RST), the number of packages showing non-zero damage is too small for the reliable estimation of the mean and sigma. This is another, more benign, problem arising from the small sample size of 17 time histories. Instead, the coefficient of variation obtained for the 90% RST and for the same PGV is used.

This is an appropriate solution, but I personally would have used the coefficient of variation for the 90% RST and for the PGV that corresponds to roughly the same mean damage area, regardless of PGV (leaving essentially the same standard deviation). This would preserve the pattern noted earlier, where low values of the mean area are accompanied by high values of the coefficient of variation (thereby yielding exponential-like distribution shapes).

Response: *As noted above by Dr. Toro, the coefficient of variation is greater at lower PGV levels with smaller mean values for the conditional nonzero damaged area. For example, at the 0.4 m/s PGV level at 90% RST, Table 6-17 indicates a coefficient of variation of (0.040/0.031) = 1.29, which is about twice as great as the coefficient of variation at 4.07 m/s PGV level at 90% RST, which is 0.673. Use of the greater value for the coefficient of variation would increase the standard deviation at the 100% RST to (1.29)(0.006) ~ 0.008, rather than the value of 0.004 in Table 6-18. However, the impact of this change on the TSPA will be very limited because: (1) the mean value is unchanged (as explained in the Response to 6.5.1.2(a), the mean value is anticipated to be a key parameter for TSPA, and a change in the standard deviation will not affect the mean damaged area or the mean dose), and (2) the magnitudes of*

the nonzero damaged areas are very small at 100% RST in comparison to 90% RST. This potential change is therefore anticipated to have an insignificant impact on the compliance case for the license application.

6.7.1.2 Conditional Probability Distributions (of Rockfall Volume) for Lithophysal Rockfall

a. **Exclusion of Category 1 Rock.** Rock Category 1 is excluded from the calculation of these distributions, despite their greater propensity to rockfall, because Category 1 constitutes only 3% of the total length of emplacement drifts. This is a difficult call. One could have weighted the volume data, as is done in Figure 6-52, but the resulting distribution would be difficult to interpret. For instance, in computing the volume generated by multiple events, one would add volumes occurring in different locations within the repository, which is not meaningful.

Response: *The decision to exclude Rock Category 1 was based on two considerations: (1) the exclusion has little impact on the conditional probability distributions for rockfall volumes at 1.05 m/s and 2.44 m/s PGV levels, and (2) there are only three nonzero observations for Rock Category 1 at the 0.4 m/s PGV level, providing a limited basis for defining the conditional probability distribution. These considerations are consistent with the physical response of the lithophysal units to ground motion, in the sense that the ground motions at the 1.05 m/s and 2.44 m/s PGV levels are large enough to cause significant rockfall for all rock categories, while the ground motions at the 0.4 m/s PGV level only cause significant rockfall for the weakest Category 1 rock. Given that Rock Category 1 constitutes only 3% of the emplacement drifts in lithophysal units and that the conditional probability distributions at higher PGV levels are insensitive to the presence of the Category 1 data, the exclusion of these data at 0.4 m/s PGV level is a reasonable compromise.*

b. **Distribution of Volume for 0.4 m per second PGV**. After the Category 1 volumes are removed, only three data points remain. As a result, it is impossible to obtain a reliable estimate of the standard deviation. The result is a non-monotonic COV[24] in Table 6-30 (recall that trend identified earlier, where lower values of damage area accompanied by higher COVs, which correspond to exponential-like distribution shapes; rockfall volume is likely to follow a similar trend), and problems when fitting a quadratic shape for the calculation of the standard deviation at intermediate values of PGV (see Figure 6-56). In my opinion, the approach of using a constant standard deviation for PGV values lower than 0.4 m per second is likely unconservative. I would have used the coefficient of variation observed for 1.05 m per second (i.e., slightly above 1.0) for PGVs lower than 1.05 m per second. On the other hand, the effect of this unconservative choice is probably not large because the mean rockfall volumes for low PGVs are so small.

[24] EDITORIAL NOTE: COV is the coefficient of variation, which is the ratio of the standard deviation to the mean of a data set.

Response: *Dr. Toro's comment about the COV is reasonable, but its impact on dose is likely to be small because the mean rockfall volumes for low values of PGV are so small, as he notes..*

6.8.1 Mathematical Formulation for Fragility Analysis (of Drip Shield)

a. **Fifth Paragraph.** The fifth paragraph is confusing to me. It speaks of pressures on the drip shield causing ultimate tensile failure. I guess this could be explained in terms of buckling. Further explanation may be useful in this paragraph.

Response: *The text in the fifth through seventh paragraphs has been revised to clarify the failure modes and to explain the use of pressure on the top of the drip shield.*

b. **Eq. 6.8-1.** The units in this inequality are not consistent. I would suggest to write the left-hand side as 1+A/g. This equation occurs in other sections.

Response: *Notation for Equations 6.8-1 and 6.8-2 has been clarified to fix this problem, and corrections have also been made in Sections 6.10.1.1 and 6.10.1.2.*

6.8.1.1 Conditional Probability Distribution for Peak Vertical Acceleration

The calculation of vertical PGA from horizontal PGV, seems somewhat unorthodox for a reviewer who has worked on ground motion prediction. Also, some of the results obtained are somewhat surprising, as follows:

a. The coefficient of 1.079 is somewhat unexpected. I would have expected a value lower than 1.0 because PGV has a stronger dependence on magnitude than PGA, and roughly the same dependence on distance.

b. The standard deviation of 0.700 is somewhat higher than what I expected. It tells us that knowing the PGV tells us somewhat less about vertical PGV than knowing the magnitude and the distance of the earthquake.

In addition, this approach has the following two drawbacks:

c. The calculated coefficients have high statistical uncertainties as a result of the residual standard deviation of 0.700 and of the small number of data (for instance, the uncertainty in the slope term in Eq. 6.8-12 is 0.15). In this regard, it would have been preferable to use some of the data that were assembled at a part to the PSHA study.

d. The approach used ignores the phenomenon of “regression to the mean” discussed earlier. This is conservative.

On the other hand, as indicated earlier, the use of rational approaches for the joint treatment of multiple components of ground motion in PSHA and in performance assessment is beyond the current state of practice.

Response: *The regression analysis in Section 6.8.1.1 determines a conditional probability distribution for PGA-Vertical, conditional on the value of horizontal PGV (denoted as PGV-H1) for a seismic event. This regression analysis is based on the existing sets of postclosure ground motions. This is a reasonable approach because: (1) a bounded hazard curve is available for PGV-H1, and (2) the first horizontal component of PGV for the existing sets of ground motions is scaled to a given value, and these sets of ground motions are a major input to the dynamic structural response calculations. In other words, the regression analysis in Section 6.8.1.1 is consistent with the data that provide the basis for the seismic damage abstractions.*

It is possible that an alternate measure of ground motion intensity would be a "better" measure of seismic-related damage. A "better" measure would provide lower variability about the mean for damaged areas and possibly lower variability about the mean for other seismic damage mechanisms, such as rupture or puncture. As an example, the vertical component of PGV or PGA may be better correlated with kinematic damaged area than PGV-H1 because vertical contact during waste package-to-pallet impacts is the main source of damage during kinematic response. The existence of a better measure does not invalidate the seismic damage abstractions based on PGV-H1, but it would mean that a simpler representation may be possible.

Selection of the alternate measure of ground motion intensity may not be straightforward. First, different intensity measures may be optimal for different damage processes. For example, damage for the waste package surrounded by rubble may be better correlated with the vector sum of several components of PGV or PGA because the presence of the rubble eliminates impacts and distributes dynamic loads over the whole surface of the waste package. In this situation, an intensity measure based on the magnitude of several components of the ground motion, rather than on a single component of ground motion, may provide the best results for a waste package surrounded by rubble. Second, an appropriate hazard curve must be available for the alternate measure of ground motion intensity. Ideally, this hazard curve should be bounded by the physical response of the host rock in a manner similar to that in Section 6.4.3. Finally, it is possible that a joint treatment with multiple components may produce a better measure of ground motion intensity, but this is beyond the state-of-the-art as noted by Dr. Toro.

6.8.1.2 Probability Distribution for Lithophysal Rubble Load

In my opinion, this section needs additional explanations. Here are some questions:

a. What quantities were varied in the six realizations?

b. What is the meaning of the segments?

c. Why do you compute the averages over segments first? (By the way, probably as a result of this averaging, the load has a rather low COV).

I assume that the text is supposed to be self-explanatory, in the sense that the reader should be able to obtain a general understanding of how the data for the abstractions were obtained (without having to consult the DTNs cited).

Response: *The discussion in Section 6.8.1.2 has been expanded to clarify items (a) and (b). With regard to item (c), we compute the average load over segments 11 through 20 because the*

small size of rubble particles compared to the dimensions of the drip shield leads to the expectation that the point loads from individual rock particles will be averaged over the much larger areas of the individual drip shield plates.

6.8.2.1 Ultimate Plastic Capacity of the (Drip-Shield) Plates

The logarithmic standard deviation of the plate capacity is computed by considering the difference between the capacities obtained with different boundary conditions at the bottom. The resulting logarithmic standard deviations are less than 10% for thicknesses of 10 and 15 cm. These logarithmic standard deviations may be too low, because other sources of uncertainty (such as non-uniform load distributions) are being neglected.

Response: *The boundary conditions are designed to represent two extremes of plate response, as discussed in the second paragraph of Section 6.8.2.1. Nonuniform load distributions are not anticipated to be a major uncertainty because the small size of rubble particles compared to the dimensions of the drip shield plates implies that the point loads from individual rock particles will be averaged over the larger areas of the individual drip shield plates. The plate fragility curves for the 10-mm-thick and 15-mm-thick plates are also insensitive to the values of the logarithmic standard deviation of plate capacity. The fragility curves depend on the logarithmic standard deviation of the ratio of plastic load capacity to rockfall load, which is defined in Equation 6.8-5 as* $\beta = \sqrt{\beta_{CAP}^2 + \beta_{STAT}^2}$, *where* β_{CAP} *and* β_{STAT} *are the logarithmic standard deviations of the plastic load capacity and the static rockfall load, respectively. The values of* β_{CAP} *are 0.067 and 0.035 for the 10-mm-thick and 15-mm-thick plates, respectively (see Table 6-35). The value of* β_{STAT} *is 0.149 (see Equation 6.8-16). If the values for* β_{CAP} *double or triple, this will produce only a minor change in the value of* β. *It follows that* β_{CAP} *is a small contributor to the net* β *for the fragility curves for plate thicknesses greater than 10 mm.*

6.8.3.3 Numerical Calculations

The first paragraph refers to equation 3-27. This equation number appears to be incorrect or incomplete because its format deviates from the format of other equations in this report.

Response: *The reference to Equation 3-27 is no longer in the document.*

6.9 ABSTRACTIONS FOR THE WASTE PACKAGE SURROUNDED BY RUBBLE

It would seem that the sharp blocks of non-lithophysal rock have the potential for puncturing the waste package. There is probably a good reason why this mechanism is not considered, and I suggest that this reason be explained in the report.

Response: *The potential for large rock blocks in nonlithophysal units to damage the waste package has been screened out of TSPA because the drip shield remains structurally intact, even for impact by the largest rock block on a drip shield with 10-mm thickness reduction for all components. The screening argument is presented in Section 6.10.2.11.*

6.9.1 Probability of Puncture (for Waste Package Surrounded by Rubble)

In describing these calculations, the text refers to 17 time histories, whereas the DTN MO0704PUNCTURE.000 readme file refers to 17 combinations of time history and block geometry. These block geometries should be described (or at least mentioned) in the report.

Response: *Text has been changed to mention the random block geometry for the lithophysal rock.*

Also, the results in Tables 6-42 and 6-43 for PGV≤2.44 m per second may be significantly affected by statistical uncertainty resulting from the small number of time histories (even in those cases where the average probability is nonzero). For instance, in Table 6-42 the columns for 1.05 m per second and 2.44 m per second show nonzero probabilities for only two of the time histories.

Response: *The probability of puncture is based on engineering judgment, and there is no simple approach to quantify the statistical uncertainty at this time.*

In addition, no justification is provided for the use of a uniform distribution for the failed area of a punctured package, or for the assumed upper bound on 0.10 m2. It would seem, for instance, that this area should depend on the value of PGV.

Response: *The sensitivity of TSPA results to the type of conditional probability distribution for failed area in a punctured package is not known at this time. The upper bound of 0.10 m^2 for the uniform distribution is based on two estimates for the area of a hypothetical puncture: one based on a sharp internal fragment that can puncture the OCB, and a second for a fuel basket plate that slices through the OCB. These estimates are an engineering judgment that indirectly incorporates the value of PGV through the probability of a seismic event eliminating the free space between the degraded internals and the OCB. Further details are discussed in Section 6.9.1.*

6.9.2 Probability of Damage

In contrast to what was done on earlier calculations of the probabilities of nonzero damaged area, some explanations and intermediate results seem to be missing from this section.

Response: *The probability of nonzero damage for the waste package surrounded by rubble is 0 for the 0.4 m/s and 1.05 m/s PGV levels. No further analysis or intermediate results are needed for this section.*

6.10.1.2 Dynamic Load on the Drip Shield

The regression of ln(PGV) on ln(1+A) suffers from the same limitations mentioned in regards to section 6.8.1.1, plus the additional limitation of being less physically meaningful. On the other hand, the fit turns out to be just as good as the one in 6.8.1.1 and provides considerable simplification in the calculations. From an engineering perspective, this additional step is acceptable.

Response: *The technical rationale for this regression is summarized in the response to Section 6.8.1.1.*

6.10.1.3 Damaged Area as a Function of Total Dynamic Load

Some of the cumulative distributions shown in Figures 6-96 and 6-97 (particularly those for 5-mm thickness) terminate on a large vertical step, suggesting bimodal distributions of damaged area. Examination of Table 6-49 and of the spreadsheets cited, however indicates that the second step corresponds to the maximum dynamic load considered for that particular plate thickness. Unless there is a justification for these maximum dynamic loads (are the maximum loads associated with failure?), it would seem that the distributions should extend to greater values of the damaged area.

Response: *The large vertical step corresponds to failure of the plates. The cumulative distributions in Figures 6-96 and 6-97 are intended to represent the damaged areas on the plates for loads below the ultimate plastic capacity. Loads at or beyond the ultimate plastic capacity are expected to rupture the drip shield plates, based on the fragility curves defined in Section 6.8.2. With this approach, the distributions do not need to extend to greater values of the damaged area.*

6.10.2.2 Drip Shield Damage - Single Block Impact

Figure C-1 shows the data from damaged area from Table 6-51 in graphical form. The next-to-last point for the 15-mm-thick plates appears to be anomalous (which is not a model-abstraction issue). Alternatively, it may be that the damaged area exhibits a significant dependence on quantities other than energy (which is a model-abstraction issue). Some discussion of this point may be necessary.

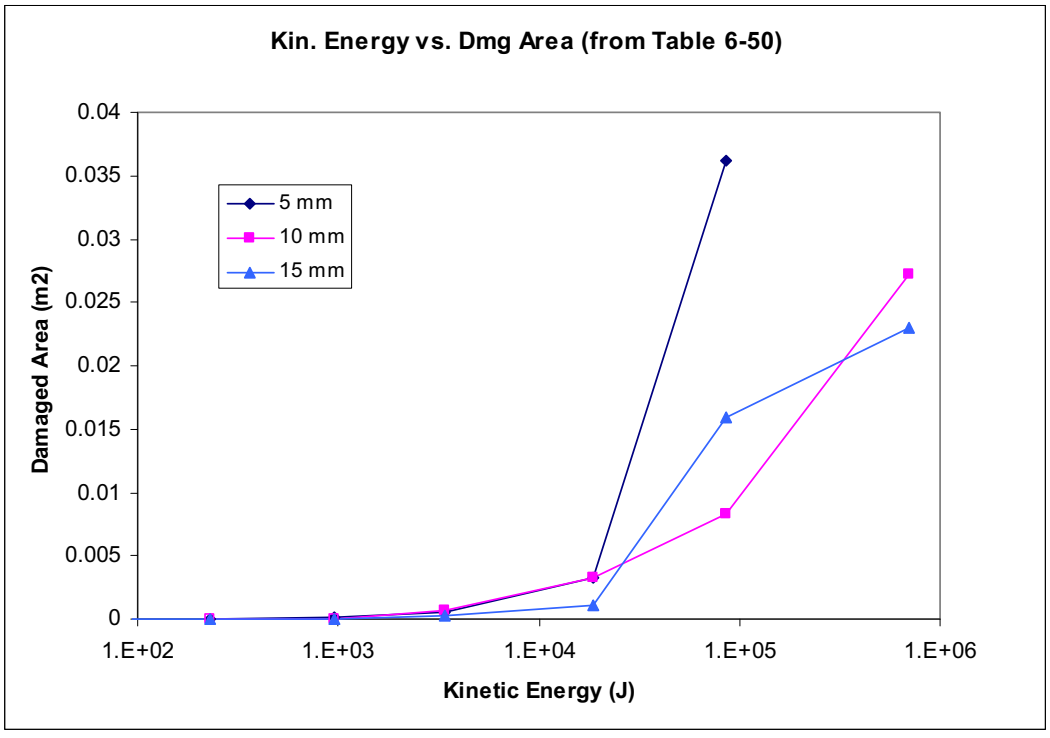

Figure C-1. Catalog data for Damaged Area from Table 6-51.

Response: *Damaged area is a function of the local plastic strain and the stiffness of the structural components of the drip shield. Increased plastic strain will result in increased damaged area for a given structure. However, for two structures with different stiffness but the same plastic strain field, the stiffer structure will have greater residual stress and a larger damaged area. The change from the 15-mm-thick plate (with no loss of thickness due to corrosion) to the 10-mm-thick plate (with a 5-mm loss of thickness in all components) alters the stiffnesses of the plates on top of the drip shield and the axial stiffeners beneath the crown of the drip shield. It is difficult to predict the combined effects of the reduced component stiffnesses from a 5-mm loss of thickness and the distribution of dynamic load between the plates and axial stiffeners of the drip shield. The rock block impact calculations and the output data for damaged area have been checked, and the "cross-over" observed in the figure represents the calculated behavior of the drip shield.*

Sections 6.11 and 6.12

I have done a brief review of section 6.11, but I have not yet prepared any review comments for it, and I have not reviewed section 6.12. It is my understanding that review of these sections was not required.

Response: *This is correct because there are no models to review in these sections.*

SUMMARY

The preceding review identifies a large number of issues, but most of them represent areas needing clarification (it may well be, however, that the reviewer failed to understand them despite their clarity or that explanations were provided elsewhere in the report), or suggestions for improvements in future versions of the report.

The only potentially serious issue that was identified in the review is the difficulty to establish the probabilities of nonzero damage for moderate and low values of PGV, given the limitation of 17 time histories. Increasing the number of time histories in order to attain a purely statistical resolution of this problem may be impractical. The preferred solution is probably to look for additional arguments to justify these probabilities of zero. If this does not succeed, one would have to devise alternative approaches that rely more on mechanics and probability and less on brute-force statistics (i.e., counting).

In addition, the effects of the cutoff of 0.0024 m^2 should be investigated, and the potential problems identified in Sections 6.10.1.3 and 6.10.2.2 should be explained or resolved.

Aside from these issues, my overall conclusion is that the abstractions contained in this report are adequate in terms of accuracy and treatment of uncertainty, despite the difficulty of this task. The approach followed is sound and it is well documented by means of Q-Q plots and plots of the data and quantiles as a function of PGV. In addition, the report contains an adequate characterization of the limitations of these abstractions.

INTENTIONALLY LEFT BLANK

APPENDIX D
ANALYSIS OF FAULT STANDOFF DISTANCE

APPENDIX D
ANALYSIS OF FAULT STANDOFF DISTANCE

D.1 INTRODUCTION

This appendix provides a summary of scientific analyses for the width of the damage zone resulting from a sliding fault that intersects an emplacement drift filled with lithophysal rubble at the Yucca Mountain site.

D.2 INTRA-BLOCK FAULT GEOMETRY

There are two primary sets of intra-block (Type II or known secondary) faults that potentially intersect emplacement drifts at the Yucca Mountain site (Figure D-1). These faults are:

- North-south trending faults such as the Ghost Dance Fault that are sub-parallel in strike to the block bounding structures. The Ghost Dance Fault exposed in Alcove 6 of the ESF has bounding edges of the 0.6-to-1.0 meter wide breccia zone of 180°/80° on the footwall and 175°/82° on the hanging wall (Eatman et al. 1997 [DIRS 157677]). Exposures of the Ghost Dance Fault at the ground surface indicate that dips vary from 75° to 85° with down-to-the-west separation (Day et al. 1998 [DIRS 101557]).
- North-west trending faults (azimuth of approximately 300^{o}) such as the Drill Hole or Pagany Wash faults. The Drill Hole Wash Fault has two splays exposed in the North Ramp of the ESF at stations 19+01 to 19+43 (Barr et al. 1996 [DIRS 100029]). The splay at 19+01 has a strike and dip of 316°/86°, and the splay at 19+43 has a strike and dip of 150°/90°. There is approximately 4 m of dip-slip separation; however, slickensides are mostly horizontal, and this is consistent with the mostly strike-slip separation. The fault zone is about 1 m wide with a minor fracture zone on the northeast (footwall) side of the fault.

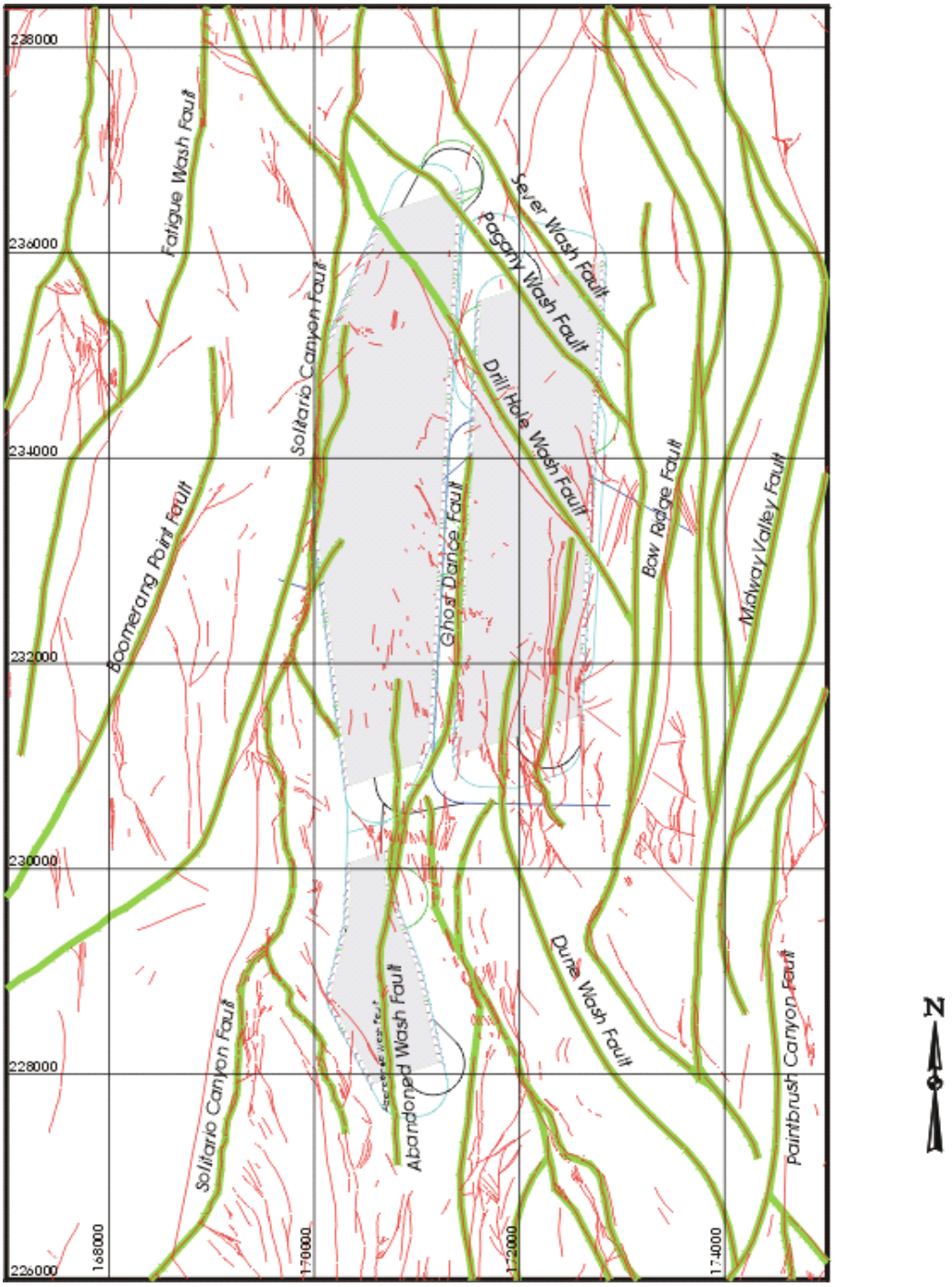

Sources: Surfaces traces of faults from *Geologic Framework Model (GFM2000)* (BSC 2004 [DIRS 170029], Figure 6-2). Facility layout for the site recommendation from *Yucca Mountain Science and Engineering Report* (DOE 2002 [DIRS 155943], Figure 2-10).

NOTES: Green lines indicate the major faults and red the minor faults. Among these, the Solitario Canyon Fault and the Bow Ridge Fault are Type I faults. The remaining named faults are Type II faults.

Figure D-1. Plan View of Yucca Mountain Area Showing Mapped Faults

D.3 ANALYSIS OF THE EMPLACEMENT TUNNEL/FAULT INTERSECTION

An analysis of the impact of shear displacement on a vertical fault through a rubble-filled drift is described here. Based on the high dip angle of the intra-block faults described in Section D.2, a vertical fault intersecting an emplacement drift is a reasonable representation for this process. For this analysis, the emplacement drifts are completely filled with rubble prior to the time of the fault displacement. This approach is reasonable for two reasons. First, the free space in a drift that is partly filled with rubble provides clearance for the translation of a waste package without damage, even if the waste package is placed directly on a fault. In other words, the case of a drift that is completely filled with rubble is conservative for rockfall loads on the waste package relative to a drift that is partly filled with rubble.

Second, emplacement drifts are expected to be significantly or completely filled with rubble from prior seismic events when a large fault displacement occurs, based on the following reasoning. As described in *Drift Degradation Analysis* (BSC 2004 [DIRS 166107], Section 6.4.2.2.2), emplacement drifts in the lithophysal rock mass are predicted to collapse for earthquake ground motions with a PGV-H1 of approximately 2 m/sec or larger. This ground motion level is characteristic of an annual exceedance frequency of 8.755×10^{-7} (see Table 6-3 in this report). Substantial lithophysal rockfall occurs for ground motions characterized by a PGV-H1 of approximately 1 m/s or larger (see Figure 6-57 in this report), which is characteristic of an annual exceedance frequency of approximately 1×10^{-5} (again, see Table 6-3). The lithophysal rock mass comprises 80% to 85% of the emplacement drift length (SNL 2007 [DIRS 179466], Table 4-1, Item Number 01-03). Additionally, in the nonlithophysal rock mass, which comprises the remaining 15% to 20% of emplacement drift area, some rockfall is predicted for ground motions associated with PGV levels of 1.05 m/s and 2.44 m/s, corresponding to annual exceedance frequencies of 1×10^{-5} and 4.5×10^{-7} (see Figure 6-58 and Table 6-3 in this report). Since emplacement drift collapse or substantial filling occurs in all emplacement drift rock mass types at greater annual exceedance frequencies than the annual exceedance frequencies associated with large fault displacement, it is reasonable to represent the drifts as filled with rockfall. The range of annual exceedance frequencies associated with large fault displacements on known secondary faults is less than or equal to 1×10^{-7}, based on the data in Table 6-61 in this report.

The two-dimensional PFC2D V2.0 program (STN: 10828-2.0-00 [DIRS 161950]) was used to simulate a 5.5-m-high longitudinal section along the axis of an emplacement drift (Figure D-2). The length of drift simulated is 33 m, containing a vertical fault through the center of the drift length. The drift length is then six drift diameters, with three diameter lengths represented on either side of the fault. The drift is represented as a two-dimensional planar slot, thus maximizing the estimate of disturbance within the rubble from the fault plane.

The drift rubble is simplified as circular particles whose diameters vary according to a normal distribution between two limits. Two cases were examined: Case 1 having a diameter represented by a normal distribution from 0.3 m to 0.6 m, and Case 2 with a diameter represented by a normal distribution from 0.15 m to 0.3 m. The particle diameter distribution for Case 1 was sized to represent the average side length of the rock blocks estimated from three-dimensional discontinuum analyses of rockfall in the nonlithophysal rock (BSC 2004 [DIRS 166107],

Section 6.3.1.2)[25]. The Case 2 particle size distribution of 0.15 m to 0.3 m represents the estimated particle size in the lithophysal rock. This size range is based on *Drift Degradation Analysis* (BSC 2004 [DIRS 166107], Section 6.4.1.1), where the spacing of the ubiquitous fracture fabric in the lithophysal rock mass is estimated to be on the order of 0.1 m, with subsequent rubble size of centimeters to decimeters.

The porosity of the rubble is approximately 15%, which represents a bulking factor of approximately 18%, which is similar to the bulking factor of approximately 20% proposed for the lithophysal rubble in *Drift Degradation Analysis* (BSC 2004 [DIRS 166107], Table P-9). The initial tangent modulus of the rubble is approximated as 150 MPa, based on empirical and numerical evidence which suggests that the initial tangent modulus lies between 50 MPa and 200 MPa for confinement between 0.1 MPa and 1 MPa (BSC 2005 [DIRS 173172], Page IX-15). The friction angle directly between rubble particles is 35° (see Assumption 5.5, Section 5).

Each simulation applies a slow, quasi-static vertical velocity to the invert of the tunnel on one side of the fault, which forces the entire drift and rubble particles upward on one side of the fault. A total vertical fault displacement of approximately 1.1 m is simulated. The depth of the zone of disturbance from the fault plane equilibrates after only a few centimeters of fault movement, so the 1.1-m shear displacement captures the maximum distance of fault influence along the longitudinal axis of the drift.

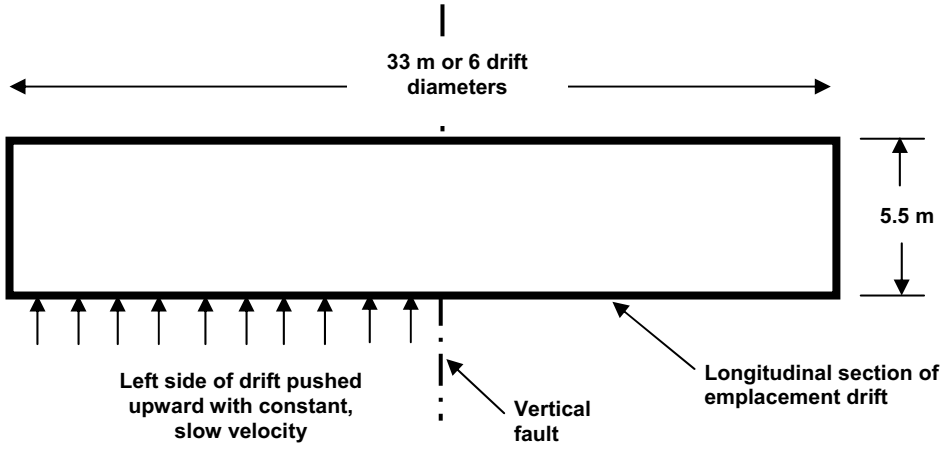

Source: Created for illustrative purposes only.

NOTES: Rubble inside the drift is not shown.
The left-hand side of the emplacement drift is pushed upward at a slow, constant velocity, which produces shear displacement on the fault and disturbance of the rubble in the drift.

Figure D-2. Two-Dimensional Conceptualization of a 33-m-Long Segment of a 5.5-m-Diameter, Rubble-Filled Emplacement Drift Cut by a Vertical Fault

[25] The mean tonnage for the 1.05 m/s, 2.44 m/s, and 5.35 m/s ground motions is given in Tables 6-11, 6-14, and 6-17, respectively, in *Drift Degradation Analysis* (BSC 2004 [DIRS 166107], Section 6.3.1.2). The average block volume was determined by dividing the tonnage by the assumed density of 2.6 tonnes/m^3. The average side length in meters was then estimated by taking the cube root of the average volume.

D.4 RESULTS

The distance of disturbance in the rubble from the fault intersection for the two cases is illustrated by two methods:

- Plots of the rubble particle geometry with superimposed particle centroid displacement vectors
- Plots of shear strain in the rubble along a drift axial line through the center of the drift.

For both Case 1 and Case 2 particle size distributions, the rubble particle displacements (Figures D-3 and D-5) are confined to two to three particle diameters from the projection of the fault dislocation plane. This result is quantified by plots of shear strain as a function of position along the axis of the drift (Figures D-4 and D-6), which indicates that the impact of fault displacement occurs within approximately 1 m from the projection of the fault plane across the rubble. Based on these results, a set-back distance from the fault of 2.5 m (approximately one-half a typical waste package length) provides a substantial safety margin to avoid excessive strain induced by fault movement in a completely collapsed drift.

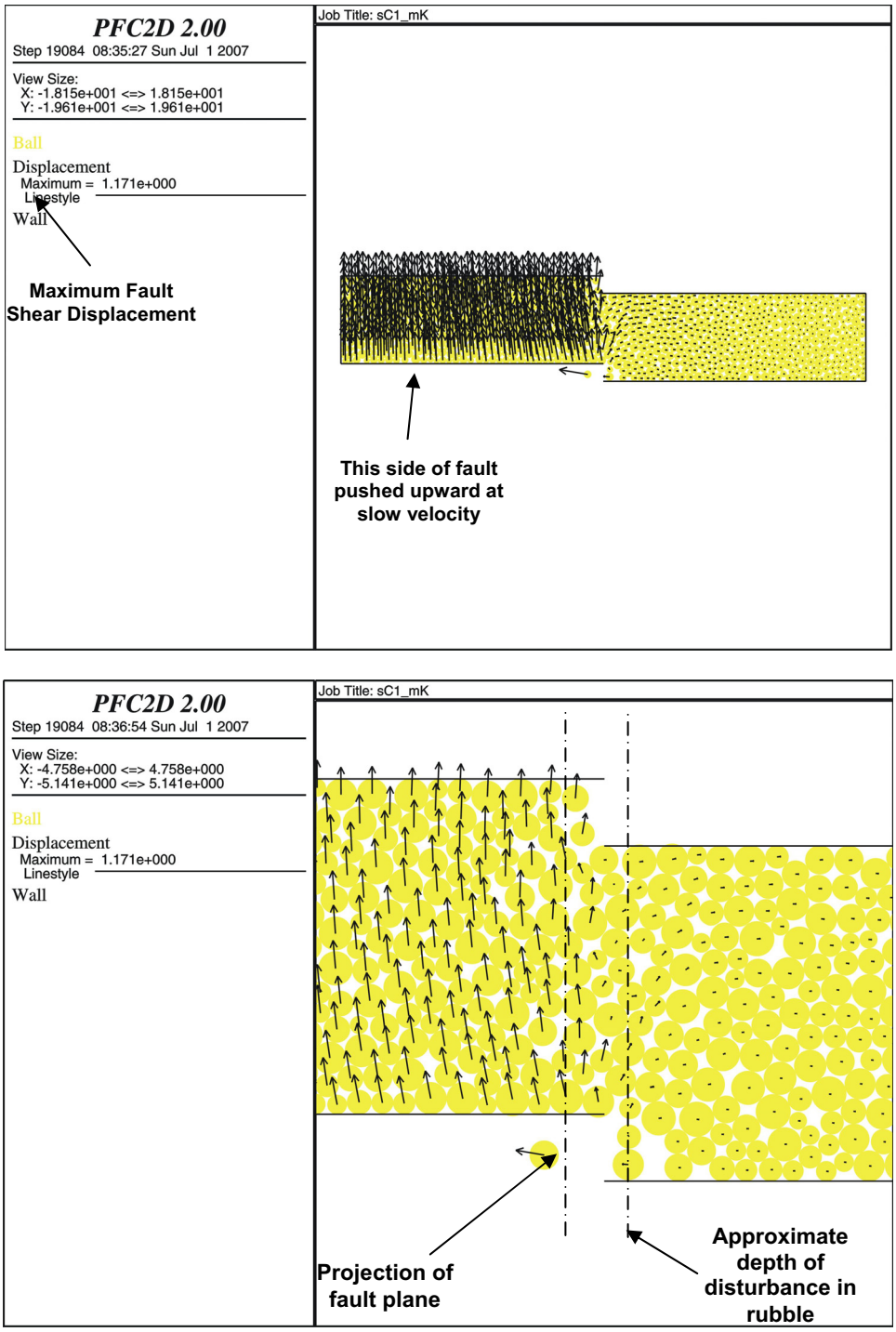

Source: Output DTN MO0707STANDOFF.000, Folder: case1, files *case1_plot1.pcx* (top plot) and *case1_plot3.pcx* (bottom plot).

NOTES: The upper figure shows the entire 33-m length, while the bottom figure shows a close-up view of the fault region.

The zone of disturbance on the right-hand side of the fault is limited to about two to three rubble particle diameters.

Figure D-3. Case 1 Displacement of Rubble Centroids after a Fault Shear Displacement of Approximately 1.1 m

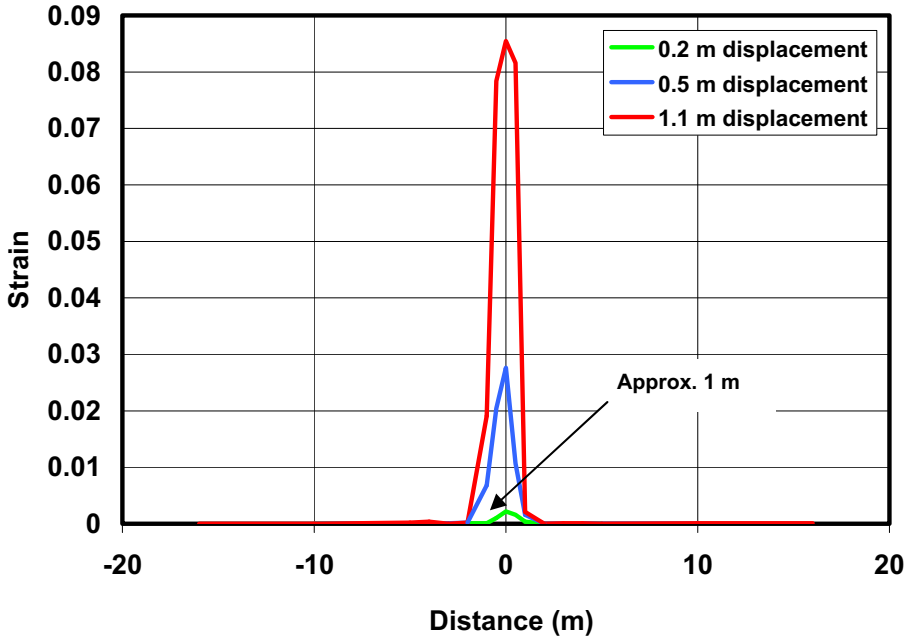

Source: Output DTN: MO0707STANDOFF.000, File *summary_case_1.xls*, worksheet "ch shear strain."

NOTE: The maximum distance of the disturbance is approximately 1 m from the fault plane.

Figure D-4. Shear Strain as a Function of Distance from the Fault for Case 1 for Three Levels of Fault Shear Displacement

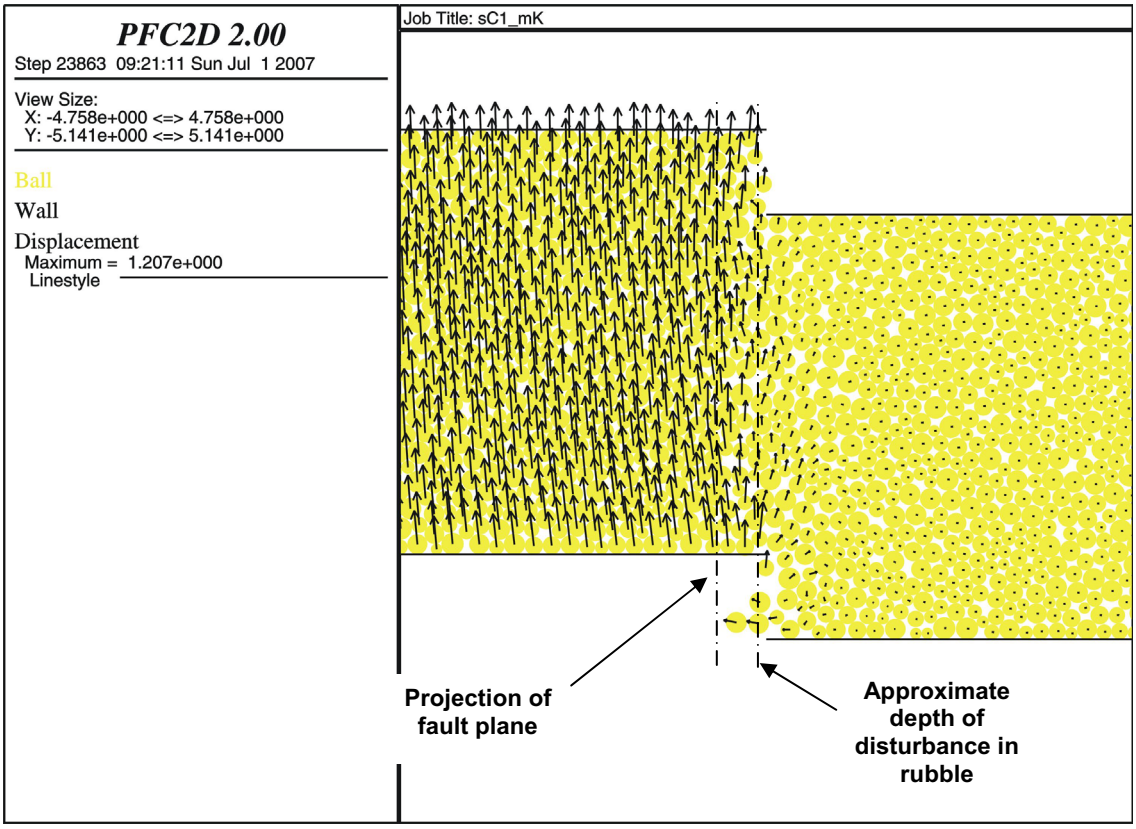

Source: Output DTN MO0707STANDOFF.000, Folder case2, file *case2_plot3.pcx*.

NOTES: This figure shows a close-up view of the fault region.

The zone of disturbance on the right-hand side of the fault is limited to about two to three rubble particle diameters.

Figure D-5. Case 2 Displacement of Rubble Centroids after a Fault Shear Displacement of 1.1 m

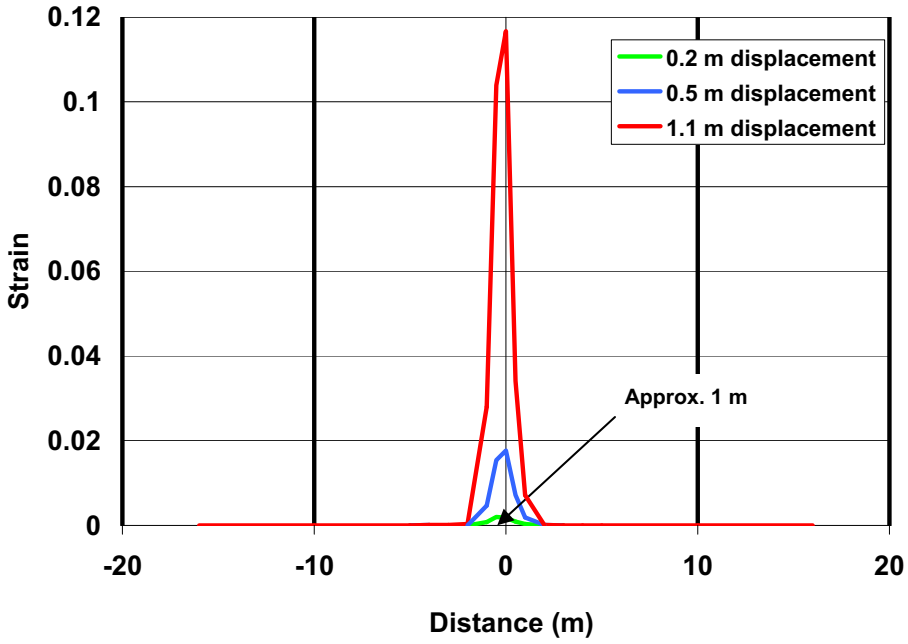

Source: Output DTN: MO0707STANDOFF.000, File *summary_case_2.xls*, worksheet "ch shear strain."

NOTE: The maximum disturbance is approximately one meter from the fault plane.

Figure D-6. Shear Strain as a Function of Distance from the Fault for Case 2 for Three Levels of Fault Shear Displacement

INTENTIONALLY LEFT BLANK